STEM CELLS IN TISSUE HOMEOSTASIS AND DISEASE

EDITED BY: Yan-Ru Lou, Wencheng Zhang, Jianjun Zhou and Zhiying He
PUBLISHED IN: Frontiers in Cell and Developmental Biology

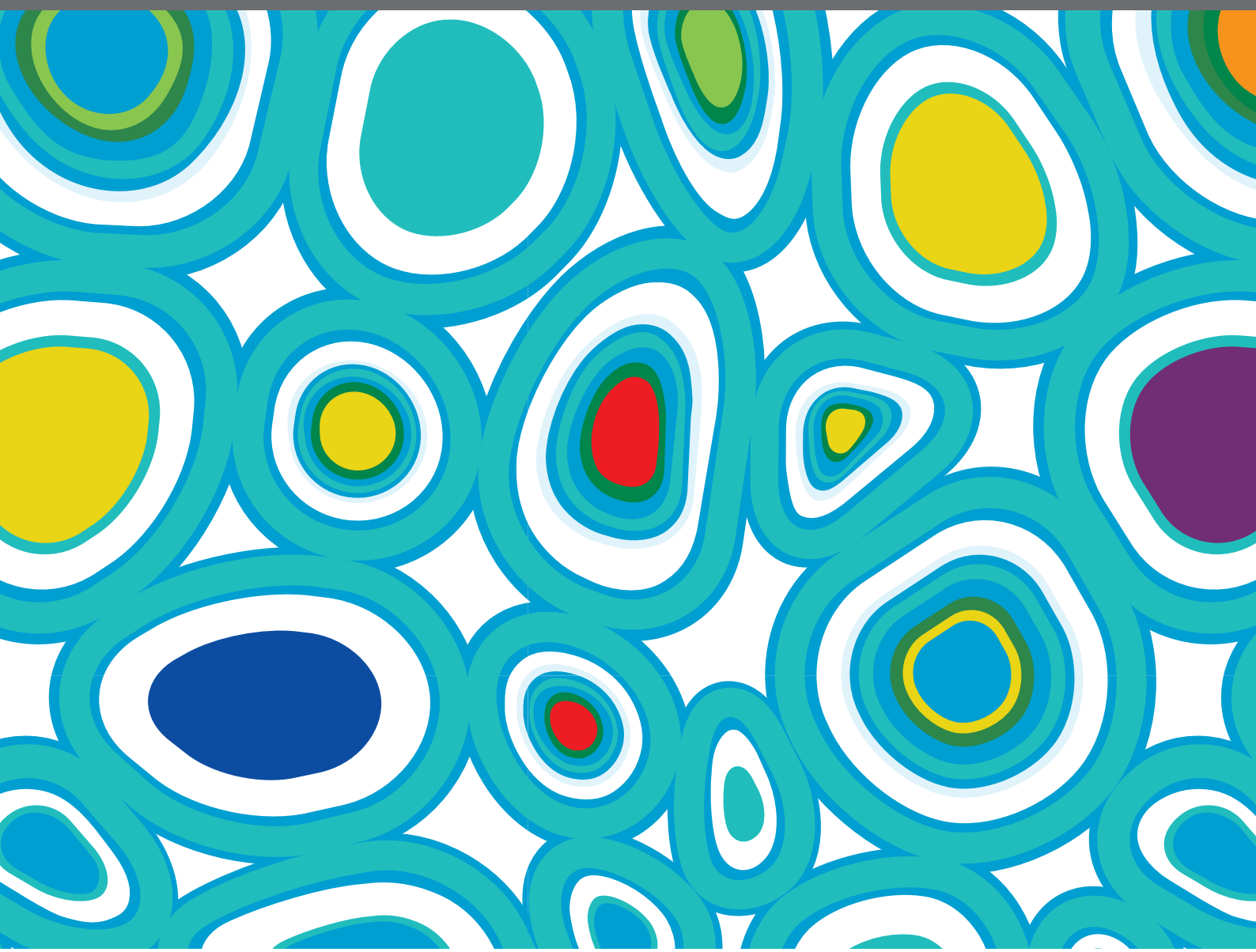

frontiers Research Topics

ISSN 1664-8714
ISBN 978-2-88974-801-3
DOI 10.3389/978-2-88974-801-3

About Frontiers

Frontiers is more than just an open-access publisher of scholarly articles: it is a pioneering approach to the world of academia, radically improving the way scholarly research is managed. The grand vision of Frontiers is a world where all people have an equal opportunity to seek, share and generate knowledge. Frontiers provides immediate and permanent online open access to all its publications, but this alone is not enough to realize our grand goals.

Frontiers Journal Series

The Frontiers Journal Series is a multi-tier and interdisciplinary set of open-access, online journals, promising a paradigm shift from the current review, selection and dissemination processes in academic publishing. All Frontiers journals are driven by researchers for researchers; therefore, they constitute a service to the scholarly community. At the same time, the Frontiers Journal Series operates on a revolutionary invention, the tiered publishing system, initially addressing specific communities of scholars, and gradually climbing up to broader public understanding, thus serving the interests of the lay society, too.

Dedication to Quality

Each Frontiers article is a landmark of the highest quality, thanks to genuinely collaborative interactions between authors and review editors, who include some of the world's best academicians. Research must be certified by peers before entering a stream of knowledge that may eventually reach the public - and shape society; therefore, Frontiers only applies the most rigorous and unbiased reviews.
Frontiers revolutionizes research publishing by freely delivering the most outstanding research, evaluated with no bias from both the academic and social point of view. By applying the most advanced information technologies, Frontiers is catapulting scholarly publishing into a new generation.

What are Frontiers Research Topics?

Frontiers Research Topics are very popular trademarks of the Frontiers Journals Series: they are collections of at least ten articles, all centered on a particular subject. With their unique mix of varied contributions from Original Research to Review Articles, Frontiers Research Topics unify the most influential researchers, the latest key findings and historical advances in a hot research area! Find out more on how to host your own Frontiers Research Topic or contribute to one as an author by contacting the Frontiers Editorial Office: frontiersin.org/about/contact

STEM CELLS IN TISSUE HOMEOSTASIS AND DISEASE

Topic Editors:
Yan-Ru Lou, Fudan University, China
Wencheng Zhang, Tongji University, China
Jianjun Zhou, Tongji University, China
Zhiying He, Tongji University, China

Citation: Lou, Y.-R., Zhang, W., Zhou, J., He, Z., eds. (2022). Stem cells in Tissue Homeostasis and Disease. Lausanne: Frontiers Media SA.
doi: 10.3389/978-2-88974-801-3

Table of Contents

frontiers in Cell and Developmental Biology

EDITORIAL
published: 09 March 2022
doi: 10.3389/fcell.2022.876060

Editorial: Stem Cells in Tissue Homeostasis and Disease

Wencheng Zhang[1,2,3], *Yan-Ru Lou*[4]*, *Jianjun Zhou*[5] *and Zhiying He*[1,2,3]

[1]*Institute for Regenerative Medicine, Shanghai East Hospital, School of Life Sciences and Technology, Tongji University, Shanghai, China,* [2]*Shanghai Engineering Research Center of Stem Cells Translational Medicine, Shanghai, China,* [3]*Shanghai Institute of Stem Cell Research and Clinical Translation, Shanghai, China,* [4]*Department of Clinical Pharmacy and Drug Administration, School of Pharmacy, Fudan University, Shanghai, China,* [5]*Cancer Stem Cell Institute, Research Center for Translational Medicine, Shanghai East Hospital, Tongji University, Shanghai, China*

Keywords: stem cell, tissue homeostasis, lineage, cancer stem cell, stem cell-based therapy, dynamic cell tracking, animal model

Editorial on the Research Topic

Stem Cells in Tissue Homeostasis and Disease

The regular cellular turning over of organs and tissues throughout life span reveals the homeostasis of an individual in multiple ways, which is commonly disrupted in disease states. Uncovering the potential mechanisms of maintaining and regulating normal status is the key to the development of strategic treatments of disorders and diseases. With the progress of regeneration theory and technology in recent years, the role of tissue-specific stem cells in tissue homeostasis has been increasingly recognized. The potential of stem cell-based cell therapies in restoring organ function and achieving tissue regeneration is fantastic. This Research Topic "Stem cells in Tissue Homeostasis and Disease" published in *Frontiers in Cell and Developmental Biology* explores recent advances in the emerging field of stem cells and regenerative medicine, and tissue engineering with a focus on revealing the mechanisms of tissue homeostasis, which enables us to better understand the causes of diseases and to develop efficient therapeutic strategies.

In order to identify proper treatments of diseases, it is essential to understand the cellular basis of healthy organs. **Stem cells lineage contribution** has been extensively studied during normal embryology development. Hematopoietic stem cells (HSCs) are the best studied stem cells. HSCs maintain the hematopoietic homeostasis via self-renewal and a well-established lineage distribution pattern with blood cell differentiation potentials. This stem cell lineage distribution is not unique to the blood system. Biliary tree stem cells located in peribiliary glands had been proved to participate in the functional regeneration of liver and pancreas. Based on this, Overi et al. had identified a cell compartment with stem/progenitor cell features within pancreatic duct glands (PDGs). These stem/progenitor cells were shown to participate in the islet injury repair in type 2 diabetic mellitus (T2DM) patients and diabetic animal models, indicating that the activation of these somatic stem cells can be a potential strategy for promoting organ regeneration. The same scenario occurs for intestinal stem cells (ISCs). ISCs located in the villi of intestinal crypts and commonly known as $Lgr5^+$ subpopulations, are also critical for natural turning over of intestinal mucosa. Song et al. discovered an active fraction of the rhizomes of Trillium tschonoskii Maxim (TT), which can promote irradiated intestinal organoid growth and increase $Lgr5^+$ intestinal stem cell numbers, to develop a potential oral drug for improving the regeneration and repair of intestinal epithelia that have intestinal radiation damage.

Besides activating retaining somatic stem cells, other researchers are focusing on targeting the **cancer stem cells (CSCs)**. Chen et al. have summarized the recent studies on the regulation and dysfunction of autophagy-related genes of stem cells which controlled cellular homeostasis of HSCs

Edited and reviewed by:
Valerie Kouskoff,
The University of Manchester, United Kingdom

***Correspondence:**
Yan-Ru Lou
yanru_lou@fudan.edu.cn

Specialty section:
This article was submitted to Stem Cell Research, a section of the journal Frontiers in Cell and Developmental Biology

Received: *15 February 2022*
Accepted: *22 February 2022*
Published: *09 March 2022*

Citation:
Zhang W, Lou Y-R, Zhou J and He Z (2022) Editorial: Stem Cells in Tissue Homeostasis and Disease. Front. Cell Dev. Biol. 10:876060. doi: 10.3389/fcell.2022.876060

or leukemia stem cells (LSCs) under different conditions. For the same types of adult stem cells but on a different aspect, Wang et al. reviewed the latest advances to better understand the biological activity of N^6-methyladenosine (m^6A), a common modification of mammalian mRNAs, in preserving the function of HSCs and LSCs. Thus, offering the field a promising therapeutic strategy for targeting M^6A modifiers in myeloid leukemia. Guo et al. discovered miR-221/222 cluster as a novel regulator of CD133+ CSCs in non-small cell lung cancer (NSCLC). Their study not only revealed the Reck-Notch1 signaling as the key mediate of miR-221/222, but also provided a potential therapeutic target for the treatment of NSCLC.

Stem cell-based therapies are the most promising strategies for diseases that cannot be treated with traditional surgery or drugs. Various candidate cell types have been explored in recent decades. Use of human pluripotent stem cells (hPSCs), referring to human embryonic stem cells (hESCs) and human induced pluripotent stem cells (iPSCs), in cell therapy still faces their challenges, such as differentiation efficiency, organoid technology, maturity of derived cells, cell expansion, Bogacheva et al. had carefully compared the spheroid size and 3D cell culture systems on spheroid morphology and the effectiveness of definitive endoderm (DE) differentiation, which highlighted the importance of choosing proper biomaterials to achieve successful human iPSC differentiation. Chang et al. have reviewed the most recent advanced development of **hPSCs-derived liver organoids (PSC-LOs)**. Emerging with new bioengineering techniques and tools, PSC-LOs show great potentials in disease modeling, drug development, and liver regeneration.

However, a number of obstacles, such as the lack of an xeno-free expansion system, low yield of *in vitro* differentiation, low maturity, lack of a non-invasive cell tracking method, have slowed the progress of PSC-LOs in clinical applications and drug development. Fortunately, two papers in this Research Topic have made great contribution to overcoming some of these challenges. **Expansion and functional maturation of stem cells** is essential for quality and quantity of cells to meet the need of translational research and clinical applications. Liu et al. reviewed the progress made in the field of *in vitro* generation of platelets from various stem cells, with some achieving large scale production. While cell fate determination post-transplanting or post-grafting has shown its importance for the translation application of stem cells as a therapeutic treatment to various diseases. Advanced technologies in stem cell fate tracking and *in vivo* imaging have been developed over the past decade. However, **dynamic cell tracking** methodology for tracing transplanted cells *in vivo* is still at its early phase. In Lu et al. study, a three-dimensional imaging technique was established to conduct the overall evaluation of transplanted hepatocytes in host liver.

Sharing major biomarkers with hPSCs, human amniotic epithelial stem cells (hAESCs) are preferrable in many clinical studies. Li et al. generated human retinal pigment epithelium (RPE) from hAESCs that had rescued the visual function of a retinal degeneration rat model. Other than hAESCs, mesenchymal stem cells (MSCs) are a commonly used candidate for stem cell-based therapies currently, given their advantages on proliferation, immunomodulation, and tissue maintenance, Yang et al. have reviewed most recent studies in MSC differentiation into specialized cell types, revealing long non-coding RNAs (lncRNAs) as master regulators during the maintenance of homeostasis and multi-differentiation functions through epigenetic, transcriptional, and post-translational mechanisms. Li et al. studied the effect of melatonin on promoting the viability of adipose-derived mesenchymal stem cells (ADMSCs) during the treatment of diabetic mellitus. The melatonin-treated ADMSCs not only performed better in controlling hyperglycemia, insulin resistance, and liver glycogen metabolism in T2DM patients, but also proved to be safe and valuable for pet clinic.

In studies of stem cell-based organ regeneration, **animal models** are critical to study diseases and to develop potential treatments. Chen et al. had established a typical hyperoxia-based Bronchopulmonary dysplasia (BPD) mouse model to mimic hallmarks of BPD, which enabled them to reveal that both cord blood-derived mononuclear cells (CB-MNCs) and umbilical cord-derived mesenchymal stem cells (UC-MSCs) are efficient in alleviating BPD (Chen et al.). In the study of stem cells in the pancreatic ductal glands, Overi et al. evaluated the pancreatic islet injury and regeneration based on the classical streptozotocin (STZ)-induced diabetic mouse model. In the 3D imaging study, Lu et al. conducted the study based on a fumarylacetoacetate hydrolase (Fah) deficiency liver injury model, which enabled them to verify the percentage of cell repopulation of donor cells in host at different time points by using pre-established histology and serology assays.

By focusing on identifying potential candidate stem cells, establishing expansion and maturation systems, and developing grafting technique and post-transplantation cell tracking techniques, the collection of studies in this Research Topic is aiming to promoting the translation of techniques and basic research on stem cells to clinical products.

AUTHOR CONTRIBUTIONS

WZ drafted the first version. Y-RL, JZ, and ZH edited it. All the authors approved the submission.

FUNDING

WZ and ZH are funded by Major Program of National Key Research and Development Project (2020YFA0112600, 2019YFA0801502), Shanghai Pujiang Program (21PJD059), Natural Science Fund Project of Shanghai 2022 "Scientific and Technological Innovation Action Plan" (22ZR1451100), National Natural Science Foundation of China (82173019, 81772954), The Key Project of Shanghai science and technology commission (17431906600), Program of Shanghai Academic/Technology Research Leader (20XD1434000), and Peak Disciplines (Type IV) of Institutions of Higher Learning in Shanghai.

ACKNOWLEDGMENTS

We thank authors of the publications collected in this Research Topic for their contributions. We also thank the Journal Manager, Dr. Katie Powis, Frontiers Specialist, Hajer Bachi, and Frontiers Submissions Specialist, Emily Kaiser, for their support.

Conflict of Interest: The authors declare that the research was conducted in the absence of any commercial or financial relationships that could be construed as a potential conflict of interest.

frontiers in Cell and Developmental Biology

ORIGINAL RESEARCH
published: 20 April 2021
doi: 10.3389/fcell.2021.663279

Reck-Notch1 Signaling Mediates miR-221/222 Regulation of Lung Cancer Stem Cells in NSCLC

Yuefan Guo[1†], Guangxue Wang[1†], Zhongrui Wang[1†], Xin Ding[1], Lu Qian[1,2], Ya Li[1,3], Zhen Ren[1,3], Pengfei Liu[1], Wenjing Ma[1], Danni Li[1], Yuan Li[1], Qian Zhao[1], Jinhui Lü[1], Qinchuan Li[1], Qinhong Wang[1]* and Zuoren Yu[1]**

[1] Research Center for Translational Medicine, Shanghai East Hospital, Tongji University School of Medicine, Shanghai, China, [2] Jinzhou Medical University, School of Basic Medical, Jinzhou, China, [3] Dalian Medical University, School of Basic Medical, Dalian, China

OPEN ACCESS

Edited by:
Yan-Ru Lou,
Fudan University, China

Reviewed by:
Rafael Rosell,
Catalan Institute of Oncology, Spain
Silvia Deaglio,
University of Turin, Italy

***Correspondence:**
Qinchuan Li
li.qinchuan@163.com
Qinhong Wang
qinhong.wang@yahoo.com
Zuoren Yu
Zuoren.yu@tongji.edu.cn

[†] These authors have contributed equally to this work

Specialty section:
This article was submitted to Stem Cell Research, a section of the journal Frontiers in Cell and Developmental Biology

Received: 02 February 2021
Accepted: 29 March 2021
Published: 20 April 2021

Citation:
Guo Y, Wang G, Wang Z, Ding X, Qian L, Li Y, Ren Z, Liu P, Ma W, Li D, Li Y, Zhao Q, Lü J, Li Q, Wang Q and Yu Z (2021) Reck-Notch1 Signaling Mediates miR-221/222 Regulation of Lung Cancer Stem Cells in NSCLC. Front. Cell Dev. Biol. 9:663279. doi: 10.3389/fcell.2021.663279

Cancer stem cells (CSCs) contribute to the cancer initiation, metastasis and drug resistance in non-small cell lung cancer (NSCLC). Herein, we identified a miR-221/222 cluster as a novel regulator of CSCs in NSCLC. Targeted overexpression or knockdown of miR-221/222 in NSCLC cells revealed the essential roles of miR-221/222 in regulation of lung cancer cell proliferation, mammosphere formation, subpopulation of $CD133^{+}$ CSCs and the expression of stemness genes including OCT4, NANOG and h-TERT. The *in vivo* animal study showed that overexpression of miR-221/222 significantly enhanced the capacity of lung cancer cells to develop tumor and grow faster, indicating the importance of miR-221/222 in tumorigenesis and tumor growth. Mechanistically, Reck was found to be a key direct target gene of miR-221/222 in NSCLC. Overexpression of miR-221/222 significantly suppressed Reck expression, activated Notch1 signaling and increased the level of NICD. As an activated form of Notch1, NICD leads to enhanced stemness in NSCLC cells. In addition, knockdown of Reck by siRNA not only mimicked miR-221/222 effects, but also demonstrated involvement of Reck in the miR-221/222-induced activation of Notch1 signaling, verifying the essential roles of the miR-221/222-Reck-Notch1 axis in regulating stemness of NSCLC cells. These findings uncover a novel mechanism by which lung CSCs are significantly manipulated by miR-221/222, and provide a potential therapeutic target for the treatment of NSCLC.

Keywords: non-small cell lung cancer, cancer stem cell, miR-221/222, Reck, Notch1 signaling

INTRODUCTION

Lung cancer is the leading cause of cancer-related deaths worldwide (Chen et al., 2016; Bray et al., 2018). It is classified into two categories including small cell lung cancer (SCLC) and non-small cell lung cancer (NSCLC). The majority of lung cancer cases (∼85%) belong to NSCLC all over the world (Wood et al., 2015; Jiang et al., 2018). Although traditional chemotherapy and molecular targeted therapeutic drugs have been widely applied to NSCLC patients after primary treatment

with surgical resection, the 5-year survival rate is still very low mostly due to tumor recurrence and drug resistance (Jiang et al., 2018). It is the small subpopulation of stem-like cells within tumors that are believed to be responsible for the tumor recurrence and drug resistance (Yu et al., 2012). They are called cancer stem cells (CSCs) or tumor initiating cells (TICs), and characterized by self-renewal, differentiation and strong ability of tumor-regeneration.

Since first evidence for CSCs was published in 1997 in leukemia (Bonnet and Dick, 1997), CSC isolation and identification in solid cancers including breast, lung and prostate cancer have been frequently reported. In lung cancer, CSCs are considered as the main reason causing tumor initiation, dormancy, recurrence, metastasis and resistance to therapy (Pardal et al., 2003; Eramo et al., 2010). As such, determination of the molecular mechanism underlying the behavior of lung CSCs and the development of target molecules against lung CSCs could potentially bring great benefits to the patients with lung cancer (MacDonagh et al., 2016). Up to date, several stem cell markers including CD133, ALDH1 and CXCR4 have been successfully applied to isolate lung CSCs from tumor tissues (Wang et al., 2013; Roudi et al., 2015; Eramo et al., 2016; Aghajani et al., 2019). However, the understanding of lung CSCs remains largely unclear.

Non-coding RNAs (ncRNAs), including long non-coding RNAs (lncRNAs) and microRNAs (miRNAs), have been well demonstrated to be crucial for gene expression regulation, as well as epigenetic regulation (Cech and Steitz, 2014; Adams et al., 2017). MiRNAs are a class of single-stranded small RNAs with 18–24 nucleotides in length, usually regulating gene expression at the post-transcriptional level through binding to the 3'UTR of target mRNAs (Krek et al., 2005; Rupaimoole and Slack, 2017). During the development and progression of cancer, miRNAs play important roles in regulating cancer cell stemness, tumor regeneration, cancer cell metastasis and chemo-resistance (Shimono et al., 2009; Bu et al., 2016; Khan et al., 2019). In NSCLC, aberrant expression of miRNAs including miR-582-3p, miR-1246, and miR-1290 have been reported to regulate CSCs and promote tumor progression (Fang et al., 2015; Zhang et al., 2016; Shukla et al., 2018).

In the current study, we performed a miRNA screening analysis on the $CD133^+$ CSC subpopulation isolated from both A549 and H1299 NSCLC cell lines, and identified a subset of miRNAs with differential expression in CSCs including upregulation of miR-221/222. Enforced overexpression of miR-221/222 in NSCLC cells enhanced cell proliferation and CSC properties *in vitro*. Xenografting of A549 cells stably expressing miR-221/222 into immune-deficient nude mice developed much bigger tumors than control cells, indicating that miR-221/222 plays an essential role in the process of tumorigenesis and tumor growth. Gene reversion-inducing cysteine-rich protein with kazal motifs (Reck) was identified as a direct target gene of miR-221/222 in NSCLC, which involves in the activation of downstream Notch1 signaling and subsequent self-renewal of lung CSCs. Our findings for the first time demonstrated that miR-221/222-Reck-Notch signaling acts as a critical regulatory mechanism underlying the stemness of CSCs in NSCLC.

MATERIALS AND METHODS

Clinical Tumor Samples

Human NSCLC tumor samples were collected from Tongji University Shanghai East Hospital. All the procedures were approved by the Institutional Review Board (IRB) of Tongji University Shanghai East Hospital. All patients were provided with a written informed consent form.

Animals

Six-week-old immunodeficient male nude mice were purchased from the Silaike Animal Company (Shanghai, China) for *in vivo* assays. 5×10^5 A549 cells with or without stable expression of miR-221/222 were transplanted into immune-deficient nude mice by subcutaneous injection to establish the NSCLC animal model. All animal studies were performed following the protocols approved by the Institutional Animal Care and Use Committee of Tongji University School of Medicine.

Cells

Human lung cancer cell lines A549, NCI-H1299 and human bronchial non-tumorigenic epithelial cell line BEAS-2B were originally purchased from ATCC, maintained in our lab, and cultured in Dulbecco's Modified Eagle's Medium (DMEM) with 100 mg/L penicillin and streptomycin and 10% fetal bovine serum (FBS). All of these cells were cultured at 37°C in a humidified environment with 5% CO2.

Vectors, Oligos, and Transfection

miR-221/222-overexpression vector for animal study is a lentivirus-based product from Novobiosci Company (Shanghai, China). Tet-inducible PB-TRE3G vector was used to prepare the tet-on 3G miR-221/222 system by inserting primary miR-221/222 sequence (chrX.c45747283-45746050). 4 μg of PB-TRE3G-miR-221/222 and 3 μg PB-Tet 3G were co-transfected into A549 cells using lipofectamine 2000 (Invitrogen, United States) cultured in the tet-free medium. In 24 h, doxycycline (Boyotime, Shanghai, China) was added into the medium (Dox+, 3 μg/ml). Another dish in parallel without treatment with doxycycline (Dox-) was used for control. Cells were collected for RNA and protein isolation in 48 h after doxycycline treatment. miRNA mimics, anti-miRNA inhibitors, siRNAs and corresponding negative controls were synthesized by GenScript (Nanjing, China). The siRNAs targeting Reck sequences are: 5′ GAACATCCTTTAGTATTGA 3′. Hiperfect transfection reagent (Qiagen Technologies) was used for cell transfection following the manufacturer's instruction. A final concentration of 30 nM of small RNA oligos was used in all *in vitro* assays.

First Strand cDNA Preparation and Real-Time PCR

Total RNAs were extracted by using Trizol reagent. 500 ng of total RNA was used for reverse transcription for miRNAs determination by using the M&G miRNA Reverse Transcription kit (miRGenes, Shanghai, China) according to

the manufacturer's instruction. 0.5–1.0 μg of total RNA was used for reverse transcription for mRNA determination by using iScript cDNA synthesis kit (Bio Rad, United States) Universal SYBR qPCR Master Mix and Applied Biosystems QuantStudio 6 (Applied Biosystem, Thermo Fisher Scientific) were used for real-time PCR assays. β-actin and GAPDH were used for mRNA normalization, and 5s rRNA was used for miRNA normalization. Forward primer sequences for miR-221: 5′ AGCUACAUUGUCUGCUGGGUUU 3′; miR-222: 5′ AGCUACAUCUGGCUACUGGG 3′; 5s rRNA, 5′ AGTACTTGGATGGGAGACCG 3′. All primer sequences for mRNAs are available upon request.

Western Blot

50 μg of cell lysates was applied to 8–10% sodium dodecyl sulfate–polyacrylamide gel electrophoresis (SDS/PAGE) for protein separation. The primary antibodies (1:2,000) was used including OCT4 (2750S, Cell Signaling Technology), NANOG (4903S, Cell Signaling Technology), Notch1 (sc-373891, Santa Cruz, United States), GAPDH (sc-47724, Santa Cruz). Reck (sc-373929, Santa Cruz), NICD (sc-373891, Santa Cruz), h-TERT (sc-377511, Santa Cruz), HRP-linked anti-rabbit IgG (7074S, Cell Signaling Technology) and HRP-linked anti-mouse IgG (7076S, Cell Signaling Technology) were used as secondary antibodies (1:3,000).

Colony Formation Assay

2,000 cells per well were seeded in a 12-well plate and cultured under regular condition for 7–10 days until visible colonies were formed. 4% paraformaldehyde was used to fix the colonies, and 0.5% crystal violet solution was used for staining. The colonies with diameter over 40 μm were counted under microscope for quantitative analysis.

Sphere Formation Assay

Cancer cells were plated in 12-well ultra-low adherent cell culture plate (Corning, United States) at a density of 2,000 cells/well, and cultured in the serum-free medium containing DMEM/F12 with 1×B27 supplement (Invitrogen, United States), 20 ng/mL human epidermal growth factor (EGF) (Sigma, United States),

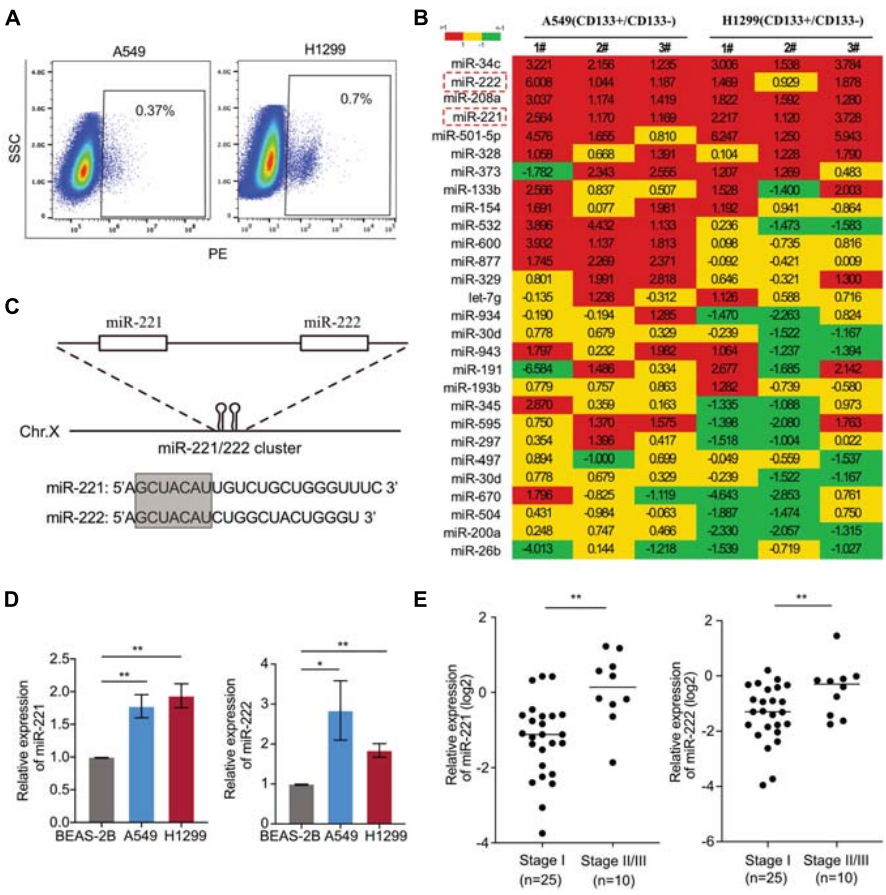

FIGURE 1 | Upregulation of miR-221/222 in the CD133$^+$ lung cancer stem cells. **(A)** CD133$^+$ CSC isolation from A549 and H1299 cells using FACS analysis. **(B)** miRNA screening analysis on the CD133$^+$ CSC subpopulation, compared with matched CD133$^-$ cells. **(C)** Chromosomal structure of the miR-221/222 cluster, in which miR-221 and miR-222 share same "seed" sequence. **(D)** Upregulation of miR-221 and miR-222 in the NSCLC cell lines A549 and H1299, compared with non-tumorigenic lung epithelial cell line BEAS-2B. Data are presented as mean SEM ($N = 3$), $^*p < 0.05$, $^{**}p < 0.01$. **(E)** Higher levels of miR-221 and miR-222 in the NSCLC tumors at stages II/III, compared with the tumors at stage I. $^{**}p < 0.01$.

and 20 ng/ml of human basic fibroblast growth factor (bFGF) (R&D Systems, United States) for 5 days without disturbing.

Luciferase Reporter Assay

pGL-3 luciferase reporter vectors carrying either wide type (WT) or miR-221/222 binding site-mutated (MU) 3′UTR of Reck were co-transfected into 293T cells with RL-TK control vector (Renilla) and miR-221/222 mimics in a 24-well plate. After 18-h culturing, Dual-Luciferase Reporter Assay kit (Promega, United States) was used to measure the luciferase activities.

Statistical Analysis

Data are presented as mean ± SEM unless otherwise stated. Statistical significance was determined by standard two-tailed student's t-test followed by least-significant difference (LSD). $P < 0.05$ was considered statistically significant.

RESULTS

Upregulation of miR-221/222 in the CD133$^+$ CSCs in NSCLC

In order to identify the key genes regulating CSCs in NSCLC, CD133$^+$ cells were isolated from two NSCLC cell lines A549 and H1299 (**Figure 1A**). A home-made cancer-associated miRNA panel was applied for the miRNA screening analysis in the CD133$^+$ CSCs, comparing to the matched CD133$^-$ cells. A subset of miRNAs differentially expressed in the CSCs

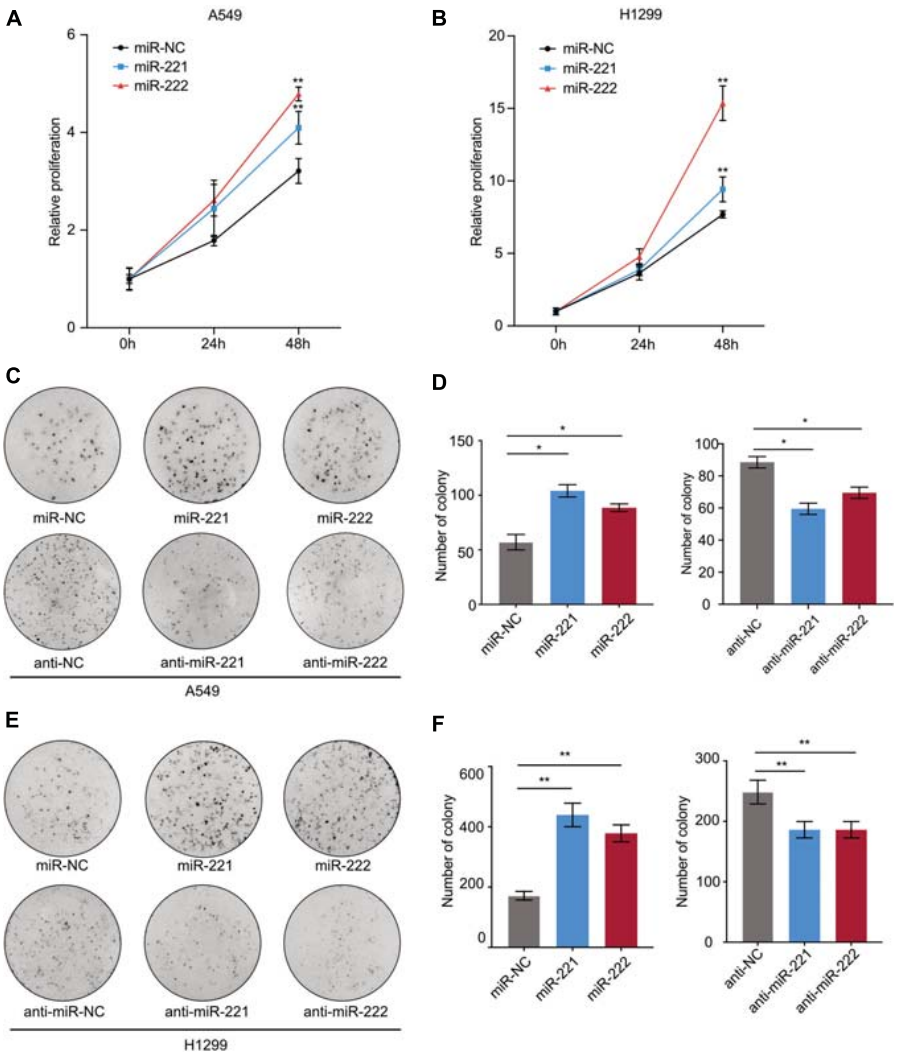

FIGURE 2 | miR-221/222 promoted cell proliferation in NSCLC. **(A,B)** CCK8 assays indicating increased cell proliferation by overexpression of miR-221 and miR-222 in A549 **(A)** and H1299 **(B)** cells. **(C)** Colony formation assays indicating the positive regulation of cell proliferation by miR-221/222 in A549 cells. Both overexpression and knockdown of miR-221 or miR-222 were applied. **(D)** Quantitative analysis of panel **(C)**. **(E)** Colony formation assays indicating the positive regulation of cell proliferation by miR-221/222 in H1299 cells. Both overexpression and knockdown of miR-221 or miR-222 were applied. **(F)** Quantitative analysis of panel **(E)**. Data are presented as mean ± SEM ($N = 3$), $^*p < 0.05$, $^{**}p < 0.01$.

were identified including upregulated miR-34c, miR-208a, miR-221/222, miR-501-5p, et al., and downregulated miR-26b, miR-200a, miR-504, et al. (**Figure 1B**). Among those top-list of miRNAs, miR-34c and miR-501-5p have been well documented to regulate cancer cell stemness, while the function of miR-221/222 in lung CSCs remains unknown. MiR-221 and miR-222 are in a cluster sharing same "seed" sequence (**Figure 1C**), so we focused on the miR-221/222 cluster to determine its regulation on CSCs in NSCLC. The expression levels of miR-221 and miR-222 in NSCLC cells were detected. Both miR-221 and miR-222 showed significantly upregulation in A549 and H1299 cells compared to non-tumorigenic bronchial epithelial cell BEAS-2B (**Figure 1D**). The miR-221/222 analysis in tumor samples from NSCLC patients further indicated a positive correlation between the miR-221/222 levels and tumor-stage. Both miR-221 and miR-222 showed a higher level in the NSCLC tumors at stages II/III, compared with the tumor samples at stage I (**Figure 1E**).

miR-221/222 Promoted Cell Proliferation in NSCLC

To determine the biological function of miR-221/222 in NSCLC, both A549 and H1299 cells were transfected with miR-221 mimic, miR-222 mimic or negative control (**Supplementary Figures 1A,B**), followed by CCK8 cell proliferation assay and colony formation assay. As shown in **Figures 2A,B**, both miR-221 and miR-222 promoted cell proliferation in NSCLC cells. In addition to miRNA overexpression, anti-miRNA inhibitor oligos targeting either miR-221 or miR-222 were applied to A549 and H1299 cells (**Supplementary Figures 2A,B**) followed by colony formation assay. As shown in **Figures 2C–F**, overexpression of miR-221 or miR-222 increased colony formation in the adhesion-independent condition. In contrast, knockdown of miR-221 or miR-222 decreased the colony formation.

miR-221/222 Promoted the Cell Stemness in NSCLC

Following overexpression or knockdown of miR-221/222 in A549 and H1299 cells, the changes of the $CD133^+$ CSC percentage were determined by flow cytometry analysis. As shown in **Figures 3A,B**, overexpression of miR-221/222 in A549 cells increased $CD133^+$ CSC subpopulation from 1.49% to 2.37–2.58%. In contrast, knockdown of miR-221/222 in A549 cells decreased $CD133^+$ CSCs from 1.55% to 0.52–0.75%. Similar results were obtained from H1299 cells (**Figures 3C,D**). In addition, sphere formation assays were performed to further determine the stemness changes after overexpression (**Figure 3E**) or knockdown (**Figure 3F**) of miR-221/222 in A549 cells. Quantitative analysis indicated a positive regulation of both sphere number and sphere size by miR-221/222 (**Figures 3G,H**). Same assays were applied to H1299 cells and generated similar results (**Supplementary Figure 3**), verifying the stemness-promoting function of miR-221/222 in NSCLC. Moreover, a group of well-defined stemness genes including Oct4, Nanog, and h-Tert were examined in A549 cells by quantitative RT-PCR and western blot analyses. The results showed that miR-221/222 remarkably increased the expression of Oct4, Nanog, and h-Tert at the both mRNA (**Figure 3I**) and protein (**Figure 3J**) levels.

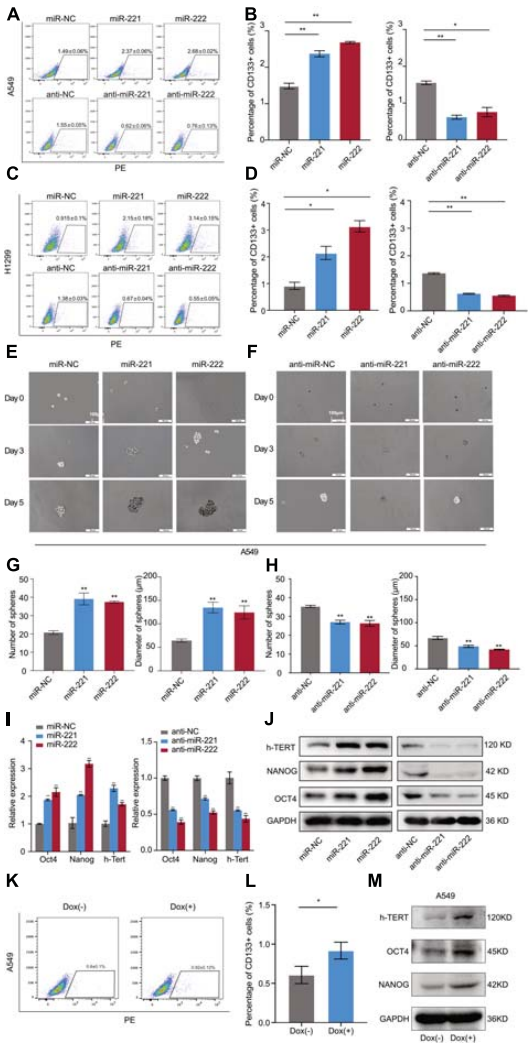

FIGURE 3 | miR-221/222 promoted the cancer cell stemness in NSCLC. **(A)** Increased percentage of $CD133^+$ CSCs in A549 cells after treatment with miR-221 or miR-222. Conversely, $CD133^+$ CSC percentage decreased after treatment with anti-miR-221 or anti-miR-222. **(B)** Quantitative analysis of panel **(A)**. **(C)** H1299 cells were applied with same assays with panel **(A)**. **(D)** Quantitative analysis of panel **(C)**. **(E)** Sphere formation assays using A549 cells treated with miR-221 or miR-222 mimics. **(F)** Sphere formation assays using A549 cells treated with anti-miR-221 or anti-miR-222. **(G)** Quantitative analysis of the number and size of the spheres in panel **(E)**. **(H)** Quantitative analysis of the number and size of the spheres in panel **(F)**. **(I,J)** Quantitative real-time PCR **(I)** and western blot **(J)** analyses indicating the increased expression of Oct4, Nanog and h-Tert in A549 cells after treatment with miR-221 or miR-222 mimics. Consistent results were obtained after treatment with anti-miR-221 or anti-miR-222. **(K,L)** Doxycycline-induced miR-221/222 overexpression promoted $CD133^+$ CSC percentage in A549 cells. **(M)** Doxycycline-induced miR-221/222 overexpression increased the expression of Oct4, Nanog, and h-Tert in A549 cells. Data are presented as mean ± SEM ($N = 3$), $^*p < 0.05$, $^{**}p < 0.01$.

In order to further validate the regulation of cancer cell stemness by miR-221/222 in NSCLC, a tetracycline-inducible

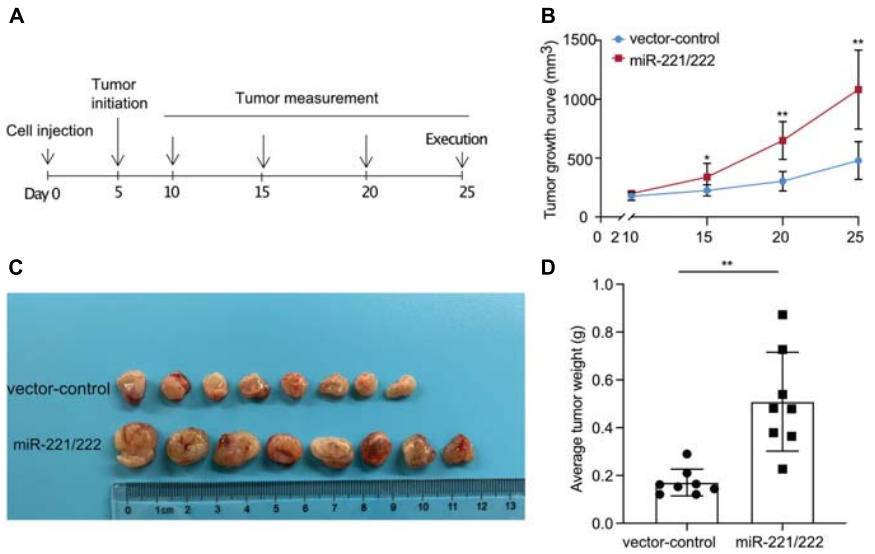

FIGURE 4 | miR-221/222 promoted tumor growth in the xenograft model with NSCLC. **(A)** Schematic representation of the procedure for *in vivo* assays. **(B)** Tumor growth curves of the two groups of mice (miR-221/222-overexpressing group and control group). **(C)** Tumor images isolated from the mice. **(D)** Weight of the tumors from both groups of mice. Data are presented as mean ± SEM ($N = 8$), $^{*}p < 0.05$, $^{**}p < 0.01$.

system was applied to miR-221/222 as shown in **Supplementary Figure 4**. Doxycycline-induced miR-221/222 overexpression in A549 cells significantly promoted $CD133^{+}$ CSC percentage (**Figures 3K,L**), and increased the expression of Oct4, Nanog, and h-Tert as well (**Figure 3M**).

Overexpression of miR-221/222 Promoted NSCLC Tumor Growth *in vivo*

In order to determine the effects of miR-221/222 on the NSCLC tumorigenesis and tumor growth *in vivo*, a NSCLC xenograft model was established by lung cancer cell xenografting into immunodeficient female nude mice. A549 cells with or without stable overexpression of miR-221/222 (**Supplementary Figure 5**) were applied for the xenografting, followed by the continuous tracking of tumor growth (**Figure 4A**). The tumor growth curves showed a significant promotion of tumor growth by overexpression of miR-221/222 (**Figure 4B**), which was further demonstrated by the average size and weight of the tumors on the day 25 after cell xenografting (**Figures 4C,D**). In addition, ki67 staining on the paraffin-embedded tumor tissue slides validated the increased tumor cell proliferation by miR-221/222 overexpression (**Supplementary Figure 6**).

Activation of Notch1 Signaling by miR-221/222 *via* Suppressing the Expression of Reck

Next we sought to determine the molecular mechanism(s) through which miR-221/222 regulates CSCs in NSCLC. Bioinformatics analyses predicted 2,313 target genes of miR-221/222, 5,346 stem cell-related genes and 87 NSCLC-regulating genes using public databases. Among them 3 genes were overlapped including Ect2, Braf and Reck (**Figure 5A**). Quantitative RT-PCR analysis revealed that overexpression or knockdown of miR-221/222 significantly decreased or increased Reck gene expression, respectively (**Figures 5B,C**), suggesting that Reck is a potential target gene of miR-221/222 in lung cancer cells. In order to verify whether Reck is a direct target of miR-221/222, luciferase reporter constructs carrying either wide type (WT) or miR-221/222-binding sites-mutated (MU) 3′UTR of Reck were co-transfected with miR-221/222 mimics into 293T cells (**Figures 5D,E**), and the results we obtained from this experiment strongly supported that the inhibition of Reck 3′UTR by miR-221/222, relying on their sequence complementary binding (**Figure 5E**).

The protein encoded by Reck is an extracellular protein with protease inhibitor-like domains with downregulation in many tumors and cells transformed by various kinds of oncogenes, functioning as a tumor suppressor. In view of cell stemness regulation by Reck by suppressing Notch1 shedding and activation in gastric cancer (Hong et al., 2014), we tested the expression changes of Reck and Notch1 in A549 cells with or without overexpression of miR-221/222. As shown in **Figure 5F**, both miR-221 and miR-222 reduced the protein levels of Reck and Notch1, but increased the expression level of Notch1 intracellular domain (NICD). Consistent results were obtained in A549 cells after knockdown of miR-221/222 (**Figure 5F**). NICD is the activated form of Notch1 after cleavage. It has been demonstrated that NICD functions as a transcriptional factor to induce cell stemness (Hong et al., 2014; Lee et al., 2016). Since Reck negatively regulates the Notch1 cleavage, and thereby suppresses the CSC properties (Hong et al., 2014), siRNA targeting Reck (si-Reck) was applied to A549 cells to test its effect on the Notch1 signaling. Significant increase of NICD was observed when Reck was knocked down by siRNA (**Figure 5G**). Furthermore, in the si-Reck-treated A549 cells, overexpression of miR-221/222 did not

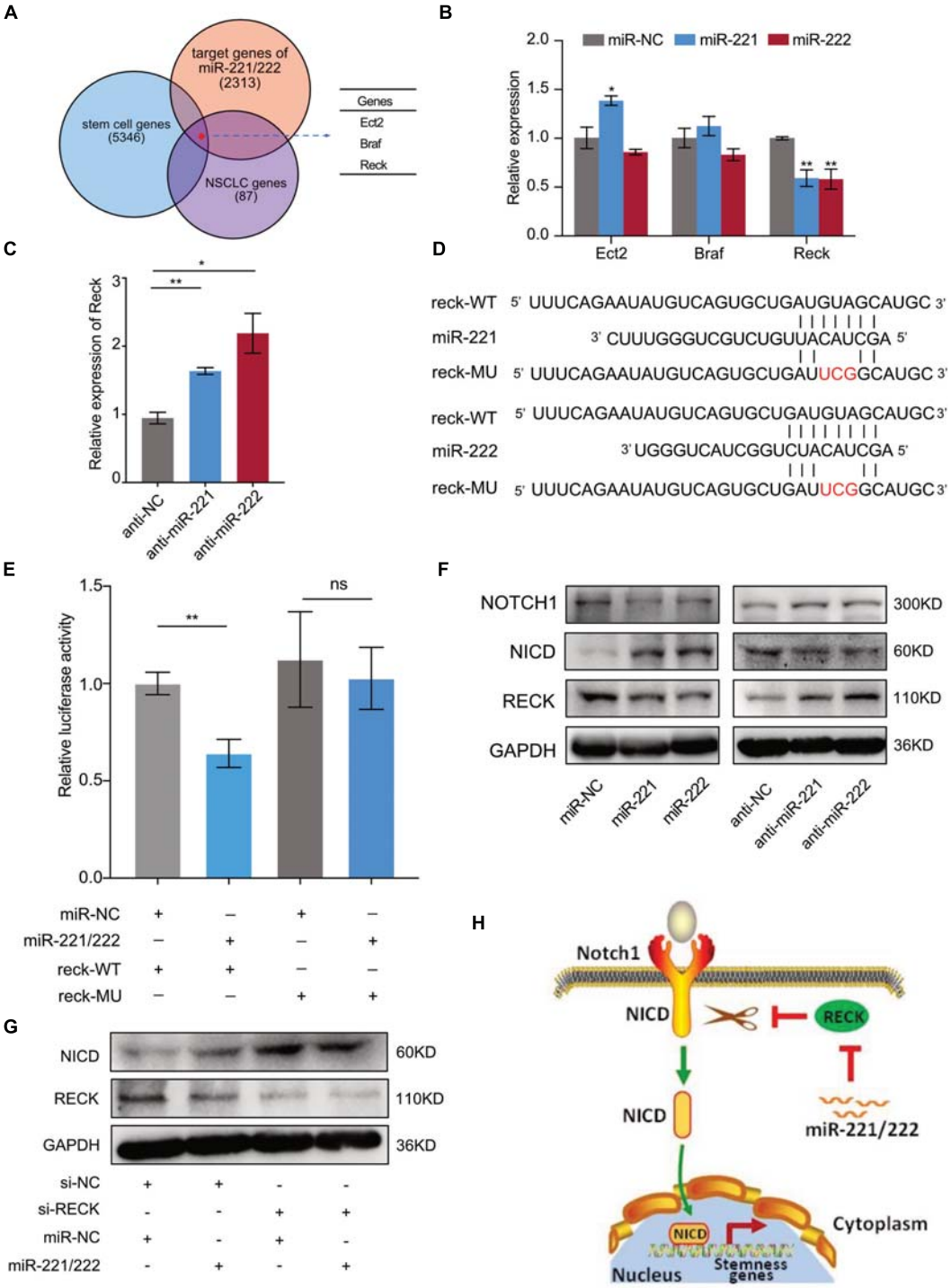

FIGURE 5 | Reck gene mediated the miR-221/222-induced Notch1 signaling activation in NSCLC. **(A)** 2,313 predicted target genes of miR-221/222, 5,346 stem cell-related genes and 87 NSCLC-regulating genes overlapped 3 genes including Ect2, Braf and Reck. **(B)** Quantitative real-time PCR analysis validated downregulation of Reck by overexpression of miR-221/222 in A549 cells. **(C)** Upregulation of Reck was shown after knockdown of miR-221/222 in A549 cells. **(D)** Wild type (WT) or point mutated (MU) Reck 3′UTR were cloned into pGL-3 Luciferase reporter vector. The miR-221/222 binding site was mutated in MU. **(E)** Luciferase reporter assays indicating the direct inhibition of Reck WT 3′UTR by miR-221/222, which was attenuated by the binding-site mutation. **(F)** Western blot analyses indicating the activation of Notch1 signaling by miR-221/222 overexpression in A549 cells, including increased level of Notch1 intracellular domain (NICD) and decreased level of uncleaved Notch1, which were associated with downregulation of Reck. Consistent results were obtained in A549 cells after knockdown of miR-221/222. **(G)** Western blot analyses indicating the increase of NICD by knockdown of Reck. But miR-221/222 did not show regulation on the level of NICD in the si-Reck-treated A549 cells. **(H)** Schematic representation of the mechanism through which miR-221/222 promoted CSCs properties in NSCLC by suppressing Reck and activating Notch1 signaling. Data are presented as mean ± SEM ($N = 3$), $^{*}p < 0.05$, $^{**}p < 0.01$, ns means non significant.

show more induction of the Notch1 activation (**Figure 5G**). These data suggest the requirement of Reck expression for the miR-221/222-induced Notch1 signaling activation and cell stemness promotion in NSCLC (**Figure 5H**).

DISCUSSION

Emerging evidences indicate that many genetic and epigenetic changes underlying the aggressive and destructive behavior of cancer cells are orchestrated by a small population of cancer cells called CSCs within tumor tissues (Easwaran et al., 2014). However, the understanding of the identification, biomarkers, and cellular properties of CSCs are limited and variable upon tumor types. Herein, we identified the miR-221/222 cluster with upregulation in $CD133^+$ CSCs as an essential positive regulator promoting the stemness of NSCLC cells, which are closely associated with tumorigenesis and tumor growth in NSCLC. Further, we demonstrated that a Reck-Notch1 signaling mediates the miR-221/222-induced increase of CSC properties in NSCLC.

It has been reported that Reck gene inhibits cell migration, invasion and angiogenesis by negatively regulating matrix metalloproteinases (MMPs) and a disintegrin and metalloproteinase 10 (ADAM10) (Hong et al., 2014). In gastric cancer, ectopic expression of Reck gene suppressed the expression of stemness genes and the sphere formation and sphere size of $CD133^+$ CSCs (Hong et al., 2014). In the current study, we are the first to demonstrate that Reck gene, a direct target of miR-221/222, is an important mediator for the miR-221/222-induced CSC properties, and verify the involvement of Reck gene in the epigenetic regulation of CSCs. Our previous work has demonstrated the oncogenic function of miR-221/222 in regulating the cellular migration, invasion, CSCs and drug-resistance in triple negative breast cancer (Li et al., 2014, 2020). However, the regulatory function and mechanism of miR-221/222 in lung CSCs remain unclear. Garofalo et al. reported in 2009 that the overexpression of miR-221/222 in aggressive NSCLC cells induced TRAIL resistance and enhanced cellular migration by targeting Pten and Timp3 (Garofalo et al., 2009). Besides this, there is no other report regarding the effect of miR-221/222 on NSCLC cells, especially CSCs.

In this study, in order to explore the fundamental mechanism(s) by which how miR-221/222 influences CSCs properties in NSCLC, we decided to look at Notch1 signaling since Reck functions as a tumor suppressor by suppressing Notch1 shedding and activation (Hong et al., 2014). Notch1 signaling has been shown to be critical for cell proliferation, cell fate specification and CSC self-renewal (Chiba, 2006; Venkatesh et al., 2018). It is also reported that a cleaved form of Notch1, NICD promoted the self-renewal capacity of CSCs in head and neck squamous cell carcinoma by activating sphere formation and increasing the expression of stem cell markers (Lee et al., 2016). Here in our study, we found that miR-221/222 downregulates Reck but increases the NICD level, suggesting that miR-221/222 enhances stemness of NSCLC cells mostly through activating Notch 1 signaling. However, how miR-221/222-Reck signaling promotes the cleavage of Notch1 into NICD needs to be further investigated. CSCs are one of the sources for cancer initiation, development and metastasis. Emerging evidences show that targeting Notch signaling pathway of CSCs represents a promising therapeutic strategy to treat cancer (Zhao et al., 2016; Venkatesh et al., 2018). Our *in vivo* study clearly showed that overexpression of miR-221/222 significantly enhanced tumor growth, providing an evidence to target miR-221/222 as an upstream regulator of Notch1 signaling in regulating CSCs and achieving potential therapeutic effects on NSCLC.

Many transcriptional factors and signaling pathways are involved in regulation of cancer cell dormancy and cancer stem cells (Talukdar et al., 2019). For example, upregulation of Forkhead box M1 (FOXM1) in cancer stem cells is associated with poor prognosis in a variety of tumor types (Zhang et al., 2017). In breast cancer, FOXM1 was found to promote the activity of YAP1 and maintain the cancer cell stemness (Sun et al., 2020). The crosstalk between YAP/TAZ and Notch signaling influences cell self-renewal, stem cell differentiation, cell fate decisions, epithelial-stromal interactions, inflammation, morphogenesis, and large-scale gene oscillations (Totaro et al., 2018). Overexpression of miR-222 has been reported to induce activation of YAP-TEAD1 signaling and promote cell proliferation and invasion in gastric cancer cells (Li et al., 2015). Although a miR-221/222 binding site was predicted in the 3′-UTR of YAP1, it remains unknown whether miR-221/222 regulate YAP1 expression in NSCLC. Nevertheless, the finding in the current study of the mir-221/222-RECK-Notch signaling adds a node to the regulatory network of CSCs in NSCLC.

Epidermal growth factor receptor (EGFR) mutation can lead to pathogenesis in NSCLC (Hsu et al., 2018). EGFR inhibitors including gefitinib and erlotinib have been applied for the first-line treatment of EGFR-mutant NSCLC (Yang et al., 2017). Targeted inhibition of miR-221/222 has been demonstrated to induce cancer cell sensitivity to TRAIL, gefitinib and erlotinib (Garofalo et al., 2009, 2011; Jang et al., 2016). In view of the close correlation between CSCs and chemoresistance, the findings in our study may provide a clue to interpret the miR-221/222-induced chemoresistance in NSCLC.

In summary, our findings indicate that miR-221/222 functions as a novel critical regulator of CSCs in NSCLC through suppressing Reck and activating Notch1 signaling. The miR-221/222-Reck-Notch1 axis not only represents a vital epigenetic mechanism in regulating CSC self-renewal and maintenance, but also provides potential targets for inhibition of CSCs in treatment of SCLC.

DATA AVAILABILITY STATEMENT

The original contributions presented in the study are included in the article/**Supplementary Material**, further inquiries can be directed to the corresponding author/s.

ETHICS STATEMENT

The studies involving human participants were reviewed and approved by the Institutional Review Board (IRB) of

Tongji University Shanghai East Hospital. The patients/participants provided their written informed consent to participate in this study. The animal study was reviewed and approved by Experimental Animal Center of Tongji University School of Medicine.

AUTHOR CONTRIBUTIONS

QW, QL, and ZY designed the project and wrote the manuscript. YG and QZ did the data analysis. YG, GW, ZW, LQ, XD, PL, WM, DL, and YLi performed the cell and molecular biology experiments. YG, JL, ZR, and YuL did the animal study. All authors contributed to the article and approved the submitted version.

FUNDING

This work was supported by grants 81672285 and 81773266 from Natural Science Foundation of China, grant 18411965900 from the Science and Technology Commission of Shanghai Municipality, grant PWZxq2017-13 from the Key Disciplines Group Construction Project of Pudong Health Bureau of Shanghai, and grant PWYgf 2018-05 from the Top-level Clinical Discipline Project of Shanghai Pudong.

SUPPLEMENTARY MATERIAL

The Supplementary Material for this article can be found online at: https://www.frontiersin.org/articles/10.3389/fcell.2021.663279/full#supplementary-material

REFERENCES

Adams, B. D., Parsons, C., Walker, L., Zhang, W. C., and Slack, F. J. (2017). Targeting noncoding RNAs in disease. *J. Clin. Invest.* 127, 761–771. doi: 10.1172/JCI84424

Aghajani, M., Mansoori, B., Mohammadi, A., Asadzadeh, Z., and Baradaran, B. (2019). New emerging roles of CD133 in cancer stem cell: Signaling pathway and miRNA regulation. *J. Cell. Physiol.* 234, 21642–21661. doi: 10.1002/jcp.28824

Bonnet, D., and Dick, J. E. (1997). Human acute myeloid leukemia is organized as a hierarchy that originates from a primitive hematopoietic cell. *Nat. Med.* 3, 730–737. doi: 10.1038/nm0797-730

Bray, F., Ferlay, J., Soerjomataram, I., Siegel, R. L., Torre, L. A., and Jemal, A. (2018). Global cancer statistics 2018: GLOBOCAN estimates of incidence and mortality worldwide for 36 cancers in 185 countries. *CA Cancer J. Clin.* 68, 394–424. doi: 10.3322/caac.21492

Bu, P., Wang, L., Chen, K. Y., Srinivasan, T., Murthy, P. K., Tung, K. L., et al. (2016). A miR-34a-numb feedforward loop triggered by inflammation regulates asymmetric stem cell division in intestine and colon cancer. *Cell Stem Cell* 18, 189–202. doi: 10.1016/j.stem.2016.01.006

Cech, T. R., and Steitz, J. A. (2014). The noncoding RNA revolution-trashing old rules to forge new ones. *Cell* 157, 77–94. doi: 10.1016/j.cell.2014.03.008

Chen, W., Zheng, R., Baade, P. D., Zhang, S., Zeng, H., Bray, F., et al. (2016). Cancer statistics in China, 2015. *CA Cancer J. Clin.* 66, 115–132. doi: 10.3322/caac.21338

Chiba, S. (2006). Notch signaling in stem cell systems. *Stem Cells* 24, 2437–2447. doi: 10.1634/stemcells.2005-0661

Easwaran, H., Tsai, H. C., and Baylin, S. B. (2014). Cancer epigenetics: tumor heterogeneity, plasticity of stem-like states, and drug resistance. *Mol. Cell* 54, 716–727. doi: 10.1016/j.molcel.2014.05.015

Eramo, A., Haas, T. L., and De Maria, R. (2010). Lung cancer stem cells: tools and targets to fight lung cancer. *Oncogene* 29, 4625–4635. doi: 10.1038/onc.2010.207

Eramo, A., Lotti, F., Sette, G., Pilozzi, E., Biffoni, M., Di Virgilio, A., et al. (2016). Identification and expansion of the tumorigenic lung cancer stem cell population. *Cell Death Differ.* 15, 504–514. doi: 10.1038/sj.cdd.4402283

Fang, L., Cai, J., Chen, B., Wu, S., Li, R., Xu, X., et al. (2015). Aberrantly expressed miR-582-3p maintains lung cancer stem cell-like traits by activating Wnt/beta-catenin signalling. *Nat. Commun.* 6:8640. doi: 10.1038/ncomms9640

Garofalo, M., Di Leva, G., Romano, G., Nuovo, G., Suh, S. S., Ngankeu, A., et al. (2009). miR-221&222 regulate TRAIL resistance and enhance tumorigenicity through PTEN and TIMP3 downregulation. *Cancer Cell* 16, 498–509. doi: 10.1016/j.ccr.2009.10.014

Garofalo, M., Romano, G., Di Leva, G., Nuovo, G., Jeon, Y. J., Ngankeu, A., et al. (2011). EGFR and MET receptor tyrosine kinase-altered microRNA expression induces tumorigenesis and gefitinib resistance in lung cancers. *Nat. Med.* 18, 74–82. doi: 10.1038/nm.2577

Hong, K. J., Wu, D. C., Cheng, K. H., Chen, L. T., and Hung, W. C. (2014). RECK inhibits stemness gene expression and tumorigenicity of gastric cancer cells by suppressing ADAM-mediated Notch1 activation. *J. Cell. Physiol.* 229, 191–201. doi: 10.1002/jcp.24434

Hsu, W. H., Yang, J. C., Mok, T. S., and Loong, H. H. (2018). Overview of current systemic management of EGFR-mutant NSCLC. *Ann. Oncol.* 29(suppl. 1), i3–i9.

Jang, J. Y., Kim, Y. G., Nam, S. J., Keam, B., Kim, T. M., Jeon, Y. K., et al. (2016). Targeting adenine nucleotide translocase-2 (ANT2) to overcome resistance to epidermal growth factor receptor tyrosine kinase inhibitor in non-small cell lung cancer. *Mol. Cancer Ther.* 15, 1387–1396. doi: 10.1158/1535-7163.MCT-15-0089

Jiang, W., Cai, G., Hu, P. C., and Wang, Y. (2018). Personalized medicine in non-small cell lung cancer: a review from a pharmacogenomics perspective. *Acta Pharm. Sin. B* 8, 530–538. doi: 10.1016/j.apsb.2018.04.005

Khan, A. Q., Ahmed, E. I., Elareer, N. R., Junejo, K., Steinhoff, M., and Uddin, S. (2019). Role of miRNA-regulated cancer stem cells in the pathogenesis of human malignancies. *Cells* 8:840. doi: 10.3390/cells8080840

Krek, A., Grün, D., Poy, M. N., Wolf, R., Rosenberg, L., Epstein, E. J., et al. (2005). Combinatorial microRNA target predictions. *Nat. Genet.* 37, 495–500. doi: 10.1038/ng1536

Lee, S. H., Do, S. I., Lee, H. J., Kang, H. J., Koo, B. S., and Lim, Y. C. (2016). Notch1 signaling contributes to stemness in head and neck squamous cell carcinoma. *Lab. Invest.* 96, 508–516. doi: 10.1038/labinvest.2015.163

Li, N., Yu, N., Wang, J., Xi, H., Lu, W., Xu, H., et al. (2015). miR-222/VGLL4/YAP-TEAD1 regulatory loop promotes proliferation and invasion of gastric cancer cells. *Am. J. Cancer Res.* 5, 1158–1168.

Li, S., Li, Q., Lü, J., Zhao, Q., Li, D., Shen, L., et al. (2020). Targeted inhibition of miR-221/222 promotes cell sensitivity to Cisplatin in triple-negative breast cancer MDA-MB-231 Cells. *Front. Genet.* 10:1278. doi: 10.3389/fgene.2019.01278

Li, Y., Liang, C., Ma, H., Zhao, Q., Lu, Y., Xiang, Z., et al. (2014). miR-221/222 promotes S-phase entry and cellular migration in control of basal-like breast cancer. *Molecules* 19, 7122–7137. doi: 10.3390/molecules19067122

MacDonagh, L., Gray, S. G., Breen, E., Cuffe, S., Finn, S. P., O'Byrne, K. J., et al. (2016). Lung cancer stem cells: the root of resistance. *Cancer Lett.* 372, 147–156. doi: 10.1016/j.canlet.2016.01.012

Pardal, R., Clarke, M. F., and Morrison, S. J. (2003). Applying the principles of stem-cell biology to cancer. *Nat. Rev. Cancer* 3, 895–902. doi: 10.1038/nrc1232

Roudi, R., Korourian, A., Shariftabrizi, A., and Madjd, Z. (2015). Differential expression of cancer stem cell markers ALDH1 and CD133 in various lung cancer subtypes. *Cancer Invest.* 33, 294–302. doi: 10.3109/07357907.2015.1034869

Rupaimoole, R., and Slack, F. J. (2017). MicroRNA therapeutics: towards a new era for the management of cancer and other diseases. *Nat. Rev. Drug Discov.* 16, 203–222. doi: 10.1038/nrd.2016.246

Shimono, Y., Zabala, M., Cho, R. W., Lobo, N., Dalerba, P., Qian, D., et al. (2009). Downregulation of miRNA-200c links breast cancer stem cells with normal stem cells. *Cell* 138, 592–603. doi: 10.1016/j.cell.2009.07.011

Shukla, S., Khan, S., Sinha, S., and Meeran, S. M. (2018). Lung cancer stem cells: an epigenetic perspective. *Curr. Cancer Drug Targets* 18, 16–31. doi: 10.2174/1568009617666170206104623

Sun, H. L., Men, J. R., Liu, H. Y., Liu, M. Y., and Zhang, H. S. (2020). FOXM1 facilitates breast cancer cell stemness and migration in YAP1-dependent manner. *Arch. Biochem. Biophys*. 685:108349.

Talukdar, S., Bhoopathi, P., Emdad, L., Das, S., Sarkar, D., and Fisher, P. B. (2019). Dormancy and cancer stem cells: an enigma for cancer therapeutic targeting. *Adv. Cancer Res.* 141, 43–84.

Totaro, A., Castellan, M., Di Biagio, D., and Piccolo, S. (2018). Crosstalk between YAP/TAZ and Notch signaling. *Trends Cell Biol*. 28, 560–573.

Venkatesh, V., Nataraj, R., Thangaraj, G. S., Karthikeyan, M., Gnanasekaran, A., Kaginelli, S. B., et al. (2018). Targeting Notch signalling pathway of cancer stem cells. *Stem Cell Investig.* 5:5. doi: 10.21037/sci.2018.02.02

Wang, S., Xu, Z. Y., Wang, L. F., and Su, W. (2013). CD133+ cancer stem cells in lung cancer. *Front. Biosci. (Landmark Ed.)* 18:447–453. doi: 10.2741/4113

Wood, S. L., Pernemalm, M., Crosbie, P. A., and Whetton, A. D. (2015). Molecular histology of lung cancer: from targets to treatments. *Cancer Treat. Rev.* 41, 361–375. doi: 10.1016/j.ctrv.2015.02.008

Yang, Z., Hackshaw, A., Feng, Q., Fu, X., Zhang, Y., Mao, C., et al. (2017). Comparison of gefitinib, erlotinib and afatinib in non-small cell lung cancer: a meta-analysis. *Int. J. Cancer* 140, 2805–2819. doi: 10.1002/ijc.30691

Yu, Z., Pestell, T. G., Lisanti, M. P., and Pestell, R. G. (2012). Cancer stem cells. *Int. J. Biochem. Cell Biol.* 44, 2144–2151. doi: 10.1016/j.biocel.2012.08.022

Zhang, S., Zhao, B. S., Zhou, A., Lin, K., Zheng, S., Lu, Z., et al. (2017). m(6)A demethylase ALKBH5 maintains tumorigenicity of glioblastoma stem-like cells by sustaining FOXM1 expression and cell proliferation program. *Cancer Cell* 31, 591–606.e6.

Zhang, W. C., Chin, T. M., Yang, H., Nga, M. E., Lunny, D. P., Lim, E. K., et al. (2016). Tumour-initiating cell-specific miR-1246 and miR-1290 expression converge to promote non-small cell lung cancer progression. *Nat. Commun.* 7:11702. doi: 10.1038/ncomms11702

Zhao, Z. L., Zhang, L., Huang, C. F., Ma, S. R., Bu, L. L., Liu, J. F., et al. (2016). NOTCH1 inhibition enhances the efficacy of conventional chemotherapeutic agents by targeting head neck cancer stem cell. *Sci. Rep*. 6:24704. doi: 10.1038/srep24704

Conflict of Interest: The authors declare that the research was conducted in the absence of any commercial or financial relationships that could be construed as a potential conflict of interest.

frontiers in Cell and Developmental Biology

REVIEW
published: 22 July 2021
doi: 10.3389/fcell.2021.711005

Long Non-coding RNA Regulation of Mesenchymal Stem Cell Homeostasis and Differentiation: Advances, Challenges, and Perspectives

Yanlei Yang[1,2], Suying Liu[1], Chengmei He[1], Zhilei Chen[1], Taibiao Lyu[1], Liuting Zeng[1], Li Wang[1], Fengchun Zhang[1], Hua Chen[1]* and Robert Chunhua Zhao[2,3]**

[1] Key Laboratory of the Ministry of Education, Department of Rheumatology and Clinical Immunology, Clinical Immunology Center, Peking Union Medical College Hospital, Chinese Academy of Medical Sciences, Peking Union Medical College, Beijing, China, [2] Beijing Key Laboratory (No. BZO381), School of Basic Medicine, Center of Excellence in Tissue Engineering, Peking Union Medical College Hospital, Institute of Basic Medical Sciences, Chinese Academy of Medical Sciences, Peking Union Medical College, Beijing, China, [3] School of Life Sciences, Shanghai University, Shanghai, China

OPEN ACCESS

Edited by:
Wencheng Zhang, Tongji University, China

Reviewed by:
Zhipeng Fan, Capital Medical University, China
Jingting Li, Sun Yat-sen University, China

***Correspondence:**
Fengchun Zhang
zhangfccra@aliyun.com
Hua Chen
chenhua@pumch.cn
Robert Chunhua Zhao
zhaochunhua@ibms.pumc.edu.cn

Specialty section:
This article was submitted to Stem Cell Research, a section of the journal Frontiers in Cell and Developmental Biology

Received: *17 May 2021*
Accepted: *21 June 2021*
Published: *22 July 2021*

Citation:
Yang Y, Liu S, He C, Chen Z, Lyu T, Zeng L, Wang L, Zhang F, Chen H and Zhao RC (2021) Long Non-coding RNA Regulation of Mesenchymal Stem Cell Homeostasis and Differentiation: Advances, Challenges, and Perspectives. Front. Cell Dev. Biol. 9:711005. doi: 10.3389/fcell.2021.711005

Given the self-renewal, multi-differentiation, immunoregulatory, and tissue maintenance properties, mesenchymal stem cells (MSCs) are promising candidates for stem cell-based therapies. Breakthroughs have been made in uncovering MSCs as key contributors to homeostasis and the regenerative repair of tissues and organs derived from three germ layers. MSC differentiation into specialized cell types is sophisticatedly regulated, and accumulating evidence suggests long non-coding RNAs (lncRNAs) as the master regulators of various biological processes including the maintenance of homeostasis and multi-differentiation functions through epigenetic, transcriptional, and post-translational mechanisms. LncRNAs are ubiquitous and generally referred to as non-coding transcripts longer than 200 bp. Most lncRNAs are evolutionary conserved and species-specific; however, the weak conservation of their sequences across species does not affect their diverse biological functions. Although numerous lncRNAs have been annotated and studied, they are nevertheless only the tip of the iceberg; the rest remain to be discovered. In this review, we characterize MSC functions in homeostasis and highlight recent advances on the functions and mechanisms of lncRNAs in regulating MSC homeostasis and differentiation. We also discuss the current challenges and perspectives for understanding the roles of lncRNAs in MSC functions in homeostasis, which could help develop promising targets for MSC-based therapies.

Keywords: mesenchymal stem cells, long non-coding RNAs, differentiation, homeostasis, exosomes

INTRODUCTION

Mesenchymal stem cells (MSCs) are heterogeneous, multipotent adult stem cells that originate in the mesoderm and that have been isolated from diverse tissues such as adipose tissue, bone marrow, and umbilical cord. Due to their self-renewal, multilineage differentiation potential, extensive immunomodulatory effects, and tissue maintenance properties, MSCs have emerged as attractive

tools for cell-based therapies and have been involved as treatment options for hematological diseases, autoimmune diseases, and peripheral nerve injuries (Chen et al., 2019; Yousefi et al., 2019; Zoehler et al., 2020). Currently, there have been breakthroughs in uncovering MSCs as key contributors to homeostasis and the regenerative repair of tissues and organs derived from three germ layers (mesoderm, ectoderm, and endoderm) (Sui et al., 2020). Notably, the MSCs present in different embryonic development stages, including postembryonic and postnatal tissues, constitute a population of sub-totipotent stem cells or progenitors, which were recently defined as MSC systems, have been confirmed to have molecular heterogeneity at single-cell transcriptomic level. MSCs maintain tissue homeostasis in three main ways. First, the MSCs residing in the major tissues, including adipose, bone, cartilage, muscles, divide and differentiate into targeted cell types to support the expansion, regeneration, and homeostasis of these tissues (Hilgendorf et al., 2019). Second, MSCs residing in tissue perivascular niches interact closely with their surroundings, which harbor varied cell types and soluble factors that further influence MSC behavior (Crisan et al., 2008; Sui et al., 2020). Third, MSCs themselves also secrete abundant types of biofactors and extracellular vesicles (EVs) to potentially affect their surroundings, including supporting hematopoiesis and modulating immune responses (Wang et al., 2014; Kfoury and Scadden, 2015; Sui et al., 2020). These functional capabilities contribute to MSC modulation in tissue homeostasis. However, the regulation of MSC function in these processes is immensely complex and tightly controlled and warrants extensive studies.

Long non-coding RNAs (lncRNAs) are transcripts with an average length of >200 nucleotides, lack protein-coding potential, and were previously considered transcriptional noise (Djebali et al., 2012). Most lncRNAs are evolutionarily conserved and species-specific, albeit less conserved across species, and they have diverse biological functions (Jin et al., 2011). According to genome-wide association studies (GWAS), non-coding intervals cover over one-third of the phenotype-associated locations. Nevertheless, lncRNAs largely remain to be identified, and their association and their functions require intensive studies (Jin et al., 2011). With the development of high-throughput sequencing, microarrays, and bioinformatics, an increasing number of lncRNAs has been identified, and increasing evidence has confirmed their roles as master regulators of various biological processes, including the maintenance of MSC homeostasis and multi-differentiation functions through diverse mechanisms at the epigenetic, transcriptional, and translational level.

In this review, we provide an overview of the MSC characteristics and their contributions to tissue homeostasis, and highlight the role of lncRNAs in modulating MSC homeostasis and differentiation. We also discuss the challenges and perspectives underlying lncRNA usage in preclinical research and clinical application. We aim to elucidate the underlying mechanisms involved in this process, which could help provide promising targets for MSC-based therapies.

MSCS CONTRIBUTE TO TISSUE HOMEOSTASIS

Mesenchymal stem cells were first identified from bone marrow by Friedenstein et al. (1976) in the 1950s; thereafter, scientists revealed that they are present in almost all connective tissues, and can also reside in fetal or adult somatic tissues, including the amniotic membrane (Parolini et al., 2008), umbilical cord (Romanov et al., 2003), adipose tissue (Zuk et al., 2002), skin (Orciani and Di Primio, 2013), peripheral blood (He et al., 2007), dental pulp (Huang et al., 2009), fetal liver (Zhang et al., 2005), and synovial membrane (De Bari et al., 2001). The source tissue from which MSCs are derived determines their differentiation potential (Xu et al., 2017). Bone marrow-derived MSCs (BMSCs) and adipose-derived MSCs (ADSCs) share similar morphological features and cell surface markers; however, many studies have indicated that significant biological differences exist, including differentiation potential. For example, BMSCs exhibit higher osteogenic but lower adipogenic differentiation capacity compared to ADSCs (Xu et al., 2017). ADSCs produce more neurosphere-derived neuron-like cells compared to BMSCs; therefore, ADSCs are a more suitable source for cell transplantation for treating spinal cord injury (Chung et al., 2013). Therefore, clarifying the intrinsic biological characteristic of MSCs derived from different sources and choosing the appropriate MSCs are important for their clinical application. To create a standard criterion for univocally defining the identity of MSCs used for scientific research and preclinical studies, the International Society for Cellular Therapy established the minimum criteria required for defining MSCs (Dominici et al., 2006; Wang et al., 2019): (1) MSCs must be fibroblast-like plastic-adherent cells when maintained in standard culture conditions; (2) ≥ 95% of the MSC population must express CD105, CD73, and CD90, and lack (≤2% positive) CD45, CD34, CD14 or CD11b, CD79a or CD19, and HLA-class II expression; (3) MSCs must have the capacity to differentiate into adipocytes, osteoblasts, and chondroblasts *in vitro*. Later studies have indicated that besides the capacity to differentiate into mesenchymal lineages, MSCs also have the potential to trans-differentiate into the unrelated germline ectodermal (neurocytes) and endodermal lineages (hepatocytes).

Recently, a new concept of MSC system was proposed by Wang et al. (2019), which was regarded as all MSCs derived from different stages of embryonic development, from postembryonic sub-totipotent stem cells to progenitors (Zhao, 2013). The MSC system well defined the important self-renewal and differentiation, immunomodulatory, and tissue homeostasis properties of MSCs, which provides a more comprehensive view of MSCs and better explains the heterogeneity of MSCs in differentiation potential and immunomodulatory functions. MSCs that reside in tissues such as bone marrow, adipose, cartilage, and muscle primarily form unique niches with a quiescent state. When exposed to stimulus such as injury, inflammation, and medicine, MSCs enter an active state to divide and differentiate into specialized cell types to support the expansion and homeostasis of these

tissues (Méndez-Ferrer et al., 2010; Hilgendorf et al., 2019; Hu et al., 2020). Besides, MSCs interact closely with their surroundings by secreting variable biofactors and EVs to support hematopoiesis and modulate immune responses; the surrounding niches in which MSCs reside also influence their behavior (Crisan et al., 2008; Zhao et al., 2014). For example, during wound healing, skin residential ADSCs divide and migrate to injured sites and differentiate into skin cells such as dermal fibroblasts (DFs) to replace and regenerate damaged cells. On the other hand, ADSCs activate wound healing via the autocrine and paracrine pathways. Together with other skin cells such as DFs, ADSCs secrete factors to form the extracellular matrix and interact with each other to promote wound healing, maintain skin structure, and modulate skin homeostasis (Mazini et al., 2020). Another example is BMSCs, which express nestin, in the perivascular stroma, can self-renew and differentiate into osteochondral lineages that form a unique niche in the bone marrow to maintain hematopoietic stem cell (HSC) homeostasis, such as modulating HSC proliferation, differentiation, and recruitment (Méndez-Ferrer et al., 2010). In the endosteal niche, these BMSCs, together with osteoblasts, maintain HSCs in a quiescent state. When subjected to injury, MSCs expressing LepR and Gli1 divide and contribute to bone repair and regeneration (Zhou et al., 2014; Shi et al., 2017). In lethally irradiated mice, the injection of MSCs deficient in nestin expression notably reduced HSC homing to the bone marrow (Méndez-Ferrer et al., 2010). BMSC dysfunction, including aberrant proliferation and differentiation, is the crucial pathogenesis of bone degeneration and hematopoiesis suppression. Moreover, MSCs are indispensable in maintaining the homeostasis of other tissues, including intestinal (Stzepourginski et al., 2017) and skeletal muscle (Wosczyna et al., 2019).

So far, there have been breakthroughs in understanding the biological characteristics and potential therapeutic values of MSCs. In general, MSCs have multi-directional differentiation potential, can secrete bioactive molecules to migrate and home to injured or inflamed sites, and have powerful immunomodulating ability, thereby making them important contributors in tissue repair and homeostasis maintenance (**Figure 1**) (Vizoso et al., 2019; Wang et al., 2019; Bulati et al., 2020).

MSCs and Their Multilineage Differentiation Potential in Tissue Repair and Homeostasis

Mesenchymal stem cells maintain tissue homeostasis based on their differentiation potential by serving as a source of renewable progenitor cells to repair injured tissues and replace cells in routine cellular turnover throughout adult life (Spees et al., 2016; Chen et al., 2017). MSCs are adult stem cells that present in many tissues and can differentiate into multiple mesenchymal lineage cell types such as adipocytes, osteoblasts, chondrocytes, and myoblasts under specific culture conditions (Boeuf and Richter, 2010; Scott et al., 2011; Westhrin et al., 2015; Chen et al., 2018). Besides, when exposed to certain extracellular cues, MSCs can also give rise to cross-lineage cell types like endodermal-hepatocyte and ectodermal-neurons, which is also known as trans-differentiate potential (Song and Tuan, 2004).

During bone tissue fracture, MSCs are recruited to the injury site and differentiate into osteoblasts to aid the repair and reconstitution of injured bone tissue (Freitas et al., 2019; Moura et al., 2020). MSCs can differentiate into cardiac cells under specific conditions *in vitro*; genetically manipulated MSCs with Akt1 and Wnt11 overexpression exhibit enhanced cardiac differentiation as verified by the elevated cardiac markers Nkx2.5, GATA4, α-MHC, and BNP, indicating that the transplantation of genetically engineered MSCs is a promising strategy for treating acute myocardial infarction (Chen et al., 2018). Moreover, MSCs also have the potential to trans-differentiate into endoderm and ectoderm cells to help repair specific tissues and organs. MSCs induced by chemically defined media containing specific cytokines and growth factors *in vitro* can trans-differentiate into hepatocyte-like cells with the functional properties of albumin synthesis and secretion, cytochrome P450 enzyme activity, glycogen storage, urea biosynthesis, and the expression of hepatocyte-specific genes (He et al., 2013; Fu et al., 2016; Maymó et al., 2018; Furuya et al., 2019), and can reconstitute liver function *in vivo* in experimental hepatic injury murine models (Xu et al., 2014; Fu et al., 2016). MSCs also have the capacity to produce pancreas-like cells under stepwise induction by cytokine cocktails (Yu et al., 2015; Mehrfarjam et al., 2016), via pancreatic extract or coculture with pancreatic adult stem cells (Lee et al., 2008; Hefei et al., 2015). MSC-derived insulin-producing cells express pancreatic β cell-related genes, respond to glucose challenge *in vitro*, and have the potential to improve glucose tolerance in diabetic 90% pancreatectomy rats *in vivo* (Yu et al., 2015). Further, MSCs can tans-differentiate into endothelial cells with the endothelial phenotype and express endothelial nitric oxide synthase, which contributed to improving endothelial function in a vascular injury rat model (Jiang et al., 2006; Yue et al., 2008).

Although the multi-differentiation capacity of MSCs ensures their tissue repair and regeneration function, the increasing application of MSCs clinically has reported that only a small amount of MSCs undergo subsequent differentiation into the targeted cell type after transplantation while still receiving functional improvement (Ferrand et al., 2011; Lai et al., 2015; Vizoso et al., 2019). Other mechanisms may confer MSCs efficacy in damaged tissues and the maintenance of tissue homeostasis.

The MSC Secretome in Tissue Homeostasis

Increasing evidence supports the idea that intravenously injected MSCs can home specifically to sites of ischemia, damage, or inflammation, while not requiring induction into a specific functional cell type in advance (Price et al., 2006; Ye and Zhang, 2017; Ben Menachem-Zidon et al., 2019). Yet, other studies have shown poor survival and transient retainment of transplanted MSCs within the host tissue (Yeo et al., 2013; Miao et al., 2017), indicating that MSCs may not exert their therapeutic effects directly; rather, it occurs through the secretion of bioactive factors

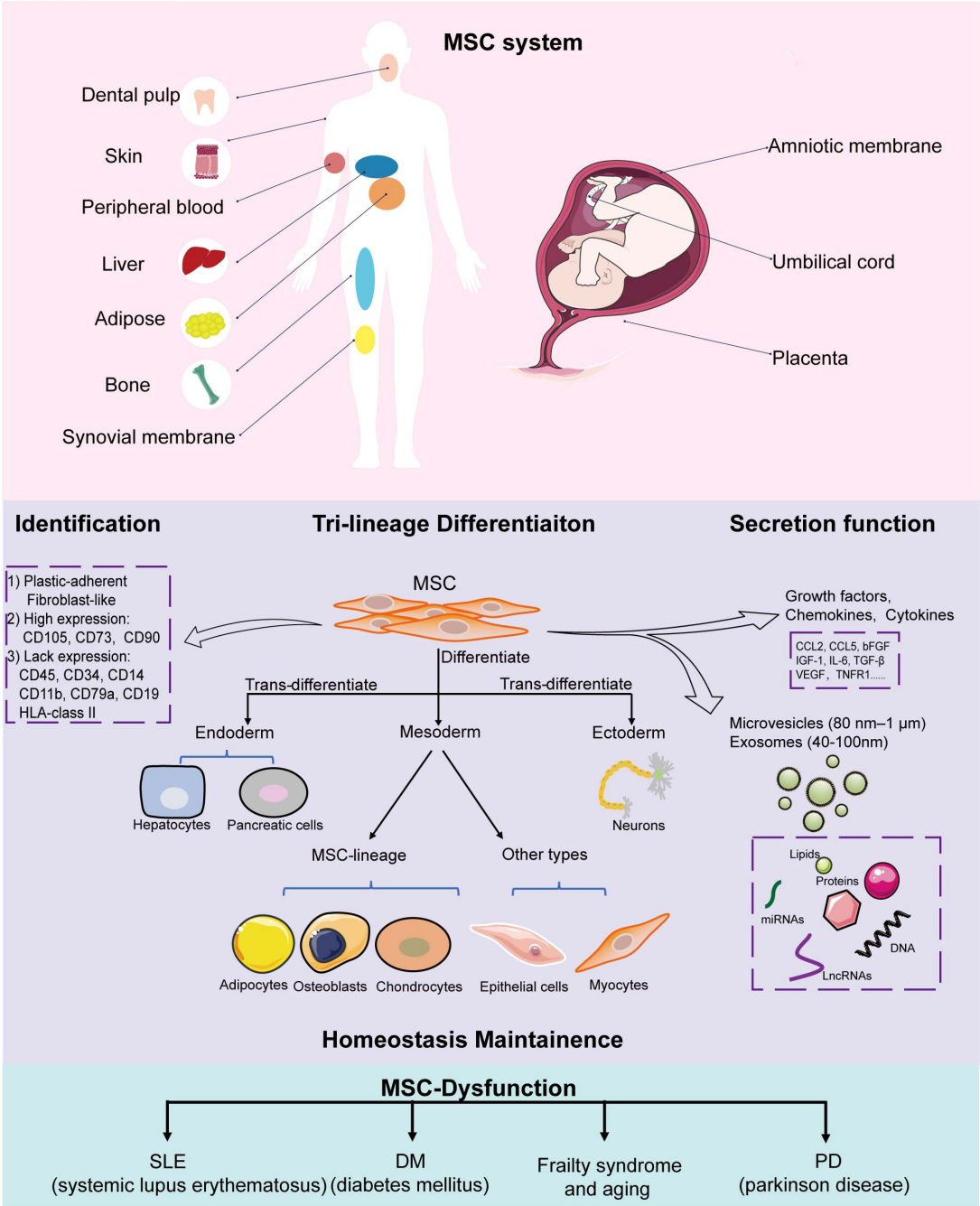

FIGURE 1 | Implications of MSCs in homeostasis. MSCs can be isolated from a variety of tissues, including the amniotic membrane, umbilical cord, placenta, adipose tissue, skin, peripheral blood, dental pulp, and fetal liver. All MSCs derived from different stages of embryonic development, from postembryonic sub-totipotent stem cells to progenitors, are defined as MSC systems. During *in vitro* culture, MSCs must: (1) be fibroblast-like and plastic-adherent; (2) express CD105, CD73, and CD90, and lack CD45, CD34, CD14 or CD11b, CD79a or CD19, and HLA class II expression; (3) differentiate into adipocytes, osteoblasts, and chondroblasts. MSCs have trilineage differentiation potential, can secrete bioactive molecules and EVs (microvesicles and exosomes) to help tissue repair and maintain homeostasis. MSC dysfunction leads to disease-related MSC alterations that induce homeostasis disorder systemic disease.

to provide a conducive microenvironment to facilitate the repair and regeneration of injured tissues.

Mesenchymal stem cells with the potential for synthesizing and secreting a variety of bioactive factors (e.g., cytokines and chemokines), and to affect nearby cells were first described by Haynesworth et al. (1996). In 2009, Bruno et al. (2009) reported that a new form of MSC secretion, termed microvesicles (80 nm to 1 μm), was protective against acute tubular injury.

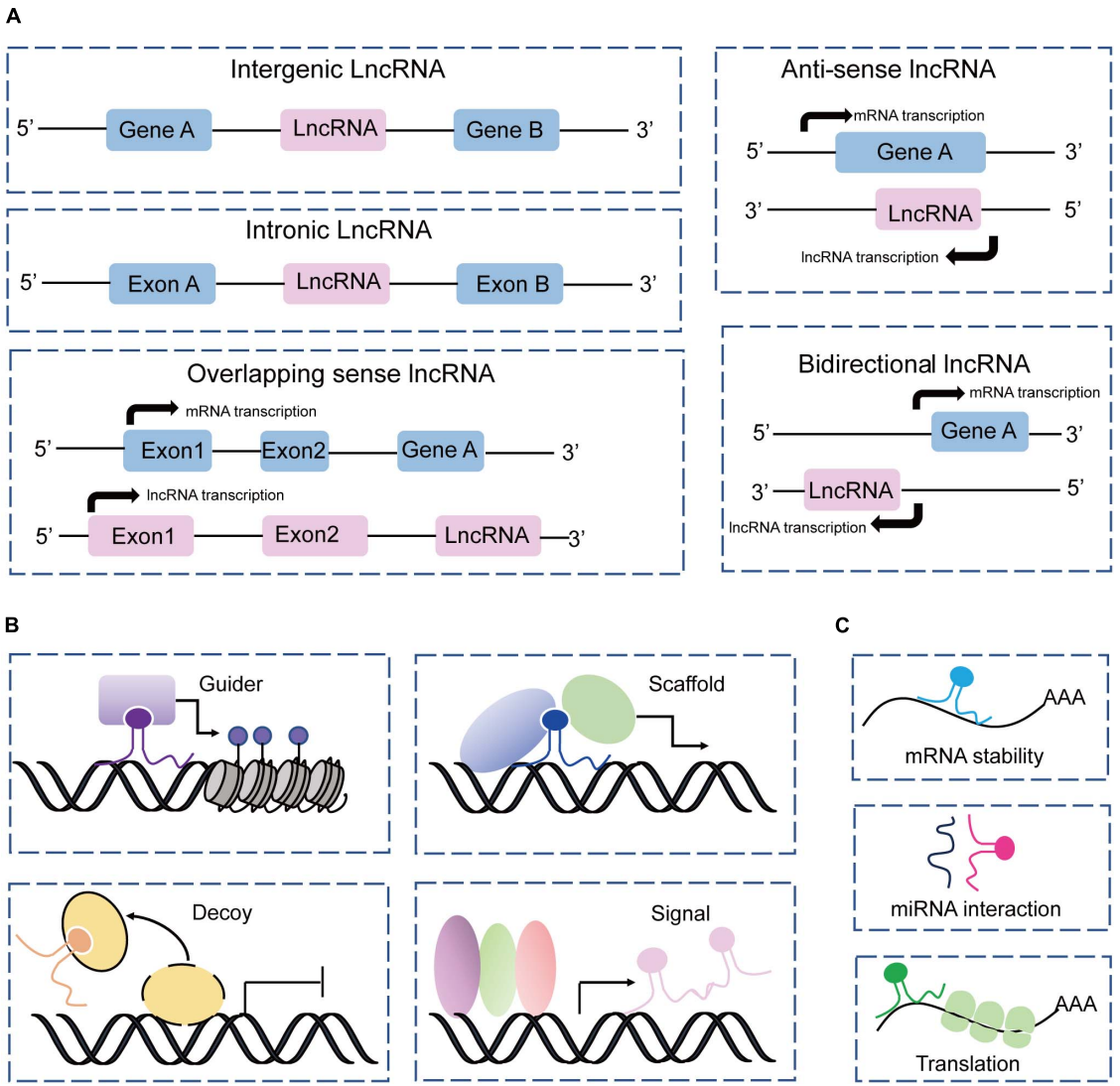

FIGURE 2 | Classification and mechanism of lncRNAs. **(A)** Classification of lncRNAs according to the protein-coding genes as intergenic, intronic, sense, antisense, and bidirectional. **(B)** LncRNAs acting as guides, scaffolds, decoys, and signals to perform their functions with DNAs and proteins. **(C)** LncRNAs interact with RNAs to regulate RNA stability, and translation, and sponge miRNAs.

The next year, Lai et al. (2010) demonstrated a specific class of extracellular vesicles (EVs) with a diameter of 40–100 nm, defined as exosomes. The multiple bioactive factors, together with the EVs (e.g., exosomes and microvesicles), are generally referred to as MSC secretome. Subsequent studies reported that the MSC secretome has important effects in promoting angiogenesis, modulating immunity, and hematopoietic support (Lai et al., 2015; Konala et al., 2016). The composition of the soluble factors of MSCs derived from different tissues may vary, but they often secrete cytokines (e.g., CCL2, CCL5, bFGF, IL-6, TGF-β, and VEGF), contributing to tissue development, cell differentiation, and tumor growth and metastasis (Wang et al., 2019). Some factors (e.g., IL-6, IL-10, PGE2, HGF, nitric oxide, and human HLA-G) account for the immunomodulatory functions of MSCs (Wang et al., 2019). MSCs can also secrete neurotrophic factors, such as brain- and glial-derived neurotrophic factors (e.g., nerve growth factor), making them attractive cellular sources for brain disorders (Lopatina et al., 2019). Moreover, MSC-derived EVs also exhibit tissue repair and immunomodulation functions. Our group demonstrated that MSC-derived exosomes can promote the angiogenesis of human brain microvascular endothelial cells and contribute to alleviating Parkinson disease (PD) in a mouse model (Xue et al., 2021). Further, MSC exosomes inhibited inflammatory responses and reactive astrogliosis *in vitro* and *in vivo*, and repaired learning and memory impairments induced by status epilepticus in a mouse model (Xian et al., 2019). In an allogeneic hematopoietic stem cell transplantation animal model, EVs derived from human umbilical cord-derived MSCs prevented acute graft-versus-host disease (GVHD) (Wang et al., 2016).

OVERVIEW OF LncRNAs

Accumulating evidence supports the role of lncRNAs as master regulators of various biological processes, including the maintenance of MSC homeostasis and multi-differentiation functions through diverse mechanisms. The recent development of genome technology opened the door to understanding their functional importance. Conventionally, lncRNAs are transcribed by RNA polymerase II, containing multi-exons, processed by alternative splicing, 3′ polyadenylated and 5′ capped, and present transcriptional activation activity like that of mRNAs (Djebali et al., 2012; Ma et al., 2013; Lagarde et al., 2017). Although lncRNAs are distributed widely across species, they are poorly conserved and exhibit low expression levels, making them species-specific features and easily regarded as transcriptional noise (Ma et al., 2013). Moreover, lncRNAs exhibit a spatiotemporal and cell-, tissue-, and development-specific expression pattern (Shi et al., 2020), and their subcellular location in the nucleus or the cytoplasm determines their functions and working mechanisms (Chen, 2016). Nuclear lncRNAs are usually involved in transcriptional regulation, including interaction with chromatin regulation and RNA processing. Cytoplasmic lncRNAs tend to affect translation, such as modulating mRNA stability and cellular signaling cascades (Schmitt and Chang, 2016).

Based on the genome location of protein-coding genes, lncRNAs can be classified into five groups: intergenic, intronic, sense, antisense, and bidirectional (Ma et al., 2013; Jarroux et al., 2017; Fernandes et al., 2019), which are described in **Figure 2A**. This classification is widely used by the GENCODE/Ensemble database in the annotation of transcript biotypes, as well as newly assembled lncRNA transcripts identified by laboratories. Initially, lncRNA transcripts can be classified as either intergenic or intragenic; the intragenic lncRNAs overlap with coding genes and are further classified into antisense, bidirectional, intronic, and overlapping sense lncRNAs. Additionally, lncRNAs commonly perform their gene expression regulatory functions by acting as signals, decoys, guides, and scaffolds through main mechanisms by interacting with DNA, protein, and RNA (Wang and Chang, 2011; Schmitt and Chang, 2016), as illustrated in **Figures 2B,C**. However, the mechanisms underlying lncRNA regulation of gene expression and biological processes are complex and not simply confined to one archetype as we have summarized, and await more extensive discoveries.

Accumulating studies have implicated lncRNAs as vital regulators of variable bioprocesses, including genomic imprinting, chromosome modification, transcriptional interference, cell cycle, proliferation, immunobiology, and differentiation (Bartolomei et al., 1991; Quinn and Chang, 2016; Yang et al., 2018). In terms of the important biological functions of lncRNAs, dysregulation such as overexpression, deficiency, or mutation is suspected in the occurrence and progression of many diseases, including autoimmune disease, cardiovascular disease, and cancer (Batista and Chang, 2013; Beermann et al., 2016; Atianand et al., 2017). Moreover, emerging evidence has confirmed the contribution of lncRNAs in MSC differentiation, homeostasis, and related diseases (Tye et al., 2015); clarifying the roles and innate mechanisms of MSC-related lncRNAs in homeostasis will help provide promising targets for MSC-based therapies.

MSC-ASSOCIATED LncRNAs IN DIFFERENTIATION AND HOMEOSTASIS

Mesenchymal stem cell differentiation is intricately regulated by multiple factors, including transcriptional factors (Runx2, PPARγ, MyoD, and GATA6), growth factors (VEGF, HGF, and EGF), and epigenetic factors such as DNA methylation, histone modification, RNA modification, and non-coding RNAs (miRNAs and lncRNAs) (Almalki and Agrawal, 2016; Sui et al., 2020). Recent studies have shown that lncRNAs are relatively new differentiation regulators that exert their functions through variable mechanisms, and await extensive studies. Herein, we mainly focus on the MSC-associated lncRNAs in differentiation and homeostasis.

LncRNAs in MSC-Derived Multilineage Differentiation

Long non-coding RNAs involved in MSC-derived lineage (adipocytes, osteoblasts and chondrocytes) differentiation have been extensively studied while remaining relatively less well studied in other directions such as endoderm and ectoderm lineage commitment and differentiation. Herein, we provide an overview of the essential lncRNAs involved in MSC lineage commitment (**Figure 3** and **Table 1**) and elaborate on the representative lncRNAs below.

LncRNAs in Mesodermal Lineage Differentiation

Mesenchymal stem cells tend to differentiate toward osteogenic, adipogenic, and chondrogenic lineages. Osteogenic and adipogenic MSC differentiation is a theoretically opposite process, during which the signaling pathways or transcription factors induced in adipogenesis occur at the cost of osteogenesis, and vice versa (Yuan et al., 2016). For example, peroxisome proliferator-activated receptor γ (PPARγ), a master regulator of MSC adipogenesis, and inhibits osteogenic differentiation. Bone morphogenetic protein (BMP) and Wnt, crucial inducers of MSC osteogenic differentiation, may hinder MSC adipogenic commitment by inactivating PPARγ. Many lncRNAs such as H19 and MEG3 act in the same manner. H19 is a paternally imprinted gene (Zhang and Tycko, 1992) that has been recently uncovered as an inhibitor during BMSC adipogenic differentiation through the epigenetic modulation of histone deacetylases (HDACs) (Huang et al., 2016). H19 also has the potential to promote MSC osteogenic differentiation by acting as a competing endogenous RNA (ceRNA) through sponging and inhibiting the expression of miR-22 and miR-141 (Liang et al., 2016). Similarly, H19 promotes tension-induced osteogenesis of BMSCs by sponging miR-138 and activates the downstream FAK pathway (Wu et al., 2018). Therefore, H19 is a key regulator in the multi-direction commitment of MSCs.

MEG3 is also an essential multi-functional regulator during MSC differentiation. During osteogenic differentiation, MSCs

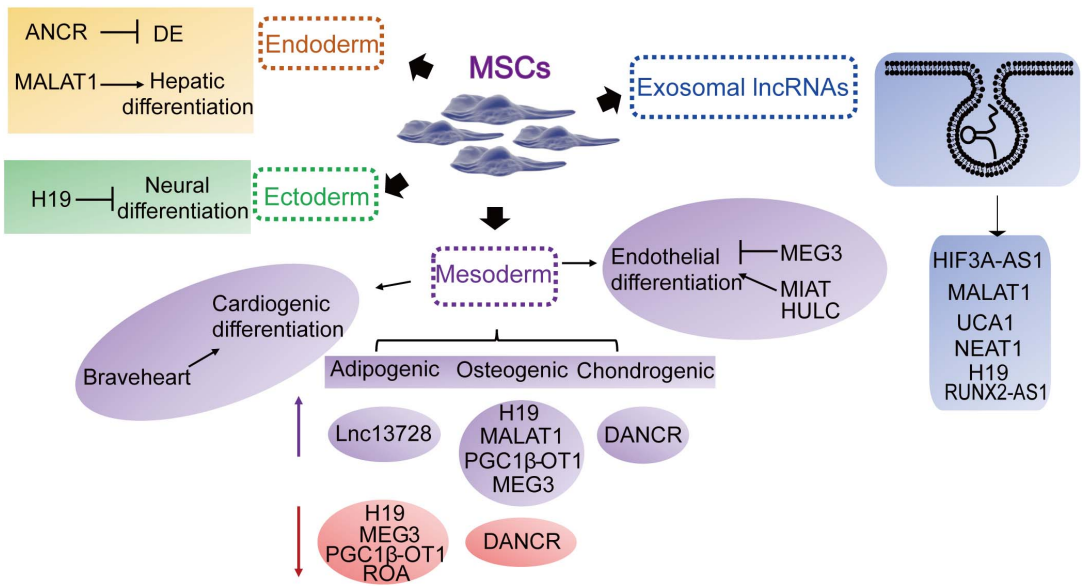

FIGURE 3 | Representative MSC differentiation- and exosome-associated lncRNAs. Endoderm: ANCR (DANCR), (differentiation) antagonizing non-protein coding RNA; MALAT1, metastasis-associated lung adenocarcinoma transcript 1. Ectoderm: H19. Mesoderm-cardiac: Braveheart. Mesoderm-adipogenic: PGC1β-OT1, peroxisome proliferator-activated receptor γ coactivator-1β-OT1; lnc13728; H19; MEG3, maternally expressed 3. Mesoderm-osteogenic: H19; MEG3; MALAT1; DANCR; PGC1β-OT1. Mesoderm-chondrogenic: DANCR. Mesoderm-endothelial: MEG3; MIAT, myocardial infarction-associated transcript; HULC, highly upregulated in liver cancer. Exosomal lncRNAs: HIF3A-AS1, HIF3A antisense 1; MALAT1; UCA1, urothelial carcinoma-associated 1; NEAT1, nuclear paraspeckle assembly transcript 1; H19; KLF3-AS1, KLF3 antisense 1.

from patients with multiple myeloma (MM) had lower MEG3 expression compared to that from normal donors (Zhuang et al., 2015). MEG3 performs its function at multiple levels. At the transcriptional level, it may act as a decoy to dissociate SOX2 binding at the BMP4 promoter, repressing BMP4 expression, thereby transcriptionally activating BMP4 promotion of MSC osteogenic differentiation (Zhuang et al., 2015). MEG3 can also act as histone methylation mediators by binding to the enhancer of zeste homolog 2 (EZH2), which can inhibit the expression of Wnt pathway genes by inducing H3K27 trimethylation to inhibit the osteogenic differentiation of human dental follicle stem cells (hDFSCs) (Deng et al., 2018). At the post-transcriptional level, MEG3 may act as a ceRNA to regulate osteogenic gene expression, and its expression level is increased in postmenopausal osteoporosis (PMOP) patients as compared to that in healthy donors (Wang et al., 2017). During the osteogenic differentiation of BMSCs from PMOP, MEG3 may target miR-133a-3p to inhibit this process (Wang et al., 2017). In addition, MEG3 may control the balance between MSC adipogenic and osteogenic differentiation; its downregulation promotes adipogenic differentiation while inhibiting the osteogenic differentiation of human ADSCs via miR-140-5p (Li et al., 2017). Moreover, MEG3 is an inhibitor of the development of many bone disorders, such as bone tumors, osteoarthritis (OA), osteoporosis, RA, and ankylosing spondylitis (AS). These findings indicate that MEG3 may act as a novel target for diagnosing or treating such bone diseases (Sun et al., 2020).

DANCR was characterized as a differentiation-antagonizing lncRNA of progenitor cells (Kretz et al., 2012). It functions as a positive regulator of chondrogenesis of human synovium-derived MSCs (through the miR-1305–Smad4 axis) (Zhang et al., 2017) while acting as an inhibitor of periodontal ligament stem cell osteogenesis (Wang et al., 2020). Another study revealed that DANCR inhibited the osteogenic differentiation of human BMSCs through the p38–MAPK pathway (Zhang et al., 2018). The lncRNA MALAT1 is another well-known abundant and conserved imprinted gene that acts as a master regulator of osteogenic differentiation via the mechanism of sponging miRNAs such as miR-143 (Gao et al., 2018) and miR-34c (Yang et al., 2019). Another newly identified lncRNA, PGC1β-OT1, reciprocally modulates MSC adipogenic and osteogenic commitment by sponging miR-148a-3p and enhancing the effect of KDM6B (Yuan et al., 2019); the lncRNA ROA inhibits MSC adipogenic differentiation by destroying hnRNPA1 binding to the PTX3 promoter, thereby transcriptionally downregulating PTX3 and the ERK pathway (Pan et al., 2020). Moreover, our lab discovered that lncRNA13728 promoted ADSC adipogenic differentiation by upregulating ZBED3 and inhibiting the WNT–β-catenin pathway (Xu et al., 2021).

The disruption of the balance between MSC osteogenesis and adipogenesis leads to disorders such as osteoporosis (Hoshiba et al., 2012). Notably, lncRNAs such as MEG3 and PGC1β-OT1 reciprocally modulate MSC commitment to adipogenic and osteogenic cells; therefore, understanding the roles and

TABLE 1 | MSCs-associated lncRNAs in multi-lineage differentiation.

Name of lncRNA	Function and MSC sources	Working model	Mechanism-effector and target	References
lncRNAs modulating MSC mesodermal lineage differentiation				
Osteogenesis, adipogenesis and chondrogenesis				
H19	Inhibit adipogenesis and BMSC	Epigenetic modulation	CTCF/H19/miR-675/HDAC	Huang et al., 2016
	Promote osteogenesis and BMSC	Sponging	miR-141, miR-22/Wnt/β-catenin pathway	Liang et al., 2016
			miR-138/FAK pathway	Wu et al., 2018
MEG3	Promote osteogenesis and BMSC (MM patients)	Decoy	SOX2/BMP4	Zhuang et al., 2015
	Inhibit osteogenesis and DFSCs	Unclassified	EZH2/Wnt genes	Deng et al., 2018
	Inhibit osteogenesis and BMSCs (PMOP patients)	Sponging	miR-133a-3p	Wang et al., 2017
	Inhibit adipogenesis, promote osteogenesis, and ADSC	Sponging	miR-140-5p.	Li et al., 2017
DANCR	Promote chondrogenesis and SMSC	Sponging	miR-1305/Smad4 axis	Zhang et al., 2017
	Inhibit osteogenesis and BMSC	Unclassified	p38 MAPK pathway	Zhang et al., 2018
MALAT1	Promote osteogenic and BMSC	Sponging	miR-34c/SATB2	Yang et al., 2019
			miR-143/OSX	Gao et al., 2018
PGC1β-OT1	Inhibit adipogenesis, promote osteogenesis, and BMSC	Sponging	miR-148a-3p/KDM6B	Yuan et al., 2019
ROA	Inhibit adipogenesis and BMSC	Decoy	hnRNP A1/PTX3/ERK	Pan et al., 2020
13728	Promote adipogenesis and ADSC	Unclassified	ZBED3/Wnt/β-catenin pathway	Xu et al., 2021
Endothelial and cardiac differentiation				
MEG3	Inhibit endothelial differentiation and BMSC	Post-transcriptional modulation	FOXM1/VEGF	Sun et al., 2018
MIAT	Promote endothelial differentiation and BMSC	Sponging	miR-200a/VEGF	Wang et al., 2018
HULC	Promote epithelial and smooth muscle-like cell differentiation and ADSC	Unclassified	BMP9/Wnt–β-catenin/Notch pathway	Li Y. et al., 2018
Braveheart	Promote cardiogenic differentiation	Unclassified	Mesp1	Hou et al., 2017
lncRNAs modulating MSC trans-differentiation into endoderm lineage				
ANCR	Inhibit DE commitment andADSC	Scaffold	ID2/PTK2B	Li et al., 2019
MALAT1	Promote trans-differentiate into hepatocyte and BMSC	Sponging	β-catenin/miR-217/ZEB1	Tan et al., 2019
lncRNAs modulating MSC trans-differentiation into ectoderm lineage				
H19	Inhibit trans-differentiate into neural-like cells and BMSC	Sponging	miR-675/IGFR	Farzi-Molan et al., 2018

underlying mechanisms of these lncRNAs may provide insights into improving the therapeutic method and effect of MSCs in diseases such as osteosarcoma, obesity, and OA.

In addition, MSCs can differentiate into mesoderm endotheliocytes and myocytes. The dysfunction of endothelial cell and myocyte generation leads to defects in angiogenesis and related cardiovascular disease. MEG3 inhibits BMSC endothelial differentiation by accelerating FOXM1 protein degradation via ubiquitination and decreasing VEGF expression (Sun et al., 2018). Moreover, the lncRNA MIAT, identified as a key contributor to development and disease, acts as a ceRNA of miR-200a and thereby targets VEGF to promote MSC endothelial differentiation (Wang et al., 2018). For MSC myogenesis, a recent study revealed that the lncRNA HULC promotes ADSC epithelial and smooth muscle-like cell differentiation by targeting BMP9, activating the Wnt–β-catenin pathway while inhibiting the Notch pathway (Li Y. et al., 2018). Another report showed the lncRNA Braveheart efficiently facilitates MSC cardiogenic differentiation by upregulating cardiac-specific transcription factors and epithelial-mesenchymal transition (EMT)-associated genes (Hou et al., 2017). Although MSCs have the potential to differentiate into all kinds of myocytes, functional lncRNAs in other types of myocyte commitment remain to be discovered.

LncRNAs in MSC Endodermal- and Ectodermal-Lineage Trans-Differentiation

Mesenchymal stem cells have tri-lineage differentiation potential; despite the mesodermal-lineage cells, MSCs can also trans-differentiate into ectodermal and endodermal lineages. Unlike the well-studied mesoderm lineage-associated lncRNAs described above, studies on the detailed functions of lncRNAs in MSC ectoderm and endoderm commitment are

relatively rare (which are summarized in **Table 1**), and further exploration is warranted.

Generating definitive endoderm (DE) and its lineage hepatocytes is a prerequisite for cell replacement therapy for liver and pancreatic diseases as well as for drug testing and toxicology studies (Li et al., 2019). According to our findings, the lncRNA ANCR (DANCR) is an inhibitor during ADSC trans-differentiation toward DE, and the mechanism linked involves it acting as a scaffold to recruit PTBP1 to ID2 mRNA, enhancing the interaction between them and subsequently stabilizing the ID2 mRNA (Li et al., 2019). This finding reveals another function of ANCR in modulating MSC DE commitment besides regulating chondrogenesis and osteogenesis. MALAT1 also performs a function in MSC trans-differentiation into hepatocyte in addition to adipogenesis and osteogenesis. Tan et al. (2019) successfully induced BMSCs into hepatocytes using HGF *in vitro* and discovered that MALAT1 coordinated with β-catenin, sponging miR-217, and upregulating ZEB1 to enhance telomerase activity during MSC hepatic trans-differentiation.

Ectoderm lineage neural cells are the foundation of our nervous system; they are relatively difficult to generate *in vitro*. Generating abundant neural cells will help promote cell-based therapy for treating neurological disorders and nerve injuries. Many studies have demonstrated that MSCs have the potential to trans-differentiate into neural-like cells under specific stimulation, making them a novel therapy for treating nervous system diseases. A study that profiled lncRNAs during BMSC neural cell differentiation found that several lncRNAs were differentially expressed, suggesting their key roles in this process (Wu et al., 2015). A subsequent study confirmed that H19 has a negative effect on BMSC neural-like differentiation through the miR-675–IGFR axis (Farzi-Molan et al., 2018). In the future, the identification of new lncRNAs in MSC neurogenesis and studies of the extensive mechanisms involved, as well as *in vivo* experiments, are needed, which will contribute to improving MSC-based therapeutic effects in treating neurological disease.

These lncRNAs, i.e., DANCR, MALAT1 MEG3, and H19, represent a subset of lncRNAs that exert various functions through multiple mechanisms in specific cell types under specific stimulations, which subsequently attach MSC unique capabilities to meet the qualifications *in vivo* and for clinical usage *in vitro*.

MSC Exosome-Derived LncRNAs and Their Implications in Clinical Usage

Increasing evidence suggests that the efficacy of MSC therapies is largely attributed to their paracrine secretion function, especially the exosomes (Dong et al., 2019). MSC-derived exosomes can shuttle a variety of bioactive molecules such as proteins, lipids, miRNA, lncRNAs, circular RNAs (circRNAs), and DNA to influence various bioprocesses, including development, immunity, and tissue homeostasis (Dong et al., 2019; Pegtel and Gould, 2019). Due to the advantages of low tumorigenic potential and low immunogenicity, exosomes are becoming novel, promising cell-free tools for tissue repair and diseases (Pegtel and Gould, 2019). Recently, functional lncRNAs derived from MSC exosomes have drawn increased attention, and some of these lncRNAs have been discovered. For example, the MSC exosomal lncRNA HIF3A-AS1 exhibits increased capacity in chondrocyte proliferation and cartilage repair in OA, which may be achieved through the miR-206–GIT1 axis (Liu et al., 2018a,b). Another study found that the exosomal lncRNA KLF3-AS1 alleviates cardiomyocyte pyroptosis and myocardial infarction through the miR-138-5p–Sirt1 axis (Mao et al., 2019). MALAT1 also resides in MSC exosomes; functional studies have shown that exosomal MALAT1 ameliorates osteoporotic by modulating the miR-34c–SATB2 axis (Yang et al., 2019) and can sponge miR-92a-3p and target ATG4a to fulfill its cardioprotective roles in doxorubicin-induced cardiac senescence and damage (Xia et al., 2020). Other exosomal lncRNAs such as UCA1 (Chen H. et al., 2020) and NEAT1 (Chen H. et al., 2020) also have a cardioprotective function by acting as ceRNAs.

The transfer of exosomes or microvesicles containing RNAs or other molecules between MSCs and the target cell type is one of the mechanisms by which MSCs perform their tissue repair functions (Spees et al., 2016). For example, H19 derived from MSC exosomes was transferred from MSCs to fibroblasts, thereby inhibiting fibroblast apoptosis and inflammation and activating the wound healing process in diabetic foot ulcers (Li et al., 2020). H19 could also be transferred to trophoblast cells via MSC-derived exosomes, enhancing trophoblast cell invasion and migration while inhibiting their apoptosis in preeclampsia (Chen Y. et al., 2020). Conversely, MSCs could also be the target cells during exosomal lncRNA transfer. MSCs derived from patients with MM had abundant exosomal lncRNA RUNX2-AS1; further studies revealed that it could be transferred from MM cells to MSCs and thereby prevent MSC osteogenesis by downregulating RUNX2 (Li B. et al., 2018), which provides a novel pathological mechanism of the bone lesion in patients with MM and could be a potential therapeutic target in the future.

These findings suggest that MSC-derived exosomes overexpressing lncRNAs such as H19 might be a novel direction for developing cell-free therapeutic strategies. Moreover, these exosomal lncRNAs are promising novel targets or biomarkers for treating and diagnosing diseases such as cardiomyopathy. In addition, understanding the tumor–stroma stem cell interactions, molecular transfer, and communication is also critical for developing novel and more effective strategies against cancer and other diseases.

CONCLUDING REMARKS

Mesenchymal stem cells are key contributors in maintaining tissue homeostasis (**Figure 1**). The regulatory mechanisms underlying MSC functions are complicated, and are intricately regulated by multiple factors, i.e., transcriptional factors, growth factors, and epigenetic factors such as DNA methylation, histone modification, RNA modification, and non-coding RNAs (lncRNAs, miRNAs, and circRNAs). Recently, lncRNAs have emerged as prominent modulators of MSC fate commitment and functional homeostasis (**Table 1**) through variable mechanisms (**Figure 2**). Understanding the roles of lncRNAs in MSC functions in homeostasis will aid the development of promising

targets for MSC-based therapies. However, issues and challenges remain to be investigated, including the conditions of MSCs used in basic research and clinical application, as well as the complex characteristics and mechanisms underlying lncRNA function.

CHALLENGES

As MSCs play an important role in tissue repair, regeneration, and homeostasis, their dysfunction may cause various systemic diseases. Clinical observation of allogenic MSC treatment of patients with autoimmune diseases, including systemic lupus erythematosus (SLE), diabetes mellitus (DM), rheumatoid arthritis (RA), and multiple sclerosis (MS) (Vizoso et al., 2019) indicates that the transplantation of external MSCs in good condition restores internal homeostasis. Further, MSC dysfunction indicates the onset of many diseases, including metabolic syndrome, DM, and RA, and aging syndromes such as Werner syndrome and Hutchinson–Gilford progeria syndrome (Liu et al., 2011; Zhang et al., 2015). Conversely, the continued inflammatory environment in these diseases may hinder MSC homing to the damage sites and probably result in MSC pool reduction and exhaustion (Shi et al., 2010), which contributes to the deterioration in MSC function and limits their use in autologous therapy.

To date, significant progress has been made in utilizing MSCs in basic preclinical research and clinical studies. However, some challenges should be overcome before the final clinical application (Wang et al., 2019). First, there is an urgent need for standard and consensus production (e.g., sources, medium, and culture conditions) to ensure the safety, reproducibility, and efficiency of MSCs administered to patients, which is also required in basic research. Second, MSCs derived from different tissues may have varying characteristics and functions; therefore, it is important to uncover the genetic background of different MSC sources and understand the specific innate characteristics of MSCs, which would aid the selection of the best seeds for fulfilling the specific clinical usage. Third, there is an urgent need to discover new genes or regulators such as the lncRNAs, as well as outstanding technologies to be developed to genetically modify MSCs and enhance their functions to boost their clinical application. Besides, the signals and mechanisms that modulate MSCs in tissue expansion, repair, and regeneration remain to be clarified, including the program that determines the balance between self-renewal and differentiation, the growth factors or signals that destroy the balance and trigger MSC expansion or differentiation, and how MSCs communicate with their surrounding niches to support a functional environment.

Mesenchymal stem cells maintain tissue homeostasis based on their differentiation potential to produce renewable progenitor cells to repair tissues and to replace cells in routine cellular turnover. MSCs tend to differentiate into mesenchymal lineage cells, while their trans-differentiation into endodermal and ectodermal lineage cells is limited. There are persistent challenges to fully understanding the underlying mechanisms in MSC differentiation, including identifying new signal and master transcription factors, and crosstalk between the signaling pathways involved in mediating and promoting MSC lineage differentiation and trans-differentiation rate. Manipulating MSCs with the overexpression of transcriptional factors increases their potential to differentiate into an intended cell type (Chen et al., 2018). However, a long journey remains before these genetically manipulated MSCs enter clinical application for treating diseases, unless safer methods are developed for manipulating MSCs with forced gene expression and to avoid activating the innate tendency of MSCs to differentiate into other unintended cell types.

Numerous lncRNAs participate in MSC lineage commitment, and lncRNAs derived from MSC exosomes exhibit enhanced tissue-protective and repair function. However, some challenges remain. On one hand, lncRNAs have multiple and varied functions and mechanisms of action, and lncRNAs largely remain unknown. e.g., H19 contributes to adipogenesis and osteogenesis, and resides in MSC exosomes to accelerate wound healing through different mechanisms. Moreover, lncRNAs may have an opposite effect on the same biological process, such as MEG3, which promotes and inhibits MSC osteogenic differentiation. First, the source of MSCs may confer the bidirectional effect on the lncRNA. lncRNAs usually display tissue- and spatiotemporal-specific expression patterns, and their aberrant expression is highly associated with disease and cancer occurrence. Therefore, lncRNAs may be differentially expressed at different stages of development, which confers their variable roles. Second, the MSC culture conditions *in vitro* may influence their stemness and functions, and the passage of MSCs used also matters. Therefore, as discussed above, there is an urgent need to establish a gold-standard approach for MSC basic research and clinical application. Taken together, extensive functional studies on one particular lncRNA can be performed in the future, and accompanying advanced molecular biotechnologies are being developed to better clarify and identify lncRNA targets and pathways and to screen for unknown lncRNA-interacting proteins. In addition, lncRNAs comprise a large proportion of the genome, and myriad functional lncRNAs remain to be discovered and studied. Moreover, most mechanisms of the existing studies on lncRNAs are focused on the downstream targets and pathways; the upstream stimulators and regulators that modulate lncRNA expression should be discovered. On the other hand, lncRNAs are poorly conserved among different species (Mirza et al., 2014), rendering it difficult or complicated to generate conditional knockout animal models to study the full function of lncRNAs, and complicating the development of lncRNAs as drug targets (Matsui and Corey, 2017). Despite these challenges, MSC-associated lncRNAs are promising targets and biomarkers for treating and diagnosing diseases. Nevertheless, opportunities coexist with challenges. There are emerging studies on lncRNA-based or -targeted drugs are emerging (Matsui and Corey, 2017), making them attractive therapeutic interventions in the future.

PERSPECTIVES

Mesenchymal stem cell exosome-derived lncRNAs such as H19 shuttle between MSCs and fibroblasts to perform their function

in facilitating wound healing in diabetic foot ulcers (Li et al., 2020), which indicates that MSC-derived exosomes with lncRNA overexpression might be a novel direction for developing cell-free therapeutic strategies and will improve MSC efficacy. With continued research in the future, genetically modified MSCs with improved tissue repair and regeneration functions will be achieved soon.

Over the last decade, non-coding RNAs (e.g., miRNAs and lncRNAs) have emerged as significant new therapeutic targets; many efforts have been dedicated to developing new oligonucleotide-based therapies aimed at promoting or antagonizing them. To date, over 100 antisense oligonucleotide (ASO)-based therapies have been developed and tested in clinical trials. The US Food and Drug Administration (FDA) has approved fomivirsen for treating cytomegalovirus retinitis and mipomersen for treating familial hypercholesterolemia (Adams et al., 2017). Unlike miRNAs, which are small and advantageous for delivering their mimics or inhibitors through synthetically modified oligoribonucleotides, lncRNAs are relatively large and usually are of a structured nature that makes it difficult to design effective mimics or inhibitors (Scacalossi et al., 2019). Although no clinical advances have been made with lncRNAs, they remain striking targets for clinical therapeutic intervention in the future. In addition, lncRNAs are relatively large and therefore more stable, rendering them suitable diagnostic and prognostic biomarkers for cancer. In recent years, it has been confirmed that circulating lncRNAs are valuable for detecting cancer types, as they are quite easily detected by common methods such as qRT-PCR, RNA sequencing (RNA-seq), and microarray in whole blood, plasma, serum, urine, saliva, and gastric juice samples; some circulating lncRNAs have been proven as sensitive biomarkers. More lncRNAs are being identified as diagnostic and prognostic biomarkers for varied diseases, especially for those caused by aberrant MSC dysfunction.

AUTHOR CONTRIBUTIONS

FZ and RZ conceived the project. YY, SL, CH, ZC, TL, LZ, and LW collected the data. YY wrote and revised the manuscript. FZ, HC, and RZ provided guidelines and edited the manuscript. All authors read and approved the final manuscript.

FUNDING

This study was supported by the National Key R&D Program of China (2016YFA0101003 and 2016YFC0903901), National Natural Science Fund (81771764), CAMS Innovation Fund for Medical Sciences (2017-I2M-3-007), and project funded by China Postdoctoral Science Foundation (2021M690461).

REFERENCES

Adams, B. D., Parsons, C., Walker, L., Zhang, W. C., and Slack, F. J. (2017). Targeting noncoding RNAs in disease. *J. Clin. Invest.* 127, 761–771. doi: 10.1172/jci84424

Almalki, S. G., and Agrawal, D. K. (2016). Key transcription factors in the differentiation of mesenchymal stem cells. *Differentiation* 92, 41–51. doi: 10.1016/j.diff.2016.02.005

Atianand, M. K., Caffrey, D. R., and Fitzgerald, K. A. (2017). Immunobiology of Long Noncoding RNAs. *Annu. Rev. Immunol.* 35, 177–198. doi: 10.1146/annurev-immunol-041015-055459

Bartolomei, M. S., Zemel, S., and Tilghman, S. M. (1991). Parental imprinting of the mouse H19 gene. *Nature* 351, 153–155. doi: 10.1038/351153a0

Batista, P. J., and Chang, H. Y. (2013). Long noncoding RNAs: cellular address codes in development and disease. *Cell* 152, 1298–1307. doi: 10.1016/j.cell.2013.02.012

Beermann, J., Piccoli, M. T., Viereck, J., and Thum, T. (2016). Non-coding RNAs in development and disease: background, mechanisms, and therapeutic approaches. *Physiol. Rev.* 96, 1297–1325. doi: 10.1152/physrev.00041.2015

Ben Menachem-Zidon, O., Gropp, M., Ben Shushan, E., Reubinoff, B., and Shveiky, D. (2019). Systemically transplanted mesenchymal stem cells induce vascular-like structure formation in a rat model of vaginal injury. *PLoS One* 14:e0218081. doi: 10.1371/journal.pone.0218081

Boeuf, S., and Richter, W. (2010). Chondrogenesis of mesenchymal stem cells: role of tissue source and inducing factors. *Stem Cell Res. Ther.* 1:31. doi: 10.1186/scrt31

Bruno, S., Grange, C., Deregibus, M. C., Calogero, R. A., Saviozzi, S., Collino, F., et al. (2009). Mesenchymal stem cell-derived microvesicles protect against acute tubular injury. *J. Am. Soc. Nephrol.* 20, 1053–1067. doi: 10.1681/asn.2008070798

Bulati, M., Miceli, V., Gallo, A., Amico, G., Carcione, C., Pampalone, M., et al. (2020). The Immunomodulatory Properties of the Human Amnion-Derived Mesenchymal Stromal/Stem Cells Are Induced by INF-γ Produced by Activated Lymphomonocytes and Are Mediated by Cell-To-Cell Contact and Soluble Factors. *Front. Immunol.* 11:54. doi: 10.3389/fimmu.2020.00054

Chen, B., Chen, X., Liu, C., Li, J., Liu, F., and Huang, Y. (2018). Co-expression of Akt1 and Wnt11 promotes the proliferation and cardiac differentiation of mesenchymal stem cells and attenuates hypoxia/reoxygenation-induced cardiomyocyte apoptosis. *Biomed. Pharmacother.* 108, 508–514. doi: 10.1016/j.biopha.2018.09.047

Chen, H., Xia, W., and Hou, M. (2020). LncRNA-NEAT1 from the competing endogenous RNA network promotes cardioprotective efficacy of mesenchymal stem cell-derived exosomes induced by macrophage migration inhibitory factor via the miR-142-3p/FOXO1 signaling pathway. *Stem Cell Res. Ther.* 11:31. doi: 10.1186/s13287-020-1556-7

Chen, Y., Ding, H., Wei, M., Zha, W., Guan, S., Liu, N., et al. (2020). MSC-Secreted Exosomal H19 Promotes Trophoblast Cell Invasion and Migration by Downregulating let-7b and Upregulating FOXO1. *Mol. Ther. Nucleic Acids* 19, 1237–1249. doi: 10.1016/j.omtn.2019.11.031

Chen, H. S., Hsu, C. Y., Chang, Y. C., Chuang, H. Y., Long, C. Y., Hsieh, T. H., et al. (2017). Benzyl butyl phthalate decreases myogenic differentiation of endometrial mesenchymal stem/stromal cells through miR-137-mediated regulation of PITX2. *Sci. Rep.* 7:186. doi: 10.1038/s41598-017-00286-6

Chen, L. L. (2016). Linking Long Noncoding RNA Localization and Function. *Trends Biochem. Sci.* 41, 761–772. doi: 10.1016/j.tibs.2016.07.003

Chen, Y., Yu, Q., Hu, Y., and Shi, Y. (2019). Current Research and Use of Mesenchymal Stem Cells in the Therapy of Autoimmune Diseases. *Curr. Stem Cell Res. Ther.* 14, 579–582. doi: 10.2174/1574888x14666190429141421

Chung, C. S., Fujita, N., Kawahara, N., Yui, S., Nam, E., and Nishimura, R. (2013). A comparison of neurosphere differentiation potential of canine bone marrow-derived mesenchymal stem cells and adipose-derived mesenchymal stem cells. *J. Vet. Med. Sci.* 75, 879–886. doi: 10.1292/jvms.12-0470

Crisan, M., Yap, S., Casteilla, L., Chen, C. W., Corselli, M., Park, T. S., et al. (2008). A perivascular origin for mesenchymal stem cells in multiple human organs. *Cell Stem Cell* 3, 301–313. doi: 10.1016/j.stem.2008.07.003

De Bari, C., Dell'Accio, F., Tylzanowski, P., and Luyten, F. P. (2001). Multipotent mesenchymal stem cells from adult human synovial membrane. *Arthritis Rheum.* 44, 1928–1942. doi: 10.1002/1529-0131(200108)44:8<1928::Aid-art331<3.0.Co;2-p

Deng, L., Hong, H., Zhang, X., Chen, D., Chen, Z., Ling, J., et al. (2018). Down-regulated lncRNA MEG3 promotes osteogenic differentiation of human dental follicle stem cells by epigenetically regulating Wnt pathway. *Biochem. Biophys. Res. Commun.* 503, 2061–2067. doi: 10.1016/j.bbrc.2018.07.160

Djebali, S., Davis, C. A., Merkel, A., Dobin, A., Lassmann, T., Mortazavi, A., et al. (2012). Landscape of transcription in human cells. *Nature* 489, 101–108. doi: 10.1038/nature11233

Dominici, M., Le Blanc, K., Mueller, I., Slaper-Cortenbach, I., Marini, F., Krause, D., et al. (2006). Minimal criteria for defining multipotent mesenchymal stromal cells. The International Society for Cellular Therapy position statement. *Cytotherapy* 8, 315–317. doi: 10.1080/14653240600855905

Dong, R., Liu, Y., Yang, Y., Wang, H., Xu, Y., and Zhang, Z. (2019). MSC-Derived Exosomes-Based therapy for peripheral nerve injury: a novel therapeutic strategy. *Biomed. Res. Int.* 2019:6458237. doi: 10.1155/2019/6458237

Farzi-Molan, A., Babashah, S., Bakhshinejad, B., Atashi, A., and Fakhr Taha, M. (2018). Down-regulation of the non-coding RNA H19 and its derived miR-675 is concomitant with up-regulation of insulin-like growth factor receptor type 1 during neural-like differentiation of human bone marrow mesenchymal stem cells. *Cell Biol. Int.* 42, 940–948. doi: 10.1002/cbin.10960

Fernandes, J. C. R., Acuña, S. M., Aoki, J. I., Floeter-Winter, L. M., and Muxel, S. M. (2019). Long Non-Coding RNAs in the Regulation of Gene Expression: physiology and Disease. *Noncoding RNA* 5:17. doi: 10.3390/ncrna5010017

Ferrand, J., Noël, D., Lehours, P., Prochazkova-Carlotti, M., Chambonnier, L., Ménard, A., et al. (2011). Human bone marrow-derived stem cells acquire epithelial characteristics through fusion with gastrointestinal epithelial cells. *PLoS One* 6:e19569. doi: 10.1371/journal.pone.0019569

Freitas, J., Santos, S. G., Gonçalves, R. M., Teixeira, J. H., Barbosa, M. A., and Almeida, M. I. (2019). Genetically Engineered-MSC Therapies for Non-unions, Delayed Unions and Critical-size Bone Defects. *Int. J. Mol. Sci.* 20:3430. doi: 10.3390/ijms20143430

Friedenstein, A. J., Gorskaja, J. F., and Kulagina, N. N. (1976). Fibroblast precursors in normal and irradiated mouse hematopoietic organs. *Exp. Hematol.* 4, 267–274.

Fu, Y., Deng, J., Jiang, Q., Wang, Y., Zhang, Y., Yao, Y., et al. (2016). Rapid generation of functional hepatocyte-like cells from human adipose-derived stem cells. *Stem Cell Res. Ther.* 7:105. doi: 10.1186/s13287-016-0364-6

Furuya, K., Zheng, Y. W., Sako, D., Iwasaki, K., Zheng, D. X., Ge, J. Y., et al. (2019). Enhanced hepatic differentiation in the subpopulation of human amniotic stem cells under 3D multicellular microenvironment. *World J. Stem Cells* 11, 705–721. doi: 10.4252/wjsc.v11.i9.705

Gao, Y., Xiao, F., Wang, C., Wang, C., Cui, P., Zhang, X., et al. (2018). Long noncoding RNA MALAT1 promotes osterix expression to regulate osteogenic differentiation by targeting miRNA-143 in human bone marrow-derived mesenchymal stem cells. *J. Cell Biochem.* 119, 6986–6996. doi: 10.1002/jcb.26907

Haynesworth, S. E., Baber, M. A., and Caplan, A. I. (1996). Cytokine expression by human marrow-derived mesenchymal progenitor cells in vitro: effects of dexamethasone and IL-1 alpha. *J. Cell Physiol.* 166, 585–592. doi: 10.1002/(sici)1097-4652(199603)166:3<585::aid-jcp13<3.0.co;2-6

He, H., Liu, X., Peng, L., Gao, Z., Ye, Y., Su, Y., et al. (2013). Promotion of hepatic differentiation of bone marrow mesenchymal stem cells on decellularized cell-deposited extracellular matrix. *Biomed. Res. Int.* 2013:406871. doi: 10.1155/2013/406871

He, Q., Wan, C., and Li, G. (2007). Concise review: multipotent mesenchymal stromal cells in blood. *Stem Cells* 25, 69–77. doi: 10.1634/stemcells.2006-0335

Hefei, W., Yu, R., Haiqing, W., Xiao, W., Jingyuan, W., and Dongjun, L. (2015). Morphological characteristics and identification of islet-like cells derived from rat adipose-derived stem cells cocultured with pancreas adult stem cells. *Cell Biol. Int.* 39, 253–263. doi: 10.1002/cbin.10387

Hilgendorf, K. I., Johnson, C. T., Mezger, A., Rice, S. L., Norris, A. M., Demeter, J., et al. (2019). Omega-3 Fatty Acids Activate Ciliary FFAR4 to Control Adipogenesis. *Cell* 179, 1289–1305.e21. doi: 10.1016/j.cell.2019.11.005

Hoshiba, T., Kawazoe, N., and Chen, G. (2012). The balance of osteogenic and adipogenic differentiation in human mesenchymal stem cells by matrices that mimic stepwise tissue development. *Biomaterials* 33, 2025–2031. doi: 10.1016/j.biomaterials.2011.11.061

Hou, J., Long, H., Zhou, C., Zheng, S., Wu, H., Guo, T., et al. (2017). Long noncoding RNA Braveheart promotes cardiogenic differentiation of mesenchymal stem cells in vitro. *Stem Cell Res. Ther.* 8:4. doi: 10.1186/s13287-016-0454-5

Hu, B., Lv, X., Chen, H., Xue, P., Gao, B., Wang, X., et al. (2020). Sensory nerves regulate mesenchymal stromal cell lineage commitment by tuning sympathetic tones. *J. Clin. Invest.* 130, 3483–3498. doi: 10.1172/jci131554

Huang, G. T., Gronthos, S., and Shi, S. (2009). Mesenchymal stem cells derived from dental tissues vs. those from other sources: their biology and role in regenerative medicine. *J. Dent. Res.* 88, 792–806. doi: 10.1177/0022034509340867

Huang, Y., Zheng, Y., Jin, C., Li, X., Jia, L., and Li, W. (2016). Long Non-coding RNA H19 Inhibits Adipocyte Differentiation of Bone Marrow Mesenchymal Stem Cells through Epigenetic Modulation of Histone Deacetylases. *Sci. Rep.* 6:28897. doi: 10.1038/srep28897

Jarroux, J., Morillon, A., and Pinskaya, M. (2017). History, Discovery, and Classification of lncRNAs. *Adv. Exp. Med. Biol.* 1008, 1–46. doi: 10.1007/978-981-10-5203-3_1

Jiang, W., Ma, A., Wang, T., Han, K., Liu, Y., Zhang, Y., et al. (2006). Intravenous transplantation of mesenchymal stem cells improves cardiac performance after acute myocardial ischemia in female rats. *Transpl. Int.* 19, 570–580. doi: 10.1111/j.1432-2277.2006.00307.x

Jin, G., Sun, J., Isaacs, S. D., Wiley, K. E., Kim, S. T., Chu, L. W., et al. (2011). Human polymorphisms at long non-coding RNAs (lncRNAs) and association with prostate cancer risk. *Carcinogenesis* 32, 1655–1659. doi: 10.1093/carcin/bgr187

Kfoury, Y., and Scadden, D. T. (2015). Mesenchymal cell contributions to the stem cell niche. *Cell Stem Cell* 16, 239–253. doi: 10.1016/j.stem.2015.02.019

Konala, V. B., Mamidi, M. K., Bhonde, R., Das, A. K., Pochampally, R., and Pal, R. (2016). The current landscape of the mesenchymal stromal cell secretome: a new paradigm for cell-free regeneration. *Cytotherapy* 18, 13–24. doi: 10.1016/j.jcyt.2015.10.008

Kretz, M., Webster, D. E., Flockhart, R. J., Lee, C. S., Zehnder, A., Lopez-Pajares, V., et al. (2012). Suppression of progenitor differentiation requires the long noncoding RNA ANCR. *Genes Dev.* 26, 338–343. doi: 10.1101/gad.182121.111

Lagarde, J., Uszczynska-Ratajczak, B., Carbonell, S., Pérez-Lluch, S., Abad, A., Davis, C., et al. (2017). High-throughput annotation of full-length long noncoding RNAs with capture long-read sequencing. *Nat. Genet.* 49, 1731–1740. doi: 10.1038/ng.3988

Lai, R. C., Arslan, F., Tan, S. S., Tan, B., Choo, A., Lee, M. M., et al. (2010). Derivation and characterization of human fetal MSCs: an alternative cell source for large-scale production of cardioprotective microparticles. *J. Mol. Cell Cardiol.* 48, 1215–1224. doi: 10.1016/j.yjmcc.2009.12.021

Lai, R. C., Yeo, R. W., and Lim, S. K. (2015). Mesenchymal stem cell exosomes. *Semin Cell Dev. Biol.* 40, 82–88. doi: 10.1016/j.semcdb.2015.03.001

Lee, J., Han, D. J., and Kim, S. C. (2008). In vitro differentiation of human adipose tissue-derived stem cells into cells with pancreatic phenotype by regenerating pancreas extract. *Biochem. Biophys. Res. Commun.* 375, 547–551. doi: 10.1016/j.bbrc.2008.08.064

Li, B., Luan, S., Chen, J., Zhou, Y., Wang, T., Li, Z., et al. (2020). The MSC-Derived Exosomal lncRNA H19 Promotes Wound Healing in Diabetic Foot Ulcers by Upregulating PTEN via MicroRNA-152-3p. *Mol. Ther. Nucleic Acids* 19, 814–826. doi: 10.1016/j.omtn.2019.11.034

Li, B., Xu, H., Han, H., Song, S., Zhang, X., Ouyang, L., et al. (2018). Exosome-mediated transfer of lncRUNX2-AS1 from multiple myeloma cells to MSCs contributes to osteogenesis. *Oncogene* 37, 5508–5519. doi: 10.1038/s41388-018-0359-0

Li, Y., Shan, Z., Yang, B., Yang, D., Men, C., Cui, Y., et al. (2018). LncRNA HULC promotes epithelial and smooth-muscle-like differentiation of adipose-derived stem cells by upregulation of BMP9. *Pharmazie* 73, 49–55. doi: 10.1691/ph.2018.7634

Li, J., Yang, Y., Fan, J., Xu, H., Fan, L., Li, H., et al. (2019). Long noncoding RNA ANCR inhibits the differentiation of mesenchymal stem cells toward definitive endoderm by facilitating the association of PTBP1 with ID2. *Cell Death Dis.* 10:492. doi: 10.1038/s41419-019-1738-3

Li, Z., Jin, C., Chen, S., Zheng, Y., Huang, Y., Jia, L., et al. (2017). Long non-coding RNA MEG3 inhibits adipogenesis and promotes osteogenesis of human adipose-derived mesenchymal stem cells via miR-140-5p. *Mol. Cell Biochem.* 433, 51–60. doi: 10.1007/s11010-017-3015-z

Liang, W. C., Fu, W. M., Wang, Y. B., Sun, Y. X., Xu, L. L., Wong, C. W., et al. (2016). H19 activates Wnt signaling and promotes osteoblast differentiation by

functioning as a competing endogenous RNA. *Sci. Rep.* 6:20121. doi: 10.1038/srep20121

Liu, G. H., Barkho, B. Z., Ruiz, S., Diep, D., Qu, J., Yang, S. L., et al. (2011). Recapitulation of premature ageing with iPSCs from Hutchinson-Gilford progeria syndrome. *Nature* 472, 221–225. doi: 10.1038/nature09879

Liu, Y., Lin, L., Zou, R., Wen, C., Wang, Z., and Lin, F. (2018a). MSC-derived exosomes promote proliferation and inhibit apoptosis of chondrocytes via lncRNA-KLF3-AS1/miR-206/GIT1 axis in osteoarthritis. *Cell Cycle* 17, 2411–2422. doi: 10.1080/15384101.2018.1526603

Liu, Y., Zou, R., Wang, Z., Wen, C., Zhang, F., and Lin, F. (2018b). Exosomal KLF3-AS1 from hMSCs promoted cartilage repair and chondrocyte proliferation in osteoarthritis. *Biochem. J.* 475, 3629–3638. doi: 10.1042/bcj20180675

Lopatina, T., Kalinina, N., Karagyaur, M., Stambolsky, D., Rubina, K., Revischin, A., et al. (2019). Correction: adipose-Derived Stem Cells Stimulate Regeneration of Peripheral Nerves: BDNF Secreted by These Cells Promotes Nerve Healing and Axon Growth De Novo. *PLoS One* 14:e0219946. doi: 10.1371/journal.pone.0219946

Ma, L., Bajic, V. B., and Zhang, Z. (2013). On the classification of long non-coding RNAs. *RNA Biol.* 10, 925–933. doi: 10.4161/rna.24604

Mao, Q., Liang, X. L., Zhang, C. L., Pang, Y. H., and Lu, Y. X. (2019). LncRNA KLF3-AS1 in human mesenchymal stem cell-derived exosomes ameliorates pyroptosis of cardiomyocytes and myocardial infarction through miR-138-5p/Sirt1 axis. *Stem Cell Res. Ther.* 10:393. doi: 10.1186/s13287-019-1522-4

Matsui, M., and Corey, D. R. (2017). Non-coding RNAs as drug targets. *Nat. Rev. Drug Discov.* 16, 167–179. doi: 10.1038/nrd.2016.117

Maymó, J. L., Riedel, R., Pérez-Pérez, A., Magatti, M., Maskin, B., Dueñas, J. L., et al. (2018). Proliferation and survival of human amniotic epithelial cells during their hepatic differentiation. *PLoS One* 13:e0191489. doi: 10.1371/journal.pone.0191489

Mazini, L., Rochette, L., Admou, B., Amal, S., and Malka, G. (2020). Hopes and Limits of Adipose-Derived Stem Cells (ADSCs) and Mesenchymal Stem Cells (MSCs) in Wound Healing. *Int. J. Mol. Sci.* 21:1306. doi: 10.3390/ijms21041306

Mehrfarjam, Z., Esmaeili, F., Shabani, L., and Ebrahimie, E. (2016). Induction of pancreatic β cell gene expression in mesenchymal stem cells. *Cell Biol. Int.* 40, 486–500. doi: 10.1002/cbin.10567

Méndez-Ferrer, S., Michurina, T. V., Ferraro, F., Mazloom, A. R., Macarthur, B. D., Lira, S. A., et al. (2010). Mesenchymal and haematopoietic stem cells form a unique bone marrow niche. *Nature* 466, 829–834. doi: 10.1038/nature09262

Miao, C., Lei, M., Hu, W., Han, S., and Wang, Q. (2017). A brief review: the therapeutic potential of bone marrow mesenchymal stem cells in myocardial infarction. *Stem Cell Res. Ther.* 8:242. doi: 10.1186/s13287-017-0697-9

Mirza, A. H., Kaur, S., Brorsson, C. A., and Pociot, F. (2014). Effects of GWAS-associated genetic variants on lncRNAs within IBD and T1D candidate loci. *PLoS One* 9:e105723. doi: 10.1371/journal.pone.0105723

Moura, S. R., Bras, J. P., Freitas, J., Osório, H., Barbosa, M. A., Santos, S. G., et al. (2020). miR-99a in bone homeostasis: regulating osteogenic lineage commitment and osteoclast differentiation. *Bone* 134:115303. doi: 10.1016/j.bone.2020.115303

Orciani, M., and Di Primio, R. (2013). Skin-derived mesenchymal stem cells: isolation, culture, and characterization. *Methods Mol. Biol.* 989, 275–283. doi: 10.1007/978-1-62703-330-5_21

Pan, Y., Xie, Z., Cen, S., Li, M., Liu, W., Tang, S., et al. (2020). Long noncoding RNA repressor of adipogenesis negatively regulates the adipogenic differentiation of mesenchymal stem cells through the hnRNP A1-PTX3-ERK axis. *Clin. Transl. Med.* 10:e227. doi: 10.1002/ctm2.227

Parolini, O., Alviano, F., Bagnara, G. P., Bilic, G., Bühring, H. J., Evangelista, M., et al. (2008). Concise review: isolation and characterization of cells from human term placenta: outcome of the first international Workshop on Placenta Derived Stem Cells. *Stem Cells* 26, 300–311. doi: 10.1634/stemcells.2007-0594

Pegtel, D. M., and Gould, S. J. (2019). Exosomes. *Annu. Rev. Biochem.* 88, 487–514. doi: 10.1146/annurev-biochem-013118-111902

Price, M. J., Chou, C. C., Frantzen, M., Miyamoto, T., Kar, S., Lee, S., et al. (2006). Intravenous mesenchymal stem cell therapy early after reperfused acute myocardial infarction improves left ventricular function and alters electrophysiologic properties. *Int. J. Cardiol.* 111, 231–239. doi: 10.1016/j.ijcard.2005.07.036

Quinn, J. J., and Chang, H. Y. (2016). Unique features of long non-coding RNA biogenesis and function. *Nat. Rev. Genet.* 17, 47–62. doi: 10.1038/nrg.2015.10

Romanov, Y. A., Svintsitskaya, V. A., and Smirnov, V. N. (2003). Searching for alternative sources of postnatal human mesenchymal stem cells: candidate MSC-like cells from umbilical cord. *Stem Cells* 21, 105–110. doi: 10.1634/stemcells.21-1-105

Scacalossi, K. R., van Solingen, C., and Moore, K. J. (2019). Long non-coding RNAs regulating macrophage functions in homeostasis and disease. *Vascul. Pharmacol.* 114, 122–130. doi: 10.1016/j.vph.2018.02.011

Schmitt, A. M., and Chang, H. Y. (2016). Long Noncoding RNAs in Cancer Pathways. *Cancer Cell* 29, 452–463. doi: 10.1016/j.ccell.2016.03.010

Scott, M. A., Nguyen, V. T., Levi, B., and James, A. W. (2011). Current methods of adipogenic differentiation of mesenchymal stem cells. *Stem Cells Dev.* 20, 1793–1804. doi: 10.1089/scd.2011.0040

Shi, T., Hu, W., Hou, H., Zhao, Z., Shang, M., and Zhang, L. (2020). Identification and Comparative Analysis of Long Non-Coding RNA in the Skeletal Muscle of Two Dezhou Donkey Strains. *Genes* 11:508. doi: 10.3390/genes11050508

Shi, Y., He, G., Lee, W. C., McKenzie, J. A., Silva, M. J., and Long, F. (2017). Gli1 identifies osteogenic progenitors for bone formation and fracture repair. *Nat. Commun.* 8:2043. doi: 10.1038/s41467-017-02171-2

Shi, Y., Hu, G., Su, J., Li, W., Chen, Q., Shou, P., et al. (2010). Mesenchymal stem cells: a new strategy for immunosuppression and tissue repair. *Cell Res.* 20, 510–518. doi: 10.1038/cr.2010.44

Song, L., and Tuan, R. S. (2004). Transdifferentiation potential of human mesenchymal stem cells derived from bone marrow. *FASEB J.* 18, 980–982. doi: 10.1096/fj.03-1100fje

Spees, J. L., Lee, R. H., and Gregory, C. A. (2016). Mechanisms of mesenchymal stem/stromal cell function. *Stem Cell Res. Ther.* 7:125. doi: 10.1186/s13287-016-0363-7

Stzepourginski, I., Nigro, G., Jacob, J. M., Dulauroy, S., Sansonetti, P. J., Eberl, G., et al. (2017). CD34+ mesenchymal cells are a major component of the intestinal stem cells niche at homeostasis and after injury. *Proc. Natl. Acad. Sci. U. S. A.* 114, E506–E513. doi: 10.1073/pnas.1620059114

Sui, B. D., Zheng, C. X., Li, M., Jin, Y., and Hu, C. H. (2020). Epigenetic Regulation of Mesenchymal Stem Cell Homeostasis. *Trends Cell Biol.* 30, 97–116. doi: 10.1016/j.tcb.2019.11.006

Sun, H., Peng, G., Wu, H., Liu, M., Mao, G., Ning, X., et al. (2020). Long non-coding RNA MEG3 is involved in osteogenic differentiation and bone diseases (Review). *Biomed. Rep.* 13, 15–21. doi: 10.3892/br.2020.1305

Sun, X., Luo, L. H., Feng, L., and Li, D. S. (2018). Down-regulation of lncRNA MEG3 promotes endothelial differentiation of bone marrow derived mesenchymal stem cells in repairing erectile dysfunction. *Life Sci.* 208, 246–252. doi: 10.1016/j.lfs.2018.07.024

Tan, Y. F., Tang, L., OuYang, W. X., Jiang, T., Zhang, H., and Li, S. J. (2019). β-catenin-coordinated lncRNA MALAT1 up-regulation of ZEB-1 could enhance the telomerase activity in HGF-mediated differentiation of bone marrow mesenchymal stem cells into hepatocytes. *Pathol. Res. Pract.* 215, 546–554. doi: 10.1016/j.prp.2019.01.002

Tye, C. E., Gordon, J. A., Martin-Buley, L. A., Stein, J. L., Lian, J. B., and Stein, G. S. (2015). Could lncRNAs be the missing links in control of mesenchymal stem cell differentiation? *J. Cell Physiol.* 230, 526–534. doi: 10.1002/jcp.24834

Vizoso, F. J., Eiro, N., Costa, L., Esparza, P., Landin, M., Diaz-Rodriguez, P., et al. (2019). Mesenchymal stem cells in Homeostasis and systemic diseases: hypothesis, evidences, and therapeutic opportunities. *Int. J. Mol. Sci.* 20:3738. doi: 10.3390/ijms20153738

Wang, H., Ding, X. G., Yang, J. J., Li, S. W., Zheng, H., Gu, C. H., et al. (2018). LncRNA MIAT facilitated BM-MSCs differentiation into endothelial cells and restored erectile dysfunction via targeting miR-200a in a rat model of erectile dysfunction. *Eur. J. Cell Biol.* 97, 180–189. doi: 10.1016/j.ejcb.2018.02.001

Wang, K. C., and Chang, H. Y. (2011). Molecular mechanisms of long noncoding RNAs. *Mol. Cell* 43, 904–914. doi: 10.1016/j.molcel.2011.08.018

Wang, L., Gu, Z., Zhao, X., Yang, N., Wang, F., Deng, A., et al. (2016). Extracellular Vesicles Released from Human Umbilical Cord-Derived Mesenchymal Stromal Cells Prevent Life-Threatening Acute Graft-Versus-Host Disease in a Mouse Model of Allogeneic Hematopoietic Stem Cell Transplantation. *Stem Cells Dev.* 25, 1874–1883. doi: 10.1089/scd.2016.0107

Wang, Q., Li, Y., Zhang, Y., Ma, L., Lin, L., Meng, J., et al. (2017). LncRNA MEG3 inhibited osteogenic differentiation of bone marrow mesenchymal stem cells from postmenopausal osteoporosis by targeting miR-133a-3p. *Biomed. Pharmacother.* 89, 1178–1186. doi: 10.1016/j.biopha.2017.02.090

Wang, S., Zhu, R., Li, H., Li, J., Han, Q., and Zhao, R. C. (2019). Mesenchymal stem cells and immune disorders: from basic science to clinical transition. *Front. Med.* 13, 138–151. doi: 10.1007/s11684-018-0627-y

Wang, Y., Chen, X., Cao, W., and Shi, Y. (2014). Plasticity of mesenchymal stem cells in immunomodulation: pathological and therapeutic implications. *Nat. Immunol.* 15, 1009–1016. doi: 10.1038/ni.3002

Wang, Z., Huang, Y., and Tan, L. (2020). Downregulation of lncRNA DANCR promotes osteogenic differentiation of periodontal ligament stem cells. *BMC Dev. Biol.* 20:2. doi: 10.1186/s12861-019-0206-8

Westhrin, M., Xie, M., Olderøy, M., Sikorski, P., Strand, B. L., and Standal, T. (2015). Osteogenic differentiation of human mesenchymal stem cells in mineralized alginate matrices. *PLoS One* 10:e0120374. doi: 10.1371/journal.pone.0120374

Wosczyna, M. N., Konishi, C. T., Perez Carbajal, E. E., Wang, T. T., Walsh, R. A., Gan, Q., et al. (2019). Mesenchymal Stromal Cells Are Required for Regeneration and Homeostatic Maintenance of Skeletal Muscle. *Cell Rep.* 27, 2029–2035.e5. doi: 10.1016/j.celrep.2019.04.074

Wu, A. M., Ni, W. F., Huang, Z. Y., Li, Q. L., Wu, J. B., Xu, H. Z., et al. (2015). Analysis of differentially expressed lncRNAs in differentiation of bone marrow stem cells into neural cells. *J. Neurol. Sci.* 351, 160–167. doi: 10.1016/j.jns.2015.03.011

Wu, J., Zhao, J., Sun, L., Pan, Y., Wang, H., and Zhang, W. B. (2018). Long non-coding RNA H19 mediates mechanical tension-induced osteogenesis of bone marrow mesenchymal stem cells via FAK by sponging miR-138. *Bone* 108, 62–70. doi: 10.1016/j.bone.2017.12.013

Xia, W., Chen, H., Xie, C., and Hou, M. (2020). Long-noncoding RNA MALAT1 sponges microRNA-92a-3p to inhibit doxorubicin-induced cardiac senescence by targeting ATG4a. *Aging* 12, 8241–8260. doi: 10.18632/aging.103136

Xian, P., Hei, Y., Wang, R., Wang, T., Yang, J., Li, J., et al. (2019). Mesenchymal stem cell-derived exosomes as a nanotherapeutic agent for amelioration of inflammation-induced astrocyte alterations in mice. *Theranostics* 9, 5956–5975. doi: 10.7150/thno.33872

Xu, D., Nishimura, T., Zheng, M., Wu, M., Su, H., Sato, N., et al. (2014). Enabling autologous human liver regeneration with differentiated adipocyte stem cells. *Cell Transplant.* 23, 1573–1584. doi: 10.3727/096368913x673432

Xu, H., Yang, Y., Fan, L., Deng, L., Fan, J., Li, D., et al. (2021). Lnc13728 facilitates human mesenchymal stem cell adipogenic differentiation via positive regulation of ZBED3 and downregulation of the WNT/β-catenin pathway. *Stem Cell Res. Ther.* 12:176. doi: 10.1186/s13287-021-02250-8

Xu, L., Liu, Y., Sun, Y., Wang, B., Xiong, Y., Lin, W., et al. (2017). Tissue source determines the differentiation potentials of mesenchymal stem cells: a comparative study of human mesenchymal stem cells from bone marrow and adipose tissue. *Stem Cell Res. Ther.* 8:275. doi: 10.1186/s13287-017-0716-x

Xue, C., Li, X. L., Ba, L., Zhang, M., Yang, Y., Gao, Y., et al. (2021). MSC-derived exosomes can enhance the engiogenesis of euman erain MECs and show eherapeutic eotential in a mouse model of Parkinson's disease. *Aging Dis.* (in press). doi: 10.14336/ad.2020.1221

Yang, Q., Jia, L., Li, X., Guo, R., Huang, Y., Zheng, Y., et al. (2018). Long Noncoding RNAs: new Players in the Osteogenic Differentiation of Bone Marrow- and Adipose-Derived Mesenchymal Stem Cells. *Stem Cell Rev. Rep.* 14, 297–308. doi: 10.1007/s12015-018-9801-5

Yang, X., Yang, J., Lei, P., and Wen, T. (2019). LncRNA MALAT1 shuttled by bone marrow-derived mesenchymal stem cells-secreted exosomes alleviates osteoporosis through mediating microRNA-34c/SATB2 axis. *Aging* 11, 8777–8791. doi: 10.18632/aging.102264

Ye, X., and Zhang, C. (2017). Effects of Hyperlipidemia and Cardiovascular Diseases on Proliferation, Differentiation and Homing of Mesenchymal Stem Cells. *Curr. Stem Cell Res. Ther.* 12, 377–387. doi: 10.2174/1574888x12666170316105805

Yeo, R. W., Lai, R. C., Zhang, B., Tan, S. S., Yin, Y., Teh, B. J., et al. (2013). Mesenchymal stem cell: an efficient mass producer of exosomes for drug delivery. *Adv. Drug Deliv. Rev.* 65, 336–341. doi: 10.1016/j.addr.2012.07.001

Yousefi, F., Lavi Arab, F., Nikkhah, K., Amiri, H., and Mahmoudi, M. (2019). Novel approaches using mesenchymal stem cells for curing peripheral nerve injuries. *Life Sci.* 221, 99–108. doi: 10.1016/j.lfs.2019.01.052

Yu, Y. B., Bian, J. M., and Gu, D. H. (2015). Transplantation of insulin-producing cells to treat diabetic rats after 90% pancreatectomy. *World J. Gastroenterol.* 21, 6582–6590. doi: 10.3748/wjg.v21.i21.6582

Yuan, H., Xu, X., Feng, X., Zhu, E., Zhou, J., Wang, G., et al. (2019). A novel long noncoding RNA PGC1β-OT1 regulates adipocyte and osteoblast differentiation through antagonizing miR-148a-3p. *Cell Death Differ.* 26, 2029–2045. doi: 10.1038/s41418-019-0296-7

Yuan, Z., Li, Q., Luo, S., Liu, Z., Luo, D., Zhang, B., et al. (2016). PPARγ and Wnt Signaling in Adipogenic and Osteogenic Differentiation of Mesenchymal Stem Cells. *Curr. Stem Cell Res. Ther.* 11, 216–225. doi: 10.2174/1574888x10666150519093429

Yue, W. M., Liu, W., Bi, Y. W., He, X. P., Sun, W. Y., Pang, X. Y., et al. (2008). Mesenchymal stem cells differentiate into an endothelial phenotype, reduce neointimal formation, and enhance endothelial function in a rat vein grafting model. *Stem Cells Dev.* 17, 785–793. doi: 10.1089/scd.2007.0243

Zhang, H., Miao, Z., He, Z., Yang, Y., Wang, Y., and Feng, M. (2005). The existence of epithelial-to-mesenchymal cells with the ability to support hematopoiesis in human fetal liver. *Cell Biol. Int.* 29, 213–219. doi: 10.1016/j.cellbi.2004.12.007

Zhang, J., Tao, Z., and Wang, Y. (2018). Long non-coding RNA DANCR regulates the proliferation and osteogenic differentiation of human bone-derived marrow mesenchymal stem cells via the p38 MAPK pathway. *Int. J. Mol. Med.* 41, 213–219. doi: 10.3892/ijmm.2017.3215

Zhang, L., Sun, X., Chen, S., Yang, C., Shi, B., Zhou, L., et al. (2017). Long noncoding RNA DANCR regulates miR-1305-Smad 4 axis to promote chondrogenic differentiation of human synovium-derived mesenchymal stem cells. *Biosci. Rep.* 37:BSR20170347. doi: 10.1042/bsr20170347

Zhang, W., Li, J., Suzuki, K., Qu, J., Wang, P., Zhou, J., et al. (2015). Aging stem cells. A Werner syndrome stem cell model unveils heterochromatin alterations as a driver of human aging. *Science* 348, 1160–1163. doi: 10.1126/science.aaa1356

Zhang, Y., and Tycko, B. (1992). Monoallelic expression of the human H19 gene. *Nat. Genet.* 1, 40–44. doi: 10.1038/ng0492-40

Zhao, C. H. (2013). [Concept of mesenchymal stem cells: bring more insights into functional research of MSC]. *Zhongguo Shi Yan Xue Ye Xue Za Zhi* 21, 263–267. doi: 10.7534/j.issn.1009-2137.2013.02.001

Zhao, H., Feng, J., Seidel, K., Shi, S., Klein, O., Sharpe, P., et al. (2014). Secretion of shh by a neurovascular bundle niche supports mesenchymal stem cell homeostasis in the adult mouse incisor. *Cell Stem Cell* 14, 160–173. doi: 10.1016/j.stem.2013.12.013

Zhou, B. O., Yue, R., Murphy, M. M., Peyer, J. G., and Morrison, S. J. (2014). Leptin-receptor-expressing mesenchymal stromal cells represent the main source of bone formed by adult bone marrow. *Cell Stem Cell* 15, 154–168. doi: 10.1016/j.stem.2014.06.008

Zhuang, W., Ge, X., Yang, S., Huang, M., Zhuang, W., Chen, P., et al. (2015). Upregulation of lncRNA MEG3 Promotes Osteogenic Differentiation of Mesenchymal Stem Cells From Multiple Myeloma Patients By Targeting BMP4 Transcription. *Stem Cells* 33, 1985–1997. doi: 10.1002/stem.1989

Zoehler, B., Fracaro, L., Senegaglia, A. C., and Bicalho, M. D. G. (2020). Infusion of Mesenchymal Stem Cells to Treat Graft Versus Host Disease: the Role of HLA-G and the Impact of its Polymorphisms. *Stem Cell Rev. Rep.* 16, 459–471. doi: 10.1007/s12015-020-09960-1

Zuk, P. A., Zhu, M., Ashjian, P., De Ugarte, D. A., Huang, J. I., Mizuno, H., et al. (2002). Human adipose tissue is a source of multipotent stem cells. *Mol. Biol. Cell* 13, 4279–4295. doi: 10.1091/mbc.e02-02-0105

Conflict of Interest: The authors declare that the research was conducted in the absence of any commercial or financial relationships that could be construed as a potential conflict of interest.

frontiers in Cell and Developmental Biology

REVIEW
published: 03 August 2021
doi: 10.3389/fcell.2021.715200

Role of Autophagy in the Maintenance of Stemness in Adult Stem Cells: A Disease-Relevant Mechanism of Action

Shanshan Chen[1†], Wenqi Wang[1†], Hor-Yue Tan[2†], Yuanjun Lu[3], Zhiping Li[1], Yidi Qu[1], Ning Wang[3] and Di Wang[1,4*]*

[1] School of Life Sciences, Jilin University, Changchun, China, [2] Centre for Chinese Herbal Medicine Drug Development, School of Chinese Medicine, Hong Kong Baptist University, Hong Kong, China, [3] School of Chinese Medicine, The University of Hong Kong, Hong Kong, China, [4] Engineering Research Center of Chinese Ministry of Education for Edible and Medicinal Fungi, Jilin Agricultural University, Changchun, China

OPEN ACCESS

Edited by:
Yan-Ru Lou,
Fudan University, China

Reviewed by:
Alexander Birbrair,
Federal University of Minas Gerais, Brazil
Tokuhiro Chano,
GF Mille Co., Ltd., Japan

***Correspondence:**
Ning Wang
ckwang@hku.hk
Di Wang
jluwangdi@jlu.edu.cn

† These authors have contributed equally to this work and share first authorship

Specialty section:
This article was submitted to Stem Cell Research, a section of the journal Frontiers in Cell and Developmental Biology

Received: 26 May 2021
Accepted: 15 July 2021
Published: 03 August 2021

Citation:
Chen S, Wang W, Tan H-Y, Lu Y, Li Z, Qu Y, Wang N and Wang D (2021) Role of Autophagy in the Maintenance of Stemness in Adult Stem Cells: A Disease-Relevant Mechanism of Action. Front. Cell Dev. Biol. 9:715200. doi: 10.3389/fcell.2021.715200

Autophagy is an intracellular scavenging mechanism induced to eliminate damaged, denatured, or senescent macromolecular substances and organelles in the body. The regulation of autophagy plays essential roles in the processes of cellular homeostasis and senescence. Dysregulated autophagy is a common feature of several human diseases, including cancers and neurodegenerative disorders. The initiation and development of these disorders have been shown to be associated with the maintenance of disease-specific stem cell compartments. In this review, we summarize recent advances in our understanding of the role of autophagy in the maintenance of stemness. Specifically, we focus on the intersection between autophagy and adult stem cells in the initiation and progression of specific diseases. Accordingly, this review highlights the role of autophagy in stemness maintenance from the perspective of disease-associated mechanisms, which may be fundamental to our understanding of the pathogeneses of human diseases and the development of effective therapies.

Keywords: autophagy, adult stem cells, self-renewal, proliferation, differentiation, cancers

INTRODUCTION

Stem cells are a group of self-renewing cells that originate during embryogenesis and persist throughout the lifespan of the organism. These cells can be classified into two main types based on the stage of origin: embryonic stem cells (ESCs) and adult stem cells (Boya et al., 2018). ESCs are characterized by unlimited proliferation and a pluripotent state, whereas adult stem cells generally originate and reside in specific tissues and have a limited differentiation capacity (Boya et al., 2018). Under physiological conditions, stem cells largely remain quiescent and retain their stemness; however, they are able to either proliferate or differentiate to meet regenerative demands and maintain tissue homeostasis. In this way, the balance between the growth and degeneration of tissues and organs can be maintained by the dynamic status of stem cells.

Abbreviations: ESCs, embryonic stem cells; ATG, autophagy-related genes; LC3, microtubule-associated protein 1 light chain 3; HSCs, hematopoietic stem cells; NSCs, neural stem cells; MSCs, mesenchymal stem cells; ISCs, intestinal stem cells; iPSCs, induced pluripotent stem cells; CSCs, cancer stem cells; LSCs, leukemia stem cells; AML, acute myeloid leukemia; CML, chronic myeloid leukemia; B-ALL, B-cell acute lymphoblastic leukemia; ZIKV, Zika virus; AD, Alzheimer's disease; BMSCs, bone marrow mesenchymal stem cells; CAFs, cancer associated fibroblasts; TNBC, triple negative breast cancer; GSCs, glioma stem cells; ROS, reactive oxygen species.

Existing evidence indicates that the fate of adult stem cells is influenced by several factors, including growth factors, the cellular niche, metabolic pathways, calcium homeostasis, and autophagy.

Growth factors are essential signaling molecules that promote the proliferation and differentiation of adult stem cells. These factors interact with cell-cell contacts and cell-matrix adhesions to engineer a microenvironment that regulates the survival and fate of stem cells. For example, in random skin flaps used to treat type 1 diabetes mellitus, the release of vascular endothelial growth factor improves the ability of mesenchymal stem cells (MSCs) to repair ischemia via angiogenesis (Chehelcheraghi et al., 2019). Fibroblast growth factor-2, a mitogen, shortens the cell cycle and improves the proliferation efficiency of neural stem cells (NSCs) (Hicks and Miller, 2019). In contrast, transforming growth factor-β1 (TGF-β1) promotes cell cycle exit and inhibits the proliferation efficiency of NSCs (Hicks and Miller, 2019).

The cellular niche, also known as the microenvironment, is composed of neighboring cells and extracellular matrix and contains a reservoir of stem cells (Vazin and Schaffer, 2010). Notably, mechanical and physical cues from the niche are required for adult stem cells to maintain their potency during tissue development and regeneration (Vining and Mooney, 2017). Accordingly, the niche facilitates the essential functions of adult stem cells in maintaining tissue homeostasis and responding to foreign stimuli.

The mitochondrion is traditionally described as the powerhouse of the cell due to its fundamental role in energy production (Xu et al., 2013). However, in the tissues and organs of an adult organism, pluripotent stem cells preferentially use non-oxidative glycolysis as the major source of energy and display reduced mitochondrial mass and oxidative phosphorylation (Rehman, 2010). Consistently, hypoxia is a potent suppressor of mitochondrial oxidation and it appears to promote the stemness of adult stem cells (Rehman, 2010). Accordingly, undifferentiated stem cells are characterized by low mitochondrial oxidative phosphorylation levels. Moreover, this cell population maintains pluripotency and self-renewal by regulating mitochondrial oxidative metabolism.

Calcium (Ca^{2+}) is a ubiquitous intracellular signaling molecule that regulates differentiation, proliferation, and apoptosis. As an intracellular messenger, Ca^{2+} plays a crucial role in cell signaling pathways during various stages of stem cell differentiation (Tonelli et al., 2012). For example, after being induced by increased extracellular Ca^{2+} levels, bone morphogenetic protein-2 promotes the osteogenic differentiation of human adipose-derived stem cells (Yanai et al., 2019).

Autophagy, which literally translates as "self-eating," is a cellular process of self-digestion, by which intracellular compartments are scavenged within the cell (Chang, 2020). Thus far, three main types of autophagy have been identified in mammalian cells: microautophagy, chaperone-mediated autophagy, and macroautophagy (Scrivo et al., 2018). Macroautophagy is the prevalent form of autophagy, and is hereby referred to as "autophagy." It is a highly conserved process for the degradation and recycling of damaged and aged proteins and organelles, which thereby prevents cellular damage.

The autophagy-mediated recycling of cellular components is a critical step in cell homeostasis and tissue remodeling during development (Chang, 2020). More than 30 autophagy-related genes (*Atgs*) have been identified by screening yeast for autophagy-absent abnormalities. These genes are also evolutionarily conserved in a diverse range of species. The proteins encoded by these genes form a series of complexes that engage in different stages of the autophagic process, including autophagy induction, autophagosome formation, and the fusion of autophagosomes and lysosomes (Wang et al., 2019). Autophagy induction is regulated by the mammalian target of rapamycin (mTOR) complex 1 (mTORC1) pathway (Wang et al., 2019). Under conditions of starvation, the inhibition of mTORC1 promotes the formation of the ULK complex, which includes Atg13, ULK (uncoordinated-51 like kinase) 1, FIP200 (an interacting protein of the focal adhesion kinase family), and Atg101, thus leading to the activation of autophagy. Studies have also shown that 5′-AMP-activated protein kinase (AMPK) is involved in autophagy induction by suppressing mTOR (Liu L. et al., 2017). The class III phosphatidylinositol 3-kinase (PI3K) complex I translocates to the endoplasmic reticulum (ER) after the formation of the ULK complex. The ULK and PI3K complexes then promote the nucleation and assembly of the isolation membrane (IM) to form the precursor of the autophagosome. Atg9 is also recruited by the ULK complex to the IM to carry membrane components used for IM expansion. Furthermore, two ubiquitin-like conjugation systems, the Atg12 conjugation system (Atg12-Atg5-Atg16) and the microtubule-associated protein light chain 3 (LC3) system, facilitate IM expansion and the final formation of the autophagosome (Geng and Klionsky, 2008). The mature autophagosome then fuses with lysosomes or endosomes to form an autolysosome. The contents of the autolysosome are degraded and recycled to the cytoplasm for further utilization (Wang et al., 2019).

In recent years, an increasing number of studies have shown that autophagy plays an essential role in the maintenance of homeostasis and stemness in both ESCs and adult stem cells under physiological conditions, as well as in the initiation and progression of human diseases (Garcia-Prat et al., 2016; Zuo et al., 2019). In ESCs, autophagy activation is important for the maintenance of their stemness (Wang et al., 2019). For example, it has been shown that the pluripotency of ESCs is inhibited by ULK1 deficiency (Gong et al., 2018). Ectopic P-granules autophagy protein 5 homolog (EPG5) is a eukaryotic-specific autophagy regulator that mediates the fusion of autophagosomes and lysosomes. Mechanistically, the non-classical K63-linked ubiquitin chain of EPG5 is removed by the ubiquitin-specific peptidase USP8, an enzyme that catalyzes deubiquitination. Once EPG5 is deubiquitinated, the interaction between EPG5 and LC3 is enhanced, which results in increased autophagy flux, thus promoting the maintenance of ECS stemness (Gu et al., 2019). However, compared to the role of autophagy in maintaining the stemness of ESCs, its role in maintaining the stemness of adult stem cells is more complicated due to different types of adult stem cells, as discussed in detail in the follow section. The involvement of autophagy-related genes and proteins in the proliferation and differentiation of stem cells, as well as the maintenance of their

stemness, has been intensively studied in several types of adult stem cells, including hematopoietic stem cells (HSCs), NSCs, MSCs, intestinal stem cells (ISCs), induced pluripotent stem cells (iPSCs), and cancer stem cells (CSCs) (**Figure 1**). More importantly, impaired autophagy has been shown to contribute to the pathogenesis of various diseases, such as cancer (Zhu et al., 2013; Yao et al., 2020), neurodegenerative disorders (Park et al., 2014), and responses to viral infections (Tiwari et al., 2020). Therefore, in this review, we will also discuss the roles that autophagy plays in stem cells from the point of view of stem cell-related diseases, to facilitate improved utilization of autophagy-related targets for clinical therapies.

THE PHYSIOLOGICAL ROLES OF AUTOPHAGY IN DIFFERENT ADULT STEM CELLS AND RELATED DISEASES

Physiological Role of Autophagy in HSCs

Hematopoietic stem cells are the primary source of all blood cells, and they maintain blood homeostasis by producing myeloid- and lymphoid-precursor cells (Birbrair and Frenette, 2016). Myeloid-precursor cells differentiate further to produce the majority of white blood cells, while lymphoid precursor cells differentiate into lymphocytes. HSCs are distributed ubiquitously in the extremely hypoxic and specialized bone marrow niche. They contain relatively few mitochondria to keep mitochondrial oxidative phosphorylation quiescent and maintain their self-renewal ability. Based on the duration of their stemness, HSCs can be divided into long-term HSCs (at least 6 months) and short-term HSCs (up to 3 months) (Zon, 2008).

The self-renewal of HSCs is regulated via various pathways. For example, in long-term HSCs, pyruvate dehydrogenase kinase activation induced by hypoxia inducible factor (HIF-1α) inhibits pyruvate dehydrogenase, which promotes the maintenance of glycolytic flow and the inhibition of mitochondrial oxidative phosphorylation, thus maintaining cell cycle quiescence in HSCs (Takubo et al., 2013). Apart from anaerobic glycolysis mentioned above, autophagy, especially mitophagy (a specific selective term for autophagy related to mitochondrial removal), also plays an important role in HSC self-renewal. Damaged and redundant mitochondria are eliminated and recycled via mitophagy to sustain the stemness of HSCs (Murakami et al., 2021). Impaired mitophagy, presenting as an increase in mitochondrial respiration and subsequent oxidative stress, causes an increase in reactive oxygen species (ROS) production and limits self-renewal potential, resulting in the transformation of long-term HSCs to short-term HSCs (Koschade and Brandts, 2020). Although short-term HSCs cannot maintain their stemness for as long as long-term HSCs, they generate hematopoietic progenitor cells, which may further differentiate into blood cells (Koschade and Brandts, 2020). In colony-forming cellular assays, when autophagosome formation is blocked with 3-methyladenine (3-MA), the number of HSCs decreases and self-renewal capacity is inhibited, which is similar to the results when Atg5 expression is blocked with an *Atg5*-specific shRNA (Salemi et al., 2012). In the *Atg12*$^{flox/flox}$:*Mx1-Cre* conditional knockout (*Atg12*^{cKO}) mouse model, enhanced mitochondrial production and accelerated oxidative phosphorylation increased the entry of HSCs into the cell cycle, which disrupted their quiescence (Ho et al., 2017). Liu et al. reported that augmented mitochondrial mass and ROS levels in FIP200-deficient fetal HSCs prevent their stemness maintenance (Liu et al., 2010). Consequently, these results indicate that autophagy contributes to the regulation of HSC stemness.

In addition to its role in stemness maintenance, exogenous TGF-β1 has been shown to increase the rate of differentiation of HSCs to red blood cells by stimulating mitophagy (Kuhikar et al., 2020). FIP200 is involved in the differentiation of HSCs to mature red blood cells, and therefore, the depletion of FIP200 inhibits erythropoiesis (Zhang et al., 2015). Similarly, the conditional deletion of Atg7 in HSCs leads to the accumulation of mitochondria and superoxide, resulting in a failure to differentiate into myeloid- and lymphoid-precursor cells (Mortensen et al., 2011).

Disease-Relevant Mechanism of Autophagy in HSCs

A defect in the balance between the self-renewal and differentiation of HSCs leads to various diseases related to the hematopoiesis system. Hematopoietic cells convert into leukemia cells at the stem cell (leukemia stem cells [LSCs]) or progenitor cell stage (Koschade and Brandts, 2020). As a double-edged sword, autophagy may delay or contribute to the initiation and progression of HSC-related diseases. Here, we will discuss three major diseases related to HSCs, namely, acute myeloid leukemia (AML), chronic myeloid leukemia (CML), and B-cell acute lymphoblastic leukemia (B-ALL), and focus on the role of autophagy in these diseases.

Atg5- or Atg7-deficient hematopoietic stem and progenitor cells exhibit defective autophagy, which leads to bone marrow hyperplasia, dysregulated glycolytic metabolism, and an increased susceptibility to AML (Watson et al., 2015). CD147 is a transmembrane protein that performs various functions in cancers, including AML. Studies have found that CD147 levels increase in cancer cells, resulting in tumor progression and chemotherapeutic resistance. Isabella et al. found that AC-73, an inhibitor of CD147, decreases leukemia cell proliferation through the inhibition of the extracellular-signal-regulated kinase (ERK)/signal transducer and activator of transcription 3 (STAT3) pathway and the activation of autophagy. They also reported that CD147 is co-expressed in leukemia cells with CD371, a surface marker of LSCs, suggesting that AC-73-induced autophagy induction in LSCs may be a promising strategy for AML treatment (Spinello et al., 2019). Accordingly, these results demonstrate that autophagy activation helps delay the progression of AML. However, autophagy can also be instrumental in LSCs, which aggravate the disease. AMPK/FIS1-mediated intrinsic mitophagy plays an important role in clearing stressed mitochondria, thus maintaining the self-renewal capacity of LSCs (Pei et al., 2018). Furthermore, autophagy helps form a drug-resistance mechanism to protect LSCs against

apoptosis. The effect of the bromodomain and extraterminal domain inhibitor JQ1 on AML is limited, partly because AMPK-ULK1-mediated autophagy is activated to decrease LSC apoptosis (Jang et al., 2017). Therefore, even though autophagy plays a dual role in AML development, targeting autophagy remains a promising therapeutic strategy for AML.

Chronic myeloid leukemia is caused by the malignant transformation of HSCs, and its pathogenesis involves BCR/ABL tyrosine kinase (Bellodi et al., 2009). Imatinib is a tyrosine kinase that has been used for CML therapy; however, the benefits are limited due to the development of drug resistance. Researchers have previously found that imatinib induces protective autophagy in LSCs (Bellodi et al., 2009). Accordingly, combined treatment with an autophagy inhibitor and a tyrosine kinase inhibitor, such as imatinib, was found to almost completely eliminate LSCs. However, a recent study confirmed that combined treatment with a histone deacetylase inhibitor and imatinib increases the apoptosis of LSCs, partly due to autophagy activation, as knockout of the autophagy-related gene *BECN1*, which encodes Beclin-1 (inducer of autophagosome formation), was found to inhibit LSC apoptosis (Lernoux et al., 2020). The effect of this type of combined therapy on LSCs requires further exploration. Collectively, these findings provide robust evidence for the need to investigate CML from the view of autophagy and LSCs.

B-cell acute lymphoblastic leukemia mostly occurs in children and is caused by the malignant transformation of B cells (Delahaye et al., 2021). In patients with B-ALL, LSCs express the phenotypic surface markers CD34 and CD19. Experimentally, treatment with bafilomycin A1 (BafA1), an inhibitor of the fusion of autophagosomes and lysosomes, leads to a significant reduction in the number of $CD34^{+}CD19^{+}$ LSCs in the G0 phase of the cell cycle (Xu et al., 2020). In other words, BafA1 induces quiescent LSCs to enter the cell cycle, while retaining normal HSCs. Autophagy inactivation eventually leads to an impaired self-renewal capacity of LSCs in primary B-ALL, which is followed by apoptosis. Nevertheless, rapamycin-mediated autophagy activation promotes the survival of animals with B-ALL via the partial restoration of HSCs and cell-cycle arrest of ALL cells (Yuan et al., 2015). Therefore, both the suppression and induction of autophagy may be instrumental in B-ALL treatment. This treatment strategy should be considered and studied extensively.

Physiological Role of Autophagy in NSCs

Neural stem cells reside in the embryonic nervous system and certain parts of the adult brain, where they generate a diverse range of new neurons to maintain homeostasis and repair damage. NSCs are mainly confined to two regions in adulthood: the subventricular zone (Yazdankhah et al., 2014) and the subgranular zone (Obernier and Alvarez-Buylla, 2019). NSCs generate a large number of neurons and glial cells during brain development, and in the subventricular and subgranular zones, they have lifelong adult neurogenesis ability, which is of great significance for learning, memory, and damage repair. Basal autophagy plays a pivotal role in brain growth, synaptic plasticity, neurodegenerative disease development, and neoplasia via its protective effects, which involve the elimination of damaged organelles and proteins. Accordingly, basal autophagy is implicated in the proliferation and differentiation of NSCs, and it also regulates the survival or death of these cells under stressful conditions. On one hand, autophagy maintains NSC homeostasis through several pathways. On the other hand, chronic restraint stress activates the autophagic cell death pathway, by which NSCs undergo programmed death (Jung et al., 2020).

Neural stem cell proliferation and differentiation are pivotal components of self-renewal and damage repair processes within the nervous system. The autophagy-related gene *EVA1A* (Eva-1 homolog A) has been shown to regulate the self-renewal and differentiation of NSCs. *In vitro* and *in vivo* studies have shown that when Eva1a is depleted, the PI3K-AKT axis is activated before mTOR activation, to inhibit autophagy, leading to embryonic neurogenic defects (Li M. et al., 2016). This study also showed that embryonic neurogenic defects caused by Eva1a depletion were recovered after adding methylpyruvate to the culture during NSC differentiation. Thus, we speculate that autophagy plays an energy-providing role during NSC differentiation. Further, Beclin-1 knockout or 3-MA treatment leads to the inhibition of autophagy and a significant suppression of NSC differentiation (Yazdankhah et al., 2014). Similarly, the conditional knockout of FIP200 in mice leads to a decrease in the number of adult NSCs, the disruption of neuronal differentiation, and the eventual disappearance of the NSC pool (Wang et al., 2013). FIP200 also regulates NSC differentiation via a novel non-cell autonomous mechanism. FIP200-deficient NSCs in the subventricular zone have increased expression levels of Ccl5 and Cxcl10, both of which are able to recruit microglia of the M1 phenotype to infiltrate this zone. Activated microglia can then indirectly inhibit the differentiation of FIP200-null NSCs (Wang et al., 2017). Other studies have also found that FIP200 activates mTOR, thus facilitating cell growth by either interfering with the formation of tuberous sclerosis complex protein (TSC)1 and TSC2 (Gan et al., 2005) or by degrading TSC1 via the ubiquitin-proteasomal pathway (Chano et al., 2006), in mouse embryonic fibroblasts and neuromuscular cells, respectively. TSC1 and TSC2 (or hamartin and tuberin, respectively) are both tumor suppressor proteins that negatively regulate mTOR. In these two studies, the finding that FIP200 regulates mTOR to promote cell growth is contradictory to previous findings that mTOR is a negative regulator of autophagy activation, which promotes cell growth and differentiation (Li M. et al., 2016). It may be interesting to explore how FIP200 regulates mTOR in NSCs and whether FIP200-mediated autophagy is involved in the control of cell growth.

Disease-Relevant Mechanism of Autophagy in NSCs

Much attention has been paid to the relationship between NSCs and autophagy during viral infections. Zika virus (ZIKV), a flavivirus, mainly infects NSCs of the growing fetus, causing brain defects, including microcephaly (Chiramel and Best, 2018). Autophagy plays a dual role in NSCs infected by ZIKV. Virophagy, a selective form of autophagy, is used by NSCs to sequester viral components in an effort to defend against ZIKV

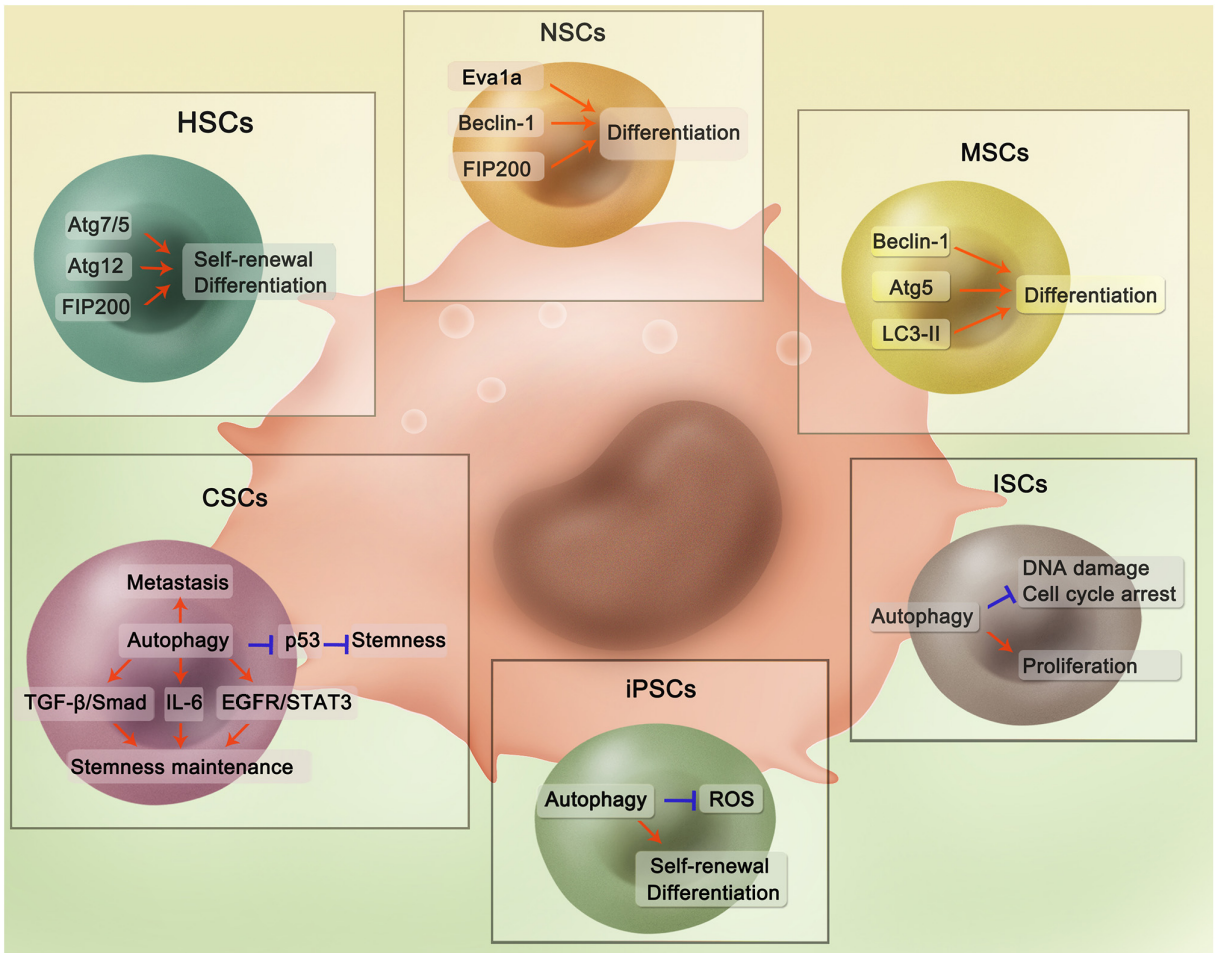

FIGURE 1 | Regulatory mechanisms of autophagy in different adult stem cells. In HSCs, Atg7/5, Atg12, and FIP200 are able to maintain stemness and promote differentiation. Autophagy-related proteins Eva1a, Beclin-1, and FIP200 could promote NSCs differentiation through activating autophagy. In MSCs, Beclin-1, Atg5, and LC3-II could contribute to differentiation. For ISCs, Autophagy could reduce DNA damage and cell cycle arrest with ISCs proliferation also promoted. For iPSCs, autophagy is implicated in the inhibition of ROS-induced injury and promotion of self-renewal and differentiation. Autophagy plays an important role in CSCs through several pathways. Specifically, in the hepatic cancer stem cells, mitophagy could suppress p53 which hampers stemness maintenance. While in the breast cancer, autophagy regulates self-renewal of several breast cancer stem cells through different pathways including TGF-β/Smad, IL-6 secretion, and EGFR/STAT3. Besides, autophagy is involved in the tumor metastasis, which is evidenced in various cancers.

infection (Tiwari et al., 2020). Autophagy in NSCs can also be used by ZIKV to promote its own replication in host cells by inhibiting the AKT-mTOR pathway through its non-structural proteins, NS4A and NS4B (Liang Q. et al., 2016).

Autophagy failure is a known characteristic of Alzheimer's disease (AD) (Nixon and Yang, 2011). Such a failure is caused by presenilin 1 deficiency, as a consequence of dysregulated ERK/CREB signaling, as evidenced by a reduction in the number of autophagosomes and autophagy-related mRNA and protein levels in presenilin 1-deficient NSCs (Chong et al., 2018). Studies have confirmed that autophagy activation can ameliorate AD. Specifically, the combination of berberine and curcumin extracted from herbal medicine effectively attenuates inflammation and oxidative stress in AD via autophagy induction through the AMPK pathway (Lin et al., 2020). Another study showed that the AMPK pathway activated by resveratrol is instrumental for NSCs to ameliorate inflammation and oxidative stress caused by amyloid-beta deposition. Although the authors of this study did not mention the involvement of autophagy in inhibiting inflammation and oxidative stress in NSCs, other studies have shown that AMPK-activated autophagy helps clear amyloid-beta deposits (Rahman et al., 2021; Wani et al., 2021), which have a strong relationship with neuroinflammation and oxidative stress (Moore and O'Banion, 2002). In conclusion, these results make it reasonable to speculate that AMPK-related autophagy in NSCs is a promising target for AD treatment.

Furthermore, based on the positive regulation of mTOR by FIP200 during cell growth (Chano et al., 2006), it has also been found that in differentiated neurons, FIP200 dysfunction leads to neurite atrophy and apoptosis and eventually exacerbates AD. These effects also occur through mTOR repression (Chano et al., 2007). NSCs have the ability to differentiate into new

neurons, while FIP200 engages in regulating cell growth. It may be interesting to explore the relationship between FIP200 and mTOR using NSCs as a model, to facilitate the development of novel AD treatments.

Physiological Role of Autophagy in MSCs

The pluripotency of MSCs was first identified using cells from murine bone marrow (Friedenstein et al., 1968). MSCs can be isolated from various tissues, including bone marrow, umbilical cord, adipose tissue, liver, and pancreas, and they exhibit varying degrees of differentiation and proliferation potential.

Autophagy regulates MSC stemness and differentiation under several conditions. Autophagy may be activated in response to extreme conditions, such as hyperglycemia, senescence, increased ROS levels, or hypoxia. In this context, autophagy may be protective or destructive for MSCs (Sbrana et al., 2016). The specialized differentiation of MSCs requires autophagy. For example, upon activation by cAMP, the ERK1/2-Beclin-1 signaling pathway induces autophagy in MSCs, thus inhibiting the proliferation of MSCs and also contributing to their differentiation into nerve cells (Ugland et al., 2011). Irisin is produced after exercise and is involved in the transformation of white adipose tissue to brown adipose tissue, thus regulating energy consumption. A recent study found that irisin promotes the osteogenic differentiation of bone marrow mesenchymal stem cells (BMSCs) by activating autophagy, as evidenced by increased levels of LC3II and Atg5 (Chen et al., 2020). ROS accumulation and radiation-induced DNA damage induce a loss of stemness in autophagy-deficient MSCs, suggesting that autophagy protects MSCs against oxidative damage, thus maintaining their stemness (Hou et al., 2013). Interestingly, another study found that under hypoxic conditions, autophagy activated by the AMPK/mTOR pathway leads to MSC apoptosis (Zhang et al., 2016).

Disease-Relevant Mechanism of Autophagy Concerning MSCs

Due to their pluripotency, the potent regenerative properties of MSCs have attracted considerable attention in research on human disease therapies. In this review, we mainly focus on the roles of autophagy in recipient cells after MSC transplantation. Specifically, Parkinson's disease, myocardial infarction, myocardial ischemia/reperfusion (I/R) injury, and cerebral I/R injury will be discussed in detail in this section.

In Parkinson's disease, abnormal proteins produced by mistranslation are not properly processed, causing aggregates to precipitate. The accumulation of α-synuclein, which is toxic to neurons and ultimately causes neuronal death, is commonly seen. In the 1-methyl-4-phenyl-1,2,3,6-tetrahydropyridine-treated animal model of Parkinson's disease, levels of α-synuclein in dopaminergic neurons have been shown to decrease after MSC administration, partly due to autophagy induction (Park et al., 2014). Specifically, MSCs release certain small molecules that activate the PI3K/AKT pathway in neurons, which upregulates autophagy-related proteins, such as Beclin-1, leading to autophagosome formation and the clearance of α-synuclein (Shin and Lee, 2020). Another study found that MSC administration promotes the fusion of autophagosomes and lysosomes (Park et al., 2014). Similarly, MSC treatment induces the clearance of amyloid-beta in AD, along with the promotion of autophagosome formation and fusion (Shin et al., 2014), which may also be a promising treatment strategy for other neurodegenerative diseases. However, further studies should also be conducted to explore the exact mechanism of MSC treatment in these diseases.

In myocardial infarction, MSC treatment also regulates autophagy. The transplanted MSCs release apoptotic bodies, which are engulfed by recipient endothelial cells. Apoptotic bodies increase the expression of transcription factor EB in recipient cells. The induction of the autophagy transcription factor EB then promotes angiogenesis and the recovery of cardiac function (Liu et al., 2020).

Myocardial ischemia is defined as a lack of blood flow to cardiac tissue, which causes an oxygen imbalance, with subsequent cardiac dysfunction and myocardial tissue damage. The effective and timely restoration of blood perfusion can reduce the associated myocardial injury and necrosis, but it may cause further tissue damage. BMSCs relieve ischemic myocardial reperfusion injury via two mechanisms (Wang and Li, 2007). First, these cells can differentiate into myocardial and vascular cells. Second, BMSCs secrete various growth factors, cytokines, and exosomes and thus mediate endogenous regeneration, particularly angiogenesis, via paracrine activation of resident cardiac stem cells and other stem cells.

In the case of myocardial ischemia and associated hypoxia, the mTOR pathway is involved in autophagy regulation in BMSCs. mTOR is negatively regulated by AMPK. Hypoxia enhances AMPK/mTOR signaling pathway activity (Liu L. et al., 2017), and BMSCs play a potential role in inhibiting myocardial apoptosis via the induction of myocardial autophagy under conditions of hypoxic stress. During myocardial ischemia and hypoxia, intracellular ATP levels significantly decrease in cardiac myocytes, leading to an increased AMP/ATP ratio (Matsui et al., 2008). Activated AMPK then phosphorylates TSC2 and thus inhibits mTOR activation (Wang et al., 2018). This signaling cascade mainly suppresses protein synthesis and induces autophagy, which enables the myocardium to adapt to the hypoxic environment. When myocardial ischemia occurs, autophagy is inhibited. BMSCs promote the activation of AMPK in cardiomyocytes to block the mTOR pathway, reactivate autophagy, and inhibit apoptosis. At this time, autophagy has a protective effect on ischemic myocardial cells (Liu L. et al., 2017). Therefore, regulation of the AMPK/mTOR signaling pathway may be the mechanism of action underlying the effects of BMSCs in the treatment of myocardial I/R injury.

However, autophagy activation exacerbates cerebral I/R injury. In a rat model of cerebral I/R injury (middle cerebral artery occlusion), the intravenous transplantation of BMSCs leads to increased p-AKT and p-mTOR levels, but decreased LC3 and Beclin-1 levels, which facilitates behavioral improvements, reduced cerebral infarction volume, and decreased neuronal apoptosis (He et al., 2019). In summary, activation of the PI3K/AKT/mTOR signaling pathway protects the brain from cerebral I/R injury by suppressing autophagy.

Physiological Role of Autophagy in ISCs

In mammals, the intestinal lumen is lined with a single layer of epithelial cells that are renewed every 2–5 days. The intestinal epithelium comprises crypts, which contain ISCs, and villi, which contain differentiated and specialized intestinal cells. The rapidly cycling ISCs are located at the basement membranes of the crypts, and they maintain continuous epithelial regeneration and epithelial homeostasis under intact circumstances (Sailaja et al., 2016).

Epithelial intestinal cells can be rapidly activated, and thus, ISCs require extraordinarily precise control. The ability of ISCs to reenter the cell cycle upon request critically depends on their ability to maintain a quiescent state. In ISCs, an elevated basal level of autophagy maintains cellular function, whereas the blockade of autophagy in the intestinal tract leads to the premature death of ISCs. Autophagy-deficient ISCs exhibit increased DNA damage and cell cycle arrest (Trentesaux et al., 2020). Knocking out *Atg5* in ISCs causes ROS accumulation, which in turn decreases the number of ISCs in the pool (Asano et al., 2017). Another study showed that mitophagy is activated by the innate immune receptor NOD2 to reduce mitochondrial ROS levels and thus protect ISCs (Levy et al., 2020). Therefore, autophagy is considered as an essential factor in sustained cell proliferation and the preservation of the stem cell pool.

Disease-Relevant Mechanism of Autophagy in ISCs

Autophagy plays a dual role in ISC-related diseases. Slit2 is a secreted glycoprotein that belongs to the Slit family. It binds to the roundabout receptor Robo1, which activates the Slit2/Robo1 pathway. In ulcerative colitis, the Slit2/Robo1 pathway regulates ISC proliferation to attenuate inflammation in the colon by activating autophagy (Xie et al., 2020).

Similarly, in the early stage of tumorigenesis, tumor suppressive autophagy inhibits the excessive proliferation and malignant transformation of ISCs by degrading epidermal growth factor receptor (EGFR) (Zhang et al., 2019a). Autonomous autophagy deficiency leads to the induction of intestinal hyperplasia and colon cancer (Zhang et al., 2019b). However, in the later stage of tumorigenesis, autophagy is hijacked by CSCs to provide energy and nutrients for themselves. Prox1 is a transcription factor involved in tumor progression (Elsir et al., 2012), and it is not expressed in normal ISCs. Under pathological conditions, Prox1 promotes ISC survival through autophagy activation, thus facilitating tumor growth (Wiener et al., 2014).

Physiological Role of Autophagy in iPSCs

In 2006, the research team of Shinya Yamanaka was the first to induce and designate "induced pluripotent stem cells." These cells are similar to embryonic stem cells with respect to morphology; gene expression profile; and many crucial functions, including cell multiplication, embryogenesis, teratogenesis, and the capacity to differentiate and form chimeras (Takahashi and Yamanaka, 2006).

The stemness of iPSCs is maintained by a high level of autophagic flux, which also prevents genomic defects and ROS-induced injury. Autophagy clears the mitochondria during iPSC reprogramming, during which a necessary metabolic transformation from mitochondrial oxidative phosphorylation to glycolysis occurs (Xu et al., 2013). In other words, autophagy protects the self-renewal and differentiation capacities of iPSCs. In a previous study, the autophagy inhibitor 3-MA was used to evaluate the induction and protective effects of autophagy in iPSCs. Notably, the authors determined that the loss of autophagy leads to a near-complete block of iPSC proliferation (Ma et al., 2015).

Disease-Relevant Mechanism of Autophagy Concerning iPSCs

Many disease and drug mechanisms have been studied in cellular and animal models. However, there are differences between animal models of disease and human disease. Due to their pluripotency, iPSCs have the ability to generate different types of tissues. Thus, iPSCs derived from patients have been extensively used to establish models of diseases, such as neurodegenerative diseases (Amin et al., 2019; Seranova et al., 2020), providing a new and powerful model for disease research.

For example, autophagy impairment has been shown to be a pathological characteristic of AD that is caused by presenilin 1 deficiency (Chong et al., 2018). These results were previously confirmed by Martin-Maestro using a patient-derived iPSC model of AD (Martin-Maestro et al., 2017). Moreover, iPSCs from AD patients can be used as an experimental model to explore the mechanism of drugs used for AD treatment. Dantrolene has been approved by the Food and Drug Administration for the treatment of malignant hyperthermia, but it has also been shown to help prevent memory decline in animal models of AD. In iPSCs from patients with AD, dantrolene restores intracellular Ca^{2+} homeostasis and physiological autophagy, thus attenuating impaired neurogenesis and synaptogenesis (Wang et al., 2020). In another pharmacological study, iPSC-derived NSCs were used to explore the effect of bexarotene, an autophagy-activation drug, on AD (Martin-Maestro et al., 2019). Taken together, these results suggest that iPSCs derived from patients may be an ideal model for research on related diseases.

Physiological Role of Autophagy in CSCs

Autophagy, as a ubiquitous survival pathway in cells, is closely linked with cancer, in which it plays a dual role as either a tumor suppressor or a tumor promoter (Yun et al., 2021). In the early stage of tumorigenesis, autophagy maintains cellular homeostasis through protein and organelle quality control mechanisms (Li et al., 2020). Autophagy sustains genomic stability and inhibits the occurrence of inflammation by degraded oncogenic proteins, thus hindering tumor initiation, development, and metastasis (Zhong et al., 2016; Chao et al., 2021). The tumor-suppressive function of autophagy can also be evidenced by the fact that knocking down *Atg7* promotes cell proliferation in non-small cell lung

cancer (NSCLC) cells (Cao et al., 2020). However, at the later stage of tumorigenesis, autophagy helps cancer cells survive and adapt to unfavorable microenvironments, such as hypoxia and nutrient deprivation (Xue et al., 2016; Guo et al., 2018). Moreover, autophagy inhibition reduces drug resistance in gastric cancer (Xin et al., 2019), multiple myeloma (Zhang et al., 2020), colorectal carcinoma (Wang and Gu, 2018), and NCSLC (Lotsberg et al., 2020). Accordingly, autophagy plays an important role in tumorigenesis. It is reasonable to speculate that autophagy is necessary for CSCs to continuously generate new cancer cells.

Cancer stem cells are functionally similar to stem cells, but they can drive tumorigenesis. Tumor cells can form a cellular hierarchy similar to that in normal tissue, in which CSCs remain at the peak and control the occurrence, malignant transformation, drug resistance, and recurrence of tumors. Compared with normal stem cells, CSCs exhibit dysregulated migration and invasion abilities, as well as an abnormal tolerance to pharmacologic and immune factors (Smith and Macleod, 2019). There is increasing evidence suggesting that CSC maintenance and differentiation rely on autophagy (Camuzard et al., 2020; Yao et al., 2020; Wang et al., 2021).

Cancer stem cells reside in the niche, which is also a part of the tumor microenvironment. However, the niche has anatomically distinct regions within the tumor microenvironment that maintain the key properties of CSCs and protect them from the immune system (Plaks et al., 2015). The microenvironment has been shown to provide some necessary factors for the stability of stem cell niches so that the stem cells retain their properties. Autophagy is a process that is necessary in the tumor microenvironment, and it may modulate the interaction between tumor cells and components of both the innate and adaptive immune systems and supply nutrients or other factors to regulate the growth of tumor cells (Levy et al., 2017). For example, autophagy promotes the release of damage-associated molecular patterns and ATP from dying tumor cells, thus recruiting $CD8^+$ cytotoxic T lymphocytes that synergize with conventional therapeutics to eliminate cancers (Michaud et al., 2011).

However, another study reported that autophagy is induced in certain other non-tumor cells in the tumor microenvironment in a manner that further promotes tumor cell growth and progression (Sousa et al., 2016). To adapt to conditions of hypoxia, cancer cells prefer to generate energy through glycolysis, a process that generates pyruvate and lactate. This is termed the "Warburg effect" (also known as aerobic glycolysis) (Gentric and Mechta-Grigoriou, 2021). However, a novel metabolite pathway known as the "reverse Warburg effect" is also used by cancer cells. Specifically, epithelial cancer cells induce oxidative stress in cancer-associated fibroblasts (CAFs), followed by mitophagy activation in CAFs. The CAFs are forced to undergo aerobic glycolysis, whose energy-rich metabolites pyruvate and lactate are utilized by cancer cells to undergo the TCA cycle for abundant energy production (Martinez-Outschoorn et al., 2011), thereby promoting the generation of new CSCs (Pavlides et al., 2009; **Figure 2**).

Disease-Relevant Mechanism of Autophagy in CSCs

During early tumorigenesis, autophagy maintains intracellular homeostasis by removing damaged mitochondria, peroxisomes, and other cytotoxic substances from normal cells, thus inhibiting the activation of oncogenes and preventing further tumorigenesis. In malignantly transformed cancer cells, however, autophagy recycles cellular components to provide nutrients that are essential for survival, thereby promoting cell proliferation, invasion, and metastasis. In this section, we will mainly focus on the role of autophagy in hepatic and breast CSCs, and discuss the intersection between autophagy and drug resistance in other types of CSCs from cancers including epithelial ovarian cancer, bladder cancer, pancreatic cancer, glioblastoma, and gastric cancer.

In hepatoma carcinoma, chloroquine, an autophagy inhibitor, reduces the formation of autophagic lysosomes, blocks pSTAT3, and inhibits the self-renewal of hepatic CSCs (Li et al., 2017). Moreover, studies have shown that mitophagy is also involved in cancer progression. Specifically, when mitophagy is impaired in hepatic CSCs, the tumor suppressor p53 is phosphorylated at S392 by PINK1, a kinase associated with mitophagy, in the mitochondria. p53 then translocates to the nucleus and binds to the *NANOG* promoter, causing a failure of OCT4, SOX2 transcription factors to activate expression of NANOG which is a pivotal transcription factor in maintenance of hepatic CSCs (Liu K. et al., 2017). Conversely, mitophagy can be enhanced under conditions such as hypoxia and starvation. After p53 is inhibited by mitophagy, it localizes in the mitochondria and is degraded in a mitophagy-dependent manner, after which it cannot affect NANOG expression, thereby promoting the self-renewal of hepatic CSCs (Lee et al., 2018). These findings suggest that autophagy activates hepatic CSCs and thus facilitates their stemness and self-renewal (**Figure 2**).

CD133 is a biomarker of stem-like cells, and its expression has been demonstrated in liver CSCs (Suetsugi et al., 2006). In low-glucose medium, CD133 has been shown to promote the uptake of glucose and the generation of sufficient energy for the survival of Huh-7 cells (human hepatoma cells), in which autophagy is activated (Chen et al., 2013a). A monoclonal anti-CD133 antibody (CD133mAb) has also been shown to promote the death of hepatoma cells expressing CD133 on their surface, by repressing autophagy (Chen et al., 2013b). Notably, the tumor-suppressive effect of CD133mAb on liver CSCs is more effective under conditions of nutrient deprivation, such as in low-glucose medium. Therefore, combined therapy with a hypoglycemic agent, which simultaneously decreases glucose concentration in the tumor microenvironment, increases the sensitivity of CSCs to CD133mAb.

In breast cancer, tumor growth and metastasis require blood vessels, whereas tumor stem cells differentiate into endothelial cells to promote the formation of new blood vessels. The levels of autophagy-related factors have been shown to be elevated during the differentiation of breast cancer stem cells (BCSCs), and the use of autophagy blockers or the conditional knockout of *Atg5* inhibits the differentiation process (Yao et al., 2020).

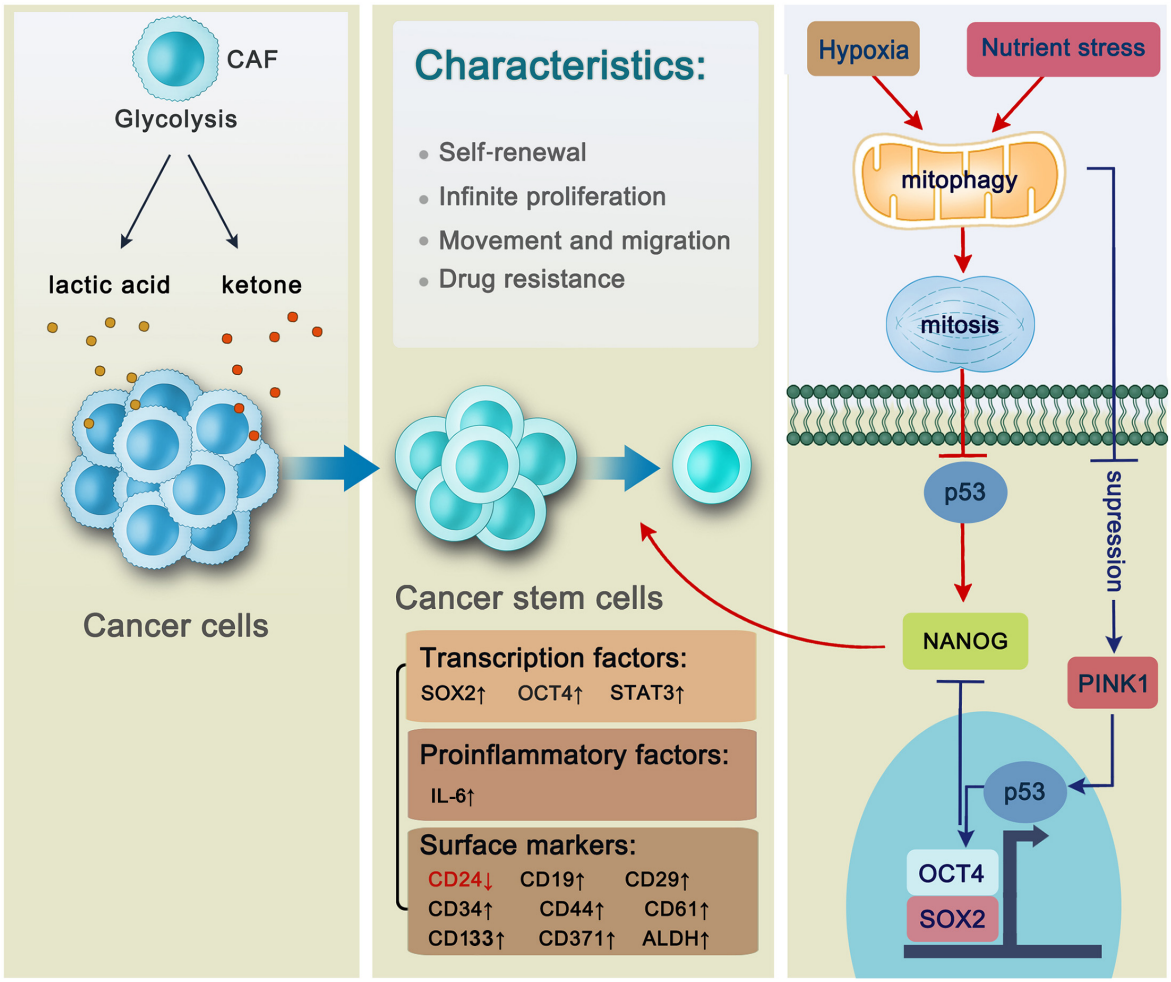

FIGURE 2 | The general characteristics of cancer stem cells and the regulation of mitophagy in hepatic cancer stem cells. Cancer cells benefit from cancer-associated fibroblasts whose products including anaerobic glycolysis lactic acid and ketone are utilized by cancer cells to generate new cancer stem cells. Cancer stem cells are characterized by self-renewal, infinite proliferation, movement and migration and drug resistance with a series of intracellular factors and surface markers changing. Transcription factors including SOX2, OCT4, and STAT3 are activated through autophagy-related pathways to be involved in the self-renewal of hepatic CSC. Autophagy promotes the maintenance of $CD44^{+}/CD24^{low/-}$ phenotype in the MDA-MB-468 breast cancer cell lines via proinflammatory factor IL-6 secretion. CD133 is a stem cell marker located on both liver cancer stem cells and pancreatic cancer stem cells. In AML, LSCs express surface markers including CD371. In B-ALL, CD34, and CD19 are located on the surface of LSCs. There are three kinds of cancer stem cells in the breast cancer, whose surface markers are characterized by $CD44^{+}/CD24^{low/-}$, $ALDH^{+}$, and $CD29^{hi}CD61^{+}$, respectively. Mitophagy plays an essential role in hepatic CSC maintenance. Specifically, mitophagy will be activated under the unfavorable condition such as hypoxia or nutrient stress followed by p53 inhibition, thus promoting NANOG expression which can facilitate stemness of liver CSCs. However, if mitophagy is suppressed, PINK1 will be activated to phosphorylate p53 at S392, making it possible for p53 to translocate into the nucleus. Then p53 binds to the NANOG promoter, leading to the failure of OCT4 and SOX2 to reach to their binding sites on the NANOG promoter, thus suppressing NANOG expression.

In the process of tumor cell metastasis, there is excessive blood supply, resulting in hypoxia, a lack of nutrients, and other unfavorable conditions. Autophagy helps BCSCs combat hypoxia and perform protein catabolism to supply BCSCs under conditions of starvation (Espina et al., 2010). When antiangiogenic drugs are used to treat breast cancer, instead of inhibiting the development of the cancer, they have been found to promote metastasis by generating intratumoral hypoxia (Conley et al., 2012). As we discussed above, the increase in BCSC metastasis may attribute to the hypoxic microenvironment formed by antiangiogenic drugs, under which autophagy is activated to provide sufficient energy for BCSC metastasis and tumor development.

Research on the relationship between autophagy and BCSCs must be designed specifically based on different types of BCSCs, because the autophagic process differs in different cell types. Based on surface markers, there are three distinct CSC types, namely $CD44^{+}/CD24^{low/-}$, $ALDH^{+}$, and $CD29^{hi}CD61^{+}$ phenotypes (Ricardo et al., 2011; Yeo et al., 2016). Although all BCSCs have the potential for tumor initiation, autophagy promotes their maintenance via different pathways. For example, autophagy promotes the maintenance of $CD44^{+}/CD24^{low/-}$

MDA-MB-468 breast cancer cells via IL-6 secretion. However, autophagy does not promote the survival of $CD44^+/CD24^{low/-}$ MCF-7 CSCs (Maycotte et al., 2015). Autophagy has also been implicated in the tumor-initiating potential of distinct BCSC subsets through different pathways (Yeo et al., 2016). Autophagy deficiency induced by FIP200 depletion causes a decrease in the number of $CD29^{hi}CD61^+$ BCSCs and their potential to initiate tumors by inhibiting the TGF-β/Smad pathway. However, the inhibition of autophagy by *FIP200* knockout reduces the number of $ALDH^+$ BCSCs as well as their tumor-initiating potential. In summary, there is a need for a comprehensive consideration of how to utilize autophagy against these three distinct types of BCSCs.

Triple-negative breast cancer (TNBC) is an important form of breast cancer. The drug resistance and recurrence of TNBC are mainly attributed to the ability of CSCs to generate an unlimited number of new cancer cells, during which autophagy plays an important role. Data from patient-derived xenograft models indicate that autophagy is activated in chemo-resistant xenografts, as evidenced by higher levels of autophagy markers (*BECN1* mRNA) than those detected in chemo-sensitive models (Bousquet et al., 2017). This study implies that autophagy inhibition may be effective for cancer therapy. Chloroquine (an autophagy inhibitor) has been used to target CSCs to inhibit autophagy, which causes damage to the mitochondrial structure, increased oxidative stress levels, and changes in the degree of DNA methylation, thereby reducing the metastatic potential of TNBC (Liang D.H. et al., 2016). Furthermore, the combination of chloroquine and standard chemotherapy exerts favorable effects. For example, chloroquine sensitizes TNBC cells to paclitaxel by inhibiting autophagy and decreasing the population of $CD44^+/CD24^{-/low}$ CSCs by blocking the Janus-activated kinase (JAK) 2/STAT3 pathway (Choi et al., 2014). The anti-tumor effect of pterostilbene, a natural demethylated analog of resveratrol from blueberries, potentiates the effect of the autophagy inhibitor 3-MA (Chen et al., 2014). Accordingly, autophagy inhibition is a promising target for TNBC treatment and a combined therapy is worth consideration.

Links have also been identified between autophagy and other types of CSCs, including those in epithelial ovarian cancer, bladder cancer, pancreatic cancer, glioblastoma, and gastric cancer. In view of the role of autophagy in the resistance of tumors to chemotherapy, the tumor suppressor gene *BRCA1* has been shown to render epithelial ovarian CSCs resistant to cisplatin (a chemotherapeutic drug) by regulating autophagy (Li D. et al., 2016). Autophagy inhibitors may attenuate the drug resistance of epithelial ovarian CSCs mediated by BRCA1 (You et al., 2019). A recent study has also demonstrated that the autophagy inhibitor chloroquine in combination with cisplatin decreases the drug resistance of epithelial cancer cells (Hwang et al., 2020). These results indicate that autophagy may be a promising target for overcoming drug resistance in epithelial ovarian cancer.

Similarly, autophagy is also linked to the drug resistance of bladder cancer cells. Greater autophagic flux has been observed in bladder CSCs (Ojha et al., 2014). Atg7 promotes the maintenance of bladder CSCs by stabilizing CD44, which serves as a classical marker of stem cells and also favors sphere formation, invasion, and lung metastasis (Zhu et al., 2019). JAK2 expression activates autophagy in CSCs, leading to increased expression levels of genes related to drug resistance in CSCs (Ojha et al., 2016). Accordingly, autophagy inhibition may be an effective therapeutic strategy. Icaritin, a flavonol glycoside, delays the progression of bladder cancer by inhibiting autophagy (Pan et al., 2016). Furthermore, autophagy inhibition can render CSCs more sensitive to the chemotherapeutic drugs, cisplatin (Ojha et al., 2014) and taxol (Ma et al., 2021).

In a hypoxic microenvironment, increased levels of HIF-1α induce autophagy to promote the transformation from non-stem pancreatic cancer cells to $CD133^+$ pancreatic CSCs (Zhu et al., 2013). Additionally, HIF-1α-induced autophagy has been shown to promote the epithelial-to-mesenchymal transition of pancreatic CSCs, resulting in increased tumor aggressiveness (Zhu et al., 2014). Rausch reported that a balanced autophagy flux, with neither hyperactivation nor over-inhibition, maintains pancreatic CSC survival (Rausch et al., 2012). The stem cell-like characteristics of pancreatic cancer cells are diminished following the inhibition of nutrient-deprivation autophagy factor-1, an important factor that regulates autophagy and oxidative stress (Qin et al., 2020). Autophagy is also involved in drug resistance, as exemplified by the negative regulation of pancreatic CSC stemness by mitophagy impairment as a result of ISGylated protein depletion (Alcala et al., 2020). The addition of chloroquine inhibits pancreatic CSC activity and increases the anti-tumor effect of gemcitabine (Yang et al., 2015).

The autophagy-related factor DRAM1 promotes to the localization of p62, an essential regulator of autophagy, to autophagosome. p62 has a short LC3-interacting region, which can promote binding with LC3, which results in the selective degradation of p62 through autophagy (Li et al., 2020). Defective autophagy causes p62 accumulation, and therefore, p62 is a negative marker of autophagy activation. DRAM1 and p62 regulate the migration and invasion of glioma stem cells (GSCs) and autophagy-mediated cell degradation (Galavotti et al., 2013). GSCs and other glioblastoma cells survive and promote tumor growth through the induction of autophagy and the inhibition of apoptosis under a hypoxic microenvironment (Chakrabarti et al., 2016). A demethoxycurcumin analog is used to inhibit the growth of glioblastomas via the activation of apoptosis, but it also induces autophagy, which protects GSCs from apoptosis (Shi et al., 2020). Therefore, the combination therapy of demethoxycurcumin and an autophagy inhibitor may be more effective than monotherapy for cancer treatment. The PI3K/AKT pathway is considered to be involved in the maintenance of GSCs. Treatment with chloroquine, while concomitantly inhibiting the PI3K/AKT pathway, significantly inhibits glioblastoma progression (Graham et al., 2014). GSCs are resistant to temozolomide, an oral anti-tumor drug. A low concentration of temozolomide can promote the growth of GSCs. A recent study suggested that GSC-derived PD-L1-containing exosomes activate AMPK/ULK1-mediated autophagy, thus increasing drug-resistance in glioblastoma (Zheng et al., 2021). Accordingly, autophagy inactivation increases the sensitivity of GSCs to drugs (Buccarelli et al., 2018).

The level of autophagy is significantly higher in $CD44^+$ $CD54^+$ gastric CSCs than in non-CSCs. There is considerable evidence to suggest that Notch signaling regulates gastric CSC resistance. Combined treatment with chloroquine (an autophagy inhibitor) and 5-fluorouracil (a chemotherapeutic agent) inhibits CSC activity, increases the expression levels of Notch1 protein, and increases the sensitivity of cells to drugs (Li et al., 2018). In *Helicobacter pylori*-infected gastric cancer, levels of the autophagy marker LC3 increase concomitantly with the upregulation of CD44 (Courtois et al., 2021), a classical marker of stem cells, indicating that autophagy plays a vital role in gastric CSCs. However, incomplete autophagy also exists in gastric CSCs to protect *H. pylori* from contact with antibiotics.

CONCLUSION

The highly conserved process of autophagy works as a "cleaner" to degrade damaged proteins and impaired organelles in cells. This process contributes to the homeostasis of adult stem cells in terms of their quiescence, self-renewal, and differentiation. Dysfunctional autophagy in adult stem cells leads to the progression of diseases, especially various types of cancers. Autophagy plays different roles in different stages of tumorigenesis, such as initiation, development, and metastasis, either inhibiting tumor growth or promoting tumor development. In the earlier stages of tumor progression, autophagy regulates cellular homeostasis by eliminating damaged mitochondria and oncogenic proteins, thus inhibiting tumor initiation and delaying tumor growth. However, in the later stages of tumorigenesis, autophagy is a survival mechanism for cancer cells, allowing them to acquire energy and materials through autophagic degradation, which helps them to adapt to unfavorable environments, thereby promoting tumor progression, metastasis, and invasion. Although autophagy inhibition has been shown to be a promising strategy for cancer treatment (Yang et al., 2015; Pan et al., 2016; Buccarelli et al., 2018; Bie et al., 2021), there are some studies indicating that autophagy activation can also be utilized in cancer treatment. For example, autophagy activation, not inhibition, increases the sensitivity of GSCs to drugs (Hung et al., 2020). Another study showed that the co-suppression of mTORC1, histone deacetylase, and estrogen receptor 1 decreases the number of CSCs via autophagy activation in TNBC (Sulaiman et al., 2018). These results are reasonable based on the dual role of autophagy in tumorigenesis. Consequently, before utilizing autophagy as a target for cancer treatment, the tumorigenesis stage, the context, microenvironment stress levels, and nutrient availability need to be taken into consideration.

A study published in 2018 showed that autophagy suppression increased the sensitivity of GSCs to temozolomide, which is used for glioblastoma treatment through the activation of ferroptosis (an iron-dependent form of programmed cell death) (Buccarelli et al., 2018). This suggests that autophagy suppression may affect other intracellular events, such as ferroptosis and apoptosis, indicating essential roles for autophagy during these cellular processes (Jang et al., 2017, 2020). In addition, in the transplantation of bone-derived MSCs for the treatment of myocardial infarction and myocardial and cerebral I/R injury, targeting autophagy may significantly improve therapeutic efficacy. Therefore, targeting autophagy is a promising strategy not only for cancer but also for transplantation treatment.

In summary, our review has comprehensively demonstrated the essential roles of autophagy in CSC regulation and CSC-related diseases, suggesting that autophagy is a promising target for clinical therapy.

AUTHOR CONTRIBUTIONS

NW and DW provided the idea, designed the structure of the manuscript and figures, and revised the manuscript. SC, WW, and H-YT collected materials, wrote and revised the manuscript, and drew the figures and revised them. YL collected materials and provided many valuable comments. ZL provided useful advice during the process of revision. YQ collected materials and revised the manuscript. YL, ZL, and YQ provided useful advice during the drawing process of figures. All authors contributed to the article and approved the submitted version.

FUNDING

This work was supported by the Natural Science Foundation of Jilin Province (20200201122JC and 20200201030JC).

REFERENCES

Alcala, S., Sancho, P., Martinelli, P., Navarro, D., Pedrero, C., Martin-Hijano, L., et al. (2020). ISG15 and ISGylation is required for pancreatic cancer stem cell mitophagy and metabolic plasticity. *Nat. Commun.* 11:2682. doi: 10.1038/s41467-020-16395-2

Amin, N., Tan, X. N., Ren, Q. N., Zhu, N., Botchway, B. O. A., Hu, Z. Y., et al. (2019). Recent advances of induced pluripotent stem cells application in neurodegenerative diseases. *Prog. Neuro Psychopharmacol. Biol. Psychiatry* 95:109674. doi: 10.1016/j.pnpbp.2019.109674

Asano, J., Sato, T., Ichinose, S., Kajita, M., Onai, N., Shimizu, S., et al. (2017). Intrinsic autophagy is required for the maintenance of intestinal stem cells and for irradiation-induced intestinal regeneration. *Cell Rep.* 20, 1050–1060. doi: 10.1016/j.celrep.2017.07.019

Bellodi, C., Lidonnici, M. R., Hamilton, A., Helgason, G. V., Soliera, A. R., Ronchetti, M., et al. (2009). Targeting autophagy potentiates tyrosine kinase inhibitor-induced cell death in Philadelphia chromosome-positive cells, including primary CML stem cells. *J. Clin. Invest.* 119, 1109–1123. doi: 10.1172/JCI35660

Bie, Q. L., Song, H., Chen, X. K., Yang, X., Shi, S., Zhang, L. H., et al. (2021). IL-17B/IL-17RB signaling cascade contributes to self-renewal and tumorigenesis of cancer stem cells by regulating Beclin-1 ubiquitination. *Oncogene* 40, 2200–2216. doi: 10.1038/s41388-021-01699-4

Birbrair, A., and Frenette, P. S. (2016). Niche heterogeneity in the bone marrow. *Ann. N. Y. Acad. Sci.* 1370, 82–96. doi: 10.1111/nyas.13016

Bousquet, G., El Bouchtaoui, M., Sophie, T., Leboeuf, C., de Bazelaire, C., Ratajczak, P., et al. (2017). Targeting autophagic cancer stem-cells to reverse chemoresistance in human triple negative breast cancer. *Oncotarget* 8, 35205–35221. doi: 10.18632/oncotarget.16925

Boya, P., Codogno, P., and Rodriguez-Muela, N. (2018). Autophagy in stem cells: repair, remodelling and metabolic reprogramming. *Development* 145:dev146506. doi: 10.1242/dev.146506

Buccarelli, M., Marconi, M., Pacioni, S., De Pascalis, I., D'Alessandris, Q. G., Martini, M., et al. (2018). Inhibition of autophagy increases susceptibility of glioblastoma stem cells to temozolomide by igniting ferroptosis. *Cell Death Dis.* 9:841. doi: 10.1038/s41419-018-0864-7

Camuzard, O., Trojani, M. C., Santucci-Darmanin, S., Pagnotta, S., Breuil, V., Carle, G. F., et al. (2020). Autophagy in osteosarcoma cancer stem cells is a critical process which can be targeted by the antipsychotic drug thioridazine. *Cancers* 12:3675. doi: 10.3390/cancers12123675

Cao, Q., You, X., Xu, L., Wang, L., and Chen, Y. (2020). PAQR3 suppresses the growth of non-small cell lung cancer cells via modulation of EGFR-mediated autophagy. *Autophagy* 16, 1236–1247. doi: 10.1080/15548627.2019.1659654

Chakrabarti, M., Klionsky, D. J., and Ray, S. K. (2016). miR-30e blocks autophagy and acts synergistically with proanthocyanidin for inhibition of AVEN and BIRC6 to increase apoptosis in glioblastoma stem cells and glioblastoma SNB19 cells. *PLoS One* 11:e0158537. doi: 10.1371/journal.pone.0158537

Chang, N. C. (2020). Autophagy and stem cells: self-eating for self-renewal. *Front. Cell Dev. Biol.* 8:138. doi: 10.3389/fcell.2020.00138

Chano, T., Okabe, H., and Hulette, C. M. (2007). RB1CC1 insufficiency causes neuronal atrophy through mTOR signaling alteration and involved in the pathology of Alzheimer's diseases. *Brain Res.* 1168, 97–105. doi: 10.1016/j.brainres.2007.06.075

Chano, T., Saji, M., Inoue, H., Minami, K., Kobayashi, T., Hino, O., et al. (2006). Neuromuscular abundance of RB1CC1 contributes to the non-proliferating enlarged cell phenotype through both RB1 maintenance and TSC1 degradation. *Int. J. Mol. Med.* 18, 425–432.

Chao, T., Shih, H. T., Hsu, S. C., Chen, P. J., Fan, Y. S., Jeng, Y. M., et al. (2021). Autophagy restricts mitochondrial DNA damage-induced release of ENDOG (endonuclease G) to regulate genome stability. *Autophagy*. doi: 10.1080/15548627.2021.1874209 [Epub ahead of print].

Chehelcheraghi, F., Chien, S., and Bayat, M. (2019). Mesenchymal stem cells improve survival in ischemic diabetic random skin flap via increased angiogenesis and VEGF expression. *J. Cell. Biochem.* 120, 17491–17499. doi: 10.1002/jcb.29013

Chen, H., Luo, Z., Dong, L., Tan, Y., Yang, J., Feng, G., et al. (2013a). CD133/prominin-1-mediated autophagy and glucose uptake beneficial for hepatoma cell survival. *PLoS One* 8:e56878. doi: 10.1371/journal.pone.0056878

Chen, H., Luo, Z., Sun, W., Zhang, C., Sun, H., Zhao, N., et al. (2013b). Low glucose promotes CD133mAb-elicited cell death via inhibition of autophagy in hepatocarcinoma cells. *Cancer Lett.* 336, 204–212. doi: 10.1016/j.canlet.2013.04.031

Chen, W. C., Hsu, K. Y., Hung, C. M., Lin, Y. C., Yang, N. S., Ho, C. T., et al. (2014). The anti-tumor efficiency of pterostilbene is promoted with a combined treatment of Fas signaling or autophagy inhibitors in triple negative breast cancer cells. *Food Funct.* 5, 1856–1865. doi: 10.1039/c4fo00145a

Chen, X., Sun, K. N., Zhao, S. J., Geng, T. X., Fan, X., Sun, S. X., et al. (2020). Irisin promotes osteogenic differentiation of bone marrow mesenchymal stem cells by activating autophagy via the Wnt//beta-catenin signal pathway. *Cytokine* 136:155292. doi: 10.1016/j.cyto.2020.155292

Chiramel, A. I., and Best, S. M. (2018). Role of autophagy in Zika virus infection and pathogenesis. *Virus Res.* 254, 34–40. doi: 10.1016/j.virusres.2017.09.006

Choi, D. S., Blanco, E., Kim, Y. S., Rodriguez, A. A., Zhao, H., Huang, T. H., et al. (2014). Chloroquine eliminates cancer stem cells through deregulation of Jak2 and DNMT1. *Stem Cells* 32, 2309–2323. doi: 10.1002/stem.1746

Chong, C. M., Ke, M., Tan, Y., Huang, Z., Zhang, K., Ai, N., et al. (2018). Presenilin 1 deficiency suppresses autophagy in human neural stem cells through reducing gamma-secretase-independent ERK/CREB signaling. *Cell Death Dis.* 9:879. doi: 10.1038/s41419-018-0945-7

Conley, S. J., Gheordunescu, E., Kakarala, P., Newman, B., Korkaya, H., Heath, A. N., et al. (2012). Antiangiogenic agents increase breast cancer stem cells via the generation of tumor hypoxia. *Proc. Natl. Acad. Sci. U.S.A.* 109, 2784–2789. doi: 10.1073/pnas.1018866109

Courtois, S., Haykal, M., Bodineau, C., Sifre, E., Azzi-Martin, L., Menard, A., et al. (2021). Autophagy induced by *Helicobacter* pylori infection is necessary for gastric cancer stem cell emergence. *Gastric Cancer* 24, 133–144. doi: 10.1007/s10120-020-01118-9

Delahaye, M. C., Salem, K. I., Pelletier, J., Aurrand-Lions, M., and Mancini, S. J. C. (2021). Toward therapeutic targeting of bone marrow leukemic niche protective signals in B-cell acute lymphoblastic leukemia. *Front. Oncol.* 10:606540. doi: 10.3389/fonc.2020.606540

Elsir, T., Smits, A., Lindstrom, M. S., and Nister, M. (2012). Transcription factor PROX1: its role in development and cancer. *Cancer Metastasis Rev.* 31, 793–805. doi: 10.1007/s10555-012-9390-8

Espina, V., Mariani, B. D., Gallagher, R. I., Tran, K., Banks, S., Wiedemann, J., et al. (2010). Malignant precursor cells pre-exist in human breast DCIS and require autophagy for survival. *PLoS One* 5:e10240. doi: 10.1371/journal.pone.0010240

Friedenstein, A. J., Petrakova, K. V., Kurolesova, A. I., and Frolova, G. P. (1968). Heterotopic of bone marrow. Analysis of precursor cells for osteogenic and hematopoietic tissues. *Transplantation* 6, 230–247. doi: 10.1097/00007890-196803000-00009

Galavotti, S., Bartesaghi, S., Faccenda, D., Shaked-Rabi, M., Sanzone, S., McEvoy, A., et al. (2013). The autophagy-associated factors DRAM1 and p62 regulate cell migration and invasion in glioblastoma stem cells. *Oncogene* 32, 699–712. doi: 10.1038/onc.2012.111

Gan, B. Y., Melkoumian, Z. K., Wu, X. Y., Guan, K. L., and Guan, J. L. (2005). Identification of FIP200 interaction with the TSC1-TSC2 complex and its role in regulation of cell size control. *J. Cell Biol.* 170, 379–389. doi: 10.1083/jcb.200411106

Garcia-Prat, L., Martinez-Vicente, M., and Munoz-Canoves, P. (2016). Autophagy: a decisive process for stemness. *Oncotarget* 7, 12286–12288. doi: 10.18632/oncotarget.7766

Geng, J., and Klionsky, D. J. (2008). The Atg8 and Atg12 ubiquitin-like conjugation systems in macroautophagy. 'Protein modifications: beyond the usual suspects' review series. *EMBO Rep.* 9, 859–864. doi: 10.1038/embor.2008.163

Gentric, G., and Mechta-Grigoriou, F. (2021). Tumor cells and cancer-associated fibroblasts: an updated metabolic perspective. *Cancers (Basel)* 13:399. doi: 10.3390/cancers13030399

Gong, J., Gu, H., Zhao, L., Wang, L., Liu, P., Wang, F., et al. (2018). Phosphorylation of ULK1 by AMPK is essential for mouse embryonic stem cell self-renewal and pluripotency. *Cell Death Dis.* 9:38. doi: 10.1038/s41419-017-0054-z

Graham, R., Benito, D., Soni, N., Uddin, R., Zhang, B. Y., Walters, W., et al. (2014). Targeting glioblastoma stem cells via inhibition of PI3K/AKT pathway alone and in combination with autophagy blockade. *Neuro Oncol.* 16, v198–v199. doi: 10.1093/neuonc/nou275.9

Gu, H., Shi, X., Liu, C., Wang, C., Sui, N., Zhao, Y., et al. (2019). USP8 maintains embryonic stem cell stemness via deubiquitination of EPG5. *Nat. Commun.* 10:1465. doi: 10.1038/s41467-019-09430-4

Guo, X. L., Hu, F., Wang, H., Fang, J. M., Zhu, Z. Z., Wei, L. X., et al. (2018). Inhibition of autophagy in hepatocarcinoma cells promotes chemotherapeutic agent-induced apoptosis during nutrient deprivation. *Oncol. Rep.* 39, 773–783. doi: 10.3892/or.2017.6115

He, H., Zeng, Q., Huang, G., Lin, Y., Lin, H., Liu, W., et al. (2019). Bone marrow mesenchymal stem cell transplantation exerts neuroprotective effects following cerebral ischemia/reperfusion injury by inhibiting autophagy via the PI3K/Akt pathway. *Brain Res.* 1707, 124–132. doi: 10.1016/j.brainres.2018.11.018

Hicks, S. D., and Miller, M. W. (2019). Ethanol-induced DNA repair in neural stem cells is transforming growth factor beta 1-dependent. *Exp. Neurol.* 317, 214–225. doi: 10.1016/j.expneurol.2019.02.003

Ho, T. T., Warr, M. R., Adelman, E. R., Lansinger, O. M., Flach, J., Verovskaya, E. V., et al. (2017). Autophagy maintains the metabolism and function of young and old stem cells. *Nature* 543, 205–210. doi: 10.1038/nature21388

Hou, J., Han, Z. P., Jing, Y. Y., Yang, X., Zhang, S. S., Sun, K., et al. (2013). Autophagy prevents irradiation injury and maintains stemness through decreasing ROS generation in mesenchymal stem cells. *Cell Death Dis.* 4:e844. doi: 10.1038/cddis.2013.338

Hung, H. C., Liu, C. C., Chuang, J. Y., Su, C. L., and Gean, P. W. (2020). Inhibition of sonic hedgehog signaling suppresses glioma stem-like cells likely through inducing autophagic cell death. *Front. Oncol.* 10:1233. doi: 10.3389/fonc.2020.01233

Hwang, J. R., Kim, W. Y., Cho, Y. J., Ryu, J. Y., Choi, J. J., Jeong, S. Y., et al. (2020). Chloroquine reverses chemoresistance via upregulation of p21(WAF1/CIP1) and autophagy inhibition in ovarian cancer. *Cell Death Dis.* 11:1034. doi: 10.1038/s41419-020-03242-x

Jang, J. E., Eom, J. I., Jeung, H. K., Cheong, J. W., Lee, J. Y., Kim, J. S., et al. (2017). AMPK-ULK1-mediated autophagy confers resistance to BET inhibitor JQ1 in acute myeloid leukemia stem cells. *Clin. Cancer Res.* 23, 2781–2794. doi: 10.1158/1078-0432.CCR-16-1903

Jang, J. E., Eom, J. I., Jeung, H. K., Chung, H., Kim, Y. R., Kim, J. S., et al. (2020). PERK/NRF2 and autophagy form a resistance mechanism against G9a inhibition in leukemia stem cells. *J. Exp. Clin. Cancer Res.* 39:66. doi: 10.1186/s13046-020-01565-3

Jung, S., Choe, S., Woo, H., Jeong, H., An, H. K., Moon, H., et al. (2020). Autophagic death of neural stem cells mediates chronic stress-induced decline of adult hippocampal neurogenesis and cognitive deficits. *Autophagy* 16, 512–530. doi: 10.1080/15548627.2019.1630222

Koschade, S. E., and Brandts, C. H. (2020). Selective autophagy in normal and malignant hematopoiesis. *J. Mol. Biol.* 432, 261–282. doi: 10.1016/j.jmb.2019.06.025

Kuhikar, R., Khan, N., Philip, J., Melinkeri, S., Kale, V., and Limaye, L. (2020). Transforming growth factor beta1 accelerates and enhances in vitro red blood cell formation from hematopoietic stem cells by stimulating mitophagy. *Stem Cell Res. Ther.* 11:71. doi: 10.1186/s13287-020-01603-z

Lee, J., Liu, K., Stiles, B., and Ou, J. J. (2018). Mitophagy and hepatic cancer stem cells. *Autophagy* 14, 715–716. doi: 10.1080/15548627.2018.1425058

Lernoux, M., Schnekenburger, M., Losson, H., Vermeulen, K., Hahn, H., Gerard, D., et al. (2020). Novel HDAC inhibitor MAKV-8 and imatinib synergistically kill chronic myeloid leukemia cells via inhibition of BCR-ABL/MYC-signaling: effect on imatinib resistance and stem cells. *Clin. Epigenetics* 12, 69. doi: 10.1186/s13148-020-00839-z

Levy, A., Stedman, A., Deutsch, E., Donnadieu, F., Virgin, H. W., Sansonetti, P. J., et al. (2020). Innate immune receptor NOD2 mediates LGR5+ intestinal stem cell protection against ROS cytotoxicity via mitophagy stimulation. *Proc. Natl. Acad. Sci. U.S.A.* 117, 1994–2003. doi: 10.1073/pnas.1902788117

Levy, J. M. M., Towers, C. G., and Thorburn, A. (2017). Targeting autophagy in cancer. *Nat. Rev. Cancer* 17, 528–542. doi: 10.1038/nrc.2017.53

Li, D., Wu, Q. J., Bi, F. F., Chen, S. L., Zhou, Y. M., Zhao, Y., et al. (2016). Effect of the BRCA1-SIRT1-EGFR axis on cisplatin sensitivity in ovarian cancer. *Am. J. Transl. Res.* 8, 1601–1608.

Li, J., Hu, S. B., Wang, L. Y., Zhang, X., Zhou, X., Yang, B., et al. (2017). Autophagy-dependent generation of Axin2+ cancer stem-like cells promotes hepatocarcinogenesis in liver cirrhosis. *Oncogene* 36, 6725–6737. doi: 10.1038/onc.2017.272

Li, L. Q., Pan, D., Zhang, S. W., Xie, D. Y., Zheng, X. L., and Chen, H. (2018). Autophagy regulates chemoresistance of gastric cancer stem cells via the Notch signaling pathway. *Eur. Rev. Med. Pharmacol. Sci.* 22, 3402–3407.

Li, M., Lu, G., Hu, J., Shen, X., Ju, J., Gao, Y., et al. (2016). EVA1A/TMEM166 regulates embryonic neurogenesis by autophagy. *Stem Cell Rep.* 6, 396–410. doi: 10.1016/j.stemcr.2016.01.011

Li, X., He, S., and Ma, B. (2020). Autophagy and autophagy-related proteins in cancer. *Mol. Cancer* 19:12. doi: 10.1186/s12943-020-1138-4

Liang, D. H., Choi, D. S., Ensor, J. E., Kaipparettu, B. A., Bass, B. L., and Chang, J. C. (2016). The autophagy inhibitor chloroquine targets cancer stem cells in triple negative breast cancer by inducing mitochondrial damage and impairing DNA break repair. *Cancer Lett.* 376, 249–258. doi: 10.1016/j.canlet.2016.04.002

Liang, Q., Luo, Z., Zeng, J., Chen, W., Foo, S. S., Lee, S. A., et al. (2016). Zika virus NS4A and NS4B proteins deregulate Akt-mTOR signaling in human fetal neural stem cells to inhibit neurogenesis and induce autophagy. *Cell Stem Cell* 19, 663–671. doi: 10.1016/j.stem.2016.07.019

Lin, L., Li, C., Zhang, D., Yuan, M., Chen, C. H., and Li, M. (2020). Synergic effects of berberine and curcumin on improving cognitive function in an Alzheimer's disease mouse model. *Neurochem. Res.* 45, 1130–1141. doi: 10.1007/s11064-020-02992-6

Liu, F., Lee, J. Y., Wei, H., Tanabe, O., Engel, J. D., Morrison, S. J., et al. (2010). FIP200 is required for the cell-autonomous maintenance of fetal hematopoietic stem cells. *Blood* 116, 4806–4814. doi: 10.1182/blood-2010-06-288589

Liu, H., Liu, S., Qiu, X., Yang, X., Bao, L., Pu, F., et al. (2020). Donor MSCs release apoptotic bodies to improve myocardial infarction via autophagy regulation in recipient cells. *Autophagy* 16, 2140–2155. doi: 10.1080/15548627.2020.1717128

Liu, K., Lee, J., Kim, J. Y., Wang, L., Tian, Y., Chan, S. T., et al. (2017). Mitophagy controls the activities of tumor suppressor p53 to regulate hepatic cancer stem cells. *Mol. Cell* 68, 281–292. doi: 10.1016/j.molcel.2017.09.022

Liu, L., Jin, X., Hu, C. F., Li, R., Zhou, Z., and Shen, C. X. (2017). Exosomes derived from mesenchymal stem cells rescue myocardial ischaemia/reperfusion injury by inducing cardiomyocyte autophagy via AMPK and Akt pathways. *Cell. Physiol. Biochem.* 43, 52–68. doi: 10.1159/000480317

Lotsberg, M. L., Wnuk-Lipinska, K., Terry, S., Tan, T. Z., Lu, N., Trachsel-Moncho, L., et al. (2020). AXL targeting abrogates autophagic flux and induces immunogenic cell death in drug-resistant cancer cells. *J. Thoracic Oncol.* 15, 973–999. doi: 10.1016/j.jtho.2020.01.015

Ma, T. H., Li, J., Xu, Y., Yu, C., Xu, T., Wang, H. X., et al. (2015). Atg5-independent autophagy regulates mitochondrial clearance and is essential for iPSC reprogramming. *Nat. Cell Biol.* 17, 1379–1387. doi: 10.1038/ncb3256

Ma, X. L., Mao, G. M., Chang, R. L., Wang, F., Zhang, X. Y., and Kong, Z. L. (2021). Down-regulation of autophagy-associated protein increased acquired radio-resistance bladder cancer cells sensitivity to taxol. *Int. J. Radiat. Biol.* 97, 507–516. doi: 10.1080/09553002.2021.1872812

Martinez-Outschoorn, U. E., Pavlides, S., Howell, A., Pestell, R. G., Tanowitz, H. B., Sotgia, F., et al. (2011). Stromal-epithelial metabolic coupling in cancer: integrating autophagy and metabolism in the tumor microenvironment. *Int. J. Biochem. Cell Biol.* 43, 1045–1051. doi: 10.1016/j.biocel.2011.01.023

Martin-Maestro, P., Gargini, R., Sproul, A. A., Garcia, E., Anton, L. C., Noggle, S., et al. (2017). Mitophagy failure in fibroblasts and iPSC-Derived neurons of Alzheimer's disease-associated presenilin 1 mutation. *Front. Mol. Neurosci.* 10:291. doi: 10.3389/fnmol.2017.00291

Martin-Maestro, P., Sproul, A., Martinez, H., Paquet, D., Gerges, M., Noggle, S., et al. (2019). Autophagy induction by bexarotene promotes mitophagy in presenilin 1 familial Alzheimer's disease iPSC-Derived neural stem cells. *Mol. Neurobiol.* 56, 8220–8236. doi: 10.1007/s12035-019-01665-y

Matsui, Y., Kyoi, S., Takagi, H., Hsu, C. P., Hariharan, N., Ago, T., et al. (2008). Molecular mechanisms and physiological significance of autophagy during myocardial ischemia and reperfusion. *Autophagy* 4, 409–415. doi: 10.4161/auto.5638

Maycotte, P., Jones, K. L., Goodall, M. L., Thorburn, J., and Thorburn, A. (2015). Autophagy supports breast cancer stem cell maintenance by regulating IL6 secretion. *Mol. Cancer Res.* 13, 651–658. doi: 10.1158/1541-7786.MCR-14-0487

Michaud, M., Martins, I., Sukkurwala, A. Q., Adjemian, S., Ma, Y. T., Pellegatti, P., et al. (2011). Autophagy-Dependent anticancer immune responses induced by chemotherapeutic agents in mice. *Science* 334, 1573–1577. doi: 10.1126/science.1208347

Moore, A. H., and O'Banion, M. K. (2002). Neuroinflammation and anti-inflammatory therapy for Alzheimer's disease. *Adv. Drug Deliv. Rev.* 54, 1627–1656. doi: 10.1016/s0169-409x(02)00162-x

Mortensen, M., Soilleux, E. J., Djordjevic, G., Tripp, R., Lutteropp, M., Sadighi-Akha, E., et al. (2011). The autophagy protein Atg7 is essential for hematopoietic stem cell maintenance. *J. Exp. Med.* 208, 455–467. doi: 10.1084/jem.20101145

Murakami, K., Kurotaki, D., Kawase, W., Soma, S., Fukuchi, Y., Kunimoto, H., et al. (2021). OGT regulates hematopoietic stem cell maintenance via PINK1-dependent mitophagy. *Cell Rep.* 34:108579. doi: 10.1016/j.celrep.2020.108579

Nixon, R. A., and Yang, D. S. (2011). Autophagy failure in Alzheimer's disease-locating the primary defect. *Neurobiol. Dis.* 43, 38–45. doi: 10.1016/j.nbd.2011.01.021

Obernier, K., and Alvarez-Buylla, A. (2019). Neural stem cells: origin, heterogeneity and regulation in the adult mammalian brain. *Development* 146:dev156059. doi: 10.1242/dev.156059

Ojha, R., Jha, V., Singh, S. K., and Bhattacharyya, S. (2014). Autophagy inhibition suppresses the tumorigenic potential of cancer stem cell enriched side population in bladder cancer. *Biochim. Biophys. Acta Mol. Basis Dis.* 1842, 2073–2086. doi: 10.1016/j.bbadis.2014.07.007

Ojha, R., Singh, S. K., and Bhattacharyya, S. (2016). JAK-mediated autophagy regulates sternness and cell survival in cisplatin resistant bladder cancer cells. *Biochim. Biophys. Acta Gen. Subj.* 1860, 2484–2497. doi: 10.1016/j.bbagen.2016.07.021

Pan, X. W., Li, U., Huang, Y., Huang, H., Xu, D. F., Gao, Y., et al. (2016). Icaritin acts synergistically with epirubicin to suppress bladder cancer growth through inhibition of autophagy. *Oncol. Rep.* 35, 334–342. doi: 10.3892/or.2015.4335

Park, H. J., Shin, J. Y., Kim, H. N., Oh, S. H., and Lee, P. H. (2014). Neuroprotective effects of mesenchymal stem cells through autophagy modulation in a parkinsonian model. *Neurobiol. Aging* 35, 1920–1928. doi: 10.1016/j.neurobiolaging.2014.01.028

Pavlides, S., Whitaker-Menezes, D., Castello-Cros, R., Flomenberg, N., Witkiewicz, A. K., Frank, P. G., et al. (2009). The reverse Warburg effect: aerobic glycolysis in cancer associated fibroblasts and the tumor stroma. *Cell Cycle* 8, 3984–4001. doi: 10.4161/cc.8.23.10238

Pei, S., Minhajuddin, M., Adane, B., Khan, N., Stevens, B. M., Mack, S. C., et al. (2018). AMPK/FIS1-mediated mitophagy is required for self-renewal of human AML stem cells. *Cell Stem Cell* 23, 86–100. doi: 10.1016/j.stem.2018.05.021

Plaks, V., Kong, N., and Werb, Z. (2015). The cancer stem cell niche: how essential is the niche in regulating stemness of tumor cells? *Cell Stem Cell* 16, 225–238. doi: 10.1016/j.stem.2015.02.015

Qin, T., Cheng, L., Xiao, Y., Qian, W., Li, J., Wu, Z., et al. (2020). NAF-1 inhibition by resveratrol suppresses cancer stem cell-like properties and the invasion of pancreatic cancer. *Front. Oncol.* 10:1038. doi: 10.3389/fonc.2020.01038

Rahman, M. A., Cho, Y., Nam, G., and Rhim, H. (2021). Antioxidant Compound, Oxyresveratrol, Inhibits APP Production through the AMPK/ULK1/mTOR-Mediated Autophagy Pathway in Mouse Cortical Astrocytes. *Antioxidants* 10:408. doi: 10.3390/antiox10030408

Rausch, V., Liu, L., Apel, A., Rettig, T., Gladkich, J., Labsch, S., et al. (2012). Autophagy mediates survival of pancreatic tumour-initiating cells in a hypoxic microenvironment. *J. Pathol.* 227, 325–335. doi: 10.1002/path.3994

Rehman, J. (2010). Empowering self-renewal and differentiation: the role of mitochondria in stem cells. *J. Mol. Med. (Berl)* 88, 981–986. doi: 10.1007/s00109-010-0678-2

Ricardo, S., Vieira, A. F., Gerhard, R., Leitao, D., Pinto, R., Cameselle-Teijeiro, J. F., et al. (2011). Breast cancer stem cell markers CD44, CD24 and ALDH1: expression distribution within intrinsic molecular subtype. *J. Clin. Pathol.* 64, 937–946. doi: 10.1136/jcp.2011.090456

Sailaja, B. S., He, X. C., and Li, L. H. (2016). The regulatory niche of intestinal stem cells. *J. Physiol. Lond.* 594, 4827–4836. doi: 10.1113/jp271931

Salemi, S., Yousefi, S., Constantinescu, M. A., Fey, M. F., and Simon, H. U. (2012). Autophagy is required for self-renewal and differentiation of adult human stem cells. *Cell Res.* 22, 432–435. doi: 10.1038/cr.2011.200

Sbrana, F. V., Cortini, M., Avnet, S., Perut, F., Columbaro, M., De Milito, A., et al. (2016). The role of autophagy in the maintenance of stemness and differentiation of mesenchymal stem cells. *Stem Cell Rev. Rep.* 12, 621–633. doi: 10.1007/s12015-016-9690-4

Scrivo, A., Bourdenx, M., Pampliega, O., and Cuervo, A. M. (2018). Selective autophagy as a potential therapeutic target for neurodegenerative disorders. *Lancet Neurol.* 17, 802–815. doi: 10.1016/s1474-4422(18)30238-2

Seranova, E., Palhegyi, A. M., Verma, S., Dimova, S., Lasry, R., Naama, M., et al. (2020). Human induced pluripotent stem cell models of neurodegenerative disorders for studying the biomedical implications of autophagy. *J. Mol. Biol.* 432, 2754–2798. doi: 10.1016/j.jmb.2020.01.024

Shi, L., Sun, G., and Zhu, H. F. (2020). Demethoxycurcumin analogue DMC-BH inhibits orthotopic growth of glioma stem cells by targeting JNK/ERK signaling. *Aging Us* 12, 14718–14735. doi: 10.18632/aging.103531

Shin, J. Y., and Lee, P. H. (2020). Mesenchymal stem cells modulate misfolded alpha-synuclein in parkinsonian disorders: a multitarget disease-modifying strategy. *Stem Cell Res.* 47:101908. doi: 10.1016/j.scr.2020.101908

Shin, J. Y., Park, H. J., Kim, H. N., Oh, S. H., Bae, J. S., Ha, H. J., et al. (2014). Mesenchymal stem cells enhance autophagy and increase beta-amyloid clearance in Alzheimer disease models. *Autophagy* 10, 32–44. doi: 10.4161/auto.26508

Smith, A. G., and Macleod, K. F. (2019). Autophagy, cancer stem cells and drug resistance. *J. Pathol.* 247, 708–718. doi: 10.1002/path.5222

Sousa, C. M., Biancur, D. E., Wang, X. X., Halbrook, C. J., Sherman, M. H., Zhang, L., et al. (2016). Pancreatic stellate cells support tumour metabolism through autophagic alanine secretion. *Nature* 536, 479–483. doi: 10.1038/nature19084

Spinello, I., Saulle, E., Quaranta, M. T., Pasquini, L., Pelosi, E., Castelli, G., et al. (2019). The small-molecule compound AC-73 targeting CD147 inhibits leukemic cell proliferation, induces autophagy and increases the chemotherapeutic sensitivity of acute myeloid leukemia cells. *Haematologica* 104, 973–985. doi: 10.3324/haematol.2018.199661

Suetsugi, A., Nagaki, M., Aoki, H., Motohashi, T., Kunisada, T., and Moriwaki, H. (2006). Characterization of CD133(+) hepatocellular carcinoma cells as cancer stem/progenitor cells. *Biochem. Biophys. Res. Commun.* 351, 820–824. doi: 10.1016/j.bbrc.2006.10.128

Sulaiman, A., McGarry, S., Lam, K. M., El-Sahli, S., Chambers, J., Kaczmarek, S., et al. (2018). Co-inhibition of mTORC1, HDAC and ESR1alpha retards the growth of triple-negative breast cancer and suppresses cancer stem cells. *Cell Death Dis.* 9:815. doi: 10.1038/s41419-018-0811-7

Takahashi, K., and Yamanaka, S. (2006). Induction of pluripotent stem cells from mouse embryonic and adult fibroblast cultures by defined factors. *Cell* 126, 663–676. doi: 10.1016/j.cell.2006.07.024

Takubo, K., Nagamatsu, G., Kobayashi, C. I., Nakamura-Ishizu, A., Kobayashi, H., Ikeda, E., et al. (2013). Regulation of glycolysis by Pdk functions as a metabolic checkpoint for cell cycle quiescence in hematopoietic stem cells. *Cell Stem Cell* 12, 49–61. doi: 10.1016/j.stem.2012.10.011

Tiwari, S. K., Dang, J. W., Lin, N., Qin, Y., Wang, S., and Rana, T. M. (2020). Zika virus depletes neural stem cells and evades selective autophagy by suppressing the Fanconi anemia protein FANCC. *EMBO Rep.* 21:e49183. doi: 10.15252/embr.201949183

Tonelli, F. M., Santos, A. K., Gomes, D. A., da Silva, S. L., Gomes, K. N., Ladeira, L. O., et al. (2012). Stem cells and calcium signaling. *Adv. Exp. Med. Biol.* 740, 891–916. doi: 10.1007/978-94-007-2888-2_40

Trentesaux, C., Fraudeau, M., Pitasi, C. L., Lemarchand, J., Jacques, S., Duche, A., et al. (2020). Essential role for autophagy protein ATG7 in the maintenance of intestinal stem cell integrity. *Proc. Natl. Acad. Sci. U.S.A.* 117, 11136–11146. doi: 10.1073/pnas.1917174117

Ugland, H., Naderi, S., Brech, A., Collas, P., and Blomhoff, H. K. (2011). cAMP induces autophagy via a novel pathway involving ERK, cyclin E and Beclin 1. *Autophagy* 7, 1199–1211. doi: 10.4161/auto.7.10.16649

Vazin, T., and Schaffer, D. V. (2010). Engineering strategies to emulate the stem cell niche. *Trends Biotechnol.* 28, 117–124. doi: 10.1016/j.tibtech.2009.11.008

Vining, K. H., and Mooney, D. J. (2017). Mechanical forces direct stem cell behaviour in development and regeneration. *Nat. Rev. Mol. Cell Biol.* 18, 728–742. doi: 10.1038/nrm.2017.108

Wang, C., Liang, C. C., Bian, Z. C., Zhu, Y., and Guan, J. L. (2013). FIP200 is required for maintenance and differentiation of postnatal neural stem cells. *Nat. Neurosci.* 16, 532–542. doi: 10.1038/nn.3365

Wang, C., Yeo, S., Haas, M. A., and Guan, J. L. (2017). Autophagy gene FIP200 in neural progenitors non-cell autonomously controls differentiation by regulating microglia. *J. Cell Biol.* 216, 2581–2596. doi: 10.1083/jcb.201609093

Wang, J. Y., Liu, D. D., Sun, Z. W., Ye, T., Li, J. Y., Zeng, B., et al. (2021). Autophagy augments the self-renewal of lung cancer stem cells by the degradation of ubiquitinated p53. *Cell Death Dis.* 12:98. doi: 10.1038/s41419-021-03392-6

Wang, L., Ye, X., and Zhao, T. (2019). The physiological roles of autophagy in the mammalian life cycle. *Biol. Rev. Camb. Philos. Soc.* 94, 503–516. doi: 10.1111/brv.12464

Wang, S. M., and Gu, K. S. (2018). Insulin-like growth factor 1 inhibits autophagy of human colorectal carcinoma drug-resistant cells via the protein kinase B/mammalian target of rapamycin signaling pathway. *Mol. Med. Rep.* 17, 2952–2956. doi: 10.3892/mmr.2017.8272

Wang, X.-J., and Li, Q.-P. (2007). The roles of mesenchymal stem cells (MSCs) therapy in ischemic heart diseases. *Biochem. Biophys. Res. Commun.* 359, 189–193. doi: 10.1016/j.bbrc.2007.05.112

Wang, Y., Liang, G., Liang, S., Mund, R., Shi, Y., and Wei, H. (2020). Dantrolene ameliorates impaired neurogenesis and synaptogenesis in induced pluripotent stem cell lines derived from patients with Alzheimer's disease. *Anesthesiology* 132, 1062–1079. doi: 10.1097/ALN.0000000000003224

Wang, Y., Xu, W. B., Yan, Z. X., Zhao, W. L., Mi, J. Q., Li, J. M., et al. (2018). Metformin induces autophagy and G0/G1 phase cell cycle arrest in myeloma by targeting the AMPK/mTORC1 and mTORC2 pathways. *J. Exp. Clin. Cancer Res.* 37:63. doi: 10.1186/s13046-018-0731-5

Wani, A., Al Rihani, S. B., Sharma, A., Weadick, B., Govindarajan, R., Khan, S. U., et al. (2021). Crocetin promotes clearance of amyloid-beta by inducing autophagy via the STK11/LKB1-mediated AMPK pathway. *Autophagy*. doi: 10.1080/15548627.2021.1872187 [Epub ahead of print].

Watson, A. S., Riffelmacher, T., Stranks, A., Williams, O., De Boer, J., Cain, K., et al. (2015). Autophagy limits proliferation and glycolytic metabolism in acute myeloid leukemia. *Cell Death Discov.* 1:15008. doi: 10.1038/cddiscovery.2015.8

Wiener, Z., Hogstrom, J., Hyvonen, V., Band, A. M., Kallio, P., Holopainen, T., et al. (2014). Prox1 promotes expansion of the colorectal cancer stem cell population to fuel tumor growth and ischemia resistance. *Cell Rep.* 8, 1943–1956. doi: 10.1016/j.celrep.2014.08.034

Xie, J., Li, L., Deng, S., Chen, J., Gu, Q., Su, H., et al. (2020). Slit2/Robo1 mitigates DSS-induced ulcerative colitis by activating autophagy in intestinal stem cell. *Int. J. Biol. Sci.* 16, 1876–1887. doi: 10.7150/ijbs.42331

Xin, L., Zhou, Q., Yuan, Y. W., Zhou, L. Q., Liu, L., Li, S. H., et al. (2019). METase/lncRNA HULC/FoxM1 reduced cisplatin resistance in gastric cancer by suppressing autophagy. *J. Cancer Res. Clin. Oncol.* 145, 2507–2517. doi: 10.1007/s00432-019-03015-w

Xu, L., Yuan, N., Liu, H., Fang, Y. X., Ge, C., Xu, F., et al. (2020). Bafilomycin A1 targets patient-derived CD34(+)CD19(+) leukemia stem cells. *Haematologica* 105, E17–E21. doi: 10.3324/haematol.2018.207258

Xu, X., Duan, S., Yi, F., Ocampo, A., Liu, G. H., and Izpisua Belmonte, J. C. (2013). Mitochondrial regulation in pluripotent stem cells. *Cell Metab.* 18, 325–332. doi: 10.1016/j.cmet.2013.06.005

Xue, H., Yuan, G., Guo, X., Liu, Q. L., Zhang, J. S., Gao, X., et al. (2016). A novel tumor-promoting mechanism of IL6 and the therapeutic efficacy of tocilizumab: hypoxia-induced IL6 is a potent autophagy initiator in glioblastoma via the p-STAT3-MIR155-3p-CREBRF pathway. *Autophagy* 12, 1129–1152. doi: 10.1080/15548627.2016.1178446

Yanai, R., Tetsuo, F., Ito, S., Itsumi, M., Yoshizumi, J., Maki, T., et al. (2019). Extracellular calcium stimulates osteogenic differentiation of human adipose-derived stem cells by enhancing bone morphogenetic protein-2 expression. *Cell Calcium* 83:102058. doi: 10.1016/j.ceca.2019.102058

Yang, M. C., Wang, H. C., Hou, Y. C., Tung, H. L., Chiu, T. J., and Shan, Y. S. (2015). Blockade of autophagy reduces pancreatic cancer stem cell activity and potentiates the tumoricidal effect of gemcitabine. *Mol. Cancer* 14:179. doi: 10.1186/s12943-015-0449-3

Yao, Z., Yang, Z. Q., Chen, F. J., Jiang, Y., Fu, C. Z., Wang, Y., et al. (2020). Autophagy is essential for the endothelial differentiation of breast cancer stem-like cells. *Int. J. Mol. Med.* 45, 255–264. doi: 10.3892/ijmm.2019.4399

Yazdankhah, M., Farioli-Vecchioli, S., Tonchev, A. B., Stoykova, A., and Cecconi, F. (2014). The autophagy regulators Ambra1 and Beclin 1 are required for adult neurogenesis in the brain subventricular zone. *Cell Death Dis.* 5:e1403. doi: 10.1038/cddis.2014.358

Yeo, S. K., Wen, J., Chen, S., and Guan, J. L. (2016). Autophagy differentially regulates distinct breast cancer stem-like cells in murine models via EGFR/Stat3 and Tgfbeta/Smad signaling. *Cancer Res.* 76, 3397–3410. doi: 10.1158/0008-5472.CAN-15-2946

You, Y., Bi, F. F., Jiang, Y., Xu, Y. T., An, Y. Y., Li, D., et al. (2019). BRCA1 affects the resistance and stemness of SKOV3-derived ovarian cancer stem cells by regulating autophagy. *Cancer Med.* 8, 656–668. doi: 10.1002/cam4.1975

Yuan, N., Song, L., Lin, W., Cao, Y., Xu, F., Liu, S., et al. (2015). Autophagy collaborates with ubiquitination to downregulate oncoprotein E2A/Pbx1 in B-cell acute lymphoblastic leukemia. *Blood Cancer J.* 5:e274. doi: 10.1038/bcj.2014.96

Yun, C. W., Jeon, J., Go, G., Lee, J. H., and Lee, S. H. (2021). The dual role of autophagy in cancer development and a therapeutic strategy for cancer by targeting autophagy. *Int. J. Mol. Sci.* 22:179. doi: 10.3390/ijms22010179

Zhang, J., Wu, K., Xiao, X., Liao, J., Hu, Q., Chen, H., et al. (2015). Autophagy as a regulatory component of erythropoiesis. *Int. J. Mol. Sci.* 16, 4083–4094. doi: 10.3390/ijms16024083

Zhang, L., Rastgoo, N., Wu, J., Zhang, M., Pourabdollah, M., Zacksenhaus, E., et al. (2020). MARCKS inhibition cooperates with autophagy antagonists to potentiate the effect of standard therapy against drug-resistant multiple myeloma. *Cancer Lett.* 480, 29–38. doi: 10.1016/j.canlet.2020.03.020

Zhang, P., Holowatyj, A. N., Roy, T., Pronovost, S. M., Marchetti, M., Liu, H., et al. (2019a). An SH3PX1-dependent endocytosis-autophagy network restrains intestinal stem cell proliferation by counteracting EGFR-ERK signaling. *Dev. Cell* 49, 574–589.e575. doi: 10.1016/j.devcel.2019.03.029

Zhang, P., Holowatyj, A. N., Ulrich, C. M., and Edgar, B. A. (2019b). Tumor suppressive autophagy in intestinal stem cells controls gut homeostasis. *Autophagy* 15, 1668–1670. doi: 10.1080/15548627.2019.1633863

Zhang, Z., Yang, M., Wang, Y., Wang, L., Jin, Z., Ding, L., et al. (2016). Autophagy regulates the apoptosis of bone marrow-derived mesenchymal stem cells under hypoxic condition via AMP-activated protein kinase/mammalian target of rapamycin pathway. *Cell Biol. Int.* 40, 671–685. doi: 10.1002/cbin.10604

Zheng, Y., Liu, L., Wang, Y., Xiao, S., Mai, R. K., Zhu, Z. F., et al. (2021). Glioblastoma stem cell (GSC)-derived PD-L1-containing exosomes activates AMPK/ULK1 pathway mediated autophagy to increase temozolomide-resistance in glioblastoma. *Cell Biosci.* 11:63. doi: 10.1186/s13578-021-00575-8

Zhong, Z. Y., Sanchez-Lopez, E., and Karin, M. (2016). Autophagy, inflammation, and immunity: a troika governing cancer and its treatment. *Cell* 166, 288–298. doi: 10.1016/j.cell.2016.05.051

Zhu, H. T., Wang, D. Q., Liu, Y. F., Su, Z. L., Zhang, L. R., Chen, F. F., et al. (2013). Role of the Hypoxia-inducible factor-1 alpha induced autophagy in the conversion of non-stem pancreatic cancer cells into CD133(+) pancreatic cancer stem-like cells. *Cancer Cell Int.* 13:119. doi: 10.1186/1475-2867-13-119

Zhu, H. T., Wang, D. Q., Zhang, L. R., Xie, X. D., Wu, Y. Y., Liu, Y. F., et al. (2014). Upregulation of autophagy by hypoxia-inducible factor-1 alpha promotes EMT and metastatic ability of CD133(+) pancreatic cancer stem-like cells during intermittent hypoxia. *Oncol. Rep.* 32, 935–942. doi: 10.3892/or.2014.3298

Zhu, J., Huang, G., Hua, X., Li, Y., Yan, H., Che, X., et al. (2019). CD44s is a crucial ATG7 downstream regulator for stem-like property, invasion, and lung metastasis of human bladder cancer (BC) cells. *Oncogene* 38, 3301–3315. doi: 10.1038/s41388-018-0664-7

Zon, L. I. (2008). Intrinsic and extrinsic control of haematopoietic stem-cell self-renewal. *Nature* 453, 306–313. doi: 10.1038/nature07038

Zuo, R., Wang, Y., Li, J., Wu, J., Wang, W., Li, B., et al. (2019). Rapamycin induced autophagy inhibits inflammation-mediated endplate degeneration by enhancing Nrf2/Keap1 signaling of cartilage endplate stem cells. *Stem Cells* 37, 828–840. doi: 10.1002/stem.2999

Conflict of Interest: The authors declare that the research was conducted in the absence of any commercial or financial relationships that could be construed as a potential conflict of interest.

Publisher's Note: All claims expressed in this article are solely those of the authors and do not necessarily represent those of their affiliated organizations, or those of the publisher, the editors and the reviewers. Any product that may be evaluated in this article, or claim that may be made by its manufacturer, is not guaranteed or endorsed by the publisher.

frontiers in Cell and Developmental Biology

REVIEW
published: 12 August 2021
doi: 10.3389/fcell.2021.713434

In vitro Generation of Megakaryocytes and Platelets

*Huicong Liu, Jiaqing Liu, Lingna Wang and Fangfang Zhu**

School of Biomedical Engineering, Shanghai Jiao Tong University, Shanghai, China

Platelets, the tiny anucleate cells responsible for stopping bleeding through thrombosis, are derived from hematopoietic stem cells through a series of differentiation steps. Thrombocytopenia, characterized by abnormally low blood platelet counts, may arise from cancer therapies, trauma, sepsis, as well as blood disorders, and could become a life-threatening problem. Platelet transfusion is the most effective strategy to treat thrombocytopenia, however, the source of platelets is in great shortage. Therefore, *in vitro* generation of platelets has become an important topic and numerous attempts have been made toward generating platelets from different types of cells, including hematopoietic stem cells, pluripotent stem cells, fibroblast cells, and adipose-derived cells. In this review, we will detail the efforts made to produce, in the *in vitro* culture, platelets from these different cell types. Importantly, as transfusion medicine requires a huge number of platelets, we will highlight some studies on producing platelets on a large scale. Although new methods of gene manipulation, new culture conditions, new cytokines and chemical compounds have been introduced in platelet generation research since the first study of hematopoietic stem cell-derived platelets nearly 30 years ago, limited success has been achieved in obtaining truly mature and functional platelets *in vitro*, indicating the studies of platelets fall behind those of other blood cell types. This is possibly because megakaryocytes, which produce platelets, are very rare in blood and marrow. We have previously developed a platform to identify new extrinsic and intronic regulators for megakaryocytic lineage development, and in this review, we will also cover our effort on that. In summary, stem cell-based differentiation is a promising way of generating large-scale platelets to meet clinical needs, and continuous study of the cellular development of platelets will greatly facilitate this.

Keywords: platelet, megakaryocyte, hematopoietic stem cell, pluripotent stem cell, lineage reprogramming, transcription factor, histone deacetylase (HDAC), GABA

OPEN ACCESS

Edited by:
Jianjun Zhou,
Tongji University, China

Reviewed by:
Gianandrea Pasquinelli,
University of Bologna, Italy
Yongping Jiang,
Chinese Academy of Medical Sciences and Peking Union Medical College, China

****Correspondence:***
Fangfang Zhu
zhuff@sjtu.edu.cn

Specialty section:
This article was submitted to Stem Cell Research, a section of the journal Frontiers in Cell and Developmental Biology

Received: *23 May 2021*
Accepted: *26 July 2021*
Published: *12 August 2021*

Citation:
Liu H, Liu J, Wang L and Zhu F (2021) In vitro Generation of Megakaryocytes and Platelets. Front. Cell Dev. Biol. 9:713434. doi: 10.3389/fcell.2021.713434

INTRODUCTION

Platelets, small and anucleate cells in the blood, are multifunctional and implicated in many pathophysiological processes, including hemostasis, thrombosis, vessel constriction and repair, and inflammations during host defense and tumor growth/metastasis (Harrison, 2005). Platelets, generated from hematopoietic stem cell-derived megakaryocytes, have a short lifespan of only 8–10 days (McArthur et al., 2018), and therefore in healthy persons, new platelets have to be produced constantly to maintain a normal level. Thrombocytopenia, defined by a platelet count of $<1.5 \times 10^{11}$/L in the blood, is not only commonly seen in some hematological diseases, for

example, leukemia, bone marrow abnormalities, and hematopoietic aplastic anemia (Squires, 2015), but also may arise from multiple other conditions including connective tissue diseases, critical care medicine, hepatopathy, infectious illnesses, as well as cancer radiotherapy and chemotherapy (Robb and Begley, 1997). To reduce the mortality caused by bleeding in these situations, platelet transfusion has become an effective and irreplaceable treatment strategy.

Currently, platelets used in the clinic are provided solely through blood donations. With the rising population of hematological cancer patients and the development of clinical treatment options for various diseases, demands for platelets in transfusion medicine have been steadily growing in the aging society. However, blood donations have not been increased proportionally, therefore, the severe shortage of platelets has become a worldwide problem. To address this issue, researchers have been focusing on pursuing alternative strategies to obtain platelets. Since the first report of *in vitro* generation of platelets from hematopoietic stem cells by Choi et al. (1995) about 30 years ago, efforts have been made to derive, from *in vitro* culture, human platelets from different types of cells, including hematopoietic stem cells, human embryonic stem cells, human induced pluripotent stem cells, fibroblast cells, and adipose tissue-derived cells. Among all these sources, stem cells have attracted the most attention because they secure an unlimited supply. To date, existing protocols have been established by the ectopic expression of key transcription factors (TFs) which control megakaryocyte and platelet cell fate during development, by the activation or inhibition of external signals with cytokines or chemical compounds, as well as by the co-culture with stromal cells or in 3D conditions to provide an environment similar to that during embryonic development. The ability to regenerate platelets *in vitro* would address the urgent and unmet needs of platelet supply in clinics and provide a promising way to solve the life-threatening bleeding problem in different diseases. Besides, these methods also have significant advantages over the current donor-dependent program, in terms of variations between donors, number of cells that could be obtained, risk of bacteria and virus contamination, cell viability, and storage, etc. **Figure 1** shows how different cell sources could be used *in vitro* for platelet-required clinical applications.

However, only limited success has been achieved so far in producing truly mature and functional platelets from these *in vitro* cultures. With various differentiation methods, platelets could be generated, and they are phenotypically similar to plasma-derived platelets, however, the *in vivo* functions of these platelets were either not tested or not as good as plasma-derived platelets. More importantly, their lifespan is much shorter than that of primary platelets. Therefore, platelet differentiation protocols require further optimization. One of the possible reasons why *in vitro* derived platelets are not as expected is our lack of knowledge on how megakaryocyte and platelet generation from hematopoietic stem cells is precisely regulated during development. Megakaryocytes in the blood are very rare, and in bone marrow, they represent only 0.01% of all nucleated cells (Nakeff and Maat, 1974), which makes it difficult to isolate and culture these cells, and therefore, the research on megakaryocyte generation and differentiation falls far behind that of other hematopoietic cell types. We have described the identification of new intrinsic and extrinsic regulators for megakaryocyte development with an established platform that is designed to identify the hematopoietic regulatory network by combining the Gene Expression Commons (GeXC), which profiles the absolute expression of any gene on the microarray (Seita et al., 2012), CRISPR/Cas9 mediated gene knockout screening and lentivirus-mediated gene overexpression.

In this review, we will first summarize the existing research progress on *in vitro* generation of platelets from stem cells and other cell types and then discuss the promising solutions to hit the final goal of generating large-scale mature platelets *in vitro* for basic research and clinical applications.

CELL SOURCES FOR *IN VITRO* MEGAKARYOCYTE AND PLATELET GENERATION

Different cells have been used as the starting materials to derive megakaryocytes and platelets *in vitro*, and these cells belong to two types: embryonic or adult stem cells including hematopoietic stem cells and human pluripotent stem cells which can directly differentiate into megakaryocytes and platelets naturally, while the other cell types including fibroblasts and adipose tissue-derived cells that are not its natural progenitors and require a conversion of cell fates from one to another. Stem cells as the cell source for platelets usually have the advantages in terms of scalability, ease of genetic modification, and platelet functions. However, different stem cells have their unique characteristics, and may require different methods to be directed to generate platelets. **Table 1** summarizes current progress in platelet production *in vitro* from these different types of cells, which covers differentiation methods, efficiency, etc., and although all groups successfully characterized the generated megakaryocytes and platelets with various *in vitro* assays, functional tests in animal models (mouse, rabbit, etc.) were performed in only one third of these studies. Of note, Guan et al. (2017) not only demonstrated generated human megakaryocytes could engraft in mice and produce functional platelets, but also showed platelet recovery in non-human primates that were transplanted with autologous megakaryocytes, bringing one step closer to the clinical applications of human platelet transfusion.

Generation of Platelets From Hematopoietic Stem Cells

Hematopoietic stem cells (HSCs), which could be found in bone marrow (BM), peripheral blood (PB), and cord blood (CB) after birth, continuously divide to provide more hematopoietic stem and progenitor cells to balance self-renewal and differentiation. Through multiple steps, HSCs differentiate into multipotent progenitors (MPPs), common myeloid progenitors (CMPs), megakaryocyte-erythroid progenitors (MEPs), megakaryocyte progenitors (MkPs), and then megakaryocytes (MKs), which finally mature and produce

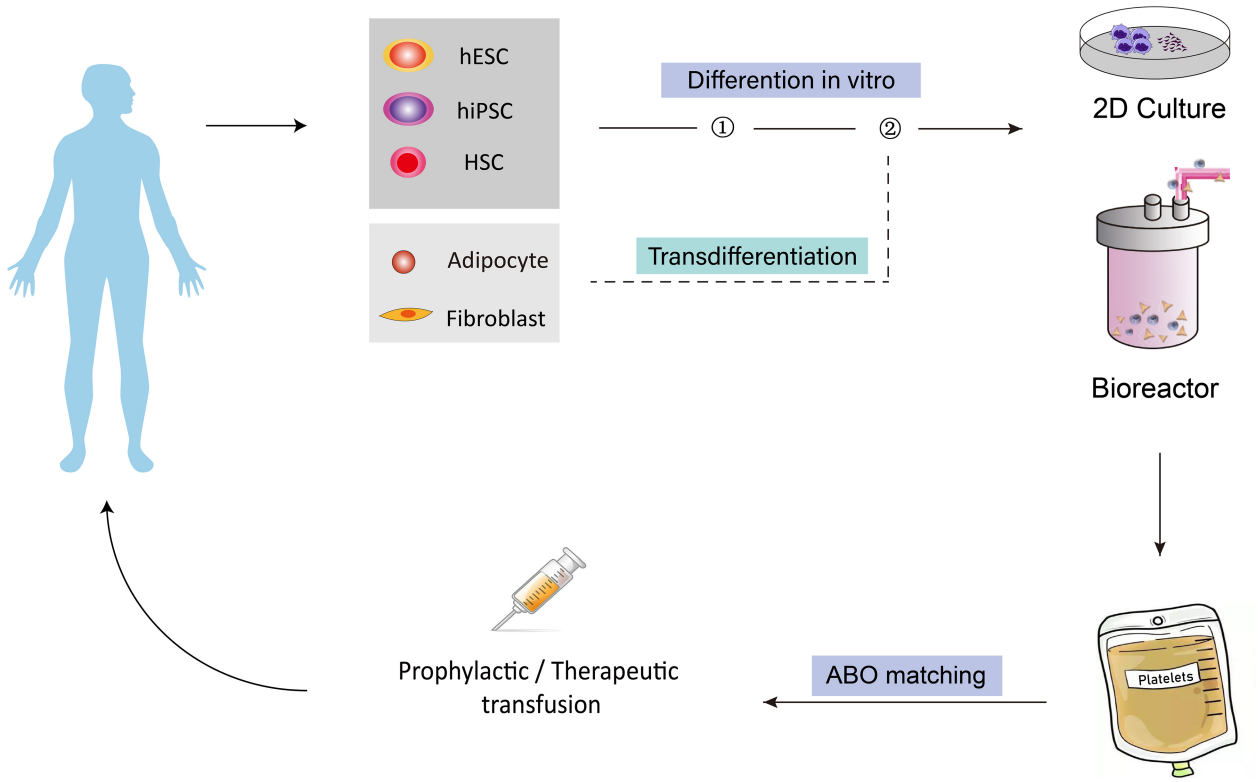

FIGURE 1 | Overview of the concept of generating human platelets *in vitro* for clinical applications. Different cell types, including HSCs, hESCs, hiPSCs, fibroblasts and adipocyte-derived cells, could be induced to differentiate into MkPs/MKs, then bioreactors could be introduced to produce platelet from MK on a larger scale for transfusion purpose. The generated platelets could finally be injected into human for platelet-related diseases. HSCs, hematopoietic stem cells; hESCs, human embryonic stem cells; hiPSCs, human induced pluripotent stem cells; MkPs, megakaryocyte progenitors; MKs, megakaryocytes.

functional platelets (Seita and Weissman, 2010; Machlus and Italiano, 2013). Therefore, the generation of HSC-derived platelets seems to be a natural process, and the earliest attempts to create platelets *in vitro* were using CD34-enriched HSCs as the starting materials. Choi et al. (1995) first described a method in which isolated HSCs from PB were cultured in conditions supplemented with human and aplastic canine serum to induce MK differentiation. Aplastic canine serum was then removed from the culture medium in which plasma factors from human serum promoted MK differentiation to platelets, which exhibited a similar ultrastructure to platelets isolated from plasma and could be aggregated after platelet agonist adenosine diphosphate (ADP) treatment. However, the differentiation efficiency is very low, with only 3×10^6 mature MKs obtained from one leukapheresis unit, and only about 40% MKs could generate platelets upon further differentiation (Choi et al., 1995).

Various optimizations were later tried to improve the differentiation efficiency. Norol et al. (1998) searched for cytokines that could stimulate the generation of MKs and platelets from HSCs. They tested the functions of megakaryocyte growth and development factor (MGDF, now commonly known as thrombopoietin, TPO), the ligand for Mpl, either alone or in various combinations with stem cell factor (SCF), interleukin-3 (IL-3), and IL-6. They found both TPO alone and its combination with these three cytokines accelerated MK differentiation, while TPO alone was able to promote platelet production by 10-fold, highlighting the critical role of TPO in MK differentiation, maturation, and platelet generation (Norol et al., 1998). Currently, TPO is regarded as one of the most important cytokines in megakaryocytopoiesis and thrombopoiesis. Proulx et al. (2004), in an interesting study, showed the unexpected effect of elevated temperature on differentiation of HSCs to MK-committed cells. Compared to those at 37°C, the differentiation cultures maintained at 39°C promoted the proliferation and differentiation efficiency of HSCs, accelerated MK maturation by 3–4 days, and improved platelets output by more than 15-fold (Proulx et al., 2004). Later, the 3D culture method, specifically the roller-bottle cell culture system, was also found to be able to improve the efficiency of platelet generation from CB HSCs by a few folds, compared with the routinely used static culture condition, either in a small research scale (Yang et al., 2016) or in a Good Manufacturing Practice (GMP) standard culture (Guan et al., 2020).

To fulfill transfusion purposes, attempts were also made to generate platelets on a large scale. Matsunaga et al. (2006) reported a 33-day three-phase culture system using HSCs isolated from CB. By combining co-culture with telomerase gene-transduced human stromal cells for MK differentiation and

TABLE 1 | Summary of current methods for *in vitro* generation of megakaryocytes and platelets from different type of cells.

Reference	Cell source	Culture condition	Differentiation steps	Cytokines	Stromal cell coculture	Gene editing	Large scale	Efficiency	*In vivo* function evaluation
Choi et al., 1995	CD34+ HSC	2D	HSC-MK-PLT	N/A	N/A	N/A	No	2.1 MKs per HSC	N/A
Norol et al., 1998		2D	HSC-MkP-MK-PLT	TPO, SCF, IL-3, IL-6	N/A	N/A	No	4.6 MKs per HSC	N/A
Proulx et al., 2004		2D	HSC-MK-PLT	TPO, SCF, IL-6, FL	N/A	N/A	No	120 PLTs per seeded cells	N/A
Matsunaga et al., 2006		2D	HSC-MK-PLT	TPO, SCF, IL-3, FL, IL-6,IL-11, IL-1β, SDF-1α, FGF-4, PDGF	hTERT	N/A	Yes	3.36×10^4 PLTs per HSC	N/A
Yang et al., 2016		Rotary vessel	HSC-MK-PLT	TPO, SCF, IL-3, IL-11	N/A	N/A	Yes	$\sim 1.9 \times 10^3$ PLTs per HSC	N/A
Guan et al., 2017		2D	HSC-MK	SCF, FL, TPO, IL-3, IL-6, IL-11, GM-CSF, SR1	N/A	N/A	No	1×10^4 MKs per HSC	MKs produced functional PLTs in mice and monkeys
Guan et al., 2020		Roller-bottle	HSC-MK	TPO, SCF, IL-6, SR1, C433, VPA	N/A	N/A	Yes	2×10^4 MKs per HSC	MKs produced functional PLTs in mice
Gaur et al., 2006	hESC	2D	hESC-MK-PLT	TPO, bFGF	OP9, MEF	N/A	No	0.05–0.2 MK per hESC	N/A
Takayama et al., 2008		2D	hESC-HPC-MK-PLT	TPO, IGF-II, VEGF, bFGF, heparin, SCF, PlGF	OP9, C3H10T1/2	N/A	No	48 PLTs per hESC	N/A
Lu et al., 2011		2D	hESC-MK-PLT	IL-6, IL-9, IL-11, bFGF, VEGF, TPO, SCF	OP9, C3H10T1/2	N/A	Yes	5.5×10^3 PLTs per hESC	PLTs contributed to thrombi in mice
Pick et al., 2013		2D	hESC-MkP-MK-PLT	TPO, SCF, IL-3, FGF2, VEGF, BMP-4	MEF	N/A	No	0.25–1.6 MkPs per 10^3 hESCs	N/A
Takayama et al., 2010	hiPSC	2D	hiPSC-HPC-MK-PLT	SCF, TPO, FL	C3H10T1/2	c-MYC	No	20 PLTs per hiPSC	PLTs contributed to thrombi in mice
Nakamura et al., 2014		2D	hiPSC-HPC-imMKCL-MK-PLT	TPO, SCF	C3H10T1/2	c-MYC, BMI1, BCL-XL	No	250 MKs per imMKCL	PLTs contributed to thrombi in mice
Ito et al., 2018		Bioreactor	hiPSC-imMKCL-MK-PLT	SCF, TA-316, Y27632/Y39983, SR1, KP-457, GNF-351	C3H10T1/2	c-MYC, BMI1, BCL-XL	Yes	70–80 PLTs per hiPSC	PLTs contributed to hemostasis in mice and rabbits
Feng et al., 2014		2D	hiPSC-MkP-MK-PLT	TPO, SCF, IL-3, IL-6, IL-9, ACF, FL, APEL, BMP-4, VEGF, bFGF	N/A	B2M KO	No	∼16 MkPs per iPSC	PLTs contributed to thrombi in mice
Moreau et al., 2016		2D	hiPSC-hPSC-MK	TPO, IL-1β, SCF, BMP4, Y-27632, FGF2, LY-294002	N/A	GATA1, FLI1, TAL1	Yes	2×10^5 MKs per hiPSC	N/A

(Continued)

TABLE 1 | Continued

Reference	Cell source	Culture condition	Differentiation steps	Cytokines	Stromal cell coculture	Gene editing	Large scale	Efficiency	*In vivo* function evaluation
Eicke et al., 2018		Bioreactor	hiPSC-MK-PLT	VEGF, BMP4, TPO, SCF, IL-3, Y27632	N/A	N/A	Yes	29.9 MKs per hiPSC	MKs produced PLTs in mice
Norbnop et al., 2020		2D	hiPSC-HPC-MK-PLT	VEGF, TPO, SCF, heparin	OP9	B2M KO	No	N/A	MKs produced PLTs in mice
Ono et al., 2012	Fibroblast	2D	Fibroblast-iMK-PLT	N/A	N/A	p45NF-E2, Maf G, MafK, CEBPα	No	0.04–0.05 iMK per fibroblast	MKs produced PLTs in mice
Pulecio et al., 2016		2D	Fibroblast-iMkP-MK-PLTs	TPO, IL-3, IL-6, IL-9, SCF	N/A	GATA1, GATA2, TAL1, LMO2, c-MYC, RUNX1	No	N/A	MkP produced MKs and PLTs in mice
Matsubara et al., 2009	Adipocyte	2D	Adipocyte-MK-PLT	LDL, TPO, dNTP, Insulin, Transferrin	N/A	N/A	No	0.2 MK and 0.015 PLT per adipocyte precursor cell	N/A
Tozawa et al., 2019		Bioreactor	Adipose-ASCL-MK-PLT	Transferrin, LDL, Insulin, dNTP, TPO	N/A	N/A	Yes	0.42 PLT per ASCL	PLTs survived in mice

HSC, hematopoietic stem cell; hESC, human embryonic stem cells; hiPSC, human induced pluripotent stem cell; MkP, megakaryocyte progenitor; MK, megakaryocyte; PLT, platelet.

expansion, and liquid culture medium for platelet production, they were able to obtain 1.26–1.68 $\times$ 10^{11} platelets from 1 unit of CB (which contains 3–5 $\times$ 10^6 $CD34^+$ HSCs). These platelets exhibited features similar to those from plasma in both morphology and *in vitro* functions, including ADP-induced aggregation (Matsunaga et al., 2006).

However, despite all the current progress, the biggest challenge of producing platelets from HSCs is still the low differentiation efficiency and the difficulty of large-scale production in a time- and cost-efficient manner. Besides, there is no detailed analysis of the production of each progenitor population (CMPs, EPs, and MkPs) during the differentiation process, which led to the incomplete establishment of the differentiation path from HSCs to platelets.

Generation of Platelets From Human Pluripotent Stem Cells

Human pluripotent stem cells (hPSCs) comprise human embryonic stem cells (hESCs) and the recently discovered human induced pluripotent stem cells (hiPSCs). hPSCs could proliferate (self-renew) infinitely *in vitro*, and under specific conditions, they can differentiate into any cell type of the human body. Therefore, hPSCs could serve as an unlimited source for platelet production *in vitro*.

Generation of hESC-Derived Platelets

Thomson et al. (1998) reported the derivation of the first hESCs from the inner cell mass of blastocyst-stage human embryos, opening the door for platelet differentiation from hESCs. Gaur et al. (2006) established an OP9 stromal cell co-culture system to increase MK production from hESCs, while the yield was unsatisfactory (less than 1 MK produced per 10 input hESCs) and no release of platelets was demonstrated. Takayama et al. (2008) further refined the scheme, in which hESCs were co-cultured with either C3H10T1/2 or OP9 stromal cells and supplemented with human vascular endothelial growth factor (VEGF) to promote the emergence of sac-lick hematopoietic progenitors, which were then further differentiated into MKs and platelets by adding TPO. The platelets displayed activation in response to ADP. This study showed that adding factors that promote mesoderm differentiation from hESCs will eventually benefit the MK and platelet generation. However, MKs generated in this system produced very few platelets (Takayama et al., 2008). Later, Lu et al. (2011) described a more competent method to obtain functional MKs and platelets from hESCs on a large scale, in which they isolated hESC-derived early hematopoietic progenitor cells, the hemangioblasts/blast cells, for further differentiation into MK lineage cells through coculture with OP9. They were able to generate over 100 $CD41a^+$ MKs per hESC, an efficiency much higher than the previous 0.05–0.2 MKs and 2–5 MKs as reported by Gaur et al. (2006) and Takayama et al. (2008), respectively. After being transplanted into a mouse model, these platelets form thrombi at the sites of injury, which is the first report demonstrating the *in vivo* function of platelets derived from hESCs. However, only fewer than 7 platelets were produced from each hESC-derived MK with this method (Lu et al., 2011). A serum- and feeder-free culture system through embryoid bodies (EBs) differentiation was also established, moving one

step forward toward using hESC-derived platelets for transfusion medicine, though the differentiation efficiency is very low, with only 100–800 MK-containing cell colonies obtained per 100,000 sorted CD41a+ cells derived from hESCs (Pick et al., 2013).

These studies above suggest that hESC-derived platelet production is feasible.

Generation of hiPSC-Derived Platelets

Human induced pluripotent stem cells possess similar self-renewal capacity and multipotency to hESCs and could be generated from somatic cells of any individual by overexpression of the TF combinations OCT3/4, SOX2, KLF4, and c-MYC (OSKM) or OCT3/4, SOX2, NANOG, and LIN28 (OSNL) (Takahashi et al., 2007; Yu et al., 2007), which is a breakthrough in the stem cell field. Therefore, hiPSCs represent another promising unlimited source to obtain platelets without the risk of immune rejection, particularly for patients with a rare HLA, and ethical concerns of embryo destruction related to hESCs. Takayama et al. (2010) first demonstrated OSKM hiPSCs could give rise to $CD41a^{+}CD42b^{+}$ platelets. They co-cultured hiPSCs with mouse cell line C3H10T1/2 for differentiation into hematopoietic progenitors, which were subsequently cultured in MK differentiation medium to produce platelets. *In vivo* imaging revealed that these $CD42b^{+}$ platelets were present in thrombi after laser-induced vessel wall injury. Importantly, they showed that c-MYC promoted megakaryopoiesis in the early stage of differentiation but later inhibited thrombopoiesis, indicating complicated roles c-MYC is playing in this differentiation process (Takayama et al., 2010). Nakamura et al. (2014) developed inducible imMKCLs cell lines to improve the consistency and efficiency of platelet generation from hiPSCs. The imMKCLs cell lines are immortalized megakaryocytic cell lines which were differentiated from hiPSCs by inducible overexpression of c-MYC, BMI1, and BCL-XL through the Tet-on system, and then the expression of these three genes would be shut down when further differentiation of imMKCLs into platelets is needed. The imMKCLs could be expanded *in vitro* for 4–5 months, after which they could still be differentiated into platelets that are similar to those isolated from blood (Nakamura et al., 2014). In 2018, turbulence, which mimics the shear stress of blood and helps cut megakaryocytes into small platelets, was introduced by Ito et al. (2018) on a large-scale generation of platelets from hiPSCs. They established a 3D differentiation system in which each hiPSC-derived MK generated 70–80 platelets, almost a 20-fold increase compared with previous reports, although it is still much less than that of 10^4 platelets per megakaryocyte in the human body (Machlus and Italiano, 2013). Nevertheless, they eventually collected 100 billion platelets from hiPSC-MKs in an 8L turbulence-controllable bioreactor, which represents a breakthrough for *in vitro* generation of platelet on a clinical scale for transfusion medicine (Ito et al., 2018).

Besides, other methods were also developed to induce the generation of platelets from hiPSCs. These methods either utilize stepwise differentiation from hiPSCs to early hematopoietic progenitors, then to MKs and finally to platelets, by using different cytokine combinations and culture media (Feng et al., 2014), or applied the microcarrier beads assisted stirred bioreactors to promote MK generation (Eicke et al., 2018), or rely on ectopic expression of key MK TFs GATA1, FLI1, and TAL1 in hiPSCs to directly promote platelet generation (Moreau et al., 2016). 2×10^{11} MKs releasing 1×10^{12} platelets – the equivalent of 3 transfusion units – could be obtained from only 1×10^{6} input hiPSCs (Moreau et al., 2016). Furthermore, by knocking out the β2-microglobulin gene, several groups have generated platelets without major histocompatibility antigens (HLA), which theoretically does not require additional HLA-match and does not cause immune rejection in clinical applications (Feng et al., 2014; Norbnop et al., 2020; Suzuki et al., 2020). Therefore, the application of hiPSC-based technology could potentially yield a consistent supply of HLA- and/or HPA-matched or even autologous platelets for clinical applications.

Generation of Platelets From Other Cell Types

Besides all studies described above to use various stem cells as the starting materials for platelet *in vitro* production, other cell types have also been used to generate megakaryocytes and platelets. However, the efficiency is low, and it is still far away from a practically feasible clinical implementation for platelet transfusion. Alternatively, they can be used for *in vitro* disease modeling and drug screening purposes for platelet-related disorders.

Generation of Fibroblast-Derived Platelets

Transdifferentiation, also known as lineage reprogramming, was recognized as the direct conversion from one mature cell type to another. After the generation of hiPSCs from fibroblasts by overexpression of OSKM or OSNL, fibroblasts or other mature cells have been successfully converted to many different types of cells, such as neurons, cardiomyocytes, hepatocytes, etc. (Wang et al., 2021). Therefore, researchers have also attempted and accomplished, through overexpression of TFs critical for megakaryocytic lineage development, the direct conversion of fibroblasts to MKs, which could further produce platelets *in vitro* or *in vivo* after transplantation into mice. In one study, 3T3 fibroblast cell line and adult human dermal fibroblasts could be transdifferentiated into induced megakaryocytes (iMKs) through the overexpression of p45NF-E2 and its binding proteins MafG and MafK (Ono et al., 2012). iMKs could further produce $CD41^{+}$ platelets which were shown to be involved in thrombosis on the collagen-coated chip *in vitro*. However, the conversion efficiency is pretty low, and they only obtained $8–10 \times 10^{5}$ iMKs from 20×10^{6} fibroblasts, indicating further optimization is required. Pulecio et al. (2016), in a previous study, identified a set of TFs GATA1, TAL-1, LMO2, and c-MYC (GTLM) that was able to convert fibroblast cells into EPs in the presence of erythropoietin (EPO). As EPs and MkPs are both derived from MEPs during development, they may share some core transcriptional regulators. Indeed, in a later study, they successfully generated MkPs from human fibroblasts by adding TFs GATA2 and RUNX1 to the GTLM combo (Pulecio et al., 2016). These MkPs could

further differentiate and produce platelets *in vitro* as well as generate $CD41^+/CD42^+$ platelets *in vivo* after transplantation into immunocompromised mice. This direct conversion to MkPs takes only 12 days and the $CD41^+/CD45^+$ cells appear in 8% cell population. Importantly, they also showed in a Fanconi Anemia patient which has extremely low HSCs and frequent thrombocytopenia, that fibroblast cells could be isolated and *in vitro* gene-corrected, and then directly converted to generate healthy megakaryocytes and platelets.

Generation of Adipose Tissue Cell-Derived Platelets

Matsubara et al. (2009) have been trying to study the capacity of adipose tissue-derived cells in differentiating into MKs and platelets. In 2009, they first showed that megakaryocytes and platelets could be generated from human subcutaneous adipose tissues (Matsubara et al., 2009). Later, to further increase the differentiation efficiency, they generated an adipose tissue-derived mesenchymal stem cell line (ASCL) from adipose-derived stromal cells. As the starting materials, these ASCL cells were able to proliferate for more than 2 months *in vitro*, and upon differentiation, these cells could generate platelets, which express typical platelet cell surface markers and could be activated by ADP. In the end, they were able to obtain one platelet from one starting ASCL (Tozawa et al., 2019).

REGULATORY NETWORK OF MEGAKARYOCYTE DEVELOPMENT

Despite all current progress, the generation of truly mature and functional platelets from *in vitro* cultures was demonstrated in few studies, and one possible reason is, the percentage of MKs in bone marrow is very low (about 0.01% of all nucleated cells) (Nakeff and Maat, 1974), therefore, although MKs were discovered over 100 years ago, it is very difficult to study their development and biology. So far, researchers have been focusing on the study of internal and external factors that affect the fate of megakaryocytic lineage cells. The external factors are exogenous signal transduction and microenvironment, and internal factors are mainly TFs and epigenetic regulators. To date, only a few TFs have been reported to be involved in this process, including GATA1 (Crispino and Horwitz, 2017), FLI1 (Li et al., 2015), MEIS1 (Zeddies et al., 2014), RUNX1 (Goldfarb, 2009), and SCL (Robb and Begley, 1997). Not surprisingly, some of these genes, including RUNX1, ERG and MEIS1, and TPO-encoding gene Thrombopoietin have all been demonstrated to be involved in hESC *in vitro* differentiation into MKs and platelets (Tu et al., 2017; Wang et al., 2018; Zhang et al., 2018), indicating that studies in MK regulators will eventually help establish methods to drive platelet *in vitro* generation.

Our laboratory is devoted to discovering more TFs and mapping the regulatory network to understand the decision-making factors during platelet development (Zhu et al., 2018). To identify the regulators for HSC differentiation to MkPs, the immediate precursor cells for MKs and platelets, we applied Gene Expression Commons (GeXC), a platform developed in Irving Weissman's laboratory at Stanford University (Seita et al., 2012), to get the candidate gene list, in which these genes have high expression level in MkPs but low in EPs and MEPs, a common progenitor for MkPs and EPs. This expression pattern indicates that genes in this list may play a role in MkP differentiation. To address this hypothesis, we deleted these candidate genes separately in HSCs using CRISPR/Cas9 and found that the knockout of some genes inhibited MkP generation from HSCs. Subsequently, 9 candidate TFs, which include MZF1, GSX2, HOXC6, HES7, FOXB1, MXD3, HOXA9, NFATC1, and PCGF2, were identified to promote MkP generation from HSCs by lentivirus-mediated overexpression. Further analysis showed that MkP generation was increased by four–five fold with this TFs overexpression. To our knowledge, the functions of these 9 TFs in MK lineages development have not been reported previously. We also found inhibition of histone deacetylase (HDAC) activity could also promote the differentiation of HSCs into MkPs and platelets, possibly through regulating some of the 9 newly identified TFs: gene expression analysis showed GSX2, MXD3, HOXC6, and HES7 were significantly up-regulated while PCGF2, FOXB1, and MZF1 were moderately up-regulated after HDAC inhibition. These results have added more players into the regulatory network of endogenous factors during MkP development and platelet generation.

In another study to identify the exogenous signals, we found the neurotransmitter GABA was involved in the occurrence of platelets, indicating there is a link between the neural and hematopoietic systems (Zhu et al., 2019). We found GABRR1 is the only GABA receptor that is expressed in subsets of HSCs and MkPs. Electrophysiological recording experiment showed that $GABRR1^+$ but not $GABRR1^-$ HSCs and MkPs respond to GABA in patch-clamp studies. Besides, GABA signaling through GABRR1 affected mouse HSC differentiating into megakaryocytic lineage cells. Stimulated by GABA agonists, including TACA and Muscimol, the mouse showed increased platelet numbers. We also found similar functions of GABRR1 in human hematopoiesis. Treatment with GABRR1 antagonist inhibited the number of MkPs and platelets generated from HSCs, while agonist treatment or overexpression of GABRR1 in HSCs significantly promoted MkP and platelet generation. Thus, this is the first study that showed the role of GABA signaling in the differentiation of HSCs and MkPs, and provides another evidence for the correlation between the neural and hematopoietic systems. This study not only indicates GABA may be a potential target in platelet-related disorders, but also shows it may help increase the MK and platelet production from HSCs (and potentially other stem cells) by adding GABA or its agonists during *in vitro* differentiation cultures.

Taken together, our studies reveal the complexity and the lack of knowledge of comprehensive MK regulators. Our laboratory is devoted to identifying more MK lineage-specific genes and signaling factors and completing the regulatory network of platelet generation, which may hopefully not only provide new drug targets related to platelet counts, activation, and aggregation, but also facilitate platelet generation *in vitro*.

DISCUSSION

Currently, various methods have been developed and great progress has been made toward the generation of platelets from different cell types *in vitro* to fulfill the transfusion medicine purpose independent of or as a supplement to blood donations. However, certain limits still exist in using each of these cell types as the starting materials for platelet *in vitro* biogenesis, and these problems and/or questions must be resolved before they could be used in clinical applications.

Due to the rareness of HSCs in PB and the difficulty in obtaining BM, HSCs from CB are now routinely used for *in vitro* platelet differentiation. Based on this, new cytokines (such as IL-11) and new chemical compounds (such as Y27632 and DAC) have been identified, a new 3D culture system (such as roller-bottle culture system), and new stromal cells (such as hTERT-transduced stroma) have been introduced to the culture conditions. These optimizations have significantly improved the differentiation efficacy, with 2×10^4 MKs obtained from 1 seeded $CD34^+$ HSC, compared with the previous 5 MKs per HSC (Norol et al., 1998; Guan et al., 2020), and 1.26×10^{11}–1.68×10^{11} platelets generated from one CB unit, which equal to 2.5–3.4 units of donor-derived platelets (Matsunaga et al., 2006). However, only a limited number of $CD34^+$ HSCs, about $3\text{-}5 \times 10^6$, could be extracted from one unit of CB, and these cells are difficult to obtain and culture. Besides, the number of platelets generated by current differentiation methods still cannot meet the requirement of transfusion medicine, therefore, more work is needed to improve the efficacy for large-scale generation of platelets *in vitro*. It has also been reported that, although CB HSCs were able to yield the highest number of MKs compared with those from PB and BM, the CB-derived MKs showed reduced ploidization indicating less maturation (van den Oudenrijn et al., 2000). Last but not least, there is no detailed analysis of the production of each progenitor population during the differentiation process, which led to the incomplete establishment of the differentiation path from HSCs to platelets.

Human embryonic stem cells and hiPSCs can proliferate indefinitely *in vitro*, which may bypass some limits associated with CB-derived HSCs as the starting materials. However, hESCs are derived from blastocyst-stage embryos (Thomson et al., 1998), so there are ethical controversies and potential risks of viral infection and congenital diseases in the human embryos. hiPSCs are derived from human somatic cells (Takahashi et al., 2007; Yu et al., 2007), thus avoid ethical controversy as in hESCs, but there are still some obstacles to use hiPSCs for *in vitro* generation of platelets, which include safety issues, long differentiation cycles, and the huge cost. One safety concern is the residual undifferentiated hiPSCs in the final products, as hiPSCs have the potential to form tumors after transplantation *in vivo*. Considering that a large number of platelets is needed for each transfusion (about 3×10^{11} platelets per unit), even contamination of 0.01% hiPSCs in platelets means 3×10^7 undifferentiated hiPSCs in a treatment unit, which is more than enough to form tumors in human. Although platelet products are usually irradiated by gamma-ray before transfusion, one still cannot exclude the possibility of hiPSC contamination after irradiation. Another safety issue is that the oncogene c-MYC was overexpressed for the best results of platelet generation (Takayama et al., 2010; Nakamura et al., 2014; Ito et al., 2018), which leads to the risk of oncogenicity. Even though regulated by Doxycycline, the c-MYC gene may be reactivated in other ways. As for the production cycle, it takes weeks or even months to establish the hiPSC cell lines and carry out various assays to identify the best clones (Takahashi et al., 2007; Yu et al., 2007). Then, the differentiation of hiPSCs into platelets involves multiple steps and a long period. For example, in a study by Ito et al. (2018), it takes about 14 days to differentiate hiPSCs into hematopoietic progenitors *in vitro*, then several weeks to establish and expand imMKCLs by overexpression of c-MYC, BMI1, and BCL-XL, finally, another 6 days are needed to obtain mature platelets from these expanded imMKCLs. In another study by Feng et al. (2014), it takes 6 days to direct hiPSCs *in vitro* to hematopoietic progenitors, after which early MkPs were generated in another 7 days, a final 7 days are then required to induce mature MKs and platelet generation. The cost associated with hPSC-derived platelets is mainly due to the use of growth factors/small molecules and plasma/serum during the cell culture medium. Some growth factors like bFGF are indispensable in the routine culture of hPSCs, and more cytokines are needed in the platelet differentiation from these hPSCs. Ito et al. (2018) introduced human plasma/serum, SCF, TA-316, KP-457SR-1, GNF-351, and Y27632 at multiple stages of their differentiation method, and Feng et al. (2014) used even more cytokines, including BMP-4, VEGF, bFGF, TPO, SCF, Flt3-L, IL-3, IL-6, and IL-9. A common issue with both hESC- and hiPSC-derived platelets is, these generated platelets have a much shorter lifespan than those from plasma (Feng et al., 2014; Moreau et al., 2016), indicating these differentiated platelets are not as fully mature and functional as primary platelets.

Transdifferentiation from fibroblasts to platelets is not feasible for making large-scale platelets due to the limited sources, difficulty in expansion of fibroblasts, as well as low conversion efficiency (Ono et al., 2012; Pulecio et al., 2016). As to using adipose tissue-derived cells for *in vitro* platelet production, although expandable cell lines could be established from adipocytes, it is difficult to use these cells in large-scale manufacture because of their limited proliferation and inefficient differentiation. Moreover, the final products not only express typical platelets cell surface markers but also possess some features of mesenchymal stem cells, such as expression of CD90, indicating that these final products are not bona fide platelets, and the mechanism of adipocytes converting to platelets is still unknown (Tozawa et al., 2019).

In summary, although significant progress has been made toward the *in vitro* generation of platelets from HSCs, hPSCs, fibroblasts, and adipose-derived cells, with various stem cells as the most promising starting materials, the current issues of scalability, cost, duration of differentiation, and cell functionality

are all hurdles to applying these *in vitro* generated platelets into clinical applications. A better understanding of the biology and development of megakaryocytes will hopefully address some of these issues and greatly facilitate *in vitro* platelet biogenesis on a large scale for transfusion medicine.

AUTHOR CONTRIBUTIONS

FZ contributed to the conception and design of the structure of the manuscript and wrote the first draft of the manuscript. HL collected information from reference literature, organized the database, and wrote some sections of the manuscript. FZ, HL, JL, and LW contributed to manuscript revision and read and approved the submitted version of the manuscript. All authors contributed to the article and approved the submitted version.

FUNDING

This study was supported by Shanghai Municipal Education Commission (ZXWF082101) and the Double First-Class Initiative startup research fund (WF220408222) to FZ from Shanghai Jiao Tong University.

ACKNOWLEDGMENTS

The authors thank colleagues for discussion during the preparation of this manuscript. They would also like to thank all the researchers, cited or not, that contributed to progress related to the discussed topic in this manuscript. Due to space limitations, the authors were not able to list all related references in this manuscript.

REFERENCES

Choi, E. S., Nichol, J. L., Hokom, M. M., Hornkohl, A. C., and Hunt, P. (1995). Platelets generated in vitro from proplatelet-displaying human megakaryocytes are functional. *Blood.* 85, 402–413. doi: 10.1182/blood.v85.2.402.bloodjournal852402

Crispino, J. D., and Horwitz, M. S. (2017). GATA factor mutations in hematologic disease. *Blood.* 129, 2103–2110. doi: 10.1182/blood-2016-09-687889

Eicke, D., Baigger, A., Schulze, K., Latham, S. L., Halloin, C., Zweigerdt, R., et al. (2018). Large-scale production of megakaryocytes in microcarrier-supported stirred suspension bioreactors. *Sci. Rep.* 8:10146. doi: 10.1038/s41598-018-28459-x

Feng, Q., Shabrani, N., Thon, J. N., Huo, H., Thiel, A., Machlus, K. R., et al. (2014). Scalable generation of universal platelets from human induced pluripotent stem cells. *Stem cell Rep.* 3, 817–831. doi: 10.1016/j.stemcr.2014.09.010

Gaur, M., Kamata, T., Wang, S., Moran, B., Shattil, S. J., and Leavitt, A. D. (2006). Megakaryocytes derived from human embryonic stem cells: a genetically tractable system to study megakaryocytopoiesis and integrin function. *J. Thromb. Haemost.* 4, 436–442. doi: 10.1111/j.1538-7836.2006.01744.x

Goldfarb, A. N. (2009). Megakaryocytic programming by a transcriptional regulatory loop: a circle connecting RUNX1, GATA-1, and P-TEFb. *J Cell Biochem.* 107, 377–382. doi: 10.1002/jcb.22142

Guan, X., Qin, M., Zhang, Y., Wang, Y., Shen, B., Ren, Z., et al. (2017). Safety and efficacy of megakaryocytes induced from hematopoietic stem cells in murine and nonhuman primate models. *Stem Cells Transl. Med.* 6, 897–909. doi: 10.5966/sctm.2016-0224

Guan, X., Wang, L., Wang, H., Wang, H., Dai, W., and Jiang, Y. (2020). Good manufacturing practice-grade of megakaryocytes produced by a novel ex vivo culturing platform. *Clin. Transl. Sci.* 13, 1115–1126. doi: 10.1111/cts.12788

Harrison, P. (2005). Platelet function analysis. *Blood Rev.* 19, 111–123. doi: 10.1016/j.blre.2004.05.002

Ito, Y., Nakamura, S., Sugimoto, N., Shigemori, T., Kato, Y., Ohno, M., et al. (2018). Turbulence activates platelet biogenesis to enable clinical scale ex vivo production. *Cell* 174, 636-648.e18. doi: 10.1016/j.cell.2018.06.011

Li, Y., Luo, H., Liu, T., Zacksenhaus, E., and Ben-David, Y. (2015). The ets transcription factor Fli-1 in development, cancer and disease. *Oncogene* 34, 2022–2031. doi: 10.1038/onc.2014.162

Lu, S. J., Li, F., Yin, H., Feng, Q., Kimbrel, E. A., Hahm, E., et al. (2011). Platelets generated from human embryonic stem cells are functional in vitro and in the microcirculation of living mice. *Cell Res.* 21, 530–545. doi: 10.1038/cr.2011.8

Machlus, K. R., and Italiano, J. E. (2013). The incredible journey: From megakaryocyte development to platelet formation. *J. Cell Biol.* 201, 785–796. doi: 10.1083/jcb.201304054

Matsubara, Y., Saito, E., Suzuki, H., Watanabe, N., Murata, M., and Ikeda, Y. (2009). Generation of megakaryocytes and platelets from human subcutaneous adipose tissues. *Biochem. Biophys. Res. Commun.* 378, 716–720. doi: 10.1016/j.bbrc.2008.11.117

Matsunaga, T., Tanaka, I., Kobune, M., Kawano, Y., Tanaka, M., Kuribayashi, K., et al. (2006). Ex vivo large-scale generation of human platelets from cord blood CD34+ cells. *Stem Cells* 24, 2877–2887. doi: 10.1634/stemcells.2006-0309

McArthur, K., Chappaz, S., and Kile, B. T. (2018). Apoptosis in megakaryocytes and platelets: the life and death of a lineage. *Blood* 131, 605–610. doi: 10.1182/blood-2017-11-742684

Moreau, T., Evans, A. L., Vasquez, L., Tijssen, M. R., Yan, Y., Trotter, M. W., et al. (2016). Large-scale production of megakaryocytes from human pluripotent stem cells by chemically defined forward programming. *Nat. Commun.* 7:11208. doi: 10.1038/ncomms11208

Nakamura, S., Takayama, N., Hirata, S., Seo, H., Endo, H., Ochi, K., et al. (2014). Expandable megakaryocyte cell lines enable clinically applicable generation of platelets from human induced pluripotent stem cells. *Cell stem cell.* 14, 535–548. doi: 10.1016/j.stem.2014.01.011

Nakeff, A., and Maat, B. (1974). Separation of megakaryocytes from mouse bone marrow by velocity sedimentation. *Blood* 43, 591–595. doi: 10.1182/blood.v43.4.591.591

Norbnop, P., Ingrungruanglert, P., Israsena, N., Suphapeetiporn, K., and Shotelersuk, V. (2020). Generation and characterization of HLA-universal platelets derived from induced pluripotent stem cells. *Sci. Rep.* 10:8472. doi: 10.1038/s41598-020-65577-x

Norol, F., Vitrat, N., Cramer, E., Guichard, J., Burstein, S. A., Vainchenker, W., et al. (1998). Effects of cytokines on platelet production from blood and marrow CD34+ cells. *Blood* 91, 830–843. doi: 10.1182/blood.v91.3.830.830_830_843

Ono, Y., Wang, Y., Suzuki, H., Okamoto, S., Ikeda, Y., Murata, M., et al. (2012). Induction of functional platelets from mouse and human fibroblasts by p45NF-E2/Maf. *Blood* 120, 3812–3821. doi: 10.1182/blood-2012-02-413617

Pick, M., Azzola, L., Osborne, E., Stanley, E. G., and Elefanty, A. G. (2013). Generation of megakaryocytic progenitors from human embryonic stem cells in a feeder- and serum-free medium. *PLoS One.* 8:e55530. doi: 10.1371/journal.pone.0055530

Proulx, C., Dupuis, N., St-Amour, I., Boyer, L., and Lemieux, R. (2004). Increased megakaryopoiesis in cultures of CD34-enriched cord blood cells maintained at 39 degrees C. *Biotechnol. Bioeng.* 88, 675–680. doi: 10.1002/bit.20288

Pulecio, J., Alejo-Valle, O., Capellera-Garcia, S., Vitaloni, M., Rio, P., Mejia-Ramirez, E., et al. (2016). Direct conversion of fibroblasts to megakaryocyte progenitors. *Cell Rep.* 17, 671–683. doi: 10.1016/j.celrep.2016.09.036

Robb, L., and Begley, C. (1997). The SCL/TAL1 gene: roles in normal and malignant haematopoiesis. *Bioessays* 19, 607–613. doi: 10.1002/bies.950190711

Seita, J., Sahoo, D., Rossi, D. J., Bhattacharya, D., Serwold, T., Inlay, M. A., et al. (2012). Gene expression commons: an open platform for absolute gene expression profiling. *PLoS One.* 7:e40321. doi: 10.1371/journal.pone.0040321

Seita, J., and Weissman, I. L. (2010). Hematopoietic stem cell: self-renewal versus differentiation. *Wiley Interdisc. Rev. Syst. Biol. Med.* 2, 640–653. doi: 10.1002/wsbm.86

Squires, J. E. (2015). Indications for platelet transfusion in patients with thrombocytopenia. *Blood Transfus.* 13, 221–226. doi: 10.2450/2014.0105-14

Suzuki, D., Flahou, C., Yoshikawa, N., Stirblyte, I., Hayashi, Y., Sawaguchi, A., et al. (2020). iPSC-derived platelets depleted of HLA class I are inert to anti-HLA class I and natural killer cell immunity. *Stem Cell Rep.* 14, 49–59. doi: 10.1016/j.stemcr.2019.11.011

Takahashi, K., Tanabe, K., Ohnuki, M., Narita, M., Ichisaka, T., Tomoda, K., et al. (2007). Induction of pluripotent stem cells from adult human fibroblasts by defined factors. *Cell* 131, 861–872. doi: 10.1016/j.cell.2007.11.019

Takayama, N., Nishikii, H., Usui, J., Tsukui, H., Sawaguchi, A., Hiroyama, T., et al. (2008). Generation of functional platelets from human embryonic stem cells in vitro via ES-sacs, VEGF-promoted structures that concentrate hematopoietic progenitors. *Blood* 111, 5298–5306. doi: 10.1182/blood-2007-10-117622

Takayama, N., Nishimura, S., Nakamura, S., Shimizu, T., Ohnishi, R., Endo, H., et al. (2010). Transient activation of c-MYC expression is critical for efficient platelet generation from human induced pluripotent stem cells. *J. Exp. Med.* 207, 2817–2830. doi: 10.1084/jem.20100844

Thomson, J. A., Itskovitz-Eldor, J., Shapiro, S. S., Waknitz, M. A., Swiergiel, J. J., Marshall, V. S., et al. (1998). Embryonic stem cell lines derived from human blastocysts. *Science* 282, 1145–1147. doi: 10.1126/science.282.5391.1145

Tozawa, K., Ono-Uruga, Y., Yazawa, M., Mori, T., Murata, M., Okamoto, S., et al. (2019). Megakaryocytes and platelets from a novel human adipose tissue-derived mesenchymal stem cell line. *Blood* 133, 633–643. doi: 10.1182/blood-2018-04-842641

Tu, Q., Liu, C. C., Wu, D., and Pei, S. U. (2017). Establishment of the screening model for highly efficient generation of megakaryocytes and platelets from human pluripotent stem cells (in Chinese). *Sci. Sin. Vitae* 47, 1363–1374. doi: 10.1360/N052017-00270

van den Oudenrijn, S., von dem Borne, A. E., and de Haas, M. (2000). Differences in megakaryocyte expansion potential between CD34(+) stem cells derived from cord blood, peripheral blood, and bone marrow from adults and children. *Exp. Hematol.* 28, 1054–1061. doi: 10.1016/s0301-472x(00)00517-8

Wang, H., Liu, C., Liu, X., Wang, M., Wu, D., Gao, J., et al. (2018). MEIS1 regulates hemogenic endothelial generation, megakaryopoiesis, and thrombopoiesis in human pluripotent stem cells by targeting TAL1 and FLI1. *Stem Cell Rep.* 10, 447–460. doi: 10.1016/j.stemcr.2017.12.017

Wang, H., Yang, Y., Liu, J., and Qian, L. (2021). Direct cell reprogramming: approaches, mechanisms and progress. *Nat. Rev. Mol. Cell Biol.* 22, 410–424. doi: 10.1038/s41580-021-00335-z

Yang, Y., Liu, C., Lei, X., Wang, H., Su, P., Ru, Y., et al. (2016). Integrated biophysical and biochemical signals augment megakaryopoiesis and thrombopoiesis in a three-dimensional rotary culture system. *Stem Cells Transl. Med.* 5, 175–185. doi: 10.5966/sctm.2015-0080

Yu, J., Vodyanik, M. A., Smuga-Otto, K., Antosiewicz-Bourget, J., Frane, J. L., Tian, S., et al. (2007). Induced pluripotent stem cell lines derived from human somatic cells. *Science* 318, 1917–1920. doi: 10.1126/science.1151526

Zeddies, S., Jansen, S. B., di Summa, F., Geerts, D., Zwaginga, J. J., van der Schoot, C. E., et al. (2014). MEIS1 regulates early erythroid and megakaryocytic cell fate. *Haematologica* 99, 1555–1564. doi: 10.3324/haematol.2014.106567

Zhang, L., Liu, C., Wang, H., Wu, D., Su, P., Wang, M., et al. (2018). Thrombopoietin knock-in augments platelet generation from human embryonic stem cells. *Stem Cell Research Therapy.* 9:194. doi: 10.1186/s13287-018-0926-x

Zhu, F., Feng, M., Sinha, R., Murphy, M. P., Luo, F., Kao, K. S., et al. (2019). The GABA receptor GABRR1 is expressed on and functional in hematopoietic stem cells and megakaryocyte progenitors. *Proc. Natl. Acad. Sci. U.S.A.* 116, 18416–18422. doi: 10.1073/pnas.1906251116

Zhu, F., Feng, M., Sinha, R., Seita, J., Mori, Y., and Weissman, I. L. (2018). Screening for genes that regulate the differentiation of human megakaryocytic lineage cells. *Proc. Natl. Acad. Sci. U.S.A.* 115, E9308–E9316. doi: 10.1073/pnas.1805434115

Conflict of Interest: The authors declare that the research was conducted in the absence of any commercial or financial relationships that could be construed as a potential conflict of interest.

Publisher's Note: All claims expressed in this article are solely those of the authors and do not necessarily represent those of their affiliated organizations, or those of the publisher, the editors and the reviewers. Any product that may be evaluated in this article, or claim that may be made by its manufacturer, is not guaranteed or endorsed by the publisher.

frontiers in Cell and Developmental Biology

REVIEW
published: 13 August 2021
doi: 10.3389/fcell.2021.710964

RNA m^{6}A Modification Plays a Key Role in Maintaining Stem Cell Function in Normal and Malignant Hematopoiesis

Peipei Wang[1,2†], Mengdie Feng[2†], Guoqiang Han[2†], Rong Yin[2], Yashu Li[2], Shuxin Yao[2], Pengbo Lu[2], Yuhua Wang[1] and Haojian Zhang[1,2,3]*

[1] The State Key Laboratory Breeding Base of Basic Science of Stomatology and Key Laboratory of Oral Biomedicine Ministry of Education, School and Hospital of Stomatology, Wuhan University, Wuhan, China, [2] Frontier Science Center for Immunology and Metabolism, School of Medicine, Medical Research Institute, Wuhan University, Wuhan, China, [3] RNA Institute, Wuhan University, Wuhan, China

OPEN ACCESS

Edited by:
Jianjun Zhou,
Tongji University, China

Reviewed by:
Xiaocheng Weng,
University of Chicago, United States
Yuan-I Chang,
National Yang Ming Chiao Tung University, Taiwan

***Correspondence:**
Haojian Zhang
haojian_zhang@whu.edu.cn

[†] These authors have contributed equally to this work

Specialty section:
This article was submitted to Stem Cell Research, a section of the journal Frontiers in Cell and Developmental Biology

Received: 17 May 2021
Accepted: 28 July 2021
Published: 13 August 2021

Citation:
Wang P, Feng M, Han G, Yin R, Li Y, Yao S, Lu P, Wang Y and Zhang H (2021) RNA m^{6}A Modification Plays a Key Role in Maintaining Stem Cell Function in Normal and Malignant Hematopoiesis. Front. Cell Dev. Biol. 9:710964. doi: 10.3389/fcell.2021.710964

N^6-methyladenosine (m^{6}A) is a commonly modification of mammalian mRNAs and plays key roles in various cellular processes. Emerging evidence reveals the importance of RNA m^{6}A modification in maintaining stem cell function in normal hematopoiesis and leukemogenesis. In this review, we first briefly summarize the latest advances in RNA m^{6}A biology, and further highlight the roles of m^{6}A writers, readers and erasers in normal hematopoiesis and acute myeloid leukemia. Moreover, we also discuss the mechanisms of these m^{6}A modifiers in preserving the function of hematopoietic stem cells (HSCs) and leukemia stem cells (LSCs), as well as potential strategies for targeting m^{6}A modification related pathways. Overall, we provide a comprehensive summary and our insights into the field of RNA m^{6}A in normal hematopoiesis and leukemia pathogenesis.

Keywords: RNA m^{6}A, hematopoietic stem cells, leukemia stem cells, hematopoiesis, myeloid leukemia

INTRODUCTION

Hematopoietic homeostasis is maintained by rare multipotent hematopoietic stem cells (HSCs) via efficient self-renewal and differentiation into all lineage blood cells. This process is tightly controlled at multilayers such as the transcriptional and post-transcriptional levels (Orkin and Zon, 2008; Olson et al., 2020; Wilkinson et al., 2020). Alterations in these regulatory mechanisms affect the function of HSCs, and frequently cause hematologic diseases. Acute myeloid leukemia (AML) is an aggressive and fatal hematologic malignancy characterized by uncontrolled expansion of poorly differentiated myeloid cells (Dohner et al., 2015), and its development is associated with accumulation of acquired genetic and epigenetic changes in hematopoietic stem/progenitor cells (HSPCs) (Cancer Genome Atlas Research Network Ley et al., 2013; Shlush et al., 2014). These alterations confer HSPCs with increased self-renewal capacity and impair their normal differentiation trajectory, thereby subsequently transforming HSPCs into leukemia stem cells (LSCs) (Lu et al., 2016; Yang et al., 2016). The existence of LSCs is also considered as the main reason for AML relapse. Therefore, exploring the underlying mechanisms of maintaining the function of HSCs and LSCs is always an attractive topic in this field.

The post-transcriptional modification of RNA plays important roles in regulating gene expression. m^{6}A was first discovered in the 1970s, and is the most abundant one among about 160

chemical marks on cellular RNA that have been discovered to date (Desrosiers et al., 1974; Helm and Motorin, 2017). About one-third of mammalian mRNAs have been identified as containing m^{6}A modification with an average of 3–5 modifications per mRNA (Huang et al., 2020). Along with the development of m^{6}A high-throughput sequencing technology that enables profiling of m^{6}A modifications at the transcriptome-wide level, it is found that m^{6}A modification sites have a typical consensus motif DRACH and are mainly enriched in the coding sequence and 3'untranslated region (Dominissini et al., 2012; Meyer et al., 2012). Moreover, m^{6}A modification is reversible and dynamically controlled by m^{6}A modifiers including writers, erasers and readers, and plays key roles in determining RNA fate by regulating RNA processing such as decay, stability, splicing, transportation, and translation. Increasing evidences including studies from our laboratory indicate that RNA m^{6}A is involved in many biological processes, including hematopoiesis and leukemogenesis (Vu et al., 2019; Wang et al., 2020). In this review, we summarize the roles of m^{6}A writers, readers and erasers in normal hematopoiesis and acute myeloid leukemia by focusing on their function in HSCs and LSCs maintenance, as well as potential strategies for targeting m^{6}A modification related pathways.

REGULATION OF RNA m^{6}A MODIFICATION

RNA m^{6}A is a dynamic and reversible modification that is executed by m^{6}A modifiers and related factors, which can be divided into three different functional groups, writers, erasers, and readers. The writers are responsible for installing m^{6}A marks to RNA, the erasers selectively remove m^{6}A marks, and the readers recognize m^{6}A marks specifically. m^{6}A methyltransferase complex, also called "m^{6}A writer," is composed of methyltransferase-like 3 (METTL3), METTL14, WT-associated protein (WTAP), RBM15/RBM15B, KIAA1429, and ZC3H13 (Liu et al., 2014; Ping et al., 2014; Knuckles et al., 2018; Wen et al., 2018; Hu et al., 2020). m^{6}A erasers, FTO and ALKBH5, are the main demethylases (Jia et al., 2011; Zheng et al., 2013). m^{6}A modifications are recognized by different m^{6}A readers, including YTH domain-containing protein 1–2 (YTHDC1/2), YTH domain-containing family member 1–3 (YTHDF1/2/3), and insulin-like growth factor-2 mRNA-binding protein (IGF2BP) family IGF2BP1/2/3 (Theler et al., 2014; Xiao et al., 2016; Hsu et al., 2017; Huang et al., 2018). They closely collaborate in controlling m^{6}A modification and determining RNA fates (**Figure 1**).

Writer of RNA m^{6}A

Writer of m^{6}A, the methyltransferase complex, is responsible for catalyzing the transfer of methyl group from S-adenosylmethionine (SAM) to the sixth N atom of RNA adenosine. It is currently believed that METTL3 is the only catalytical protein in this complex, whereas METTL14 maintains the activity and structural stability of METTL3/METTL14 heterodimer (Wang P. et al., 2016). METTL3 contains the leading helix structure (LH) domain, nuclear localization signal (NLS) domain, CCH-type zinc finger domain (ZFD), and two SAM structure binding domains–methyltransferase domain (MTD). LH and NLS mediate the interaction of METTL3 with METTL14 (Liu et al., 2014; Wang P. et al., 2016; Wang X. et al., 2016). ZFD serves as the target recognition domain and fulfills the methyltransferase activity of the METTL3-METTL14 complex (Huang J. et al., 2019).

The activity and specificity of m^{6}A writer also relies on the subunits of this complex. As an important subunit of m^{6}A writer complex, WTAP promotes METTL3-METTL14 heterodimer to enter the nuclear plaque and stabilize it (Ping et al., 2014). Biochemical experiments have proved that WTAP protein alone does not function as a methyltransferase *in vitro* but as an indispensable subunit for the complex. RBM15 is another important subunit and facilitates the recruitment of m^{6}A writer complex to specific RNA (Patil et al., 2016). ZC3H13 exists in an evolutionarily conserved complex ZC3H13-WTAP-Virilizer-Hakai. ZC3H13 loss promotes the transfer of WTAP from nucleus to cytoplasm accompanying with decreased nuclear METTL13 and METTL14, thus blocking m^{6}A installation (Knuckles et al., 2018; Wen et al., 2018). VIRMA contains the RBP domain, and facilitates m^{6}A writer complex to the 3′UTR region, suggesting that VIRMA plays a significant role in m^{6}A modification concentrated near 3′UTR and stop codon (Yue et al., 2018). Together, RNA m^{6}A installation is a complicated process, and multiple factors involved in this process guarantee its accuracy.

Erasers of RNA m^{6}A

Currently, two m^{6}A demethylases have been reported, FTO and ALKBH5, and both belong to the ALKB family (Jia et al., 2011; Zheng et al., 2013). Although FTO is a member of the ALKB family, its C-terminus has a specific domain (long loop) that can demethylate methylated bases (Zhang et al., 2019). Beyond m^{6}A, FTO can also catalyze the demethylation of m^{6}Am on mRNA and m^{1}A on tRNA. Recent study showed that the cellular distribution of FTO is distinct among different cell lines, which affects the access of FTO to different RNA substrates. FTO in the nucleus has a higher affinity for m^{6}A, while FTO in the cytoplasm has a higher affinity for m^{6}Am (Wei et al., 2018). Although a nuclear localization signal at the N-terminus guides FTO into the nucleus, factors that influence FTO location remain unknown yet. ALKBH5 is another demethylated enzyme that specifically recognizes the m^{6}A on RNA. Knockout of ALKBH5 in mice does not affect the health status except for the defect of spermatogenesis in mice, which makes ALKBH5 more suitable as a therapeutic target (Zheng et al., 2013; Shen et al., 2020; Wang et al., 2020). Notably, α-KG and Fe^{2+} are essential for the demethylation activity of FTO and ALKBH5, however, it remain elusive how the activities of these m^{6}A erasers are regulated in different contexts.

Readers of RNA m^{6}A

Identification of m^{6}A readers has provided important information about how m^{6}A acts in determining RNA fates, and the list of m^{6}A readers is still expanding. Both YTHDF1/2/3 and

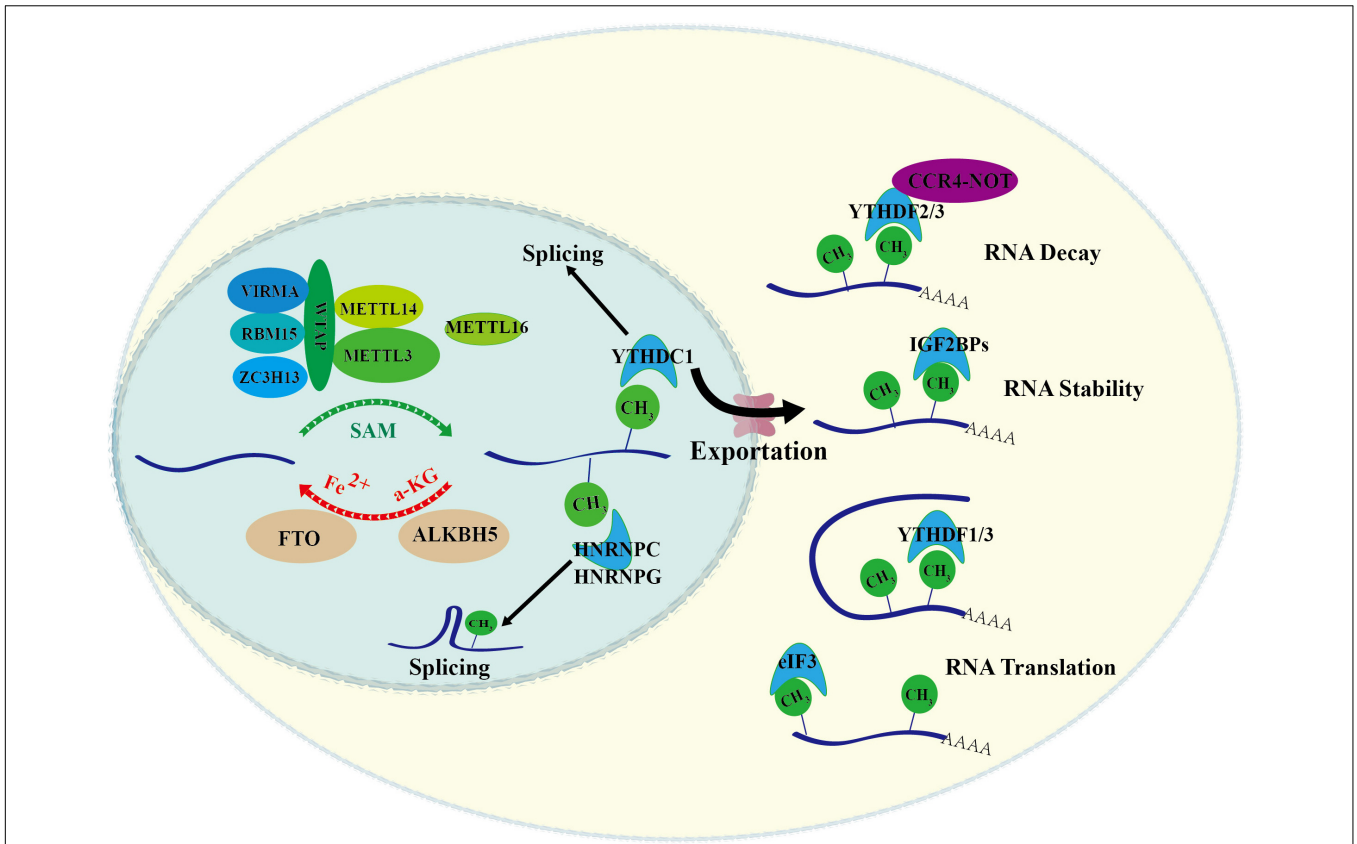

FIGURE 1 | Overview of RNA m^{6}A modification. m^{6}A methylation is catalyzed by the writer complex that is composed by METTL3, METTL14, WTAP, METTL16, VIRMA, RBM15, ZC3H13, and KIAA1429. m^{6}A methylation is removed by erasers including ALKBH5 and FTO. The m^{6}A-modified RNA reader proteins include YTHDF1/2/3, YTHDC1/2, IGF2BP1/2/3, and HNRNPs. These readers bind to the target RNA in an m^{6}A-dependent manner, and affects the metabolic processes of RNA, such as pre-mRNA splicing, nuclear export, RNA decay, RNA stability and RNA translation.

YTHDC1/2 can be grouped into one class, as they all contain the same YTH domain that is responsible for recognizing m^{6}A. YTHDF2 mainly promotes degradation of m^{6}A-tagged mRNAs (Du et al., 2016), while YTHDF1 and YTHDF3 affect the translation of their target transcripts (Shi et al., 2017). The different consequences brought by these different readers may result from their associated regulatory machinery or related factors. For instance, YTHDF1 interacts with eukaryotic initiation factor 3 (eIF3) in the 48S translation initiation complex and further recruits other translational factors for facilitating translation (Lee et al., 2015); YTHDF3 recruits eIF4G2 directly bound to internal ribosome entry sites to initiate eIF4E-independent translation (Yang et al., 2017; Di Timoteo et al., 2020); YTHDF2 recruits CCR4-NOT deadenylase complex for mRNA decay (Du et al., 2016). Similarly, YTHDC1/2 executes a distinct function in fine-tuning m^{6}A-tagged transcripts, although they share the same sequence pattern with YTHDF1/2/3. YTHDC1 mainly locates in the nucleus and participates in m^{6}A-tagged mRNA export from the nucleus to the cytoplasm (Zhang et al., 2010; Xu et al., 2014; Xiao et al., 2016; Roundtree et al., 2017). Recent studies indicate that YTHDC1 also mediates mRNA splicing by recruiting two competitive mRNA splicing factors serine/arginine-rich splicing factor 3 (SRSF3) and SRSF10 (Xiao et al., 2016). YTHDC2 affects the stability and translation of mRNA by recognizing m^{6}A modification (Xu et al., 2015; Wojtas et al., 2017; Kretschmer et al., 2018).

IGF2BPs form another group of m^{6}A readers as they use common RNA binding domains (RBDs) for recognizing m^{6}A-tagged RNA. IGF2BPs contains 4 repetitive KH protein domains, and the third and fourth KH protein domains are essential for IGF2BPs to recognize m^{6}A. IGF2BPs mainly regulate the stability of their target mRNA in an m^{6}A-dependent manner, and in Hela cells they share about 60% target transcripts (Huang et al., 2018). But the regulatory machinery of IGF2BPs remains elusive. Our recent work revealed that YBX1 cooperates with IGF2BPs to promote the stability of m^{6}A-tagged transcripts (Feng et al., 2021), suggesting YBX1 is one component of IGF2BP regulatory machinery. However, what the other factors are involved in the machinery still needs investigation in the future. Several heterogeneous nuclear ribonucleoproteins (HNRNPs) including HNRNPC, HNRNPG, and HNRNPA2/B1 also function as m^{6}A reader. For instance, HNRNPA2B1 can directly bind to the primary miRNA (pri-miRNA) that carry m^{6}A mark, and promotes the processing of the mature of pri-miRNA through cooperating with miRNA microprocessing complex DGCR8 (Alarcón et al., 2015).

Open Scientific Questions

The biology of RNA modification has attracted burst interests, and the important role of m^{6}A modification in regulating RNA fates has been appreciated. While the field become flourishing, some key scientific questions remain unknown. First, how are the activities of m^{6}A modifiers regulated? Changing the expression levels of m^{6}A modifiers in different cells may be a major approach for fine-tuning their activities. For instance, increased expression of several m^{6}A modifiers such as METTL3, FTO, and ALKBH5 have been observed in leukemia cells (discussed in the following) (Li et al., 2017; Vu et al., 2017; Wang et al., 2020). In addition, the activities of m^{6}A modifiers may be affected by metabolites. Recent study showed that oncometabolite 2-hydroxyglutarate (2HG) inhibits FTO (Su et al., 2018). Moreover, the cellular distribution and post-translational modification of m^{6}A modifiers also regulate their activities (Lin et al., 2016; Du et al., 2018; Wei et al., 2018; Sun et al., 2020). Second, what determines the transcript specificity of m^{6}A modifiers? It is known that m^{6}A is installed on mRNA co-transcriptionally by m^{6}A writer complex (Yang et al., 2018), but it is still unknown how the transcripts are selected by m^{6}A writer. Same question is also applicable to m^{6}A erasers and readers. Increasing evidence shows that diverse regulatory machinery can be recruited to m^{6}A-tagged mRNA through m^{6}A readers, and RBPs involved in these machineries might convey specificity of m^{6}A readers toward certain m^{6}A sites or m^{6}A-tagged RNA. Thus, identifying the cofactors of m^{6}A modifiers may be more important in the future. Last, we should appreciate the importance of context issue in RNA modification biology. From this point, it becomes reasonable that RNA m^{6}A is highly dynamic and context-dependent.

RNA m^{6}A IN MAINTAINING THE FUNCTION OF HSCs AND LSCs

HSCs locate at the top of the hematopoietic hierarchy and are responsible for replenishing blood system throughout life. LSCs transformed from normal HSCs initiate the development of myeloid leukemia such as AML. Increasing evidence show that RNA m^{6}A plays key roles in sustaining the function of HSCs and LSCs in normal and malignant hematopoiesis. In the following, we summarize the research advances in this field (**Figure 2**).

RNA m^{6}A Is Essential for HSC Maintenance in Normal Hematopoiesis

Both the emergence and functional maintenance of HSCs in hematopoiesis are delicately controlled. HSCs are derived early from embryonic precursors, such as hemogenic endothelial cells and pre-hematopoietic stem cells (Zhou et al., 2016). The first HSC appears in mid-gestational mouse embryos at embryonic day 10.5 (E10.5), and progressively colonizes fetal liver and dramatically expands there from E12. Before birth, HSCs migrate into bone marrow, where they maintain the homeostasis of hematopoietic system by extensively self-renewing and differentiating into entire blood lineages throughout lifetime.

RNA m^{6}A modification controls the fate determination of HSCs and progenitor cells during vertebrate definitive hematopoiesis. Using a zebrafish model and deleting Mettl3 expression by morpholino (MO), a recent study found that HSPCs differentiation toward erythroid, myeloid, and lymphoid cells is substantially impaired in *mettl3* morphants, while the primitive hematopoiesis is relatively unaltered (Zhang et al., 2017). Mettl3 loss abolishes the transition of endothelial cells into HSCs, as showing the decreased number of hemogenic endothelium and emerging HSPCs in *mettl3* morphants. They investigated the molecular mechanisms by integrating RNA-seq with m^{6}A-seq, and found that deletion of mettl3 in endothelial cells upregulates the Notch and vascular endothelial growth factor pathways, and identified that notch1a as one of the downstream targets of mettl3. They confirmed that Mettl3-mediated m^{6}A modification regulates HSPC generation through inhibiting endothelial Notch signaling, which is mediated by m^{6}A reader Ythdf2 (Zhang et al., 2017). Thus, m^{6}A modulates HSPC specification in early definitive hematopoiesis of zebrafish embryogenesis. Recent studies showed that Mettl3 is also essential for mammalian hematopoiesis (Gao et al., 2020; Jiang et al., 2021). Deletion of *Mettl3* and m^{6}A in *Vav-Cre;Mettl3$^{fl/fl}$* mice caused hematopoietic failure with expansion of phenotypical Lin$^-$Sca-1$^+$c-Kit$^+$ (LSK) HSPCs in the fetal liver that were functionally defective. Further analysis revealed that loss of m^{6}A results in robust transcriptional upregulation of interferon-stimulated genes (ISGs) and 2′, 5′-oligoadenylate synthetase (*Oas*) genes and induces a dsRNA-mediated innate immune response, showing activation of the OAS-RNase L and PKR-eIF2a pathways and upregulation of the dsRNA sensors MDA5 and RIG-I (Gao et al., 2020). These studies reveal that RNA m^{6}A plays key role in embryonic hematopoiesis.

In adult hematopoiesis, m^{6}A is essential for maintaining HSC function. Inducible deletion of *Mettl3* in adult hematopoietic system in *Mx1-Cre;Mettl3$^{fl/fl}$* mice does not significantly change the production ratio of mature myeloid cells, but blocks the normal differentiation and causes accumulation of phenotypical HSCs with long-term hematopoietic disorder and impaired hematopoietic reconstitution potential (Yao et al., 2018; Cheng et al., 2019; Lee et al., 2019). Knockdown of METTL3 or METTL14 by shRNAs can also significantly inhibit the proliferation and promote the differentiation of human umbilical cord blood derived CD34$^+$ HSPCs (Vu et al., 2017; Martin and Park, 2018). Using single-cell RNA-seq in combination with transcriptomic profiling of HSPCs, researchers found that m^{6}A-deficient HSCs fails to symmetrically differentiate due to alteration of *Myc* mRNA abundance, and enforced expression of Myc rescues differentiation defect of *Mettl3*-deficient HSCs (Cheng et al., 2019; Lee et al., 2019). Thus, these studies reveal a key role of m^{6}A in governing HSC differentiation in adult hematopoietic system, which is distinct to its function in embryonic hematopoiesis, indicating a developmental stage-specific requirement for m^{6}A in hematopoiesis.

Interestingly, recent works further add the complexity about the role of m^{6}A in hematopoiesis. Two early studies found that YTHDF2 depletion significantly expands hematopoietic stem

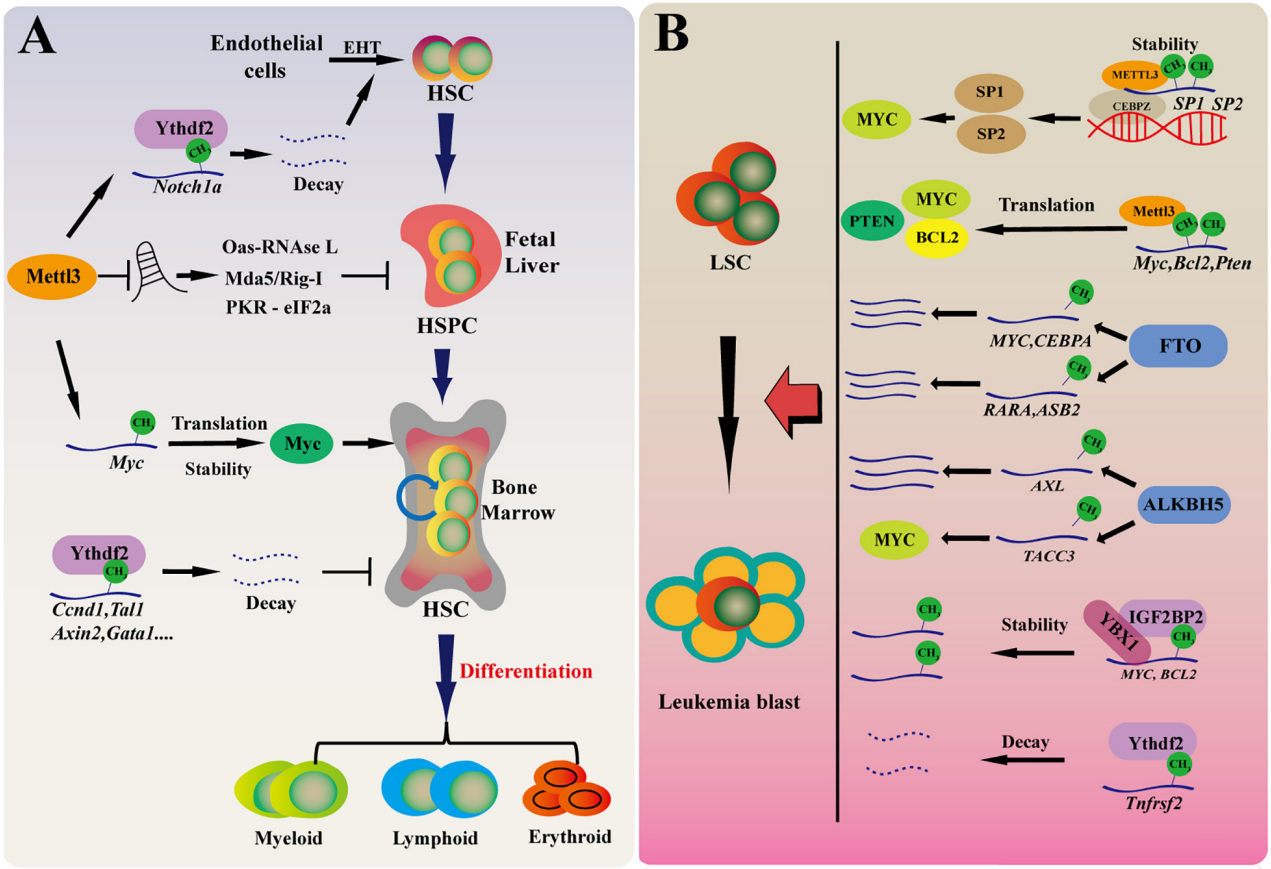

FIGURE 2 | RNA m^{6}A in maintaining HSCs and LSCs function in normal and malignant hematopoiesis. **(A)** m^{6}A modification regulates normal hematopoietic system. Mettl3 mediated m^{6}A modification regulates HSPC fate specification by inhibiting Notch signaling during early definitive hematopoiesis. During HSPC expansion in fetal liver, Mettl3 deletion promotes dsRNA formation, activates OAS RNase L and PKR-eIF2a pathways, and upregulates MDA5/RIG-I, leading to hematopoietic failure. In adult HSCs, Mettl3 regulates the translation of c-Myc and promotes the proliferation of hematopoietic stem cells. Ythdf2-deficient HSCs display chronic activation of inflammatory pathways, resulting in a progressive myeloid bias. EHT, endothelial-to-hematopoietic transition. **(B)** The role of RNA m^{6}A for LSCs in myeloid leukemia. The m^{6}A level of cancer-related genes are affected with m^{6}A "writer," "reader," and "eraser" by regulating mRNA translation, decay, stability in the development of AML. These cancer-related genes promote the development of leukemia by affecting proliferation, differentiation, cancer self-renewal, and apoptosis.

cells in mouse and human umbilical cord blood without skewing lineage differentiation preference or leading to hematopoietic malignancy (Li et al., 2018; Paris et al., 2019). Intriguingly, Mapperley et al. (2021) recently analyzed the long-term effect of Ythdf2 deletion on HSC maintenance and multilineage hematopoiesis. They found that HSCs from young mice with *Ythdf2* deficiency cannot be transplanted continuously. Furthermore, *Ythdf2*-deficient HSCs displays chronic activation of inflammatory pathways, resulting in a progressive myeloid bias, loss of lymphoid potential and HSC expansion with functional defect of long-term reconstitution (Mapperley et al., 2021). Of course, the roles of other m^{6}A readers in hematopoiesis remain unknown. However, it becomes clear that m^{6}A eraser AlKBH5 is not dispensable for adult hematopoiesis and HSC function. Using Mx1-Cre to conditional delete *Albkh5* in mouse hematopoietic cells, we found that Alkbh5 deficiency does not affect normal hematopoiesis. We also performed serial transplantation and confirmed that loss of Alkbh5 does not affect HSCs self-renewal, differentiation and long-term hematopoietic function (Shen et al., 2020; Wang et al., 2020). Knockdown of ALKBH5 also does not affect the colony forming ability of HSPCs derived from human umbilical cord blood (Wang et al., 2020). We speculate that FTO, another m^{6}A eraser, may compensate the function of Alkbh5 in *Alkbh5*-deficient cells, thus loss of Alkbh5 alone does not significant affect normal hematopoiesis and HSC function. Overall, we believe that m^{6}A acts much more complex role in hematopoiesis (**Figure 2A**).

The Role of RNA m^{6}A for LSCs in Myeloid Leukemia

Most myeloid leukemia is initiated by LSCs that are transformed from dysregulated HSCs. Similarly, RNA m^{6}A also plays essential roles in leukemia and LSC function. Compared with normal HSPCs or other types of tumor cells, the expression level of METTL3 is obviously higher in AML (Barbieri et al., 2017; Vu et al., 2017). Overexpression of METTL3 inhibits leukemia cell differentiation and increases cell growth; conversely, deletion

of METTL3 in human myeloid leukemia cells can induce cell differentiation and promote apoptosis, and delay *in vivo* leukemia development (Barbieri et al., 2017; Vu et al., 2017; Guirguis et al., 2020). Single-nucleotide-resolution mapping coupled with RNA-seq and ribosome profiling revealed that m^{6}A promotes the translation of downstream targets including *c-MYC*, *BCL2,* and *PTEN* (Vu et al., 2017). METTL3 may act in another way. In another study, ChIP-seq experiment showed that METTL3, independently of METTL14, binds to chromatin and localizes to transcriptional start site (TSS) of active genes. Promoter-bound METTL3 recruits CEBPZ and regulates the translation of downstream oncogenic drivers SP1 and SP2. SP1 in turn regulates the expression of c-MYC and ultimately promotes the occurrence and development of leukemia (Barbieri et al., 2017). Another subunit of m^{6}A writer core complex, METTL14 is also highly expressed in AML cells and is required for leukemia. In mechanism, transcription factor SPI1 negatively regulates METTL14 expression, and MYB and MYC are functional downstream targets of METTL14 (Weng et al., 2018).

Actually, FTO is the first m^{6}A modifier that is reported to play an oncogenic role in AML (Li et al., 2017). FTO is highly expressed in leukemia cells from different subtypes of AML, and especially in leukemia stem cells. FTO knockout or inhibition can significantly inhibit the self-renewal of leukemia stem cells, thus hindering the occurrence and development of AML; conversely, high expression of FTO promotes the growth of leukemia cells and accelerates leukemogenesis. Mechanistically, FTO regulates the degradation of *ASB2* and *RARA* mRNA in an m^{6}A-dependent manner (Li et al., 2017). IDH1/2 catalyze the oxidative decarboxylation of isocitrate to α-ketoglutarate (α-KG). IDH1/2 mutations occur in about 20% of AML, resulting in increased production of R-2-hydroglutarate (R-2HG). Thus, R-2HG is considered as an oncometabolite. Interestingly, as R-2HG is structurally close to α-KG, it competitively inhibits the activity of α-KG-dependent dioxygease, FTO, thereby increasing the overall level of m^{6}A without affecting FTO expression and decreasing the stability of *MYC* and *CEBPA* mRNA in R-2HG-sensitive leukemia cells (Su et al., 2018). Moreover, a recent study found that R-2HG also suppresses glycolysis in leukemia cells by abrogating FTO/m^{6}A/YTHDF2-mediated upregulation of two critical glycolytic genes *phosphofructokinase platelet (PFKP)* and *lactate dehydrogenase B (LDHB)* (Qing et al., 2021). Thus, these works provide rationale for FTO as a potential therapeutic target for AML treatment.

ALKBH5 is regarded as the major demethylase for most mRNA m^{6}A, as FTO only demethylates 5–10% of mRNA m^{6}A in common cells (maybe up to 40% in some AML cells). Recent works from our group and Dr. Chen's group simultaneously revealed the key and selective role of ALKBH5 in self-renewal and maintenance of leukemia stem cells (Shen et al., 2020; Wang et al., 2020). We found that ALKBH5 expression is regulated by chromatin state alteration during leukemogenesis of human AML, which is mediated by histone demethylase KDM4C. KDM4C reduces H3K9me3 levels and promotes recruitment of MYB and Pol II to *ALKBH5* promoter region (Wang et al., 2020). Using MLL-AF9 mouse model and a series of leukemia reconstitution experiments in the *Alkbh5* conditional knockout mice, we confirmed that *Alkbh5* deletion could significantly inhibit the occurrence and development of AML and prolong the survival time of the knockout mice. Furthermore, integration of m^{6}A-seq, SLAM-seq, Ribo-seq data analysis showed that ALKBH5 knockdown significantly increases the overall level of m^{6}A modification, decreases the stability of the overall mRNA, and does not affect the overall mRNA translation. We focused on a receptor tyrosine kinase AXL and found that ALKBH5 affects *AXL* mRNA stability in an m^{6}A-dependent way. AXL belongs to the TAM (TYRO3, AXL, MER) receptor kinase family, and has been reported that AXL can phosphorylate FLT3 in AML to promote the pathological progress of AML. At the same time, AML patients with high expression of AXL have poor prognosis (Park et al., 2015). We confirmed that AXL activates downstream PI3K/AKT pathway in AML and mediates the function of ALKBH5 in AML. Meanwhile, Cheng et al. (2020) and Shen et al. (2020) found that ALKBH5 knockdown accelerates the degradation of *TACC3* mRNA, an oncogenic factor described to be critical in the growth of various cancer cells. These two complimentary studies clearly uncover the important role of ALKBH5 in the pathogenesis of AML and LSCs maintenance, but has no significant effect on normal hematopoietic differentiation. The findings from our group also link chromatin state dynamics with expression regulation of m^{6}A modifiers.

The roles of other m^{6}A modifiers in LSC maintenance and leukemogenesis are also being recognized recently. It has been reported that WTAP is highly expressed in AML and is associated with poor prognosis. Knockdown of WTAP inhibits cell proliferation, induces apoptosis and enhances myeloid differentiation, and plays a oncogenic role in leukemia (Bansal et al., 2014; Naren et al., 2021). Importantly, upregulation of WTAP is not enough to promote the proliferation of leukemia cells when the function of METTL3 is absent, indicating that the oncogenic role of WTAP depends on METTL3 and RNA m^{6}A (Sorci et al., 2018). Paris et al. (2019) found that YTHDF2 is highly expressed in AML and is required for disease initiation as well as propagation in mouse and human AML. Ythdf2 loss decreases the half-life of diverse m^{6}A transcripts that contribute to the overall integrity of LSC function, including the tumor necrosis factor receptor Tnfrsf2, whose upregulation in *Ythdf2*-deficient LSCs primes cells for apoptosis (Paris et al., 2019). IGF2BPs promote mRNA stability and translation (Huang et al., 2018). It has been found that IGF2BP1 affects the proliferation and tumorigenic potential of leukemia cells by regulating the key factors of self-renewal, such as HOXB4, MYB, and ALDH1A1 (Elcheva et al., 2020; Schuschel et al., 2020). Overall, while the function of the remaining m^{6}A modifiers in hematologic malignancies is being exploited, the studies so far clearly show that RNA m^{6}A is essential for the development of myeloid leukemia and LSCs maintenance (**Figure 2B**).

Targeting m^{6}A Modifiers: A Promising Therapeutic Strategy for Myeloid Leukemia

Current studies have established a rationale for developing therapeutic approaches against leukemia by targeting RNA m^{6}A

modifiers. In a recent study, via a high throughput screen of 250,000 diverse drug-like compounds, a highly potent and selective first-in-class catalytic inhibitor of METTL3, STM2457, was identified (Yankova et al., 2021). STM2457 can directly bind to the SAM binding site of METTL3, thereby blocking its methyltransferase activity and affecting the translation of BRD4, c-Myc, SP1 and other genes. STM2457 treatment significantly inhibits proliferation, induces differentiation and increase apoptosis of leukemia cells. Surprisingly, STM2457 has no significant effect on normal HSCs and other normal cells, although previous studies showed that genetic deletion of METTL3 impairs HSC differentiation and damage normal hematopoiesis (Vu et al., 2017; Martin and Park, 2018). This study may present a promising targeting strategy for AML treatment. Notably, given that METTL3 is the core subunit of RNA m^{6}A writer complex and is essential for various physiological processes, it needs to pay much attention to the possible side effects resulting from targeting METTL3 in the future.

FTO is another potential target for cancer therapy, and small molecules against FTO are being developed. Meclofenamic acid (MA) is an inhibitor of FTO (Huang et al., 2015), and based on the structural principles underlying FTO/MA interaction, recently. Huang Y. et al. (2019) developed new FTO inhibitors FB23 and FB23-2, and found that FB23-2 displays inhibitory effects on leukemia cells *in vitro* and *in vivo*. They further conducted a structure-based virtual screening of the 260,000 compounds, and identified two small molecule inhibitors CS1 (bisantrene) and CS2 (brequinara). Inhibition of FTO by these two compounds attenuates LSC self-renewal and reprograms immune response (Su et al., 2020). The inhibition of immune escape of leukemia cells with targeting FTO is mainly associated with the immunosuppressive molecule LILRB4, which is highly expressed in leukemia cells. These studies may provide a model for identifying potential inhibitors for m^{6}A modifiers. In the future, it is necessary to further clarify the role of FTO in normal hematopoiesis and HSCs. Strikingly, recent studies of our group and Dr. Chen's group have clearly showed that ALKBH5 is essential for AML stem cells but dispensable for normal HSCs and hematopoiesis, which signify ALKBH5 as a novel target for AML treatment. In addition, genetic deletion of Alkbh5 has no significant effect on the whole life span and physiological status of mice except spermatogenesis (Zheng et al., 2013). From this point, we believe ALKBH5 might be another very promising therapeutic target.

Open Scientific Questions

It becomes clear that RNA m^{6}A modification and the related modifiers play critical roles in maintaining stem cell function in normal and malignant hematopoiesis. However, some key scientific questions remain unclear. For instance, in term of definitive hematopoiesis during mammalian embryogenesis, which developmental stages are really affected by RNA m^{6}A? Why does m^{6}A play distinct roles in embryonic and adult hematopoiesis? What is the underlying mechanism? Interestingly, some m^{6}A modifiers are selectively essential for LSCs and leukemia but are dispensable for normal hematopoiesis. What is the underlying rationale for these different effects on LSCs and normal HSCs of certain m^{6}A modifiers, such as ALKBH5? Moreover, genomic instability is one of main mechanisms for cancer development and progression, and various genetic deletions, insertions or chromosome translocations have been found in leukemia. Recent studies have shown that m^{6}A involves in DNA damage repair and genomic stability (Xiang et al., 2017; Zhang et al., 2020), it will be interesting to explore whether RNA m^{6}A modification regulates genomic instability during leukemogenesis. Rapidly accumulating evidence also shows the crosstalk between RNA methylation and histone/DNA epigenetic mechanisms (Huang H. et al., 2019; Liu et al., 2020; Wei and He, 2021), which guides the recruitment of chromatin modifiers or RNA m^{6}A machinery, and regulates the transcriptional activity and translation. Thus, further exploring the underlying mechanisms might provide more information for the specification of RNA m^{6}A in normal and malignant hematopoiesis. In addition, m^{6}A writers and erasers are all required for hematologic malignancies, and deletion of either one results in similar phenotypes. From the biochemical or molecular view, m^{6}A writers and erasers act in totally opposite ways in m^{6}A modification, why do they function similarly at the pathological context? We propose that m^{6}A plays a protective role under stress setting, such as oncogene transformation, which induces higher level of transcription during leukemogenesis. In response to this higher oncogenesis-induced transcriptional stress, cells strengthen the regulatory networks including RNA m^{6}A pathway to maintain the homeostasis of RNA metabolism. Thus, interfering RNA m^{6}A pathway by altering either m^{6}A writers or erasers results in the similar cellular consequence under pathogenesis. Overall, these questions need to be addressed in the future.

CONCLUSION AND PERSPECTIVES

In summary, accumulated evidences in the past few years show that m^{6}A modification plays essential role in normal hematopoiesis and leukemia pathogenesis. However, the underlying molecular mechanisms are still unclear. How does RNA m^{6}A specifically and precisely regulate the physiological and pathological processes of hematopoiesis. RBPs such as YBX1 regulate the interaction between m^{6}A-tagged RNA substrates and m^{6}A modifiers (Feng et al., 2021), suggesting that RBPs or cofactors for m^{6}A modifiers may act key roles in determining the precision and specificity of RNA m^{6}A. In addition, it is necessary to investigate the dynamics of RNA m^{6}A profiling during normal and malignant hematopoiesis. Unfortunately, current approaches of m^{6}A-seq are not suitable for rare stem cells. Therefore, developing a highly sensitive m^{6}A-seq is urgent and very useful in the future. Given the important role of RNA m^{6}A in AML, it will be very exciting to explore the therapeutic potentials and clinical benefit by targeting m^{6}A modifiers in AML treatment. Indeed, small molecule compounds that target m^{6}A regulators (METTL3 and FTO) have been developed (Qiao et al., 2016; Huang Y. et al., 2019; Yankova et al., 2021). In the next, developing effective therapeutic strategies by targeting

RNA m^{6}A pathway and clarifying their feasibility in the clinical should be paid much attention. Taken together, these studies shed light on the role of RNA m^{6}A in normal and malignant hematopoiesis, and we believe this just opens the door for us to explore the unknown RNA modification world.

AUTHOR CONTRIBUTIONS

PW, MF, GH, and HZ wrote the manuscript. GH prepared the figures. RY, YL, SY, PL, and YW contributed to critically discussing the manuscript. All authors contributed to the article and approved the submitted version.

FUNDING

This work was supported by grants to HZ from the National Natural Science Foundation of China (81870124 and 81722003), the Natural Science Foundation of Hubei Province (2019CFA073), and the Medical Science Advancement Program (Basic Medical Sciences) of Wuhan University (TFJC2018005).

ACKNOWLEDGMENTS

We acknowledge the members of our laboratory for helpful discussion.

REFERENCES

Alarcón, C. R., Goodarzi, H., Lee, H., Liu, X., Tavazoie, S., and Tavazoie, S. F. (2015). HNRNPA2B1 is a mediator of m(6)A-dependent nuclear RNA processing events. *Cell* 162, 1299–1308. doi: 10.1016/j.cell.2015.08.011

Bansal, H., Yihua, Q., Iyer, S. P., Ganapathy, S., Proia, D. A., Penalva, L. O., et al. (2014). WTAP is a novel oncogenic protein in acute myeloid leukemia. *Leukemia* 28, 1171–1174. doi: 10.1038/leu.2014.16

Barbieri, I., Tzelepis, K., Pandolfini, L., Shi, J., Millan-Zambrano, G., Robson, S. C., et al. (2017). Promoter-bound METTL3 maintains myeloid leukaemia by m(6)A-dependent translation control. *Nature* 552, 126–131. doi: 10.1038/nature24678

Cancer Genome Atlas Research Network Ley, T. J., Miller, C., Ding, L., Raphael, B. J., Mungall, A. J., et al. (2013). Genomic and epigenomic landscapes of adult de novo acute myeloid leukemia. *N. Engl. J. Med.* 368, 2059–2074. doi: 10.1056/NEJMoa1301689

Cheng, Y., Luo, H., Izzo, F., Pickering, B. F., Nguyen, D., Myers, R., et al. (2019). m(6)A RNA methylation maintains hematopoietic stem cell identity and symmetric commitment. *Cell Rep.* 28, 1703–1716. doi: 10.1016/j.celrep.2019.07.032

Cheng, Y., Luo, H., and Kharas, M. G. (2020). Rubbing out leukemia stem cells by erasing the eraser. *Cell Stem Cell* 27, 3–5. doi: 10.1016/j.stem.2020.06.009

Desrosiers, R., Friderici, K., and Rottman, F. (1974). Identification of methylated nucleosides in messenger RNA from Novikoff hepatoma cells. *Proc. Natl. Acad. Sci. U.S.A.* 71, 3971–3975. doi: 10.1073/pnas.71.10.3971

Di Timoteo, G., Dattilo, D., Centrón-Broco, A., Colantoni, A., Guarnacci, M., Rossi, F., et al. (2020). Modulation of circRNA Metabolism by mA modification. *Cell Rep.* 31:107641. doi: 10.1016/j.celrep.2020.107641

Dohner, H., Weisdorf, D. J., and Bloomfield, C. D. (2015). Acute Myeloid Leukemia. *N. Engl. J. Med.* 373, 1136–1152. doi: 10.1056/NEJMra1406184

Dominissini, D., Moshitch-Moshkovitz, S., Schwartz, S., Salmon-Divon, M., Ungar, L., Osenberg, S., et al. (2012). Topology of the human and mouse m6A RNA methylomes revealed by m6A-seq. *Nature* 485, 201–206. doi: 10.1038/nature11112

Du, H., Zhao, Y., He, J., Zhang, Y., Xi, H., Liu, M., et al. (2016). YTHDF2 destabilizes m(6)A-containing RNA through direct recruitment of the CCR4-NOT deadenylase complex. *Nat. Commun.* 7:12626. doi: 10.1038/ncomms12626

Du, Y., Hou, G., Zhang, H., Dou, J., He, J., Guo, Y., et al. (2018). SUMOylation of the m6A-RNA methyltransferase METTL3 modulates its function. *Nucleic Acids Res.* 46, 5195–5208. doi: 10.1093/nar/gky156

Elcheva, I. A., Wood, T., Chiarolanzio, K., Chim, B., Wong, M., Singh, V., et al. (2020). RNA-binding protein IGF2BP1 maintains leukemia stem cell properties by regulating HOXB4, MYB, and ALDH1A1. *Leukemia* 34, 1354–1363. doi: 10.1038/s41375-019-0656-9

Feng, M., Xie, X., Han, G., Zhang, T., Li, Y., Li, Y., et al. (2021). YBX1 is required for maintaining myeloid leukemia cell survival by regulating BCL2 stability in an m6A-dependent manner. *Blood* 138, 71–85. doi: 10.1182/blood.2020009676

Gao, Y., Vasic, R., Song, Y., Teng, R., Liu, C., Gbyli, R., et al. (2020). m(6)a modification prevents formation of endogenous double-stranded RNAs and deleterious innate immune responses during hematopoietic development. *Immunity* 52, 1007–1021. doi: 10.1016/j.immuni.2020.05.003

Guirguis, A. A., Liddicoat, B. J., and Dawson, M. A. (2020). The old and the new: DNA and RNA methylation in normal and malignant hematopoiesis. *Exp. Hematol.* 90, 1–11. doi: 10.1016/j.exphem.2020.09.193

Helm, M., and Motorin, Y. (2017). Detecting RNA modifications in the epitranscriptome: predict and validate. *Nat. Rev. Genet.* 18, 275–291. doi: 10.1038/nrg.2016.169

Hsu, P. J., Zhu, Y., Ma, H., Guo, Y., Shi, X., Liu, Y., et al. (2017). Ythdc2 is an N(6)-methyladenosine binding protein that regulates mammalian spermatogenesis. *Cell Res.* 27, 1115–1127. doi: 10.1038/cr.2017.99

Hu, Y., Ouyang, Z., Sui, X., Qi, M., Li, M., He, Y., et al. (2020). Oocyte competence is maintained by m(6)A methyltransferase KIAA1429-mediated RNA metabolism during mouse follicular development. *Cell Death Differ.* 27, 2468–2483. doi: 10.1038/s41418-020-0516-1

Huang, H., Weng, H., and Chen, J. (2020). m(6)a modification in coding and non-coding RNAs: roles and therapeutic implications in cancer. *Cancer Cell* 37, 270–288. doi: 10.1016/j.ccell.2020.02.004

Huang, H., Weng, H., Sun, W., Qin, X., Shi, H., Wu, H., et al. (2018). Recognition of RNA N(6)-methyladenosine by IGF2BP proteins enhances mRNA stability and translation. *Nat. Cell Biol.* 20, 285–295. doi: 10.1038/s41556-018-0045-z

Huang, H., Weng, H., Zhou, K., Wu, T., Zhao, B. S., Sun, M., et al. (2019). Histone H3 trimethylation at lysine 36 guides m(6)A RNA modification co-transcriptionally. *Nature* 567, 414–419. doi: 10.1038/s41586-019-1016-7

Huang, J., Dong, X., Gong, Z., Qin, L. Y., Yang, S., Zhu, Y. L., et al. (2019). Solution structure of the RNA recognition domain of METTL3-METTL14 N(6)-methyladenosine methyltransferase. *Protein Cell* 10, 272–284. doi: 10.1007/s13238-018-0518-7

Huang, Y., Su, R., Sheng, Y., Dong, L., Dong, Z., Xu, H., et al. (2019). Small-molecule targeting of oncogenic FTO demethylase in acute myeloid leukemia. *Cancer Cell* 35, 677–691. doi: 10.1016/j.ccell.2019.03.006

Huang, Y., Yan, J., Li, Q., Li, J., Gong, S., Zhou, H., et al. (2015). Meclofenamic acid selectively inhibits FTO demethylation of m6A over ALKBH5. *Nucleic Acids Res.* 43, 373–384. doi: 10.1093/nar/gku1276

Jia, G., Fu, Y., Zhao, X., Dai, Q., Zheng, G., Yang, Y., et al. (2011). N6-methyladenosine in nuclear RNA is a major substrate of the obesity-associated FTO. *Nat. Chem. Biol.* 7, 885–887. doi: 10.1038/nchembio.687

Jiang, X., Liu, B., Nie, Z., Duan, L., Xiong, Q., Jin, Z., et al. (2021). The role of m6A modification in the biological functions and diseases. *Signal Transduct. Target Ther.* 6:74. doi: 10.1038/s41392-020-00450-x

Knuckles, P., Lence, T., Haussmann, I. U., Jacob, D., Kreim, N., Carl, S. H., et al. (2018). Zc3h13/Flacc is required for adenosine methylation by bridging the mRNA-binding factor Rbm15/Spenito to the m(6)A machinery component Wtap/Fl(2)d. *Genes Dev.* 32, 415–429. doi: 10.1101/gad.309146.117

Kretschmer, J., Rao, H., Hackert, P., Sloan, K. E., Höbartner, C., and Bohnsack, M. T. (2018). The mA reader protein YTHDC2 interacts with the small ribosomal subunit and the 5'-3' exoribonuclease XRN1. *RNA* 24, 1339–1350. doi: 10.1261/rna.064238.117

Lee, A. S. Y., Kranzusch, P. J., and Cate, J. H. D. (2015). eIF3 targets cell-proliferation messenger RNAs for translational activation or repression. *Nature* 522, 111–114. doi: 10.1038/nature14267

Lee, H., Bao, S., Qian, Y., Geula, S., Leslie, J., Zhang, C., et al. (2019). Stage-specific requirement for Mettl3-dependent m(6)A mRNA methylation during haematopoietic stem cell differentiation. *Nat. Cell Biol.* 21, 700–709. doi: 10.1038/s41556-019-0318-1

Li, Z., Qian, P., Shao, W., Shi, H., He, X. C., Gogol, M., et al. (2018). Suppression of m(6)A reader Ythdf2 promotes hematopoietic stem cell expansion. *Cell Res.* 28, 904–917. doi: 10.1038/s41422-018-0072-0

Li, Z., Weng, H., Su, R., Weng, X., Zuo, Z., Li, C., et al. (2017). FTO plays an oncogenic role in acute myeloid leukemia as a N(6)-methyladenosine RNA demethylase. *Cancer Cell* 31, 127–141. doi: 10.1016/j.ccell.2016.11.017

Lin, S., Choe, J., Du, P., Triboulet, R., and Gregory, R. I. (2016). The m(6)A methyltransferase METTL3 promotes translation in human cancer cells. *Mol. Cell.* 62, 335–345. doi: 10.1016/j.molcel.2016.03.021

Liu, J., Dou, X., Chen, C., Chen, C., Liu, C., Xu, M. M., et al. (2020). N (6)-methyladenosine of chromosome-associated regulatory RNA regulates chromatin state and transcription. *Science* 367, 580–586. doi: 10.1126/science.aay6018

Liu, J., Yue, Y., Han, D., Wang, X., Fu, Y., Zhang, L., et al. (2014). A METTL3-METTL14 complex mediates mammalian nuclear RNA N6-adenosine methylation. *Nat. Chem. Biol.* 10, 93–95. doi: 10.1038/nchembio.1432

Lu, R., Wang, P., Parton, T., Zhou, Y., Chrysovergis, K., Rockowitz, S., et al. (2016). Epigenetic perturbations by Arg882-mutated DNMT3A potentiate aberrant stem cell gene-expression program and acute leukemia development. *Cancer Cell* 30, 92–107. doi: 10.1016/j.ccell.2016.05.008

Mapperley, C., Van De Lagemaat, L. N., Lawson, H., Tavosanis, A., Paris, J., Campos, J., et al. (2021). The mRNA m6A reader YTHDF2 suppresses proinflammatory pathways and sustains hematopoietic stem cell function. *J. Exp. Med.* 218:e20200829. doi: 10.1084/jem.20200829

Martin, G. H., and Park, C. Y. (2018). Meddling with METTLs in normal and leukemia stem cells. *Cell Stem Cell* 22, 139–141. doi: 10.1016/j.stem.2018.01.013

Meyer, K. D., Saletore, Y., Zumbo, P., Elemento, O., Mason, C. E., and Jaffrey, S. R. (2012). Comprehensive analysis of mRNA methylation reveals enrichment in 3' UTRs and near stop codons. *Cell* 149, 1635–1646. doi: 10.1016/j.cell.2012.05.003

Naren, D., Yan, T., Gong, Y., Huang, J., Zhang, D., Sang, L., et al. (2021). High Wilms' tumor 1 associating protein expression predicts poor prognosis in acute myeloid leukemia and regulates m(6)A methylation of MYC mRNA. *J. Cancer Res. Clin. Oncol.* 147, 33–47. doi: 10.1007/s00432-020-03373-w

Olson, O. C., Kang, Y. A., and Passegue, E. (2020). Normal hematopoiesis is a balancing act of self-renewal and regeneration. *Cold Spring Harb. Perspect. Med.* 10:a035519. doi: 10.1101/cshperspect.a035519

Orkin, S. H., and Zon, L. I. (2008). Hematopoiesis: an evolving paradigm for stem cell biology. *Cell* 132, 631–644. doi: 10.1016/j.cell.2008.01.025

Paris, J., Morgan, M., Campos, J., Spencer, G. J., Shmakova, A., Ivanova, I., et al. (2019). Targeting the RNA m(6)A reader YTHDF2 selectively compromises cancer stem cells in acute myeloid leukemia. *Cell Stem Cell* 25, 137–148. doi: 10.1016/j.stem.2019.03.021

Park, I. K., Mundy-Bosse, B., Whitman, S. P., Zhang, X., Warner, S. L., Bearss, D. J., et al. (2015). Receptor tyrosine kinase Axl is required for resistance of leukemic cells to FLT3-targeted therapy in acute myeloid leukemia. *Leukemia* 29, 2382–2389. doi: 10.1038/leu.2015.147

Patil, D. P., Chen, C.-K., Pickering, B. F., Chow, A., Jackson, C., Guttman, M., et al. (2016). m(6)A RNA methylation promotes XIST-mediated transcriptional repression. *Nature* 537, 369–373. doi: 10.1038/nature19342

Ping, X. L., Sun, B. F., Wang, L., Xiao, W., Yang, X., Wang, W. J., et al. (2014). Mammalian WTAP is a regulatory subunit of the RNA N6-methyladenosine methyltransferase. *Cell Res.* 24, 177–189. doi: 10.1038/cr.2014.3

Qiao, Y., Zhou, B., Zhang, M., Liu, W., Han, Z., Song, C., et al. (2016). A Novel Inhibitor of the Obesity-Related Protein FTO. *Biochemistry* 55, 1516–1522. doi: 10.1021/acs.biochem.6b00023

Qing, Y., Dong, L., Gao, L., Li, C., Li, Y., Han, L., et al. (2021). R-2-hydroxyglutarate attenuates aerobic glycolysis in leukemia by targeting the FTO/m(6)A/PFKP/LDHB axis. *Mol. Cell.* 81, 922.e9–939.e9. doi: 10.1016/j.molcel.2020.12.026

Roundtree, I. A., Luo, G.-Z., Zhang, Z., Wang, X., Zhou, T., Cui, Y., et al. (2017). YTHDC1 mediates nuclear export of N-methyladenosine methylated mRNAs. *eLife* 6:e31311. doi: 10.7554/eLife.31311

Schuschel, K., Helwig, M., Huttelmaier, S., Heckl, D., Klusmann, J. H., and Hoell, J. I. (2020). RNA-binding proteins in acute leukemias. *Int. J. Mol. Sci.* 21:3409. doi: 10.3390/ijms21103409

Shen, C., Sheng, Y., Zhu, A. C., Robinson, S., Jiang, X., Dong, L., et al. (2020). RNA demethylase ALKBH5 selectively promotes tumorigenesis and cancer stem cell self-renewal in acute myeloid leukemia. *Cell Stem Cell* 27, 64–80. doi: 10.1016/j.stem.2020.04.009

Shi, H., Wang, X., Lu, Z., Zhao, B. S., Ma, H., Hsu, P. J., et al. (2017). YTHDF3 facilitates translation and decay of N-methyladenosine-modified RNA. *Cell Res.* 27, 315–328. doi: 10.1038/cr.2017.15

Shlush, L. I., Zandi, S., Mitchell, A., Chen, W. C., Brandwein, J. M., Gupta, V., et al. (2014). Identification of pre-leukaemic haematopoietic stem cells in acute leukaemia. *Nature* 506, 328–333. doi: 10.1038/nature13038

Sorci, M., Ianniello, Z., Cruciani, S., Larivera, S., Ginistrelli, L. C., Capuano, E., et al. (2018). METTL3 regulates WTAP protein homeostasis. *Cell Death Dis.* 9:796. doi: 10.1038/s41419-018-0843-z

Su, R., Dong, L., Li, C., Nachtergaele, S., Wunderlich, M., Qing, Y., et al. (2018). R-2HG exhibits anti-tumor activity by targeting FTO/m(6)A/MYC/CEBPA signaling. *Cell* 172, 90–105. doi: 10.1016/j.cell.2017.11.031

Su, R., Dong, L., Li, Y., Gao, M., Han, L., Wunderlich, M., et al. (2020). Targeting FTO suppresses cancer stem cell maintenance and immune evasion. *Cancer Cell* 38, 79–96. doi: 10.1016/j.ccell.2020.04.017

Sun, H. L., Zhu, A. C., Gao, Y., Terajima, H., Fei, Q., Liu, S., et al. (2020). Stabilization of ERK-phosphorylated METTL3 by USP5 increases m(6)A methylation. *Mol. Cell.* 80, 633.e7–647.e7. doi: 10.1016/j.molcel.2020.10.026

Theler, D., Dominguez, C., Blatter, M., Boudet, J., and Allain, F. H. (2014). Solution structure of the YTH domain in complex with N6-methyladenosine RNA: a reader of methylated RNA. *Nucleic Acids Res.* 42, 13911–13919. doi: 10.1093/nar/gku1116

Vu, L. P., Cheng, Y., and Kharas, M. G. (2019). The biology of m(6)A RNA methylation in normal and malignant hematopoiesis. *Cancer Discov.* 9, 25–33. doi: 10.1158/2159-8290.CD-18-0959

Vu, L. P., Pickering, B. F., Cheng, Y., Zaccara, S., Nguyen, D., Minuesa, G., et al. (2017). The N(6)-methyladenosine (m(6)A)-forming enzyme METTL3 controls myeloid differentiation of normal hematopoietic and leukemia cells. *Nat. Med.* 23, 1369–1376. doi: 10.1038/nm.4416

Wang, J., Li, Y., Wang, P., Han, G., Zhang, T., Chang, J., et al. (2020). Leukemogenic chromatin alterations promote AML leukemia stem cells via a KDM4C-ALKBH5-AXL signaling axis. *Cell Stem Cell* 27, 81–97. doi: 10.1016/j.stem.2020.04.001

Wang, P., Doxtader, K. A., and Nam, Y. (2016). Structural basis for cooperative function of Mettl3 and Mettl14 methyltransferases. *Mol. Cell.* 63, 306–317. doi: 10.1016/j.molcel.2016.05.041

Wang, X., Feng, J., Xue, Y., Guan, Z., Zhang, D., Liu, Z., et al. (2016). Structural basis of N(6)-adenosine methylation by the METTL3-METTL14 complex. *Nature* 534, 575–578. doi: 10.1038/nature18298

Wei, J., and He, C. (2021). Chromatin and transcriptional regulation by reversible RNA methylation. *Curr. Opin. Cell Biol.* 70, 109–115. doi: 10.1016/j.ceb.2020.11.005

Wei, J., Liu, F., Lu, Z., Fei, Q., Ai, Y., He, P. C., et al. (2018). Differential m(6)A, m(6)Am, and m(1)A demethylation mediated by FTO in the cell nucleus and cytoplasm. *Mol. Cell.* 71, 973–985. doi: 10.1016/j.molcel.2018.08.011

Wen, J., Lv, R., Ma, H., Shen, H., He, C., Wang, J., et al. (2018). Zc3h13 regulates nuclear RNA m(6)A methylation and mouse embryonic stem cell self-renewal. *Mol. Cell.* 69, 1028–1038. doi: 10.1016/j.molcel.2018.02.015

Weng, H., Huang, H., Wu, H., Qin, X., Zhao, B. S., Dong, L., et al. (2018). METTL14 inhibits hematopoietic stem/progenitor differentiation and promotes leukemogenesis via mRNA m(6)A modification. *Cell Stem Cell* 22, 191–205. doi: 10.1016/j.stem.2017.11.016

Wilkinson, A. C., Igarashi, K. J., and Nakauchi, H. (2020). Haematopoietic stem cell self-renewal in vivo and ex vivo. *Nat. Rev. Genet.* 21, 541–554. doi: 10.1038/s41576-020-0241-0

Wojtas, M. N., Pandey, R. R., Mendel, M., Homolka, D., Sachidanandam, R., and Pillai, R. S. (2017). Regulation of mA Transcripts by the 3′→5′ RNA Helicase

YTHDC2 is essential for a successful meiotic program in the mammalian germline. *Mol. Cell.* 68, 374.e12–387.e12. doi: 10.1016/j.molcel.2017.09.021

Xiang, Y., Laurent, B., Hsu, C. H., Nachtergaele, S., Lu, Z., Sheng, W., et al. (2017). RNA m(6)A methylation regulates the ultraviolet-induced DNA damage response. *Nature* 543, 573–576. doi: 10.1038/nature21671

Xiao, W., Adhikari, S., Dahal, U., Chen, Y. S., Hao, Y. J., Sun, B. F., et al. (2016). Nuclear m(6)A Reader YTHDC1 regulates mRNA splicing. *Mol. Cell.* 61, 507–519. doi: 10.1016/j.molcel.2016.01.012

Xu, C., Liu, K., Ahmed, H., Loppnau, P., Schapira, M., and Min, J. (2015). Structural basis for the discriminative recognition of N6-methyladenosine RNA by the human YT521-B homology domain family of proteins. *J. Biol. Chem.* 290, 24902–24913. doi: 10.1074/jbc.M115.680389

Xu, C., Wang, X., Liu, K., Roundtree, I. A., Tempel, W., Li, Y., et al. (2014). Structural basis for selective binding of m6A RNA by the YTHDC1 YTH domain. *Nat. Chem. Biol.* 10, 927–929. doi: 10.1038/nchembio.1654

Yang, L., Rodriguez, B., Mayle, A., Park, H. J., Lin, X., Luo, M., et al. (2016). DNMT3A loss drives enhancer hypomethylation in FLT3-ITD-associated leukemias. *Cancer Cell* 30, 363–365. doi: 10.1016/j.ccell.2016.07.015

Yang, Y., Fan, X., Mao, M., Song, X., Wu, P., Zhang, Y., et al. (2017). Extensive translation of circular RNAs driven by N-methyladenosine. *Cell Res.* 27, 626–641. doi: 10.1038/cr.2017.31

Yang, Y., Hsu, P. J., Chen, Y. S., and Yang, Y. G. (2018). Dynamic transcriptomic m(6)A decoration: writers, erasers, readers and functions in RNA metabolism. *Cell Res.* 28, 616–624. doi: 10.1038/s41422-018-0040-8

Yankova, E., Blackaby, W., Albertella, M., Rak, J., De Braekeleer, E., Tsagkogeorga, G., et al. (2021). Small molecule inhibition of METTL3 as a strategy against myeloid leukaemia. *Nature* 593, 597–601. doi: 10.1038/s41586-021-03536-w

Yao, Q. J., Sang, L., Lin, M., Yin, X., Dong, W., Gong, Y., et al. (2018). Mettl3-Mettl14 methyltransferase complex regulates the quiescence of adult hematopoietic stem cells. *Cell Res.* 28, 952–954. doi: 10.1038/s41422-018-0062-2

Yue, Y., Liu, J., Cui, X., Cao, J., Luo, G., Zhang, Z., et al. (2018). VIRMA mediates preferential mA mRNA methylation in 3'UTR and near stop codon and associates with alternative polyadenylation. *Cell Discov.* 4:10. doi: 10.1038/s41421-018-0019-0

Zhang, C., Chen, L., Peng, D., Jiang, A., He, Y., Zeng, Y., et al. (2020). METTL3 and N6-methyladenosine promote homologous recombination-mediated repair of DSBs by modulating DNA-RNA hybrid accumulation. *Mol. Cell.* 79, 425–442. doi: 10.1016/j.molcel.2020.06.017

Zhang, C., Chen, Y., Sun, B., Wang, L., Yang, Y., Ma, D., et al. (2017). m(6)A modulates haematopoietic stem and progenitor cell specification. *Nature* 549, 273–276. doi: 10.1038/nature23883

Zhang, X., Wei, L.-H., Wang, Y., Xiao, Y., Liu, J., Zhang, W., et al. (2019). Structural insights into FTO's catalytic mechanism for the demethylation of multiple RNA substrates. *Proc. Natl. Acad. Sci. U.S.A.* 116, 2919–2924. doi: 10.1073/pnas.1820574116

Zhang, Z., Theler, D., Kaminska, K. H., Hiller, M., De La Grange, P., Pudimat, R., et al. (2010). The YTH domain is a novel RNA binding domain. *J. Biol. Chem.* 285, 14701–14710. doi: 10.1074/jbc.M110.104711

Zheng, G., Dahl, J. A., Niu, Y., Fedorcsak, P., Huang, C. M., Li, C. J., et al. (2013). ALKBH5 is a mammalian RNA demethylase that impacts RNA metabolism and mouse fertility. *Mol. Cell.* 49, 18–29. doi: 10.1016/j.molcel.2012.10.015

Zhou, F., Li, X., Wang, W., Zhu, P., Zhou, J., He, W., et al. (2016). Tracing haematopoietic stem cell formation at single-cell resolution. *Nature* 533, 487–492. doi: 10.1038/nature17997

Conflict of Interest: The authors declare that the research was conducted in the absence of any commercial or financial relationships that could be construed as a potential conflict of interest.

Publisher's Note: All claims expressed in this article are solely those of the authors and do not necessarily represent those of their affiliated organizations, or those of the publisher, the editors and the reviewers. Any product that may be evaluated in this article, or claim that may be made by its manufacturer, is not guaranteed or endorsed by the publisher.

frontiers in Cell and Developmental Biology

BRIEF RESEARCH REPORT
published: 07 September 2021
doi: 10.3389/fcell.2021.698795

A Three-Dimensional Imaging Method for the Quantification and Localization of Dynamic Cell Tracking Posttransplantation

Fengfeng Lu[1,2,3†], Xin Pan[1,2,3†], Wencheng Zhang[1,2,3†], Xin Su[1,2,3], Yuying Gu[4], Hua Qiu[1,5], Shengwei Shen[1,6], Changcheng Liu[1,2,3], Wei Liu[1,2,3], Xicheng Wang[1,2,3], Zhenzhen Zhan[7], Zhongmin Liu[1,2,3,7] and Zhiying He[1,2,3]**

[1] Institute for Regenerative Medicine, Shanghai East Hospital, School of Life Sciences and Technology, Tongji University, Shanghai, China, [2] Shanghai Engineering Research Center of Stem Cells Translational Medicine, Shanghai, China, [3] Shanghai Institute of Stem Cell Research and Clinical Translation, Shanghai, China, [4] Department of Cardiology, Shanghai East Hospital, Tongji University, Shanghai, China, [5] The First Affiliated Hospital of Nanchang University, Nanchang, China, [6] Department of Hepatobiliary and Pancreatic Surgery, Shanghai East Hospital, School of Medicine, Tongji University, Shanghai, China, [7] Institute of Heart Failure, Shanghai East Hospital, Tongji University, Shanghai, China

Cell transplantation has been proposed as a promising therapeutic strategy for curing the diseases requiring tissue repairing and functional restoration. A preclinical method to systematically evaluate the fates of donor cells in recipients, spatially and temporally, is demanded for judging therapeutic potentials for the particularly designed cell transplantation. Yet, the dynamic cell tracking methodology for tracing transplanted cells *in vivo* is still at its early phase. Here, we created a practical protocol for dynamically tracking cell *via* a three-dimensional (3D) technique which enabled us to localize, quantify, and overall evaluate the transplanted hepatocytes within a liver failure mouse model. First, the capacity of 3D bioluminescence imaging for quantifying transplanted hepatocytes was defined. Images obtained from the 3D bioluminescence imaging module were then combined with the CT scanner to reconstruct structure images of host mice. With those reconstructed images, precise locations of transplanted hepatocytes in the liver of the recipient were dynamically monitored. Immunohistochemistry staining of transplanted cells, and the serology assay of liver panel of the host mice were applied to verify the successful engraftment of donor cells in the host livers. Our protocol was practical for evaluating the engraftment efficiency of donor cells at their preclinical phases, which is also applicable as a referable standard for studying the fates of other transplanted cells, such as stem cell-derived cell types, during preclinical studies with cell transplantation therapy.

Keywords: cell transplantation, *in vivo* tracking, bioluminescence imaging (BLI), computer tomography (CT), cell distribution

OPEN ACCESS

Edited by:
Melissa R. Andrews, University of Southampton, United Kingdom

Reviewed by:
Ragai Mitry, King's College London, United Kingdom
Vanderson Rocha, University of São Paulo, Brazil

***Correspondence:**
Zhongmin Liu
liu.zhongmin@tongji.edu.cn
Zhiying He
zyhe@tongji.edu.cn

† These authors have contributed equally to this work

Specialty section:
This article was submitted to Stem Cell Research, a section of the journal Frontiers in Cell and Developmental Biology

Received: *22 April 2021*
Accepted: *03 August 2021*
Published: *07 September 2021*

Citation:
Lu F, Pan X, Zhang W, Su X, Gu Y, Qiu H, Shen S, Liu C, Liu W, Wang X, Zhan Z, Liu Z and He Z (2021) A Three-Dimensional Imaging Method for the Quantification and Localization of Dynamic Cell Tracking Posttransplantation. Front. Cell Dev. Biol. 9:698795. doi: 10.3389/fcell.2021.698795

INTRODUCTION

Today, cell transplantation therapy plays important roles in clinical therapies for many types of diseases. Since 1967, the well-known success of bone marrow transplantation had started a new era of cell transplantation for the therapies of blood diseases (Thomas, 1987, 2005; Cossu et al., 2018). Later, hepatocyte transplantation was also successfully used in the clinical trials for some liver diseases (Ott and Castell, 2019). The current studies in the fields of stem cells and regenerative medicine are hoped to provide the adequate sources of donor cells and bring the cell transplantation therapy into even newer era, which have widely opened the scope to forecast its potential applications into therapies of many injuries or diseases for tissue repairing or replacements. Especially, stem cell-derived functional cells for various tissues are increasingly considered sources of donor cells for cell transplantation therapy in the future.

To evaluate the therapeutic effects of cell transplantation, the dynamic migration and movements of donor cells in the hosts are required to be comprehensively analyzed during preclinical studies. Therefore, a practical method to track the state and fate of donor cells posttransplantation spatially and temporally is highly demanded in many current and future studies on the preclinical applications of cell transplantation-based therapies (Nguyen et al., 2014).

The dynamic study with comprehensive analyses on transplanted cells through using the new technology of *in vivo* tracking has become a powerful strategy to judge the fate of transplanted cells (Feigenbaum et al., 2009). Such new technology is under a non-invasive condition, which does not require the multiple rounds of sacrificing animals and harvesting samples. Especially, non-invasive tracking has many common advantages to perform the dynamic cell tracking in a real-time process, which were able to monitor the fate of transplanted cells *in vivo* during various dynamic processes, including the stages of cell homing and engraftments, as well as target tissue repairing or replacements for functional recoveries of many tissues (Kircher et al., 2011).

Bioluminescence imaging (BLI) technique system carries many potential advantages for dynamic tracking on cells *in vivo*. Most used bioluminescence is firefly luciferase, with Mg^{2+}, ATP, and O_2, which catalyze its substrate luciferin to generate bioluminescence signals. Luciferase has been used as a reporter gene product to recognize those luciferase-expressing cells during their biological processes (Dubey, 2012). With a set of optical inspection instruments, dynamic activities of the transplanted luciferase-expressing cells in the body of recipients can be directly monitored, based on the luciferase-induced bioluminescence signal (Herter-Sprie et al., 2014).

Normally, BLI could only be used at the mode of two dimensions (2D), which was successfully applied in the studies on observations of tumor growth *in vivo* (Yao et al., 2018). However, BLI of 2D mode (2D BLI) could not reach to the enough depths of tissues to track signals of detected cells that located deeply in the body of recipients (Kocher and Piwnica-Worms, 2013). Recently, BLI of 3D mode (3D BLI) has been developed with significant improvements, which enable scientists to capture both the information more accurately about localization and quantification of donor cells during the dynamic cell tracking after cell transplantation.

Based on the latest generation of instrument for IVIS® Spectrum computed tomography (CT) scanner that combines optical imaging and CT in one platform (Aalipour et al., 2019), we investigated how to establish a practical protocol to perform 3D cell tracking of transplanted hepatocytes in mice. This protocol was also expected to be a useful and referable standard for the 3D tracking of other cell types during their dynamic process of cell transplantation.

In our study, the fumarylacetoacetate hydrolase-deficient ($Fah^{-/-}$) mouse model was used as the preferable system for hepatocyte transplantation and liver repopulation. $Fah^{-/-}$ mice can undergo induced liver failure and animal death once lacking enough 2-(2-nitro-4-trifluoromethylbenzoyl)-1,3-cyclohexanedione (NTBC) water. However, they can also be successfully rescued from death by restoring their liver function through the liver repopulation after transplantation of hepatocytes from wild-type animals. In our experiment, the dynamic process, including the stages of cell engraftment, migration, proliferation, and liver regeneration in final, was continuously tracked in a real-time manner after transplanting luciferase-expressing hepatocytes into the body of $Fah^{-/-}$ mouse.

METHOD

Animals

All mice received humane care according to the guidelines of Tongji University Animal Care and Use Committees. Luciferase transgenic mice were purchased from Shanghai Model Organisms Center, Inc., maintained under specific pathogen-free conditions and used at 8–10 weeks of age.

Mice Model With Liver Failure

As described in previous studies (He et al., 2010; Wang et al., 2018), $Fah^{-/-}$ mice undergo liver failure and death. To survive, the mice need to be maintained with continuous supplement of 2-(2-nitro-4-trifluoromethylbenzoyl)-1,3-cyclohexanedione (NTBC) in their drinking water (7.5 mg/L). To induce liver injury, NTBC was totally withdrawn from the drinking water of $Fah^{-/-}$ mice.

Hepatocyte Isolation and Transplantation

Donor luciferase-expressing hepatocytes were isolated from luciferase transgenic mice (Shanghai Model Organisms Center, Inc., Shanghai, China) with the perfusion protocol that is established in previous studies (He et al., 2012; Wang et al., 2014). Briefly, the liver was preperfused with 1 × Earle's balanced salt solution (EBSS) (Gibco, Amarillo, TX, United States) with 5 mM 4-(2-hydroxyethyl)-1-piperazineethanesulfonic acid (HEPES) (Gibco) for 10 min at 37°C, and then perfused with 1 × EBSS with 5 mM HEPES with collagenase D (Sigma-Aldrich, St. Louis, MO, United States) for 10 min

at 37°C. The dissociated cells were filtered through a 70-μm Nylon cell strainer (BD Biosciences, San Jose, CA, United States), and then centrifuged twice for 2 min at 50 g to remove clumps. Furthermore, viability of isolated hepatocytes was above 80% evaluated by Trypan blue stain (Sigma-Aldrich). Harvested hepatocytes were resuspended in DMEM and injected into $Fah^{-/-}$ recipient animals through the spleen (1×10^6 cells/recipient) as described (Wang et al., 2014).

CT for Three-Dimensionally Localizing Luciferase-Expressing Hepatocytes

Computed tomography scanning was carried out with IVIS® Spectrum CT *in vivo* Imaging System (PerkinElmer, Waltham, MA, United States). CT images were captured with 50 kVp X-rays at a tube current of 1 mA, with exposure time of 50 ms, and with an aluminum filter. CT images were reconstructed with Living Image 4.5 software, which not only provided a field of view (FOV) of 20 cm × 20 cm × 20 cm but also allowed an isotropic resolution of 0.15 mm for the anatomical location of transplanted cells with bioluminescence.

Bioluminescence Imaging of Transplanted Hepatocytes

In vitro BLI of Luciferase-Expressing Hepatocytes in 2D System

The isolated luciferase-expressing hepatocytes were seeded in 96-well plates with different densities (1×10^3, 1×10^4, and 1×10^5). After being attached in the CO_2 incubator for 4 h under 37°C, the value of bioluminescence excited by cells was measured for depleting the background signals. D-Luciferin (250 μM) was then added to the attached hepatocytes in the 96-well plate. After reacting for 5 min, the plate with cells was placed in the IVIS® Lumina III *In Vivo* Imaging System (PerkinElmer) for detecting the intensity of bioluminescence. The imaging data were analyzed by Living Image software to determine correlations between signal intensity (p/s/cm^2/sr) and cell numbers.

In vivo BLI of Luciferase-Expressing Hepatocytes in Host Mice After Transplanting

Bioluminescence imaging of $Fah^{-/-}$ mice were captured at different intervals after transplantation (3 days, 1, 3, 5, 8, and 10 weeks). To conduct the BLI, host $Fah^{-/-}$ mice were intraperitoneally injected with D-luciferin (100 mM) right after anesthesia. After reaction for 5 min (for 2D BLI) or 8 min (for 3D BLI), the mice were placed in the light-tight chamber in the IVIS® Spectrum CT *in vivo* Imaging System. Dorsal imaging was performed for all host mice at different time points. For 2D BLI, no emission filter was used during the imaging process. For 3D BLI, five bandpass open emission filters were centered at 560, 580, 600, 620, and 640 nm to collect the optical signal, respectively.

The imaging signals collected within 5 min were used to locate the transplanted luciferase-expressing hepatocytes under 3D BLI, and the density of proliferating cell groups or nodules could be distinguished by different colors intuitively. Those colors indicated diverse intensity level and corresponding color scale at the right side of every picture. Beforehand, the reconstructed 3D whole-body structure image of $Fah^{-/-}$ mouse recipient was captured by CT scanner. By combining the 3D BLI with CT-reconstructed whole-body structure images, the results of the real-time distributions of transplanted luciferase-expressing hepatocytes in the liver and other organs of each $Fah^{-/-}$ mouse recipient were collected for further analysis. FOV = 13.2 × 13.2 cm, f/stop = 1, binning = 8.

Analysis of BLI

Bioluminescence signal intensity was calculated by Living Image 4.5 Software (PerkinElmer). The photon radiance was measured as photons per second per square centimeter per steradian (p/s/cm^2/sr) within the regions of interest (ROIs) (Kuo et al., 2007; Thompson et al., 2013). Bioluminescence unit was showed as total flux radiance which is a calibrated measurement based on photon emission.

Real-Time Quantitative PCR

Real-time quantitative PCR (RT-qPCR) was performed with the TB Green Premix Ex Taq II (Takara, Kusatsu, Japan). The expression of glyceraldehyde 3-phosphate dehydrogenase (GAPDH) was used as control. PCRs were performed under the following conditions: 95°C for 15 s followed by 40 cycles at 95°C for 5 s, 60°C for 34 s, 95°C for 1 min, and 55°C for 1 min. The primers used for the assay include luciferase-Forward 5′-TTACCAGGGATTTCAGTCG-3′; luciferase-Reverse 5′-CCTT TAGGCAGACCAGTAGA-3′; GAPDH-Forward 5′-AGGTCGG TGTGAACGGATTTG-3′; GAPDH-Reverse 5′-GGGGTCGTT GATGGCAACA-3′.

Immunohistochemistry Assay

The transplanted $Fah^{-/-}$ mice were sacrificed at experimental time points. The liver samples were harvested, and immunohistochemistry with FAH antibody was conducted to examine the percentage of liver repopulations. For immunohistochemistry staining, the fresh liver samples were fixed in 4% paraformaldehyde, embedded in paraffin, and cut into 2-μm-thick slices. Sections were baked, deparaffinized, rehydrated, permeabilized with 3% H_2O_2 solution for 15 min, and blocked by 1% BSA for 30 min. The sections were then incubated with rabbit antimouse FAH primary antibody (HepatoScience, 1:3,000) at 4°C overnight and with secondary antibodies conjugated with HRP (Sangon Biotech) at 37°C for 30 min. After staining with DAB (MXB) in proper intensity, the sections were counterstained with hematoxylin (Beyotime, Jiangsu, China), dehydrated rapidly, and mounted with neutral resin (SolarBio, Beijing, China). Finally, the samples were examined under optical microscope (Leica, Wetzlar, Germany).

Aperio ImageScope software of pathological section scanner (Leica SDPTOP HS6) was served for immunohistochemistry stain imaging and statistics of FAH^+ area and liver area. We picked no less than three discontinuous sections in each liver to

calculate FAH^+ area and liver area. In the analysis, regions of interest (ROIs) were calculated by software automatically.

Statistical Analysis

Data are presented as mean ± SD or mean ± SEM from at least three independent experiments unless otherwise indicated. One-way ANOVA with Tukey's *post hoc* test was used for multiple groups and Student's *t*-test for two groups. $p < 0.05$ was considered statistically significant ($^*p < 0.05$, $^{**}p < 0.01$, $^{***}p < 0.001$. $N = 3$).

RESULTS

A Positive Linear Correlation Between Bioluminescence Intensity and Number of Luciferase-Expressing Hepatocytes Is Established Both *in vitro* and *in vivo*

Donor hepatocytes expressing luciferase were obtained from the luciferase transgenic mouse generated from our previous study (Wangensteen et al., 2008). Expression of luciferase enabled liver cells to be detected based on the bioluminescence released from biochemical induction of luciferase with luciferin (**Supplementary Figure 1A**). The viability of luciferase-expressing hepatocytes was evaluated based on vitality and healthy morphology compared with healthy wild-type hepatocytes. The correlation between the level intensity of induced bioluminescence releasing and the number of luciferase-expressing hepatocytes was determined (**Supplementary Figure 1B**). Results indicated that the total flux of bioluminescence intensity for 1×10^3, 1×10^4, and 1×10^5 of hepatocytes were 6.222×10^5, 1.255×10^7, and 5.5265×10^7 p/s/cm^2/sr, respectively (**Supplementary Figure 1A**). The results revealed a positive linear correlation between bioluminescence intensity and number of luciferase-expressing hepatocytes existed ($R^2 = 0.9959$) (**Supplementary Figure 1B**). In the calculated averages, total bioluminescent photons emitted by each luciferase-expressing hepatocyte were approximately 8.152×10^2 p/s/cm^2/sr.

Then, luciferase-expressing hepatocytes were transplanted into *Fah*$^{-/-}$ mice with acute liver failure *via* spleen injection (1×10^6 hepatocytes/mouse). For monitoring the process of surviving, engrafting, and proliferating of transplanted luciferase-expressing hepatocytes, 2D BLI on *Fah*$^{-/-}$ mice was performed at different time points (3 days, 1, 3, 5, 8, and 10 weeks) after transplantation. Evident bioluminescence signal was observed in *Fah*$^{-/-}$ mice on the third day after transplantation, suggesting that the luciferase-expressing hepatocytes were successfully transplanted into *Fah*$^{-/-}$ mice recipients (**Supplementary Figure 1C**).

After a slightly decreasing in *Fah*$^{-/-}$ mice recipients at the first week posttransplantation, bioluminescence signals started to increase significantly at the third week posttransplantation. From the fifth-week to eighth-week posttransplantation, the bioluminescence signals in *Fah*$^{-/-}$ mice recipients increased continually (Krohn et al., 2009). Based on this linear correlation between the bioluminescence intensity and number of luciferase-expressing hepatocytes obtained from the above experiments, the number of luciferase-expressing hepatocytes in *Fah*$^{-/-}$ mice recipients were calculated by the measured bioluminescence values (**Supplementary Figures 1D,E**).

Developing a 3D BLI and CT Combined Real-Time Localizing and Quantification Methodology for Tracking the Transplanted Hepatocytes in Livers of *Fah*$^{-/-}$ Mouse Recipients

Next, the combined methods of 3D BLI and CT were performed to make a dynamic tracking on the localization and quantification of transplanted luciferase-expressing hepatocytes. The same animal recipients used during above 2D BLI were further analyzed in the process of 3D BLI and the comparisons between 3D and 2D imaging were specially performed.

For 3D BLI, open emission filters were performed within a range of 560–640 nm (every 20 nm bandpass) to collect the optical signal for five times. Images that the signals collected within 5 min were used to locate and quantify the luciferase-expressing cells in the recipients in real time. Meanwhile, CT scanning was carried out to scan mouse stereo body to visually reconstruct their 3D internal structures. Thus, the distribution of transplanted hepatocyte *in vivo* could be presented vividly (**Supplementary Movie 1**).

During the process, the midpoint in every dimensional of recipient mouse was regarded as initial point. Every bioluminescent cell or cell-composed cluster *in vivo*, such as single luciferase-expressing repopulation nodules, could be positioned and analyzed on horizontal plane (*Z*), vertical plane (*Y*), and longitudinal plane (*X*), respectively (**Supplementary Movie 2**). Through these analyses, the transplanted luciferase-expressing hepatocytes could be precisely located (*x*, *y*, *z*) cm from the initial point at each detection time point. The total number could be quantified at the same detection time point according to the optical signal values of single hepatocyte/cluster with bioluminescence tomography (**Figure 1A** and **Supplementary Movie 2**). With the established protocol, luciferase-expressing hepatocytes were precisely localized in *Fah*$^{-/-}$ mice at six time points (3 days, 1, 3, 5, 8, and 10 weeks) after transplantation (**Figure 1B** and **Supplementary Movie 1**).

To further localize the numbers of cells engrafted in livers of *Fah*$^{-/-}$ mice at detection time points, a liver module was calculated and added to the images according to the parameters of the liver sizes and its distances to the abdominal surface (**Figure 1C**). With such module, engrafted numbers of luciferase-expressing hepatocytes were determined. As shown in the **Figure 1D**, on the third day of transplantation, less than 1×10^5 hepatocytes could be successfully engrafted into the livers of *Fah*$^{-/-}$ mouse recipients. However, by 10 weeks after transplantation, the number of luciferase-expressing hepatocytes in *Fah*$^{-/-}$ mice expended to 1.84×10^7. Of note, there are no consideration of degradation or maldistribution when using luciferase expression as a marker, and therefore a long-term and timelessness of cell tracking can be performed.

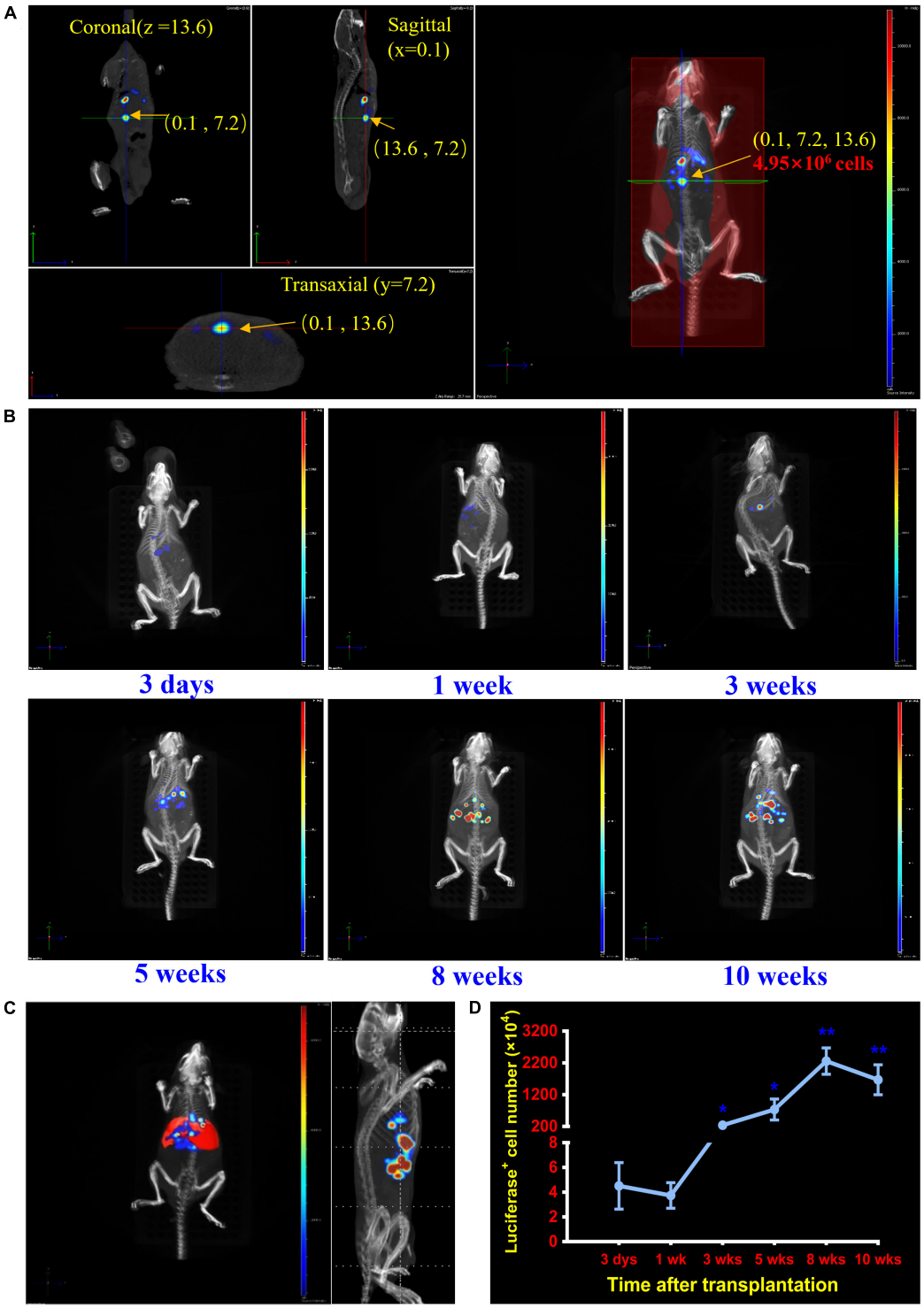

FIGURE 1 | Localization and quantification analysis of transplanted cells in the liver of *Fah*$^{-/-}$ mice. **(A)** Establishment of the dynamic cell-tracking strategy for posttransplantation localizing and quantifying of grafted cells *in vivo*. A combination of 3D BLI and CT is established to locate and quantify the transplanted hepatocytes in livers of *Fah*$^{-/-}$ mouse recipients at any time point of detection. Representative image of accurate localization (0.1, 7.2, 13.6) cm and cell quantification (4.95 × 10^6) of one nodule repopulated by transplanted hepatocytes (pointed by the arrow). **(B)** Dynamically localizing transplanted hepatocytes at different time points posttransplantation. Representative merged images of transplanted hepatocytes of *Fah*$^{-/-}$ mice at 3 days, 1, 3, 5, 8, and 10 weeks after hepatocyte transplantation. **(C)** Spectrum CT image of mouse liver was reconstructed by Living Image 4.5 software in *Fah*$^{-/-}$ mouse. **(D)** Quantification of transplanted hepatocytes in livers of *Fah*$^{-/-}$ mice at 3 days, 1, 3, 5, 8, and 10 weeks. Quantitative analyses of transplanted hepatocytes in liver of *Fah*$^{-/-}$ mice. Data are shown as mean ± SEM. $^*p < 0.05$, $^{**}p < 0.01$. $N = 3$. Student's *t*-test.

Traditional Assessment of Posttransplantation Hepatocytes *via* 3D Cell Dynamic Tracking Process

Finally, to validate the results from 3D cell dynamic tracking process, the results from the traditional methods that are still routinely used in detection processes, involving conventional BLI imaging of isolated organs (liver, spleen, kidney), quantitative PCR test and the histochemical observations, were performed. In the liver of transplanted $Fah^{-/-}$ mice, BLI signal analysis showed the signal value was significantly improved at 10 weeks compared with that at 3 days. In contrast, the BLI value was significantly decreased in the spleen at 10 weeks compared with that at 3 days. There was no evident difference between the BLI values in the kidney of $Fah^{-/-}$ mice between 10 weeks and 3 days (**Supplementary Figure 2A**).

FAH protein, the donor cell-specific marker, was used to prove the existence of donor-derived hepatocytes in transplanted $Fah^{-/-}$ mice. To unravel the detailed number of regenerative hepatocytes, we assessed the regeneration efficiency *via* FAH^{+} area/liver area based on the immunohistochemistry staining of FAH antibody. The results showed that FAH^{+} hepatocytes was about 0.77% after 3 days posttransplantation, while it reached to approximately 80% after 10 weeks of repopulation (**Supplementary Figures 2B,C**). Consistently, the expression level of *luciferase* gene at 10 weeks was obviously higher than that at 3 days after cell transplantation (**Supplementary Figure 2D**).

To further validate regenerative status, we also examined liver functions of donor-derived hepatocytes grafted $Fah^{-/-}$ mice. Results showed that several parameters of liver function, including alanine aminotransferase (ALT), aspartate aminotransferase (AST), total bilirubin (T-BIL), and albumin (ALB), were recovered to the normal ranges at 10 weeks posttransplantation (**Supplementary Figure 2E**).

DISCUSSION

For the first time, a 3D BLI imaging system was established and was successfully used in combination with CT scanning to evaluate the dynamic process of *in vivo* cell tracking for the transplanted cells, which can precisely assess the localization and quantification of transplanted cells in the relative animal recipients.

Previously, several traditional methods had been developed for judging the transplanted donor cells during preclinical studies, which required enormous experimental animals while still only capable of conducting limited numbers of assays, and analyses for evaluating expected outcomes of cell transplantation. Moreover, these analytical processes could only rely on the multiple rounds of animal sacrificing and sample harvesting at limited time points after cell transplantations (Massoud and Gambhir, 2003). Therefore, a large number of animals were required for one study. In addition, these traditional methods also have chances of mistaken organ collections and misinterpretations due to inaccurate observations during necropsy and animal harvesting, partially because of the indirect or delayed interpretations for the real-time facts of those *in situ* and dynamic occurrences (Phair and Misteli, 2001). Therefore, the non-invasive tracking methods are crucial for achieving the goal of evaluating the cell fate posttransplantation.

Among several non-invasive tracking methods, the two representative ones used currently are magnetic particle imaging (MPI) and photoacoustic imaging (PAI). MPI is a method based on tomography for detecting the spatial distribution of superparamagnetic iron oxide nanoparticles (SPIONs) (Haegele et al., 2012; Wei et al., 2018). When labeled with Resovit, a particular type of SPIONs, a minimum of 200 mesenchymal stem cells can be successfully detected after transplantation during a tracking period up to 3 months (Bulte et al., 2015). However, both traceability and accuracy of SPIONs for MPI could be susceptibly influenced from gas, calcification, and blood flow in tissues (Bourquin et al., 2018; Zhou et al., 2018).

On the other hand, the method of PAI combines high optical contrast with high ultrasound resolution in a single imaging modality (Knox and Chan, 2018). During PAI analyses, the transplanted cells are labeled by the nanogold particles with photoacoustic effects. After transplantation, the nanogold particle-labeled cells could be dynamically tracked in real time by photoacoustic signal for 4 weeks (Jokerst et al., 2012; Zheng et al., 2015; Zhang et al., 2017). In similar with MPI, PAI also has some limitations. For instance, the nanomaterials used in PAI can be mainly distributed in the lysosomes after entering cells through endocytosis. Therefore, it may become difficult to ensure the equal distributions in the offspring cells derived from original donor cells that carry nanomaterials with such limitations (Knox and Chan, 2018).

Bioluminescence imaging is another currently used technology to detect the signal of luminescence light emitted from enzyme-catalyzed reactions. In our previous study, the 2D BLI was performed to measure numbers of repopulating hepatocytes during liver repopulation (Wangensteen et al., 2008). However, these results from 2D BLI could only provide the information on survival and proliferation tendency for the transplanted luciferase-expressing hepatocytes. The key information on localization and quantification of the transplanted luciferase-expressing hepatocytes in $Fah^{-/-}$ mice recipients could not be obtained under 2D BLI. Notably, the combined methods of both 3D BLI and CT developed in this study enabled us to make a dynamic tracking on the localization and quantification of transplanted luciferase-expressing hepatocytes. Here, 3D BLI was tested for its first use to dynamically monitor the transplanted luciferase-expressing hepatocytes in $Fah^{-/-}$ mice recipients in real time. In addition, our results indicated that the combined technologies with both 3D BLI and CT made it possible to monitor the spatial and temporal distribution of transplanted cells in recipient and to determine the exact number of cells in different distributive regions during cell transplantation assay. Furthermore, with our model system, a new analysis program for localization and quantitation was established for our following studies, to finalize a standard protocol for transplanting any luciferase-expressing cells when 3D BLI and CT were performed simultaneously.

Although our method has achieved the *in vivo* localization and quantification of transplanted hepatocytes, there are still some issues to be further addressed. Firstly, the detection sensitivity of the current system still needs to be improved. With our 3D dynamic cell tracking system, clusters of ∼50 cells can be detected, but it is not sufficient to localize and quantitatively detect a single cell. The establishment of AkaLuc mutagenesis from luciferase may help us to achieve this goal (Iwano et al., 2018). AkaLuc can pair with its optical substrate AkaLumine hydrochloride, which produces a roughly fourfold improvement in the expression level than luciferase. This ultra-enhanced signal enables scientists to non-invasively visualize single cells deep inside freely moving animals (Iwano et al., 2018). Secondly, the resolution of CT also needs to be improved. We are currently improving our resolution by establishing a Bruker micro-CT-based system, which enable us to convert images into a complete microscopic visualization solution with the specialized software for further analysis. Finally, the *in vivo* depth of transplanted cells currently established for detection is limited. Our method is commonly used for posttransplant internal localization in small animals such as mice and rats; the application of the system on large animal or in human will be tested in the future study.

Taken together, the combination of 3D BLI and CT scanning could be used to analyze transplanted hepatocytes on several parameters in real time, including cell distribution, quantification, and location. Significantly, a protocol for such study process could be applied to judge whether the donor hepatocytes were qualified candidates for the potential clinical cell transplantation to liver failure patients, on considering both safety, and therapeutic efficiency. In addition, our established protocol is also expected to become a valuable and referable standard for visually analyzing other cell candidates, which were used for transplantation therapies in any kinds of animal models during their preclinical studies (He et al., 2010).

DATA AVAILABILITY STATEMENT

The original contributions presented in the study are included in the article/**Supplementary Material**, further inquiries can be directed to the corresponding author/s.

ETHICS STATEMENT

The animal study was reviewed and approved by Tongji University Animal Care and Use Committees.

AUTHOR CONTRIBUTIONS

FL and XP conducted most of the experiments and imaging analysis. XS, YG, HQ, SS, and CL conducted the $Fah^{-/-}$ mice management and hepatocytes grafting with FL and XP. WL and ZZ conducted the *in vitro* assays which were provided as controls of this study. ZH designed the study. ZH and ZL supported and supervised the study. ZH, FL, WZ, XP, and XW wrote the manuscript with help from the other authors. All authors contributed to the article and approved the submitted version.

FUNDING

This study was funded by Major Program of National Key Research and Development Project (2020YFA0112600 and 2019YFA0801502), Shanghai Zhangjiang National Innovtaion Demonstration Zone (ZJ2018-ZD-004), National Natural Science Foundation of China (81772954 and 82002945), the Top-Level Clinical Discipline Project of Shanghai Pudong (PWYgf2018-04), Program of Shanghai Academic/Technology Research Leader (20XD1434000), Peak Disciplines (Type IV) of Institutions of Higher Learning in Shanghai, and Shanghai Engineering Research Center of Stem Cells Translational Medicine (20DZ2255100).

ACKNOWLEDGMENTS

We are thankful to PerkinElmer and Sinoneural (Shanghai) Cell and Gene Engineering Holdings Co., Ltd. for their technical support.

SUPPLEMENTARY MATERIAL

The Supplementary Material for this article can be found online at: https://www.frontiersin.org/articles/10.3389/fcell.2021.698795/full#supplementary-material

Supplementary Figure 1 | Analysis of bioluminescence intensity of luciferase hepatocytes *in vitro* and *in vivo* after transplanting into $Fah^{-/-}$ mice. **(A)** BLI image of luciferase hepatocytes *in vitro*. **(B)** The linear correlation assay between the number of luciferase hepatocytes and BLI signal intensity, respectively. **(C)** Representative pictures of 2D BLI imaging of $Fah^{-/-}$ mice (3 days, 1, 3, 5, 8, and 10 weeks). **(D)** Quantified analysis of 2D BLI signal intensity of $Fah^{-/-}$ mice *in vivo*. **(E)** Quantified analysis of transplanted hepatocytes in 2D of $Fah^{-/-}$ mice *in vivo*. Data are shown as mean ± SEM. $*p < 0.05$, $**p < 0.01$, $***p < 0.001$. $N = 3$. Student's *t*-test.

Supplementary Figure 2 | Assessment of posttransplantation hepatocytes in $Fah^{-/-}$ mice. **(A)** Bioluminescence intensity of isolated livers, spleen, kidney of $Fah^{-/-}$ mice, respectively. **(B)** Immunohistochemistry staining of histological sections of the livers from $Fah^{-/-}$ mice with luciferase-hepatocyte transplantation. $N = 3$. Scale bars, 200 μm (up) and 50 μm (down). **(C)** Quantification analysis for liver regeneration of $Fah^{-/-}$ mice at 3 days and 10 weeks after transplantation, respectively. **(D)** The relative expression level of luciferase gene in the liver of $Fah^{-/-}$ mice. **(E)** Serum levels of ALT **(a)**, AST **(b)**, ALB **(c)**, and total bilirubin **(d)** in $Fah^{-/-}$, $Fah^{-/-}$ + luciferase hepatocytes ($Fah^{-/-}$ + Luc-Heps). Data are presented as mean ± SD. $*p < 0.05$, $**p < 0.01$, $***p < 0.001$. $N = 3$. Student's *t*-test.

Supplementary Movie 1 | 3D-BLI signal intensity of $Fah^{-/-}$ mice after transplantation. Real-time 3D BLI imaging and CT scanning of transplanted hepatocytes in $Fah^{-/-}$ mice at 3 days, 1, 3, 5, 8, and 10 weeks after transplantation, respectively.

Supplementary Movie 2 | Localization analysis of transplanted cells. 3D localization analysis of transplanted cells from horizontal (*Z*), vertical (*Y*), and longitudinal plane (*X*) *in vivo*.

REFERENCES

Aalipour, A., Chuang, H. Y., Murty, S., D'Souza, A. L., Park, S. M., Gulati, G. S., et al. (2019). Engineered immune cells as highly sensitive cancer diagnostics. *Nat. Biotechnol.* 37, 531–539. doi: 10.1038/s41587-019-0064-8

Bourquin, J., Milosevic, A., Hauser, D., Lehner, R., Blank, F., Petri-Fink, A., et al. (2018). Biodistribution, clearance, and long-term fate of clinically relevant nanomaterials. *Adv. Mater.* 30:e1704307. doi: 10.1002/adma.201704307

Bulte, J. W., Walczak, P., Janowski, M., Krishnan, K. M., Arami, H., Halkola, A., et al. (2015). Quantitative "Hot Spot" imaging of transplanted stem cells using superparamagnetic tracers and Magnetic Particle Imaging (MPI). *Tomography* 1, 91–97. doi: 10.18383/j.tom.2015.00172

Cossu, G., Birchall, M., Brown, T., De Coppi, P., Culme-Seymour, E., Gibbon, S., et al. (2018). Lancet commission: stem cells and regenerative medicine. *Lancet* 391, 883–910. doi: 10.1016/s0140-6736(17)31366-1

Dubey, P. (2012). Reporter gene imaging of immune responses to cancer: progress and challenges. *Theranostics* 2, 355–362. doi: 10.7150/thno.3903

Feigenbaum, G. S., Lemberg, L., and Hare, J. M. (2009). Tracking cell fate with noninvasive imaging. *J. Am. Coll. Cardiol.* 54, 1627–1628. doi: 10.1016/j.jacc.2009.05.067

Haegele, J., Rahmer, J., Gleich, B., Borgert, J., Wojtczyk, H., Panagiotopoulos, N., et al. (2012). Magnetic particle imaging: visualization of instruments for cardiovascular intervention. *Radiology* 265, 933–938. doi: 10.1148/radiol.12120424

He, Z., Zhang, H., Zhang, X., Xie, D., Chen, Y., Wangensteen, K. J., et al. (2010). Liver xeno-repopulation with human hepatocytes in Fah-/-Rag2-/- mice after pharmacological immunosuppression. *Am. J. Pathol.* 177, 1311–1319. doi: 10.2353/ajpath.2010.091154

He, Z. Y., Deng, L., Li, Y. F., Xiang, D., Hu, J. K., Chen, Y. X., et al. (2012). Murine embryonic stem cell-derived hepatocytes correct metabolic liver disease after serial liver repopulation. *Int. J. Biochem. Cell Biol.* 44, 648–658. doi: 10.1016/j.biocel.2012.01.002

Herter-Sprie, G. S., Koridеck, H., Christensen, C. L., Herter, J. M., Rhee, K., Berbeco, R. I., et al. (2014). Image-guided radiotherapy platform using single nodule conditional lung cancer mouse models. *Nat. Commun.* 5:5870. doi: 10.1038/ncomms6870

Iwano, S., Sugiyama, M., Hama, H., Watakabe, A., Hasegawa, N., Kuchimaru, T., et al. (2018). Single-cell bioluminescence imaging of deep tissue in freely moving animals. *Science* 359, 935–939. doi: 10.1126/science.aaq1067

Jokerst, J. V., Thangaraj, M., Kempen, P. J., Sinclair, R., and Gambhir, S. S. (2012). Photoacoustic imaging of mesenchymal stem cells in living mice via silica-coated gold nanorods. *ACS Nano* 6, 5920–5930. doi: 10.1021/nn302042y

Kircher, M. F., Gambhir, S. S., and Grimm, J. (2011). Noninvasive cell-tracking methods. *Nat. Rev. Clin. Oncol.* 8, 677–688. doi: 10.1038/nrclinonc.2011.141

Knox, H. J., and Chan, J. (2018). Acoustogenic probes: a new frontier in photoacoustic imaging. *Acc. Chem. Res.* 51, 2897–2905. doi: 10.1021/acs.accounts.8b00351

Kocher, B., and Piwnica-Worms, D. (2013). Illuminating cancer systems with genetically engineered mouse models and coupled luciferase reporters in vivo. *Cancer Discov.* 3, 616–629. doi: 10.1158/2159-8290.Cd-12-0503

Krohn, N., Kapoor, S., Enami, Y., Follenzi, A., Bandi, S., Joseph, B., et al. (2009). Hepatocyte transplantation-induced liver inflammation is driven by cytokines-chemokines associated with neutrophils and Kupffer cells. *Gastroenterology* 136, 1806–1817. doi: 10.1053/j.gastro.2009.01.063

Kuo, C., Coquoz, O., Troy, T. L., Xu, H., and Rice, B. W. (2007). Three-dimensional reconstruction of in vivo bioluminescent sources based on multispectral imaging. *J. Biomed. Opt.* 12:024007. doi: 10.1117/1.2717898

Massoud, T. F., and Gambhir, S. S. (2003). Molecular imaging in living subjects: seeing fundamental biological processes in a new light. *Genes Dev.* 17, 545–580. doi: 10.1101/gad.1047403

Nguyen, P. K., Riegler, J., and Wu, J. C. (2014). Stem cell imaging: from bench to bedside. *Cell Stem Cell* 14, 431–444. doi: 10.1016/j.stem.2014.03.009

Ott, M., and Castell, J. V. (2019). Hepatocyte transplantation, a step forward? *J. Hepatol.* 70, 1049–1050. doi: 10.1016/j.jhep.2019.03.022

Phair, R. D., and Misteli, T. (2001). Kinetic modelling approaches to in vivo imaging. *Nat. Rev. Mol. Cell Biol.* 2, 898–907. doi: 10.1038/35103000

Thomas, E. D. (1987). Bone marrow transplantation. *CA Cancer J. Clin.* 37, 291–301. doi: 10.3322/canjclin.37.5.291

Thomas, E. D. (2005). Bone marrow transplantation from the personal viewpoint. *Int. J. Hematol.* 81, 89–93. doi: 10.1532/ijh97.04197

Thompson, S. M., Callstrom, M. R., Knudsen, B. E., Anderson, J. L., Sutor, S. L., Butters, K. A., et al. (2013). Molecular bioluminescence imaging as a noninvasive tool for monitoring tumor growth and therapeutic response to MRI-guided laser ablation in a rat model of hepatocellular carcinoma. *Invest. Radiol.* 48, 413–421. doi: 10.1097/RLI.0b013e31827a4a3f

Wang, C., Chen, W. J., Wu, Y. F., You, P., Zheng, S. Y., Liu, C. C., et al. (2018). The extent of liver injury determines hepatocyte fate toward senescence or cancer. *Cell Death Dis.* 9:575. doi: 10.1038/s41419-018-0622-x

Wang, M. J., Chen, F., Li, J. X., Liu, C. C., Zhang, H. B., Xia, Y., et al. (2014). Reversal of hepatocyte senescence after continuous in vivo cell proliferation. *Hepatology* 60, 349–361. doi: 10.1002/hep.27094

Wangensteen, K. J., Wilber, A., Keng, V. W., He, Z., Matise, I., Wangensteen, L., et al. (2008). A facile method for somatic, lifelong manipulation of multiple genes in the mouse liver. *Hepatology* 47, 1714–1724. doi: 10.1002/hep.22195

Wei, Y., Zhou, L., Yang, D., Yao, T., and Shi, S. (2018). Stem cells controlling, imaging and labeling by functional nanomaterials. *Nano LIFE* 08, 1841007. doi: 10.1142/S1793984418410076

Yao, Z., Zhang, B. S., and Prescher, J. A. (2018). Advances in bioluminescence imaging: new probes from old recipes. *Curr. Opin. Chem. Biol.* 45, 148–156. doi: 10.1016/j.cbpa.2018.05.009

Zhang, Y., Zhang, Y., Yin, L., Xia, X., Hu, F., Liu, Q., et al. (2017). Synthesis and bioevaluation of iodine-131 directly labeled cyclic RGD-PEGylated gold nanorods for tumor-targeted imaging. *Contrast Media Mol. Imaging* 2017:6081724. doi: 10.1155/2017/6081724

Zheng, B., Vazin, T., Goodwill, P. W., Conway, A., Verma, A., Saritas, E. U., et al. (2015). Magnetic particle imaging tracks the long-term fate of in vivo neural cell implants with high image contrast. *Sci. Rep.* 5:14055. doi: 10.1038/srep14055

Zhou, X. Y., Tay, Z. W., Chandrasekharan, P., Yu, E. Y., Hensley, D. W., Orendorff, R., et al. (2018). Magnetic particle imaging for radiation-free, sensitive and high-contrast vascular imaging and cell tracking. *Curr. Opin. Chem. Biol.* 45, 131–138. doi: 10.1016/j.cbpa.2018.04.014

Conflict of Interest: The authors declare that the research was conducted in the absence of any commercial or financial relationships that could be construed as a potential conflict of interest.

frontiers in Cell and Developmental Biology

ORIGINAL RESEARCH
published: 09 September 2021
doi: 10.3389/fcell.2021.726499

Differentiation of Human Pluripotent Stem Cells Into Definitive Endoderm Cells in Various Flexible Three-Dimensional Cell Culture Systems: Possibilities and Limitations

Mariia S. Bogacheva[1†], Riina Harjumäki[1†], Emilia Flander[1‡], Ara Taalas[1‡], Margarita A. Bystriakova[1], Marjo Yliperttula[1], Xiaoqiang Xiang[2], Alan W. Leung[3] and Yan-Ru Lou[1,2*$]*

[1] Division of Pharmaceutical Biosciences, Drug Research Program, Faculty of Pharmacy, University of Helsinki, Helsinki, Finland, [2] Department of Clinical Pharmacy and Drug Administration, School of Pharmacy, Fudan University, Shanghai, China, [3] Yale Stem Cell Center, Department of Genetics, Yale University, New Haven, CT, United States

The generation of human stem cell-derived spheroids and organoids represents a major step in solving numerous medical, pharmacological, and biological challenges. Due to the advantages of three-dimensional (3D) cell culture systems and the diverse applications of human pluripotent stem cell (iPSC)-derived definitive endoderm (DE), we studied the influence of spheroid size and 3D cell culture systems on spheroid morphology and the effectiveness of DE differentiation as assessed by quantitative PCR (qPCR), flow cytometry, immunofluorescence, and computational modeling. Among the tested hydrogel-based 3D systems, we found that basement membrane extract (BME) hydrogel could not retain spheroid morphology due to dominant cell–matrix interactions. On the other hand, we found that nanofibrillar cellulose (NFC) hydrogel could maintain spheroid morphology but impeded growth factor diffusion, thereby negatively affecting cell differentiation. In contrast, suspension culture provided sufficient mass transfer and was demonstrated by protein expression assays, morphological analyses, and mathematical modeling to be superior to the hydrogel-based systems. In addition, we found that spheroid size was reversely correlated with the effectiveness of DE formation. However, spheroids of insufficient sizes failed to retain 3D morphology during differentiation in all the studied culture conditions. We hereby demonstrate how the properties of a chosen biomaterial influence the differentiation process and the importance of spheroid size control for successful human iPSC differentiation. Our study provides critical parametric information for the generation of human DE-derived, tissue-specific organoids in future studies.

Keywords: definitive endoderm, human pluripotent stem cell, suspension cell culture, nanofibrillar cellulose hydrogel, computational modeling, spheroid, organoid, basement membrane extract hydrogel

OPEN ACCESS

Edited by:
Gianluca Carnevale, University of Modena and Reggio Emilia, Italy

Reviewed by:
Hong Ouyang, Sun Yat-sen University, China
Marco Tatullo, University of Bari Medical School, Italy
Kazuo Takayama, Kyoto University, Japan

***Correspondence:**
Yan-Ru Lou
yanru_lou@fudan.edu.cn
Xiaoqiang Xiang
xiangxq@fudan.edu.cn

[†] These authors have contributed equally to this work and share first authorship

[‡] These authors have contributed equally to this work and share second authorship

[$] Lead contact

Specialty section:
This article was submitted to Stem Cell Research, a section of the journal Frontiers in Cell and Developmental Biology

Received: *17 June 2021*
Accepted: *10 August 2021*
Published: *09 September 2021*

Citation:
Bogacheva MS, Harjumäki R, Flander E, Taalas A, Bystriakova MA, Yliperttula M, Xiang X, Leung AW and Lou Y-R (2021) Differentiation of Human Pluripotent Stem Cells Into Definitive Endoderm Cells in Various Flexible Three-Dimensional Cell Culture Systems: Possibilities and Limitations. Front. Cell Dev. Biol. 9:726499. doi: 10.3389/fcell.2021.726499

INTRODUCTION

Spheroids and organoids are three-dimensional (3D) clusters of cells. Spheroids can be made from a variety of cells including stem cells, tumor cells, and organ-specific cells. Organoids are made from stem cells or progenitors that can self-organize into organ-specific structures (Fatehullah et al., 2016; Lou and Leung, 2018). Both spheroids and organoids can produce *in vivo*–like structures and thus hold great potential in human development research, disease modeling, drug research, and tissue replacement *via* transplantation. Spheroids and organoids can be cultured and differentiated in a 3D biomaterial or in suspension without the use of a biomaterial. The selection of an appropriate biomaterial is important for successful 3D culture. Basement membrane extract (BME), such as Matrigel™, is the most widely utilized biomaterial for the formation of spheroids/organoids from many cell types (Spence et al., 2011; Chua et al., 2014; Dye et al., 2015; Hohwieler et al., 2017). BME hydrogel is an animal-derived biomaterial and can interact with various types of cells *via* cell membrane receptors. For potential applications of spheroids/organoids in regenerative medicine, several xeno-free and chemically defined hydrogels have been developed (Gjorevski et al., 2016; Nowak et al., 2017; Broguiere et al., 2018; Candiello et al., 2018). Some of these systems generate spheroid/organoid-hydrogel constructs, which may cause issues in *in vivo* applications, such as hydrogel biocompatibility and biodegradation. For this reason, xeno-free hydrogels that can generate biomaterial-free cell or tissue constructs have been developed. Among them, nanofibrillar cellulose (NFC) hydrogel has been shown to support the 3D spheroid formation of human embryonic stem cells (ESCs; Lou et al., 2014), induced pluripotent stem cells (iPSCs; Lou et al., 2014), liver cancer cells HepG2 (Bhattacharya et al., 2012), and HepaRG (Malinen et al., 2014). Intact spheroids formed in NFC hydrogel can be harvested after removal of the hydrogel by utilizing a cellulase enzyme (Lou et al., 2014), thereby facilitating various downstream analyses and applications (Lou et al., 2014). NFC hydrogel displayed weak interactions with human ESCs and HepG2 cells compared with natural extracellular matrix proteins including collagens and laminins (Harjumaki et al., 2019). In contrast, suspension culture is a biomaterial-free system, usually performed in a low-adhesive culture dish or a flask for scaled-up production. Like the NFC hydrogel, suspension culture can generate scaffold-free spheroids/organoids. Suspension culture has been reported to be effective in the formation of cell aggregates and organoids (Kim et al., 2016; Bergmann et al., 2018; Kumar et al., 2019; Wimmer et al., 2019).

Although spheroid/organoid technology has been rapidly developing during the past decade, several challenges remain (Lou and Leung, 2018). One of the major challenges facing organoid technology is heterogeneity and inefficient differentiation due to uncontrolled parameters such as spheroid size and mass transfer. The heterogeneity can result in variable phenotypes and inconsistent results in downstream analyses and applications. This prompted us to study factors affecting spheroid/organoid formation. We devised the current study to investigate the 3D differentiation of human iPSCs into definitive endoderm (DE) cells using spheroids of different sizes cultured in various 3D systems. Human iPSC differentiation toward DE represents a critical step on the way to generate cell models for the liver, gut, pancreas, lungs, trachea, and thyroid (Zorn and Wells, 2009). Great strides have been made in the development of DE differentiation methods in the previous decades (D'Amour et al., 2005; Hay et al., 2008; Wang et al., 2015; Bogacheva et al., 2018). DE cells are generally characterized by the expression of specific markers: SRY-box 17 (SOX17), Cerberus 1 (CER1), hepatocyte nuclear factor 3β (HNF3B, also known as FOXA2), and chemokine receptor type 4 (CXCR4). In our previous study of DE differentiation in two-dimensional (2D) culture, we found the most efficient protocol to involve the use of activin A in a serum-free B-27-supplemented medium for 6 days (Bogacheva et al., 2018).

The current study compares three types of 3D cell culture systems: inert hydrogel-based (NFC hydrogel), cell-interacting hydrogel-based (reduced growth factor BME), and biomaterial-free (suspension) systems for their contribution to the DE differentiation of human iPSC spheroids in different sizes.

MATERIALS AND METHODS

Cell Lines

The human iPSC line iPS(IMR90)-4 was purchased from WiCell Research Institute Inc (Madison, WI, United States), and GM23720B was purchased from Coriell Institute (United States). They were cultured on Matrigel™ (BD Biosciences) with daily replenishment of the mTeSR™1 medium (STEMCELL™ Technologies). Subculture was performed every 4 days using Versene solution 1:5,000 (Invitrogen, 15040033) for cell detachment. Cultures were maintained at 37°C and at 5% CO_2. Mycoplasma testing was carried out regularly by the Division of Pharmaceutical Biosciences at the University of Helsinki, Finland.

Formation of Spheroids and SC Differentiation to DE

The human iPSCs cultured on Matrigel™ in the mTeSR™1 medium were dissociated into single cells by Accutase™ (Millipore, SCR005). Spheroids containing a different number of cells (200, 500, and 1,000 cells per spheroid) were generated in AggreWell™400 (STEMCELL™ Technologies, 27845 and 34411) in the mTeSR™1 medium in the presence of 10 μM Rho-associated protein kinase (ROCK)-inhibitor Y-27632 (Selleck Chemicals, S1049). After 24 h, spheroids were collected from the AggreWell™400 and transferred in three different conditions for further culturing. Suspension culture condition was performed in a low-attachment 3.5-cm dish (Thermo Scientific Nunc, 174913). Hydrogel culturing was performed either in 0.55% NFC hydrogel GrowDex® (UPM-Kymmene Corporation, Helsinki, Finland) in a non-adhesive 96-well plate (Corning, 3474) or in Cultrex® Reduced Growth Factor BME (R&D Systems, 3533-005-02) in angiogenesis 15-well slides (ibidi, Cat# 81501, uncoated). The cell-number-to-medium-volume ratio was kept

the same under all the conditions. The day when DE induction started was set as day 0. DE induction was performed for 6 days in the RPMI-1640 medium (Gibco, 31870-025) supplemented with 1× GlutaMAX™ (Gibco, 35050-038), 1× B-27 (Gibco, 17504-044), 100 ng/ml activin A (PeproTech, 120-14E), and 10 μM ROCK-inhibitor Y-27632. The medium was renewed daily.

Live/Dead Cell Staining

At the end of the differentiation experiment, spheroids cultured in BME were stained with a LIVE/DEAD™ Viability/Cytotoxicity Kit for mammalian cells (Thermo Fisher Scientific, L3224) according to the instruction of the manufacturer. The dye solution consisted of Calcein AM (the final concentration was 0.5 μM) and Ethidium homodimer-1 (the final concentration was 1 μM) in the RPMI-1640 medium. The cells treated with 1% Triton X-100 for 5 min at room temperature were used as dead cell control. Spheroids were imaged within 30–60 min after staining using a confocal microscope Leica TCS SP5II HCS A with a HC PL APO 20×/0.7 CS (air) objective. Fluorescent Calcein AM (ex/em ∼495 nm/∼515 nm) produces green fluorescence in live cells. Ethidium homodimer-1 penetrates cells with damaged membranes, binds to nucleic acids, and provides red fluorescence in dead cells (ex/em ∼495 nm/∼635 nm).

Measurement of Spheroid Diameter

The images of spheroid morphology were taken with a phase contrast microscope (Leica DM IL LED) at 5× and 10× magnifications. Spheroid diameters were then measured with the LAS EZ software (Leica Microsystems) and ImageJ (National Institutes of Health, United States).

Collection of Spheroids From the NFC Hydrogel Culture

For downstream analyses including RNA isolation, immunofluorescence staining, and flow cytometry, spheroids were collected after removing NFC hydrogel. NFC hydrogel was removed by approximately 20-h treatment with cellulase (UPM-Kymmene Corporation, Helsinki, Finland) by following a previously described procedure (Lou et al., 2014).

RNA Isolation and cDNA Conversion

We collected RNA samples at six time points: undifferentiated stem cells cultured in 2D (2D SC), undifferentiated stem cells in spheroids (3D SC), day 1, day 2, day 4, and day 6 of differentiation. Cells and spheroids were lysed using TRI-reagent (Zymo-research, R2050-1-50), and then RNA was isolated with a Direct-zol RNA MicroPrep kit (Zymo-research, R2060) according to the instruction of the manufacturer. The concentrations of RNA samples were measured with NanoDrop™ One (Thermo Fisher Scientific). The cDNA conversion was made with a High Capacity cDNA reverse transcription kit (Applied Biosystems, 4368814) following the instructions of the manufacturer.

Quantitative PCR

The quantitative PCR (qPCR) reactions of the obtained cDNA samples were performed on a StepOnePlus Real-Time PCR System (Applied Biosystems) using either a PowerUp SYBR Green Master Mix (Applied Biosystems, A25741) or a TaqMan® Gene Expression Master Mix (Applied Biosystems, 4369016). Ribosomal protein, large, P0 (*RPLP0*) was used as a housekeeping gene. All the used primers and TaqMan Gene Expression Assay mixes are listed in **Supplementary Table 1**. All primers were designed by the Primer Express v2.0 software (Applied Biosystems) (Kanninen et al., 2016a) except the primers for *OCT4* (Yu et al., 2007) and *HNF3B* (D'Amour et al., 2005), and they were synthesized by Oligomer Oy (Helsinki, Finland) or Metabion (Planegg, Germany). The relative quantification of each target gene in comparison with the housekeeping gene was made by a standard curve method based on a published mathematical model (Pfaffl, 2001). The relative gene expression was calculated with reference to the undifferentiated human iPSCs in 2D culture condition.

Immunofluorescent Staining of 2D Cell Culture

After the formation of SC spheroids in AggreWell™400 for 24 h, they were collected, dissociated into single cells using Accutase™ (Millipore, SCR005), suspended in the mTeSR™1 medium with 10 μM ROCK-inhibitor Y-27632, and seeded on laminin-521 (LN521, Biolamina) coated black 96-well μ-plates (ibidi, 89626) to form a 2D cell monolayer. LN521 coating was prepared by incubating 10 μg/ml LN521 diluted in 1× DPBS with Ca^{+} and Mg^{+} either overnight at 4°C (slow coating) or for 2 h at 37°C (fast coating). After cells attached for 3 h, they were fixed in 4% paraformaldehyde for 10 min, permeabilized with 0.1% Triton X-100 for 10 min, and thereafter blocked with 10% normal goat or donkey serum (Millipore, Burlington, MA, United States) for 1 h. Cells were incubated with primary antibodies overnight at 4°C and then with secondary antibodies conjugated with Alexa Fluor 594 or Alexa Fluor 488 (Invitrogen) for 1 h at room temperature. Cell nuclei were stained with DAPI (Sigma-Aldrich, D8417, 12.5 μg/ml in MilliQ water) for 2 min. Primary and secondary antibodies used for immunostaining in this study are listed in **Supplementary Table 2**.

Immunofluorescent Staining of 3D Spheroids

After 4 days of differentiation experiments, spheroids were collected from the culture dishes and fixed in 4% paraformaldehyde for 24 h. The next day, they were treated with 100% methanol for 2 min, then with 20% DMSO in methanol for 2 min, and again with methanol for 2 min. After that, the cells were permeabilized with 1% Triton X-100 in 1× DPBS for 2 min and then incubated in a Penetration Buffer (0.3 M Glycine + 20% DMSO + 0.2% (wt.) Triton X-100 in 1× DPBS) for 15 min with shaking. Blocking was performed with a Blocking Buffer (6% donkey serum (Southern Biotech, 0030-01) or goat serum (Gibco, 16210) + 10% DMSO + 0.2% (wt.) Triton X-100 in 1×

DPBS) at 37°C for 15 min with shaking. Then the spheroids were incubated with primary antibodies diluted in an Antibody Buffer (3% donkey serum or goat serum + 5% DMSO + 0.2% Tween 20 + 10 μg/ml Heparin in 1× DPBS) at 37°C for 30 min with shaking. Thereafter, the spheroids were washed in 1× Washing Buffer (0.2% Tween 20 + 10 μg/ml Heparin in 1× DPBS) five times for 5 min each at 37°C with shaking. Then the spheroids were incubated with secondary antibody diluted in the Antibody Buffer at 37°C for 30 min with shaking followed by washing in the same way as after the primary antibody treatment. Nuclei were stained with DAPI (Sigma-Aldrich, D8417, 12.5 μg/ml in MilliQ water) for 2 min. Finally, the spheroids were treated with 100% methanol for 2 min. Visikol HISTO-M (Visikol Inc.) was added to the spheroids. Primary and secondary antibodies used for immunostaining in this study are listed in **Supplementary Table 2**.

Imaging of Immunostaining

Imaging was performed on a confocal microscope Leica TCS SP5II HCS A with a HC PL APO 20×/0.7 CS (air) objective. DAPI was excited with UV (diode 405 nm/50 mW), Alexa Fluor 488 with an Argon 488 nm laser, and Alexa Fluor 594 with a DPSS (561 nm/20 mW) laser.

Flow Cytometry

The spheroids were dissociated using Accutase™ (Millipore, SCR005) at each time point as indicated. For CXCR4 and viability measurement, single cells were incubated with either PE Mouse Anti-Human CD184 (CXCR4) IgG2a (BD Biosciences, 561733) or PE Mouse IgG2a (BD Biosciences, 555574) at the concentrations according to the instruction of the manufacturer for 40 min in the dark on ice. After washing with 2% FBS (Gibco, 10270-106) in 1× DPBS, the cells were treated with 0.05 mg/ml 7-AAD Viability Staining Solution (eBioscience, 00-6993-50) for 5 min in the dark on ice. Unstained cells were used to adjust FSC, SSC, and PE-Cy5. Fluorescence compensation for the CXCR4 signal in the PE channel and the 7-AAD signal in the PE-Cy5 channel was set in an experiment using DE cells derived in 2D culture by following a previously described procedure (Bogacheva et al., 2018) and dead cells produced by the treatment with various concentrations of ethanol.

Analysis of the SSEA-4 surface marker was conducted at the same time points as for CXCR4. After treatment with Accutase™, single cells were incubated with primary Mouse Anti-SSEA-4 (Developmental Studies Hybridoma Bank, MC-813-70) or Mouse IgG (PeproTech, 500-M00) at 0.2 μg/ml for 40 min on ice followed by washing with 2% FBS in 1× DPBS. Thereafter, the cells were stained with F(ab')2-Goat Anti-Mouse-PE (eBioscience, 12-4010-82) at the concentration according to the instruction of the manufacturer for 40 min in the dark on ice.

Flow cytometric analysis was carried out on a BD LSRII flow cytometer (YellGrn Laser, with filter PE (586/15) or PE-Cy5 (670/30)) using the BD FACSDiva software. The calculation of positive cell percentage and cell viability and the visualization of the results were performed using the FlowLogic software (Inivai Technologies). An isotype control signal was used for gating the false-positive peak caused by unspecific binding. Unstained cells' signal was used for gating living cells.

Concentration Modeling

Nanofibrillar cellulose hydrogel-based DE differentiation was performed in 96-well plates (Corning 3474). In each well, the lower phase B contained 100 μl NFC hydrogel diluted in a medium and mixed with 3D cell spheroids (**Supplementary Figure 1**). The upper phase A contained a 100 μl medium supplemented with activin A whose half-life *in vivo* is 5.5 min (fast) and 20.3 min (slow) (Johnson et al., 2016). Since only phase A could be renewed daily, we used a 2× medium for phase A, which contained the RPMI-1640 medium supplemented with 2× GlutaMAX™, 2× B-27, 200 ng/ml activin A, and 20 μM ROCK-inhibitor Y-27632. To model the diffusion of the key growth factor activin A from the interface between phase A and phase B into phase B, we used a computational model based on the Fick's second law of diffusion (Berg, 1993), the general formula for half-life in exponential decay (Nelson, 2013), and the linear estimation of the diffusion constant from the literature (Bhattacharya et al., 2012).

Below is the derivation of the model. First is the Fick's second law of diffusion written in terms of finite difference approximations to the derivatives as (Adams and Essex, 2009):

$$\frac{c_j^{n+1} - c_j^n}{\Delta t} = D\frac{c_{j+1}^n - 2c_j^n + c_{j-1}^n}{\Delta x^2} \quad (1)$$

where c is the concentration at time point $n = \{0, \Delta t, 2\Delta t, \ldots N\Delta t\}$, at position $j = \{0, \Delta x, 2\Delta x, \ldots J\Delta x\}$, and D is the diffusion constant. By defining the constant $= \frac{D\Delta t}{\Delta x^2}$, Equation 1 can be expressed as:

$$c_j^{n+1} = S\left(c_{j+1}^n + c_{j-1}^n\right) + (1 - 2S)\, c_j^n \quad (2)$$

Denaturation of protein growth factors is considered by including the general formula for exponential degradation, with half-life λ for time step Δt:

$$c_j^{n+1} = \left[S\left(c_{j+1}^n + c_{j-1}^n\right) + (1 - 2S)\, c_j^n\right]\left(\frac{1}{2}\right)^{\Delta t/\lambda} \quad (3)$$

By combining the Einstein relation of kinetic theory with the definition of the viscous friction coefficient (Nelson, 2013), the diffusion coefficient can be expressed in terms of the Boltzmann constant k_B, temperature T, time step Δt, and mass m:

$$D = \frac{k_B T \Delta t}{2m} \quad (4)$$

A previous study (Bhattacharya et al., 2012) had measured the diffusion constants of Dextran with different masses in NFC hydrogel. Since we can assume that the temperature of the hydrogel had been constant in each study for Dextran diffusion, we can consider T as a constant in the above equation. As all the other terms are constants, we can infer that the diffusion constant D and the mass of the diffusing particle m have an inverse linear correlation. Derived from the publication (Bhattacharya et al., 2012) *via* linear regression (R^2 0.999), the function takes the form:

$$D = 1.76 \cdot 10^{-7}\frac{1}{m} + 1.44 \cdot 10^{-5} \quad (5)$$

With these definitions, the diffusion constant D could be estimated for an object of mass m in NFC hydrogel. Diffusion was modeled based on Equation 3, with the diffusion constant estimated as in Equation 5 by using MatLab R2014a (8.3.0.532).

Statistical Analysis

Statistical analyses were performed using the GraphPad Prism 8 software. Statistical significance was determined by one-way analysis of variance (ANOVA) followed by Sidak's multiple comparisons test or Tukey's multiple comparisons test as recommended by the software. Kruskal–Wallis test followed by Dunn's multiple comparisons test was used in case a one-way ANOVA test could not be performed because the data did not pass a normality test. Correlation analysis was performed using a Pearson's correlation test. Differences of adjusted $p < 0.05$ (*), adjusted $p < 0.01$ (**), adjusted $p < 0.001$ (***), and adjusted $p < 0.0001$ (****) were considered significant.

RESULTS

Initial Spheroid Size (Cell Number) Affects Spheroid Survival During DE Differentiation

In subconfluent 2D cell culture where cells are well spread into monolayers, soluble factors in differentiation media are accessible to every cell. In contrast, in 3D cell culture, only cells in the outermost layer of spheroids/organoids are directly accessible by media components, but cells apart from the outermost layer must rely on other means such as diffusion or active transport in order to gain access to the media. To study the influence of cell layer thickness during cell differentiation, we generated spheroids using five different initial cell numbers (50, 100, 200, 500, and 1,000 cells per spheroid) using AggreWell^{TM}400 plates that contain microfabricated wells for the formation of homogenous spheroids. The initial size of each formed spheroid can be controlled by adjusting the input cell number, which requires the dissociation of stem cell colonies into single cells. This procedure results in the breakage of cell–cell interactions and cell–membrane junctions. The consequence of these events is the change in the balance between the actin-myosin anchoring force and the contraction force. The predominance of the contraction force stimulates cell death in the case of failure on re-adhesion (Chen et al., 2010). Rho-associated protein kinase (ROCK) is involved in the process of actin-myosin contraction. Treatment with the ROCK inhibitor Y-27632 improves stem cell viability in single cell status (Watanabe et al., 2007). Prior to the spheroid formation, we treated single human iPSCs iPS(IMR90)-4 cells with Y-27632 to prevent cell death. We initially chose two 3D culture conditions, suspension (without biomaterial) and NFC hydrogel. To differentiate human iPSCs into DE cells, we adopted an activin A-based protocol that was shown to be the most effective under 2D cell culture condition (Bogacheva et al., 2018). After 24 h in AggreWell^{TM}400 plates, the formed spheroids were transferred either into NFC hydrogel or into suspension in a differentiation medium supplemented with Y-27632. Y-27632 was used up to day 2 of differentiation.

We obtained only a few aggregates with the initial cell number of 50 and 100 cells per spheroid in both suspension and NFC hydrogel cultures (**Figure 1**). Most of the survived aggregates did not acquire a round shape and were surrounded by detached cells at day 1. Subsequently, all of them dissociated within 2 days. Due to the low survival rate of spheroids with the initial cell number of 50 and 100 cells per spheroid, we excluded them from further studies.

Spheroids with the initial cell number of 200 cells survived better in suspension culture than in NFC hydrogel with spheroid yield in suspension culture being 5.5-fold more than in NFC hydrogel at day 3. Spheroids with the initial cell number of

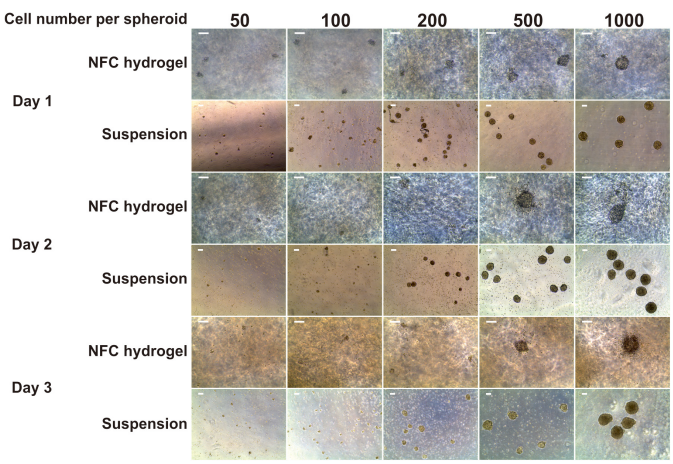

FIGURE 1 | Morphology of iPS(IMR90)-4-derived spheroids in five sizes: 50, 100, 200, 500, and 1,000 cells per spheroid cultured in suspension and nanofibrillar cellulose (NFC) hydrogel. Days 1, 2, and 3 of definitive endoderm (DE) differentiation are presented. The cell number in spheroids was controlled using the AggreWell400 plate for 24-h spheroid formation. Afterward, spheroids were collected from AggreWell400 and seeded in either low-adhesive Petri dishes in suspension or in NFC hydrogel in low-adhesive 96-well plates. Scale bars = 100 μm.

500 and 1,000 cells survived well in both conditions (**Figure 1**). They remained round by day 3. The DE differentiation medium can induce cell death as observed in our previous 2D DE differentiation study (Bogacheva et al., 2018). As expected, we also noticed dead cells in the 3D cultures. This phenomenon was more obvious around spheroids in NFC hydrogel culture probably because dead cells were more physically restricted within the hydrogel environment.

ROCK Inhibitor Y-27632 Improves Spheroid Survival During DE Differentiation

Initially, we treated iPS(IMR90)-4-derived spheroids with Y-27632 up to day 2 of differentiation but observed massive cell death (**Figure 2A**, single cells between spheroids) and loss of spheroid shape (**Figure 2A**, arrows) from day 4 onward. To obtain higher cell viability, we used Y-27632 in differentiation media for the entire period of the experiment (**Figure 2B**). In the presence of Y-27632, spheroids were well maintained during the 6-day differentiation. To investigate whether Y-27632 may have any negative effect on DE differentiation, we studied its effect on gene expression in iPS(IMR90)-4 cells cultured under conventional 2D condition. Undifferentiated stem cells grown in colonies were dissociated with Accutase™ and were cultured in the mTeSR™1 medium supplemented with Y-27632 for the first day or for 7 days (**Supplementary Figure 2A**). There were no statistically significant changes in the mRNA expression of all the studied genes in 1-day treated cells compared with day 0 cells (**Supplementary Figure 2B**). Treatment with Y-27632 for 7 days did not significantly change the gene expression of *OCT4*, *HNF3B*, *CXCR4*, *BRACHYURY*, and *SOX1* (**Supplementary Figure 2B**). However, it significantly increased the mRNA expression of *NANOG* by 2.3-folds (adjusted $p = 0.0327$) and *CER1* by 4.2-folds (adjusted $p = 0.0028$). Earlier studies have shown the increased expression of *NANOG* during

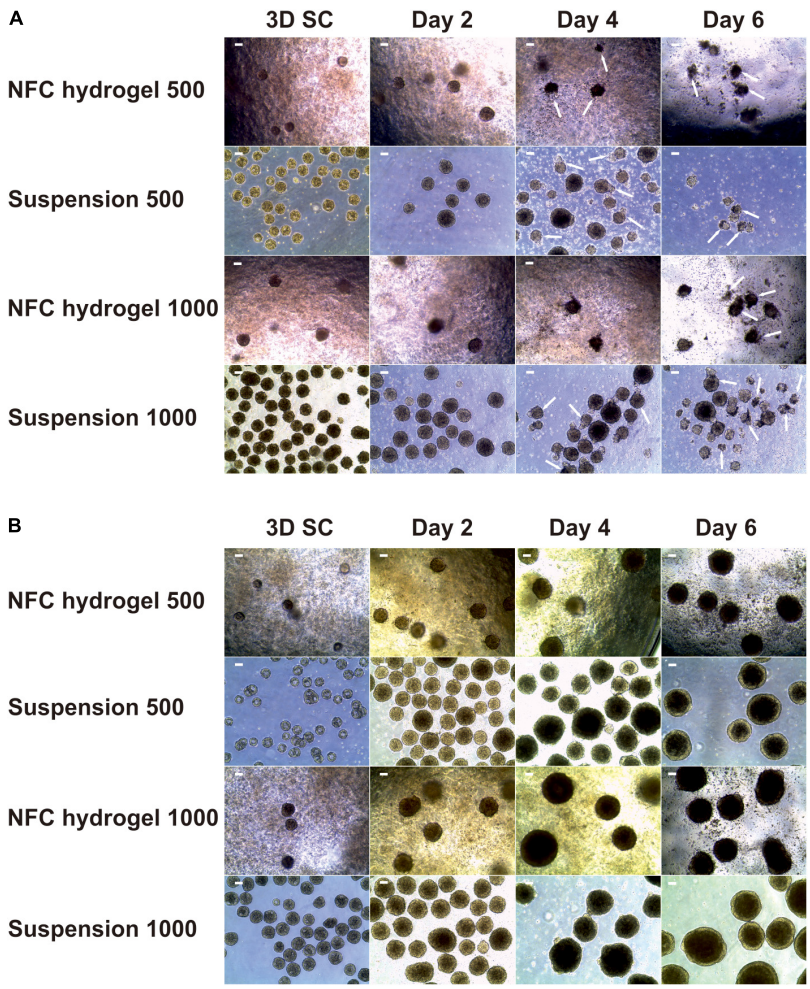

FIGURE 2 | Morphology of iPS(IMR90)-4 cell spheroids with the initial cell number of 500 and 1,000 cells per spheroid at the undifferentiated stage (3D SC) and at days 2, 4, and 6 of DE differentiation in suspension and NFC hydrogel. **(A)** Spheroids treated with a 10 μM Rho-associated protein kinase (ROCK) inhibitor Y-27632 up to day 2 of differentiation procedure. Arrows show some of damaged spheroids. Scale bars = 100 μm. **(B)** Spheroids treated with 10 μM Y-27632 throughout the entire differentiation experiment. Scale bars = 100 μm.

DE differentiation in 2D culture (Bogacheva et al., 2018), and NANOG was shown to be involved in early differentiation, for example, by participating in DE specification and repressing embryonic ectoderm differentiation (Teo et al., 2011; Wang et al., 2012). The upregulation of the specific DE marker *CER1* is a strong indication for DE differentiation. Therefore, we chose to use Y-27632 during the entire differentiation period.

3D Conditions Influence Spheroid Morphology During DE Differentiation

Based on the results from the 2D DE differentiation experiments showing that 6-day DE induction is the most effective method (Bogacheva et al., 2018), we performed 6-day DE differentiation of iPS(IMR90)-4 cells in three 3D conditions. Suspension culture in this study represents a biomaterial/scaffold-free 3D culture condition, while NFC hydrogel is an inert biomaterial that exhibits weak nonspecific interactions with cells (Harjumaki et al., 2019). Conversely, BME interacts with stem cells and DE cells directly *via* cell membrane receptors, so it represents an active cell-interacting biomaterial. We differentiated spheroids with the initial cell number of 500 and 1,000 cells in reduced growth factor BME and 200, 500, and 1,000 cells per spheroid in suspension or NFC hydrogel. Y-27632 was used throughout the entire experiment. At day 0, spheroids under all three culture conditions were transparent and round (**Supplementary Figure 3**). Hollow structures were seen in some of the spheroids at day 0, but these structures disappeared from day 2 onward. Spheroids in BME started to disintegrate and to lose their typical spherical shape morphology from day 2 onward as a result of cell migration out of the spheroids, thereby turning part of 3D culture to resemble 2D culture (**Supplementary Figures 3E,H**, arrows). On the contrary, spheroids in both suspension and NFC hydrogel retained a clear spherical shape during the entire differentiation experiment (**Supplementary Figures 3A–D,F,G**). Some larger spheroids in suspension and NFC hydrogel became darker in the center after day 2. At day 6, we observed an increase in the spheroid size and condensed darker area in the center of spheroids grown in both NFC hydrogel and in suspension. From day 4 to day 6, cells that had migrated out of the spheroids in BME started to die, as seen by cell morphology and live/dead staining (**Supplementary Figure 3**). Since BME did not support the morphology of the spheroids, we excluded the BME condition from this study.

Changes in Spheroid Size (Diameter) During DE Differentiation

After excluding BME from the study, we chose suspension and NFC hydrogel conditions in the following experiments. We differentiated iPS(IMR90)-4 spheroids with the initial cell number of 200, 500, and 1,000 cells per spheroid in suspension, named 200S, 500S, and 1000S, and in NFC hydrogel, named 200N, 500N, and 1000N, respectively. We monitored the diameters of spheroids during the 6-day differentiation (**Figure 3**). Spheroids under all the conditions gradually increased in size every day as measured by their diameters (**Figure 3B** and **Supplementary Figure 4**). Significant diameter increase day by day was seen more frequently in suspension culture than in NFC hydrogel culture (**Supplementary Figure 4**). At day 0, undifferentiated 3D SC spheroids under the conditions 200S, 500S, and 1000S were significantly different in size (adjusted $p < 0.0001$, **Figure 3A**), whereas in NFC hydrogel, a significant difference in size was only detected between 200N and 1000N (adjusted $p < 0.0001$, **Figure 3A**). At day 1, 200S or 200N spheroids were significantly different from 500S/500N to 1000S/1000N spheroids in both suspension and NFC hydrogel (**Figure 3A**). At days 2 and 3, we found statistically significant differences between the spheroids of all sizes in suspension (adjusted $p < 0.0001$), but the difference in NFC hydrogel was similar to that at day 1 (**Figure 3A**). At day 4, we did not observe a significant difference between 500S and 1000S, but we found a significant difference between 200S and 500S, as well as between 200S and 1000S. In NFC hydrogel, a significant difference was detected among all the conditions at day 4 (**Figure 3A**). Moreover, at day 4, 500S spheroids had significantly greater diameters than 500N (adjusted $p = 0.0452$). At day 5, 200S or 200N spheroids were significantly different from 500S/500N to 1000S/1000N spheroids in both suspension and NFC hydrogel. At day 6, spheroids in suspension were all different, while in NFC hydrogel, the difference remained only between 200N and 500N, as well as between 200N and 1000N. In addition, 200S and 500S were bigger than 200N and 500N, respectively (**Figure 3A**).

In summary, we found that 200S/200N spheroids were significantly smaller than 1000S/1000N spheroids in both suspension and NFC hydrogel during the entire differentiation experiment. However, we did not detect a significant difference between 500N and 1000N spheroids in NFC hydrogel at most days except at day 4. Therefore, we decided to compare 200S and 200N with 1000S and 1000N spheroids in terms of the effectiveness of DE differentiation in the subsequent immunostaining and flow cytometry experiments.

We repeated this experiment using another human iPSC line GM23720B. We differentiated GM23720B spheroids with the initial cell number of 200 and 1,000 cells per spheroid in suspension and NFC hydrogel during 4 days and assessed the dynamics of their diameter changes (**Supplementary Figures 5**, **6**). Similar to iPS(IMR90)-4, GM23720B spheroids have gradually increased in diameters during the differentiation (**Supplementary Figures 5B, 6**). Also, a significant diameter increase day by day was seen more frequently in suspension culture than in NFC hydrogel culture (**Supplementary Figure 6**). Undifferentiated 3D SC spheroids containing 200 and 1,000 cells were significantly different in size in both suspension and NFC hydrogel (adjusted $p < 0.0001$, **Supplementary Figure 5A**). In suspension, the difference between 200S and 1000S spheroids remained until day 4 (adjusted $p < 0.0001$, **Supplementary Figure 5A**). In NFC hydrogel, 200N were significantly smaller in diameter than 1000N until day 2 (adjusted $p < 0.0001$, **Supplementary Figure 5A**). At day 4, a significant difference between 200N and 1000N was detected again (adjusted $p < 0.05$, **Supplementary Figure 5A**). At day 3 and day 4, the diameter of 1000S spheroids

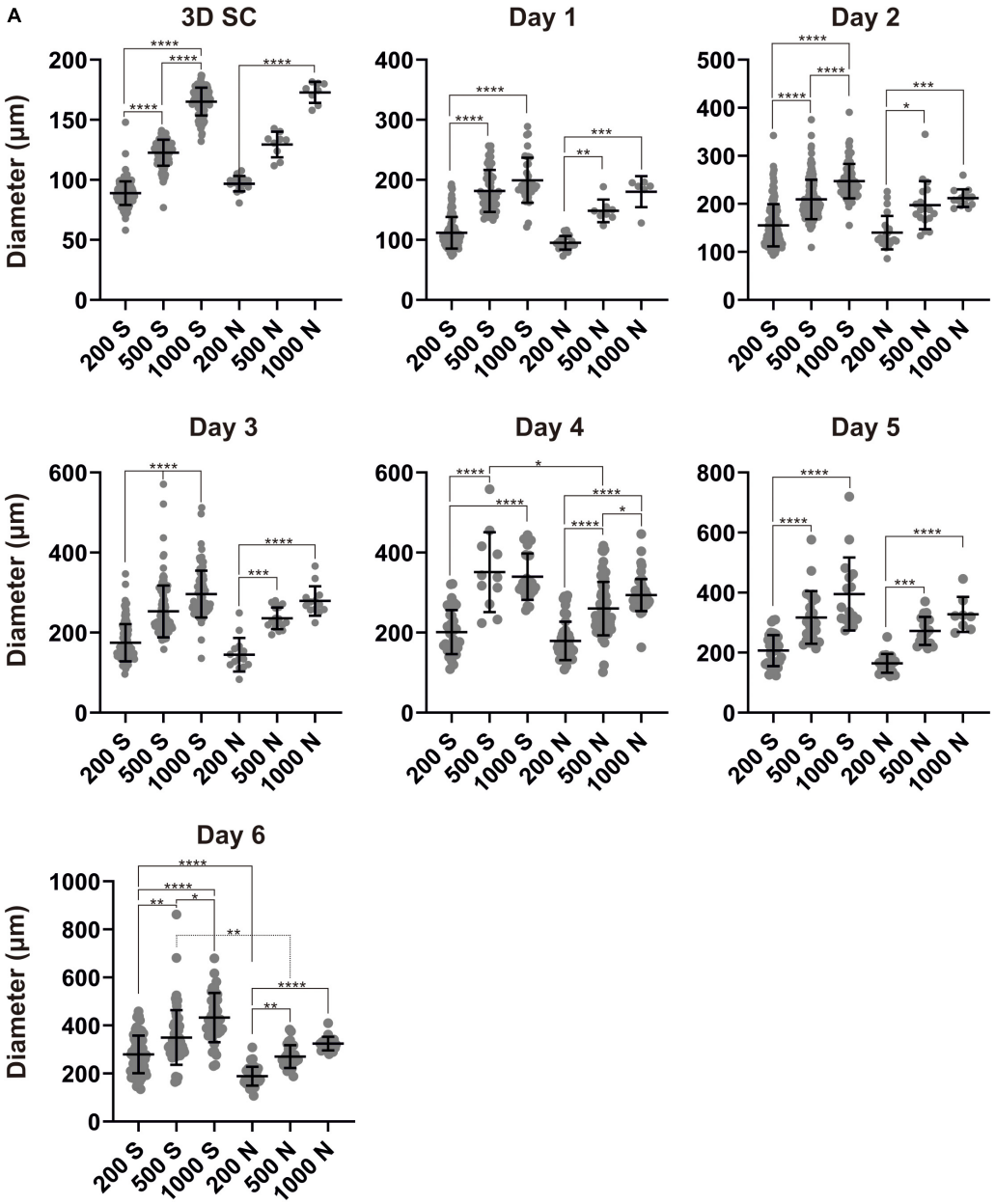

B

Condition/ Timepoint	200S	500S	1000S	200N	500N	1000N
3D SC	88.9 ± 9.8	122.6 ± 10.8	165.1 ± 11.6	96.8 ± 6.4	129.4 ± 10.7	172.8 ± 8.8
Day 1	111.8 ± 26.4	181.6 ± 35.0	199.3 ± 37.4	95.1 ± 11.4	148.4 ± 18.8	180.3 ± 25.9
Day 2	155.3 ± 44.0	209.2 ± 41.0	247.1 ± 35.8	140.1 ± 34.7	197.2 ± 49.9	211.9 ± 18.4
Day 3	174.9 ± 46.4	253.1 ± 64.6	296.3 ± 58.6	144.8 ± 42.1	235.7 ± 27.2	279.0 ± 36.8
Day 4	201.3 ± 55.2	351.2 ± 99.7	339.9 ± 58.0	179.0 ± 48.0	260.1 ± 66.8	293.9 ± 40.1
Day 5	206.7 ± 51.8	317.3 ± 87.4	395.3 ± 121.6	164.3 ± 31.3	272.2 ± 46.6	327.5 ± 58.3
Day 6	279.4 ± 78.1	350.0 ± 113.5	432.8 ± 102.5	189.0 ± 39.0	270.3 ± 47.5	324.8 ± 28.4

FIGURE 3 | Spheroid sizes during differentiation. **(A)** Size distribution of iPS(IMR90)-4 cell spheroids with the initial cell number of 200, 500, and 1,000 cells per spheroid during DE differentiation in suspension (S) and NFC hydrogel (N). Diameters (µm) were measured daily during the experiment. Horizontal lines are mean values, and vertical lines are SD. Because a normality test indicates that the data were not sampled from a Gaussian population, Kruskal–Wallis test followed by Dunn's multiple comparisons test was used. Statistical significance * adjusted $p < 0.05$, ** adjusted $p < 0.01$, *** adjusted $p < 0.001$, and **** adjusted $p < 0.0001$ are shown above lines. **(B)** Average diameter of spheroids with the initial cell number of 200, 500, and 1,000 cells per spheroid (µm) ± SD at each day of the DE differentiation of iPS(IMR90)-4 cells.

was significantly bigger than 1000N (adjusted $p < 0.05$, **Supplementary Figure 5A**).

Gene Expression Profiles in iPS(IMR90)-4 Cells and Their Derivatives During DE Differentiation in 3D Conditions

To study how spheroid size and 3D culture condition affect DE differentiation, we analyzed the gene expression profiles of mesendoderm, DE, and hepatic endoderm specific markers (**Figure 4A**) in 200S, 200N, 500S, 500N, 1000S, and 1000N at day 0, day 1, day 2, day 4, and day 6 of the differentiation experiment. Mesendoderm is a progenitor cell stage established prior to DE specification when differentiating PSCs still retain developmental plasticity to generate either mesoderm or DE.

We first validated our approach in DE differentiation by normalizing the transcript expression levels of individual genes to their highest level during DE differentiation (**Supplementary Figure 7**). We confirmed that the induction of these genes followed the sequence *BRACHYURY* (day 1) → *SOX17* (day 2) → *HNF3B*/*CER1* (day 2-4) → *CXCR4* (day 4) → *HNF4A* (day 6), which was also previously observed from other DE differentiation studies (D'Amour et al., 2005; McLean et al., 2007; Teo et al., 2012).

Next, we examined the expression of individual mesendoderm and endoderm genes according to their relative expression levels to 2D SC controls, which represent undifferentiated human iPSCs, to reveal differences among conditions for different initial cell numbers and different 3D culture strategies, namely NFC hydrogel versus suspension cultures (**Figures 4B–G**). *BRACHYURY* (*BRA* or *TBXT*) is a specific marker for mesendoderm lineage cells, and its expression turns off once cells become specified as DE. As expected, we observed a strong upregulation of its expression at day 1 in 200N and 500N cells, followed by downregulation on the next day (**Figure 4B**). Its expression stayed low or further reduced at day 4 and day 6, corroborating that by day 4, the cells were specified as DE under all the conditions.

The gene expression of the DE marker *SOX17* was significantly higher in the cells at day 2 and day 4 in all the conditions in comparison with the stem cells and the cells at day 1 of differentiation (**Figure 4C**). At day 2, 200S and 200N cells had higher *SOX17* gene expression than 1000S (adjusted $p = 0.034$) and 1000N cells (adjusted $p = 0.0123$), respectively. 500N cells also showed a higher *SOX17* level than 1000N cells (adjusted $p = 0.0271$). At day 4, *SOX17* expression significantly dropped in 200S (adjusted $p = 0.0128$), 200N (adjusted $p = 0.0374$), 500S (adjusted $p = 0.0002$), and 500N cells (adjusted $p = 0.0055$) compared to the day 2 level. By day 6, all the conditions did not exhibit a significant difference in *SOX17* expression compared with the undifferentiated stem cells, and 1000S cells even had significantly lower expression than that at day 4 (adjusted $p = 0.0016$).

The gene expression of the DE marker *HNF3B* significantly increased at day 2 in all suspension conditions and 200N except 500N and 1000N, but by day 4, it increased in all the conditions (**Figure 4D**). It was significantly upregulated in 1000S cultures by day 4 compared with day 2 (adjusted $p = 0.0161$). 1000S cultures at day 4 also had higher *HNF3B* expression than 500S cultures (adjusted $p = 0.016$). There was no significant increase from day 4 to day 6. The expression of *HNF3B* in 200S, 500S, and 500N cells at day 6 was not significantly different in comparison with the undifferentiated stem cells.

The gene expression of another DE marker *CER1* (Iwashita et al., 2013) significantly increased in all six conditions at day 2 when compared with the stem cells and the cells at day 1 (**Figure 4E**). On the following days, *CER1* expression did not increase significantly or even dropped in 200S cells at day 6 in comparison with day 4 (adjusted $p = 0.0209$). 1000N cells at day 6 had higher *CER1* expression than 500N (adjusted $p = 0.0038$) and 1000S cells (adjusted $p = 0.0044$).

CXCR4 is a well-characterized DE marker (D'Amour et al., 2005). Its expression was significantly upregulated under all the conditions at day 4 (**Figure 4F**). By day 6, it remained at the same level in 500N, 1000S, and 1000N cells and decreased in 500S cells. 1000N spheroids at day 4 showed higher *CXCR4* expression than 200N spheroids (adjusted $p = 0.016$). 1000S spheroids at day 6 displayed higher *CXCR4* expression than 200S (adjusted $p = 0.0073$) and 500S spheroids (adjusted $p = 0.0079$). Similarly, 1000N spheroids had higher *CXCR4* expression than 500N cells (adjusted $p < 0.0001$).

HNF4A isoforms are differentially expressed during development. HNF4A 1D isoform (transcribed from the P2 promoter) was earlier shown to increase in DE cells and promote DE differentiation (Hanawa et al., 2017). In the current study, we measured total *HNF4A* isoforms and found that their expression significantly increased at day 4 in 200S, 500S, 1000S, and 1000N cells, whereas 1000S cells had higher *HNF4A* expression than 500S cells (adjusted $p = 0.0217$; **Figure 4G**). By day 6, *HNF4A* increased in 1000N cells compared to the day 4 level (adjusted $p = 0.0039$). 1000S cells at day 6 showed higher *HNF4A* expression than 200S (adjusted $p = 0.0179$) and 500S cells (adjusted $p = 0.0004$). 1000N cells had higher *HNF4A* expression than 500N cells (adjusted $p = 0.0003$).

Taken together, we found that the studied DE markers were significantly increased at day 2 or day 4 in comparison with the undifferentiated stem cells. Only *HNF4A* expression was further increased from day 4 to day 6. Intriguingly, the expression of the DE markers *SOX17*, *CER1*, and *CXCR4* started to decrease at day 6 suggesting an accelerated differentiation program compared with 2D adherent differentiation (Bogacheva et al., 2018). Hence, we selected the 4-day differentiation protocol in the following experiments. Since the PCR method determines gene expression in bulk cell populations, we next used flow cytometry and immunofluorescence staining to assess DE differentiation in individual cells.

Spheroid Size and 3D Culture Conditions Affect the Efficiency and the Effectiveness of DE Formation

Before DE differentiation, we stained pluripotency markers in iPS(IMR90)-4 spheroids after their formation in AggreWell^{TM}400 plates. All the spheroids with 50, 100,

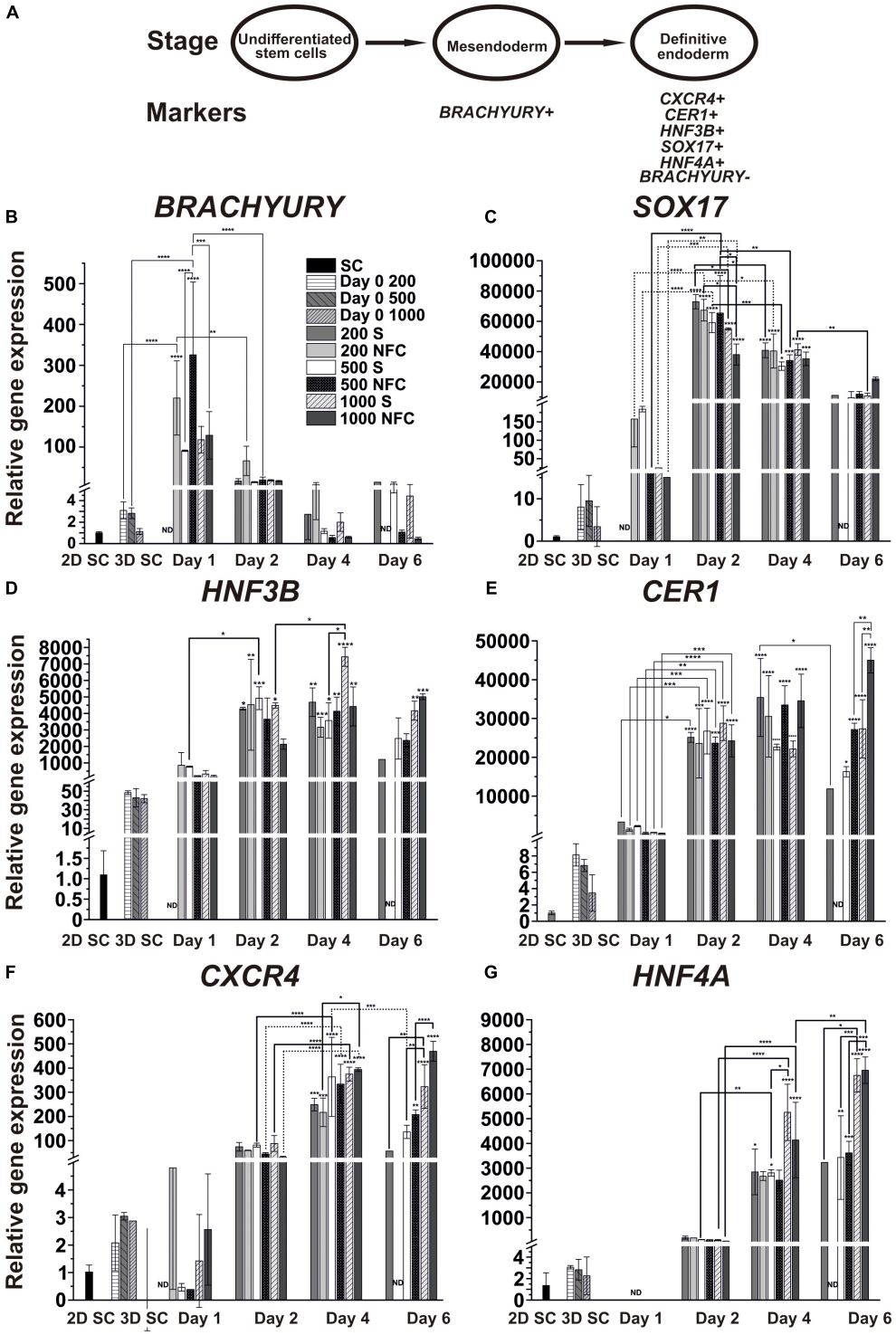

FIGURE 4 | (A) Schematic of the characteristic markers at the studied differentiation stages. **(B–G)** The mRNA expression patterns of the mesendoderm (*BRACHYURY*), DE (*SOX17*, *HNF3B*, *CER1*, and *CXCR4*), and hepatic endoderm (*HNF4A*) specific markers during DE differentiation of iPS(IMR90)-4 cells in 3D spheroids with the initial cell number of 200, 500, and 1000 cells per spheroid in suspension (S) and NFC hydrogel (N). Relative gene expression was measured by qPCR and normalized with RPLP0 housekeeping gene. Fold inductions were calculated with the reference to the stem cell samples (2D SC). $N = 2$ or 3 biological repeats. ND, no data. Error bars are SD. One-way ANOVA followed by Tukey's multiple comparisons test was used to compare between any pairs. Statistical significance *adjusted $P < 0.05$, **adjusted $P < 0.01$, ***adjusted $P < 0.001$, and ****adjusted $P < 0.0001$ in comparison with 2D SC are shown above bars. Statistically significant differences *adjusted $P < 0.05$, **adjusted $P < 0.01$, ***adjusted $P < 0.001$, and ****adjusted $P < 0.0001$ between days 1 and 2, days 2 and 4, and days 4, and 6 are shown above lines. Breaks in *Y*-axis in the figure panels are *BRACHYURY*: 5–7, *SOX17*: 16–26 and 200–9000, *HNF3B*: 2–5 and 60–150, *CER1*: 10–50, *CXCR4*: 5–30, and *HNF4A*: 5–30.

200, 500, and 1,000 cells per spheroid were positive for OCT4 and NANOG proteins (**Supplementary Figure 8**).

We evaluated the efficiency and the effectiveness of the DE formation by image-based analysis of SOX17, HNF3B, and HNF4A protein expression and quantitative analysis of CXCR4 expression. We conducted immunofluorescence staining for the DE markers SOX17, HNF3B, and HNF4A and the pluripotency marker OCT4 in day 4 spheroids (**Figure 5** and

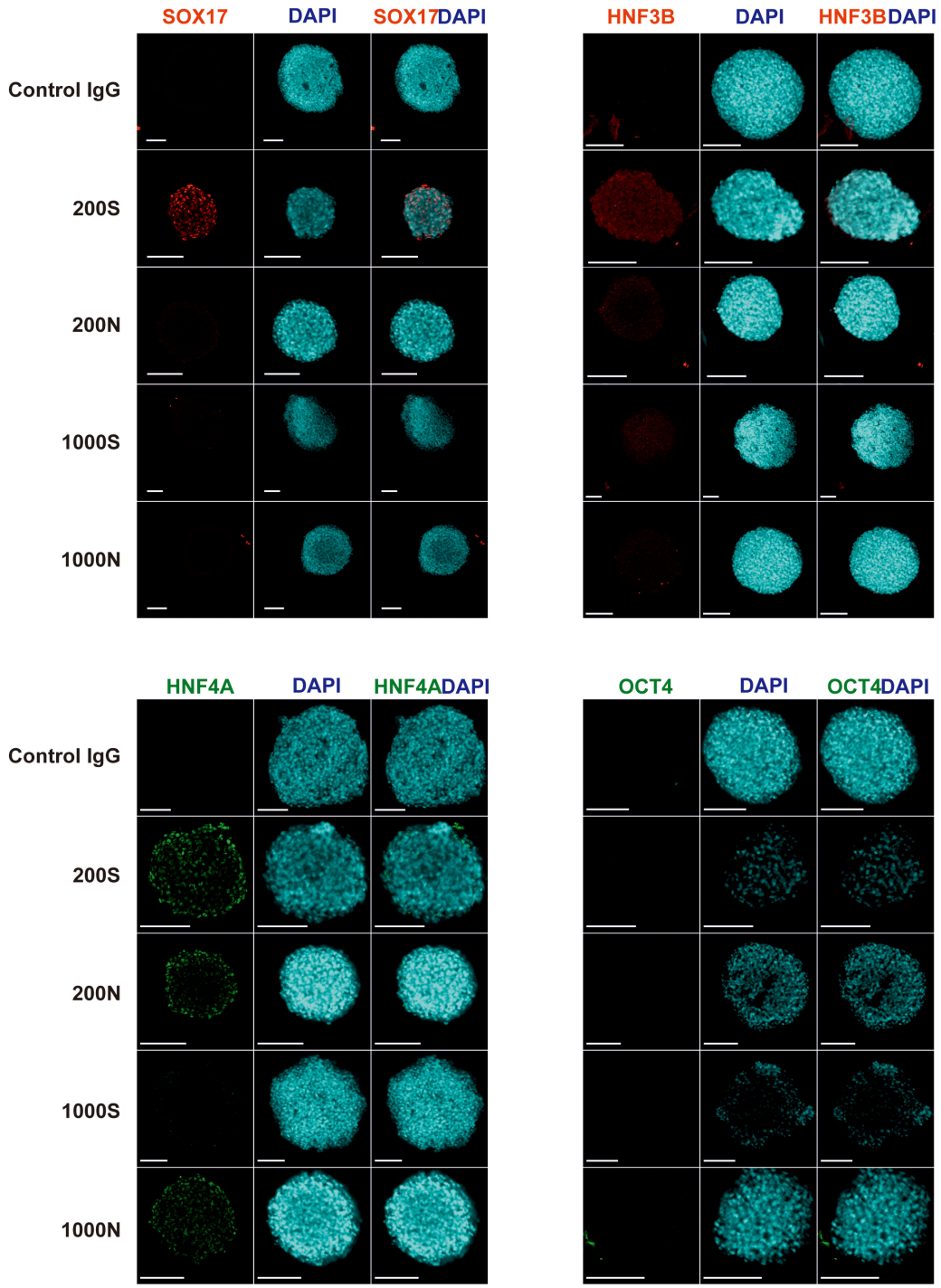

FIGURE 5 | Expression of SOX17, HNF3B, HNF4A, and OCT4 proteins in iPS(IMR90)-4 cell spheroids at day 4 of 3D DE differentiation in suspension (S) or NFC hydrogel (N). Nuclei of cells were stained with DAPI (blue). Proteins of interest were stained either with Alexa Fluor 488 (HNF4A and OCT4), showed in green, or with Alexa Fluor 594 (SOX17 and HNF3B), showed in red. Scale bars = 100 μm.

Supplementary Figure 9). 200S iPS(IMR90)-4 spheroids were positive for SOX17, HNF3B, and HNF4A (**Figure 5**). 200N spheroids were strongly positive for HNF4A protein and weakly so for HNF3B in the cells of the outer layers (**Figure 5**), which displayed similar intensity to what was observed in 2D DE differentiation previously (Bogacheva et al., 2018), but 200N spheroids were negative for SOX17 (**Figure 5**). 1000S spheroids had the weakly positive expression of HNF3B and HNF4A proteins and did not express SOX17 (**Figure 5**). 1000N spheroids showed strong HNF4A expression and were negative for SOX17 and HNF3B (**Figure 5**). None of the conditions showed OCT4 protein expression (**Figure 5**).

Similar to iPS(IMR90)-4 DE spheroids, OCT4 protein expression was not observed in day 4 GM23720B cell spheroids in all the conditions (**Supplementary Figure 9**). 200S spheroids were positive for SOX17 and HNF3B proteins while negative for HNF4A (**Supplementary Figure 9**). 200N and 1000S spheroids had positive signals for SOX17 (**Supplementary Figure 9**). 1000N spheroids demonstrated low or no expression for the stained protein markers (**Supplementary Figure 9**).

To quantify the differentiation in individual cells, we performed flow cytometry analysis of iPS(IMR90)-4 and GM23720B spheroids and their derivatives differentiated in suspension or NFC hydrogel at day 1, day 2, and day 4 of DE differentiation (**Supplementary Figure 10**). We examined the pluripotency marker SSEA4 and the DE marker CXCR4 in iPS(IMR90)-4 spheroids (**Figures 6**, **7**, and **Supplementary Figure 11**) and the DE marker CXCR4 in GM23720B spheroids (**Supplementary Figure 12**).

The percentage of $SSEA4^+$ cells in iPS(IMR90)-4 cell spheroids before differentiation was more than 99% (**Figures 6A**, **7A**), and it significantly dropped by day 4 only in spheroids cultured in suspension (adjusted $p < 0.0001$ for 200S and adjusted $p = 0.0003$ for 1000S, **Figure 7A**). We also observed that the fluorescent intensity peaks in all histograms shift to the left during the differentiation (**Figure 6A** and **Supplementary Figure 11**). At day 4, 1000S spheroids had significantly less $SSEA4^+$ cells than 1000N spheroids (adjusted $p = 0.0139$, **Figure 7A**).

Spheroids with the initial cell number of 200 and 1,000 cells per spheroid at the stem cell stage were negative for CXCR4 protein (**Figures 6B**, **7B**, and **Supplemetary Figure 12A**). The percentage of $CXCR4^+$ iPS(IMR90)-4 cells did not change at day 1 but rose at day 2 and then reached its maximum by day 4 (**Figures 6B**, **7B**). Similarly, the percentage of $CXCR4^+$ GM23720B cells also increased at day 2 and day 4 (**Supplemetary Figure 12A**). At day 2, 200S iPS(IMR90)-4 spheroids displayed the highest percentage of $CXCR4^+$ cells ($67.7 \pm 8.6\%$, **Figure 7B**). This percentage was significantly higher than that for 200N ($49.5 \pm 4.9\%$, adjusted $P = 0.0056$) and 1000S spheroids ($25.9 \pm 8.6\%$, adjusted $P < 0.0001$, **Figure 7B**). Similarly, 200S GM23720B spheroids also displayed higher percentage of $CXCR4^+$ cells ($62.7 \pm 5.8\%$) than that for 200N ($54.0 \pm 5.0\%$) and 1000S spheroids ($55.8 \pm 5.5\%$, **Supplemetary Figure 12A**). For the iPS(IMR90)-4 spheroids in NFC hydrogel, a similar trend to suspension cultures was observed: 200N spheroids ($49.5 \pm 4.9\%$) displayed a significantly higher percentage of $CXCR4^+$ cells than 1000N spheroids ($15.2 \pm 12.4\%$, adjusted $p < 0.0001$, **Figure 7B**).

Furthermore, we found a negative correlation between iPS(IMR90)-4 spheroids' size and percentage of $CXCR4^+$ cells in both NFC hydrogel ($p = 0.0225$, **Figure 7C**) and suspension ($p = 0.0024$, **Figure 7D**) at day 2 of the differentiation. For GM23720B spheroids, the correlation was found between spheroids' size and percentage of $CXCR4^+$ cells in suspension at day 4 of the differentiation ($p = 0.0251$, **Supplementary Figure 12C**).

When measuring the CXCR4 expression by flow cytometry, we also stained the cells with 7-AAD fluorescent dye to assess cell death in spheroids. We did not detect a significant difference in cell death between time points or culture conditions (**Supplementary Figure 13**). The percentage of dead cells in spheroids was averaged $4.6\% \pm 1.6\%$ under all the conditions. This indicates that poor differentiation performance of spheroids under certain culture conditions was not caused by decreased cell viability.

In summary, these data demonstrate that smaller hPSC spheroids differentiate to DE cells more efficiently than bigger spheroids, and suspension culture promotes more effective DE differentiation than NFC hydrogel.

Computational Simulation of Activin A Diffusion

Activin A used in the differentiation media is crucial for DE formation. Earlier studies showed that its effect is concentration-dependent, with high concentrations (100 ng/ml) specifying DE (D'Amour et al., 2005) and low concentrations specifying mesoderm (Schuldiner et al., 2000). The poor efficiency and effectiveness of DE formation from the bigger spheroids cultured in NFC hydrogel could indicate a poor diffusion of activin A due to mass transfer limitation caused either by cell masses in spheroids or by biomaterials. Simulating the diffusion of proteins within a spheroid is technically difficult to perform; thus, our model is focused on simulating the diffusion of activin A within the NFC hydrogel layer. By establishing a computational model based on Fick's second law of diffusion and an NFC hydrogel-specific linear regression model based on the Einstein relation of kinetic theory and the viscous friction coefficient, we found that only the top 0.25 mm (8%) of the NFC hydrogel layer received 100 ng/ml activin A (**Figure 8**). Since protein half-lives in cell culture and in tissues are different (Rahman and Sadygov, 2017), our simulation using the *in vivo* half-life of activin A might overestimate or underestimate the activin A diffusion *in vitro*. Nonetheless, the simulation result indicates that activin A encountered considerable resistance to its transfer across NFC hydrogel, presumably due to hydrogel's high viscosity (Bhattacharya et al., 2012). The limited mass transfer may explain the low effectiveness of the DE differentiation in NFC hydrogel (**Figure 9**).

DISCUSSION

To overcome the major challenges in spheroid and organoid technology and increase the effectiveness of stem cell differentiation in 3D environments, we examined how 3D cell

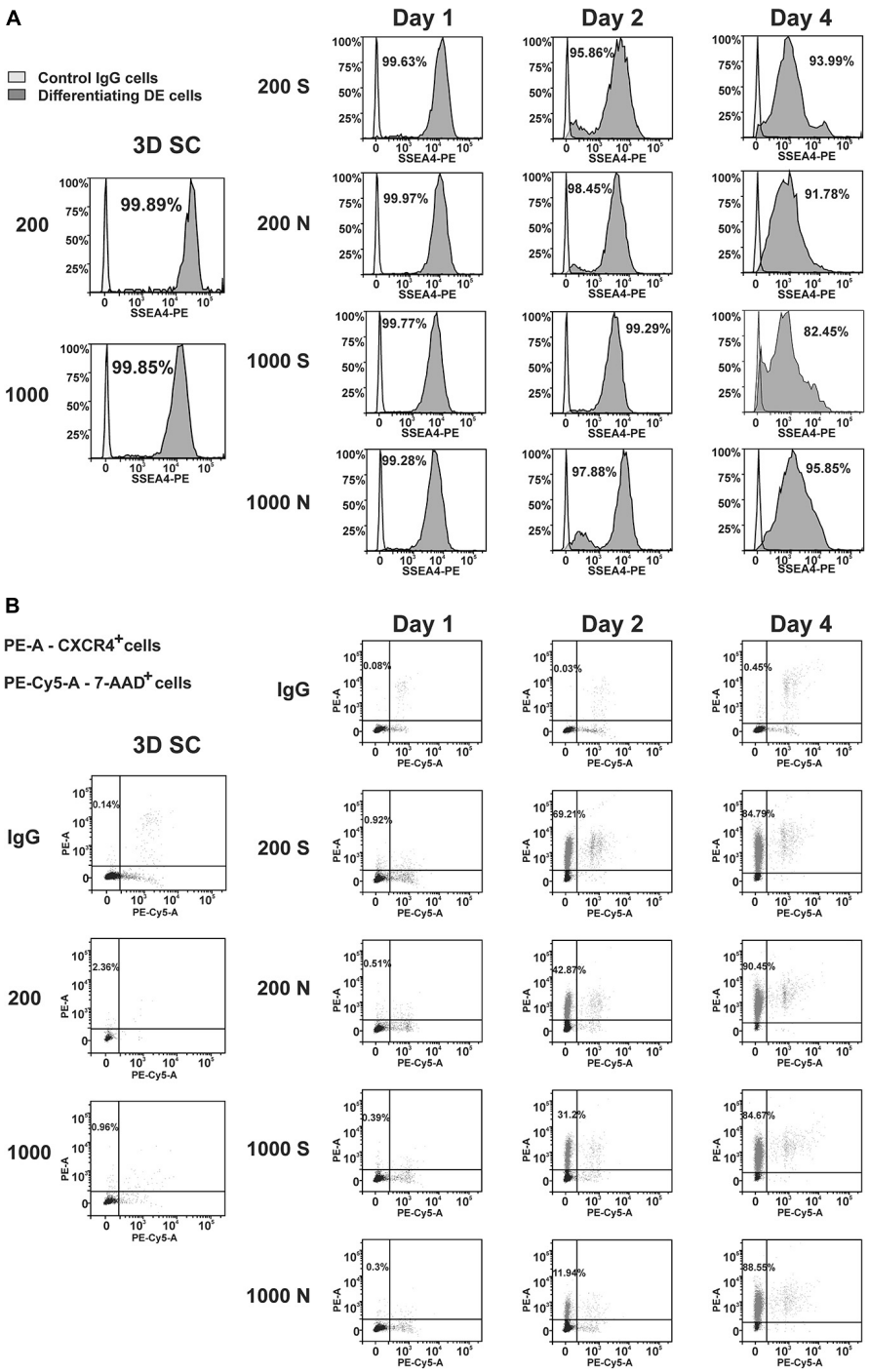

FIGURE 6 | Dynamic expression of the pluripotency (SSEA4) and DE (CXCR4) protein markers in iPS(IMR90)-4 cells and their derivatives during DE differentiation of 3D spheroids with the initial cell number of 200 and 1,000 cells per spheroid in suspension (S) and NFC hydrogel (N). Graphic results from one out of four biological repeats are presented in the figure. Graphics are generated using the Flowlogic software (Inivai Technologies). **(A)** SSEA4 protein expression at the stage of undifferentiated cells (3D SC) and day 1, day 2, and day 4 in differentiation experiments, in which the same number of spheroids was harvested from suspension (S) and NFC hydrogel (N). Cells stained with an SSEA4 antibody or normal IgG were measured in the PE channel by flow cytometry. Gating was done based on IgG control as $SSEA4^-$. Percentage on each histogram means a percent of $SSEA4^+$ cells. **(B)** CXCR4 protein expression at the stage of undifferentiated cells (3D SC) and day 1, day 2, and day 4 in differentiation experiments, in which the same number of spheroids was harvested from suspension (S) and NFC hydrogel (N). The percentage of $CXCR4^+$ cells was calculated by flow cytometry analysis. Cells were stained with PE mouse anti-human CD184 (CXCR4) IgG2a or PE mouse IgG2a that was detected in the PE channel and then with 7-AAD Viability Staining Solution that was detected in the PE-Cy5 channel. The percentage of live $CXCR4^+$ cells is presented in the upper left quadrant of each dot-blot. This experiment was performed four times, and only one of the experimental results is shown here.

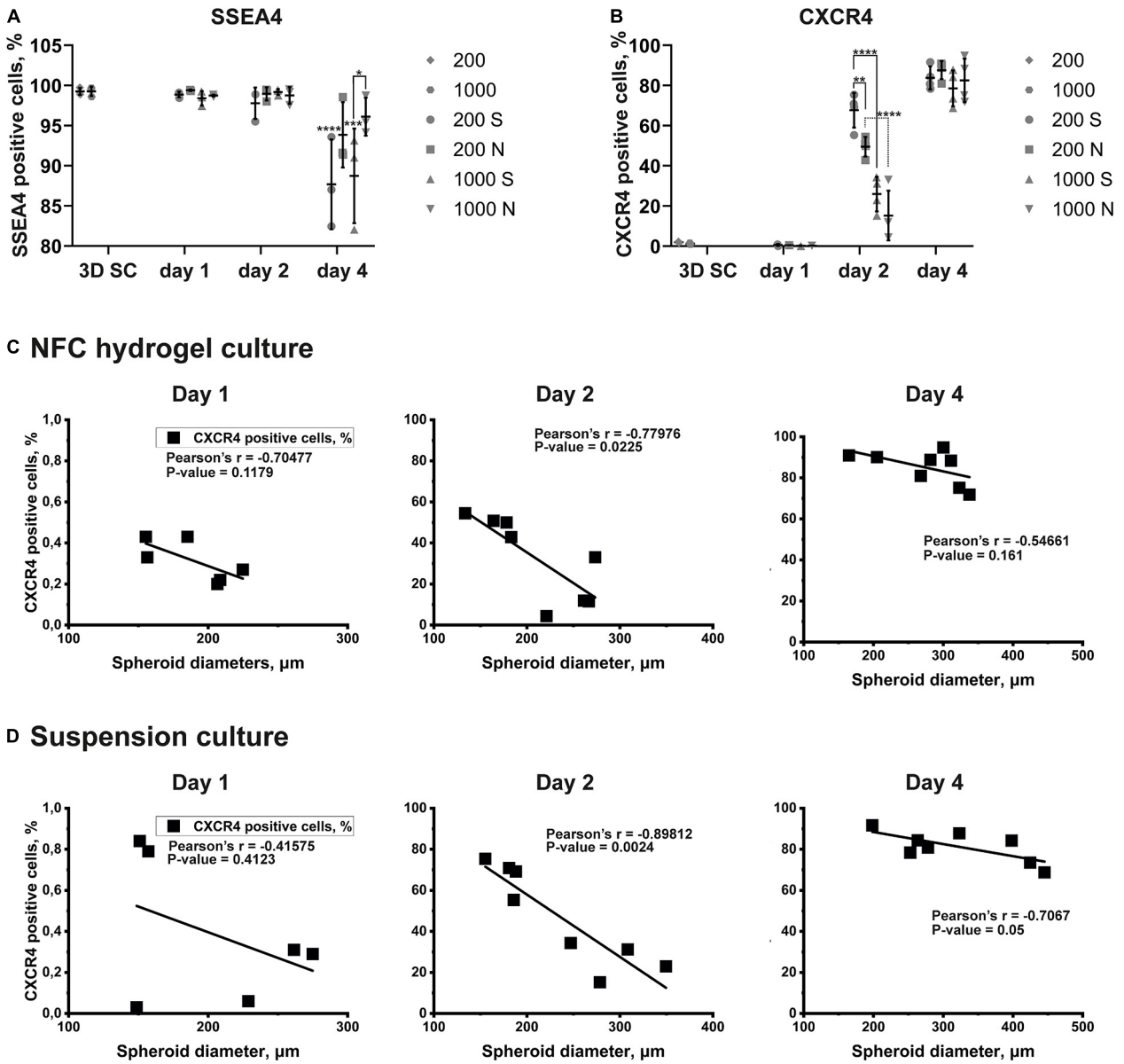

FIGURE 7 | The quantitative expression of markers and the correlation between spheroid diameters and the effectiveness of the DE differentiation in iPS(IMR90)-4 cells. **(A)** SSEA4 protein expression pattern in iPS(IMR90)-4 cell spheroids (3D SC) and their derivatives during 3D DE differentiation in suspension (S) and NFC hydrogel (N). *N* = 3 biological repeats. Data were analyzed by one-way ANOVA followed by Sidak's multiple comparisons test. Statistical significance *** adjusted $p < 0.001$ and **** adjusted $p < 0.0001$ in comparison with 3D SC are shown above scatters. Statistically significant difference * adjusted $p < 0.05$ between conditions 1000S and 1000N at day 4 is shown above the line. **(B)** CXCR4 protein expression pattern in iPS(IMR90)-4 cell spheroids (3D SC) and their derivatives during 3D DE differentiation in suspension (S) and NFC hydrogel (N). *N* = 4 biological repeats. One-way ANOVA followed by Sidak's multiple comparisons test was used. Statistically significant differences ** adjusted $p < 0.01$ and **** adjusted $p < 0.0001$ between conditions are shown above lines. **(C)** Pearson correlation between spheroid diameters and percentages of live CXCR4$^+$ cells during 3D DE differentiation in NFC hydrogel. Statistically significant negative Pearson correlation is detected at day 2. **(D)** Pearson correlation between spheroid diameters and percentages of live CXCR4$^+$ cells during 3D DE differentiation in suspension. Statistically significant negative Pearson correlation is detected at day 2.

culture systems and spheroid size influence DE differentiation of human iPSCs. Here we show that suspension culture can effectively generate DE cells from 3D human iPSC spheroids, whereas the use of biomaterials in DE differentiation may cause issues with mass transfer and spheroid formation. These findings are summarized in a schematic diagram (**Figure 9**). BME, a biomaterial with cell-interacting properties, produced strong cell–matrix interactions that caused 3D spheroids to spread out into monolayers (**Figure 9**). NFC hydrogel, a biomaterial with poor cell-interacting properties, was able to maintain 3D

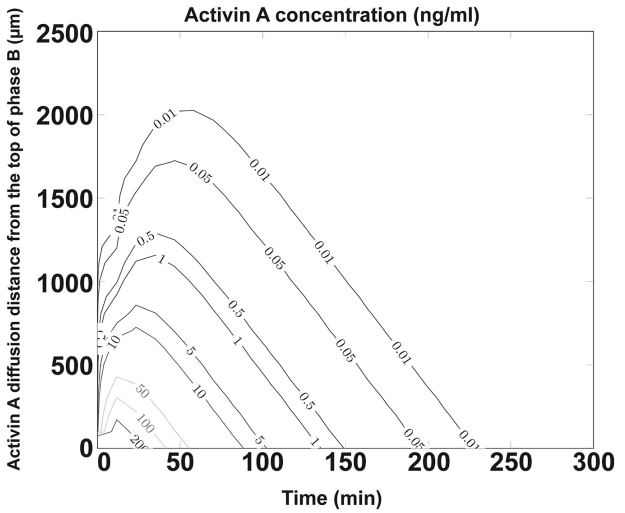

FIGURE 8 | Concentration profile of activin A protein. Diffusion coefficient set as $D_{Regression} = 7.31 \times 10^{-7}$ cm^2/s for 26.0 kDa activin A protein and half-life $\lambda = 20.3$ min (slow estimation). Activin A was diffused from the interface between phase A and phase B into phase B. Phases A and B are illustrated in **Supplementary Figure 1**. *Y*-axis shows the activin A diffusion distance (μm) from the top of phase B. Activin A concentrations (ng/ml) at different positions in phase B during 250 min after the addition of the activin A-containing differentiation medium are shown by curves. Only the top 250 μm (8%) of the NFC hydrogel layer received 100 ng/ml activin A.

spheroid morphology during DE differentiation (**Figure 9**). However, NFC hydrogel impeded growth factor diffusion presumably due to its high viscosity, and therefore DE formation was less effective than in suspension culture. We also found an inverse correlation between spheroid size and the effectiveness of DE formation; smaller spheroids (with initial 200 cells per spheroid) differentiated more effectively than the larger ones (with initial 1,000 cells per spheroid). In addition, bigger spheroids (with initial 200, 500, and 1,000 cells per spheroid) formed stable cell aggregates after 24 h, while spheroids that are too small (with initial 50 or 100 cells per spheroid) did not retain their 3D morphology in suspension or in NFC hydrogel possibly due to poor cell–cell interactions. The importance of cell–cell interaction in the formation of dermal fibroblast spheroids has recently been demonstrated by using a micropatterned hydrogel (Kim et al., 2019).

Mass transfer, also known as mass transport, is important for successful 3D cell culture and tissue engineering (Antoni et al., 2015). Sufficient mass transfer ensures the proper supply of nutrients and regulatory factors to cells and therefore generates desired cell and tissue products. Insufficient mass transfer can be caused by the presence of biomaterials and cells. Mass transfer is particularly critical when growth factors are involved because many growth factors have short half-lives, and delayed delivery to target cells results in reduced dosage to cells. By establishing a computational model to simulate growth factor diffusion, we found that activin A poorly diffused across NFC hydrogel, which may be due to the short half-life of activin A and the high viscosity of NFC hydrogel. This problem may be common for all 3D cell culture systems combining growth factors with short half-lives and highly viscose biomaterials. This issue may be solved by stabilizing growth factors or increasing the permeability of NFC hydrogel. The half-life of Wnt-3a increases when using liposomal packaging (Dhamdhere et al., 2014), so similar approaches may be applicable for activin A. However, liposomal packaging increases the radii of said growth factors, potentially hindering diffusion. Fortunately, the effect of such packaging could be predicted with the computational model described in this study. Replacing growth factors with stable small molecules is another solution. We have previously tested IDE1 as a substitute for activin A in DE differentiation, but unfortunately, it was ineffective (Bogacheva et al., 2018). Another study tested several small molecules in DE differentiation but still did not find an equally effective chemical to replace activin A (Tasnim et al., 2015). A high-content screening study identified two ROCK inhibitors as DE inducers in human and mouse ESCs (Korostylev et al., 2017). However, the undifferentiated ESCs used in their study were positive for DE markers, which may indicate intrinsic bias of the DE marker-positive ESC population toward endoderm differentiation as shown in an earlier study (Allison et al., 2018). Hydrogel permeability is an intrinsic property. Therefore, increasing permeability requires extensive investigation and may involve undesired changes in other hydrogel properties.

Basement membrane extract, representing another class of biomaterials that have cell-interacting properties, was also used in this study. The finding that BME could not maintain 3D spheroid morphology during DE differentiation is interesting. We speculate that this was the result of the imbalance between cell–matrix interactions and cell–cell interactions (**Figure 9**). It is known that undifferentiated ESCs and iPSCs can interact with BME (Xu et al., 2001). Upon embedding iPSC spheroids in BME, strong cell–BME interactions may override cell-cell interactions, thereby causing disruption of spheroid morphology. Decreasing E-cadherin expression during DE differentiation (D'Amour et al., 2005) further reduces cell–cell interactions, thereby contributing to disrupted spheroid morphology. In contrast, NFC hydrogel has negligible adhesion forces to stem cells (Harjumaki et al., 2019)—minimizing cell–matrix interactions. Thus, the predominance of cell–cell interactions may account for the well maintenance of the spheroid shape in NFC hydrogel (**Figure 9**). These conclusions are supported by Nie et al. (2020) who previously showed with human keratinocytes that decreased cell-substrate adhesion was the main driving force in the spheroid formation and at the same time cell–cell interaction forces increased and exceeded cell–biomaterial interaction force levels.

The migrating cells in BME are presumably DE cells as shown by the immunofluorescence of SOX17 (data not shown). The reason for their death from day 4 onward could be due to the nonsupportive environment. Although DE cells can be derived from human PSCs on BME in 2D culture, DE cells, in fact, have limited ability to attach to BME as shown by the downregulation of laminin 111-specific integrins in DE cells (Kanninen et al., 2016a) and failure on re-attachment to BME after detachment (Kanninen et al., 2016b). Derivation of DE

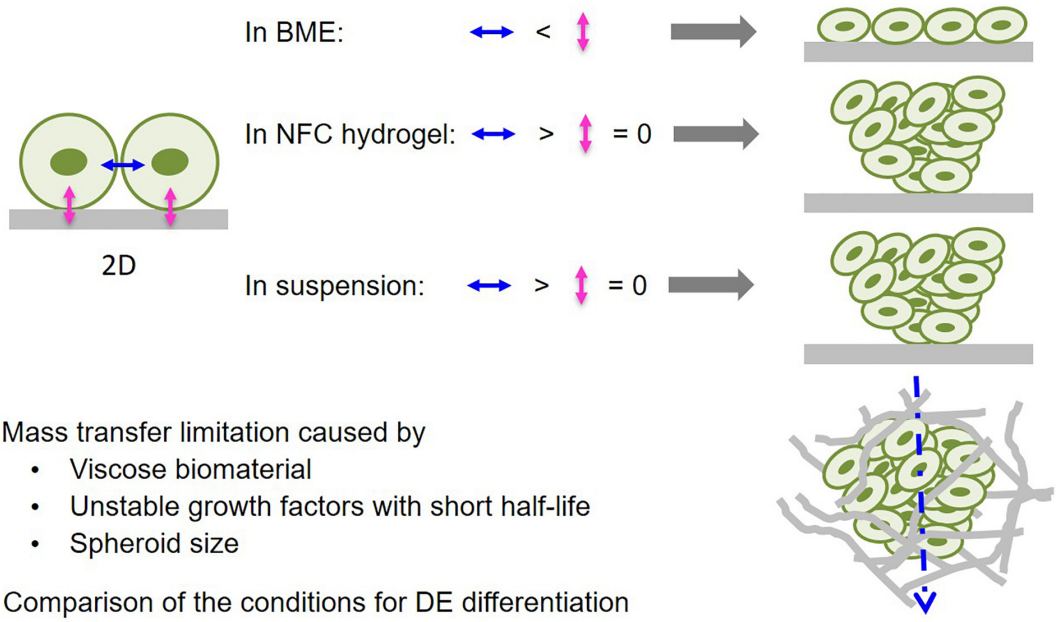

C Comparison of the conditions for DE differentiation

Condition	Dominant cell-cell interactions	Sufficient mass transfer in the environment	Optimal spheroid size
200 S	+	+	+
1000 S	+	+	-
200 N	+	-	+
1000 N	+	-	-
200 BME	-	Not studied	Not studied
1000 BME	-	Not studied	Not studied

FIGURE 9 | The critical influencing parameters in 3D DE differentiation. **(A)** Predominance of cell–biomaterial interactions in basement membrane extract (BME) leads to disintegration of 3D spheroid morphology, while predominance of cell–cell interactions in NFC hydrogel and suspension culture retains 3D spheroid morphology. **(B)** Viscose biomaterial and cell mass can limit mass transfer, thereby impairing differentiation that is mediated by growth factors with short half-lives. **(C)** Comparison of the studied 3D culture systems in terms of their properties affecting DE differentiation effectiveness.

cells on BME in 2D culture may involve an undifferentiated PSC-produced niche, which requires further investigation.

Suspension culture is a biomaterial/scaffold-free system, meaning that there is no potential mass transfer limitation caused by biomaterials. In some cases, cells are attached to floating microcarriers. Nonetheless, all suspension cultures ensure equal supply to all spheroids. Another biomaterial/scaffold-free system that has been used in spheroid technology is the hanging-drop system. It has been used to form spheroids of dermal papilla cells in a controllable and scalable manner (Lin et al., 2016). By performing DE differentiation that involves the use of growth factor, we clearly demonstrate that suspension culture is a superior 3D culture system to biomaterial-based 3D systems because it provides equal molecular diffusion among all the spheroids, and therefore produces efficient DE differentiation. Suspension culture is scalable (Amit et al., 2010; Li et al., 2018) and can be performed in a bioreactor with tight control of cell culture conditions for mass production (Lock and Tzanakakis, 2009). Unlike biomaterial-based culture systems, suspension culture does not provide physical constraint and therefore spheroids grew faster, as shown by more significant increases in diameter in suspension culture than in NFC hydrogel culture (**Supplementary Figures 4, 6**).

In addition to biomaterials, cells can also limit mass transfer. Earlier studies have found that hepatocyte spheroids with diameters of more than 100 μm (Glicklis et al., 2004) or human ESC and iPSC spheroids with diameters of more than 350 μm (Amit et al., 2010) had cell viability rates below

90%. Our 4-day protocol for DE differentiation generated more than 90% viable cells (**Supplementary Figure 13**) in spheroids with the average diameters below 350 μm (**Figure 3B** and **Supplementary Figure 5**) in all the conditions studied. Despite the high cell viability, we found that iPSC spheroids with a higher cell number had lower differentiation effectiveness. Our finding agrees with an earlier report showing that large spheroids generated fewer SOX17- and HNF3B-positive cells (Farzaneh et al., 2018). The low effectiveness of differentiation in large spheroids is presumably due to the insufficient supply of growth factors. Computational simulation of growth factor diffusion through spheroids is not straightforward because growth factor can bind to any cells on its route of diffusion. There have been computational models for oxygen permeation into a spheroid (Aleksandrova et al., 2016; Grimes and Currell, 2018), and more comprehensive models could be established to estimate protein diffusion in a cell spheroid with consideration of growth factor-receptor binding and receptor abundance. Although smaller spheroids ensure a sufficient supply of growth factor, they may not survive during DE differentiation, as shown in the current study. It is known that cadherins mediate homophilic binding between the same types of cells. DE cells express a lower level of E-cadherin and a higher level of N-cadherin than undifferentiated ESCs and iPSCs (D'Amour et al., 2005). During DE differentiation, weaker cadherin-mediated interactions could have been generated between undifferentiated PSCs and differentiating cells leading to the failure of smaller spheroids to retain their 3D morphology.

We found that cell viability inside the spheroids can be improved with the constant presence of the ROCK inhibitor Y-23720 in the differentiation media. An earlier study found a priming effect of a high concentration of Y-23720 on mesendoderm differentiation (Maldonado et al., 2016); to ensure the use of Y-23720 does not have a negative effect on DE differentiation, we analyzed its influence on the gene expression of specific pluripotency, DE, mesendoderm, and ectoderm markers. Among the three studied DE markers, only *CER1* was significantly altered by 4.2-folds by the 7-day treatment with 10 μM Y-23720 (**Supplementary Figure 2**). Cer1 is a secreted protein participating in the regulation of Nodal, Wnt, and BMP signaling pathways and is a marker of the endoderm specification (Iwashita et al., 2013). However, the 4.2-fold increase is much less than the 30,000-fold increase observed during the directed DE differentiation (**Figure 4E**). Based on our data, the effect of Y-23720 on the DE differentiation of human PSCs was relatively mild, but its biological impact needs further investigation.

Several studies have demonstrated that 3D cell culture systems can produce DE cells from human ESCs and iPSCs. A small molecule IDE1 was shown to induce DE differentiation of human iPSCs in a poly(ε-caprolactone)-based scaffold, but the expression of *HNF3B* and *SOX17* was only induced no more than 20-folds (Hoveizi et al., 2014). In contrast to 3D culture, IDE1 (Bogacheva et al., 2018) and its analog IDE2 (Tasnim et al., 2015) were found to be ineffective in 2D DE differentiation. Another study produced DE cells in alginate hydrogel using activin A and Wnt-3a with 800- and 300-fold induction of *HNF3B* and *SOX17*, respectively (Chayosumrit et al., 2010), whereas we observed more than 4000- and 40,000-fold increase in the expression of *HNF3B* and *SOX17*, respectively. A recent study showed that 3D DE differentiation in suspension culture has an increased proliferation coefficient and higher speed of the upregulation of DE markers in comparison with adherent culture (Yabe et al., 2019). Another study successfully produced DE aggregates in chemically defined, xeno-free suspension culture, which was demonstrated to be scalable by using bioreactors (Sahabian et al., 2019). In addition, 3D culture has been proven to improve the maturation of hepatic cells (Miki et al., 2011; Freyer et al., 2016) and pancreatic cells (Wang and Ye, 2009).

We found that the remaining problem with NFC hydrogel culture is high viscosity. Utilization of chemically stable small molecules to replace growth factors would potentially solve mass transfer limitation and thus would allow more effective use of NFC hydrogel in stem cell differentiation and spheroid formation. The fast growth kinetic in suspension culture might yield larger spheroids that can inhibit mass transfer. Dissociating spheroids followed by making smaller spheroids, for example 200 cells per spheroid, would be a strategy to maintain sufficient mass transfer during differentiation experiments.

This study demonstrates that the spheroids with initial 200 cells per spheroid in suspension culture can efficiently produce DE cells (**Figure 9C**). However, further work is required to quantitatively demonstrate the inverted correlation between the size of the spheroids and the expression of nuclear DE markers, which was not demonstrated in the current study due to technical limitations in flow cytometry detecting intracellular proteins. Moreover, it is necessary to assess the potential of these cells in further differentiation into endoderm derivatives, such as hepatic, pancreatic, and intestinal cells. To further differentiate DE spheroids generated in the current study, we could continue using suspension culture system to ensure sufficient mass transfer. If stable small molecules to replace growth factors are available, hydrogel-based 3D culture systems can also be utilized to provide physical support and constraint.

CONCLUSION

In the current study, we show how the size of the human iPSC spheroids and 3D culture conditions influence DE differentiation. We found that the ROCK inhibitor improves human iPSC spheroid viability and can be applied for the entire length of DE differentiation. The spheroid size determines the availability of growth factors as well as nutrients and oxygen supply to all the cells. Suspension culture provides sufficient mass transfer and thus generates more effective DE differentiation than NFC hydrogel-based culture. When using biomaterials, cell–matrix interaction and mass transfer should be considered because they can affect 3D cell spheroid morphology and the effectiveness of growth factor-mediated differentiation, respectively. Our findings are beneficial for the development of human iPSC-derived 3D cell models, which have applications in drug research

field for the evaluation of toxicity and efficacy of drug candidates, developmental biology studies, and regenerative medicine.

DATA AVAILABILITY STATEMENT

The original contributions presented in the study are included in the article/**Supplementary Material**, further inquiries can be directed to the corresponding author/s.

AUTHOR CONTRIBUTIONS

Y-RL conceived, designed, and supervised the research, carried out some of the experiments presented in the manuscript, analyzed the data, and wrote the Introduction, Results, and Discussion sections of the manuscript. MSB carried out most of the experiments presented in the manuscript, analyzed most of the data, made the figures, and wrote the Materials and Methods section and part of the Results section. RH performed preliminary DE differentiation of human PSC spheroids without spheroid size control in NFC hydrogel and suspension culture (data not shown). EF carried out some of the experiments presented in the manuscript, measured spheroid diameters, and analyzed qPCR data. AT performed preliminary DE differentiation of human PSC spheroids without spheroid size control in NFC hydrogel and suspension culture (data not shown), performed computational simulation of activin A diffusion, and wrote the modeling part of the Methods section. MAB helped in some experiments and measured spheroid diameters. AL provided valuable advice during research planning, analyzed qPCR data, and edited the manuscript. All authors commented on the final version of the manuscript.

FUNDING

This work was supported by grants from the Academy of Finland (Nos. 294193 and 294194 to Y-RL), Finnish National Agency for Education (decision 10.10.2018/TM-18-10922 to Y-RL for MAB), and Faculty of Pharmacy, University of Helsinki to Y-RL and MY.

ACKNOWLEDGMENTS

Y-RL acknowledges Fudan University for providing research grant. MSB and Y-RL acknowledge the Doctoral Programme in Drug Research for providing MSB a Ph.D. student position at the Faculty of Pharmacy, University of Helsinki. XX acknowledges the National Natural Science Foundation of China (81473409) and Shanghai Science and Technology Innovation Fund (18140900900). We would like to thank the Light Microscopy Unit at the Institute of Biotechnology for providing confocal microscopy, Flow Cytometry Unit at the University of Helsinki for providing BD LSRFortessa Cell Analyzer, and Päivi Tammela for providing the NanoDrop spectrophotometer. The antibody MC-813-70 (SSEA-4) developed by Solter D/Knowles BB was obtained from the Developmental Studies Hybridoma Bank developed under the auspices of the NICHD and maintained by The University of Iowa, Department of Biology, Iowa City, IA, United States.

SUPPLEMENTARY MATERIAL

The Supplementary Material for this article can be found online at: https://www.frontiersin.org/articles/10.3389/fcell.2021.726499/full#supplementary-material

REFERENCES

Adams, R., and Essex, C. (2009). *Calculus: A Complete Course*. North York, ON: Pearson Education Canada.

Aleksandrova, A. V., Pulkova, N. P., Gerasimenko, T. N., Anisimov, N. Y., Tonevitskaya, S. A., and Sakharov, D. A. (2016). Mathematical and experimental model of oxygen diffusion for HepaRG cell spheroids. *Bull. Exp. Biol. Med.* 160, 857–860. doi: 10.1007/s10517-016-3326-1

Allison, T. F., Smith, A. J. H., Anastassiadis, K., Sloane-Stanley, J., Biga, V., Stavish, D., et al. (2018). Identification and single-cell functional characterization of an endodermally biased pluripotent substate in human embryonic stem cells. *Stem Cell Rep.* 10, 1895–1907. doi: 10.1016/j.stemcr.2018.04.015

Amit, M., Chebath, J., Margulets, V., Laevsky, I., Miropolsky, Y., Shariki, K., et al. (2010). Suspension culture of undifferentiated human embryonic and induced pluripotent stem cells. *Stem Cell Rev.* 6, 248–259.

Antoni, D., Burckel, H., Josset, E., and Noel, G. (2015). Three-dimensional cell culture: a breakthrough in vivo. *Int. J. Mol. Sci.* 16, 5517–5527. doi: 10.3390/ijms16035517

Berg, H. (1993). *Random Walks in Biology*. Princeton, NJ: Princeton University Press.

Bergmann, S., Lawler, S. E., Qu, Y., Fadzen, C. M., Wolfe, J. M., Regan, M. S., et al. (2018). Blood-brain-barrier organoids for investigating the permeability of CNS therapeutics. *Nat. Protoc.* 13, 2827–2843. doi: 10.1038/s41596-018-0066-x

Bhattacharya, M., Malinen, M. M., Lauren, P., Lou, Y. R., Kuisma, S. W., Kanninen, L., et al. (2012). Nanofibrillar cellulose hydrogel promotes three-dimensional liver cell culture. *J. Control. Release* 164, 291–298. doi: 10.1016/j.jconrel.2012.06.039

Bogacheva, M. S., Khan, S., Kanninen, L. K., Yliperttula, M., Leung, A. W., and Lou, Y. R. (2018). Differences in definitive endoderm induction approaches using growth factors and small molecules. *J. Cell. Physiol.* 233, 3578–3589. doi: 10.1002/jcp.26214

Broguiere, N., Isenmann, L., Hirt, C., Ringel, T., Placzek, S., Cavalli, E., et al. (2018). Growth of epithelial organoids in a defined hydrogel. *Adv. Mater.* 30:e1801621.

Candiello, J., Grandhi, T. S. P., Goh, S. K., Vaidya, V., Lemmon-Kishi, M., Eliato, K. R., et al. (2018). 3D heterogeneous islet organoid generation from human embryonic stem cells using a novel engineered hydrogel platform. *Biomaterials* 177, 27–39. doi: 10.1016/j.biomaterials.2018.05.031

Chayosumrit, M., Tuch, B., and Sidhu, K. (2010). Alginate microcapsule for propagation and directed differentiation of hESCs to definitive endoderm. *Biomaterials* 31, 505–514. doi: 10.1016/j.biomaterials.2009.09.071

Chen, G., Hou, Z., Gulbranson, D. R., and Thomson, J. A. (2010). Actin-myosin contractility is responsible for the reduced viability of dissociated human embryonic stem cells. *Cell Stem Cell* 7, 240–248. doi: 10.1016/j.stem.2010.06.017

Chua, C. W., Shibata, M., Lei, M., Toivanen, R., Barlow, L. J., Bergren, S. K., et al. (2014). Single luminal epithelial progenitors can generate prostate organoids in culture. *Nat. Cell Biol.* 16, 951–954. doi: 10.1038/ncb3047

D'Amour, K. A., Agulnick, A. D., Eliazer, S., Kelly, O. G., Kroon, E., and Baetge, E. E. (2005). Efficient differentiation of human embryonic stem cells to definitive endoderm. *Nat. Biotechnol.* 23, 1534–1541. doi: 10.1038/nbt1163

Dhamdhere, G. R., Fang, M. Y., Jiang, J., Lee, K., Cheng, D., Olveda, R. C., et al. (2014). Drugging a stem cell compartment using Wnt3a protein as a therapeutic. *PLoS One* 9:e83650. doi: 10.1371/journal.pone.0083650 doi: 10.1371/journal.pone.0083650

Dye, B. R., Hill, D. R., Ferguson, M. A., Tsai, Y. H., Nagy, M. S., Dyal, R., et al. (2015). In vitro generation of human pluripotent stem cell derived lung organoids. *Elife* 4:e05098.

Farzaneh, Z., Najarasl, M., Abbasalizadeh, S., Vosough, M., and Baharvand, H. (2018). Developing a cost-effective and scalable production of human hepatic competent endoderm from size-controlled pluripotent stem cell aggregates. *Stem Cells Dev.* 27, 262–274. doi: 10.1089/scd.2017.0074

Fatehullah, A., Tan, S. H., and Barker, N. (2016). Organoids as an in vitro model of human development and disease. *Nat. Cell Biol.* 18, 246–254. doi: 10.1038/ncb3312

Freyer, N., Knospel, F., Strahl, N., Amini, L., Schrade, P., Bachmann, S., et al. (2016). Hepatic differentiation of human induced pluripotent stem cells in a perfused three-dimensional multicompartment bioreactor. *Biores. Open Access* 5, 235–248. doi: 10.1089/biores.2016.0027

Gjorevski, N., Sachs, N., Manfrin, A., Giger, S., Bragina, M. E., Ordonez-Moran, P., et al. (2016). Designer matrices for intestinal stem cell and organoid culture. *Nature* 539, 560–564. doi: 10.1038/nature20168

Glicklis, R., Merchuk, J. C., and Cohen, S. (2004). Modeling mass transfer in hepatocyte spheroids via cell viability, spheroid size, and hepatocellular functions. *Biotechnol. Bioeng.* 86, 672–680. doi: 10.1002/bit.20086

Grimes, D. R., and Currell, F. J. (2018). Oxygen diffusion in ellipsoidal tumour spheroids. *J. R. Soc. Interface* 15:20180256. doi: 10.1098/rsif.2018.0256

Hanawa, M., Takayama, K., Sakurai, F., Tachibana, M., and Mizuguchi, H. (2017). Hepatocyte nuclear factor 4 alpha promotes definitive endoderm differentiation from human induced pluripotent stem cells. *Stem Cell Rev. Rep.* 13, 542–551. doi: 10.1007/s12015-016-9709-x

Harjumaki, R., Nugroho, R. W. N., Zhang, X., Lou, Y. R., Yliperttula, M., Valle-Delgado, J. J., et al. (2019). Quantified forces between HepG2 hepatocarcinoma and WA07 pluripotent stem cells with natural biomaterials correlate with in vitro cell behavior. *Sci. Rep.* 9:7354.

Hay, D. C., Fletcher, J., Payne, C., Terrace, J. D., Gallagher, R. C., Snoeys, J., et al. (2008). Highly efficient differentiation of hESCs to functional hepatic endoderm requires ActivinA and Wnt3a signaling. *Proc. Natl. Acad. Sci. U.S.A.* 105, 12301–12306. doi: 10.1073/pnas.0806522105

Hohwieler, M., Illing, A., Hermann, P. C., Mayer, T., Stockmann, M., Perkhofer, L., et al. (2017). Human pluripotent stem cell-derived acinar/ductal organoids generate human pancreas upon orthotopic transplantation and allow disease modelling. *Gut* 66, 473–486. doi: 10.1136/gutjnl-2016-312423

Hoveizi, E., Khodadadi, S., Tavakol, S., Karima, O., and Nasiri-Khalili, M. A. (2014). Small molecules differentiate definitive endoderm from human induced pluripotent stem cells on PCL scaffold. *Appl. Biochem. Biotechnol.* 173, 1727–1736. doi: 10.1007/s12010-014-0960-9

Iwashita, H., Shiraki, N., Sakano, D., Ikegami, T., Shiga, M., Kume, K., et al. (2013). Secreted cerberus1 as a marker for quantification of definitive endoderm differentiation of the pluripotent stem cells. *PLoS One* 8:e64291. doi: 10.1371/journal.pone.0064291

Johnson, K. E., Makanji, Y., Temple-Smith, P., Kelly, E. K., Barton, P. A., Al-Musawi, S. L., et al. (2016). Biological activity and in vivo half-life of pro-activin A in male rats. *Mol. Cell. Endocrinol.* 422, 84–92. doi: 10.1016/j.mce.2015.12.007

Kanninen, L. K., Harjumaki, R., Peltoniemi, P., Bogacheva, M. S., Salmi, T., Porola, P., et al. (2016a). Laminin-511 and laminin-521-based matrices for efficient hepatic specification of human pluripotent stem cells. *Biomaterials* 103, 86–100. doi: 10.1016/j.biomaterials.2016.06.054

Kanninen, L. K., Porola, P., Niklander, J., Malinen, M. M., Corlu, A., Guguen-Guillouzo, C., et al. (2016b). Hepatic differentiation of human pluripotent stem cells on human liver progenitor HepaRG-derived acellular matrix. *Exp. Cell Res.* 341, 207–217. doi: 10.1016/j.yexcr.2016.02.006

Kim, E. M., Lee, Y. B., Byun, H., Chang, H. K., Park, J., and Shin, H. (2019). Fabrication of spheroids with uniform size by self-assembly of a micro-scaled cell sheet (muCS): the effect of cell contraction on spheroid formation. *ACS Appl. Mater. Interfaces* 11, 2802–2813. doi: 10.1021/acsami.8b18048

Kim, Y., Kim, H., Ko, U. H., Oh, Y., Lim, A., Sohn, J. W., et al. (2016). Islet-like organoids derived from human pluripotent stem cells efficiently function in the glucose responsiveness in vitro and in vivo. *Sci. Rep.* 6:35145.

Korostylev, A., Mahaddalkar, P. U., Keminer, O., Hadian, K., Schorpp, K., Gribbon, P., et al. (2017). A high-content small molecule screen identifies novel inducers of definitive endoderm. *Mol. Metab.* 6, 640–650. doi: 10.1016/j.molmet.2017.04.009

Kumar, S. V., Er, P. X., Lawlor, K. T., Motazedian, A., Scurr, M., Ghobrial, I., et al. (2019). Kidney micro-organoids in suspension culture as a scalable source of human pluripotent stem cell-derived kidney cells. *Development* 146:dev172361.

Li, X., Ma, R., Gu, Q., Liang, L., Wang, L., Zhang, Y., et al. (2018). A fully defined static suspension culture system for large-scale human embryonic stem cell production. *Cell Death Dis.* 9:892.

Lin, B., Miao, Y., Wang, J., Fan, Z., Du, L., Su, Y., et al. (2016). Surface tension guided hanging-drop: producing controllable 3D spheroid of high-passaged human dermal papilla cells and forming inductive microtissues for hair-follicle regeneration. *ACS Appl. Mater. Interfaces* 8, 5906–5916. doi: 10.1021/acsami.6b00202

Lock, L. T., and Tzanakakis, E. S. (2009). Expansion and differentiation of human embryonic stem cells to endoderm progeny in a microcarrier stirred-suspension culture. *Tissue Eng. Part A* 15, 2051–2063. doi: 10.1089/ten.tea.2008.0455

Lou, Y. R., Kanninen, L., Kuisma, T., Niklander, J., Noon, L. A., Burks, D., et al. (2014). The use of nanofibrillar cellulose hydrogel as a flexible three-dimensional model to culture human pluripotent stem cells. *Stem Cells Dev.* 23, 380–392. doi: 10.1089/scd.2013.0314

Lou, Y. R., and Leung, A. W. (2018). Next generation organoids for biomedical research and applications. *Biotechnol. Adv.* 36, 132–149. doi: 10.1016/j.biotechadv.2017.10.005

Maldonado, M., Luu, R. J., Ramos, M. E., and Nam, J. (2016). ROCK inhibitor primes human induced pluripotent stem cells to selectively differentiate towards mesendodermal lineage via epithelial-mesenchymal transition-like modulation. *Stem Cell Res.* 17, 222–227. doi: 10.1016/j.scr.2016.07.009

Malinen, M. M., Kanninen, L. K., Corlu, A., Isoniemi, H. M., Lou, Y. R., Yliperttula, M. L., et al. (2014). Differentiation of liver progenitor cell line to functional organotypic cultures in 3D nanofibrillar cellulose and hyaluronan-gelatin hydrogels. *Biomaterials* 35, 5110–5121. doi: 10.1016/j.biomaterials.2014.03.020

McLean, A. B., D'Amour, K. A., Jones, K. L., Krishnamoorthy, M., Kulik, M. J., Reynolds, D. M., et al. (2007). Activin a efficiently specifies definitive endoderm from human embryonic stem cells only when phosphatidylinositol 3-kinase signaling is suppressed. *Stem Cells* 25, 29–38. doi: 10.1634/stemcells.2006-0219

Miki, T., Ring, A., and Gerlach, J. (2011). Hepatic differentiation of human embryonic stem cells is promoted by three-dimensional dynamic perfusion culture conditions. *Tissue Eng. Part C Methods* 17, 557–568. doi: 10.1089/ten.tec.2010.0437

Nelson, P. (2013). *Biological Physics*. New York, NY: W. H. Freeman.

Nie, Y., Xu, X., Wang, W., Ma, N., and Lendlein, A. (2020). Spheroid formation of human keratinocyte: balancing between cell-substrate and cell-cell interaction. *Clin. Hemorheol. Microcirc.* 76, 329–340. doi: 10.3233/ch-209217

Nowak, M., Freudenberg, U., Tsurkan, M. V., Werner, C., and Levental, K. R. (2017). Modular GAG-matrices to promote mammary epithelial morphogenesis in vitro. *Biomaterials* 112, 20–30. doi: 10.1016/j.biomaterials.2016.10.007

Pfaffl, M. W. (2001). A new mathematical model for relative quantification in real-time RT-PCR. *Nucleic Acids Res.* 29:e45.

Rahman, M., and Sadygov, R. G. (2017). Predicting the protein half-life in tissue from its cellular properties. *PLoS One* 12:e0180428. doi: 10.1371/journal.pone.0180428

Sahabian, A., Sgodda, M., Naujok, O., Dettmer, R., Dahlmann, J., Manstein, F., et al. (2019). Chemically-defined, xeno-free, scalable production of hPSC-derived definitive endoderm aggregates with multi-lineage differentiation potential. *Cells* 8:1571. doi: 10.3390/cells8121571

Schuldiner, M., Yanuka, O., Itskovitz-Eldor, J., Melton, D. A., and Benvenisty, N. (2000). Effects of eight growth factors on the differentiation of cells derived from human embryonic stem cells. *Proc. Natl. Acad. Sci. U.S.A.* 97, 11307–11312. doi: 10.1073/pnas.97.21.11307

Spence, J. R., Mayhew, C. N., Rankin, S. A., Kuhar, M. F., Vallance, J. E., Tolle, K., et al. (2011). Directed differentiation of human pluripotent stem cells into intestinal tissue in vitro. *Nature* 470, 105–109.

Tasnim, F., Phan, D., Toh, Y. C., and Yu, H. (2015). Cost-effective differentiation of hepatocyte-like cells from human pluripotent stem cells using small molecules. *Biomaterials* 70, 115–125. doi: 10.1016/j.biomaterials.2015.08.002

Teo, A. K., Ali, Y., Wong, K. Y., Chipperfield, H., Sadasivam, A., Poobalan, Y., et al. (2012). Activin and BMP4 synergistically promote formation of definitive endoderm in human embryonic stem cells. *Stem Cells* 30, 631–642. doi: 10.1002/stem.1022

Teo, A. K., Arnold, S. J., Trotter, M. W., Brown, S., Ang, L. T., Chng, Z., et al. (2011). Pluripotency factors regulate definitive endoderm specification through eomesodermin. *Genes Dev.* 25, 238–250. doi: 10.1101/gad.607311

Wang, H., Luo, X., Yao, L., Lehman, D. M., and Wang, P. (2015). Improvement of cell survival during human pluripotent stem cell definitive endoderm differentiation. *Stem Cells Dev.* 24, 2536–2546. doi: 10.1089/scd.2015.0018

Wang, X., and Ye, K. (2009). Three-dimensional differentiation of embryonic stem cells into islet-like insulin-producing clusters. *Tissue Eng. Part A* 15, 1941–1952. doi: 10.1089/ten.tea.2008.0181

Wang, Z., Oron, E., Nelson, B., Razis, S., and Ivanova, N. (2012). Distinct lineage specification roles for NANOG, OCT4, and SOX2 in human embryonic stem cells. *Cell Stem Cell* 10, 440–454. doi: 10.1016/j.stem.2012.02.016

Watanabe, K., Ueno, M., Kamiya, D., Nishiyama, A., Matsumura, M., Wataya, T., et al. (2007). A ROCK inhibitor permits survival of dissociated human embryonic stem cells. *Nat. Biotechnol.* 25, 681–686. doi: 10.1038/nbt1310

Wimmer, R. A., Leopoldi, A., Aichinger, M., Wick, N., Hantusch, B., Novatchkova, M., et al. (2019). Human blood vessel organoids as a model of diabetic vasculopathy. *Nature* 565, 505–510. doi: 10.1038/s41586-018-0858-8

Xu, C., Inokuma, M. S., Denham, J., Golds, K., Kundu, P., Gold, J. D., et al. (2001). Feeder-free growth of undifferentiated human embryonic stem cells. *Nat. Biotechnol.* 19, 971–974. doi: 10.1038/nbt1001-971

Yabe, S. G., Nishida, J., Fukuda, S., Takeda, F., Nashiro, K., Ibuki, M., et al. (2019). Definitive endoderm differentiation is promoted in suspension cultured human iPS-derived spheroids more than in adherent cells. *Int. J. Dev. Biol.* 63, 271–280. doi: 10.1387/ijdb.180251sy

Yu, J., Vodyanik, M. A., Smuga-Otto, K., Antosiewicz-Bourget, J., Frane, J. L., Tian, S., et al. (2007). Induced pluripotent stem cell lines derived from human somatic cells. *Science* 318, 1917–1920.

Zorn, A. M., and Wells, J. M. (2009). Vertebrate endoderm development and organ formation. *Annu. Rev. Cell Dev. Biol.* 25, 221–251. doi: 10.1146/annurev.cellbio.042308.113344

Conflict of Interest: The authors declare that the research was conducted in the absence of any commercial or financial relationships that could be construed as a potential conflict of interest.

Publisher's Note: All claims expressed in this article are solely those of the authors and do not necessarily represent those of their affiliated organizations, or those of the publisher, the editors and the reviewers. Any product that may be evaluated in this article, or claim that may be made by its manufacturer, is not guaranteed or endorsed by the publisher.

frontiers in Cell and Developmental Biology

ORIGINAL RESEARCH
published: 28 September 2021
doi: 10.3389/fcell.2021.737242

Human Amniotic Epithelial Stem Cell-Derived Retinal Pigment Epithelium Cells Repair Retinal Degeneration

Jinying Li[1,2], Chen Qiu[1,2], Yang Wei[3], Weixin Yuan[1], Jia Liu[1,2], Wenyu Cui[1,2], Jiayi Zhou[1,2], Cong Qiu[1,2], Lihe Guo[4], Liquan Huang[2], Zhen Ge[3] and Luyang Yu[1,2]**

[1] Key Laboratory of Cardiovascular Intervention and Regenerative Medicine of Zhejiang Province of Sir Run Run Shaw Hospital, MOE Laboratory of Biosystems Homeostasis & Protection of College of Life Sciences, Zhejiang University, Hangzhou, China, [2] College of Life Sciences-iCell Biotechnology Regenerative Biomedicine Laboratory, Joint Research Centre for Engineering Biology, Zhejiang University-University of Edinburgh Institute, Zhejiang University, Haining, China, [3] School of Pharmaceutical Sciences, Hangzhou Medical College, Hangzhou, China, [4] Institute of Biochemistry and Cell Biology, Shanghai Institutes for Biological Sciences, Chinese Academy of Sciences (CAS), Shanghai, China

OPEN ACCESS

Edited by:
Wencheng Zhang,
Tongji University, China

Reviewed by:
Furong Gao,
Tongji University, China
Gianpaolo Papaccio,
Second University of Naples, Italy

***Correspondence:**
Zhen Ge
2020000291@hmc.edu.cn
Luyang Yu
luyangyu@zju.edu.cn

Specialty section:
This article was submitted to Stem Cell Research, a section of the journal Frontiers in Cell and Developmental Biology

Received: 06 July 2021
Accepted: 06 September 2021
Published: 28 September 2021

Citation:
Li J, Qiu C, Wei Y, Yuan W, Liu J, Cui W, Zhou J, Qiu C, Guo L, Huang L, Ge Z and Yu L (2021) Human Amniotic Epithelial Stem Cell-Derived Retinal Pigment Epithelium Cells Repair Retinal Degeneration. Front. Cell Dev. Biol. 9:737242. doi: 10.3389/fcell.2021.737242

Age-related macular degeneration (AMD), featured with dysfunction and loss of retinal pigment epithelium (RPE), is lacking efficient therapeutic approaches. According to our previous studies, human amniotic epithelial stem cells (hAESCs) may serve as a potential seed cell source of RPE cells for therapy because they have no ethical concerns, no tumorigenicity, and little immunogenicity. Herein, trichostatin A and nicotinamide can direct hAESCs differentiation into RPE like cells. The differentiated cells display the morphology, marker expression and cellular function of the native RPE cells, and noticeably express little MHC class II antigens and high level of HLA-G. Moreover, visual function and retinal structure of Royal College of Surgeon (RCS) rats, a classical animal model of retinal degeneration, were rescued after subretinal transplantation with the hAESCs-derived RPE like cells. Our study possibly makes some contribution to the resource of functional RPE cells for cell therapy. Subretinal transplantation of hAESCs-RPE could be an optional therapeutic strategy for retinal degeneration diseases.

Keywords: immune privilege, retinal pigment epithelium, retinal degeneration, human amniotic epithelial stem cells, cell therapy

INTRODUCTION

Age-related macular degeneration (AMD), the typical retinal degeneration disease, is the major cause of irreversible vision loss among senior citizens. The projected number of people with AMD globally is approximately 200 million in 2020, and it is expected to increase to nearly 300 million in 2040 (Wong et al., 2014). Especially, it has been estimated that by 2050, 55.19 million people will be affected by AMD in China (Song et al., 2017). In AMD, the early events of retinal pigment epithelium (RPE) dysfunction usually lead to photoreceptor degeneration, resulting in progressive visual loss and blindness (Luthert, 2011). Patients with wet AMD lose vision because of the growth of abnormal blood vessels (choroidal neovascularization, CNV), while patients with dry AMD, which represents approximately 90% of AMD cases, suffer vision loss as a result of geographic atrophy (GA) of the PRs, RPE, and choriocapillaris in the macular area (Ambati and Fowler, 2012).

Currently, antiangiogenic medicine has been well established for CNV. However, there are no effective treatments available for GA (Mitchell et al., 2018). With the development of stem cell technology, cell therapy is a promising therapeutic strategy for retinal degenerative diseases (Ramsden et al., 2013; Trounson and McDonald, 2015; Zarbin, 2016).

Recently, several sources of human pluripotent stem cells (hPSCs) have been tested for their ability to replace damaged or lost RPE cells with seed cells. Human embryonic stem cells (hESCs)- and human induced pluripotent stem cells (hiPSCs)-derived RPE cells have been reported to rescue visual function after subretinal transplantation into animal models, such as Royal College of Surgeon (RCS) rats (Idelson et al., 2009; Hazim et al., 2017; Sharma et al., 2019). Clinical trials that used hESCs- and hiPSCs-derived RPE demonstrated some preliminary, encouraging results (Schwartz et al., 2012, 2015). Both hESCs and hiPSCs possess considerable potential for clinical trials in the treatment of retinal degeneration diseases. However, they are currently limited by their immunogenicity and long-term safety, with chronic immune reaction, macular edema and even DNA aberrations (Mandai et al., 2017; da Cruz et al., 2018; Mehat et al., 2018).

Human amniotic epithelial stem cells (hAESCs), sharing the developmental origin of the pluripotent inner cell mass of blastocysts with hESCs, might be a more useful seed cell source for the replacement of RPE, according to our and other's previous studies (Li et al., 2018; Miki, 2018; Tan et al., 2018; Yang et al., 2018). First, hAESCs can be isolated from discarded placental tissue without the ethical concerns normally associated with hESCs (Parolini et al., 2008). Second, hAESCs express stem cell surface markers, such as embryonic antigen-3 and -4 (SSEA-3, SSEA-4), tumor rejection antigen 1-60 (TRA1-60), TRA1-81 and molecular markers of pluripotent stem cells, including octamer-binding protein 4 (OCT-4), SRY-related HMG-box gene 2 (SOX-2) and NANOG. Therefore, hAESCs possess the ability to differentiate into all three germ layers, including neurons (ectoderm), cardiomyocytes (mesoderm), and hepatocytes (endoderm), as previously reported (Miki et al., 2005; Miki and Strom, 2006). Additionally, the low immunogenicity of hAESCs is enabled by their high expression of human leukocyte antigen G (HLA-G), a non-classic major histocompatibility complex (MHC) class I molecule, and low expression of MHC class II molecules HLA-DR and HLA-DQ (Strom and Gramignoli, 2016). Finally, hAESCs show no tumorigenicity upon transplantation into both volunteers and patients, which is the key obstacle for the safe clinical use of cell-based regenerative therapies (Akle et al., 1981). This unique property may be due to the lack of telomerase; and the global DNA methylation status of hAESCs is intermediated between hESCs and somatic cells, suggesting that they are genetically stable, in contrast to hESCs (Miki, 2018). These unique characteristics of hAESCs, including pluripotency, low immunogenicity and non-tumorigenicity, make them attractive for the clinical application of retinal diseases.

Here, we report for the first time the direct differentiation of hAESCs into functional RPE like cells, which could rescue retinal function after subretinal transplantation into an animal model of retinal degeneration. The current study might provide a novel cost-efficient and safe therapeutic strategy for the treatment of retinal degeneration diseases.

MATERIALS AND METHODS

Separation of Human Amniotic Epithelial Stem Cells

Human placentas were obtained from healthy mothers who provided written informed consent after undergoing an uncomplicated elective cesarean section as described in our previous methods (Yang et al., 2018). The procedure was approved by the Institutional Patients and Ethics Committee of the International Peace Maternity and Child Health Hospital, Shanghai Jiao Tong University School of Medicine. All donors were negative for hepatitis A, B, C, and D as well as HIV-I and Treponema pallidum (TPAB) antibodies. Briefly, amniotic membranes were isolated and washed with fresh PBS, which was followed by incubation with 0.25% trypsin for 20 min at 37°C in a water bath. Then, hAESCs were centrifuged for 10 min at 300 × *g* and counted. hAESCs were cultured in complete culture medium F12/DMEM containing 10% KnockOut Serum Replacement (KSR), 2 mM L-glutamine, 1% non-essential amino acid, 55 μM 2-mercaptoethanol, 1 mM sodium pyruvate, 1% antibiotic-antimycotic (all from Thermo Scientific, Waltham, MA, United States) and 10 ng mL^{-1} human EGF (Peprotech, Rocky Hill, NJ, United States, Cat# AF-100-15) in a humidified atmosphere of 5.5% CO_2 at 37°C for three to five days. When cells reached 80% – 90% confluence, they were harvested by incubation with 0.25% trypsin at 37°C for approximately 5 min.

Differentiation of Retinal Pigment Epithelium Like Cells From Human Amniotic Epithelial Stem Cells

In our study, P0-P1 hAESCs were chosen for investigation. For identification RPE inducer, hAESCs were seeded in 24-well plates and cultured for 7 days with four different concentrations (0.5 μM, 1 μM, 2 μM, and 4 μM) of trichostatin A (TSA). Then, the expression levels of three RPE markers, microphthalmia-associated transcription factor (MITF), orthodenticle homeobox 2 (OTX2), and premelanosome protein (PMEL17), were measured by q-PCR. The transcription factors MITF and OTX2 are early RPE markers, while PMEL17 is a matrix protein present in the melanosome precursors of pigmenting cells. For RPE cell differentiation, hAESCs were seeded in 6-well plates and cultured in DMEM/F12, 15% KnockOut serum, 2 mM glutamine, 1 × non-essential amino acids, and 1 × antibiotic-antimycotic. And When cells reached 80% – 90% confluence, 10 mM NIC (Sigma-Aldrich, Cat# N3376) and 1 μM TSA (APExBIO, Cat# A8183) were added for approximately two weeks, while the medium was changed every day.

Quantitative Real-Time PCR

Total RNA was extracted from undifferentiated, differentiating hAESCs with an E.N.Z.A. total RNA kit (Omega) according

to the manufacturer's instructions. Reverse transcription was performed using a ReverTra Ace qPCR RT kit (Toyobo). Quantitative real-time PCR was performed with the BioRad iCycler real-time PCR detection system (Bio-Rad) with the primers listed in **Supplementary Table 1**. PCRs were performed under the following conditions: 95°C for 10 min followed by 40 cycles at 95°C for 10 s, 60°C for 20 s, and 72°C for 15 s. To normalize expression levels, glyceraldehyde 3-phosphate dehydrogenase (GAPDH) was used as an internal control. Quantitative PCR analysis was performed on three biological replicates.

Immunostaining

After fixation with 4% paraformaldehyde in PBS for 15 min, cells were permeabilized using 0.25% Triton X-100 in PBS for 5–10 min and were blocked for 60 min in 5% goat serum. Then, the cells were incubated for 60 min at room temperature with the following primary antibodies: anti-MITF antibody (Sangon, Cat# D120988, 1:100), anti-ZO-1 antibody (Thermo Fisher Scientific Cat# 40-2200, RRID:AB_2533456, 1:200), anti-Bestrophin antibody (Novus Cat# NB300-164, RRID:AB_10003019, 1:100), anti-RPE65 antibody (Abcam, Cat# ab78036, RRID:AB_1566691, 1:100), anti-PMEL-17 antibody (Abcam, Cat# ab137078, RRID:AB_2732921, 1:100), Cells were then incubated for 120 min at room temperature with the corresponding secondary antibodies: Alexa Fluor 594-conjugated donkey anti-rabbit IgG (Jackson ImmunoResearch, Cat# 711-586-152, RRID:AB_2340622), Alexa Fluor 594-conjugated donkey anti-mouse IgG (Jackson ImmunoResearch, Cat# 715-586-150, RRID:AB_2340857), Alexa Fluor 488-conjugated donkey anti-rabbit IgG (Jackson ImmunoResearch, Cat# 711-546-152, RRID:AB_2340619) and Alexa Fluor 488-conjugated donkey anti-mouse IgG (Jackson ImmunoResearch, Cat# 715-545-150, RRID:AB_2340846). Fluorescence images were acquired with a confocal microscope (Zeiss LSM 800, Carl Zeiss).

Transmission Electron Microscopy

Cells were fixed with 2.5% glutaraldehyde in 0.1 M cacodylate buffer (pH 7.4) overnight. After washed twice with 0.1 M PBS, cells were fixed with 1% osmium tetroxide for 1 h and then were washed twice with ddH_2O. Samples were stained with 2% uranyl acetate for 30 min, dehydrated with increasing concentrations of ethanol, and embedded in Agar 100 resin. Ultrathin sections were cut using a diamond knife (Diatome, United States), and sections were stained with 2% uranyl acetate and 2% lead citrate. Micrographs were taken with a JEM-1400 Plus (JEOL) electron microscope.

Digital Gene Expression Profile

Total RNA was extracted from hfRPE-1, hfRPE-2, and hfRPE-3 cells using TRIzol (Invitrogen) and was provided as a kind gift from Army Medical University (Chongqing, China); and RNA was similarly extracted from hAESCs-RPE-1, hAESCs-RPE-2, and hAESCs-RPE-3 cells. Sequencing libraries were generated using a NEBNext® Ultra™ RNA Library Prep kit for Illumina® (NEB) following the manufacturer's recommendations, and the quality of libraries was assessed on an Agilent 2100 Bioanalyzer system and ABI StepOnePlus Real-Time PCR System. After cluster generation, the library preparations were sequenced on an Illumina HiSeqTM 4000 platform, and 150 bp single-end reads were generated. Reads per kb per million reads (RPKM) were used to estimate gene expression levels.

Flow Cytometry

To analyze the expression levels of MHC class II antigens (HLA-DR, BioLegend, Cat# 307603, RRID:AB_314681 and HLA-DQ, BioLegend, Cat#318104, RRID:AB_604128) and HLA-G (BioLegend, Cat# 335909, RRID:AB_10900805), ARPE19 cells (ATCC, RRID:CVCL_0145), human umbilical cord mesenchymal stem cells (hUMSCs, Cat# SHTBA0009C1BAC23 obtained from iCell Biological Technology Co., Ltd), hAESCs, hAESCs-RPE like cells were collected after incubation with 10 ng mL^{-1} IFN-γ (Peprotech, Cat# 300-02-100) for 72 h. Cells were stained with FITC-anti-HLA-DR (isotype control was IgG2a, BioLegend, Cat# 400207, RRID:AB_2884007), FITC-anti-HLA-DQ (isotype control was IgG1, BioLegend, Cat# 400109, RRID:AB_2861401) and APC-anti-HLA-G (isotype control was IgG2a, BioLegend, Cat# 400220, RRID:AB_326468) according to the manufacturer's instructions, and then they were analyzed by flow cytometry (FACSCalibur; BD Biosciences, Franklin Lakes, NJ). Analyses were performed on five biological replicates.

Phagocytosis of Photoreceptor Outer Segment

Photoreceptor outer segments (POSs) phagocytosis were performed as described in a previous study (Subrizi et al., 2012). Briefly, the POSs of non-dystrophic RCS rats at 8 weeks of age were detached under dim red light. To assess the specificity of POS phagocytosis, hAESCs-RPE like cells were incubated with POS explants for 6–8 h at 37°C and 5% CO_2. The internalization of rat POSs by RPE cells was immunostained using an anti-Rhodopsin antibody (Abcam, Cat# ab5417, RRID:AB_304874, 1:200), while ZO-1 (Thermo Fisher Scientific Cat# 40-2200, RRID:AB_2533456, 1:200) was detected to demonstrate the cell morphology. In the Z-stack model, we used a Zeiss LSM 800 confocal microscope to show the location of internalized POS. Five independent experiments were conducted.

Enzyme-Linked Immunosorbent Assay

hAESCs and hUMSCs (2×10^6) were seeded onto 10 cm dish and were cultured for 72 h. Then the culture medium were collected and telomerase concentration was detected by enzyme-linked immunosorbent assay (ELISA) kit (R&D Systems). hAESCs-RPE like cells were plated at 250,000 cells per cm^2 and were grown on Transwell membranes (Corning). Cell culture media from the apical and basal sides were collected after 48 h of cell culture. Measurements were performed using five biological replicates. A standard ELISA protocol was followed using vascular endothelial growth factor (VEGF) and pigment epithelium-derived factor (PEDF) ELISA kits (R&D Systems).

Animals

Royal College of Surgeon (RCS) rats (RRID:RGD_1358258, 3 week old at the time of testing, regardless of sex),a known model of retinal disease, were obtained from the Experimental

Animal Center of Army Medical University (Chongqing, China), and they were housed under pathogen-free conditions with a 12 h day-night cycle (lights on at 08:00AM). The animals had access to food and water *ad libitum*, except during test phases. This animal model was chosen because the primary dysfunction of the RPE, a result of a mutation in the receptor tyrosine kinase gene Mertk, leads to secondary degeneration and loss of photoreceptors, which is similar to the progression of human retinal degeneration diseases (D'Cruz et al., 2000). Animals were randomly assigned to the experimental groups. Data collection and evaluation of all experiments were performed blindly. All procedures involving rats were approved by the Laboratory Animal Care and the Use Committee of Zhejiang University (approval number, ZJU20190038). All efforts were made to minimize animal suffering and to reduce the number of animals.

Transplantation of Human Amniotic Epithelial Stem Cells-Retinal Pigment Epithelium Like Cells in Royal College of Surgeon Rats

After 14 days differentiation, hAESCs-RPE like cells were transplanted into 3-week-old RCS rats. In some experiments, hAESCs-RPE like cells were infected with GFP adenovirus for the convenience of detection. Rats were anesthetized by intraperitoneal injection with a mixture of ketamine (Sigma-Aldrich, 70 mg kg^{-1}) and xylazine (Sigma-Aldrich, 6 mg kg^{-1}). Local anesthetic drops (benoxinate HCl 0.4%; Fischer Pharmaceuticals, Israel) were administered. To reduce the efflux of cells, the cornea was punctured with a 30-gauge sterile needle (BD). Cell suspensions (1.5×10^5 cells in 2 μL of PBS) were injected into the subretinal space through a small scleral incision with a glass pipette (34-gauge, Hamilton). A sham group was injected with medium alone.

Electroretinograms

Full-field ERGs were recorded after overnight (> 12 h) dark adaptation as in previously reported (Huo et al., 2012). In brief, rats were anesthetized in dim red light, and the pupils were dilated with compound tropicamide eye drops. The corneal electrodes were placed on each eye after ophthalmic topical anesthesia, with a subdermal reference electrode and a ground electrode placed in the cheek and tail, respectively. A computerized ERG system (Q450, ROLAND CONSMLT, Germany) was used to record retinal responses to full-field stimuli. Dim white flashes (−40, −25, −10, 0 and + 5 db) under scotopic conditions were used to elicit mixed cone-rod responses (a largely rod-driven response), and signal averaging was used.

Histological and Immunohistochemical Evaluation of Transplanted Eyes

The eyeballs were fixed in 4% formaldehyde for 24 h, dehydrated with 70% alcohol, embedded in paraffin and serially cut to produce 3 μm-thick sections. Slides were stained with hematoxylin and eosin (H&E) according to a standard protocol. For immunostaining, eyecups were directly frozen in OCT (Tissue-Tek) and were cut to generate 3 μm-thick sections. Sections were fixed in acetone for 10 min at −20°C and then were washed with PBS, which was followed by incubation with blocking buffer (1% BSA and 5% HBS in PBS) for one h at room temperature. After blocking, sections were incubated for 1 h in a humidified chamber with the following primary antibodies: anti-CRALBP (Abcam, Cat# ab15051, RRID:AB_2269474, 1:100), anti-RPE65 (Abcam, Cat# ab78036, RRID:AB_1566691, 1:100), Then, the sections were incubated for 14 h with secondary antibodies. Nuclei were counterstained with DAPI (DAKO). Fluorescence images were acquired with a confocal microscope (Zeiss LSM 800, Carl Zeiss).

Quantification of Retinal Thickness

The full length of the retina was scanned from high-resolution microscopic images of H&E-stained sections with NDP.view2 software. Total retinal and ONL thicknesses were measured in proximity to subretinal injection site and corresponding opposite side of the retina via the ImageJ (NIH). In each area, 3 equally spaced measurements were taken.

Statistical Analysis

Studies were designed to generate groups of almost equal size by using randomization and blinded analysis. The statistical analysis was undertaken only for studies where each group size was at least $n = 3$. All experimental animals were treated with independent values without technical replicates. Statistical analysis was performed using GraphPad Prism 6 (GraphPad, RRID:SCR_002798). Data are presented as the mean ± SEM. Comparisons were performed using unpaired *t* tests, one-way ANOVA or two-way ANOVA followed by Tukey's multiple comparisons test. *Post hoc* tests were conducted only if *F* in ANOVA achieved $p < 0.05$. The significance level for all tests was set at $^*p < 0.05$.

RESULTS

The Characterization of Human Amniotic Epithelial Stem Cells

According to our previous studies (Li et al., 2018; Tan et al., 2018), we first confirmed the purity, pluripotency and non-tumorigenicity of isolated hAESCs, and we cultured them in a serum-free system for further study. The cultured hAESCs showed the typical appearance of epithelial cells and high expression of representative epithelial marker pan-cytokeratin (**Figures 1A,B**). Meanwhile, negative expression of the hematopoietic lineage markers CD45, CD34 and endothelial marker CD31 were detected by flow cytometry, indicating the purity of hAESCs without contamination (**Figures 1C–E**). As reported, hAESCs were partly positive for the mesenchymal stem cells (MSCs) markers CD73, CD90 and CD105 (**Figures 1F–H**). The expression of pluripotent markers NANOG and SSEA4 proved the plasticity of hAESCs as seed cells (**Figures 1I–K**). Moreover, no tumor formation was observed in Balb/c nude mice with subcutaneous injection of hAESCs for 55 days, compared with obvious tumor formation in positive control mice receiving non-small lung cancer A549 cells (**Figure 1L**). The low expression of telomerase compared with MSCs may explain the non-tumorigenicity (**Figure 1M**). In summary, these results

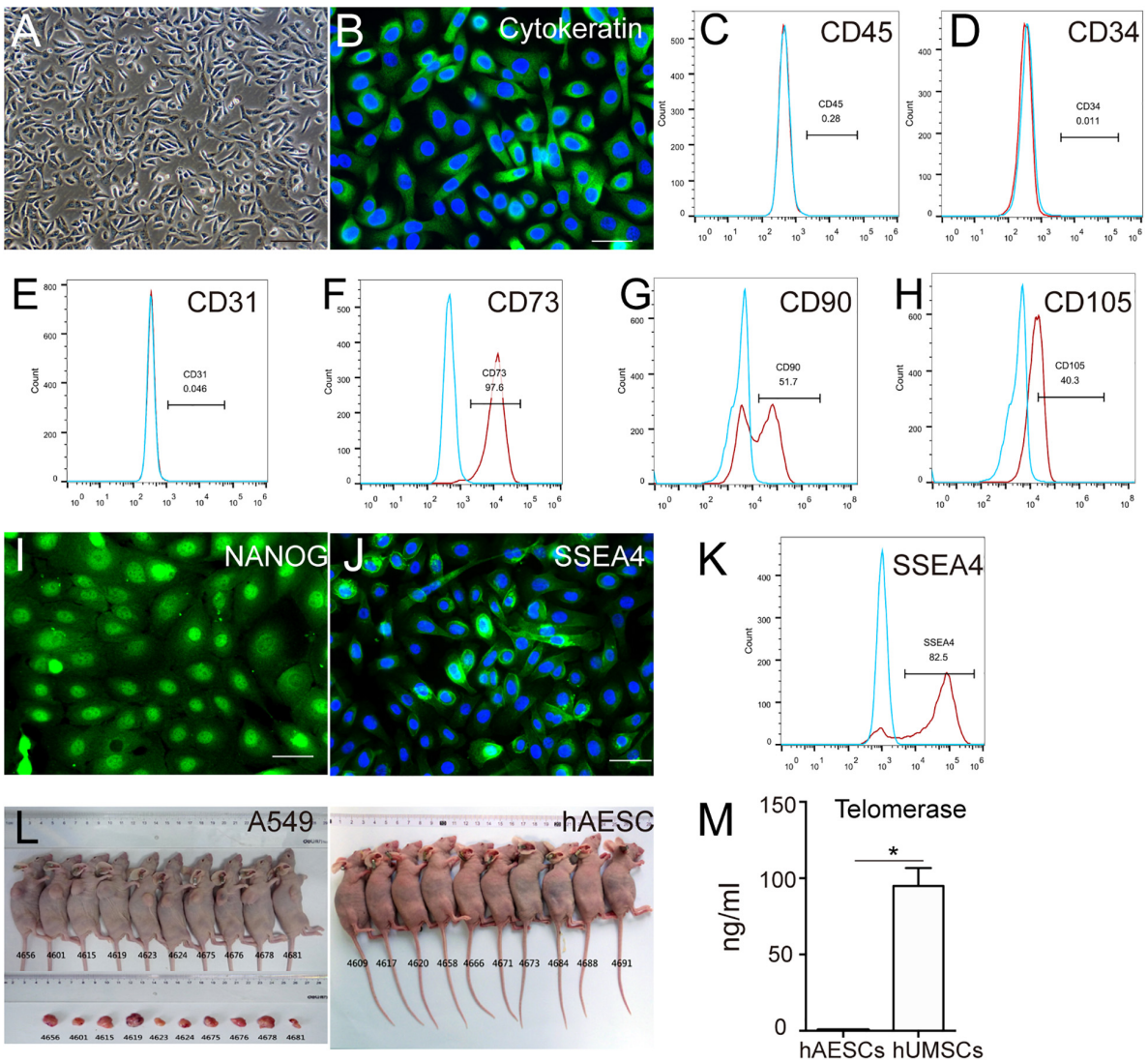

FIGURE 1 | Characteristics of hAESCs. **(A)** Phase-contrast microscope image showed the isolated hAESCs as a homogeneous population with cobblestone appearance. **(B–E)** Nearly all cells demonstrated persistent expression of representative epithelial marker cytokeratin as determined by immunofluorescence microscopy and negative for hematopoietic lineage marker CD45 and CD34, endothelial cells markers CD31 as determined by flow cytometry. **(F–H)** MSC markers CD73, CD90, CD105 were detected by flow cytometry. **(I–K)** Strong expression of pluripotency markers NANOG and SSEA4 were determined by immunofluorescence microscopy and flow cytometry. **(L)** No tumor formation was observed in Balb/c nude mice with subcutaneous injection of hAESCs for 55 days, compared with obvious tumor formation in positive control mice receiving non-small lung cancer A549 cells. **(M)** ELISA analysis showed the low expression of telomerase compared with mesenchymal stem cells (MSCs). Score bars, 100 μm in **(A)**, 50 μm in **(B)** and **(I–J)**, error bars represent mean ± SEM of three biological replicates ($n = 3$), $^*p < 0.05$, unpaired t-test.

indicate that hAESCs are a novel type of epithelial stem cells without tumorigenicity.

Trichostatin A Plus Nicotinamide Were Determined as Appropriate Chemical Cocktail for Human Amniotic Epithelial Stem Cells Differentiation Toward Retinal Pigment Epithelium Fate

To determine the scheme for RPE differentiation, hAESCs were cultured for 7 days with four different concentrations of compounds. One compound, trichostatin A (TSA), was identified as an inducer of RPE differentiation from hAESCs, according to the expression levels of three RPE markers, microphthalmia-associated transcription factor (MITF), orthodenticle homeobox 2 (OTX2), and premelanosome protein (PMEL17) as described in the Methods and Materials. Upon the administration of TSA, all three RPE markers in treated hAESCs were upregulated consistently in a dose-dependent pattern. The expression levels of MITF and OTX2 were upregulated in the presence of TSA alone, while the expression of PMEL17 was even strikingly upregulated (**Figure 2A**). Meanwhile, high concentrations of TSA

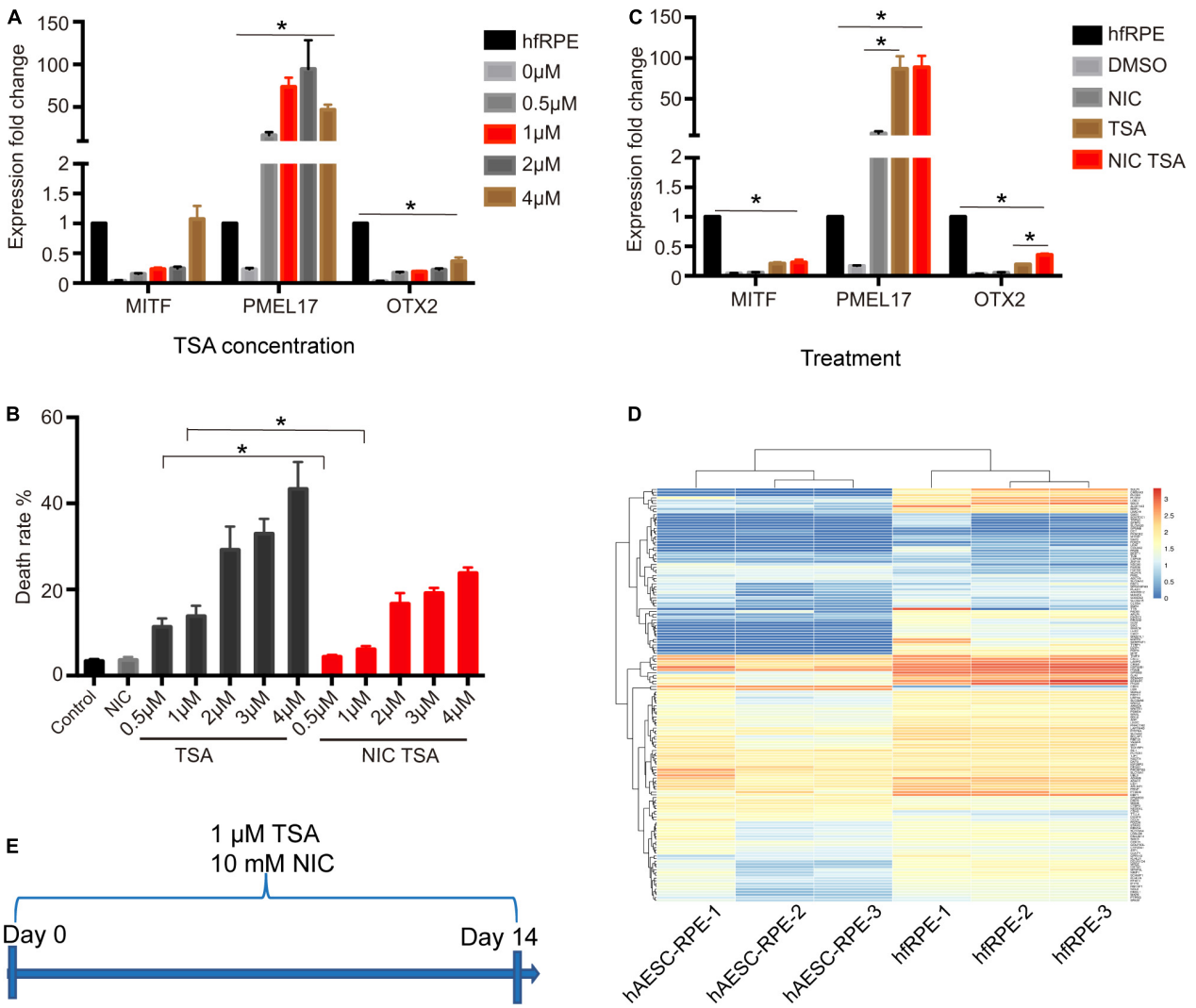

FIGURE 2 | Identification of TSA as a potent promoter of RPE differentiation. **(A)** RPE markers expression in hAESCs at day 7 following TSA treatment, as measured by quantitative PCR. Expression levels of TSA treated hAESCs were normalized by expression levels of hfRPE. **(B)** The cell death rates of hAESCs in the presence of NIC with different concentrations of TSA at day 7 following treatment. **(C)** RPE markers expression in hAESCs at day 7 following 10 mM NIC and 1 μM TSA treatment alone or combined, as measured by quantitative PCR. Expression levels of treated hAESCs were normalized by expression levels of hfRPE. **(D)** Heat map of 149 RPE signature genes in hAESCs-RPE and native human fetal RPE (hfRPE). Normalized expression levels are shown in a blue-white-red gradient. **(E)** Schematic of hAESCs differentiation into hAESCs-RPE using a chemical cocktail of NIC and TSA. Error bars represent mean ± SEM of three biological replicates ($n = 3$). MITF, microphthalmia-associated transcription factor; PMEL17, premelanosome protein; OTX2, orthodenticle homeobox 2; *$p < 0.05$, compared with control group; unpaired *t*-test, one-way ANOVA followed by Tukey's multiple comparisons test.

caused obvious cell death. Considering the induction efficiency and cell death rates, 1 μM was determined as the optimum concentration of TSA for RPE differentiation. Given the role of nicotinamide (NIC) in protecting hPSCs from cell death during neuroectoderm differentiation and the positive effect on RPE differentiation (Idelson et al., 2009; Maruotti et al., 2015), we tested the effect of NIC on the differentiation of hAESCs. As expected, NIC could prevent excessive cell death and augment the expression of OTX2 during TSA-directed RPE differentiation (**Figures 2B,C**). Altogether, these data suggest that during NIC and TSA differentiation, RPE markers are strongly up-regulated without excessive cell death.

To determine the optimal time period of the combined treatment, the expression of key markers during RPE differentiation was further assessed in the presence of NIC and TSA at sequential time points. Most RPE markers were upregulated, while dopachrome tautomerase (DCT) was downregulated after 2 weeks of differentiation (**Supplementary Figures 2A–E**). To comprehensively investigate hAESCs differentiation, their transcriptomes were examined after 2 weeks of induction. According to previous reports (Strunnikova et al., 2010), the levels of 149 representative genes during RPE differentiation were analyzed in differentiated hAESCs, and they were compared with native human fetal RPE (hfRPE)

cells. A heat map of normalized expression levels of each group showed a similar expression pattern between hAESCs-RPE cells and hfRPE cells (**Figure 2D**). To investigate the efficiency of the differentiation of hAESCs into RPE, RPE related markers were detected by flow cytometry. Results showed that more than 90% differentiated cells were positive for MITF, PMEL17, Bestrophin and RPE65 (**Supplementary Figures 3A–D**). In summary, the optimal scheme for inducing hAESCs differentiation into RPE cells was determined and is shown in schematic diagram (**Figure 2E**).

Human Amniotic Epithelial Stem Cells-Derived Retinal Pigment Epithelium Like Cells Demonstrated Typical Retinal Pigment Epithelium Cellular Characteristics and Functions *in vitro*

After 2 weeks of culture with NIC and TSA, the induced hAESCs developed an RPE like morphology that was pigmented and polygonal (**Figure 3A**). Immunostaining indicated the strong expression of signature early RPE markers such as MITF and PMEL17 in differentiated cells on day 7 after the combined treatment (**Figures 3B,C** and **Supplementary Figure 2F**). Staining also demonstrated abundant F-actin distribution adjacent to the cell membrane and high expression of the tight junction protein ZO-1 among differentiated cells on day 10 after combined treatment, which are data that are similar to those of naturally developing RPE cells (**Figures 3D,E**). At the late stage of differentiation (after 2 weeks of combined treatment), strong expression of the mature RPE markers of chloride channel-related protein Bestrophin 1 (BEST1) and retinal pigment epithelium-specific protein of 65 kids (RPE65) was detected in the differentiated cells (**Figures 3F–G** and **Supplementary Figure 2F**). Additionally, RPE ultrastructure's, including the presence of apical microvilli, pigment granules and tight junctions and well-developed apical microvilli, were revealed by transmission electron microscopys (TEM) and scanning electron microscopy (SEM), respectively (**Figures 3H,I**).

The RPE functions of the differentiated cells were further examined *in vitro*. As a polar monolayer between the neural retina and the choriocapillaris, RPE cells play crucial roles by secreting nutrition factors, phagocytosing the photoreceptor outer segment (POS) and forming the blood-retinal barrier. According to a previous report, vascular endothelial growth factor (VEGF) and pigment epithelium-derived factor (PEDF) were secreted preferentially to the basal and apical sides, respectively, by native RPE cells (Maruotti et al., 2015). Consistently, ELISA results verified similar VEGF and PEDF expression patterns in differentiated cells (**Figures 3J,K**). Z-stack images of confocal microscopy showed that Na/K ATPase is largely apical *in situ* in differentiated cells, indicating polarity that is similar to that of RPE cells (Lehmann et al., 2014) (**Figure 3L**). To determine the phagocytosis function, the differentiated cells were incubated with rat POSs and were then examined by confocal microscopy. The Z-stack images showed that ZO-1-labeled differentiated cells could phagocytose rhodopsin-labeled POSs (**Figure 3M**). Herein, these results demonstrate that hAESCs progress into a polarized and functional monolayer of RPE like cells following small molecule induction for about14 days.

The Immune Privilege of Human Amniotic Epithelial Stem Cells-Derived Retinal Pigment Epithelium Like Cells

Additionally, the immunogenicity of the differentiated cells was examined before subretinal transplantation. The flow cytometry results showed very low levels of HLA-DR and HLA-DQ and high expression of HLA-G (that counteracts NK cell function) in hAESCs-RPE like cells, similar to what were observed in hAESCs with or without IFN-γ treatment (**Figures 4E–H** and **Supplementary Figures 4C,D**). However, significant expression of HLA-DR and HLA-DQ was detected in the human retinal epithelial cell line ARPE-19, and significant expression of HLA-DR was detected in IFN-γ-treated human umbilical cord mesenchymal stem cells (hUMSCs), while very low level of HLA-G were detected in both ARPE-19 and hUMSCs (**Figures 4A–D** and **Supplementary Figures 4A,B**).

Subretinal Transplantation of Human Amniotic Epithelial Stem Cells-Retinal Pigment Epithelium Rescued Retinal Structure and Visual Function *in vivo*

To further determine whether hAESCs-RPE like cells had a therapeutic effect on retinal degeneration *in vivo*, hAESCs-RPE like cells, differentiated for 14 days *in vitro*, were transplanted into the subretinal space of RCS rats, which are an animal model of retinal degeneration in which the defect of RPE to phagocytize POSs leads to further degeneration and progressive loss of PRs (D'Cruz et al., 2000). Immunohistochemistry demonstrated the subretinal localization of the GFP-labeled engrafted cells, which expressed RPE-specific markers RPE65 and CRALBP (**Figures 5A,B**). In addition, color fundus imaging illustrated that the transplantation of hAESCs-RPE cells mitigated the retinal disorder comparing to the pale retina with unnormal pigment in control eyes (**Supplementary Figure 5**). Of note, the differential interference contrast combined with the fluorescent image indicated the presence of the transplanted hAESCs-RPE within the host RPE layer.

Importantly, an electroretinographic (ERG) response assay at 4 weeks after transplant revealed a significant preservation of visual function in cell-grafted eyes compared with medium-injected eyes (**Figure 5C**). There were significantly greater b-wave amplitudes detected at a series of luminance levels in the dark-adapted state of cell-grafted eyes than there were in the control groups (**Figure 5D**).

Furthermore, histological analysis demonstrated that organized retina structure, especially the outer nuclear layer (ONL), was extensively preserved in a region adjacent to the cell injection site compared with obvious ONL loss in opposite non-transplantation regions (**Figures 5E,F**). This was confirmed

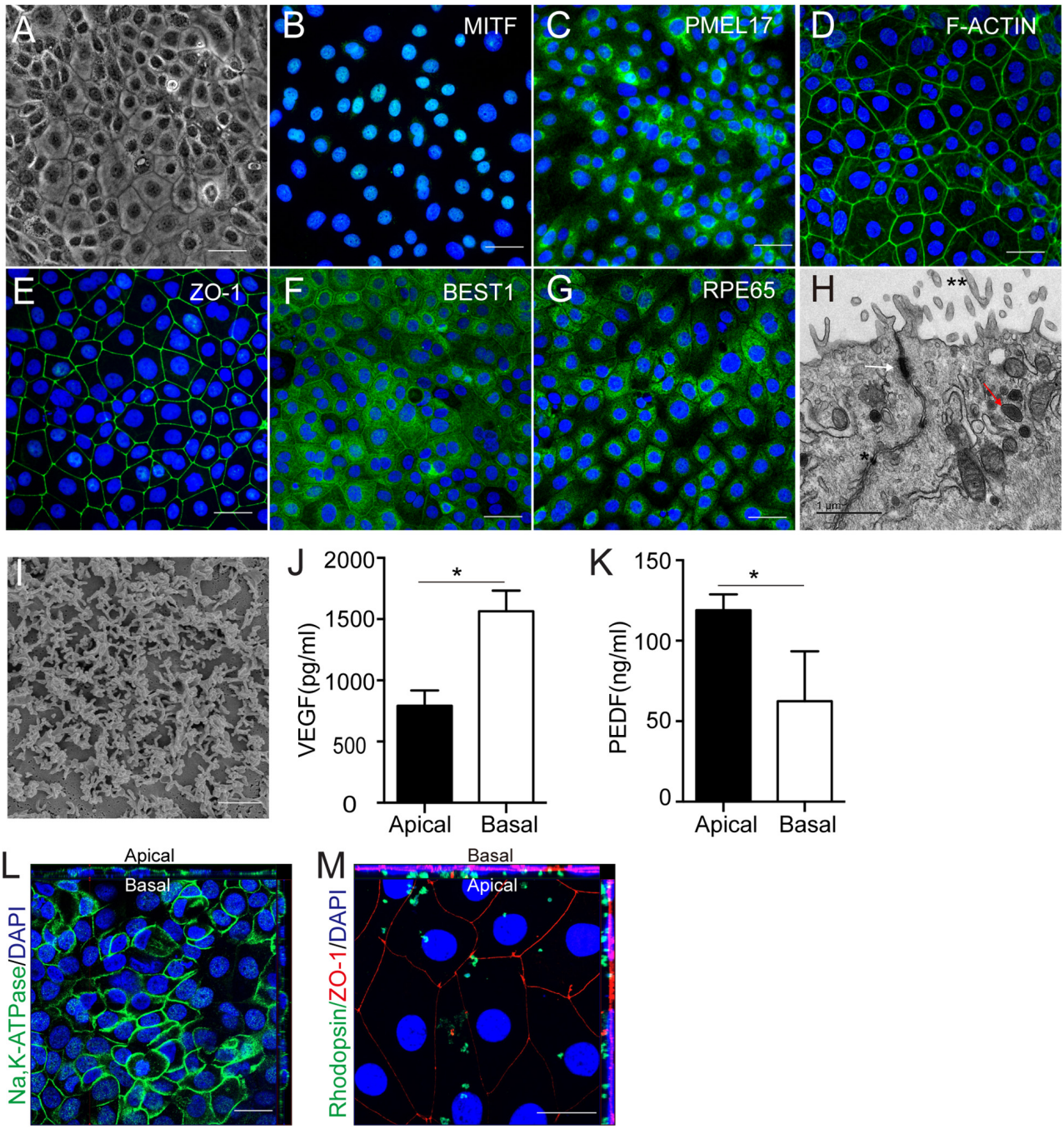

FIGURE 3 | Cellular characteristics and functions of hAESCs-RPE like cells obtained by combined induction of NIC and TSA. **(A)** Morphology of hAESCs-RPE cells after 2 weeks induction as shown in phase-contrast microscope image, with pigmented and polygonal pattern. **(B–C)** The expression of signature early RPE markers MITF, PMEL17 in hAESCs-RPE after 1 week induction were demonstrated by immunofluorescence microscopy. **(D–E)** Phalloidine staining indicated distribution of F-actin adjacent to the cell membrane and the expression of mature RPE marker ZO-1 indicated the tight junction formation in hAESCs-RPE after 10 days induction. **(F–G)** The expression of signature mature RPE markers BEST1, RPE65 in hAESCs-RPE like cells after 2 weeks induction were demonstrated by immunofluorescence microscopy. **(H–I)** Detailed feature characteristic of RPE in hAESCs-RPE after 2 weeks induction were shown by electron microscopy: apical microvilli (double asterisk), melanin granules (red arrowhead) and tight junctions (asterisk and white arrowhead) by transmission electron microscopy, and the apical microvilli by scanning electron microscopy. **(J–K)** Polarized secretion of VEGF-A and PEDF from the apical and basal sides of hAESCs-RPE after 2 weeks induction were shown by ELISA analysis. **(L)** Confocal Z-stack fluorescent image with cross-section side views showing the typical apical localization of Na-K ATPase in hAESCs-RPE after 2 weeks induction. **(M)** Confocal Z-stack fluorescent image with cross-section side views showing phagocytosis of photoreceptor outer segment purified from non-dystrophic RCS rats (green-rhodopsin) by hAESCs-RPE after 2 weeks induction. Nuclei were counterstained with DAPI (blue) in panel **(C,D,E,G,L,M)**. Score bars, 50 μm in **(A–G,L–M)**,1 μm in **(H)**, 2 μm in **(I)**, error bars represent mean ± SEM of three biological replicates ($n = 3$), $^*p < 0.05$, unpaired *t*-test.

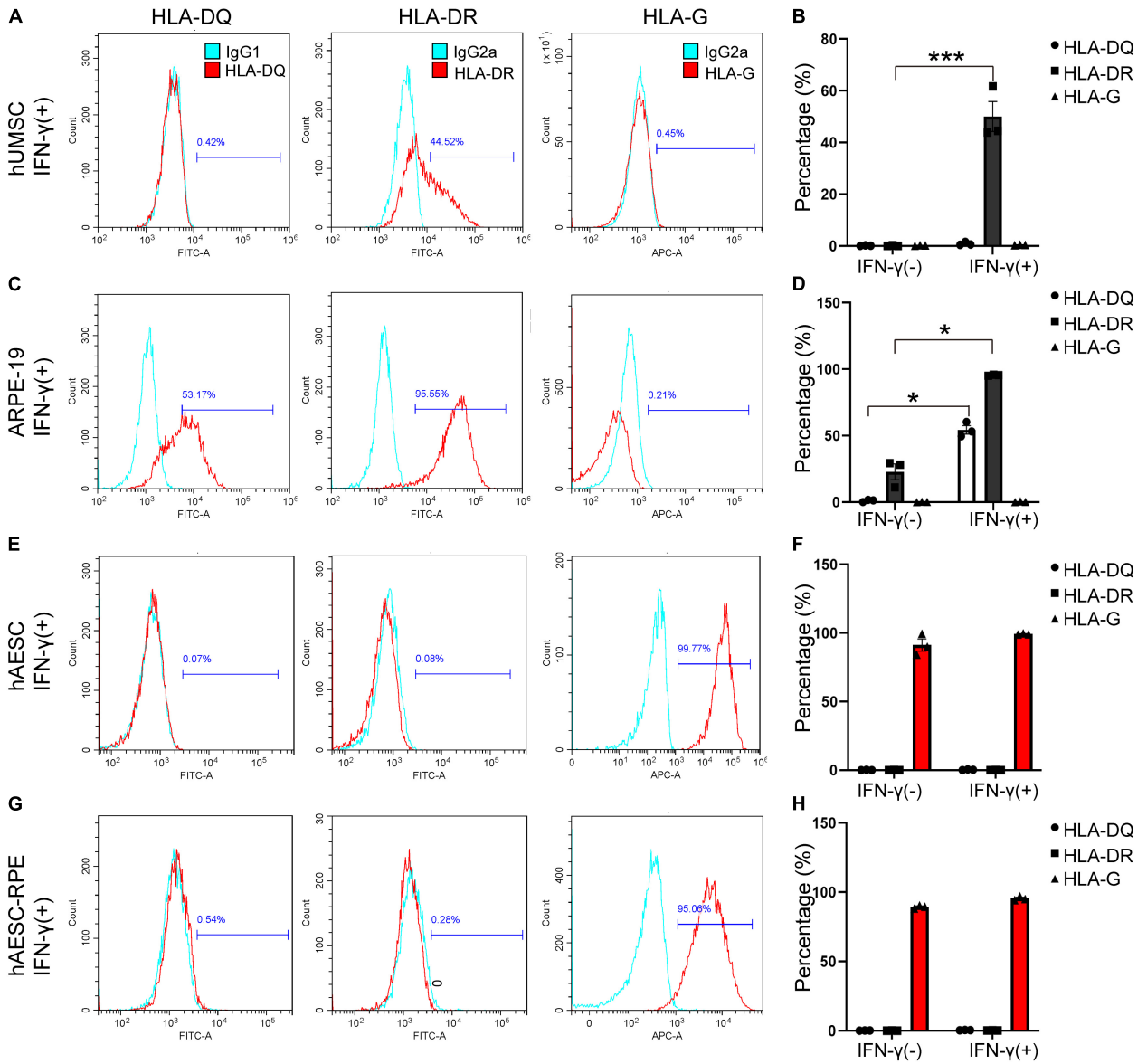

FIGURE 4 | Consistent low immunogenicity in hAESCs and their derived cells under proinflammatory condition. Flow cytometry analysis of HLA-DQ, HLA-DR, and HLA-G in human umbilical cord mesenchymal stem cells (hUMSC), human retinal epithelial cell line ARPE-19, hAESCs, hAESCs-RPE like cells with 10 ng/mL IFN-γ treatment for 72 h **(A,C,E,G)**, indicating consistent low immunogenicity in hAESCs and their derived cells under proinflammatory condition. Representative histograms of HLA-DQ, HLA-DR, and HLA-G are shown in red and the isotype controls are shown in blue. Under normal and proinflammatory conditions, the quantitative results were shown in **(B,D,F,H)**. Error bars represent mean ± SEM of three biological replicates ($n = 3$). $^{*}p < 0.05$, $^{***}p < 0.001$, unpaired t-test.

by the quantification of the ONL thickness in both groups (**Figure 5G**) and retinal length affected by the cell transplantation was quantificated by ImageJ (**Figure 5H**). Around 20% of the retina is affected by the hAESCs-RPE transplantation.

To assess the long-term therapeutic effects of hAESCs-RPE cells and to substantiate the efficacy and safety of the cell transplantation, cell-grafted and matching control groups were followed up to 8 weeks after subretinal transplantation. Immunostaining and histological analysis indicated the survival of transplanted RPE cells and showed their protective effect in retinal degeneration (**Supplementary Figures 6A–E**).

DISCUSSION

Cell transplantation of RPE cells is one of the most promising therapeutic strategies for incurable retinal degenerative diseases (Jones et al., 2017; Stern et al., 2018). Our study indicated that hAESCs might serve as an optional source for retinal cells, and they could be induced into RPE like cells under defined culture conditions. Human amniotic epithelial stem cells-derived RPE like cells exhibit the morphology and marker expression of native retinal cells and can partially improve retinal structure and function after subretinal transplantation into a classical animal

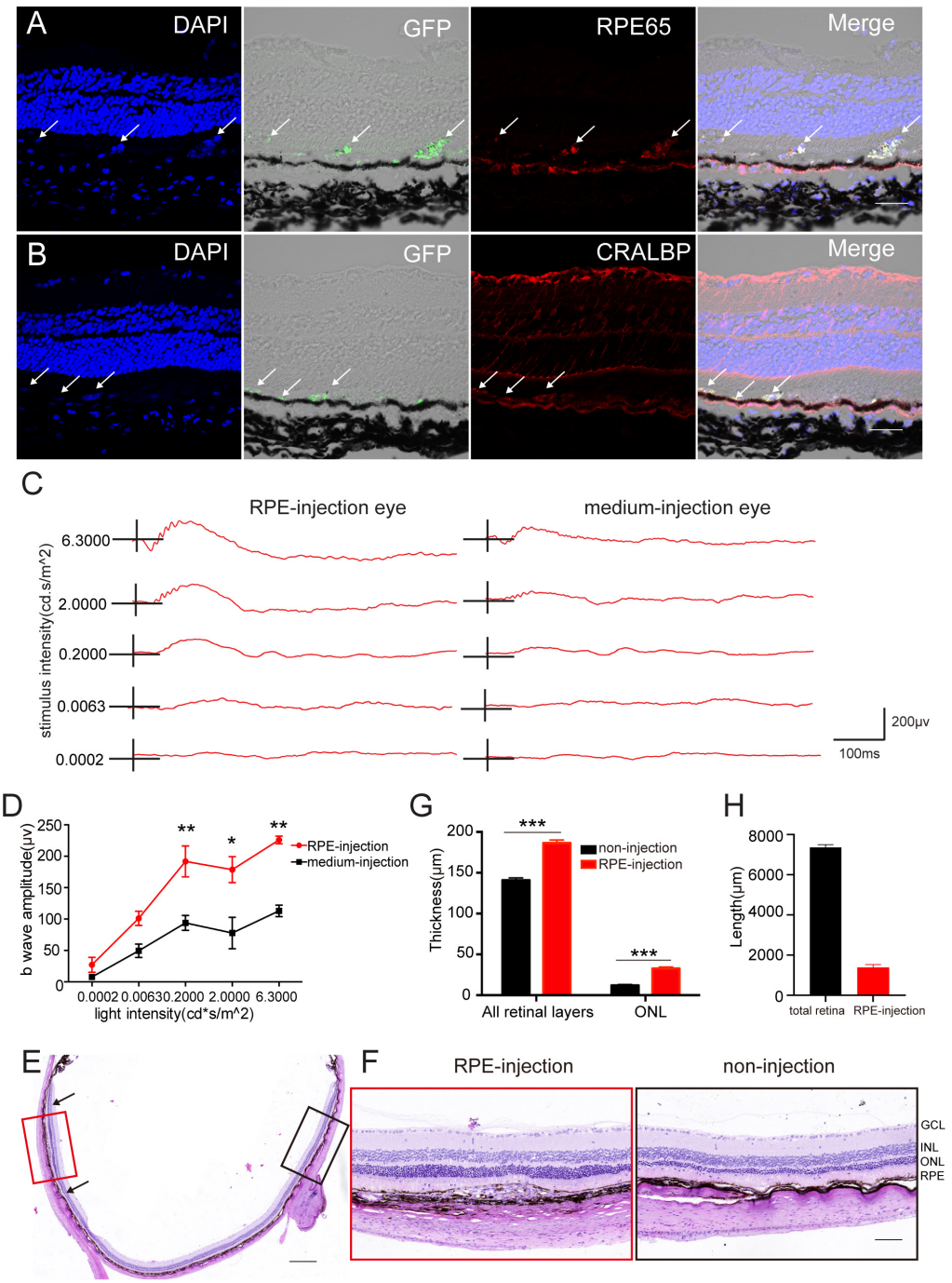

FIGURE 5 | Subretinal transplantation of hAESCs-RPE like cells rescued retinal structure and visual function in RCS rats. Retinal structure and function were examined 4 weeks after subretinal transplantation of hAESCs-RPE. **(A–B)** Immunofluorescence microscopy showed GFP-labeled transplanted hAESCs-RPE coexpressing RPE markers RPE65 and CRALBP. Nuclei were counterstained with DAPI (blue). Note differential interference contrast combined with fluorescent image indicating the integration of GFP + hAESCs-RPE within the host RPE layer; arrows showing transplanted hAESCs-RPE. **(C)** Representative ERG responses to a series of white flashes of increasing intensity in the dark-adapted state in a transplantation eye and its fellow un-treatment eye. **(D)** Mean b-wave amplitudes in response to white flashes of increasing intensity, showing significantly higher read in transplanted eyes (red line) as compared to groups of control eyes. **(E–G)** Representative images of H&E stained retina sections with histological quantifications, showing preservation of ONL and thicker whole retina in subretinal transplantation region (indicated by red frame in E and higher-magnification image in the left panel of **F**, with quantification in **G**) as compared with thinner ONL and whole retina in the region distant from graft in the same eye (indicated by black frame in E with higher-magnification image in the right panel of **F**, with quantification in **G**). **(H)** The length of the retina affected by the cell transplantation was quantificated by ImageJ (located between black arrowheads). Score bars, 50 μm in **(A–B)**, 500 μm in **(E)** and 100 μm in **(F)**, error bars represent mean ± SEM of three biological replicates, $*p < 0.05$, $**p < 0.01$, $***p < 0.001$; two-way ANOVA followed by Tukey's multiple comparisons test **(D)**; unpaired *t*-test **(G)**; $n = 3$ rats per group.

model of retinal degeneration. But we need to be aware that the induced cells are not comparable to the native RPE cells, especially lower expression of some of the RPE signature markers. Therefore, the induced cells are termed as "RPE like cells." Longer differentiation time, 3D culture carrier and additional screening of small molecules aiming the low expression markers may improve the quality of the induced cells, which will be conducted in our future studies. According to our previous studies, hAESCs possessed special properties as seed cells for cell therapy, which mainly include no ethical concerns related to their harvest and clinical application, their immunomodulatory properties, and their absence of tumorigenicity because of lack of telomerase (Li et al., 2018; Yang et al., 2018).

One of the major concerns for cell therapy is graft rejection. Employing autologous stem cells seems to be a feasible way to overcome this obstacle, but in some cases, patients with dry AMD were reported to lose light perception caused by retinal detachment after receiving an intravitreal transplantation of autologous human adipose-derived stem cells (hADSCs) (Kuriyan et al., 2017). Moreover, there are currently no reliable endogenous differentiation strategies for retinal cells, and their collection requires invasive extraction (Moviglia et al., 2012; Rezanejad et al., 2014). Additionally, their immunogenicity induction abilities are unpredictable and there is even debate regarding their tumorigenicity in pathological microenvironments in some cases (Barkholt et al., 2013; Casiraghi et al., 2013; Veceric-Haler et al., 2017). Thus, allogeneic stem cells, especially hiPSCs and hESCs, are considered the main choice as seed cells for retinal disease therapy. Along with research and development, retinal cells derived from hiPSCs and hESCs, however, cannot avoid confronting an increased risk of rejection and the challenge of tumorigenicity. Clinical trials have reported that immunosuppression is always required after hES-RPE transplantation (da Cruz et al., 2018; Mehat et al., 2018). Moreover, macular edema and even DNA aberrations occurred in the hiPSCs-RPE recipient (Mandai et al., 2017). In the present study, we also paid attention to the immunogenicity of hAESCs-derived retinal cells. Our work and others' demonstrated the immune tolerance capacity of hAESCs due to high expression of a non-classic MHC class I molecule HLA-G that impairs NK cell recognition and killing, and the weak expression of MHC class II antigens (Strom and Gramignoli, 2016; Tan et al., 2018; Yang et al., 2018). To our surprise, the differentiated cells still kept low levels of HLA-DR, DQ and high expression of HLA-G that were similar to the levels in undifferentiated hAESCs, in spite of proinflammatory stimulation. However, obvious immunogenicity was observed in the human ARPE19 cell line and IFN-γ treated human MSCs in the present study, suggesting potential graft rejection and correlated immune reactions during cell therapy. These result to not administer immunosuppressive agents to the host rats of cell transplantation. Moderate survival of engrafted cells and their effect on retinal function restoration were observed even 2 months later, while human cell rejection was observed in animal models to some extent. Coupling with the non-tumorigenicity property of hAESCs that were mentioned, our results may indicate the low immunogenicity and potential safety of hAESCs-derived RPE like cells. The success of long-term xenotransplantation may herein lead to the expectation of a better performance of hAESCs-derived RPE in clinical use. Moreover, we infer that the combined transplantation of non-differentiated hAESCs with hAESCs-RPE may achieve a better therapeutic effect, because non-differentiated hAESCs could improve the microenvironment based on their immunomodulatory properties. It is worthy to investigate the co-transplantation strategy in our future studies.

In the present study, we identified TSA, a histone deacetylase inhibitor, as an inducer of RPE differentiation. On the other hand, during hAESCs-RPE like cells differentiation, the key RPE markers were upregulated by TSA in a dose-dependent pattern (0.5 μM to 4 μM), indicating that a high concentration of TSA promoted differentiation efficiency. Nevertheless, a high ratio of cell death was observed in that circumstance. To solve this problem, NIC was introduced in the culture medium, as NIC has been reported to protect hPSCs from cell death during neuroectoderm differentiation through PARP1 inhibition (Idelson et al., 2009). Indeed, the cotreatment of TSA and NIC seem to facilitate both efficiency and viability of hAESCs-RPE like cell differentiation. The attractive findings in the current study are the preservation of vision function and retinal structure by hAESCs-derived RPE like cells. These rescue abilities are closely correlated with the f ate of differentiated cells within the host RPE layer *in vivo*.

In summary, we may contribute to expansion of RPE cell resources for replacement therapy. The hAESCs-RPE differentiation and subretinal transplantation could be a potential therapeutic strategy for treating retinal diseases such as AMD. Further preclinical studies are required to determine the effect of hAESCs-RPE cells on different types of retinal diseases such as AMD, retinitis pigmentosa (RP) and stargardt disease (SD). Although these retinal diseases have different causes and demographics, they share common pathology of RPE degeneration at their end-stage. Thus, it is worthy to investigate the therapeutic effect of the hAESCs-RPE in a wider range of animal models that correspond to retinal degeneration disease in clinic. On the other hand, more details of cell delivery need to be determined to pave the road for the fulfillment of clinical treatment in future. In this category, the comparisons may focus on the cellular product forms as cell suspension, cell preparations on a biocompatible scaffold or cell preparation in a sheet without a subjacent scaffold, the administration approaches by intravitreal injection or subretinal injection, as well as the optimal doses for single or multiple injections.

Limitation

Several limitations of the present study need to be noticed. First, the detailed working mechanism of TSA need to be dissected, in the direction of epigenetic regulation. Second, a systemic safety evaluation of the hAESCs-RPE is required for the aim of clinical application, although their proper homogeneity and low immunogenecity has been identified. Third, the time points for observation *in vivo* is limited, especially lack of longer time points more than 3 months, which is important for defining the survival duration of the transplanted cells. Fourth, further investigation is required to determine the details of the transplanted cells such as

their integration within the host RPE layer and their interaction with host cells.

DATA AVAILABILITY STATEMENT

The datasets presented in this study can be found in online repositories. The names of the repository/repositories and accession number(s) can be found below: Gene Expression Omnibus, accession number: GSE180616.

ETHICS STATEMENT

The studies involving human participants were reviewed and approved by the Institutional Patients and Ethics Committee of the International Peace Maternity and Child Health Hospital, Shanghai Jiao Tong University School of Medicine. The patients/participants provided their written informed consent to participate in this study. The animal study was reviewed and approved by the Laboratory Animal Care and the Use Committee of Zhejiang University (approval number, ZJU20190038).

AUTHOR CONTRIBUTIONS

LY and ZG: study design, review and edited the manuscript. JYL and ChQ: wrote the manuscript, data generation, and analysis. YW, WY, JL, WC, CoQ, LG, and LH: data interpretation and review the manuscript. All authors approved the final version of the manuscript.

FUNDING

This work was supported by the National Natural Science Foundation of China (81770444 and 81600354, 81970372), the National Key R&D Program of China (2018YFA0800504), the Zhejiang Provincial Natural Science Foundation of China (LZ20H020002), the Medical and Health Science and Technology Program of Health Commission of Zhejiang Province, China (2021KY633), the Project of Health Collaborative Innovation of Guangzhou City (201704020214), the China Postdoctoral Science Foundation (2019M662036), and the Fundamental Research Funds for the Central Universities of China.

ACKNOWLEDGMENTS

We thank Xiangtian Zhou at Wenzhou Medical University for constructive comments on the manuscript; Beibei Wang at the Center of Cryo-Electron Microscopy (CCEM), Zhejiang University for her excellent technical support on transmission electron microscopy; and Jianhong An and Xiaowen Cao at Wenzhou Medical University for their excellent technical support of the electroretinograms.

SUPPLEMENTARY MATERIAL

The Supplementary Material for this article can be found online at: https://www.frontiersin.org/articles/10.3389/fcell.2021.737242/full#supplementary-material

REFERENCES

Akle, C. A., Welsh, K. I., Adinolfi, M., and Leibowitz, S. (1981). Immunogenicity of human amniotic epithelial-cells after transplantation into volunteers. *Lancet* 2, 1003–1005.

Ambati, J., and Fowler, B. J. (2012). Mechanisms of age-related macular degeneration. *Neuron* 75, 26–39. doi: 10.1016/j.neuron.2012.06.018

Barkholt, L., Flory, E., Jekerle, V., Lucas-Samuel, S., Ahnert, P., Bisset, L., et al. (2013). Risk of tumorigenicity in mesenchymal stromal cell-based therapies-bridging scientific observations and regulatory viewpoints. *Cytotherapy* 15, 753–759.

Casiraghi, F., Remuzzi, G., Abbate, M., and Perico, N. (2013). Multipotent mesenchymal stromal cell therapy and risk of malignancies. *Stem Cell Rev. Rep.* 9, 65–79.

da Cruz, L., Fynes, K., Georgiadis, O., Kerby, J., Luo, Y. H., Ahmado, A., et al. (2018). Phase 1 clinical study of an embryonic stem cell-derived retinal pigment epithelium patch in age-related macular degeneration. *Nat. Biotechnol.* 36, 328–337. doi: 10.1038/nbt.4114

D'Cruz, P. M., Yasumura, D., Weir, J., Matthes, M. T., Abderrahim, H., LaVail, M. M., et al. (2000). Mutation of the receptor tyrosine kinase gene Mertk in the retinal dystrophic RCS rat. *Hum. Mol. Genet.* 9, 645–651. doi: 10.1093/hmg/9.4.645

Hazim, R. A., Karumbayaram, S., Jiang, M., Dimashkie, A., Lopes, V. S., Li, D., et al. (2017). Differentiation of RPE cells from integration-free iPS cells and their cell biological characterization. *Stem Cell Res. Ther.* 8, 217. doi: 10.1186/s13287-017-0652-9

Huo, S. J., Li, Y. C., Xie, J., Li, Y., Raisman, G., Zeng, Y. X., et al. (2012). Transplanted olfactory ensheathing cells reduce retinal degeneration in royal college of surgeons rats. *Curr. Eye Res.* 37, 749–758. doi: 10.3109/02713683.2012.697972

Idelson, M., Alper, R., Obolensky, A., Ben-Shushan, E., Hemo, I., Yachimovich-Cohen, N., et al. (2009). Directed differentiation of human embryonic stem cells into functional retinal pigment epithelium cells. *Cell Stem Cell* 5, 396–408. doi: 10.1016/j.stem.2009.07.002

Jones, M. K., Lu, B., Girman, S., and Wang, S. (2017). Cell-based therapeutic strategies for replacement and preservation in retinal degenerative diseases. *Prog. Retin. Eye Res.* 58, 1–27. doi: 10.1016/j.preteyeres.2017.01.004

Kuriyan, A. E., Albini, T. A., Townsend, J. H., Rodriguez, M., Pandya, H. K., Leonard, R. E. II, et al. (2017). Vision loss after intravitreal injection of autologous "stem cells" for AMD. *N. Engl. J. Med.* 376, 1047–1053. doi: 10.1056/NEJMoa1609583

Lehmann, G. L., Benedicto, I., Philp, N. J., and Rodriguez-Boulan, E. (2014). Plasma membrane protein polarity and trafficking in RPE cells: past, present and future. *Exp. Eye Res.* 126, 5–15. doi: 10.1016/j.exer.2014.04.021

Li, J., Qiu, C., Zhang, Z., Yuan, W., Ge, Z., Tan, B., et al. (2018). Subretinal Transplantation of human amniotic epithelial cells in the treatment of autoimmune uveitis in rats. *Cell Transplant.* 27, 1504–1514. doi: 10.1177/0963689718796196

Luthert, P. J. (2011). Pathogenesis of age-related macular degeneration. *Diagn. Histopathol.* 17, 10–16. doi: 10.1016/j.mpdhp.2010.10.004

Mandai, M., Watanabe, A., Kurimoto, Y., Hirami, Y., Morinaga, C., Daimon, T., et al. (2017). Autologous induced stem-cell-derived retinal cells for macular degeneration. *N. Engl. J. Med.* 376, 1038–1046. doi: 10.1056/NEJMoa1608368

Maruotti, J., Sripathi, S. R., Bharti, K., Fuller, J., Wahlin, K. J., Ranganathan, V., et al. (2015). Small-molecule-directed, efficient generation of retinal pigment epithelium from human pluripotent stem cells. *Proc. Natl. Acad. Sci. U. S. A.* 112, 10950–10955. doi: 10.1073/pnas.1422818112

Mehat, M. S., Sundaram, V., Ripamonti, C., Robson, A. G., Smith, A. J., Borooah, S., et al. (2018). Transplantation of human embryonic stem cell-derived retinal pigment epithelial cells in macular degeneration. *Ophthalmology* 125, 1765–1775. doi: 10.1016/j.ophtha.2018.04.037

Miki, T. (2018). Stem cell characteristics and the therapeutic potential of amniotic epithelial cells. *Am. J. Reprod. Immunol.* 80:e13003. doi: 10.1111/aji.13003

Miki, T., Lehmann, T., Cai, H., Stolz, D. B., and Strom, S. C. (2005). Stem cell characteristics of amniotic epithelial cells. *Stem Cells* 23, 1549–1559. doi: 10.1634/stemcells.2004-0357

Miki, T., and Strom, S. C. (2006). Amnion-derived pluripotent/multipotent stem cells. *Stem Cell Rev.* 2, 133–142. doi: 10.1007/s12015-006-0020-0

Mitchell, P., Liew, G., Gopinath, B., and Wong, T. Y. (2018). Age-related macular degeneration. *Lancet* 392, 1147–1159. doi: 10.1016/s0140-6736(18)31550-2

Moviglia, G. A., Blasetti, N., Zarate, J. O., and Pelayes, D. E. (2012). In vitro differentiation of adult adipose mesenchymal stem cells into retinal progenitor cells. *Ophthalmic Res.* 48(Suppl. 1), 1–5. doi: 10.1159/000339839

Parolini, O., Alviano, F., Bagnara, G. P., Bilic, G., Buhring, H. J., Evangelista, M., et al. (2008). Concise review: isolation and characterization of cells from human term placenta: outcome of the first international workshop on placenta derived stem cells. *Stem Cells* 26, 300–311. doi: 10.1634/stemcells.2007-0594

Ramsden, C. M., Powner, M. B., Carr, A. J., Smart, M. J., da Cruz, L., and Coffey, P. J. (2013). Stem cells in retinal regeneration: past, present and future. *Development* 140, 2576–2585. doi: 10.1242/dev.092270

Rezanejad, H., Soheili, Z. S., Haddad, F., Matin, M. M., Samiei, S., Manafi, A., et al. (2014). In vitro differentiation of adipose-tissue-derived mesenchymal stem cells into neural retinal cells through expression of human PAX6 (5a) gene. *Cell Tissue Res.* 356, 65–75. doi: 10.1007/s00441-014-1795-y

Schwartz, S. D., Hubschman, J. P., Heilwell, G., Franco-Cardenas, V., Pan, C. K., Ostrick, R. M., et al. (2012). Embryonic stem cell trials for macular degeneration: a preliminary report. *Lancet* 379, 713–720.

Schwartz, S. D., Regillo, C. D., Lam, B. L., Eliott, D., Rosenfeld, P. J., Gregori, N. Z., et al. (2015). Human embryonic stem cell-derived retinal pigment epithelium in patients with age-related macular degeneration and Stargardt's macular dystrophy: follow-up of two open-label phase 1/2 studies. *Lancet* 385, 509–516. doi: 10.1016/S0140-6736(14)61376-3

Sharma, R., Khristov, V., Rising, A., Jha, B. S., Dejene, R., Hotaling, N., et al. (2019). Clinical-grade stem cell-derived retinal pigment epithelium patch rescues retinal degeneration in rodents and pigs. *Sci. Transl. Med.* 11:eaat5580. doi: 10.1126/scitranslmed.aaw7624

Song, P., Du, Y., Chan, K. Y., Theodoratou, E., and Rudan, I. (2017). The national and subnational prevalence and burden of age-related macular degeneration in China. *J. Glob. Health* 7, 020703. doi: 10.7189/jogh.07.020703

Stern, J. H., Tian, Y., Funderburgh, J., Pellegrini, G., Zhang, K., Goldberg, J. L., et al. (2018). Regenerating eye tissues to preserve and restore vision. *Cell Stem Cell* 22, 834–849. doi: 10.1016/j.stem.2018.05.013

Strom, S. C., and Gramignoli, R. (2016). Human amnion epithelial cells expressing HLA-G as novel cell-based treatment for liver disease. *Hum. Immunol.* 77, 734–739. doi: 10.1016/j.humimm.2016.07.002

Strunnikova, N. V., Maminishkis, A., Barb, J. J., Wang, F., Zhi, C., Sergeev, Y., et al. (2010). Transcriptome analysis and molecular signature of human retinal pigment epithelium. *Hum. Mol. Genet.* 19, 2468–2486. doi: 10.1093/hmg/ddq129

Subrizi, A., Hiidenmaa, H., Ilmarinen, T., Nymark, S., Dubruel, P., Uusitalo, H., et al. (2012). Generation of hESC-derived retinal pigment epithelium on biopolymer coated polyimide membranes. *Biomaterials* 33, 8047–8054. doi: 10.1016/j.biomaterials.2012.07.033

Tan, B., Yuan, W. X., Li, J. Y., Yang, P. J., Ge, Z., Liu, J., et al. (2018). Therapeutic effect of human amniotic epithelial cells in murine models of Hashimoto's thyroiditis and Systemic lupus erythematosus. *Cytotherapy* 20, 1247–1258. doi: 10.1016/j.jcyt.2018.04.001

Trounson, A., and McDonald, C. (2015). Stem cell therapies in clinical trials: progress and challenges. *Cell Stem Cell* 17, 11–22. doi: 10.1016/j.stem.2015.06.007

Veceric-Haler, Z., Cerar, A., and Perse, M. (2017). (Mesenchymal) Stem cell-based therapy in cisplatin-induced acute kidney injury animal model: risk of immunogenicity and tumorigenicity. *Stem Cells Int.* 2017:7304643. doi: 10.1155/2017/7304643

Wong, W. L., Su, X., Li, X., Cheung, C. M. G., Klein, R., Cheng, C.-Y., et al. (2014). Global prevalence of age-related macular degeneration and disease burden projection for 2020 and 2040: a systematic review and meta-analysis. *Lancet Glob. Health* 2, e106–e116. doi: 10.1016/s2214-109x(13)70145-1

Yang, P. J., Yuan, W. X., Liu, J., Li, J. Y., Tan, B., Qiu, C., et al. (2018). Biological characterization of human amniotic epithelial cells in a serum-free system and their safety evaluation. *Acta Pharmacol. Sin.* 39, 1305–1316. doi: 10.1038/aps.2018.22

Zarbin, M. (2016). Cell-based therapy for degenerative retinal disease. *Trends Mol. Med.* 22, 115–134. doi: 10.1016/j.molmed.2015.12.007

Conflict of Interest: JYL, ChQ, WY, JL, and LY are coinventors on the patent application related to the use of hAESCs for RPE differentiation (China Patent Serial No. ZL201910310260.1).

The remaining authors declare that the research was conducted in the absence of any commercial or financial relationships that could be construed as a potential conflict of interest.

Publisher's Note: All claims expressed in this article are solely those of the authors and do not necessarily represent those of their affiliated organizations, or those of the publisher, the editors and the reviewers. Any product that may be evaluated in this article, or claim that may be made by its manufacturer, is not guaranteed or endorsed by the publisher.

frontiers in Cell and Developmental Biology

REVIEW
published: 01 October 2021
doi: 10.3389/fcell.2021.748576

Challenges for the Applications of Human Pluripotent Stem Cell-Derived Liver Organoids

*Mingyang Chang[1], Mariia S. Bogacheva[2] and Yan-Ru Lou[1]**

[1] Department of Clinical Pharmacy and Drug Administration, School of Pharmacy, Fudan University, Shanghai, China,
[2] Division of Pharmaceutical Biosciences, Faculty of Pharmacy, University of Helsinki, Helsinki, Finland

The current organoid culture systems allow pluripotent and adult stem cells to self-organize to form three-dimensional (3D) structures that provide a faithful recapitulation of the architecture and function of *in vivo* organs. In particular, human pluripotent stem cell-derived liver organoids (PSC-LOs) can be used in regenerative medicine and preclinical applications, such as disease modeling and drug discovery. New bioengineering tools, such as microfluidics, biomaterial scaffolds, and 3D bioprinting, are combined with organoid technologies to increase the efficiency of hepatic differentiation and enhance the functional maturity of human PSC-LOs by precise control of cellular microenvironment. Long-term stabilization of hepatocellular functions of *in vitro* liver organoids requires the combination of hepatic endodermal, endothelial, and mesenchymal cells. To improve the biological function and scalability of human PSC-LOs, bioengineering methods have been used to identify diverse and zonal hepatocyte populations in liver organoids for capturing heterogeneous pathologies. Therefore, constructing engineered liver organoids generated from human PSCs will be an extremely versatile tool in *in vitro* disease models and regenerative medicine in future. In this review, we aim to discuss the recent advances in bioengineering technologies in liver organoid culture systems that provide a timely and necessary study to model disease pathology and support drug discovery *in vitro* and to generate cell therapy products for transplantation.

Keywords: human pluripotent stem cells, liver organoid, regenerative medicine, disease modeling, drug development

OPEN ACCESS

Edited by:
Mirella Dottori,
University of Wollongong, Australia

Reviewed by:
Ranran Zhang,
Rutgers, The State University of New Jersey, United States
Bang Manh Tran,
The University of Melbourne, Australia

****Correspondence:***
Yan-Ru Lou
yanru_lou@fudan.edu.cn

Specialty section:
This article was submitted to Stem Cell Research, a section of the journal Frontiers in Cell and Developmental Biology

Received: *28 July 2021*
Accepted: *08 September 2021*
Published: *01 October 2021*

Citation:
Chang M, Bogacheva MS and Lou Y-R (2021) Challenges for the Applications of Human Pluripotent Stem Cell-Derived Liver Organoids. Front. Cell Dev. Biol. 9:748576. doi: 10.3389/fcell.2021.748576

INTRODUCTION

An organoid is a self-assembled three-dimensional (3D) structure formed by stem/progenitor cells *in vitro*, which can reproduce many structures and functions of an organ (Lou and Leung, 2018). Organoids can be generated from pluripotent stem cells (PSCs), including embryonic stem cells (ESCs) and induced pluripotent stem cells (iPSCs), and tissue-specific adult stem cells. To date, various types of organoids have been generated to mimic tissues of heart, intestine, liver, lung, brain, etc. (Mansour et al., 2018; Miller et al., 2019; Serra et al., 2019; Wang S. et al., 2019; Rossi et al., 2021). Organoid technology represents a significant enhancement of the 3D culture system. The advantage of organoid cultures is that they are combined with bioengineering technology to mimic target organ structure and environment (Yin et al., 2016), and they contain cell types with *in vivo*

properties suitable as development and disease models (Collins et al., 2019; Wörsdörfer et al., 2020; Ogoke et al., 2021). Despite the wide applications of organoids, tissue microenvironment, such as cell-cell and cell-matrix interactions, need to support complicated regulatory network, which is important to maintain the homeostasis of an organ. Biological engineering methods have enabled us to guide cell communication and cell behavior to analyze how organs work and to reconstruct the system, which are essential processes in organoid establishment.

Human liver is a structurally and functionally complex organ (Popper and Schaffner, 1957; Weiss et al., 1988), involving distinct cell types and microenvironment and possessing more than 500 functions. The liver consists of endoderm-derived hepatocytes (parenchymal cells) and cholangiocytes and mesoderm-derived sinusoidal endothelial cells, hepatic stellate cells, Kupffer cells, periportal fibroblasts, etc. The liver development requires self-organization of the cells, the process involving biochemical and biophysical cues for morphogenesis and coordinated gene activation/repression, leading to organogenesis (Koepsell et al., 2007; Tam and Loebel, 2007). Therefore, in terms of structural resemblance and functional generalization of the liver organ, liver organoids are superior to cells cultured in two-dimension (2D).

The term liver organoid (LO) refers to 3D multicellular spherical structure made of one or more liver cell types, for example, hepatocyte organoid refers to an organoid formed by hepatocytes. LOs with multiple cell types can better mimic the liver organ while LOs with single cell type are easier to form. LOs can be established from PSCs, fetal, or adult liver cells, and the latter two can be generated directly from human biopsy specimens (Hendriks et al., 2021). Like liver development *in vivo*, PSC-derived liver organoids (PSC-LOs) resemble the structure and functionality of the liver at certain developmental stage depending on the differentiation condition. The crucial problem of PSC-LOs is known to be immature characteristics. Therefore, optimized organoid engineering protocols are continuously being developed to terminally differentiate PSCs into hepatocyte-like organoids (Touboul et al., 2010; Takebe et al., 2017; Pettinato et al., 2019). Mun et al. (2021) claimed for the first time that treatment of human PSC-LOs with short-chain fatty acid mixture of acetate, propionate, and butyrate improved metabolic maturation which may help to accurately assess the CYP3A4-dependent drug toxicity.

LOs are useful for a diverse range of applications, such as studying causes and processes of diseases, gene functions, and cell interaction with tissue environments (van Ineveld et al., 2020; Zhu et al., 2020; Brooks et al., 2021; Thompson and Takebe, 2021; Wang et al., 2021). For *in vitro* applications, LOs have great potential in screening drug hepatotoxicity and modeling liver diseases. One of the causes of high attrition rates is drug-induced liver injury (DILI). In terms of human models of hepatotoxicity, Davidson and Khetani (2020) have developed a scalable culture of human LOs in 384-well plates, which are fully predictive of human DILI and facilitate high-throughput compound screening. For *in vivo* applications, LOs provide hope for cell therapy to treat end-stage liver diseases. However, LOs still face several limitations before they can be used in these applications. Current organoid systems are translationally disadvantaged by variability in self-organization, morphology, and function (Lou and Leung, 2018). Matrigel, used in most cases of organogenesis, still poses the limitation to *in vivo* applications of organoids (Ng et al., 2018; Klotz et al., 2019; Krüger et al., 2020). In this review, we aim to discuss the recent advances in bioengineering technologies in LO culture systems and how bioengineering methods can increase the value of LOs in fundamental research and translational research, such as drug development, precision medicine, and regenerative medicine.

Types of Liver Organoids

Adult Stem Cell-Derived Liver Organoids

Organoid technology has been used to establish hepatic stem cell populations *in vitro* (Schneeberger et al., 2020). A standard adult stem cell-derived LO culture system is a highly potent platform for modeling adult liver from patients' tissue specimens (Schene et al., 2020). LOs can be established from single $EpCAM^+$ cholangiocytes and expanded for several months, while retaining key functional and molecule features after long-term expansion (Huch et al., 2015). It is well-known that adult primary hepatocytes do not replicate *in vitro*, but recent LO studies have allowed them to become highly proliferative, resembling proliferating hepatocytes upon partial hepatectomy or inflammation. Hu et al. (2018) have reported long-term culture of adult hepatocyte-derived organoids that consist of progenitors and differentiated hepatocytes. The researchers confirmed that these hepatocyte organoids were derived from albumin-positive hepatocytes rather than $EpCAM^+$ and $SOX9^+$ ductal cells. In another study, researchers utilized a regenerative cytokine TNFα to establish long-term expansion of hepatocyte organoids from adult hepatocytes, which mimics inflammation-induced liver regeneration (Peng et al., 2018).

Adult stem cell-derived LOs can be expanded seemingly indefinitely, however, these organoids are derived from a single germ layer, i.e., endoderm, which have limited potential, for example, in modeling complicated liver diseases that involves endoderm- and mesoderm-derived cells. It is tempting to expect that appropriate conditions can facilitate co-culture with mesoderm-derived cells to form liver organoids with significant degree of cellular functionality and architectural complexity.

Cancer Derived Liver Organoids

The liver cancer cell line hepatoma G2 (HepG2) and patient-derived tumor xenografts (PDTXs) have long been used as tumor models and have significantly contributed to drug discovery for cancer therapy. 2D immortalized cell lines can easily proliferate *in vitro*, but their gene expression characteristics are highly altered that cannot recapitulate the function of cell types *in vivo*. Generation of PDTXs is labor intensive and time consuming. On the other hand, the generation of patient-derived tumor organoids (PDTOs) is faster. PDTOs have heterogeneous genetic features and can completely simulate tumor characteristics *in vivo*. Thus, PDTOs have enormous potential for modeling human cancers (Kuo and Curtis, 2018; Muthuswamy, 2018) and have been increasingly used in drug development and clinics for personalized drug treatment.

Broutier et al. (2017) have established primary cancer LOs that recapitulate parental tumors, even after long-term expansion *in vitro*. Diverse *in vitro* culture methods, such as bioengineering organoid, allow modeling of tumor heterogeneity or immunity. Cancer LO platform combined with the immune system, angiogenesis, and fibroblasts that retain tumor cell heterogeneity has become a cancer model for cancer microenvironment research and will unleash great potential in evaluating anti-cancer drug efficacy (Papapetrou, 2016; Pauli et al., 2017; Vlachogiannis et al., 2018).

Human Pluripotent Stem Cell-Derived Liver Organoids

The hepatic differentiation of human PSCs starts with definitive endoderm (DE) differentiation followed by the formation and expansion of hepatic progenitors and the formation and maturaton of fetal hepatocytes. The generation of PSC-LOs may be performed either partly in 3D, for example, the formation of DE cells (Akbari et al., 2019), hepatic progenitors (Wang S. et al., 2019), or hepatocyte-like cells (Sgodda et al., 2017) in 2D condition followed by the transfer of obtained cells into 3D condition for the maturation, or completely in 3D from the beginning of the PSC stage (Guan et al., 2017). Hepatic endoderm cells can aggregate into 3D structures in certain conditions, particularly as a result of the activation of FGF and BMP signaling pathways (Takebe et al., 2013).

Human PSCs-LOs can contain single or multiple cell types, such as hepatocytes, cholangiocytes, and other non-parenchymal cells, which self-organize to form the structural units present in the liver. As a result, they are closely mimicking the complex structure and functionality of the liver.

Human PSC-LOs rely on the self-organizing ability of stem cells and progenitors to form organized structures for modeling developmental processes of liver organogenesis. To better control the differentiation processes and decrease heterogeneity, organoids should be designed to generate a specific liver region according to liver zonation. *In vitro* models mimicking liver zonation have been established by HepaRG cells and hepatocytes from neonatal rats (Ahn et al., 2019; Janani and Mandal, 2021).

Liver Diseases

Liver disease is one of the leading causes of death worldwide. According to the National Center for Health Statistics in the US, the morbidity of adults with diagnosed liver disease is 1.8% and is expected to continue in the next decades (National Center For Health Statistics, 2021). Common causes of chronic liver disease and cirrhosis are viruses, genetics, autoimmune disease, excessive alcohol use, and obesity. Acute liver failure, also known as fulminant hepatic failure, is caused by drugs or toxic chemicals. These are severe damage factors to the liver, and at a certain point in the progression of liver disease, the injury can become irreversible and lead to end-stage liver disease, liver failure, liver cancer, or death. Liver transplant is the only effective treatment for end-stage liver diseases. The number of patients on waiting lists well exceeds organ donation rates and therefore people have high expectation for human PSC-derived liver cells as an alternative treatment. Earlier studies have demonstrated the feasibility of human PSC-derived liver cells as cell therapy (Takebe et al., 2017). Additionally, human PSC-LOs have potential as *in vitro* models in drug discovery and development.

CHALLENGES FOR THE APPLICATIONS OF HUMAN PLURIPOTENT STEM CELL-DERIVED LIVER ORGANOIDS

Regenerative Medicine

As human PSC-derived cells represent a substitute to cadaver and organ transplantation, human PSC-LOs provides an avenue toward cell therapy. By using improved organoid technology and transplantation techniques, transplanted human PSC-LOs could potentially integrate and grow *in vivo* into functional liver tissue to replace injured hepatocytes and non-parenchymal cells that are caused by liver diseases. Nevertheless, before human PSC-LOs are suitable for regenerative treatment, many issues must first be solved.

Xenogeniciy of Biomatrices

In the process of organoid formation, one aspect is the induction of stem cell differentiation that requires a large number of growth factors or small molecules that are tissue-specific and can change signaling pathways for cell survival, migration, and proliferation. The other aspect is the formation of 3D tissue-like structures that rely on 3D cell culture environments. When building a 3D cell culture environment, it is necessary to consider extracellular cues influenced by the scaffold, the composition of extracellular matrix (ECM) proteins, and the stiffness of the matrix. Matrigel-based matrix is often used for the generation and culture of various PSC-derived and tissue-specific stem cell-derived organoids including liver (Mun et al., 2020), brain (Lancaster et al., 2013), kidney (Takasato et al., 2015), and intestine (Sugimoto and Sato, 2017). Matrigel provides scaffolding and signaling by forming basement membranes to support cell attachment and functionality, including organoid formation (Xu and Zeger, 2001). Ouchi et al. (2019) embedded human PSC-derived foregut spheroids into Matrigel to create LOs. The resultant LOs consist of hepatocytes, hepatic stellate cells, and Kupffer cells with specific polarity and more mature characteristics in comparison with fetal human hepatocytes. A simultaneous induction of DE and mesoderm cells on Matrigel is another approach resulting in the formation of LOs containing two cell types—hepatocytes and biliary cells (Wu et al., 2019). Although Matrigel has great potential to support the generation of LOs, it is a basement membrane extracted from the Engelbreth-Holm-Swarm mouse sarcoma (Orkin et al., 1977), which severely limits organoid application in clinical practice.

Xeno-free biomatrices

Efforts have recently been made in developing clinically acceptable matrices or biomaterials for LOs (**Table 1**). The first class is animal-derived matrix, such as collagen type I, decellularized matrix, and hyaluronic acid. Collagen type I is the key component of the liver ECM that affects cell growth, viability,

TABLE 1 | 3D cell culture systems for human LOs.

3D cell culture system	Xenogenicity	Type	Cell types in LOs	Aim	Limitation	References
Matrigel	Mouse-derived	Natural	Human iPSC-derived hepatocyte-, stellate-, and Kupffer-like cells	Fibrosis model	Clinically unacceptable	Ouchi et al., 2019
Matrigel	Mouse-derived	Natural	Human iPSC-derived hepatocytes and biliary cells	Hepatobiliary organogenesis	Clinically unacceptable	Wu et al., 2019
Collagen hydrogel	Animal-derived	Natural	Human iPSC-derived hepatocyte-like cells	Hepatic maturation		Gieseck et al., 2014
Decellularized matrix	Porcine intestine-derived	Natural	Human liver duct cells or fetal hepatocytes	Clinical applications	Batch-to-batch variation	Giobbe et al., 2019
Alginate capsules	Plant-derived	Natural	PSC-derived hepatocytes and stromal cells	Functional engraftment		Song et al., 2015
Nanofibrillar cellulose hydrogel	Plant-derived	Natural	Human adult liver cells	Clinical applications	Non-biodegradable	Krüger et al., 2020
Colloidal crystal scaffolds with collagen type I	Partially animal-derived	Synthetic/natural	Human iPSC-derived hepatic progenitors	Fully defined matrix for clinical applications		Ng et al., 2018
Poly isocyanopeptides and laminin-111	Not animal-derived	Synthetic/natural	Human adult liver cells	Clinical applications		Ye et al., 2020
Poly (ethylene glycol) (PEG) hydrogels	Not animal-derived	Synthetic	Human adult liver cells	Chemically defined for clinical applications		Sorrentino et al., 2020
Matrix-free suspension	None	None	Human ESC-derived hepatocyte-like cells	Hepatic maturation		Ogawa et al., 2013
Matrix-free suspension	None	None	Human ESC- derived hepatocyte-like cells	Large-scale expansion		Sgodda et al., 2017

differentiation, and overall tissue organization. As xenogeneic collagen and hyaluronic acid are clinically acceptable, they can be used as a scaffold for the generation of LOs. Mixing of iPSC-derived hepatocyte-like cells with collagen solution followed by heating for the induction of vitellogenesis led to the generation of a 3D structure with an *in vivo*-like architecture (Gieseck et al., 2014). The transfer of clumps of 2D iPSC-derived hepatocyte-like cells into 3D collagen-based scaffold doubled the percentage of glycogen-synthesizing cells, increased the expression of mature hepatic genes, decreased the expression of fetal liver markers AFP and CYP3A7, and promoted the establishment of cell polarity. The long-term stable functionality of cells in 3D makes this model a promising tool for toxicity assessment. Moreover, this model is suitable for high-throughput screening studies (Gieseck et al., 2014).

Owing to its complex *in vivo*-like properties, decellularized matrix is used more often to support cell expansion and differentiation than any existing matrix components (Giobbe et al., 2019). After decades of research, especially in recent years, the need for complex forms of ECM has been clarified (Manou et al., 2019). So far, better results have been obtained using matrix extracts prepared by decellularizing cartilage and myocardium tissues (Schwarz et al., 2012; Oberwallner et al., 2014). Ott et al. (2008) have previously developed a technology for organ decellularization that uses a detergent for cell removal from the heart. Decellularized scaffold retains tissue-specific 3D architecture and vascular network. The decellularized scaffolds have a wide variety of applications in reconstruction of liver tissue or organ (Uygun et al., 2010; Baptista et al., 2011; Minami et al., 2019). The low immunogenicity makes decellularized matrix clinically applicable.

Rat decellularized liver scaffold has been used for the formation of human iPSC-derived hepatocyte grafts after differentiation of the iPSCs into hepatocytes in 2D culture. Recellularization of the scaffold with iPSC-derived hepatocytes led to the expression of CYP3A4 enzyme and secretion of albumin but in a lower amount than 2D iPSC-derived hepatocytes (Minami et al., 2019). Although the maturity of the recellularized iPSCs-derived grafts was not high enough and needs more study for the improvement of the protocol, the important outcome of this research is the demonstration of the suitability of the xenogeneic decellularized scaffold for human liver engineering. Effective engraftment and high induction of hepatocyte and cholangiocyte markers were reached in hepatic stem cells cultured and differentiated in the decellularized liver matrix (Wang et al., 2011), showing the potential of decellularized scaffold for liver bioengineering. Decellularized ECM promotes higher CYP enzyme activity in iPSC-derived hepatocytes compared with cells cultured in synthetic poly-l-lactic acid scaffold covered with collagen (Wang et al., 2016).

Decellularized ECM in combination with a linear polysaccharide hyaluronic acid has been shown to support the tight junction formation and possessed a lower immune response compared to other natural hydrogels (Deegan et al., 2016). Immunotolerance is one of the advantages of decellularized ECM, allowing its use in transplantation. Hyaluronic acid is an important component of the natural ECM. It is easy to modify hyaluronic acid *in vitro* to adjust its stiffness and other physical parameters according to its intended application. Particularly, hepatocytes grown in the hyaluronic acid hydrogel in 3D condition possessed high viability and growth rate (Burdick and Prestwich, 2011).

It remains challenging to obtain scalable and well-controlled organoids due to the complex composition and batch-to-batch variability of human or animal-derived matrices. Therefore, some plant-based biomaterials have been developed. Alginate, a marine algae water-soluble polysaccharide copolymer, has been successfully used for 3D cell culture. Alginate hydrogels are biocompatible, non-immunogenic, and hydrophilic (Fedorovich et al., 2007). Song et al. (2015) differentiated iPSCs into hepatocyte-like cells in a 2D environment, then co-aggregated them with stromal cells in a matrix-free environment, and then encapsulated the generated 3D organoids in alginate capsules and transplanted them into mice. The transplanted organoids demonstrated high albumin and α-antitrypsin secretion compared with primary human hepatocytes. Nanofibrillar cellulose hydrogel (also called cellulose nanofibril hydrogel, CNF) is a plant-origin xeno-free, non-toxic, and biocompatible hydrogel that has been successfully implemented for the 3D culture of human PSCs (Lou et al., 2014). Recently, CNF hydrogel was used to generate human adult liver-derived LOs (Krüger et al., 2020). The CNF was used for LO expansion due to its mechanical properties. It also provides a supportive environment to induce LOs to functional hepatocyte-like cells. Thus, the CNF hydrogel presents a viable alternative to Matrigel for clinical use.

Unlike natural biomaterials mentioned above, synthetic scaffolds possess adjustable features and users can modify stiffness, swelling rate, etc., as well as modify the scaffold with functional groups. A well-defined composition of synthetic scaffolds provides reproducible results. Ng et al. (2018) used inverted colloidal crystal scaffolds with type I collagen coating for the maturation of iPSC-derived hepatic progenitors. They have proved that the morphological and transcriptomic features of those hepatic progenitors were reached and overrode the liver characteristics level of the spheroids cultured on Matrigel. Pore size was claimed as an important factor that allowed cells to form spheroids. They demonstrated that the most optimal pore diameter for this purpose is 140 μm. The appropriate ECM-mimicking coating was shown necessary for the cell attachment when the scaffold is formed from the biologically inert material.

Ye et al. (2020) have recently provided a novel hydrogel based on polyisocyanopeptides and recombinant human laminin-111, which is promising for human adult liver-derived LO culture over at least 14 passages. Moreover, they have recently shown that the elasticity of tissue ECM is critical to many cell types. It is believed that ECM elasticity can help cells develop and function (Sorrentino et al., 2020). By adjusting the composition and elasticity of an artificial matrix, we can simulate the properties (e.g., elasticity, extensibility) of the target tissue through the composition of the ECM. This result is of great significance to the maintenance of cell viability and function, the establishment of disease models, and tissue repair and regeneration.

In summary, matrix-based culture condition needs to be further improved to exclude immunogenic and clinically unacceptable matrix and biomaterials, so as to be used for regenerative medicine and transplantation.

Matrix-free systems

Matrix-free or biomaterial-free 3D culture does not have any problems related to xenogeneic matrix and thus can be easily adapted for clinical applications. Ogawa et al. (2013) demonstrated that the maturation of hepatocyte-like cells can be increased through the transferring of human ESC-derived hepatocyte-like cells to the matrix-free suspension environment. Another study also formed LOs by aggregating PSC-derived hepatocyte-like cells (Sgodda et al., 2017). In this case, hepatocytes aggregated into organoids within 12 h. This protocol allows better control of the differentiation in 2D, and subsequent transfer into 3D culture led to the continuation of the differentiation that was determined by the change of the expression pattern of maturation genes. The authors also demonstrated the importance of size control of the LOs, indicating that the increase in the size is associated with the decrease in the hepatic functions.

In conclusion, for applications in regenerative medicine, the major xenogenic materials used in PSC-LO generation are biomaterials, such as Matrigel, which should be replaced with clinically acceptable biomaterial or removed when using suspension culture system.

Genetic and Epigenetic Instability

The iPSC technology offers full of promise for cell therapy (Takahashi et al., 2007; Yu et al., 2007; Mandai et al., 2017). The differentiation of iPSCs can generate tissue-specific cells for transplantation, and can also apply to *in vitro* studies and drug development (Grskovic et al., 2011; Inoue and Yamanaka, 2011; Plummer et al., 2019). One of the most important safety issues particularly related to the *in vivo* applications of PSC-derived cells are genetic and epigenetic instability, resulting in variations. These variations can occur at distinct levels, mainly during the generation and maintenance of iPSCs and the differentiation and expansion of iPSC-derived cells. The genetic and epigenetic variations or unstable chromosomes may change the characteristic of iPSCs and affect differentiation capacity (Nishizawa et al., 2016), yet the instability has not been fully elucidated.

Variations introduced into induced pluripotent stem cells

The variations may originate from the heterogeneous genetics of source cell population (Huang, 2009). Moreover, if some specific variations in source cells effectively promote reprogramming, these variations will be amplified in the derived iPSCs

(Cahan and Daley, 2013; Kilpinen et al., 2017). Burrows et al. (2016) compared human iPSC lines from two somatic cell types of four donors in terms of DNA methylation and gene expression and found that genetic variation between donors, but not between cell types, is the main cause for the differences between iPSC lines. By studying 711 human iPSC lines, Kilpinen et al. (2017) have found that 5–46% of variations were originated from differences between individuals (Cahan and Daley, 2013).

In addition, reprogramming protocols may introduce new variations by increasing mutations. Integrative vectors, such as lentivirus and retrovirus, can randomly integrate into the genome of iPSCs to interrupt endogenous gene expression and reactivate transgenes to lead to tumorigenesis, whereas non-integrating vectors, such as Sendai virus, adenovirus, and adeno-associated virus, induce transient expression of transcription factors. A whole exome sequencing study identified mutations in human iPSCs, of which 75% occurred during reprogramming process (Ji et al., 2012). Although the exact reason for mutagenesis was not identified in the study, retrovirus used in reprogramming could be one of the drivers. On the contrary, a later study compared three reprogramming methods, namely retrovirus, Sendai virus, and synthetic mRNA and found that the number of genetic variants identified by whole genome sequencing was moderate and did not differ between reprogramming methods (Bhutani et al., 2016). The authors concluded that reprogramming was unlikely to make human iPSCs unacceptable in cell therapy. Nonetheless, non-integrative vectors are recommended in clinical applications.

Like ESCs, iPSCs maintenance may introduce genetic or epigenetic alterations into cells. During iPSC culture, there were genetic variations among different passages or among different populations (Mayshar et al., 2010; Amps et al., 2011). These studies found that the level of overexpressed genes increased with the increased passage number and in some case, normal iPSCs at lower passage number exhibited gains in some chromosomes. Genetic and epigenetic variations preexisting in source cells or being introduced during reprogramming are subjected to selection in prolonged culture (Liang and Zhang, 2013). A high-resolution single nucleotide polymorphism genotyping study has found that duplications of oncogenes tend to accumulate during prolonged passaging of human iPSCs (Laurent et al., 2011). An unbiased study using clonal culture has identified oxidative stress as the trigger for mutation accumulation during passaging and showed that the mutation rate in human iPSCs was lower than that in human intestinal and liver stem cells (Kuijk et al., 2020).

Variations introduced into induced pluripotent stem cells-derived cells

Genetic and epigenetic instability introduced during the differentiation of human PSCs has not been well investigated. A study using human parthenogenetic stem cells has accessed instability during a serial round of differentiation and reprogramming, i.e., differentiating parthenogenetic stem cells into parthenogenetic mesenchymal stem cells via the formation of embryoid body and reprogramming parthenogenetic mesenchymal stem cells into iPSCs using retrovirus-mediated delivery of OCT4, SOX2, KLF4, and c-Myc (Vassena et al., 2012). When comparing the first-round parthenogenetic mesenchymal stem cells with the second-round parthenogenetic mesenchymal stem cells by microarray analysis, the authors found more than 3,000 differentially expressed genes and concluded that these differences were introduced during reprogramming, though no evidence was provided to show the differences appeared during reprogramming, not during differentiation. Nonetheless, this study draws our attention that genetic and epigenetic instability should be examined throughout the process of reprogramming and differentiation to ensure safe cell therapy in regenerative medicine.

Impact of genomic instability and coping strategies

Many researchers have proven that different lines of iPSCs have diverse differentiation and developmental capability (Polo et al., 2010; Tsuji et al., 2010; Boulting et al., 2011; Kim et al., 2011; Liang and Zhang, 2013). This diversity is caused by cell of origin or genetic and epigenetic variations in iPSCs. Some of these variations may result in potential abnormalities in iPSC differentiation and induction, and thereby causing phenotypic changes and functional deficiencies, which pose risks in their *in vivo* applications as well as problems in disease modeling and drug development (Mekhoubad et al., 2012).

There are some coping strategies to reduce the iPSC variability, such as reducing the causes of variations in source cells and optimizing reprogramming methods and culture conditions. First, the preexisting mutations in source cells vary with the cell of origin. Ultraviolet-induced somatic mutations in skin fibroblasts were found in fibroblast-derived human iPSCs (D'Antonio et al., 2018). For this reason, hematopoietic stem cells show advantages over skin fibroblasts as a safe cell source (Wang K. et al., 2019). Second, reprogramming method should be carefully selected regarding integration, genomic instability, and tumorigenesis issues. Third, it is necessary to acquire enough cell numbers of iPSCs for differentiation studies and applications. In light of this purpose, genetic and epigenetic variations in iPSCs should be detected and monitored throughout passages (Martins-Taylor et al., 2011). Assou et al. (2020) have developed a test which can potentially detect more than 90% of human PSC recurrent genetic abnormalities from long-term culture and can be used to routinely screen genomic integrity in human PSCs. The test was established based on a large dataset of reported genetic and epigenetic abnormalities and uses droplet digital PCR technology which greatly simplifies the regular and systematic hPSC monitoring. In addition, it would be ideal to set up a bank of human iPSC and ESC lines, in which each line is maintained as a homogeneous and genetically stable population. To set up a transgene-free human iPSC bank enabling high-throughput generation and rapid expansion to meet industrial and clinical demands, Valamehr et al. (2014) have established a platform using small molecule pathway inhibitors in feeder-free culture condition. Further studies should focus on clarifying the genetic and epigenomic stability during the *in vitro* differentiation process, such as using chemically defined reagents to reduce variability and optimal

oxygen condition, for the safe application of iPSCs-derived cells in regenerative medicine.

Genome Editing

Genome editing can be used to add, remove, or edit DNA of cellular genome to alter the characteristics of a cell or an organism, and it has the potential to both improve our understanding of human genetics and cure genetic diseases (Hou et al., 2013; Ran et al., 2015). The most used tool of genome editing is the RNA-guided CRISPR-Cas9 nuclease system that has emerged in recent years representing a system that is easy to design, highly specific, efficient, and suitable for high-throughput and multiplexed gene editing.

Since the establishment of human iPSCs, researchers had hoped to use patient's own iPSC-derived cells in regenerative medicine. However, there are four problems in autologous iPSC-based cell therapy: (1) the process of establishing autologous cell therapy is complex, time-consuming, and costly. This expensive treatment is difficult to promote and attract pharmaceutical companies to develop. (2) Autologous cell therapy is difficult to standardize. Quality control faces great challenges. (3) Autologous cell therapy cannot treat acute diseases, such as acute liver failure. (4) In the process of differentiation, the immunogenicity of autologous iPSCs will change, and the generated cells may not be immunotolerant as reported earlier (Zhao et al., 2015). On the contrary, allogeneic cells are easier to be standardized as a treatment, and can be mass produced into off-the-shelf products. However, immune rejection in allogeneic cell transplantation remains to be overcome. HLA matching iPSC lines have been established for allogeneic cell transplantation (Okita et al., 2011; Taylor et al., 2012). In recent years, scientists have established several methods to overcome the immune rejection of allogeneic PSCs. For example, CRISPR-Cas9-mediated destruction of HLA gene enhanced the immune compatibility of iPSCs (Hong et al., 2017; Xu et al., 2019; Lee et al., 2020). These studies about allogeneic human PSC-derived cells without immune responses as cell therapy open a new avenue toward regenerative medicine.

Allogeneic PSC-LO-induced immune rejection is primarily mediated by T cells. Strategies to regulate T cell costimulatory and inhibitory pathways can prevent immune rejection. A study using monoclonal antibodies to block T cell costimulation has shown immune tolerance of human ESC-derived pancreatic endoderm cells in mice (Szot et al., 2015). However, this strategy has a potential risk for cancer and infection.

Despite the obvious advantages that gene-edited iPSC-based cell therapy has, challenges like off-target, mutagenesis, tumorigenesis, and ethical debate may still exist. One of the major causes of the off-target effects of the CRISPR system is the continusly expressed Cas9 proteins in cells (Fu et al., 2013). Random integration resulted from off-target effects can potentially develop insertional mutagenesis and subsequent tumorigenesis of transplanted cells. Thus, in order to reduce the off-target effects caused by Cas9 overexpression, strategies, such as decreasing the amount of undesirable DNA cleavage or suppressing the activity of Cas9 protein, have been suggested (Nuñez et al., 2016). The use of a high-fidelity Cas9 variant is another strategy to reduce off-target events (Kleinstiver et al., 2016). We recently developed a Cas9 mRNA-based CRISPR genome editing method to efficiently edit human PSCs (Leung et al., 2020). We show that Cas9 existed in cells in a short period time. Like Cas9 ribonucleoprotein, our method can produce cells without foreign gene integration and thus can be easily translated into clinical applications. Thus, gene-edited PSCs together with organoid technology provide more opportunities in regenerative medicine.

Large-Scale Expansion for Transplantation

For future therapeutic applications of human PSC-derived liver cells, the number of cells required for each transplantation will be quite large, about one tenth of the liver mass which is approximately 10^9 cells (Sharma et al., 2011). An earlier strategy was to expand human PSCs, and more recently researchers have found some ways to expand differentiating PSCs at certain developmental stages, such as endodermal cells using defined growth factors (Raju et al., 2017) and hepatoblasts by combining growth factors and small molecules (Zhang et al., 2015). These expanding hepatoblasts maintain phenotypes during long-term culture and can differentiate into mature hepatocytes and bile duct cells. The aim was to generate a source for cell therapy of liver diseases.

Organoid technology has recently been used to expand various types of cells *in vitro*. Wang S. et al. (2019) developed a differentiation cocktail medium for the differentiation of human ESCs into LOs with high expansion ability. Hepatic progenitors derived in 2D culture conditions were embedded in Matrigel and treated with a unique combination of B27, EGF, Wnt-3A, Forskolin, N2, Nicotinamide, N-acetylcysteine, R-spondin, Gastrin, and A83-01 compound. This approach allowed long-term subculture of the resultant organoids (up to 20 passages) that remained stable after freezing-thawing procedures and mass-scale production of cells which is necessary for industrial applications. Another study showed that self-aggregated PSC spheroids formed in agarose microplates can differentiate in suspension into 3D liver tissue whose phenotype was stable for over 1 year without detectable tumorigenic activity after transplantation (Rashidi et al., 2018). The ability of the long-term culture of human PSC-LOs that remain their functional activity is one of the main advantages over primary human hepatocyte-derived organoids due to the limited supply of primary human liver tissue from healthy or diseased liver donors. Other researchers have generated LOs from human PSC-derived endoderm cells in 2 weeks and expanded them in Matrigel for more than 16 months without loss of differentiation capacity (Akbari et al., 2019). LOs spontaneously formed from 2D culture of differentiating human PSCs were expanded in Matrigel for 1 year while maintaining their karyotype and phenotype (Mun et al., 2020).

In summary, great efforts have been made to expand differentiating cells for large-scale production. However, the use of Matrigel must be replaced by a xeno-free matrix or biomaterial to meet clinical requirements. For regenerative

medicine, expansion in suspension culture (Rashidi et al., 2018) seems superior than Matrigel culture.

Transplantation and *in vivo* Engraftment

Cell transplantation has potential for end-stage liver diseases (Tsuchida et al., 2020). Human PSC-LOs as a new source for cell transplantation is innovative but still at the preclinical stage. During the process of transplantation, the homing and survival of transplanted cells are major factors determining the success of transplantation. At present, there are no standard protocols defining the differentiation status of transplanted cells (fetal stage or mature stage), cell formulation (single cell suspension, organoid suspension, or biomaterial-based construct), transplantation site (systematic, orthotopic, or ectopic), and delivery technique (injection, infusion, or implantation).

The most commonly used method to deliver liver cells or LOs is injection, which involves intraportal injection, intravenous infusion, intramuscular injection, or intrasplenic injection. Intrasplenic or portal venous infusion can hardly control engraftment efficiency and avoid ectopic engraftment because transplanted cells first enter the blood circulation before reaching the liver. A recent preclinical study in pigs has reported that the ligation of the patent ductus venosus before portal venous infusion can inhibit extrahepatic translocation (Tsuchida et al., 2020). In intrasplenic transplantation, more than 70% transplanted cells are rapidly removed by resident immune cells (Gupta et al., 1999). An earlier study has found that the disruption of sinusoidal endothelium can facilitate the integration of transplanted cells into the liver (Gupta et al., 1999). Rashidi et al. (2018) transplanted human PSC-LOs in two ways, intraperitoneal injection and subcutaneous implantation with the aid of a polycaprolactone scaffold. Both methods improved the liver functions of diseased recipient mice, but the authors did not compare these two methods, only suggesting that ectopic implantation is less invasive. Tsuchida et al. (2019) recently reported that human iPSC-LO transplantation via the portal vein had good retention of organoids in the liver, whereas single cells of LOs translocated to the lung. Some studies have found that immature cells can further become mature once transplanted *in vivo* (Takebe et al., 2013), but there is still no solid evidence on the differentiation status of transplanted cells for the best functional engraftment while avoiding tumorigenesis of immature cells.

As an alternative to liver organ transplantation for liver failure, liver cells or LOs could directly implanted to the liver orthotopically. Nagamoto et al. (2016) have implanted a cell sheet composed of human iPSC-derived hepatocytes onto the liver surface of recipient mice with acute liver injury induced by CCl_4. The orthotopic cell sheet transplantation exhibited better cell retention than intrasplenic injection, and thus had increased engraftment rate and efficacy. The authors also pointed out that a large number of cells can be transplanted using the cell sheet technology. To deliver LOs by the cell sheet technology, LOs need to be dissociated into single cells and then cultured in 2D to form a cell sheet. However, dissociation of LOs will disrupt tissue structure and may be incompatible with LO technology.

Despite many innovative transplantation methods, the low engraftment efficiency might be due to poor integration of human iPSC-derived cells to the local environment or the lack of vasculature in LOs. To evaluation transplantation and engraftment efficiency, we need non-invasive *in vivo* cell tracking methods (see the section below) (Tsuchida et al., 2020).

In vivo Cell Tracking

Real-time monitor of transplanted cells or organoids *in vivo* is necessary to study the fate of transplanted cells and evaluate engraftment during preclinical studies (Watson et al., 2014; Jung et al., 2018; Hsia et al., 2021). Ideally a reporter with highly sensitive 3D tomography is needed to non-invasively measure the engraftment of transplanted hepatic cells. Non-invasive measurement allows short, long-term, and repeated monitoring transplanted cells *in vivo*. The signal of an ideal reporter needs to last long and have resolution in certain depth to reach internal organs and at micrometer scale to localize cells. A study showed that human sodium iodide symporter (hNIS) can serve as such a reporter and can utilize radiotracers already available for clinical use to enable positron emission tomography or single photon emission computed tomography (Ashmore-Harris et al., 2019). In this study, human iPSC-derived immature hepatocytes were transduced with lentivirus containing dual-mode radionuclide-fluorescence hNIS-mGFP reporter gene followed by further differentiation *in vitro* and transplantation *in vivo*. The signal of hNIS-mGFP reporter was stable and indicating the transplanted cells precisely homing to the liver, but the signal became undetectable 1 week later due to cell death in the *in vivo* environment.

Another *in vivo* tracing technology is Raman spectroscopy-based modality that can mine data, such as proteomic and chemogenomic data. Coherent Raman scattering (CRS) microscopy is a high-speed vibrational imaging system that can visualize the chemical content of a living specimen. The major technique in CRS is coherent anti-Stokes Raman scattering (CARS) (Reintjes et al., 1982). With technical advances on hyperspectral CARS microscopy, researchers have provided many innovation studies on organoids. Pope et al. (2021) have investigated a complex multicellular system of LOs by using correlative two-photon fluorescence and hyperspectral CARS microscopy. Their most interesting finding is that organoids could be maintained alive under hyperspectral CARS measurements. In addition, they have established a method for label-free identification of chemically distinct subpopulations, which can be used to analyze and validate the quality of clinical cell transplantation. These studies emphasize the future of quantitative hyperspectral CARS microscopy as an empowering technology in regenerative medicine, showing the way to novel possibilities for non-invasive disease diagnosis.

In conclusion, to develop human PSC-LOs as a therapeutic product, safety, efficacy, and controllable quality must be fulfilled. Safety consideration includes genetic and epigenetic stability, non-xenogenicity, immune tolerance, and non-tumorigenesis. Efficacy is influenced by PSC-LO quality and delivery method. It still remains unclear on the effect of human PSC-LOs

transplanted into the liver. Non-invasive *in vivo* cell tracking methods can help evaluate engraftment efficiency and cell fate.

Disease Modeling and Drug Development

Organoid technology is a powerful tool for the study of human diseases. LOs generated from patient-derived or genome-edited PSCs have the ability to model liver diseases, to screen drug candidates, and to test their toxicity. Liver is the main organ for drug metabolism and transport. It is also the main target organ of drug toxicity. An adverse drug reaction Peng et al. (2018) is an undesirable side effect of a drug and is classified as dose-dependent or idiosyncratic drug-induced damage. Historically, toxicology research has relied on animal models to characterize the toxicity of new compounds. However, animal models are not perfect systems for human toxicity, and it can only predict 50% of DILI in humans. Thus, human toxicity prediction models are urgently needed. Primary adult human hepatocytes are the "gold standard" for evaluating drug metabolism and toxicity. However, due to their limited availability and proliferation capacity, alternative *in vitro* models are needed. Human PSCs represents an unlimited cell source for all the cell types in human body and are expected to generate *in vitro* models for drug discovery and development (Lin et al., 2021). The applications of human PSC-derived liver cells include liver disease modeling, drug metabolism, and hepatotoxicity study. As mentioned in see section "Introduction," PSC-LOs show superior structural and functional advantages over 2D cultured PSC-derived liver cells. Guan et al. (2017) estabilished a disease model of JAG1 mutations based on human iPSC-LOs with bile duct–like structures. They adopted iPSC-based organoid system and genome editing technology to show the effect of mutations on human genetic diseases. For disease modeling and drug development, a number of challenges related to human PSC-LOs remain to be overcome. The major challenge of human PSC-LOs is immaturity of hepatocytes derived from current differentiation protocols (Lynch et al., 2019). Heterogeneity is another problem related to organoid technology in general (Lou and Leung, 2018), which reduces reproducibility of drug screening and testing. Building PSC-LOs with multiple cell types to mimic liver tissue complexity is another goal, which is particularly necessary when modeling liver diseases involving several cell types or studying DILI as hepatocyte damage is caused not only by direct toxic effect of drugs but also by indirect effect of non-parenchymal cell response.

Immaturity

Mature PSC-LO models should show basic liver functions and tissue environmental characteristics. The studies focusing on liver development have contributed to establishing PSC induction methods and mimicking the environment for fetal liver cell development and growth. Liver matures during perinatal period. However, due to the limited knowledge on perinatal human liver development, the immaturity of human PSC-LOs still remains an unsolved problem. This problem hinders their applications in disease modeling and drug development. Currently, the differentiation of hepatic progenitors is mediated by HGF, oncostatin M (Prodanov et al., 2016), and dexamethasone, but the resultant hepatocytes exhibit fetal liver features (Baxter et al., 2015), such as the expression of fetal marker alpha-fetoprotein (Lucendo-Villarin et al., 2020) and lower activity of CYP3A4 than primary hepatocytes (Lee et al., 2021).

In recent years, researchers have improved the hepatic maturation of human PSC-LOs by using different factors and small molecules. According to the changes in liver microenvironment at postnatal stage, researchers have found that microbial short-chain fatty acids could improve the metabolic functions of human PSC-LOs (Mun et al., 2021). Wu et al. (2019) have firstly established functional hepatobiliary organoids from human iPSCs. 25% of mTeSRTM culture medium was replaced with RPMI-1640/B27 minus insulin at differentiation stages to induce hepatic and biliary co-differentiation, then 10% cholesterol^{+} MIX was added to promote maturation. Cholesterol^{+} MIX is a preparation from Chinese medicine products, mainly comprised of cholesterol and other small molecules.

In addition, the role of non-parenchymal cells in liver maturation has also drawn attention. Asai et al. (2017) observed that iPSC-derived hepatic endoderm cells directly interacted with human umbilical vein endothelial cells (HUVECs) and mesenchymal stem cells during liver organoid morphogenesis. At the same time, HUVECs might also exert paracrine effects, such as secreting HGF, to promote hepatocyte differentiation. Another study shows that non-parenchymal cells, namely mesenchymal stromal cells and endothelial cells, improved the hepatic maturation of human PSC-LOs by decreasing TGF-β and Wnt signaling pathways (Goulart et al., 2019).

ECM plays an important role in cell differentiation and organogenesis and may improve hepatic maturation of PSC-LOs. Zahmatkesh et al. (2021) efficiently improved hepatic maturation of LOs by mixing microparticles made of decellularized liver matrix with human PSC-derived endoderm cells, mesenchymal stromal cells, and HUVECs.

In conclusion, researchers in the past few years have made efforts to improve hepatic maturation of human PSC-LOs by applying small molecules found in the liver microenvironment during postnatal stage, incorporating non-parenchymal cells, and utilizing ECM components or bioengineering techniques (**Table 2**). The measurements indicating liver maturity vary a lot among different studies, from synthetic functions to metabolic functions. In some studies, the measurements were not compared with the primary adult human hepatocytes, and thus it is uncertain how mature these LOs are and whether they can be a valid model in disease modeling and drug development. The liver mature features should be selectively measured according to the intended applications of human PSC-LOs. We believe that with the better understanding of *in vivo* liver maturation, we will be able to generate PSC-LOs mature enough for drug screening and toxicity testing.

Heterogeneity

Heterogeneity refers to cellular, morphological, and functional non-uniformity of PSC-LOs. Heterogeneity during multi-step

TABLE 2 | Strategies for improving maturity of human PSC-LOs.

Strategies	Cell types	Key methods	Representative maturation measures	Model	Comparison	References
Soluble factors	iPSC-derived hepatocytes	Acetate, propionate, and butyrate combination in hepatic medium and differentiation medium	Increased CYP3A4 activity and ALB secretion	Drug-induced liver injury	iPSC-LOs were less sensitive than PHHs to troglitazone-induced toxicity, but HepG2 was not sensitive.	Mun et al., 2021
	iPSC-derived hepatocyte- and cholangiocyte-like cells	25% mTeSR in endoderm medium and 10% cholesterol+ MIX (Chinese medicine) to maturation medium	Bile duct structure and production and transport of bile acids	Hepatobiliary organogenesis	The maturity of iPSC-LOs was between fetal liver and adult liver.	Wu et al., 2019
Co-induction	PSC-derived hepatocytes and cholangiocytes	Hepatic endoderm spheroids were differentiated into hepatoblast spheroids, which were dissociated and seeded in an ultra-low attachment plate to form LOs.	Functional bile canaliculi system	NASH model	Free fatty acid-treated PSC-LOs showed similar gene expression signatures to NASH patients.	Ramli et al., 2020
	Healthy and Wolman diseased PSC-derived hepatocytes-, stellate-, and Kupffer-like cells	PSC spheroids embedded in Matrigel were stepwise differentiated into LOs.	LOs can be induced by free fatty acid to have inflammatory and fibrotic responses. All cell types in LOs are functional.	NASH/Fibrosis model; Wolman LO model	Wolman LOs exhibited more aggressive fibrosis phenotypes than Wolman disease patients.	Ouchi et al., 2019
Co-culture	iPSC-derived hepatocytes, HUVECs, and MSCs	iPSC-derived hepatic endoderm, HUVECs, and MSCs self-organized into 3D liver buds (LBs).	Vascularized and functional human liver	Regenerative medicine	iPSC-LBs produced higher levels of albumin than human adult hepatocytes *in vivo*.	Takebe et al., 2013
	iPSC-derived hepatocyte-like cells, HUVECs, and MSCs	Hepatic-specified endoderm co-cultured with HUVECs and MSCs without cell-cell contact.	After no cell-cell contact co-culture, hepatocyte-like cells had polarity and bile acid transport structure.		Some genes were not upregulated when compared with primary hepatocytes.	Asai et al., 2017
	iPSC-derived hepatocyte-, endothelial-, and MSC-like cells, dental pulp-derived-MSCs, and human aortic endothelial cells	Five different cell types were mixed to generate four organoid groups.	The greatest difference between four groups is the expression of phase I and phase II enzymes.		Both iPSC-derived non-parenchymal cells and adult non-parenchymal cells improved hepatic functions by mediating Wnt and TGF-β pathways. No comparison with primary hepatocytes was shown.	Goulart et al., 2019

(Continued)

TABLE 2 | (Continued)

Strategies	Cell types	Key methods	Representative maturation measures	Model	Comparison	References
Biomaterials and bioengineering	PSC-derived hepatocyte-like cells, HUVECs, and UC-MSCs	PSC-derived hepatic endoderm, HUVECs, and MSCs were mixed with liver decellularized matrix-derived microparticles to form LOs	Microparticles improved the maturation and metabolic capacity of PSC-derived hepatocytes.	Transplantation	No comparison with primary hepatocytes was shown.	Zahmatkesh et al., 2021
	iPSC-derived hepatocytes and iPSC-derived endothelial cells	Hepatocytes and endothelial cells were encapsulated in separate domains of fibers containing chitin, alginate, galactose, and collagen.	Integration with host vasculature *in vivo*	Liver tissue engineering	No comparison with primary hepatocytes was shown.	Du et al., 2014
	PSC-derived hepatoblasts	Hepatoblasts seeded in 500-μm diameter microwells to form uniformly sized hepatocyte-like cell (HLC) spheroids	HLC spheroids had sensitivity to various hepatotoxicants	Drug hepatotoxicity	Eight of the fifteen compounds showed higher cytotoxic activity to HLC spheroids when compared with primary hepatocytes	Lee et al., 2021

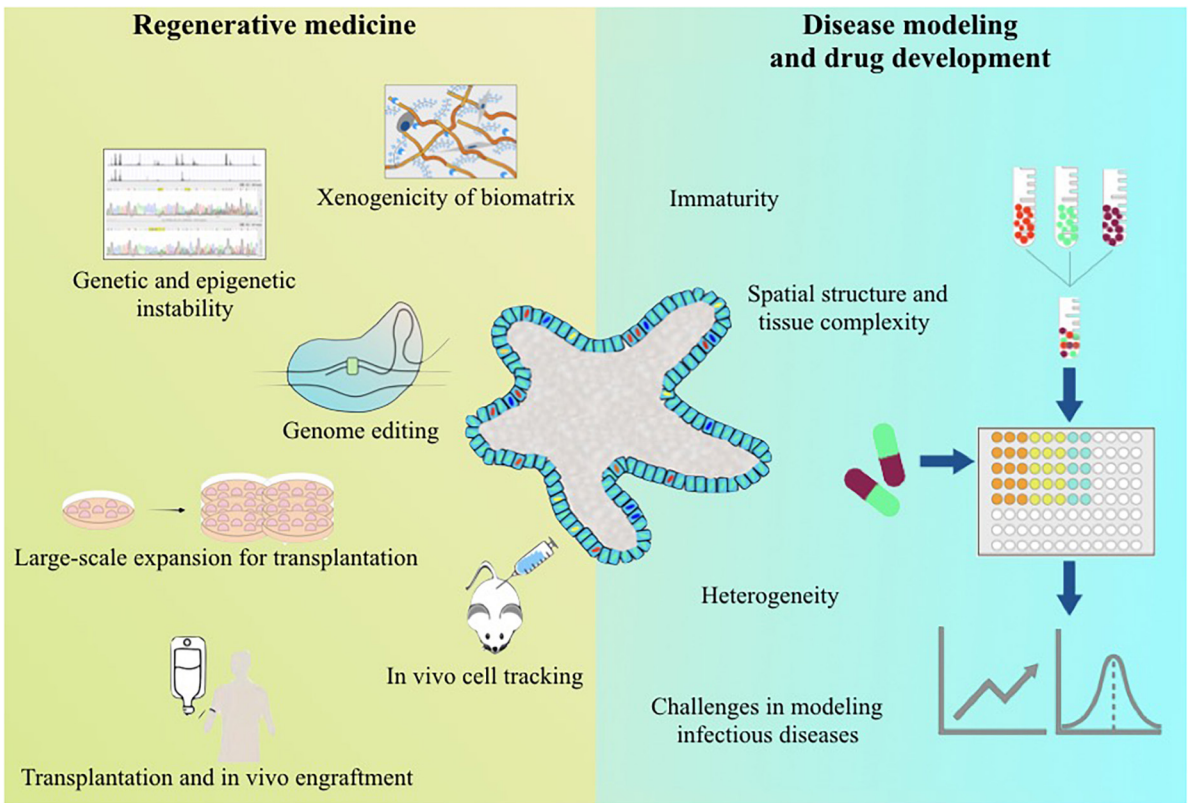

FIGURE 1 | Summary of the current challenges for the applications of human pluripotent stem cell-derived liver organoids.

stem cell differentiation is a common problem and becomes even more problematic at the maturation stage of PSC differentiation into LOs. In disease modeling and drug testing, LO heterogeneity can decrease reproducibility of screens and tests. To overcome this issue, researchers have fabricated microwells to control spheroid size and uniformity (Takebe et al., 2017). Silicone microwells were recently used to generate uniform hepatocyte spheroids from human PSCs (Lee et al., 2021). These spheroids were more sensitive to liver toxins than 2D hepatocytes in image-based testing. Another study using agarose microplates also generated uniformly sized liver spheres containing human PSC-derived hepatic progenitors, hepatic stellate cells, and endothelial cells (Lucendo-Villarin et al., 2020). By utilizing automated platform, the researchers showed reduced variation and increased throughput. 3D bioprinting is a technology that uses thin layers of the cells and other components arranged on top of each other to form a complex biological structure. Because of the tools for the precise control of the process of tissue generation, and, therefore, the ability to create complex tissue patterns, 3D bioprinting has become a promising technology for transplantation, fundamental and applicable research. The most known bioprinting methods are laser pulses, extrusion, and inkjet (Kryou et al., 2019). One of the issues of 3D bioprinting for today is promoting the vascularization of a printed organ because organoids often fail to recapitulate the functionality of primary hepatocytes in the absence of vascularization. This can be solved by integrating microfluidics into bioprinting. Another issue is the stress to cells generated by 3D bioprinting tools (Faulkner-Jones et al., 2015).

Spatial Structure and Tissue Complexity

The majority of studies have focused on the generation of hepatocyte-like cells. However, the liver consists of multiple cell types, and for the better replication of liver structure, many recent projects have developed protocols that can produce LOs consisting of different liver cell types. A pioneer study generated 3D human liver buds by combining human iPSC-derived hepatic endoderm cells, mesenchymal stem cells, and HUVECs (Takebe et al., 2013). The hepatic functions of the generated liver buds were assessed both *in vitro* and after transplantation in mice with a liver failure model. Interestingly, interactions between multiple germ layer derivatives not only increased organoid complexity but also improved functionality. *In vivo* transplantation showed a spatial pattern expressed by these liver buds and reversed drug-induced lethal liver failure (Takebe et al., 2013, 2017). However, the organoid structure did not fully recapitulate the spatial organization of the liver, and the spatial structure also varies among organoids. Other studies also demonstrated that the combination of hepatocytes with non-parenchymal cells provided signaling interactions between cells that positively affected hepatic functions (Du et al., 2014).

Recently, Ramli et al. (2020) embedded single posterior foregut cells derived from human PSCs in Matrigel to form hepatic endoderm spheroids. Further treatment with BMP4, BMP7, and FGF7 resulted in the formation of hepatoblasts spheroids. Then, the dissociated hepatoblast spheroids were seeded into 96-well plates to form hepatic organoids consisting of hepatocytes and biliary cells with bile canaliculi. These two-cell type LOs were used in the study of nonalcoholic steatohepatitis (NASH) (Ganesh et al., 2019). Ouchi et al. (2019) took a different approach to generate multicellular LOs for the study of steatohepatitis. They first established foregut organoids from PSCs, which consisted of both endoderm and mesoderm derivatives. The foregut organoids were further differentiated into LOs composed of hepatocytes, stellate cells, and Kupffer cells. These LOs exhibited the feature of steatohepatitis when stimulated by free fatty acids. Diseased PSC-LOs were shown to be suitable for studying individualized therapy of human liver fibrosis.

Metabolic zonation is a unique feature of the liver. Liver zonation is regulated by oxygen gradient (Kietzmann, 2017), Wnt/β-catenin signaling (Planas-Paz et al., 2016), and other pathways. Liver zonation makes liver structure highly complex and spatially heterogenous and also makes *in vitro* LO generation more challenging. To our knowledge, the current technology has not been able to generate PSC-LOs mimicking a specific liver metabolic zone. This could be a future research direction to obtain LOs with desired metabolic functions for certain studies. For example, NASH affects lipid zonation and causes cell damage in the pericentral region (Hall et al., 2017). Thus, PSC-LOs representing the pericentral region would be useful in modeling NASH. Oxygen and lipid gradient created by a microfluidic chip was used to study the progress of NASH in rat primary hepatocytes (Bulutoglu et al., 2019). This microfluidic device could be integrated with human PSC-LOs consisting multiple cell types to study intercellular crosstalk during the development of NASH. Ahn et al. (2019) developed a channel system in which HepaRG cells were grown under a concentration gradient of CHIR99021, an inducer of Wnt/β-catenin pathway. This gradient created hepatic zonal environment that made HepaRG cells respond to toxic drugs differently, cells in the zone-3 region showing sensitivity to hepatotoxic drugs. It is known that ECM composition exhibits zone-dependent distribution. By adjusting ECM proportion on silk scaffold, researchers have created a hepatic zonation model that was tested with rat hepatocytes (Janani and Mandal, 2021). These are interesting models worth exploiting with human PSC-LOs to test zonal toxicity of drugs.

Challenges in Modeling Infectious Diseases

Due to species-dependent features of many human hepatotropic pathogens, human cells *in vitro* or in humanized chimeric animals are the only valid models to study pathogen infection and to develop therapies. Various models based on 2D or 3D cultured human primary hepatocytes, immortalized hepatic cells, and human PSC-derived hepatocytes either alone or combined with non-parenchymal cells have been established (Gural et al., 2018; Arez et al., 2021).

Earlies studies have shown the infection and replication of hepatitis C virus (HCV) in human PSC-derived hepatocytes, though these cells were not fully mature as evidenced by the expression of fetal liver markers (Roelandt et al., 2012; Schwartz et al., 2012). By closely examining HCV infection during differentiation, Wu et al. (2012) have found that undifferentiated

human PSCs and DE cells were not permissive for HCV infection, but hepatic progenitors were readily infected with HCV. These studies present the application value of human PSC-derived hepatocytes in modeling HCV infection despite their unsatisfying maturity. Additionaly, when using iPSCs from patients with genetic diseases, this model can be used to study how genetic alteration affects HCV infection. Because 3D models can mimic the complexicity of the liver tissue, they show advantages in recapitulating some liver functions that 2D models cannot. However, to our knowledge, human PSC-LOs have not been used in the study of HCV-host interactions.

Primary adult human hepatocytes are the only host cell type for hepatitis B virus (HBV) infection *in vivo*, and thus they are the gold-standard for studying HBV-host interactions (Galle et al., 1994). An earlier study showed that HBV entered differentiated and polarized hepatocytes via basolateral membrane (Schulze et al., 2012). Sodium taurocholate cotransporting polypeptide (NTCP), mediating most of the Na^+-dependent uptake of bile salts in the liver (Stieger, 2011) and being expressed on the basolateral membrane of highly differentiated hepatocytes, has been identified as a receptor for HBV (Yan et al., 2012). Because primary adult human hepatocytes were not able to maintain and expand in long-term culture, improved cell culture systems have been established to study HBV-host interactions *in vitro*. A micropatterned coculture of primary hepatocytes with stromal cells has shown support for HBV infection and enabled to study long-term HBV-host interactions (Shlomai et al., 2014). With this system, the authors have found variations of HBV infection among different donors. To study such variations in an isogenic background, the authors used human iPSC-derived hepatocytes and found that HBV infection occurred in fully differentiated hepatocytes, not in cells at earlier stages of differentiation. The maturation of hepatocytes in PSC-LOs requires assistance of their interactions with non-parenchymal cells (Si-Tayeb et al., 2010). Therefore, reconstruction of these interactions might be a feasible approach to promoting the modeling of infectious disease development. To better understand the life cycle of HBV and to develop effective anti-HBV drugs, Nie et al. (2018) have established a HBV infection model generated from human iPSC-LOs containing PSC-derived hepatocytes, mesenchymal stem cells, and HUVECs in a 3D microwell system. This infection model could support long-term replication of HBV and at the same time exhibit phenotypic alterations in hepatic functions and ultrastructure. Human iPSC-LO may still have some characteristics different from adult hepatocytes, which limits the modeling of authentic infection.

Malaria, caused by *Plasmodium* protozoan parasites, is another infectious disease related to liver. Careful examination of *Plasmodium* infection in differentiating human PSCs has demonstrated that malaria infection started from the hepatoblst stage to hepatocytes (Ng et al., 2015). However, due to the immaturity of human PSC-derived hepatocytes, they have limited potential to test anti-malaria prodrugs that require activation by hepatocyte-specific metabolizing enzymes. Using small chemicals to improve maturation, the authors showed cell response to anti-malaria prodrug primaquine, which indicates the importance of maturity for drug tesing.

In conclusion, human PSC-LOs have not yet been widely used in modeling infectious diseases partly due to their immaturity and shortage of recognition. With the improvement of maturation, PSC-LOs are expected to show more values in the study of infectious diseases and the development of therapies.

CONCLUSION

There is no doubt about the potential values of human PSC-LOs in regenerative medicine, disease modeling, and drug development. However, it has been very slow for human PSC-LOs moving to applications. For regenerative medicine, human PSC-LOs must be safe and effective *in vivo*, which requires the use of xeno-free materials in the generation and expansion of human PSC-LOs, reliable genome editing technique, and effective *in vivo* delivery methods (**Figure 1**). Meanwhile, genetic and epigenetic stability must be monitored thoroughout the generation and culture of PSC-LOs. For disease modeling and drug development, improving maturity, reducing heterogeneity, and increasing complexity are current challenges to be solved (**Figure 1**). By working with biomaterial scientists, bioengineers, pharmacists, and physicists, researchers can nowadays design novel 3D cell culture platforms to make human PSC-LOs suitable for intended applications. All of these will contribute to treating patients with liver diseases.

AUTHOR CONTRIBUTIONS

Y-RL: conceptualization, supervision, project administration, and funding acquisition. Y-RL, MC, and MB: writing—original draft preparation. Y-RL and MC: writing—review and editing. All authors have read and agreed to the published version of the manuscript.

ACKNOWLEDGMENTS

We would like to thank the research funding from Fudan University.

REFERENCES

Ahn, J., Ahn, J.-H., Yoon, S., Nam, Y. S., Son, M.-Y., and Oh, J.-H. (2019). Human three-dimensional in vitro model of hepatic zonation to predict zonal hepatotoxicity. *J. Biol. Eng.* 13, 1–15. doi: 10.1186/s13036-019-0148-5

Akbari, S., Sevinç, G. G., Ersoy, N., Basak, O., Kaplan, K., Sevinç, K., et al. (2019). Robust, long-term culture of endoderm-derived hepatic organoids for disease modeling. *Stem Cell Rep.* 13, 627–641. doi: 10.1016/j.stemcr.2019.08.007

Amps, K., Andrews, P. W., Anyfantis, G., Armstrong, L., Avery, S., Baharvand, H., et al. (2011). Screening ethnically diverse human embryonic stem cells identifies a chromosome 20 minimal amplicon conferring growth advantage. *Nat. Biotechnol.* 29, 1132–1144. doi: 10.1038/nbt.2051

Arez, F., Rodrigues, A. F., Brito, C., and Alves, P. M. (2021). Bioengineered liver cell models of hepatotropic infections. *Viruses* 13:773.

Asai, A., Aihara, E., Watson, C., Mourya, R., Mizuochi, T., Shivakumar, P., et al. (2017). Paracrine signals regulate human liver organoid maturation from induced pluripotent stem cells. *Development* 144, 1056–1064. doi: 10.1242/dev.142794

Ashmore-Harris, C., Blackford, S. J., Grimsdell, B., Kurtys, E., Glatz, M. C., Rashid, T. S., et al. (2019). Reporter gene-engineering of human induced pluripotent stem cells during differentiation renders in vivo traceable hepatocyte-like cells accessible. *Stem Cell Res.* 41:101599. doi: 10.1016/j.scr.2019.101599

Assou, S., Girault, N., Plinet, M., Bouckenheimer, J., Sansac, C., Combe, M., et al. (2020). Recurrent genetic abnormalities in human pluripotent stem cells: definition and routine detection in culture supernatant by targeted droplet digital PCR. *Stem Cell Rep.* 14, 1–8. doi: 10.1016/j.stemcr.2019.12.004

Baptista, P. M., Siddiqui, M. M., Lozier, G., Rodriguez, S. R., Atala, A., and Soker, S. (2011). The use of whole organ decellularization for the generation of a vascularized liver organoid. *Hepatology* 53, 604–617.

Baxter, M., Withey, S., Harrison, S., Segeritz, C.-P., Zhang, F., Atkinson-Dell, R., et al. (2015). Phenotypic and functional analyses show stem cell-derived hepatocyte-like cells better mimic fetal rather than adult hepatocytes. *J. Hepatol.* 62, 581–589. doi: 10.1016/j.jhep.2014.10.016

Bhutani, K., Nazor, K. L., Williams, R., Tran, H., Dai, H., Džakula, Ž, et al. (2016). Whole-genome mutational burden analysis of three pluripotency induction methods. *Nat. Commun.* 7:10536. doi: 10.1038/ncomms10536

Boulting, G. L., Kiskinis, E., Croft, G. F., Amoroso, M. W., Oakley, D. H., Wainger, B. J., et al. (2011). A functionally characterized test set of human induced pluripotent stem cells. *Nat. Biotechnol.* 29, 279–286.

Brooks, A., Liang, X., Zhang, Y., Zhao, C. X., Roberts, M. S., Wang, H., et al. (2021). Liver organoid as a 3D in vitro model for drug validation and toxicity assessment. *Pharmacol. Res.* 169, 105608. doi: 10.1016/j.phrs.2021.105608

Broutier, L., Mastrogiovanni, G., Verstegen, M. M. A., Francies, H. E., Gavarró, L. M., Bradshaw, C. R., et al. (2017). Human primary liver cancer–derived organoid cultures for disease modeling and drug screening. *Nat. Med.* 23, 1424–1435. doi: 10.1038/nm.4438

Bulutoglu, B., Rey-Bedón, C., Kang, Y. B. A., Mert, S., Yarmush, M. L., and Usta, O. B. (2019). A microfluidic patterned model of non-alcoholic fatty liver disease: applications to disease progression and zonation. *Lab Chip* 19, 3022–3031. doi: 10.1039/c9lc00354a

Burdick, J. A., and Prestwich, G. D. (2011). Hyaluronic acid hydrogels for biomedical applications. *Adv. Mater.* 23, H41–H56.

Burrows, C. K., Banovich, N. E., Pavlovic, B. J., Patterson, K., Gallego Romero, I., Pritchard, J. K., et al. (2016). Genetic variation, not cell type of origin, underlies the majority of identifiable regulatory differences in iPSCs. *PLoS Genet.* 12:e1005793. doi: 10.1371/journal.pgen.1005793

Cahan, P., and Daley, G. Q. (2013). Origins and implications of pluripotent stem cell variability and heterogeneity. *Nat. Rev. Mol. Cell Biol.* 14, 357–368.

Collins, S. D., Yuen, G., Tu, T., Budzinska, M. A., Spring, K., Bryant, K., et al. (2019). "In vitro models of the liver: disease modeling, drug discovery and clinical applications," in *Hepatocellular Carcinoma*, ed. J. E. E. Tirnitz-Parker (Brisbane, QLD: Codon Publications).

D'Antonio, M., Benaglio, P., Jakubosky, D., Greenwald, W. W., Matsui, H., Donovan, M. K., et al. (2018). Insights into the mutational burden of human induced pluripotent stem cells from an integrative multi-omics approach. *Cell Rep.* 24, 883–894. doi: 10.1016/j.celrep.2018.06.091

Davidson, M. D., and Khetani, S. R. (2020). Intermittent starvation extends the functional lifetime of primary human hepatocyte cultures. *Toxicol. Sci.* 174, 266–277. doi: 10.1093/toxsci/kfaa003

Deegan, D. B., Zimmerman, C., Skardal, A., Atala, A., and Shupe, T. D. (2016). Stiffness of hyaluronic acid gels containing liver extracellular matrix supports human hepatocyte function and alters cell morphology. *J. Mech. Behav. Biomed. Mater.* 55, 87–103. doi: 10.1016/j.jmbbm.2015.10.016

Du, C., Narayanan, K., Leong, M. F., and Wan, A. C. (2014). Induced pluripotent stem cell-derived hepatocytes and endothelial cells in multi-component hydrogel fibers for liver tissue engineering. *Biomaterials* 35, 6006–6014. doi: 10.1016/j.biomaterials.2014.04.011

Faulkner-Jones, A., Fyfe, C., Cornelissen, D.-J., Gardner, J., King, J., Courtney, A., et al. (2015). Bioprinting of human pluripotent stem cells and their directed differentiation into hepatocyte-like cells for the generation of mini-livers in 3D. *Biofabrication* 7:044102. doi: 10.1088/1758-5090/7/4/044102

Fedorovich, N. E., Alblas, J., de Wijn, J. R., Hennink, W. E., Verbout, A. J., and Dhert, W. J. (2007). Hydrogels as extracellular matrices for skeletal tissue engineering: state-of-the-art and novel application in organ printing. *Tissue Eng.* 13, 1905–1925. doi: 10.1089/ten.2006.0175

Fu, Y., Foden, J. A., Khayter, C., Maeder, M. L., Reyon, D., Joung, J. K., et al. (2013). High-frequency off-target mutagenesis induced by CRISPR-Cas nucleases in human cells. *Nat. Biotechnol.* 31, 822–826.

Galle, P. R., Hagelstein, J., Kommerell, B., Volkmann, M., Schranz, P., and Zentgraf, H. (1994). In vitro experimental infection of primary human hepatocytes with hepatitis B virus. *Gastroenterology* 106, 664–673.

Ganesh, K., Wu, C., O'Rourke, K. P., Szeglin, B. C., Zheng, Y., Sauvé, C. G., et al. (2019). A rectal cancer organoid platform to study individual responses to chemoradiation. *Nat. Med.* 25, 1607–1614. doi: 10.1038/s41591-019-0584-2

Gieseck, R. L. III, Hannan, N. R., Bort, R., Hanley, N. A., Drake, R. A., Cameron, G. W., et al. (2014). Maturation of induced pluripotent stem cell derived hepatocytes by 3D-culture. *PLoS One* 9:e86372. doi: 10.1371/journal.pone.0086372

Giobbe, G. G., Crowley, C., Luni, C., Campinoti, S., Khedr, M., Kretzschmar, K., et al. (2019). Extracellular matrix hydrogel derived from decellularized tissues enables endodermal organoid culture. *Nat. Commun.* 10, 1–14. doi: 10.1038/s41467-019-13605-4

Goulart, E., de Caires-Junior, L. C., Telles-Silva, K. A., Araujo, B. H. S., Kobayashi, G. S., Musso, C. M., et al. (2019). Adult and iPS-derived non-parenchymal cells regulate liver organoid development through differential modulation of Wnt and TGF-β. *Stem Cell. Res. Ther.* 10, 1–11. doi: 10.1186/s13287-019-1367-x

Grskovic, M., Javaherian, A., Strulovici, B., and Daley, G. Q. (2011). Induced pluripotent stem cells—opportunities for disease modelling and drug discovery. *Nat. Rev. Drug Discov.* 10, 915–929. doi: 10.1038/nrd3577

Guan, Y., Xu, D., Garfin, P. M., Ehmer, U., Hurwitz, M., Enns, G., et al. (2017). Human hepatic organoids for the analysis of human genetic diseases. *JCI Insight* 2:e94954.

Gupta, S., Rajvanshi, P., Sokhi, R., Slehria, S., Yam, A., Kerr, A., et al. (1999). Entry and integration of transplanted hepatocytes in rat liver plates occur by disruption of hepatic sinusoidal endothelium. *Hepatology* 29, 509–519. doi: 10.1002/hep.510290213

Gural, N., Mancio-Silva, L., He, J., and Bhatia, S. N. (2018). Engineered livers for infectious diseases. *Cell. Mol. Gastroenterol. Hepatol.* 5, 131–144.

Hall, Z., Bond, N. J., Ashmore, T., Sanders, F., Ament, Z., Wang, X., et al. (2017). Lipid zonation and phospholipid remodeling in nonalcoholic fatty liver disease. *Hepatology* 65, 1165–1180. doi: 10.1002/hep.28953

Hendriks, D., Artegiani, B., Hu, H., de Sousa Lopes, S. C., and Clevers, H. (2021). Establishment of human fetal hepatocyte organoids and CRISPR-Cas9-based gene knockin and knockout in organoid cultures from human liver. *Nat. Protoc.* 16, 182–217. doi: 10.1038/s41596-020-00411-2

Hong, C.-H., Sohn, H.-J., Lee, H.-J., Cho, H.-I., and Kim, T.-G. (2017). Antigen presentation by individually transferred HLA class i genes in HLA-A, HLA-B, HLA-C null human cell line generated using the multiplex CRISPR-Cas9 system. *J. Immunother.* 40, 201–210. doi: 10.1097/CJI.0000000000000176

Hou, Z., Zhang, Y., Propson, N. E., Howden, S. E., Chu, L.-F., Sontheimer, E. J., et al. (2013). Efficient genome engineering in human pluripotent stem cells using Cas9 from *Neisseria meningitidis*. *Proc. Natl. Acad. Sci. U.S.A.* 110, 15644–15649. doi: 10.1073/pnas.1313587110

Hsia, G. S. P., Esposito, J., da Rocha, L. A., Ramos, S. L. G., and Okamoto, O. K. (2021). Clinical application of human induced pluripotent stem cell-derived organoids as an alternative to organ transplantation. *Stem Cells Int.* 2021, 6632160. doi: 10.1155/2021/6632160

Hu, H., Gehart, H., Artegiani, B., LÖpez-Iglesias, C., Dekkers, F., Basak, O., et al. (2018). Long-term expansion of functional mouse and human hepatocytes as 3D organoids. *Cell* 175, 1591–1606.e1519.

Huang, S. (2009). Non-genetic heterogeneity of cells in development: more than just noise. *Development* 136, 3853–3862.

Huch, M., Gehart, H., Van Boxtel, R., Hamer, K., Blokzijl, F., Verstegen, M. M., et al. (2015). Long-term culture of genome-stable bipotent stem cells from adult human liver. *Cell* 160, 299–312. doi: 10.1016/j.cell.2014.11.050

Inoue, H., and Yamanaka, S. (2011). The use of induced pluripotent stem cells in drug development. *Clin. Pharmacol. Ther.* 89, 655–661.

Janani, G., and Mandal, B. B. (2021). Mimicking physiologically relevant hepatocyte zonation using immunomodulatory silk liver extracellular matrix scaffolds toward a bioartificial liver platform. *ACS Appl. Mater. Interfaces* 13, 24401–24421. doi: 10.1021/acsami.1c00719

Ji, J., Ng, S. H., Sharma, V., Neculai, D., Hussein, S., Sam, M., et al. (2012). Elevated coding mutation rate during the reprogramming of human somatic cells into induced pluripotent stem cells. *Stem Cells* 30, 435–440. doi: 10.1002/stem.1011

Jung, K. B., Lee, H., Son, Y. S., Lee, M.-O., Kim, Y.-D., Oh, S. J., et al. (2018). Interleukin-2 induces the in vitro maturation of human pluripotent stem cell-derived intestinal organoids. *Nat. Commun.* 9:3039. doi: 10.1038/s41467-018-05450-8

Kietzmann, T. (2017). Metabolic zonation of the liver: the oxygen gradient revisited. *Redox Biol.* 11, 622–630. doi: 10.1016/j.redox.2017.01.012

Kilpinen, H., Goncalves, A., Leha, A., Afzal, V., Alasoo, K., Ashford, S., et al. (2017). Common genetic variation drives molecular heterogeneity in human iPSCs. *Nature* 546, 370–375.

Kim, K., Zhao, R., Doi, A., Ng, K., Unternaehrer, J., Cahan, P., et al. (2011). Donor cell type can influence the epigenome and differentiation potential of human induced pluripotent stem cells. *Nat. Biotechnol.* 29, 1117–1119.

Kleinstiver, B. P., Pattanayak, V., Prew, M. S., Tsai, S. Q., Nguyen, N. T., Zheng, Z., et al. (2016). High-fidelity CRISPR–Cas9 nucleases with no detectable genome-wide off-target effects. *Nature* 529, 490–495. doi: 10.1038/nature16526

Klotz, B. J., Oosterhoff, L. A., Utomo, L., Lim, K. S., Vallmajo-Martin, Q., Clevers, H., et al. (2019). A versatile biosynthetic hydrogel platform for engineering of tissue analogues. *Adv. Healthcare Mater.* 8:e1900979. doi: 10.1002/adhm.201900979

Koepsell, H., Lips, K., and Volk, C. (2007). Polyspecific organic cation transporters: structure, function, physiological roles, and biopharmaceutical implications. *Pharm. Res.* 24, 1227–1251. doi: 10.1007/s11095-007-9254-z

Krüger, M., Oosterhoff, L. A., van Wolferen, M. E., Schiele, S. A., Walther, A., Geijsen, N., et al. (2020). Cellulose nanofibril hydrogel promotes hepatic differentiation of human liver organoids. *Adv. Healthcare Mater.* 9:e1901658. doi: 10.1002/adhm.201901658

Kryou, C., Leva, V., Chatzipetrou, M., and Zergioti, I. (2019). Bioprinting for liver transplantation. *Bioengineering* 6:95. doi: 10.3390/bioengineering6040095

Kuijk, E., Jager, M., van der Roest, B., Locati, M. D., Van Hoeck, A., Korzelius, J., et al. (2020). The mutational impact of culturing human pluripotent and adult stem cells. *Nat. Commun.* 11:2493.

Kuo, C. J., and Curtis, C. (2018). *Organoids Reveal Cancer Dynamics*. Berlin: Nature Publishing Group.

Lancaster, M. A., Renner, M., Martin, C.-A., Wenzel, D., Bicknell, L. S., Hurles, M. E., et al. (2013). Cerebral organoids model human brain development and microcephaly. *Nature* 501, 373–379.

Laurent, L. C., Ulitsky, I., Slavin, I., Tran, H., Schork, A., Morey, R., et al. (2011). Dynamic changes in the copy number of pluripotency and cell proliferation genes in human ESCs and iPSCs during reprogramming and time in culture. *Cell Stem Cell* 8, 106–118. doi: 10.1016/j.stem.2010.12.003

Lee, G., Kim, H., Park, J. Y., Kim, G., Han, J., Chung, S., et al. (2021). Generation of uniform liver spheroids from human pluripotent stem cells for imaging-based drug toxicity analysis. *Biomaterials* 269, 120529. doi: 10.1016/j.biomaterials.2020.120529

Lee, J., Sheen, J. H., Lim, O., Lee, Y., Ryu, J., Shin, D., et al. (2020). Abrogation of HLA surface expression using CRISPR/Cas9 genome editing: a step toward universal T cell therapy. *Sci. Rep.* 10, 1–10. doi: 10.1038/s41598-020-74772-9

Leung, A. W., Broton, C., Bogacheva, M. S., Xiao, A. Z., Garcia-Castro, M. I., and Lou, Y.-R. (2020). RNA-based CRISPR-mediated loss-of-function mutagenesis in human pluripotent stem cells. *J. Mol. Biol.* 432, 3956–3964. doi: 10.1016/j.jmb.2020.04.017

Liang, G., and Zhang, Y. (2013). Genetic and epigenetic variations in iPSCs: potential causes and implications for application. *Cell Stem Cell* 13, 149–159.

Lin, X., Tang, J., and Lou, Y.-R. (2021). Human pluripotent stem-cell-derived models as a missing link in drug discovery and development. *Pharmaceuticals* 14:525. doi: 10.3390/ph14060525

Lou, Y.-R., and Leung, A. W. (2018). Next generation organoids for biomedical research and applications. *Biotechnol. Adv.* 36, 132–149.

Lou, Y.-R., Kanninen, L., Kuisma, T., Niklander, J., Noon, L. A., Burks, D., et al. (2014). The use of nanofibrillar cellulose hydrogel as a flexible three-dimensional model to culture human pluripotent stem cells. *Stem Cells Dev.* 23, 380–392. doi: 10.1089/scd.2013.0314

Lucendo-Villarin, B., Meseguer-Ripolles, J., Drew, J., Fischer, L., Ma, E., Flint, O., et al. (2020). Development of a cost-effective automated platform to produce human liver spheroids for basic and applied research. *Biofabrication* 13:015009. doi: 10.1088/1758-5090/abbdb2

Lynch, S., Pridgeon, C. S., Duckworth, C. A., Sharma, P., Park, B. K., and Goldring, C. E. P. (2019). Stem cell models as an in vitro model for predictive toxicology. *Biochem. J.* 476, 1149–1158. doi: 10.1042/BCJ20170780

Mandai, M., Watanabe, A., Kurimoto, Y., Hirami, Y., Morinaga, C., Daimon, T., et al. (2017). Autologous induced stem-cell–derived retinal cells for macular degeneration. *N. Engl. J. Med.* 376, 1038–1046.

Manou, D., Caon, I., Bouris, P., Triantaphyllidou, I.-E., Giaroni, C., Passi, A., et al. (2019). The complex interplay between extracellular matrix and cells in tissues. *Extracell. Matrix* 1952, 1–20.

Mansour, A. A., Gonçalves, J. T., Bloyd, C. W., Li, H., Fernandes, S., Quang, D., et al. (2018). An in vivo model of functional and vascularized human brain organoids. *Nat. Biotechnol.* 36, 432–441.

Martins-Taylor, K., Nisler, B. S., Taapken, S. M., Compton, T., Crandall, L., Montgomery, K. D., et al. (2011). Recurrent copy number variations in human induced pluripotent stem cells. *Nat. Biotechnol.* 29, 488–491.

Mayshar, Y., Ben-David, U., Lavon, N., Biancotti, J.-C., Yakir, B., Clark, A. T., et al. (2010). Identification and classification of chromosomal aberrations in human induced pluripotent stem cells. *Cell Stem Cell* 7, 521–531. doi: 10.1016/j.stem.2010.07.017

Mekhoubad, S., Bock, C., De Boer, A. S., Kiskinis, E., Meissner, A., and Eggan, K. (2012). Erosion of dosage compensation impacts human iPSC disease modeling. *Cell Stem Cell* 10, 595–609.

Miller, A. J., Dye, B. R., Ferrer-Torres, D., Hill, D. R., Overeem, A. W., Shea, L. D., et al. (2019). Generation of lung organoids from human pluripotent stem cells in vitro. *Nat. Protoc.* 14, 518–540.

Minami, T., Ishii, T., Yasuchika, K., Fukumitsu, K., Ogiso, S., Miyauchi, Y., et al. (2019). Novel hybrid three-dimensional artificial liver using human induced pluripotent stem cells and a rat decellularized liver scaffold. *Regen. Ther.* 10, 127–133. doi: 10.1016/j.reth.2019.03.002

Mun, S. J., Hong, Y.-H., Ahn, H.-S., Ryu, J.-S., Chung, K.-S., and Son, M. J. (2020). Long-term expansion of functional human pluripotent stem cell-derived hepatic organoids. *Int. J. Stem Cells* 13:279.

Mun, S. J., Lee, J., Chung, K. S., Son, M. Y., and Son, M. J. (2021). Effect of microbial short-chain fatty acids on CYP3A4-mediated metabolic activation of human pluripotent stem cell-derived liver organoids. *Cells* 10:126. doi: 10.3390/cells10010126

Muthuswamy, S. K. (2018). Organoid models of cancer explode with possibilities. *Cell Stem Cell* 22, 290–291. doi: 10.1016/j.stem.2018.02.010

Nagamoto, Y., Takayama, K., Ohashi, K., Okamoto, R., Sakurai, F., Tachibana, M., et al. (2016). Transplantation of a human iPSC-derived hepatocyte sheet increases survival in mice with acute liver failure. *J. Hepatol.* 64, 1068–1075. doi: 10.1016/j.jhep.2016.01.004

National Center For Health Statistics (2021). *Health, United States, 2019*. Hyattsville, MD: National Center For Health Statistics.

Ng, S. S., Saeb-Parsy, K., Blackford, S. J. I., Segal, J. M., Serra, M. P., Horcas-Lopez, M., et al. (2018). Human iPS derived progenitors bioengineered into liver organoids using an inverted colloidal crystal poly (ethylene glycol) scaffold. *Biomaterials* 182, 299–311. doi: 10.1016/j.biomaterials.2018.07.043

Ng, S., Schwartz, R. E., March, S., Galstian, A., Gural, N., Shan, J., et al. (2015). Human iPSC-derived hepatocyte-like cells support Plasmodium liver-stage infection in vitro. *Stem Cell Rep.* 4, 348–359. doi: 10.1016/j.stemcr.2015.01.002

Nie, Y.-Z., Zheng, Y.-W., Miyakawa, K., Murata, S., Zhang, R.-R., Sekine, K., et al. (2018). Recapitulation of hepatitis B virus–host interactions in liver organoids from human induced pluripotent stem cells. *EBioMedicine* 35, 114–123.

Nishizawa, M., Chonabayashi, K., Nomura, M., Tanaka, A., Nakamura, M., Inagaki, A., et al. (2016). Epigenetic variation between human induced pluripotent stem cell lines is an indicator of differentiation capacity. *Cell Stem Cell* 19, 341–354. doi: 10.1016/j.stem.2016.06.019

Nuñez, J. K., Harrington, L. B., and Doudna, J. A. (2016). Chemical and biophysical modulation of Cas9 for tunable genome engineering. *ACS Chem. Biol.* 11, 681–688. doi: 10.1021/acschembio.5b01019

Oberwallner, B., Brodarac, A., Choi, Y. H., Saric, T., Anić, P., Morawietz, L., et al. (2014). Preparation of cardiac extracellular matrix scaffolds by decellularization of human myocardium. *J. Biomed. Mater. Res. Part A* 102, 3263–3272.

Ogawa, S., Surapisitchat, J., Virtanen, C., Niapour, M., Sugamori, K. S., Wang, S., et al. (2013). Three-dimensional culture and cAMP signaling promote the maturation of human pluripotent stem cell-derived hepatocytes. *Development* 140, 3285–3296. doi: 10.1242/dev.090266

Ogoke, O., Maloy, M., and Parashurama, N. (2021). The science and engineering of stem cell-derived organoids-examples from hepatic, biliary, and pancreatic tissues. *Biol. Rev. Camb. Philos. Soc.* 96, 179–204. doi: 10.1111/brv.12650

Okita, K., Matsumura, Y., Sato, Y., Okada, A., Morizane, A., Okamoto, S., et al. (2011). A more efficient method to generate integration-free human iPS cells. *Nat. Methods* 8, 409–412.

Orkin, R., Gehron, P., Mcgoodwin, E. B., Martin, G., Valentine, T., and Swarm, R. (1977). A murine tumor producing a matrix of basement membrane. *J. Exp. Med.* 145, 204–220.

Ott, H. C., Matthiesen, T. S., Goh, S.-K., Black, L. D., Kren, S. M., Netoff, T. I., et al. (2008). Perfusion-decellularized matrix: using nature's platform to engineer a bioartificial heart. *Nat. Med.* 14, 213–221. doi: 10.1038/nm1684

Ouchi, R., Togo, S., Kimura, M., Shinozawa, T., Koido, M., Koike, H., et al. (2019). Modeling steatohepatitis in humans with pluripotent stem cell-derived organoids. *Cell Metab.* 30, 374–384.e376.

Papapetrou, E. P. (2016). Patient-derived induced pluripotent stem cells in cancer research and precision oncology. *Nat. Med.* 22, 1392–1401.

Pauli, C., Hopkins, B. D., Prandi, D., Shaw, R., Fedrizzi, T., Sboner, A., et al. (2017). Personalized in vitro and in vivo cancer models to guide precision medicine. *Cancer Discov.* 7, 462–477.

Peng, W. C., Logan, C. Y., Fish, M., Anbarchian, T., Aguisanda, F., Álvarez-Varela, A., et al. (2018). Inflammatory cytokine TNFα promotes the long-term expansion of primary hepatocytes in 3D culture. *Cell* 175, 1607–1619. e1615 doi: 10.1016/j.cell.2018.11.012

Pettinato, G., Lehoux, S., Ramanathan, R., Salem, M. M., He, L.-X., Muse, O., et al. (2019). Generation of fully functional hepatocyte-like organoids from human induced pluripotent stem cells mixed with endothelial cells. *Sci. Rep.* 9, 1–21. doi: 10.1038/s41598-019-45514-3

Planas-Paz, L., Orsini, V., Boulter, L., Calabrese, D., Pikiolek, M., Nigsch, F., et al. (2016). The RSPO–LGR4/5–ZNRF3/RNF43 module controls liver zonation and size. *Nat. Cell Biol.* 18, 467–479.

Plummer, S., Wallace, S., Ball, G., Lloyd, R., Schiapparelli, P., Quiñones-Hinojosa, A., et al. (2019). A human iPSC-derived 3D platform using primary brain cancer cells to study drug development and personalized medicine. *Sci. Rep.* 9, 1–11. doi: 10.1038/s41598-018-38130-0

Polo, J. M., Liu, S., Figueroa, M. E., Kulalert, W., Eminli, S., Tan, K. Y., et al. (2010). Cell type of origin influences the molecular and functional properties of mouse induced pluripotent stem cells. *Nat. Biotechnol.* 28, 848–855. doi: 10.1038/nbt.1667

Pope, I., Masia, F., Ewan, K., Jimenez-Pascual, A., Dale, T. C., Siebzehnrubl, F. A., et al. (2021). Identifying subpopulations in multicellular systems by quantitative chemical imaging using label-free hyperspectral CARS microscopy. *Analyst* 146, 2277–2291. doi: 10.1039/d0an02381g

Popper, H., and Schaffner, F. (1957). *Liver: Structure And Function*. New York, NY: McGraw Hill.

Prodanov, L., Jindal, R., Bale, S. S., Hegde, M., McCarty, W. J., Golberg, I., et al. (2016). Long-term maintenance of a microfluidic 3D human liver sinusoid. *Biotechnol. Bioeng.* 113, 241–246. doi: 10.1002/bit.25700

Raju, R., Chau, D., Cho, D. S., Park, Y., Verfaillie, C. M., and Hu, W.-S. (2017). Cell expansion during directed differentiation of stem cells toward the hepatic lineage. *Stem Cells Dev.* 26, 274–284.

Ramli, M. N. B., Lim, Y. S., Koe, C. T., Demircioglu, D., Tng, W., Gonzales, K. A. U., et al. (2020). Human pluripotent stem cell-derived organoids as models of liver disease. *Gastroenterology* 159, 1471–1486 e1412. doi: 10.1053/j.gastro.2020.06.010

Ran, F. A., Cong, L., Yan, W. X., Scott, D. A., Gootenberg, J. S., Kriz, A. J., et al. (2015). In vivo genome editing using Staphylococcus aureus Case. *Nature* 520, 186–191.

Rashidi, H., Luu, N. T., Alwahsh, S. M., Ginai, M., Alhaque, S., Dong, H., et al. (2018). 3D human liver tissue from pluripotent stem cells displays stable phenotype in vitro and supports compromised liver function in vivo. *Arch. Toxicol.* 92, 3117–3129. doi: 10.1007/s00204-018-2280-2

Reintjes, J., Duncan, M. D., and Manuccia, T. J. (1982). "Picosecond coherent anti-stokes raman scattering (CARS) Microscope," in *Proceedings of the SPIE 0322, Picosecond Lasers and Applications*, Los Angeles, CA.

Roelandt, P., Obeid, S., Paeshuyse, J., Vanhove, J., Van Lommel, A., Nahmias, Y., et al. (2012). Human pluripotent stem cell-derived hepatocytes support complete replication of hepatitis C virus. *J. Hepatol.* 57, 246–251. doi: 10.1016/j.jhep.2012.03.030

Rossi, G., Broguiere, N., Miyamoto, M., Boni, A., Guiet, R., Girgin, M., et al. (2021). Capturing cardiogenesis in gastruloids. *Cell Stem Cell* 28, 230–240. e236. doi: 10.1016/j.stem.2020.10.013

Schene, I. F., Joore, I. P., Oka, R., Mokry, M., van Vugt, A. H. M., van Boxtel, R., et al. (2020). Prime editing for functional repair in patient-derived disease models. *Nat. Commun.* 11:5352. doi: 10.1038/s41467-020-19136-7

Schneeberger, K., Sánchez-Romero, N., Ye, S., van Steenbeek, F. G., Oosterhoff, L. A., Pla Palacin, I., et al. (2020). Large-scale production of LGR5-positive bipotential human liver stem cells. *Hepatology* 72, 257–270. doi: 10.1002/hep.31037

Schulze, A., Mills, K., Weiss, T. S., and Urban, S. (2012). Hepatocyte polarization is essential for the productive entry of the hepatitis B virus. *Hepatology* 55, 373–383. doi: 10.1002/hep.24707

Schwartz, R. E., Trehan, K., Andrus, L., Sheahan, T. P., Ploss, A., Duncan, S. A., et al. (2012). Modeling hepatitis C virus infection using human induced pluripotent stem cells. *Proc. Natl. Acad. Sci. U.S.A.* 109, 2544–2548.

Schwarz, S., Koerber, L., Elsaesser, A. F., Goldberg-Bockhorn, E., Seitz, A. M., Dürselen, L., et al. (2012). Decellularized cartilage matrix as a novel biomatrix for cartilage tissue-engineering applications. *Tissue Eng. Part A* 18, 2195–2209. doi: 10.1089/ten.TEA.2011.0705

Serra, D., Mayr, U., Boni, A., Lukonin, I., Rempfler, M., Meylan, L. C., et al. (2019). Self-organization and symmetry breaking in intestinal organoid development. *Nature* 569, 66–72. doi: 10.1038/s41586-019-1146-y

Sgodda, M., Dai, Z., Zweigerdt, R., Sharma, A. D., Ott, M., and Cantz, T. (2017). A scalable approach for the generation of human pluripotent stem cell-derived hepatic organoids with sensitive hepatotoxicity features. *Stem Cells Dev.* 26, 1490–1504. doi: 10.1089/scd.2017.0023

Sharma, S., Raju, R., Sui, S., and Hu, W. S. (2011). Stem cell culture engineering–process scale up and beyond. *Biotechnol. J.* 6, 1317–1329. doi: 10.1002/biot.201000435

Shlomai, A., Schwartz, R. E., Ramanan, V., Bhatta, A., de Jong, Y. P., Bhatia, S. N., et al. (2014). Modeling host interactions with hepatitis B virus using primary and induced pluripotent stem cell-derived hepatocellular systems. *Proc. Natl. Acad. Sci. U.S.A.* 111, 12193–12198. doi: 10.1073/pnas.1412631111

Si-Tayeb, K., Lemaigre, F. P., and Duncan, S. A. (2010). Organogenesis and development of the liver. *Dev. Cell* 18, 175–189.

Song, W., Lu, Y.-C., Frankel, A. S., An, D., Schwartz, R. E., and Ma, M. (2015). Engraftment of human induced pluripotent stem cell-derived hepatocytes in immunocompetent mice via 3D co-aggregation and encapsulation. *Sci. Rep.* 5, 1–13. doi: 10.1038/srep16884

Sorrentino, G., Rezakhani, S., Yildiz, E., Nuciforo, S., Heim, M. H., Lutolf, M. P., et al. (2020). Mechano-modulatory synthetic niches for liver organoid derivation. *Nat. Commun.* 11, 1–10. doi: 10.1038/s41467-020-17161-0

Stieger, B. (2011). The role of the sodium-taurocholate cotransporting polypeptide (NTCP) and of the bile salt export pump (BSEP) in physiology and pathophysiology of bile formation. *Drug Transporters* 201, 205–259.

Sugimoto, S., and Sato, T. (2017). "Establishment of 3D intestinal organoid cultures from intestinal stem cells," in *3D Cell Culture. Methods in Molecular Biology*, ed. Z. Koledova (Berlin: Springer), 97–105.

Szot, G. L., Yadav, M., Lang, J., Kroon, E., Kerr, J., Kadoya, K., et al. (2015). Tolerance induction and reversal of diabetes in mice transplanted with human embryonic stem cell-derived pancreatic endoderm. *Cell Stem Cell* 16, 148–157. doi: 10.1016/j.stem.2014.12.001

Takahashi, K., Tanabe, K., Ohnuki, M., Narita, M., Ichisaka, T., Tomoda, K., et al. (2007). Induction of pluripotent stem cells from adult human fibroblasts by defined factors. *Cell* 131, 861–872.

Takasato, M., Pei, X. E., Chiu, H. S., Maier, B., Baillie, G. J., Ferguson, C., et al. (2015). Kidney organoids from human iPS cells contain multiple lineages and model human nephrogenesis. *Nature* 526, 564–568.

Takebe, T., Sekine, K., Enomura, M., Koike, H., Kimura, M., Ogaeri, T., et al. (2013). Vascularized and functional human liver from an iPSC-derived organ bud transplant. *Nature* 499, 481–484. doi: 10.1038/nature12271

Takebe, T., Sekine, K., Kimura, M., Yoshizawa, E., Ayano, S., Koido, M., et al. (2017). Massive and reproducible production of liver buds entirely from human pluripotent stem cells. *Cell Rep.* 21, 2661–2670. doi: 10.1016/j.celrep.2017.11.005

Tam, P. P. L., and Loebel, D. A. F. (2007). Gene function in mouse embryogenesis: get set for gastrulation. *Nat. Rev. Genet.* 8, 368–381. doi: 10.1038/nrg2084

Taylor, C. J., Peacock, S., Chaudhry, A. N., Bradley, J. A., and Bolton, E. M. (2012). Generating an iPSC bank for HLA-matched tissue transplantation based on known donor and recipient HLA types. *Cell Stem Cell* 11, 147–152. doi: 10.1016/j.stem.2012.07.014

Thompson, W. L., and Takebe, T. (2021). Human liver model systems in a dish. *Dev. Growth Differ.* 63, 47–58. doi: 10.1111/dgd.12708

Touboul, T., Hannan, N. R. F., Corbineau, S., Martinez, A., Martinet, C., Branchereau, S., et al. (2010). Generation of functional hepatocytes from human embryonic stem cells under chemically defined conditions that recapitulate liver development. *Hepatology* 51, 1754–1765. doi: 10.1002/hep.23506

Tsuchida, T., Murata, S., Hasegawa, S., Mikami, S., Enosawa, S., Hsu, H.-C., et al. (2020). Investigation of clinical safety of human iPS cell-derived liver organoid transplantation to infantile patients in porcine model. *Cell Transplant* 29:0963689720964384. doi: 10.1177/0963689720964384

Tsuchida, T., Murata, S., Matsuki, K., Mori, A., Matsuo, M., Mikami, S., et al. (2019). The Regenerative effect of portal vein injection of liver organoids by retrorsine/partial hepatectomy in rats. *Int. J. Mol. Sci.* 21:178. doi: 10.3390/ijms21010178

Tsuji, O., Miura, K., Okada, Y., Fujiyoshi, K., Mukaino, M., Nagoshi, N., et al. (2010). Therapeutic potential of appropriately evaluated safe-induced pluripotent stem cells for spinal cord injury. *Proc. Natl. Acad. Sci. U.S.A.* 107, 12704–12709. doi: 10.1073/pnas.0910106107

Uygun, B. E., Soto-Gutierrez, A., Yagi, H., Izamis, M.-L., Guzzardi, M. A., Shulman, C., et al. (2010). Organ reengineering through development of a transplantable recellularized liver graft using decellularized liver matrix. *Nat. Med.* 16:814.

Valamehr, B., Robinson, M., Abujarour, R., Rezner, B., Vranceanu, F., Le, T., et al. (2014). Platform for induction and maintenance of transgene-free hiPSCs resembling ground state pluripotent stem cells. *Stem Cell Rep.* 2, 366–381. doi: 10.1016/j.stemcr.2014.01.014

van Ineveld, R. L., Ariese, H. C. R., Wehrens, E. J., Dekkers, J. F., and Rios, A. C. (2020). Single-cell resolution three-dimensional imaging of intact organoids. *J. Vis. Exp.* doi: 10.3791/60709

Vassena, R., Montserrat, N., Carrasco Canal, B., Aran, B., de Oñate, L., Veiga, A., et al. (2012). Accumulation of instability in serial differentiation and reprogramming of parthenogenetic human cells. *Hum. Mol. Genet.* 21, 3366–3373. doi: 10.1093/hmg/dds168

Vlachogiannis, G., Hedayat, S., Vatsiou, A., Jamin, Y., Fernández-Mateos, J., Khan, K., et al. (2018). Patient-derived organoids model treatment response of metastatic gastrointestinal cancers. *Science* 359, 920–926.

Wang, B., Jakus, A. E., Baptista, P. M., Soker, S., Soto-Gutierrez, A., Abecassis, M. M., et al. (2016). Functional maturation of induced pluripotent stem cell hepatocytes in extracellular matrix—a comparative analysis of bioartificial liver microenvironments. *Stem Cells Transl. Med.* 5, 1257–1267. doi: 10.5966/sctm.2015-0235

Wang, H., Calvisi, D. F., and Chen, X. (2021). Organoids for the study of liver cancer. *Semin. Liver Dis.* 41, 19–27. doi: 10.1055/s-0040-1719176

Wang, K., Guzman, A. K., Yan, Z., Zhang, S., Hu, M. Y., Hamaneh, M. B., et al. (2019). Ultra-high-frequency reprogramming of individual long-term hematopoietic stem cells yields low somatic variant induced pluripotent stem cells. *Cell Rep.* 26, 2580–2592. E2587. doi: 10.1016/j.celrep.2019.02.021

Wang, S., Wang, X., Tan, Z., Su, Y., Liu, J., Chang, M., et al. (2019). Human ESC-derived expandable hepatic organoids enable therapeutic liver repopulation and pathophysiological modeling of alcoholic liver injury. *Cell Res.* 29, 1009–1026. doi: 10.1038/s41422-019-0242-8

Wang, Y., Cui, C. B., Yamauchi, M., Miguez, P., Roach, M., Malavarca, R., et al. (2011). Lineage restriction of human hepatic stem cells to mature fates is made efficient by tissue-specific biomatrix scaffolds. *Hepatology* 53, 293–305. doi: 10.1002/hep.24012

Watson, C. L., Mahe, M. M., Múnera, J., Howell, J. C., Sundaram, N., Poling, H. M., et al. (2014). An in vivo model of human small intestine using pluripotent stem cells. *Nat. Med.* 20, 1310–1314. doi: 10.1038/nm.3737

Weiss, M. J., Ray, K., Henthorn, P. S., Lamb, B., Kadesch, T., and Harris, H. (1988). Structure of the human liver/bone/kidney alkaline phosphatase gene. *J. Biol. Chem.* 263, 12002–12010.

Wörsdörfer, P. I. T., Asahina, I., Sumita, Y., and Ergün, S. (2020). Do not keep it simple: recent advances in the generation of complex organoids. *J. Neural Transm. (Vienna)* 127, 1569–1577. doi: 10.1007/s00702-020-02198-8

Wu, F., Wu, D., Ren, Y., Huang, Y., Feng, B., Zhao, N., et al. (2019). Generation of hepatobiliary organoids from human induced pluripotent stem cells. *J. Hepatol.* 70, 1145–1158.

Wu, X., Robotham, J. M., Lee, E., Dalton, S., Kneteman, N. M., Gilbert, D. M., et al. (2012). Productive hepatitis C virus infection of stem cell-derived hepatocytes reveals a critical transition to viral permissiveness during differentiation. *PLoS Pathog.* 8:e1002617. doi: 10.1371/journal.ppat.1002617

Xu, H., Wang, B., Ono, M., Kagita, A., Fujii, K., Sasakawa, N., et al. (2019). Targeted disruption of HLA genes via CRISPR-Cas9 generates iPSCs with enhanced immune compatibility. *Cell Stem Cell* 24, 566–578 e567. doi: 10.1016/j.stem.2019.02.005

Xu, J., and Zeger, S. L. (2001). The evaluation of multiple surrogate endpoints. *Biometrics* 57, 81–87.

Yan, H., Zhong, G., Xu, G., He, W., Jing, Z., Gao, Z., et al. (2012). Sodium taurocholate cotransporting polypeptide is a functional receptor for human hepatitis B and D virus. *elife* 1:e00049.

Ye, S., Boeter, J. W., Mihajlovic, M., van Steenbeek, F. G., van Wolferen, M. E., Oosterhoff, L. A., et al. (2020). A chemically defined hydrogel for human liver organoid culture. *Adv. Funct. Mater.* 30:2000893.

Yin, X., Mead, B. E., Safaee, H., Langer, R., Karp, J. M., and Levy, O. (2016). Engineering stem cell organoids. *Cell Stem Cell* 18, 25–38. doi: 10.1016/j.stem.2015.12.005

Yu, J., Vodyanik, M. A., Smuga-Otto, K., Antosiewicz-Bourget, J., Frane, J. L., Tian, S., et al. (2007). Induced pluripotent stem cell lines derived from human somatic cells. *Science* 318, 1917–1920.

Zahmatkesh, E., Ghanian, M. H., Zarkesh, I., Farzaneh, Z., Halvaei, M., Heydari, Z., et al. (2021). Tissue-specific microparticles improve organoid microenvironment for efficient maturation of pluripotent stem-cell-derived hepatocytes. *Cells* 10:1274. doi: 10.3390/cells10061274

Zhang, M., Sun, P., Wang, Y., Chen, J., Lv, L., Wei, W., et al. (2015). Generation of self-renewing hepatoblasts from human embryonic stem cells by chemical approaches. *Stem Cells Transl. Med.* 4, 1275–1282. doi: 10.5966/sctm.2015-0051

Zhao, T., Zhang, Z.-N., Westenskow, P. D., Todorova, D., Hu, Z., Lin, T., et al. (2015). Humanized mice reveal differential immunogenicity of cells derived from autologous induced pluripotent stem cells. *Cell Stem Cell* 17, 353–359. doi: 10.1016/j.stem.2015.07.021

Zhu, M., Huang, Y., Bian, S., Song, Q., Zhang, J., Zheng, W., et al. (2020). Organoid: current implications and pharmaceutical applications in liver diseases. *Curr. Mol. Pharmacol.* doi: 10.2174/1874467213666201217115854

Conflict of Interest: The authors declare that the research was conducted in the absence of any commercial or financial relationships that could be construed as a potential conflict of interest.

Publisher's Note: All claims expressed in this article are solely those of the authors and do not necessarily represent those of their affiliated organizations, or those of the publisher, the editors and the reviewers. Any product that may be evaluated in this article, or claim that may be made by its manufacturer, is not guaranteed or endorsed by the publisher.

frontiers in Cell and Developmental Biology

ORIGINAL RESEARCH
published: 15 October 2021
doi: 10.3389/fcell.2021.722365

Melatonin Promotes the Therapeutic Effect of Mesenchymal Stem Cells on Type 2 Diabetes Mellitus by Regulating TGF-β Pathway

*Balun Li[1], Xuedi Cheng[1], Aili Aierken[1], Jiaxin Du[2,3], Wenlai He[1], Mengfei Zhang[1], Ning Tan[1], Zheng Kou[1], Sha Peng[1], Wenwen Jia[4], Haiyang Tang[1,5] and Jinlian Hua[1]**

[1] Shaanxi Centre of Stem Cells Engineering and Technology, College of Veterinary Medicine, Northwest A&F University, Xianyang, China, [2] Department of Animal Engineering, Yangling Vocational and Technical College, Xianyang, China, [3] Department of Veterinary Medicine, College of Animal Sciences, Institute of Preventive Veterinary Sciences, Zhejiang University, Hangzhou, China, [4] Shanghai East Hospital, East Hospital Affiliated to Tongji University, Shanghai, China, [5] State Key Laboratory of Respiratory Disease, Guangzhou Institute of Respiratory Health, The First Affiliated Hospital of Guangzhou Medical University, Guangzhou, China

Abundant evidence proves the therapeutic effect of adipose-derived mesenchymal stem cells (ADMSCs) in the treatment of diabetes mellitus. However, the problems have not been solved that viability of ADMSCs were inconsistent and the cells quickly undergo senescence after *in vitro* cell culture. In addition, the therapeutic effect of ADMSCs is still not satisfactory. In this study, melatonin (MLT) was added to canine ADMSC culture medium, and the treated cells were used to treat type 2 diabetes mellitus (T2DM). Our research reveals that adding MLT to ADMSC culture medium can promote the viability of ADMSCs. This effect depends on the binding of MLT and MLT receptors, which activates the transforming growth factor β (TGF-β) pathway and then changes the cell cycle of ADMSCs and improves the viability of ADMSCs. Since ADMSCs were found to be used to treat T2DM by anti-inflammatory and anti-endoplasmic reticulum (ER) stress capabilities, our data demonstrate that MLT augment several effects of ADMSCs in remission hyperglycemia, insulin resistance, and liver glycogen metabolism in T2DM patients. This suggest that ADMSCs and MLT-ADMSCs is safe and vabulable for pet clinic.

Keywords: melatonin, adipose-derived mesenchymal stem cells, type 2 diabetes mellitus, TGF-β, inflammation, canine

OPEN ACCESS

Edited by:
Yan-Ru Lou,
Fudan University, China

Reviewed by:
Gianandrea Pasquinelli,
University of Bologna, Italy
Francesco Galli,
University of Perugia, Italy

****Correspondence:***
Jinlian Hua
jinlianhua@nwsuaf.edu.cn

Specialty section:
This article was submitted to Stem Cell Research, a section of the journal Frontiers in Cell and Developmental Biology

Received: *08 June 2021*
Accepted: *27 September 2021*
Published: *15 October 2021*

Citation:
Li B, Cheng X, Aierken A, Du J, He W, Zhang M, Tan N, Kou Z, Peng S, Jia W, Tang H and Hua J (2021) Melatonin Promotes the Therapeutic Effect of Mesenchymal Stem Cells on Type 2 Diabetes Mellitus by Regulating TGF-β Pathway. Front. Cell Dev. Biol. 9:722365. doi: 10.3389/fcell.2021.722365

INTRODUCTION

The pathogenesis of type 2 diabetes mellitus (T2DM) includes glucose metabolism disorder, oxidative stress, endoplasmic reticulum (ER) stress, and inflammation (Hu et al., 2018; Elshemy et al., 2021). Therefore, the interaction among multiple mechanisms leads to liver glucose metabolism disorder, insulin resistance, damage to the function of islet cells and hyperinsulinism. Islet β cells are the only cells that produce insulin in the body, and their functional damage directly leads to T2DM. Notably, the levels of ER and inflammation are critical for maintaining β-cell survival, and islet β-cell damage caused by ER damage and chronic inflammation has become an important factor in T2DM (Oyadomari et al., 2002). The ER is an organelle in eukaryotic cells and is involved in protein synthesis, modification, processing, and quality control (Saito and Imaizumi, 2018). ER stress at the normal level can promote cell self-renewal, while long-term or severe ER stress can cause

cell dysfunction and death (Li et al., 2020). Inflammation promotes the body to activate adaptive immunity and repair damaged tissues. However, excessive inflammation and chronic inflammation are also the causes of many chronic diseases, including chronic inflammatory rheumatism, diabetes mellitus (DM), and neurodegenerative diseases. ER stress is usually associated with inflammation. Both ER stress and inflammation represent short-term adjustments to body imbalance and are harmful when they are persistent or chronic (Chovatiya and Medzhitov, 2014). Studies have shown that inflammation occurs during ER stress and causes body damage, but the mechanism is still unclear (Cai et al., 2016; Cao et al., 2016; Wei et al., 2018).

Mesenchymal stem cells (MSCs) are pluripotent stem cells belonging to the mesoderm. MSCs have the potential to differentiate into bone cells, chondrocytes, adipocytes, muscle cells and other cells (Strem et al., 2005). MSC transplantation has been proven feasible for the treatment of severe traumatic diseases, autoimmune diseases, DM, and neurodegenerative diseases (Xie et al., 2017; Yang et al., 2021). There are many types of MSCs. Currently, most studies focus on umbilical cord blood mesenchymal stem cells (UCBMSCs), bone marrow mesenchymal stem cells (BMSCs), adipose-derived mesenchymal stem cells (ADMSCs), dental pulp MSCs, and limbal MSCs. Compared with MSCs from other sources, ADMSCs are obtained by liposuction and have the advantages of wide sources, convenient acquisition, low immunogenicity, and low ethical controversy.

Studies have shown that BMSC therapy improved insulin secretion, activate the insulin signaling pathway and enhance glucose transport, thereby reversing hyperglycemia in T2DM rats (Si et al., 2012; Hao et al., 2013). Fat derived MSCs improve hyperglycemia by regulating hepatic glucose metabolism in T2DM rats. Cell-free therapy (MSC-CM) based on biologically active factors secreted by stem cells and progenitor cells restore hyperglycemia and improve oxidative stress in T2DM rats (Elshemy et al., 2021). In addition, studies have revealed that autologous UCBMSC therapy can reduce patients' insulin dosage (Guan et al., 2015). However, the current MSC transplantation treatment still has some problems, including an uneven quality of MSCs used for treatment, an incomplete quality evaluation system for MSCs, and unclear treatment mechanism (Zakrzewski et al., 2019). For example, studies have shown that MSCs derived from T2DM patients contain more oxysterols, affecting the differentiation ability of MSCs (Luchetti et al., 2009; Murdolo et al., 2013). The source and quality of cells become major factors limiting the use of MSCs in clinical treatment. There is an urgent need for further explorations of the mechanism of MSC therapy to provide strong evidence for the application of MSCs in clinical medicine.

Melatonin (MLT) is an endogenous indolamine synthesized by tryptophan that is secreted by the pineal gland into blood circulation and regulates many physiological functions (Luchetti et al., 2010; Kumar Jha et al., 2015). Regarding its physiological role, MLT is a key regulator of the circadian rhythm (Reiter et al., 2010). For example, MLT plays a protective role in the body, including protecting the kidneys, through its powerful anti-inflammatory and antioxidative stress capabilities (Reiter et al., 1994, 2010; Sener et al., 2002; Luchetti et al., 2010; Galano et al., 2011; Mauriz et al., 2013). In addition, numerous studies have confirmed that MLT affects the occurrence and development of cells and the biological functions of MSCs and oocytes in various ways (Luchetti et al., 2009, 2014; Shi et al., 2009; Rocha et al., 2013; Tian et al., 2014; Maria et al., 2018; Liu et al., 2019). Studies have found that MLT acts as a mitochondrial antioxidant through the ERK-MAPK signaling pathway preventing apoptosis (Luchetti et al., 2009). MLT promotes the osteogenic differentiation of MSCs and protects BMSCs from bone injury (Knani et al., 2019). In addition, studies have shown that MLT predominantly regulates the differentiation and survival of MSCs through the Wnt/β-catenin pathway, MAPKs and TGF-β signaling (Luchetti et al., 2014). Our previous studies show that MLT prevents canine-derived ADMSCs from aging by activating NRF2 and inhibiting ER stress, restores the bone differentiation ability of aging ADMSCs, and promotes the effect of MSC therapy (Fang et al., 2018). MLT plays an important role in the *in vitro* culture of MSCs. However, the mechanism by which MLT affects the viability of MSCs remains unclear. Transforming growth factor β (TGF-β) family promotes cell proliferation, differentiation, migration and survival by controlling the expression and activity of key transcription factors in the TGF-β pathway (Blobe et al., 2000; Li et al., 2006). The upstream TGF-β pathway comprises the TGF-β ligand, type 1 TGF-β receptor (TGF-βR1) and type 2 TGF-β receptor (TGF-βR2), and the downstream TGF-β pathway comprises Smad and Smad-related transcription factors, which participate in cell proliferation and differentiation through transcriptional regulation (Budi et al., 2017; Derynck and Budi, 2019). Studies have shown that TGF-β plays a key role in the proliferation of MSCs, and the inhibition of TGF-β receptors slows the proliferation of MSCs (Ng et al., 2008; Luchetti et al., 2014).

In this study, canine-derived ADMSCs were cultured in a medium containing MLT *in vitro,* and the results showed that MLT promoted the viability of the ADMSCs by regulating the TGF-β pathway. This study shows that MLT promotes ADMSCs to treat T2DM by restoring islet and liver ER stress and inflammation. This study provides reliable and complete evidence supporting the use of MLT pretreatment as a part of MSC therapy. In addition, dogs are used as a DM model, and the usage of canine-derived ADMSCs can indirectly reflect the effect of the allogeneic transplantation of ADMSCs. Our research provides new evidence for clinical MSC therapy.

MATERIALS AND METHODS

Experimental Animals

Sixty-five 8-week-old Kun-Ming (KM) male mice (25 ± 2 g) were purchased from Chengdu Dossy Experimental Animal Co., Ltd. Eighteen 1-year-old male hybrid dogs weighing 5.0 ± 0.5 kg, provided by the Experimental Animal Center of Northwest A&F University, were used to establish canine DM models and perform safety tests. Two 6-month-old female hybrid dogs weighing 3.0 ± 0.5 kg, provided by the Experimental Animal Center of Northwest A&F University, were used for the ADMSC

separation. All animal experimental protocols were performed in strict accordance with the Guide for the Care and Use of Laboratory Animals (Ministry of Science and Technology of the People's Republic of China, Policy No. 2006 398). All animals were maintained in a conventional sanitary facility with the required consistent temperature and relative humidity. All animal experimental protocols were reviewed and approved by the Ethics Committee (no. 2015-mkrm01) of Northwest A&F University for the Use of Laboratory Animals. This experiment followed the international guidelines for animal studies (National Research Council (US) Institute for Laboratory Animal Research, 2004).

Cell Separation and Culture

Adipose-derived mesenchymal stem cells were derived from the abdominal subcutaneous adipose tissue of two 6-month-old female hybrid dogs. The detailed ADMSC separation steps and ADMSC identification were described in our previous report (Wei et al., 2016). The cells were cultured in α-MEM (Invitrogen, Carlsbad, CA, United States) complete medium at 37°C in a 5% CO_2 incubator (Peng et al., 2012; Fang et al., 2018). When the cells were attached to the bottom of the plate at approximately 80%, a 1:3 passage was performed. We treated and used the fourth-passage cells. MLT was added to the culture medium 72 h before transplantation, sample collection, and staining.

Melatonin Treatment of Adipose-Derived Mesenchymal Stem Cells

At the P4 passage, 1×10^5 cells were inoculated into a 48-well plate. ADMSCs were treated with 1 μM MLT, and the MLT-containing medium was replaced every 24 h for three times. After 72 h of MLT treatment, bright field images of cells were taken and Giemsa staining and ethynyldeoxyuridine (EdU) staining were performed. We used 60 mm cell dishes to culture the ADMSCs and collect the total cell RNA to complete the subsequent experiments (Fang et al., 2018).

Ethynyldeoxyuridine Staining

According to the instructions provided by the reagent supplier, (RiboBio, Guangzhou, China) we used logarithmic growth phase cells; we inoculated 0.5×10^4 cells into each well of a 96-well plate and cultured the cells to a density of 60–70% (Peng et al., 2012). EdU solution (1000:1) was diluted with serum-containing α-MEM medium and added to a 96-well plate. Then, the cells were incubated for 2 h, and the culture medium was discarded. The cells were washed with phosphate-buffered saline (PBS) (washed twice for 5 min per wash), cell fixation solution (4% paraformaldehyde in PBS) was added, and the samples were incubated at room temperature. Thirty minutes later, 2 mg/mL glycine were added to the cells, and the samples were incubated on a decolorizing shaker for 5 min, glycine was discarded, and the cells were washed with PBS for 5 min. Apollo staining solution was added to the cells, the samples were incubated for 30 min in the dark at room temperature, and then, the staining solution was discarded. Then, the cells were added to a 0.5% Triton X-100 decolorizing shaker and washed three times for 10 min per wash, and the permeate was discarded. Hoechst 33342 was added to the cells, and the samples were incubated for 30 min in the dark at room temperature. The staining solution was discarded, and the cells were washed once with PBS.

Cell Growth Curve

Adipose-derived mesenchymal stem cells were cultured in 24-well plates at a density of 0.5×10^4 cells per well. A cell growth curve was used to investigate the proliferation ability every 24 h. The ADMSCs were trypsinized every day, and the total number of cells was determined for seven consecutive days (Wei et al., 2016; Wu et al., 2021).

Giemsa Stain

According to the instructions provided by the reagent supplier (ZHONGHUIHECAI, China), we used logarithmic growth phase cells, inoculated 0.5×10^4 cells into each well of a 96-well plate and cultured the cells to a density of 60–70%. The Giemsa mother solution was diluted ten times with PBS to obtain the Giemsa working solution. We used 100 μL of the Giemsa working solution to fix the cells. After 1 min, 100 μL PBS were added to the cell culture dish. After 30 min, the staining solution was discarded, the cells were washed twice with PBS, and the cell status was observed under a microscope.

Quantitative Real-Time Polymerase Chain Reaction Analysis

According to the manufacturer's instructions, the total RNA was extracted from the ADMSCs by TRIzol reagent (Takara, Japan), and a reverse transcriptase reagent kit (Thermo Fisher Scientific) was used. Quantitative real-time polymerase chain reaction (qRT-PCR) was carried out using a CFX96 Real-Time polymerase chain reaction (PCR) system as follows: predenaturation at 94°C for 5 min, followed by 39 cycles for 30 s at 94°C, annealing for 30 s at 58°C and 30 s at 70°C for extension. β-Actin was used as an internal control. The comparative CT values from the qRT-PCR were used to measure the relative gene expression (Wei et al., 2016; Zhu et al., 2021). The primers are listed in **Supplementary Table 1**.

Type 2 Diabetes Mellitus Animal Model

Twelve 1-year-old male hybrid dogs and 65 KM male mice were used in the T2DM animal model. All animals were placed in the Animal Experiment Center of Northwest A&F University at constant temperature (25 ± 2°C) and constant photoperiod (12:12 h light-dark cycle) and were given adequate drinking water. To eliminate external factors, the dogs were bred adaptively before the experiment.

Twelve 1-year-old male hybrid dogs and 65 KM male mice were divided into the following five groups: (1) normal control, (2) T2DM, (3) ADMSCs, (4) MLT-ADMSCs, and (5) SB-MLT-ADMSCs. The first four groups included three dogs and 15 mice, and the fifth group included five mice. To induce the T2DM model, the last four groups were fed a high fat diet for 8 weeks combined with intravenous transplantation of streptozotocin (STZ). The transplant amount per dog was 25 mg/kg/day for 2 days, and that per mouse was 35 mg/kg/day for 2 days (Sun et al., 2018). The STZ dose for the dogs was obtained by

using different doses of STZ transplantation (**Supplementary Figure 1**). STZ was diluted with sodium citrate buffer, and the dogs and mice were fasted for 24 h before injection. After 1 week of modeling, the modeling effect was identified. In the latter three groups, ADMSCs (dogs: transplant 1×10^7 cells suspended in 10 mL sterile 0.9% NaCl, mice: transplant 2×10^6 cells suspended in 0.2 mL sterile 0.9% NaCl) were injected through the brachial vein of the dogs' forearm and tail vein in the mice. During the model preparation and treatment, we continuously monitored the changes in body weight and water and food intake.

Safety Test

Six 1-year-old male hybrid dogs were divided into three groups: (1) Normal Control, (2) ADMSCs, (3) MLT-ADMSCs. All dogs were bred adaptively for 1 week. In the latter two groups, ADMSCs (ADMSCs: transplanted 1 × 107 ADMSCs suspended in 10 mL sterile 0.9% NaCl, MLT-ADMSCs: transplanted 1 × 107 MLT-ADMSCs suspended in 10 mL sterile 0.9% NaCl) passed through the dog's forearm Brachial vein injection. To determine trace the ADMSCs transplanted into the body, the ADMSCs were digested with 0.25% trypsin and resuspended before transplantation. Then the PKH26 red fluorescent cell linker kit was used to label the ADMSCs (Sigma-Aldrich, United States) before transplantation. On the 0th day, 30th day and 60th day of cell transplantation, the blood of each group of dogs was collected for blood routine examination (Prokan, China) and blood biochemical test (Mindray, China). After the 60th day of cell transplantation, all dogs were euthanized (intravenous overdose of KCl). Collect dog liver, spleen, kidney, and pancreas tissues for frozen section. Subsequently, sections were stained with Hoechst 33342 at 0.5 μg/mL before being observed under a microscope.

Histological Analysis

The liver and pancreas tissues were fixed in 4% paraformaldehyde, gradually dehydrated, embedded in paraffin, cut into 4 μm sections, and subjected to hematoxylin/eosin (H&E) staining. Periodic acid Schiff (PAS) staining was performed according to the manufacturer's protocols for liver sections (Solarbio, China) (Fang et al., 2018; Yan et al., 2019).

For the cellular immunofluorescence, the cells were fixed in 4% paraformaldehyde in phosphate-buffered saline (PBS) at room temperature (RT) for 10 min, washed three times with PBS, and then permeabilized for 15 min with 0.1% Triton-X 100 (Sigma-Aldrich, St. Louis, MO, United States) in PBS at RT. The cells were blocked with PBS supplemented with 4% bovine serum albumin for 30 min and incubated with primary antibodies against MT1 (1:100, Boster, China) and MT2 (1:100, Boster, China) at 4°C for 16 h. After washing with PBS three times, the cells were incubated with secondary antibodies for 1 h at 37°C in the dark. Following another three washing steps with PBS, nuclear counterstaining was performed with 1 μg/mL Hoechst 33342 (Sigma-Aldrich). The fluorescence images were obtained by Evos f1 fluorescence microscopy (AMG, United States).

For the tissue immunofluorescence, liver and pancreas sections were subjected to baking, dewaxing, and repair of antigens with sodium citrate buffer (0.01 M, pH 6.0). The liver sections were incubated with a rabbit anti-rat glucose transporter 4 (GLUT4) antibody, and the pancreas sections were incubated with a rabbit anti-rat insulin antibody (1:100, Proteintech, China) at 4°C overnight. Then, the sections were washed and incubated with Alexa Fluor 555-conjugated donkey anti-rabbit IgG or FITC-conjugated goat anti-rabbit IgG (Invitrogen) for 1 h. Subsequently, the sections were stained with Hoechst 33342 at 0.5 μg/mL before being observed under a microscope.

For the immunohistochemistry, liver and pancreas sections were subjected to baking, dewaxing, and repair of antigens with sodium citrate buffer (0.01 M, pH 6.0). The tissue was blocked with animal serum after eliminating the effects of endogenous peroxidase with 3% H_2O_2. The liver and pancreas sections were incubated with rabbit anti-rat interleukin-10 (IL-10) (1:200, Proteintech, China), tumor necrosis factor-α (TNF-α), interleukin-6 (IL-6) (1:200, CST, United States), glucose-regulated protein 78 (GRP78), C/EBP-homologous protein (CHOP), and activating transcription factor 6 (ATF-6) (1:200, Bioss, China) antibodies at 4°C overnight. Then, the cells were incubated with horseradish peroxidase-labeled streptavidin working solution after washing three times with PBS. The detection was performed using 3′-diaminobenzidine (ZLI-9018; Beijing Zhongshan Golden Bridge Biotechnology Co., Ltd.), and the nucleus was stained with hematoxylin. Finally, the samples were dehydrated and covered. The tissues were analyzed under a light microscope (Nikon, Japan) (Wei et al., 2021).

Statistical Analysis

When the main effects were significant, a one-way analysis of variance (ANOVA) was used, followed by Newman–Keuls multiple range tests. A Student's *t*-test was used when comparing the means of two groups. All data are presented as the mean ± SE, and statistical significance is shown as follows: ns > 0.05; $^{*}p < 0.05$; $^{**}p < 0.01$; and $^{***}p < 0.001$. All data were analyzed by GraphPad Prism software (La Jolla, CA, United States) and represent a minimum of three different experiments.

RESULTS

Melatonin Treatment Can Enhance the Viability of Adipose-Derived Mesenchymal Stem Cells Cultured *in vitro*

Compared with the normal cultured ADMSCs, the MLT treatment did not change the morphology but increased the number of the ADMSCs (**Figure 1A**). The ADMSCs maintained rapid proliferation. and MLT treated ADMSCs proliferated faster than the control group in the first 5 days and particularly be observed in the first 4 days (**Figure 1B**). As shown in the results of the EdU staining, the cell proliferation rate of the MLT treatment group was faster than that in the normal ADMSC group (**Figures 1C,D**). The main MLT receptors include MLT receptor 1A (MT1) and MLT receptor 1B (MT2). By staining MT1/MT2 with immunofluorescence, we found that MLT bound MLT-ADMSCs effectively in the MLT treatment group (**Figure 1E**). The results show that MLT binds the MT1/MT2 receptors of ADMSCs and promotes the viability of ADMSCs cultured *in vitro*.

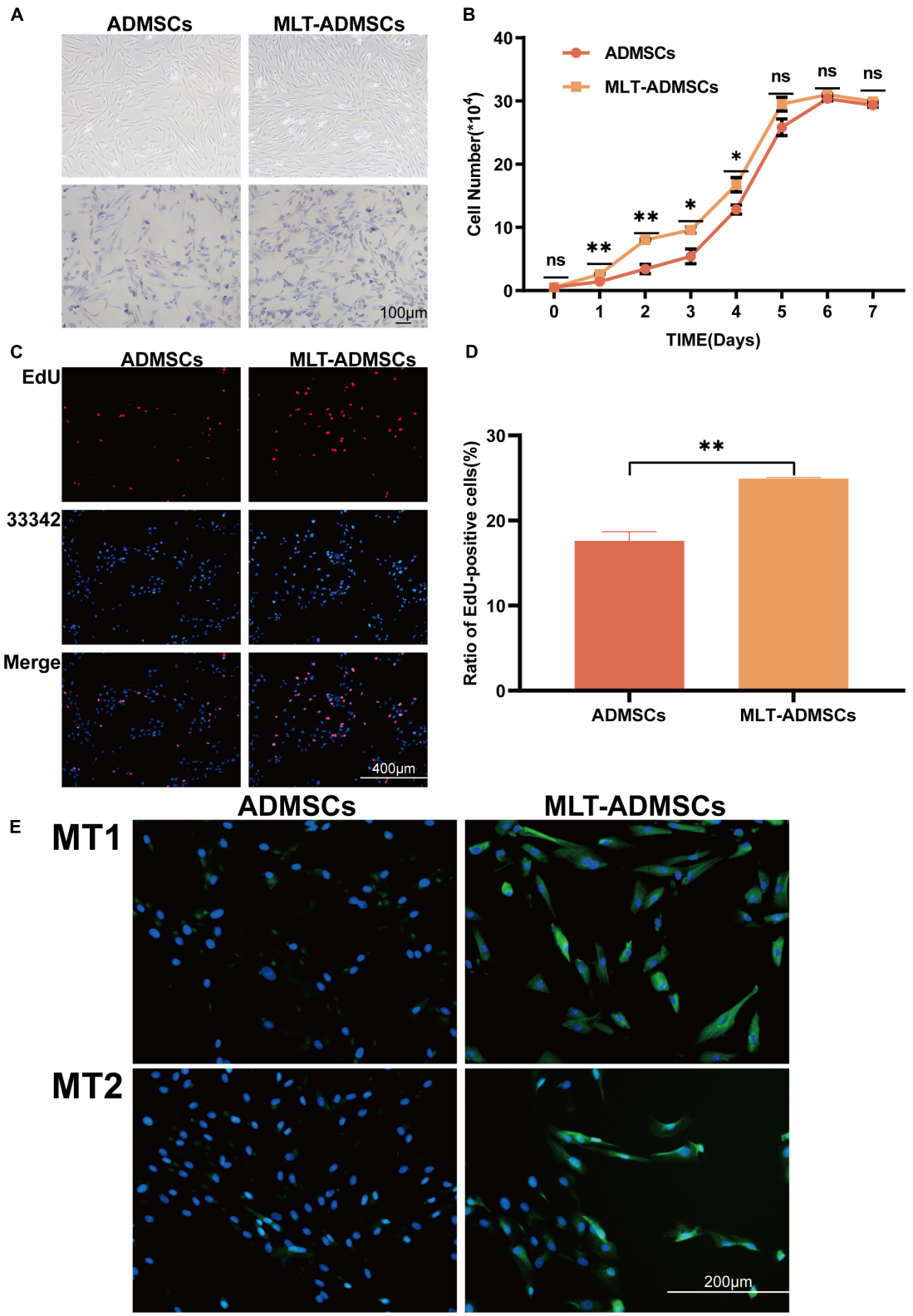

FIGURE 1 | MLT treatment can enhance the viability of ADMSCs cultured *in vitro*. **(A)** Cell morphology (ADMSCs and MT-ADMSCs). **(B)** Cell growth curve. **(C)** EdU staining. **(D)** Quantitative analysis of EdU. **(E)** MT1/MT2 immunofluorescence staining. Values in this figure are the mean ± SE; $n = 3$ per group; ns > 0.05, $^{*}p < 0.05$, $^{**}p < 0.01$ determined by a repeated-measures ANOVA.

Melatonin Enhances the Recovery Effect of Adipose-Derived Mesenchymal Stem Cells on Clinical Symptoms and Hyperglycemia in Type 2 Diabetes Mellitus Mice and Promotes Islet Reconstruction

To determine the therapeutic effect of ADMSCs on T2DM, T2DM model mice were prepared by a high-fat diet (HFD) combined with low-dose STZ injection. The data show that we successfully established a T2DM mouse model (**Figures 2A–F**). The weight of the mice reached approximately 40 g after 8 weeks of the HFD and was significantly reduced after the STZ injection (**Figure 2G**). In addition, the diet of the mice increased, and the blood sugar level exceeded 16.7 mmol/L, which is consistent with the typical symptoms of T2DM (**Figures 2A–D**). The ADMSCs and MLT-ADMSCs effectively reduced the weight of the mice (**Figure 2A**). Similarly, the increase in the diet of the mice caused by T2DM was alleviated in the ADMSC group and MLT-ADMSC group (**Figures 2B,C**). The occurrence of T2DM is mainly assumed in the presence of hyperglycemia and insulin resistance. The data show that treatment with ADMSCs alleviates hyperglycemia in mice, which was manifested by inhibiting the further deterioration of the disease and maintaining the blood sugar level at the initial level of T2DM. Surprisingly, ADMSCs treated with MLT had a stronger hypoglycemic effect on T2DM. After treatment with MLT-ADMSC, the hyperglycemia of the mice was significantly improved (**Figure 2D**). The hyperglycemia that occurs in T2DM is mainly caused by islet damage and insulin resistance in peripheral tissues. In this study, H&E staining and immunofluorescence staining were used to detect pancreatic islet damage and insulin secretion in mice. The results showed that after the HFD combined with the STZ injection, the pancreatic islets were damaged in the mice, and the amount of insulin secretion was significantly reduced. The results showed that after T2DM was treated with PBS sham operation, blood sugar continued to rise, pancreatic islets decreased, β cells were lost, and insulin secretion was significantly reduced. After treatment with ADMSC treatments, the mice's pancreatic islet injury was significantly recovered, the island structure was clear, the number of β cells was restored, and the amount of insulin secretion was significantly restored. In addition, we found that insulin secretion after the MLT-ADMSC treatment was significantly restored and basically returned to the normal levels (**Figures 2E,F**). Various data show that the ADMSC treatment restored the typical symptoms of T2DM in mice, including restoring their diet, improving their weight, lowering the blood sugar levels, rebuilding islets, and restoring insulin secretion.

Melatonin Enhances the Recovery Effect of Adipose-Derived Mesenchymal Stem Cells on Insulin Resistance in Type 2 Diabetes Mellitus Mice

When T2DM occurs, the body develops insulin resistance, and the utilization rate of insulin is reduced, resulting in an increase in blood sugar that cannot be reduced. In addition, insulin resistance causes islet β cell fatigue and further damages islet β cells. The relative lack of insulin changes to an absolute lack of insulin and aggravates T2DM. Related indicators of insulin resistance, including the OTGG, IRT, IPITT, and HOME-IR index, were used to assess the therapeutic effect of ADMSCs. In addition, the differences in the therapeutic effects of ADMSCs and MLT-ADMSCs were compared. After the treatment with ADMSCs, insulin resistance in the T2DM mice was reduced. Interestingly, compared with the ADMSCs, the MLT-ADMSCs had a stronger recovery effect on insulin resistance (**Figures 3A,C**). When the body produces insulin resistance, its sensitivity to insulin decreases. ADMSCs treatment restored the secretion and utilization of insulin. MLT enhances the effect of ADMSCs (**Figure 3B**). The HOME-IR index results showed that the ADMSCs restored the insulin sensitivity of the mice, and the MLT-ADMSC group exhibited a stronger effect (**Figure 3D**). These various data indicate that ADMSCs can promote the recovery of insulin resistance and significantly restore insulin sensitivity in mice. Surprisingly, the MLT treatment significantly enhanced this role of ADMSCs.

Melatonin Enhanced the Recovery Effect of Adipose-Derived Mesenchymal Stem Cells on Glucose Metabolism in Type 2 Diabetes Mellitus Mice and Repaired Liver Damage and Lipid Metabolism Disorder Caused by Type 2 Diabetes Mellitus

The liver is an important organ of glucose metabolism. The liver plays an important role in maintaining blood sugar balance by regulating the absorption, storage, production and metabolism of glucose. When T2DM occurs, the liver is damaged, which leads to impaired glucose metabolism. The results revealed that when T2DM occurred, the liver was damaged, and the biochemical indicators changed, manifesting as increases in ALT and AST (**Figures 4A–C**). ADMSCs treatment restored the liver function of mice, and MLT-ADMSCs had better effect (**Figures 4A–C**). In addition, when T2DM occurs, the liver is damaged, the liver cells are fused necrotic, swollen, nucleus loose, and balloon-like degeneration. ADMSCs treatment promote liver damage repair and liver cell regeneration, MLT enhances this effect (**Figure 4F**). Our previous studies have shown that ADMSCs restored liver damage caused by carbon tetrachloride (Yan et al., 2019). In this study, the ADMSC treatment alleviated the liver damage caused by T2DM, proving the extensive therapeutic effects of ADMSCs on the liver. When T2DM occurs, with the decreasing ratio of insulin to glucagon, lipolysis accelerates, and numerous fatty acids and glycerol enter the liver. Too many fatty acids esterified into triglycerides causes hyperlipidemia and easily leads to complications of T2DM, such as atherosclerosis. The ADMSC treatment promoted the recovery of the serum TC and TG levels, and MLT enhanced this effect (**Figures 4D,E**). Previous studies have shown that ADMSCs promoted the body's sensitivity to insulin and improve the body's insulin resistance

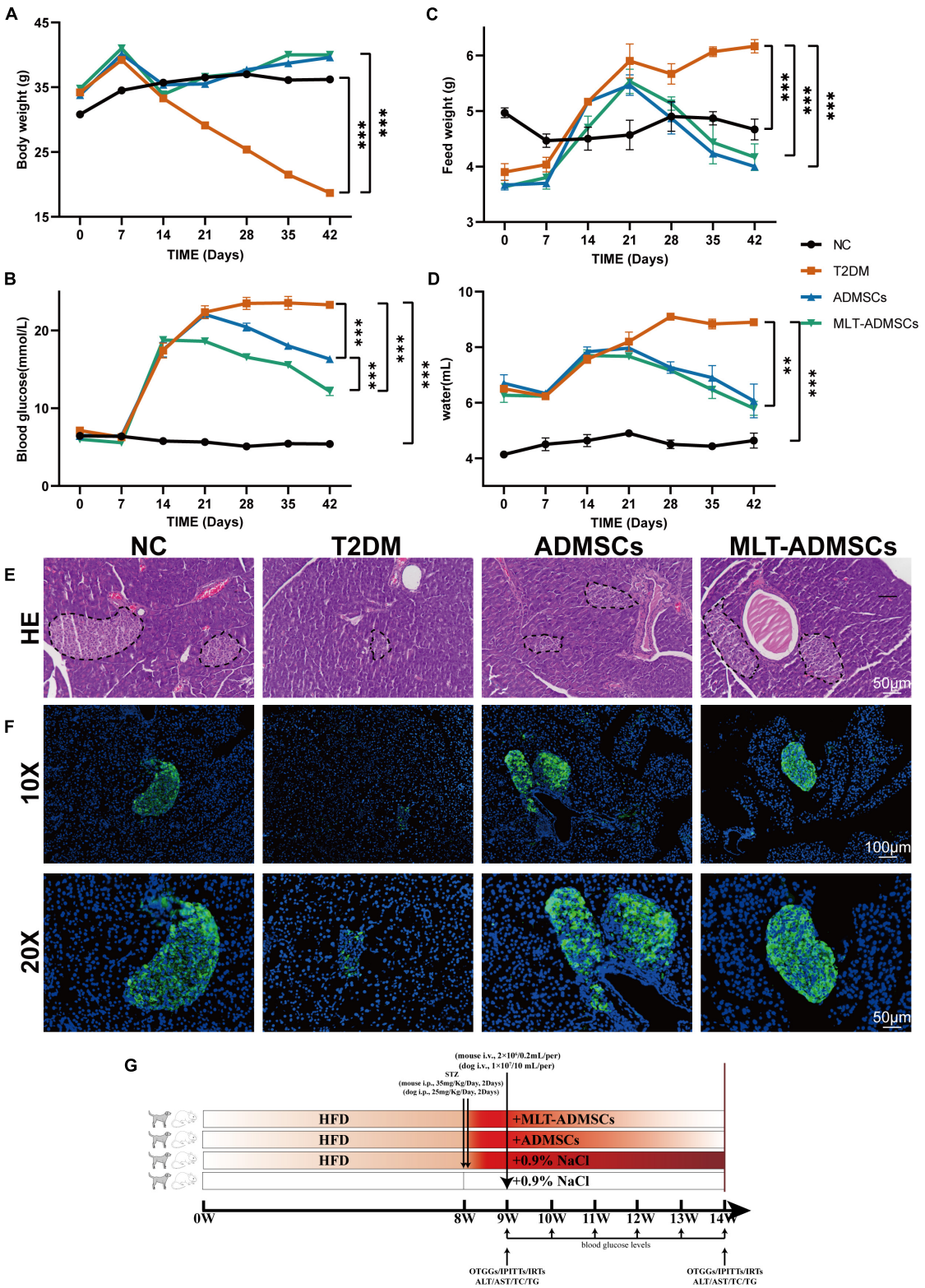

FIGURE 2 | MLT enhances the recovery effect of ADMSCs on clinical symptoms and hyperglycemia in T2DM mice and promotes islet reconstruction. **(A)** Continuous monitoring of the weight level of mice. **(C)** Changes in the feed intake of mice. **(D)** Changes in the water intake of mice. **(B)** Random blood glucose changes in mice. **(E)** Pancreas H&E staining. **(F)** Pancreas immunofluorescence insulin. **(G)** Experimental design. Values in this figure are the mean ± SE; $n = 10$ mice per group; $^{**}p < 0.01$, $^{***}p < 0.001$ determined by a repeated-measures ANOVA.

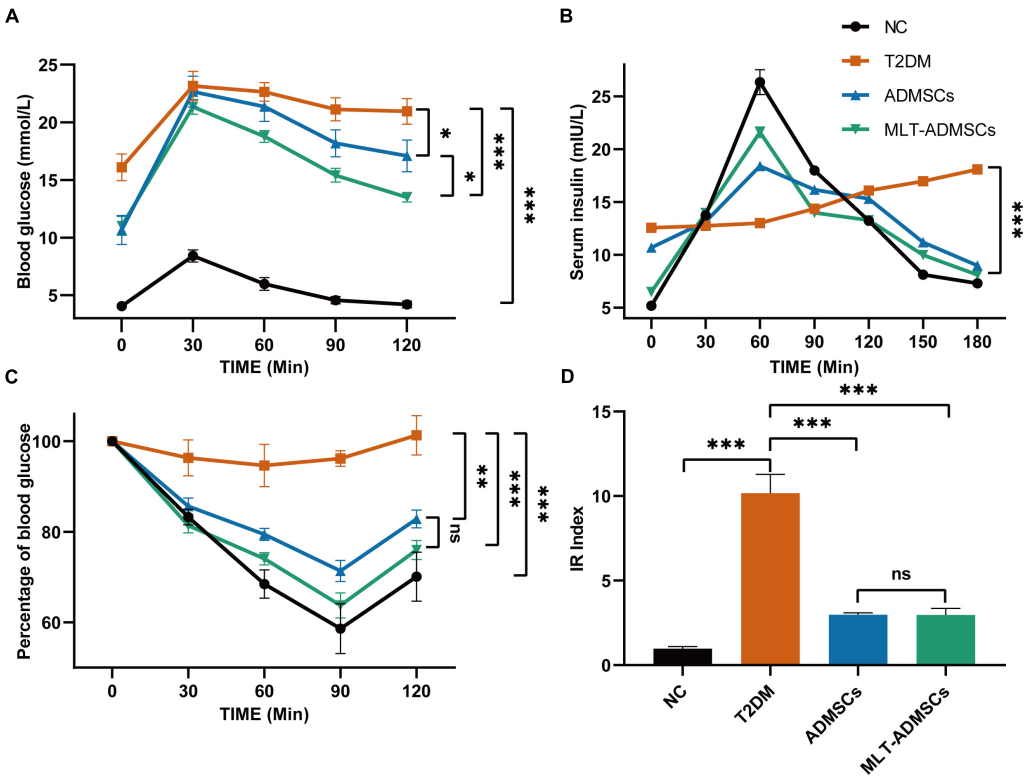

FIGURE 3 | MLT enhances the recovery effect of ADMSCs on insulin resistance in T2DM mice. **(A)** OTGG. **(B)** IRTs. **(C)** IPITT. **(D)** IR index in each group, HOMA-IR index = [FBG (in mmol/L) × FINS (in units/L)]/22.5. The blood glucose level in each group was detected after fasting for 3 h. Values in this figure are the mean ± SE; n = 10 mice per group; ns > 0.05, $^{*}p < 0.05$, $^{**}p < 0.01$, $^{***}p < 0.001$ determined by a repeated-measures ANOVA.

(**Figure 3**), MLT promote the effect of ADMSCs. To study how ADMSCs improve insulin resistance and insulin sensitivity, hepatic glycogen accumulation and GLUT4 expression were detected, and the ADMSC treatment restored the glycogen synthesis disorder and GLUT4 expression caused by T2DM (**Figures 4G,H**). These results indicate that ADMSCs repaired liver damage caused by T2DM and restored the glucose metabolism and lipid metabolism functions of the liver. The repair of liver leads to the recovery of glucose and lipid metabolism, thereby alleviating insulin resistance, restoring insulin sensitivity, promoting islet regeneration, and restoring insulin secretion. In summary, ADMSCs treat T2DM by restoring liver function and rebuilding islets. Moreover, MLT-ADMSCs exhibit a stronger therapeutic effect.

Melatonin Promotes the Therapeutic Effect of Adipose-Derived Mesenchymal Stem Cells by Enhancing the Anti-inflammatory and Anti-endoplasmic Reticulum Stress Abilities of Islets and Liver Function

Patients with T2DM often experience ER stress and chronic inflammation. The immunohistochemical staining showed that the ADMSCs alleviated islet inflammation and ER stress (**Figures 5A–F**). Inflammation and ER stress in islets can lead to injury to islet β cells. Restoring ER stress and inflammation in the islet microenvironment is beneficial for rebuilding islet β cells. ADMSCs promote the remodeling of pancreatic β-cells by repairing inflammation and ER stress levels in the islet microenvironment.

Type 2 diabetes mellitus causes liver disease and liver dysfunction. The mechanism involves the stimulation of liver glycogen metabolism and lipid metabolism disorders through hyperglycemia. Previous data have confirmed that ADMSCs alleviate liver damage caused by T2DM, but how they work remains unclear. The immunohistochemical staining showed that the therapeutic effect of ADMSCs in the liver was also related to the recovery of ER stress and inflammation (**Figures 6A–F**). In summary, the results show that the therapeutic effect of ADMSCs on T2DM is by restoring inflammation and ER stress. It is speculated that ADMSCs promote the recovery of multiple organs and have a therapeutic effect on T2DM from the perspective of the overall organ microenvironment.

Melatonin Promotes the Therapeutic Effect of Adipose-Derived Mesenchymal Stem Cells in Canine DM

The dog DM model was established by HFD and STZ. Seven days after the STZ injection, the dogs' weight decreased, the blood

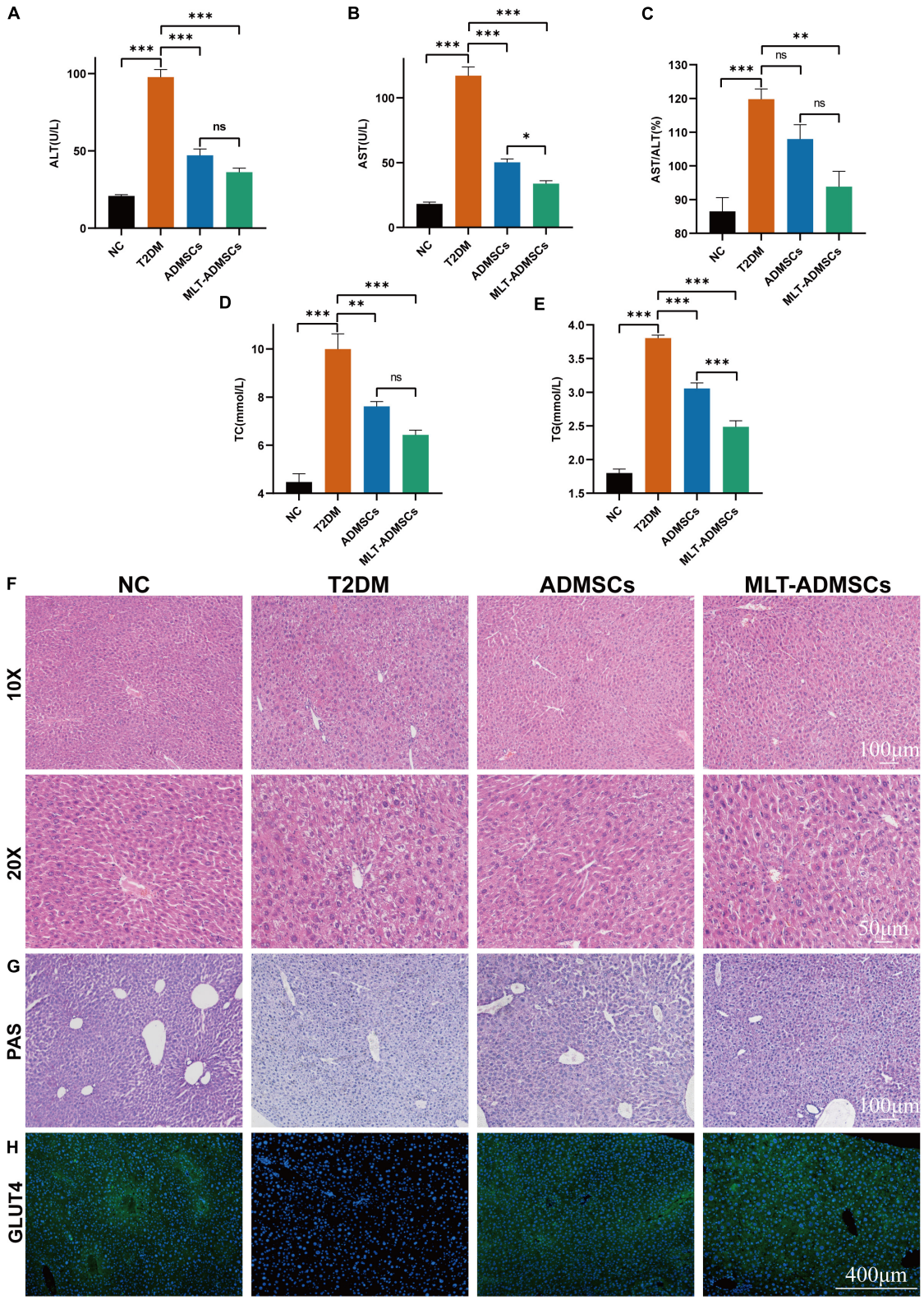

FIGURE 4 | MLT enhanced the recovery effect of ADMSCs on glucose metabolism in T2DM mice and repaired the liver damage and lipid metabolism disorders caused by T2DM. **(A)** Serum ALT. **(B)** Serum AST. **(C)** AST/ALT. **(D)** Serum TC. **(E)** Serum TG. **(F)** Liver H&E staining. **(G)** Liver PAS staining. **(H)** Liver immunofluorescence GLUT4. Values in this figure are the mean ± SE; $n = 10$ mice per group; ns > 0.05, $^{*}p < 0.05$, $^{**}p < 0.01$, $^{***}p < 0.001$ determined by a repeated-measures ANOVA.

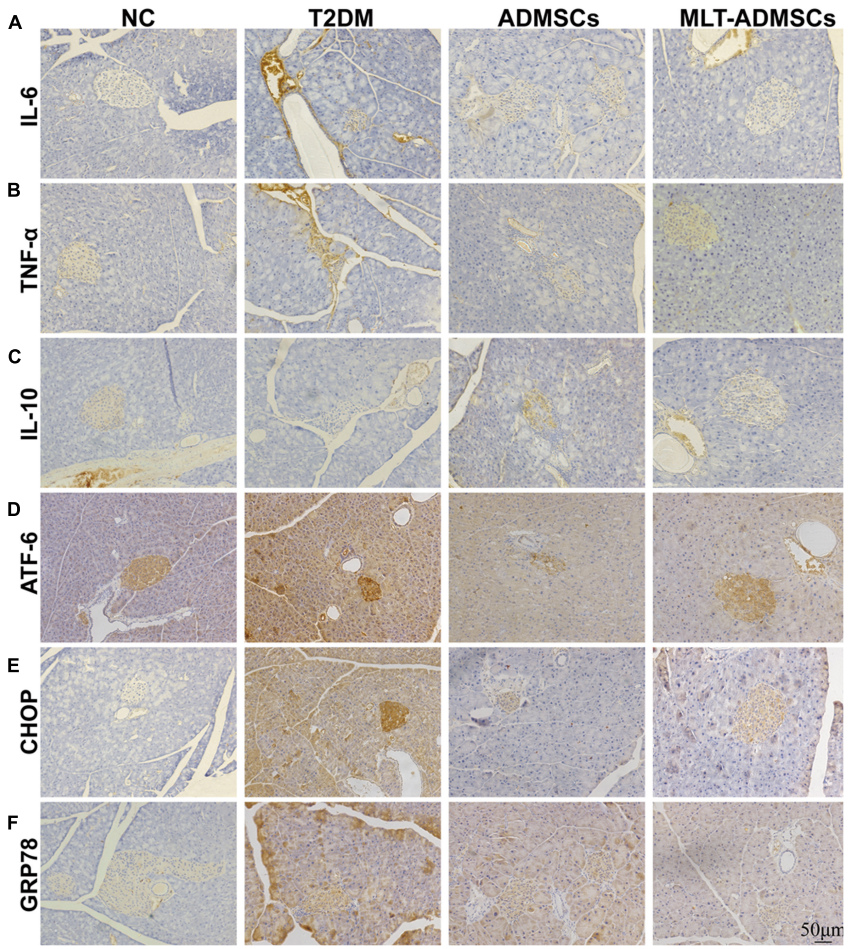

FIGURE 5 | MLT promotes the therapeutic effect of ADMSCs through stronger anti-inflammatory and anti-ER stress abilities to restore pancreatic islet function. **(A)** Pancreatic IL-6 expression. **(B)** Pancreatic TNF-α expression. **(C)** Pancreatic IL-10 expression. **(D)** Pancreatic ATF-6 expression. **(E)** Pancreatic CHOP expression. **(F)** Pancreatic GRP78 expression.

glucose level increased, and the ADMSC treatment alleviated these symptoms (**Figures 7A,B**). In addition, H&E staining and insulin immunofluorescence staining were performed using each group of pancreases. The data show that MLT in dogs can also promote the recovery of hyperglycemia and insulin secretion by ADMSCs in dogs (**Figures 7C,D**). Similarly, the results of the liver H&E staining and PAS staining further confirmed the recovery effect of ADMSCs on liver damage and glucose metabolism in canine diabetes (**Figures 7E,F**). In dogs with DM, ADMSCs and MLT-ADMSCs have effects similar to those in mice.

The Ability of Melatonin to Promote the Proliferation of Adipose-Derived Mesenchymal Stem Cells Depends on the Transforming Growth Factor β Pathway

Previous data have confirmed that MLT promotes the viability of ADMSCs *in vitro* (**Figure 1**), but the mechanism by which MLT regulates the viability of ADMSCs is unknown. The MLT receptor inhibitor luzindole and the TGF-βR1/ALK5 inhibitor SB431542 were combined with MLT to treat ADMSCs. When luzindole was used to inhibit MT1/MT2, the expression of MT1/MT2 in the ADMSCs was inhibited (**Figure 8A**), and cell proliferation slowed (**Figures 8B–D**). This finding explains why the effect of MLT on the activity of ADMSCs depends on its combination with MT1/MT2. The TGF-β pathway includes TGF-β ligands (TGF-β1, TGF-β2, and TGF-β3), TGF-β receptors (TGF-βR1 and TGF-βR2) and downstream Smad and Smad-related transcription factors. When the TGF-β inhibitor SB431542 was added, the cell proliferation caused by MLT was inhibited (**Figures 8B–D**). Inhibited TGF-β receptor, MLT still binds to MT1/MT2 (**Figure 8A**). The above results indicated that MLT firstly binds to the MT1/MT2 of ADMSCs, thereby affecting the TGF-β pathway. The expression of genes related to the TGF-β pathway was detected; it was found that MLT activated the TGF-β pathway (**Figure 9A**). With the activation of the cell cycle-related genes MYC/CREBBP/EP300, it is speculated that MLT activates the TGF-β pathway to

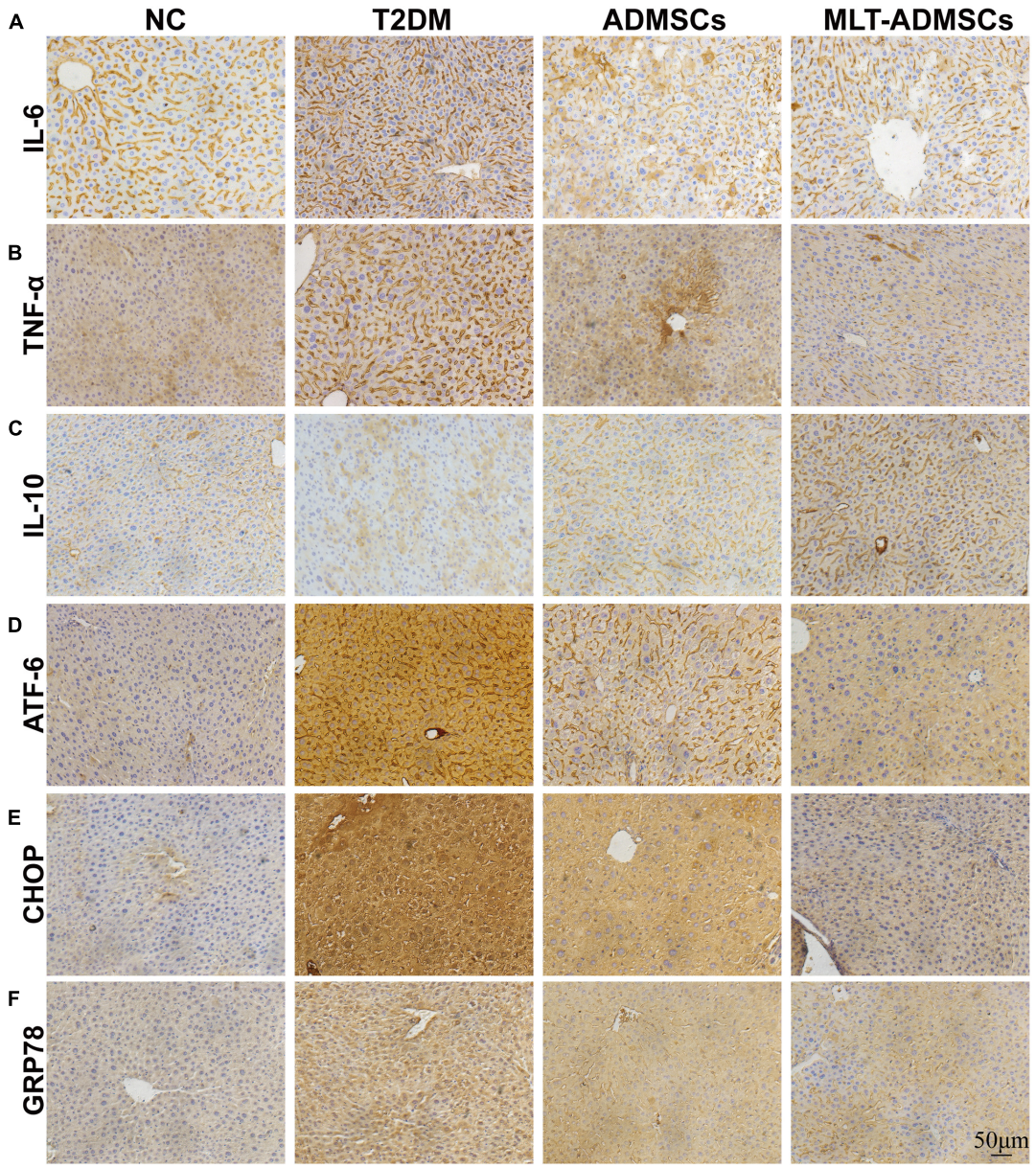

FIGURE 6 | MLT promotes the therapeutic effect of ADMSCs through stronger anti-inflammatory and anti-ER abilities to restore liver function. **(A)** Liver IL-6 expression. **(B)** Liver TNF-α expression. **(C)** Liver IL-10 expression. **(D)** Liver ATF-6 expression. **(E)** Liver CHOP expression. **(F)** Liver GRP78 expression.

promote the cell cycle renewal of ADMSCs, thereby promoting the viability of ADMSCs (**Figure 9A**). In addition, when the binding of MLT to MT1/MT2 was inhibited, the overall expression of TGF-β family and downstream genes was decreased (**Figure 9B**). The above results proved that MLT first combines with MT1/MT2 and then activates the TGF-β family, thereby affecting the cell cycle and promoting cell viability. Surprisingly, MLT promoted the ADMSCs to secrete more TGF-β, which explains the increased expression of the TGF-β receptors TGF-βR1 and TGF-βR2 and may be related to the mechanism by which MLT promotes the efficacy of ADMSCs (**Figure 9C**).

Inhibition of the Transforming Growth Factor β Pathway Blocked the Promotion of Adipose-Derived Mesenchymal Stem Cell Efficacy by Melatonin

To determine the function of TGF-β on the therapeutic effect of ADMSCs, MLT-ADMSCs treated with SB431542 were used to treat T2DM mice (**Figure 10G**). When TGF-β is inhibited, the recovery effect of ADMSCs on blood sugar levels, insulin resistance levels and islet remodeling is weakened (**Figures 10A,C,D** and **Supplementary Figure 2**). When TGF-β is inhibited, the recovery of liver function

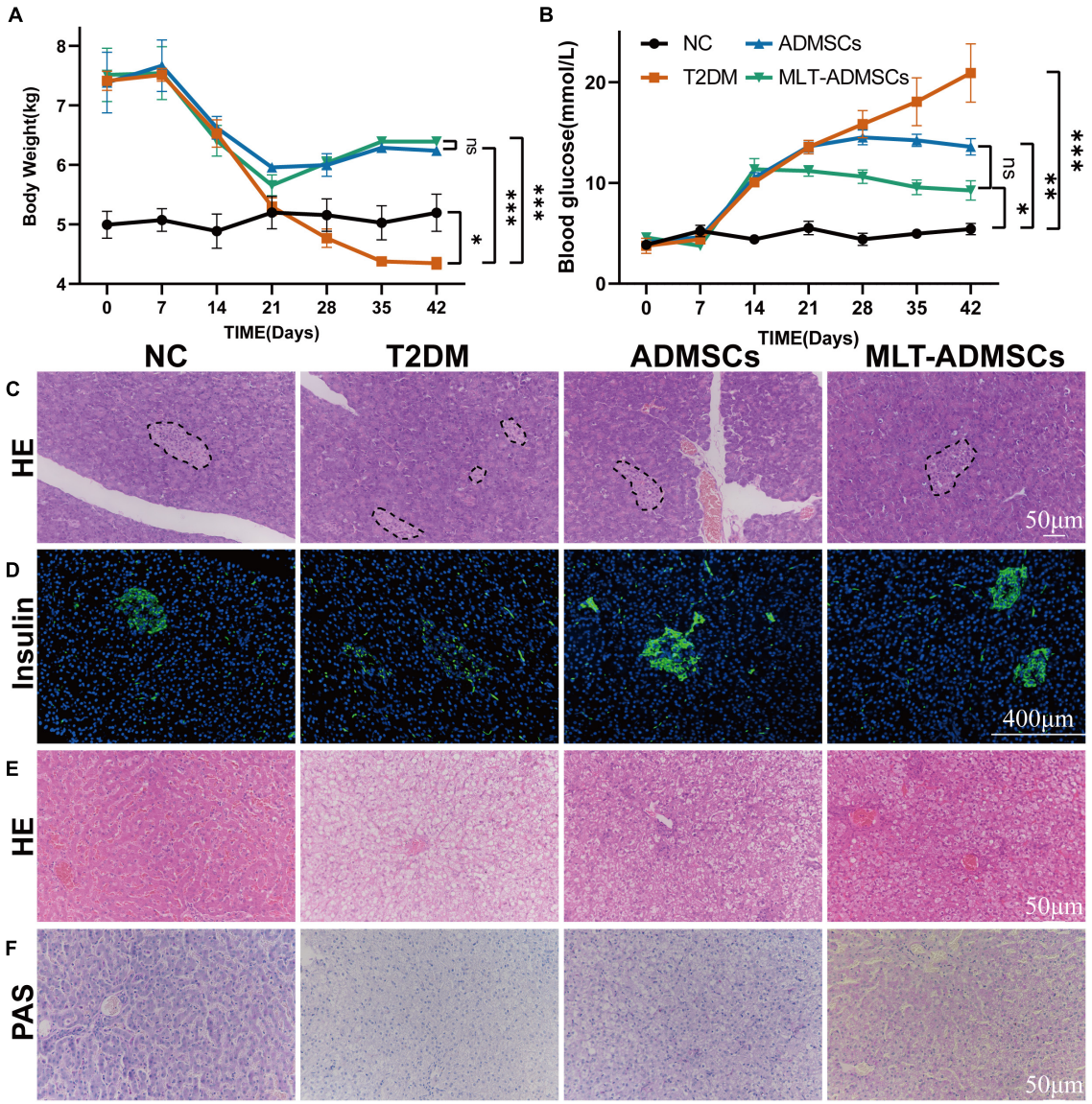

FIGURE 7 | MLT promotes the therapeutic effect of ADMSCs in canine DM. **(A)** Weight changes. **(B)** Random blood glucose changes. **(C)** Islet H&E staining. **(D)** Insulin immunofluorescence staining. **(E)** Liver H&E staining. **(F)** Liver PAS staining. Values in this figure are the mean ± SE; $n = 3$ per group; ns > 0.05, $^{*}p < 0.05$, $^{**}p < 0.01$, $^{***}p < 0.001$ determined by a repeated-measures ANOVA. The dotted ellipse includes the location and size of the islets.

is weakened (**Figures 10B,E**). In addition, inhibiting TGF-β reduced the recovery effect on liver glycogen metabolism (**Figure 10F**). In summary, TGF-β is the key factor by which MLT impacts ADMSCs.

Transplantation of Adipose-Derived Mesenchymal Stem Cells and Melatonin-Adipose-Derived Mesenchymal Stem Cells Is Safe for Animals

To determine the safety of ADMSCs and MLT-ADMSCs, healthy dogs were injected with ADMSCs and MLT-ADMSCs. The dogs' physiological data were regularly checked, and residual ADMSCs were detected after 60 days. The physiological indicators of all dogs were within the normal range (**Figures 11A,B**). After 60 days, the residual status of ADMSCs was detected. ADMSCs and MLT-ADMSCs were not detected in the liver, kidney, pancreas, or spleen (**Figure 11C**). In general, all MSCs were cleared after 60 days, and there were no side effects in the dogs.

DISCUSSION

Thus far, many studies investigated the effect of MSCs treatment on various diseases. The main point of view

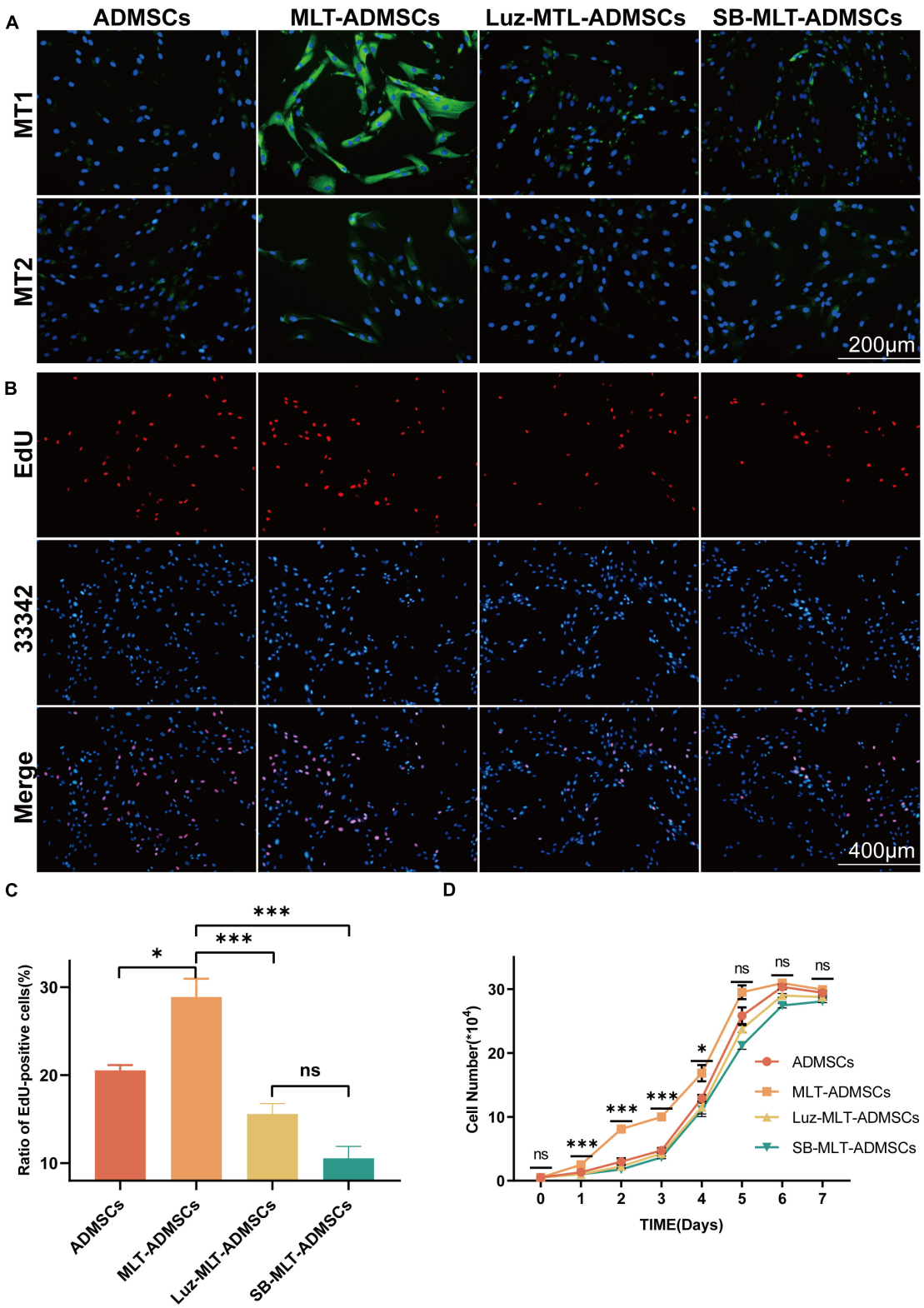

FIGURE 8 | MLT depends on the MT1/MT2 receptor and activates the TGF-β pathway to promote the viability of ADMSCs. **(A)** MT1/MT2 immunofluorescence staining. **(B)** EdU staining. **(C)** EdU quantitative analysis. **(D)** Cell growth curve. Values in **(C,D)** are the mean ± SE; $n = 3$ per group; ns > 0.05, $^{*}p < 0.05$, $^{***}p < 0.001$ determined by a repeated-measures ANOVA.

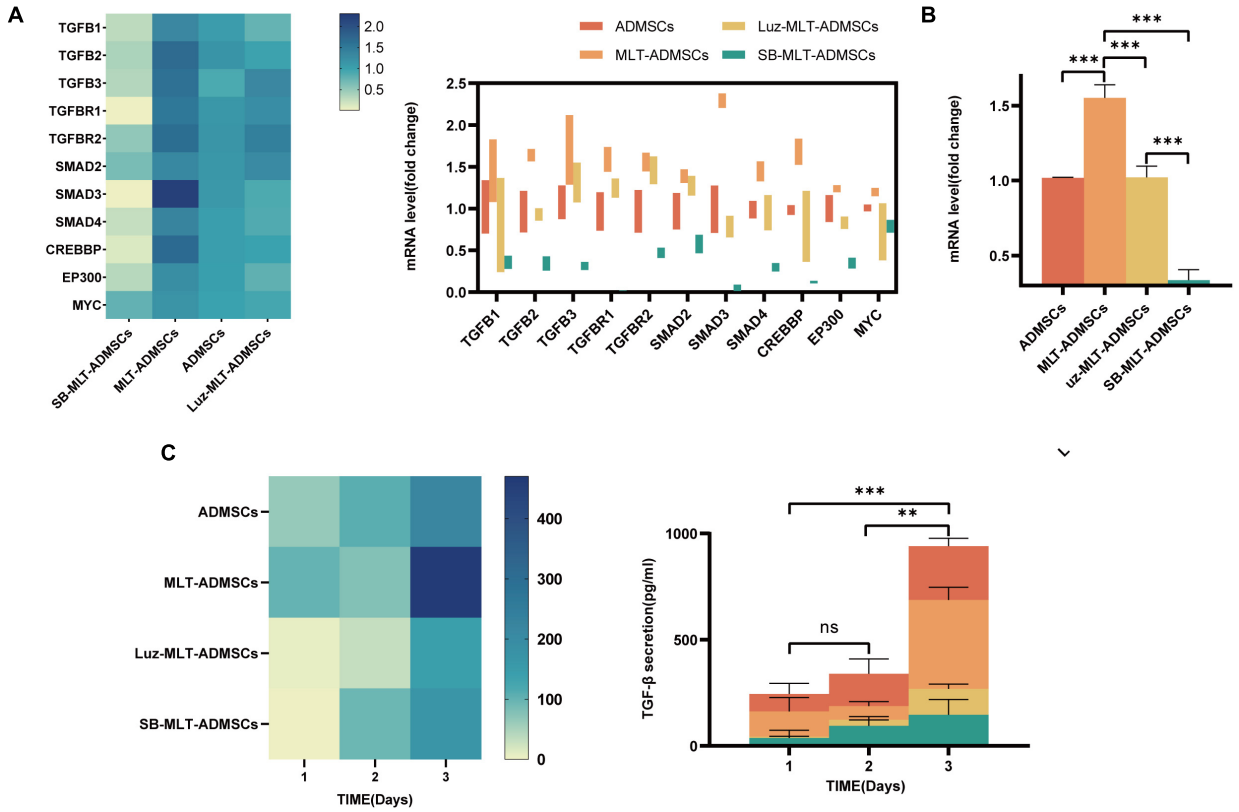

FIGURE 9 | MLT activates the TGF-β pathway in ADMSCs. **(A)** TGFB expression level. **(B)** TGF-β pathway expression level. **(C)** ELISA was used to detect the amount of TGF-β secretion. Values in this figure are the mean ± SE; $n = 3$ per group; ns > 0.05, *$p < 0.05$, **$p < 0.01$, ***$p < 0.001$ determined by a repeated-measures ANOVA.

is that MSCs differentiate into insulin-secreting cells, promote the regeneration of pancreatic islet β cells, protect endogenous pancreatic β cells, restore insulin resistance, improve glucose metabolism, etc., to achieve therapeutic effects (Rodríguez-Lozano et al., 2015; Zang et al., 2017; Hu and Li, 2019; Li et al., 2021; Xue et al., 2021). Studies have shown that MSC treat diseases by restoring body inflammation, ER stress, oxidative stress, autophagy, etc (Volarevic et al., 2011; Davey et al., 2014; Zang et al., 2017; Yu et al., 2019; He et al., 2020; Elshemy et al., 2021). However, there are still many problems in treatment using MSCs. Various unfavorable factors *in vivo* and *in vitro* affect the cell state of MSCs and hinder their therapeutic effect (Farahzadi et al., 2018; Hu and Li, 2019). Long-term *in vitro* culture leads to reduced MSC proliferation ability, senescence, and morphological changes (Danisovic et al., 2017; Farahzadi et al., 2018). Furthermore, 80–90% of ADMSCs died within 72 h after transplantation (Liu et al., 2009; Jeong and Cho, 2016; Danisovic et al., 2017). The low survival rate and proliferation rate of MSCs after transplantation are mainly due to the lack of nutrients or growth factors needed by MSCs in the body. Furthermore, adverse factors, such as oxidative stress and chronic inflammation in the body, affect the survival of MSCs *in vivo* (Han et al., 2016). Thus far, studies have attempted to promote the viability of MSCs *in vivo* and *in vitro*, but the effect is still not satisfactory, and research aiming to promote cell viability is lacking (Liu et al., 2009; Chen et al., 2014; Lee et al., 2014; Tang et al., 2014; Han et al., 2016; Shuai et al., 2016; Kadry et al., 2018).

Melatonin plays an important physiological role in the human body, and it has been determined that MLT plays an important role in the regulation of the circadian rhythm (Redman et al., 1983; McArthur et al., 1997). There are many advantages to using MLT for MSC culture. MLT are used as a component of cytoprotective agents to protect MSCs from oxidative stress, inflammation, apoptosis, and aging to regulate the cellular state of MSCs *in vivo* and *in vitro* (Calvo et al., 2013; Ma et al., 2013). Studies have shown that MLT promotes the proliferation and osteogenic differentiation of MSCs *in vitro* (Luchetti et al., 2010, 2014; Rodríguez-Lozano et al., 2015). In this study, we used MLT as an additive in the culture of ADMSCs *in vitro*. The results indicate that MLT promotes the viability of ADMSCs cultured *in vitro*. To explore how MLT affects ADMSCs, we used luzindole combined with MLT to treat ADMSCs. When the two receptors MT1/MT2 of MLT are inhibited, the pro-proliferation effect of MLT on ADMSCs disappears.

The TGF-β family is an important cytokine in the body that regulates cell proliferation and differentiation (Blobe et al., 2000).

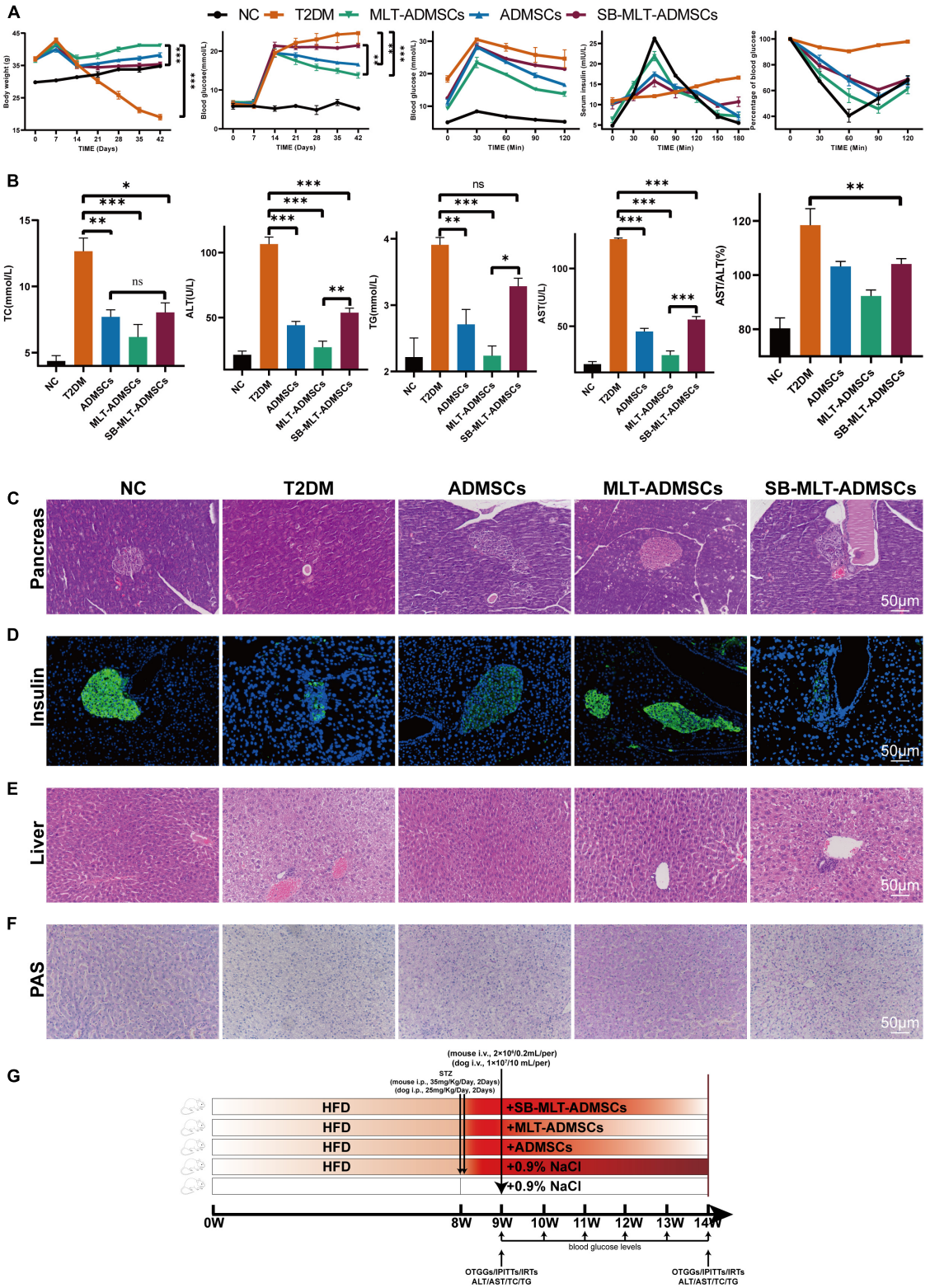

FIGURE 10 | Inhibition of the TGF-β pathway blocked the promotion of the efficacy of ADMSCs by MLT. **(A)** Levels of blood glucose metabolism and insulin resistance, including random blood glucose levels, OTGG, IRTs, and IPITT. **(B)** Liver function and glucose metabolism, including TC, TG, ALT, AST, and AST/ALT. **(C)** Pancreas H&E staining. **(D)** Pancreas immunofluorescence of insulin. **(E)** Liver H&E staining. **(F)** Liver PAS staining. **(G)** Experimental design. Values in this figure are the mean ± SE; $n = 5$ mice per group; ns > 0.05, *$p < 0.05$, **$p < 0.01$, ***$p < 0.001$ determined by a repeated-measures ANOVA.

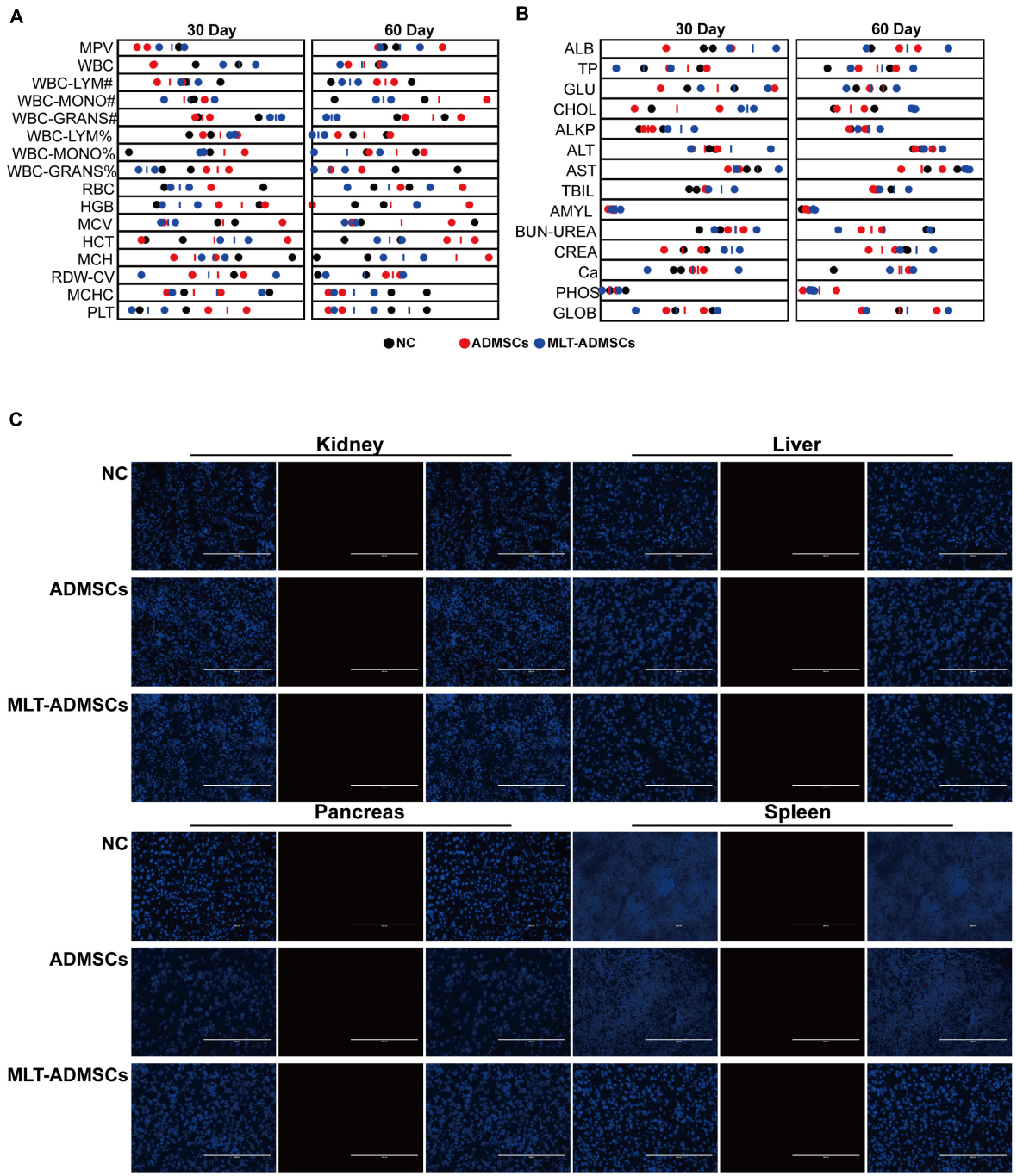

FIGURE 11 | Transplantation of ADMSCs and MLT-ADMSCs is safe for animals. **(A)** Routine blood examination. **(B)** Biochemical analysis. **(C)** PKH26 staining.

Studies have noted that TGF-β is essential for the proliferation of ADMSCs (Ng et al., 2008). We tested the expression of the TGF-β family and its downstream Smad and cell cycle-related transcription factors. After the MLT treatment, the ADMSCs expressed more TGF-β; the expression levels of TGF-βR1, TGF-βR2 and downstream Smad and cell cycle-related transcription factors also increased. We speculate that the proliferation of ADMSCs by MLT may be related to TGF-β. Then, we inhibited the TGF-βR1 of ADMSCs. It was found that when TGF-β was inhibited, the promotion of MLT on ADMSCs disappeared. Interestingly, the inhibition of TGF-β does not affect the expression of MT1/MT2. We also detected TGF-β in the culture medium of ADMSCs after MLT treatment. The above results explain the mechanism by which MLT promotes the

activity of ADMSCs. The combination of MLT and MT1/MT2 promotes the secretion of TGF-β from ADMSCs. MLT improves the cell viability of ADMSCs through the TGF-β pathway.

Subsequently, we used ADMSCs pretreated with MLT to treat T2DM mice and dogs. We found that ADMSCs ameliorated the islet damage and liver damage caused by T2DM. The pancreas and liver are the key organs in T2DM, and their damage leads to T2DM. Two characteristics of T2DM are hyperglycemia and insulin resistance. Damage to pancreatic β cells leads to a decrease in insulin secretion, while liver damage leads to a decrease in the sensitivity of the liver to insulin, leading to hyperglycemia and insulin resistance. The underlying mechanism is mainly due to impaired liver glucose metabolism caused by hyperglycemia stimulation, resulting in insulin resistance, which, in turn, leads to pancreatic β cell damage (American Diabetes Association, 2015).

To determine whether TGF-β is a key factor in MLT function, we used MLT-ADMSCs that inhibit TGF-β to treat T2DM. The results showed the key role of TGF-β. After inhibiting the secretion of TGF-β, the effect of MLT almost disappeared and was even weaker than that of ADMSCs. This result reveals the key role of TGF-β in MLT function. Moreover, the inhibition of TGF-β reduces the efficacy of ADMSCs to a lower level, implying that TGF-β plays a key role in the treatment of MSCs.

Some studies report that ER stress and chronic inflammation are also potential killers of T2DM and cause other complications of T2DM (Hu et al., 2018). Inflammation and ER stress are self-protection measures caused by the body to resist unfavorable factors, but their abnormal occurrence is harmful to the body. We detected the inflammation and ER stress levels in T2DM mice. When T2DM occurs, inflammation and ER stress coexist. After the ADMSC treatment, liver and pancreas inflammation and ER stress were improved. The MLT pretreatment of ADMSCs strengthens these effects. We detected more TGF-β in the culture medium of the ADMSCs after the MLT treatment. The promoting effect of MLT on the efficacy of ADMSCs includes two aspects. First, MLT promotes cell viability and achieves a better therapeutic effect in the body. Second, MLT promotes ADMSCs to secrete more TGF-β, which may be related to a stronger anti-inflammatory and anti-ER stress. In addition, existing studies mostly use human-derived MSCs to treat mouse T2DM models, and xenogeneic therapy has many defects. We used canine-derived ADMSCs to treat mouse and canine disease models, which simulated xenogeneic therapy and allogeneic therapy well, provided a new solution for clinical research concerning MSC therapy and solved the ethical limitations of MSC homologous therapy. Furthermore, as a companion animal of humans, dogs have a living environment and habits that are closer to those of humans. Dogs are a good animal disease model and serve as good subjects for the clinical advancement of MSC treatment.

Melatonin promotes the differentiation ability of MSCs. Off-target differentiation and cancer cell transformation have always plagued the treatment of MSCs. In previous studies, the effect of MLT on the differentiation ability of ADMSCs was partially identified, proving the salvage effect of MLT on the osteogenic differentiation potential of aging ADMSCs. In this study, we observed the cell morphology of ADMSCs treated with MLT, performed morphological staining (**Figures 1A,B**), and confirmed that the morphology of MSCs was normal. We transplanted ADMSCs and MLT-ADMSCs into healthy dogs, and the results showed that ADMSCs and MLT-ADMSCs are safe. There was no residual phenomenon 60 days after the treatment.

Unfortunately, this experiment did not further explore whether TGF-β is directly related to the efficacy of MSCs. More research concerning the function of TGF-β in the treatment of MSCs is needed in the future. There is still a lack of stronger evidence exploring more mechanisms by which MLT promotes the efficacy of ADMSCs. Our research did not prove the relationship between ADMSCs' anti-inflammatory effect and anti-endoplasmic reticulum stress. We know that ADMSCs were anti-inflammatory and anti-ER stress in the body. Since ER stress and inflammation often occur at the same time, it is urgent to research the relationship between endoplasmic reticulum stress and inflammation. Furthermore, as a new animal disease model, more research is needed to establish canine disease models that mimic human diseases. It is necessary to further explore the treatment mechanism of ADMSCs to support the use of ADMSCs in clinical treatment.

CONCLUSION

In this study, MLT was used as an additive to culture ADMSCs *in vitro*. MLT binds MT1/MT2 and activates the TGF-β pathway, thereby affecting the cell cycle changes of ADMSCs and promoting the viability of ADMSCs. ADMSCs primed with MLT were used to treat T2DM in mice and dogs. ADMSCs restore hyperglycemia, insulin resistance, insulin sensitivity, and glucose metabolism in T2DM by restoring inflammation and ER stress in the pancreas and liver. The MLT improved the anti-inflammatory and anti-ER stress abilities of ADMSCs through TGF-β and improved the therapeutic effect, and which is safe and valuable for pet clinic.

DATA AVAILABILITY STATEMENT

The original contributions presented in the study are included in the article/**Supplementary Material**, further inquiries can be directed to the corresponding author.

ETHICS STATEMENT

The animal study was reviewed and approved by the Ethics Committee of Northwest A&F University for the Use of Laboratory Animals.

AUTHOR CONTRIBUTIONS

BL and JH conceived and designed the study. BL, XC, WH, and AA performed the animal experiments. BL, XC, and AA carried out the cell experiments. BL, MZ, NT, and ZK performed the

molecular biology experiments. JD, BL, WJ, SP, and HT analyzed the data. BL drafted the manuscript. JH, BL, and JD revised and edited the manuscript. All authors have read and approved the final version of the manuscript.

FUNDING

This work was supported by grants from the Program of the National Natural Science Foundation of China (32072806), Program of Shaanxi Province Science and Technology Innovation Team (2019TD-036), Program of State Key Laboratory of Respiratory Disease (SKLRD-OP-202114), Program of Animal Hospital Company of Northwest A&F University (K4040121227), and First-class University and Academic Program from Northwest A&F University (Z1010221003).

ACKNOWLEDGMENTS

The authors appreciate Jiaxin Li's excellent comments and revision for this manuscript.

SUPPLEMENTARY MATERIAL

The Supplementary Material for this article can be found online at: https://www.frontiersin.org/articles/10.3389/fcell.2021.722365/full#supplementary-material

REFERENCES

American Diabetes Association (2015). (2) Classification and diagnosis of diabetes. *Diabet. Care* 38(Suppl.), S8–S16.

Blobe, G. C., Schiemann, W. P., and Lodish, H. F. (2000). Role of transforming growth factor beta in human disease. *N. Engl. J. Med.* 342, 1350–1358.

Budi, E. H., Duan, D., and Derynck, R. (2017). Transforming growth factor-β receptors and smads: regulatory complexity and functional versatility. *Trends Cell Biol.* 27, 658–672. doi: 10.1016/j.tcb.2017.04.005

Cai, M., Wang, H., Li, J. J., Zhang, Y. L., Xin, L., Li, F., et al. (2016). The signaling mechanisms of hippocampal endoplasmic reticulum stress affecting neuronal plasticity-related protein levels in high fat diet-induced obese rats and the regulation of aerobic exercise. *Brain Behav. Immunity* 57, 347–359. doi: 10.1016/j.bbi.2016.05.010

Calvo, J. R., González-Yanes, C., and Maldonado, M. D. (2013). The role of melatonin in the cells of the innate immunity: a review. *J. Pineal Res.* 55, 103–120. doi: 10.1111/jpi.12075

Cao, S. S., Luo, K. L., and Shi, L. (2016). Endoplasmic reticulum stress interacts with inflammation in human diseases. *J. Cell. Physiol.* 231, 288–294. doi: 10.1002/jcp.25098

Chen, H. H., Lin, K. C., Wallace, C. G., Chen, Y. T., Yang, C. C., Leu, S., et al. (2014). Additional benefit of combined therapy with melatonin and apoptotic adipose-derived mesenchymal stem cell against sepsis-induced kidney injury. *J. Pineal Res.* 57, 16–32. doi: 10.1111/jpi.12140

Chovatiya, R., and Medzhitov, R. (2014). Stress, inflammation, and defense of homeostasis. *Mol. Cell* 54, 281–288. doi: 10.1016/j.molcel.2014.03.030

Danisovic, L., Oravcova, L., Krajciova, L., Varchulova Novakova, Z., Bohac, M., Varga, I., et al. (2017). Effect of long-term culture on the biological and morphological characteristics of human adipose tissue-derived stem Cells. *J. Physiol. Pharmacol.* 68, 149–158.

Davey, G. C., Patil, S. B., O'Loughlin, A., and O'Brien, T. (2014). Mesenchymal stem cell-based treatment for microvascular and secondary complications of diabetes mellitus. *Front. Endocrinol.* 5:86. doi: 10.3389/fendo.2014.00086

Derynck, R., and Budi, E. H. (2019). Specificity, versatility, and control of TGF-β family signaling. *Sci. Signal.* 12:eaav5183. doi: 10.1126/scisignal.aav5183

Elshemy, M. M., Asem, M., Allemailem, K. S., Uto, K., Ebara, M., and Nabil, A. (2021). Antioxidative capacity of liver- and adipose-derived mesenchymal stem cell-conditioned media and their applicability in treatment of type 2 diabetic rats. *Oxid. Med. Cell. Longev.* 2021:8833467.

Fang, J., Yan, Y., Teng, X., Wen, X., Li, N., Peng, S., et al. (2018). Melatonin prevents senescence of canine adipose-derived mesenchymal stem cells through activating NRF2 and inhibiting ER stress. *Aging* 10, 2954–2972. doi: 10.18632/aging.101602

Farahzadi, R., Fathi, E., Mesbah-Namin, S. A., and Zarghami, N. (2018). Anti-aging protective effect of L-carnitine as clinical agent in regenerative medicine through increasing telomerase activity and change in the hTERT promoter CpG island methylation status of adipose tissue-derived mesenchymal stem cells. *Tissue Cell* 54, 105–113. doi: 10.1016/j.tice.2018.08.012

Galano, A., Tan, D. X., and Reiter, R. J. (2011). Melatonin as a natural ally against oxidative stress: a physicochemical examination. *J. Pineal Res.* 51, 1–16. doi: 10.1111/j.1600-079x.2011.00916.x

Guan, L. X., Guan, H., Li, H. B., Ren, C. A., Liu, L., Chu, J. J., et al. (2015). Therapeutic efficacy of umbilical cord-derived mesenchymal stem cells in patients with type 2 diabetes. *Exp. Ther. Med.* 9, 1623–1630. doi: 10.3892/etm.2015.2339

Han, D., Huang, W., Li, X., Gao, L., Su, T., Li, X., et al. (2016). Melatonin facilitates adipose-derived mesenchymal stem cells to repair the murine infarcted heart via the SIRT1 signaling pathway. *J.Pineal Res.* 60, 178–192. doi: 10.1111/jpi.12299

Hao, H., Liu, J., Shen, J., Zhao, Y., Liu, H., Hou, Q., et al. (2013). Multiple intravenous infusions of bone marrow mesenchymal stem cells reverse hyperglycemia in experimental type 2 diabetes rats. *Biochem. Biophys. Res. Commun.* 436, 418–423. doi: 10.1016/j.bbrc.2013.05.117

He, Q., Wang, L., Zhao, R., Yan, F., Sha, S., Cui, C., et al. (2020). Mesenchymal stem cell-derived exosomes exert ameliorative effects in type 2 diabetes by improving hepatic glucose and lipid metabolism via enhancing autophagy. *Stem Cell Res. Ther.* 11:223.

Hu, C., and Li, L. (2019). Melatonin plays critical role in mesenchymal stem cell-based regenerative medicine in vitro and in vivo. *Stem Cell Res. Ther.* 10:13.

Hu, Y., Liu, J., Yuan, Y., Chen, J., Cheng, S., Wang, H., et al. (2018). Sodium butyrate mitigates type 2 diabetes by inhibiting PERK-CHOP pathway of endoplasmic reticulum stress. *Environ. Toxicol. Pharmacol.* 64, 112–121. doi: 10.1016/j.etap.2018.09.002

Jeong, S. G., and Cho, G. W. (2016). Accumulation of apoptosis-insensitive human bone marrow-mesenchymal stromal cells after long-term expansion. *Cell Biochem. Funct.* 34, 310–316. doi: 10.1002/cbf.3191

Kadry, S. M., El-Dakdoky, M. H., Haggag, N. Z., Rashed, L. A., and Hassen, M. T. (2018). Melatonin improves the therapeutic role of mesenchymal stem cells in diabetic rats. *Toxicol. mech. Methods* 28, 529–538. doi: 10.1080/15376516.2018.1471634

Knani, L., Bartolini, D., Kechiche, S., Tortoioli, C., Murdolo, G., Moretti, M., et al. (2019). Melatonin prevents cadmium-induced bone damage: first evidence on an improved osteogenic/adipogenic differentiation balance of mesenchymal stem cells as underlying mechanism. *J. Pineal Res.* 67:e12597.

Kumar Jha, P., Challet, E., and Kalsbeek, A. (2015). Circadian rhythms in glucose and lipid metabolism in nocturnal and diurnal mammals. *Mol. Cell. Endocrinol.* 418(Pt 1), 74–88. doi: 10.1016/j.mce.2015.01.024

Lee, S. J., Jung, Y. H., Oh, S. Y., Yun, S. P., and Han, H. J. (2014). Melatonin enhances the human mesenchymal stem cells motility via melatonin receptor 2 coupling with Gαq in skin wound healing. *J. Pineal Res.* 57, 393–407. doi: 10.1111/jpi.12179

Li, B., Cheng, Y., Yin, Y., Xue, J., Yu, S., Gao, J., et al. (2021). Reversion of early- and late-stage β-cell dedifferentiation by human umbilical cord-derived mesenchymal stem cells in type 2 diabetic mice. *Cytotherapy* 23, 510–520. doi: 10.1016/j.jcyt.2021.01.005

Li, M. O., Wan, Y. Y., Sanjabi, S., Robertson, A. K., and Flavell, R. A. (2006). Transforming growth factor-beta regulation of immune responses. *Ann. Rev. Immunol.* 24, 99–146.

Li, W., Cao, T., Luo, C., Cai, J., Zhou, X., Xiao, X., et al. (2020). Crosstalk between ER stress, NLRP3 inflammasome, and inflammation. *Appl. Microbiol. Biotechnol.* 104, 6129–6140. doi: 10.1007/s00253-020-10614-y

Liu, X. B., Wang, J. A., Ogle, M. E., and Wei, L. (2009). Prolyl hydroxylase inhibitor dimethyloxalylglycine enhances mesenchymal stem cell survival. *J. Cell. Biochem.* 106, 903–911. doi: 10.1002/jcb.22064

Liu, Y., Yang, Y., Li, W., Ao, H., Zhang, Y., Zhou, R., et al. (2019). Effects of melatonin on the synthesis of estradiol and gene expression in pig granulosa cells. *J. Pineal Res.* 66:e12546. doi: 10.1111/jpi.12546

Luchetti, F., Betti, M., Canonico, B., Arcangeletti, M., Ferri, P., Galli, F., et al. (2009). ERK MAPK activation mediates the antiapoptotic signaling of melatonin in UVB-stressed U937 cells. *Free Rad. Biol. Med.* 46, 339–351. doi: 10.1016/j.freeradbiomed.2008.09.017

Luchetti, F., Canonico, B., Bartolini, D., Arcangeletti, M., Ciffolilli, S., Murdolo, G., et al. (2014). Melatonin regulates mesenchymal stem cell differentiation: a review. *J. Pineal Res.* 56, 382–397.

Luchetti, F., Canonico, B., Betti, M., Arcangeletti, M., Pilolli, F., Piroddi, M., et al. (2010). Melatonin signaling and cell protection function. *FASEB J.* 24, 3603–3624. doi: 10.1096/fj.10-154450

Ma, Y., Feng, Q., Ma, J., Feng, Z., Zhan, M., Ouyang, L., et al. (2013). Melatonin ameliorates injury and specific responses of ischemic striatal neurons in rats. *J. Histochem. Cytochem.* 61, 591–605.

Maria, S., Samsonraj, R. M., Munmun, F., Glas, J., Silvestros, M., Kotlarczyk, M. P., et al. (2018). Biological effects of melatonin on osteoblast/osteoclast cocultures, bone, and quality of life: implications of a role for MT2 melatonin receptors, MEK1/2, and MEK5 in melatonin-mediated osteoblastogenesis. *J. Pineal Re.* 64:e12465. doi: 10.1111/jpi.12465

Mauriz, J. L., Collado, P. S., Veneroso, C., Reiter, R. J., and González-Gallego, J. (2013). A review of the molecular aspects of melatonin's anti-inflammatory actions: recent insights and new perspectives. *J. Pineal Res.* 54, 1–14. doi: 10.1111/j.1600-079x.2012.01014.x

McArthur, A. J., Hunt, A. E., and Gillette, M. U. (1997). Melatonin action and signal transduction in the rat suprachiasmatic circadian clock: activation of protein kinase C at dusk and dawn. *Endocrinology* 138, 627–634. doi: 10.1210/endo.138.2.4925

Murdolo, G., Bartolini, D., Tortoioli, C., Piroddi, M., Iuliano, L., and Galli, F. (2013). Lipokines and oxysterols: novel adipose-derived lipid hormones linking adipose dysfunction and insulin resistance. *Free Rad. Biol. Med.* 65, 811–820. doi: 10.1016/j.freeradbiomed.2013.08.007

National Research Council (US) Institute for Laboratory Animal Research (2004). "The national academies collection: reports funded by national institutes of health," in *Proceedings of the November 2003 International Workshop: The Development of Science-based Guidelines for Laboratory Animal Care, National Academies Press (US) Copyright © 2004* (Washington, DC: National Academy of Sciences).

Ng, F., Boucher, S., Koh, S., Sastry, K. S., Chase, L., Lakshmipathy, U., et al. (2008). PDGF, TGF-beta, and FGF signaling is important for differentiation and growth of mesenchymal stem cells (MSCs): transcriptional profiling. *Blood* 112, 295–307. doi: 10.1182/blood-2007-07-103697

Oyadomari, S., Araki, E., and Mori, M. (2002). Endoplasmic reticulum stress-mediated apoptosis in pancreatic beta-cells. *Apoptosis* 7, 335–345.

Peng, F., Wu, H., Zheng, Y., Xu, X., and Yu, J. (2012). The effect of noncoherent red light irradiation on proliferation and osteogenic differentiation of bone marrow mesenchymal stem cells. *Lasers Med. Sci.* 27, 645–653. doi: 10.1007/s10103-011-1005-z

Redman, J., Armstrong, S., and Ng, K. T. (1983). Free-running activity rhythms in the rat: entrainment by melatonin. *Science (New York, N.Y.)* 219, 1089–1091. doi: 10.1126/science.6823571

Reiter, R. J., Tan, D. X., and Fuentes-Broto, L. (2010). Melatonin: a multitasking molecule. *Prog. Brain Res.* 181, 127–151. doi: 10.1016/s0079-6123(08)81008-4

Reiter, R. J., Tan, D. X., Poeggeler, B., Menendez-Pelaez, A., Chen, L. D., and Saarela, S. (1994). Melatonin as a free radical scavenger: implications for aging and age-related diseases. *Ann. N. Y. Acad. Sci.* 719, 1–12. doi: 10.1111/j.1749-6632.1994.tb56817.x

Rocha, R. M., Lima, L. F., Alves, A. M., Celestino, J. J., Matos, M. H., Lima-Verde, I. B., et al. (2013). , Interaction between melatonin and follicle-stimulating hormone promotes in vitro development of caprine preantral follicles. *Domestic Anim. Endocrinol.* 44, 1–9. doi: 10.1016/j.domaniend.2012.07.001

Rodríguez-Lozano, F. J., García-Bernal, D., Ros-Roca Mde, L., Algueró Mdel, C., ñate-Sánchez, R. E. O., Camacho-Alonso, F., et al. (2015). Cytoprotective effects of melatonin on zoledronic acid-treated human mesenchymal stem cells in vitro. *J. Cranio Maxillo Facial Surg.* 43, 855–862. doi: 10.1016/j.jcms.2015.04.012

Saito, A., and Imaizumi, K. (2018). Unfolded protein response-dependent communication and contact among endoplasmic reticulum, mitochondria, and plasma membrane. *Int. J. Mol. Sci.* 19:3215. doi: 10.3390/ijms19103215

Sener, G., Sehirli, A. O., Keyer-Uysal, M., Arbak, S., Ersoy, Y., and Yeğen, B. C. (2002). The protective effect of melatonin on renal ischemia-reperfusion injury in the rat. *J. Pineal Res.* 32, 120–126. doi: 10.1034/j.1600-079x.2002.1848.x

Shi, J. M., Tian, X. Z., Zhou, G. B., Wang, L., Gao, C., Zhu, S. E., et al. (2009). Melatonin exists in porcine follicular fluid and improves in vitro maturation and parthenogenetic development of porcine oocytes. *J. Pineal Res.* 47, 318–323. doi: 10.1111/j.1600-079x.2009.00717.x

Shuai, Y., Liao, L., Su, X., Yu, Y., Shao, B., Jing, H., et al. (2016). Melatonin treatment improves mesenchymal stem cells therapy by preserving stemness during long-term in vitro expansion. *Theranostics* 6, 1899–1917. doi: 10.7150/thno.15412

Si, Y., Zhao, Y., Hao, H., Liu, J., Guo, Y., Mu, Y., et al. (2012). Infusion of mesenchymal stem cells ameliorates hyperglycemia in type 2 diabetic rats: identification of a novel role in improving insulin sensitivity. *Diabetes* 61, 1616–1625. doi: 10.2337/db11-1141

Strem, B. M., Hicok, K. C., Zhu, M., Wulur, I., Alfonso, Z., Schreiber, R. E., et al. (2005). Multipotential differentiation of adipose tissue-derived stem cells. *Keio J. Med.* 54, 132–141.

Sun, Y., Shi, H., Yin, S., Ji, C., Zhang, X., Zhang, B., et al. (2018). Human mesenchymal stem cell derived exosomes alleviate type 2 diabetes mellitus by reversing peripheral insulin resistance and relieving β-cell destruction. *ACS Nano* 12, 7613–7628. doi: 10.1021/acsnano.7b07643

Tang, Y., Cai, B., Yuan, F., He, X., Lin, X., Wang, J., et al. (2014). Melatonin pretreatment improves the survival and function of transplanted mesenchymal stem cells after focal cerebral ischemia. *Cell Transpl.* 23, 1279–1291. doi: 10.3727/096368913x667510

Tian, X., Wang, F., He, C., Zhang, L., Tan, D., Reiter, R. J., et al. (2014). Beneficial effects of melatonin on bovine oocytes maturation: a mechanistic approach. *J. Pineal Res.* 57, 239–247. doi: 10.1111/jpi.12163

Volarevic, V., Arsenijevic, N., Lukic, M. L., and Stojkovic, M. (2011). Concise review: mesenchymal stem cell treatment of the complications of diabetes mellitus. *Stem Cells (Dayton, Ohio)* 29, 5–10. doi: 10.1002/stem.556

Wei, X., Gu, N., Feng, N., Guo, X., and Ma, X. (2018). Inhibition of p38 mitogen-activated protein kinase exerts a hypoglycemic effect by improving β cell function via inhibition of β cell apoptosis in db/db mice. *J. Enzyme Inhibition Med. Chem.* 33, 1494–1500. doi: 10.1080/14756366.2018.1477138

Wei, Y. D., Du, X. M., Yang, D. H., Ma, F. L., Yu, X. W., Zhang, M. F., et al. (2021). Dmrt1 regulates the immune response by repressing the TLR4 signaling pathway in goat male germline stem cells. *Zool. Res.* 42, 14–27.

Wei, Y., Fang, J., Cai, S., Lv, C., Zhang, S., and Hua, J. (2016). Primordial germ cell-like cells derived from canine adipose mesenchymal stem cells. *Cell Prolif.* 49, 503–511. doi: 10.1111/cpr.12271

Wu, X. L., Zhu, Z. S., Xiao, X., Zhou, Z., Yu, S., Shen, Q. Y., et al. (2021). LIN28A inhibits DUSP family phosphatases and activates MAPK signaling pathway to maintain pluripotency in porcine induced pluripotent stem cells. *Zool. Res.* 42, 377–388. doi: 10.24272/j.issn.2095-8137.2020.375

Xie, M., Hao, H. J., Cheng, Y., Xie, Z. Y., Yin, Y. Q., Zhang, Q., et al. (2017). Adipose-derived mesenchymal stem cells ameliorate hyperglycemia through regulating hepatic glucose metabolism in type 2 diabetic rats. *Biochem. Biophys. Res. Commun.* 483, 435–441. doi: 10.1016/j.bbrc.2016.12.125

Xue, B., Xiao, X., Yu, T., Xiao, X., Xie, J., Ji, Q., et al. (2021). Mesenchymal stem cells modified by FGF21 and GLP1 ameliorate lipid metabolism while reducing blood glucose in type 2 diabetic mice. *Stem Cell Res. Ther.* 12:133.

Yan, Y., Fang, J., Wen, X., Teng, X., Li, B., Zhou, Z., et al. (2019). Therapeutic applications of adipose-derived mesenchymal stem cells on acute liver injury in canines. *Res. Vet. Sci.* 126, 233–239. doi: 10.1016/j.rvsc.2019.09.004

Yang, M., Cui, Y., Song, J., Cui, C., Wang, L., Liang, K., et al. (2021). Mesenchymal stem cell-conditioned medium improved mitochondrial function and alleviated inflammation and apoptosis in non-alcoholic fatty liver disease by regulating SIRT1. *Biochem. Biophys. Res. Commun.* 546, 74–82. doi: 10.1016/j.bbrc.2021.01.098

Yu, S., Cheng, Y., Zhang, L., Yin, Y., Xue, J., Li, B., et al. (2019). Treatment with adipose tissue-derived mesenchymal stem cells exerts anti-diabetic effects, improves long-term complications, and attenuates inflammation in type 2 diabetic rats. *Stem Cell Res. Ther.* 10:333.

Zakrzewski, W., Dobrzyński, M., Szymonowicz, M., and Rybak, Z. (2019). Stem cells: past, present, and future. *Stem Cell Res. Ther.* 10:68.

Zang, L., Hao, H., Liu, J., Li, Y., Han, W., and Mu, Y. (2017). Mesenchymal stem cell therapy in type 2 diabetes mellitus. *Diabetol. Metab. Syndr.* 9:36.

Zhu, Z., Wu, X., Li, Q., Zhang, J., Yu, S., Shen, Q., et al. (2021). Histone demethylase complexes KDM3A and KDM3B cooperate with OCT4/SOX2 to define a pluripotency gene regulatory network. *FASEB J.* 35:e21664.

Conflict of Interest: The authors declare that the research was conducted in the absence of any commercial or financial relationships that could be construed as a potential conflict of interest.

frontiers in Cell and Developmental Biology

CORRECTION
published: 07 December 2021
doi: 10.3389/fcell.2021.799571

Corrigendum: Melatonin Promotes the Therapeutic Effect of Mesenchymal Stem Cells on Type 2 Diabetes Mellitus by Regulating TGF-β Pathway

*Balun Li[1], Xuedi Cheng[1], Aili Aierken[1], Jiaxin Du[2,3], Wenlai He[1], Mengfei Zhang[1], Ning Tan[1], Zheng Kou[1], Sha Peng[1], Wenwen Jia[4], Haiyang Tang[1,5] and Jinlian Hua[1]**

[1]Shaanxi Centre of Stem Cells Engineering and Technology, College of Veterinary Medicine, Northwest A&F University, Xianyang, China, [2]Department of Animal Engineering, Yangling Vocational and Technical College, Xianyang, China, [3]Department of Veterinary Medicine, College of Animal Sciences, Institute of Preventive Veterinary Sciences, Zhejiang University, Hangzhou, China, [4]Shanghai East Hospital, East Hospital Affiliated to Tongji University, Shanghai, China, [5]State Key Laboratory of Respiratory Disease, Guangzhou Institute of Respiratory Health, The First Affiliated Hospital of Guangzhou Medical University, Guangzhou, China

Keywords: melatonin, adipose-derived mesenchymal stem cells, type 2 diabetes mellitus, TGF-β, inflammation, canine

OPEN ACCESS

Edited and reviewed by:
Frontiers in Cell and Developmental Biology Editorial Office, Frontiers Media SA, Switzerland

****Correspondence:***
Jinlian Hua
jinlianhua@nwsuaf.edu.cn

Specialty section:
This article was submitted to Stem Cell Research, a section of the journal Frontiers in Cell and Developmental Biology

Received: *21 October 2021*
Accepted: *15 November 2021*
Published: *07 December 2021*

Citation:
Li B, Cheng X, Aierken A, Du J, He W, Zhang M, Tan N, Kou Z, Peng S, Jia W, Tang H and Hua J (2021) Corrigendum: Melatonin Promotes the Therapeutic Effect of Mesenchymal Stem Cells on Type 2 Diabetes Mellitus by Regulating TGF-β Pathway. Front. Cell Dev. Biol. 9:799571. doi: 10.3389/fcell.2021.799571

A Corrigendum on

Melatonin Promotes the Therapeutic Effect of Mesenchymal Stem Cells on Type 2 Diabetes Mellitus by Regulating TGF-β Pathway

by Li, B., Cheng, X., Aierken, A., Du, J., He, W., Zhang, M., Tan, N., Kou, Z., Peng, S., Jia, W., Tang, H., and Hua, J. (2021). Front. Cell Dev. Biol. 9:722365. doi: 10.3389/fcell.2021.722365

In the published article, there was an error regarding the affiliation for Haiyang Tang. As well as having affiliation 1, they should also have "*State Key Laboratory of Respiratory Disease, Guangzhou Institute of Respiratory Health, The First Affiliated Hospital of Guangzhou Medical University, Guangzhou, China.*"

The authors apologize for this error and state that this does not change the scientific conclusions of the article in any way. The original article has been updated.

frontiers in Cell and Developmental Biology

ORIGINAL RESEARCH
published: 02 November 2021
doi: 10.3389/fcell.2021.745412

An Active Fraction of *Trillium tschonoskii* Promotes the Regeneration of Intestinal Epithelial Cells After Irradiation

Feiling Song[1†], Sihan Wang[2,3†], Xu Pang[4], Zeng Fan[2], Jie Zhang[4], Xiaojuan Chen[4], Lijuan He[2,3], Baiping Ma[4], Xuetao Pei[2,3*] and Yanhua Li[1,3*]*

[1] Experimental Hematology and Biochemistry Lab, Beijing Institute of Radiation Medicine, Beijing, China, [2] Stem Cells and Regenerative Medicine Lab, Institute of Health Service and Transfusion Medicine, Beijing, China, [3] South China Research Center for Stem Cell & Regenerative Medicine, SCIB, Guangzhou, China, [4] Department of Pharmaceutical Sciences, Beijing Institute of Radiation Medicine, Beijing, China

OPEN ACCESS

Edited by:
Yan-Ru Lou,
Fudan University, China

Reviewed by:
Marco Tatullo,
University of Bari Medical School, Italy
Hyosun Jang,
Korea Institute of Radiological and Medical Sciences, South Korea
Sripathi Sureban,
University of Oklahoma Health Sciences Center, United States

***Correspondence:**
Baiping Ma
mabaiping@sina.com
Xuetao Pei
peixt@bmi.ac.cn
Yanhua Li
shirlylyh@126.com

[†] These authors have contributed equally to this work and share first authorship

Specialty section:
This article was submitted to Stem Cell Research, a section of the journal Frontiers in Cell and Developmental Biology

Received: 22 July 2021
Accepted: 11 October 2021
Published: 02 November 2021

Citation:
Song F, Wang S, Pang X, Fan Z, Zhang J, Chen X, He L, Ma B, Pei X and Li Y (2021) An Active Fraction of Trillium tschonoskii Promotes the Regeneration of Intestinal Epithelial Cells After Irradiation. Front. Cell Dev. Biol. 9:745412. doi: 10.3389/fcell.2021.745412

Despite significant scientific advances toward the development of safe and effective radiation countermeasures, no drug has been approved for use in the clinic for prevention or treatment of radiation-induced acute gastrointestinal syndrome (AGS). Thus, there is an urgent need to develop potential drugs to accelerate the repair of injured intestinal tissue. In this study, we investigated that whether some fractions of Traditional Chinese Medicine (TCM) have the ability to regulate intestinal crypt cell proliferation and promotes crypt regeneration after radiation. By screening the different supplements from a TCM library, we found that an active fraction of the rhizomes of *Trillium tschonoskii* Maxim (TT), TT-2, strongly increased the colony-forming ability of irradiated rat intestinal epithelial cell line 6 (IEC-6) cells. TT-2 significantly promoted the proliferation and inhibited the apoptosis of irradiated IEC-6 cells. Furthermore, in a small intestinal organoid radiation model, TT-2 promoted irradiated intestinal organoid growth and increased $Lgr5^+$ intestinal stem cell (ICS) numbers. More importantly, the oral administration of TT-2 remarkably enhanced intestinal crypt cell proliferation and promoted the repair of the intestinal epithelium of mice after abdominal irradiation (ABI). Mechanistically, TT-2 remarkably activated the expression of ICS-associated and proliferation-promoting genes and inhibited apoptosis-related gene expression. Our data indicate that active fraction of TT can be developed into a potential oral drug for improving the regeneration and repair of intestinal epithelia that have intestinal radiation damage.

Keywords: intestinal epithelium, active fractions of *Trillium tschonoskii*, intestinal organoid, radiation, regeneration

INTRODUCTION

A high dosage of ionizing radiation in pelvic and abdominal cancer radiotherapy or radiological emergency scenarios can cause acute gastrointestinal syndrome (AGS) in those affected (Booth et al., 2012; Chapel et al., 2013). Under irradiation, epithelial cells in intestinal villi and crypts are easily injured; this causes cell apoptosis or death. As the gastrointestinal epithelial integrity is

destroyed, patients with AGS suffer from different degrees of nausea, vomiting, disturbance of water and electrolytes, loss of the intestinal immune barrier, bacteremia and sepsis, and even death (Shadad et al., 2013). Thus, it is essential to use radiation countermeasure agents to ameliorate AGS symptoms or rescue patients. However, so far, there is no effective drug approved for application in the clinical setting for prevention and treatment of AGS.

Several labs have been devoted to develop effective radiation protectants or mitigators. A variety of agents that function differently, including blockers of oxygen consumption, free radical scavengers, somatostatin analogs, growth factors, TLR5 agonists, endothelial protection drugs, vitamin E analogs, and Chinese herbal medicine have shown protective or mitigative effects in animal models with multiple types of intestinal radiation damage (Berbee and Hauer-Jensen, 2012; Shadad et al., 2013; Choi et al., 2019). However, it remains an unmet target to develop radiation countermeasure drugs to accelerate the regeneration of radiation-injured intestinal tissue. *In vitro* drug screening systems based on cell lines or primary cells are often used for drug discovery (Ayehunie et al., 2018; Dutton et al., 2019). The rat intestinal crypt cell line, rat intestinal epithelial cell line 6 (IEC-6), is a good cell model for the discovery of new chemical compound with the ability to mitigate the effects of radiation-induced intestinal epithelial damage (Wang S. et al., 2020). The stem cell population in intestinal crypts is responsible for intestinal villi renewal and regeneration after injury *in vivo*. This process is mainly driven by intestinal crypt base columnar cells, which are active, fast-cycling intestinal stem cells (ISCs) marked by Lgr5, CD133, and Sox9 expression (Rizk and Barker, 2012; Roche et al., 2015). Recently, using a three-dimensional extracellular matrix culture system, ISCs were cultured to grow into self-organizing mini-gut structures, e.g., intestinal organoids (Sato and Clevers, 2013; Sugimoto and Sato, 2017; Wallach and Bayrer, 2017; Rahmani et al., 2019). The intestinal organoid culture technique provides a real intestinal epithelium model to evaluate the effect of radiation countermeasure agents (Kim et al., 2020; Martin et al., 2020).

Some Traditional Chinese Medicine (TCM) have been reported to play a protective or mitigative role in radiation-induced intestinal toxicity (Kim et al., 2002; Liu et al., 2006; Dutta et al., 2012; Rockwell et al., 2013; Yang et al., 2019). It is valuable and meaningful to find more effective TCM that can modulate intestinal epithelial cell function. Hence, we performed a preliminary screening experiment using an intestinal crypt cell line (IEC-6) culture and colony-forming assays after irradiation to evaluate the function of some TCM and their fractions collected in our lab. Notably, we found that an active fraction of the rhizomes of *Trillium tschonoskii* Maxim (TT), strongly increased the colony-forming ability of irradiated IEC-6 cells. TT is a perennial herb plant distributed in most areas of central and western mainland China (Wang B. et al., 2020). The rhizomes of this plant are used as a folk medicine ("Yanlingcao") for the treatment of neurasthenia, cancer, headache, and some inflammatory diseases in the clinic (Wang S. et al., 2020). Here, we firstly reported that an active fraction of TT with the ability to decrease the apoptosis and enhance the proliferation of irradiated intestinal epithelia *in vitro*. Using an *in vitro* intestinal organoid culture system and a high-dose abdominal irradiation (ABI) model, we characterized the role of the active fraction of TT in intestinal epithelia repair following radiation injury. Herein, we provide scientific evidence for the use of the active fraction of TT as a potential drug to ameliorate AGS.

MATERIALS AND METHODS

Separation and Extraction of the Fractions of *Trillium tschonoskii*

Rhizomes of TT (collected from the Shennongjia, Hubei province; 3 kg) were crushed and extracted using 50% EtOH with three refluxes (24 L, 24 L, 24 L, each for 2 h). The filtered solution was concentrated *in vacuo* and centrifugated to obtain the supernatant and sediment. The supernatant was passed through an SP825 macroporous resin column (column volume 6 L) and eluted using a gradient condition of EtOH-H_2O (*v*/*v*, 0:100 → 15:85 → 30:70 → 50:50 → 75:25 → 95:5, three column volumes per concentration) to yield six fractions (TT-1 to TT-6). TT-2 (15% EtOH elution) was lyophilized to yield 20.0 g powder, and half of TT-2 was dissolved in water and then subjected to an HP20 macroporous resin column (column volume 2 L) and eluted using a gradient condition of EtOH-H_2O (v/v, 0:100 → 15:85 → 50:50, three column volumes per concentration) to yield three fractions named TT-2-0 (8.1 g), TT-2-15 (1.1 g), and TT-2-50 (0.5 g).

Cells, Mice, and Radiation Treatment

IEC-6 cells were obtained from the American Type Culture Collection (ATCC) and cultured in Dulbecco's Modified Eagle Medium (DMEM) supplemented with 10% fetal bovine serum (FBS) at 37°C and 5% (v/v) CO_2 under a humidified atmosphere. The cells were irradiated at a rate of 54.22 cGy/min using a ^{60}Co irradiator with a total dose of 10 Gy. The irradiated cells were cultured in a medium with or without the addition of TT-2 (10 μg/mL), and TT-2 was dissolved in water to configure different concentrations.

C57BL/6 mice were obtained from a commercial vendor (Beijing Vital River Laboratory Animal Technology Co., Ltd.) and housed under standardized conditions with controlled temperature and humidity and a 12/12-h day/night light cycle for 7 days. The mice were anesthetized by intraperitoneal injection of pentobarbital, and then the abdomen part or mice were exposed to irradiation (non-abdomen body parts including the skeleton were shielded with lead blocks) at a rate of 54.22 cGy/min using a ^{60}Co irradiator (Beijing Institute of Radiation Medicine, Beijing, China) with a total dose of 14 Gy. For oral delivery, TT-2 was dissolved in water at a concentration of 10 mg/kg and administered by gavage every day from day −2 to 4. C57BL/6 mice were exposed to 14 Gy ABI on day 0. After irradiation, 200 μL water with or without TT-2 was delivered by gavage to each mouse. The irradiated mice were kept in sterile water containing antibiotics after irradiation.

Irradiated IEC-6 cells (∼1,000) were seeded in six-well plates and incubated for 7 days with or without fractions derived from a TCM bank collected in our lab. After the colonies were fixed and

stained with crystal violet, colony numbers were counted. Three repeated experiments were carried out in each group.

5-Ethynyl-2′-Deoxyuridine Incorporation and Detection

The EdU assay was performed using an EdU Kit (RiboBio, C10310-1). Irradiated IEC-6 cells were cultured with or without TT-2 (10 μg/mL) for 48 h in DMEM supplemented with 10% FBS, and then switched to fresh DMEM supplemented with EdU (50 μM) and incubated for 2 h; this was followed by fixation, permeabilization, and EdU staining with Apollo567 (RiboBio, C00031). The nuclei were stained with DAPI, and the staining of EdU-positive cells was observed using fluorescent reverse microscopy (UltraVIEW VOX, PerkinElmer). The percentage of incorporation of EdU in the nucleus of irradiated IEC-6 cells in each field was calculated and expressed as the mean ± SD. For flow cytometry assays, the cells were exposed to 10 μM EdU for 2 h at 37°C, and were prepared and treated using a Click-iT^{TM} Plus EdU Alexa Fluor^{TM} 647 Flow Cytometry Assay Kit (C10635, Thermo Fisher Scientific) according to the manufacturer's instructions. Flow cytometry analysis was performed using the FACSCalibur platform (BD Biosciences) to detect EdU incorporation.

Apoptosis Assays

Irradiated IEC-6 cells were cultured with or without TT-2 (10 μg/mL) in DMEM supplemented with 10% FBS. After 48 h of incubation, an apoptosis detection kit (AD10, DOJINDO) was used according to the manufacturer's instructions to test the apoptosis rate. In brief, after the cells were collected and washed with PBS, then were labeled with Annexin V [Fluorescein Isothiocyanate (FITC)] and PI Solution, and incubated for 15 min in the dark at room temperature. Then the apoptosis rate was measured in a flow cytometer. All the experiments were repeated three times.

TUNEL staining was carried out according to the manufacturer's instructions (Promega). The mouse intestinal slides were incubated with proteinase K for 20 min at room temperature and washed with PBS, then incubated in TdT buffer containing TUNEL reaction mixture at 37°C for 1 h. Afterward, the slides were counterstained with DAPI to label DNA and thus the cell nucleus and mounted for fluorescent microscopy with Nikon fluorescence microscope. Quantitation analysis of the TUNEL assay results was done by counting DAPI-staining cell numbers and the TUNEL-positive cell numbers in the intestinal crypts and villi to calculate the apoptotic cells. There are 3 mice in each group, and at least 30 villi or crypts in the small intestine were counted for the number of positive cells.

qRT-PCR Assays

Cells were collected and total RNA was isolated using TRIzol reagent (15596018, Invitrogen) according to the manufacturer's instructions. Then, 800 ng of total RNA was reverse-transcribed into cDNA. Real-time quantitative PCR analysis was performed on a Bio-Rad CFX Connect Real-time System thermocycler using the SYBR Green PCR Master Mix (TaKaRa). The RNA levels were normalized using HPRT or GAPDH as an internal control. All the experiments were repeated three times. The primers are shown in detail in **Supplementary Table 1**.

Crypt Isolation and Organoid Culture

The small intestines of mice were opened longitudinally and washed repeatedly with cold PBS (containing 100 U/mL or 100 μg/mL penicillin/streptomycin) until there were no visible impurities. The tissue was cut into 2–3 mm pieces, which were placed in cold 2.5 mM EDTA (AM9261, Invitrogen) at 4°C for 30 min. After removal of the EDTA medium, the tissue fragments were shaken to release crypts and then passed through a 70 μm cell strainer to remove the remaining villi. Isolated crypts were washed with cold PBS containing 0.1% BSA (A3311, Sigma) and centrifuged (∼290 × *g*) 10 times for enrichment. The crypts were buried in 30 μL cold Matrigel® matrix (356231, Corning) and 30 μL IntestiCult^{TM} Organoid Growth Medium (06005, STEMCELL) at a density of 200 crypts per well. Fresh medium was replaced every 3 days.

Hematoxylin and Eosin Staining Assays

Paraffin sections of the small intestine were melted at 56°C for 30–60 min and hydrated in 100, 90, and 70% ethanol for 5 min. The sections were immersed in Mayer hematoxylin (ZLI-9610, Zsbio) for 5 min without differentiation, and then immersed in acidified eosin ethanol solution (ZLI-9613, Zsbio) for 2–5 min. The length of villus or crypt in each group was determined by counting 30 intact villi or crypts and reported as the mean ± SD. Three mice were used in each group.

Immunohistochemistry Assays

Paraffin sections were incubated overnight with primary antibodies in 1% horse serum albumin (PK-6200, Vector) at 4°C. The next day, the samples were washed with PBS and incubated with secondary antibodies at 25°C for 1 h. After washing with PBS, the sections were developed using ImmPACT® NovaRED® Substrate, Peroxidase (HRP) (SK-4805, Vector) for color reaction, and then observed under a microscope. The number of positive cells in 30 complete crypts was counted and expressed as the mean ± SD. Three mice were used in each group. The antibodies used were anti-BrdU (5292, CST), anti-Ki67 (9129, CST), anti-Cyclin D1 (2978, CST), anti-Lgr5/GPR49 (MAB8240, R&D Systems), anti-Sox9 (82630, CST), anti-Lysozyme (ab108508, Abcam), anti-Chromogranin A (GTX113165, GeneTex), and anti-Muc2 (GTX100664, GeneTex).

In situ Hybridization

A small section of the intestine was embedded and made into paraffin sections. Then the RNA scope *in situ* hybridization 2.5 HD red detection kit (Advanced Cell Diagnostic, Newark, CA, United States) was used according to the manufacturer's instructions to process the intestinal sections. In brief, the intestinal tissue underwent target retrieval, permeabilization, hybridization of Lgr5 (MAB8240, R&D Systems), amplification, and visualization using DAB-A and DAB-B. And then the

intestinal sections were observed under a microscope. The expression of Lgr5 was quantitatively analyzed according to the five-grade scoring system recommended by the manufacturer (0, no staining; 1, 1–3 dots/cell; 2, 4–10 dots/cell; 3, >10 dots/cell; 4, >15 dots/cell with >10% of dots in clusters). The H-score was calculated as: (% of grade 1 cells × 1) + (% of grade 2 cells × 2) + (% of grade 3 cells × 3) + (% of grade 4 cells × 4). In addition, a cell with one or more dots was regarded as Lgr5-positive. Three mice were used in each group.

Fluorescein Isothiocyanate-Dextran Test

C57BL/6 mice were orally administrated with 200 μL water with or without 10 mg/kg TT-2 from day −2 to 4. These mice were exposed to 14 Gy ABI on day 0. Four days after irradiation, FITC-Dextran (Sigma-Aldrich, St. Louis, MO, United States) was administered to the mice by oral gavage at a concentration of 0.6 mg/g body weight and a volume of 20 μL. Four hours after gavage, the serum of mice was collected, and 50 μL of both diluted serum samples and standards as well as blanks (PBS and diluted serum from untreated animals), were transferred to black 96-well microplates. FITC-Dextran concentrations were analyzed with a fluorescence spectrophotometer and fluorescence intensity was measured (excitation, 492 nm; emission, 525 nm).

Statistical Analysis

Data were expressed as means ± SD. The paired *t*-test was used to determine the statistical significance between the two groups. One-way ANOVA followed by Dunnett's *post hoc* test was used to compare the means of three or more independent groups. Results with $p < 0.05$ were considered statistically significant.

RESULTS

Active Fraction of *Trillium tschonoskii* Increases Colony-Forming Ability of Irradiated IEC-6 Cells

To discover traditional Chinese herbs that may enhance intestinal epithelial repair after irradiation, we firstly chose a TCM library to screen potential effective fractions by performing the colony-forming assay of IEC-6 cells after 10 Gy irradiation (**Figure 1A**). We found that over 10 fractions from the TCM library increased the number of colonies formed by irradiated IEC-6 cells (data not shown). Notably, the active fractions of *Trillium tschonoskii* extracts (TT) numbered TT-2 caused 1.4-fold increases in the number of colonies formed by irradiated IEC-6 cells (**Figure 1B**). TT-2 was then isolated into three kinds of active fractions after elution with different concentrations of ethanol (0, 15, and 50%), these were named TT-2-0, TT-2-15, and TT-2-50. All these active fractions significantly increased the number of colonies formed by irradiated IEC-6 cells (**Figure 1C**). TT-2 and TT-2-0 were the same fraction from the TCM, and showed a better effect on increasing the colony-forming ability of irradiated IEC-6 cells than TT-2-15 and TT-2-50. These results indicated that the active fractions of TT might have the ability to promote intestinal cell regeneration after irradiation.

Active Fraction of *Trillium tschonoskii* Promotes Proliferation and Inhibits Apoptosis of Irradiated IEC-6 Cells

We performed EdU incorporation experiments to further evaluate whether the active fraction of TT could directly regulate the proliferation of intestinal crypt cells after irradiation. The results of immunostaining of incorporated EdU showed that TT-2 and TT-2-0 notably increased the incorporation of EdU in the nucleus of irradiated IEC-6 cells compared to that in the control group (**Figure 2A**). Flow cytometry data of EdU-incorporated cell percentages also demonstrated a similar role of TT-2 and TT-2-0 in enhancing incorporation (**Figure 2B**). Next, we assessed the apoptosis rate of irradiated IEC-6 cells after TT-2 or TT-2-0 treatment for 48 h. The apoptotic cell percentage of irradiated cells was significantly lower in the TT-2 or TT-2-0 treatment group than in the controls (**Figure 2C**). Given that TT-2 and TT-2-0 were the same active fraction from TT, we chose TT-2 to further evaluate its role in proliferation- and apoptosis-related gene expression. The qPCR results demonstrated that TT-2 treatment significantly enhanced the expression of the proliferation-related genes, *Cyclin D1* and *Myc* (**Figure 2D**). The expression levels of the anti-apoptosis-related gene, *Bcl-2*, significantly increased after TT-2 treatment. In contrast, the expression of the *p53* gene was inhibited by TT-2 (**Figure 2E**). These results indicated that TT-2 might have enhanced intestinal crypt cell regeneration mainly by regulating irradiated crypt cell proliferation and inhibiting cell apoptosis.

Trillium tschonoskii-2 Promotes Intestinal Organoid Growth After Irradiation

To determine whether TT-2 could directly act on *in vitro* ISC proliferation, freshly isolated small intestinal crypts of normal mice were cultured for 4 days to form organoids, and then exposed to 6 Gy radiation (**Figure 3A**). After irradiation, cells were incubated in TT-2 containing culture medium for 3 days. The imaging data showed that TT-2 significantly increased the total organoid number, budding number, and surface area of each organoid at 0.7-, 1.9-, and 1.1-fold, respectively, compared to those in the control group on day 3 after 6 Gy irradiation (**Figure 3B**). By employing Lgr5-EGFP-IRES-creERT2 mice, we found that the irradiated organoids cultured with TT-2 showed a markedly increased percentage of Lgr5-EGFP^{+} cells at 1.9-fold (**Figure 3C**). The EdU incorporation percentage of TT-2-treated organoids was increased by 0.5-fold compared with the controls (**Figure 3D**). Gene expression analysis of these irradiated organoids showed that TT-2 significantly upregulated the transcription of ISC-related and proliferation-promoting genes such as *Ascl2*, *Bmi1*, *Mam1*, *Cyclin D1*, *Myc*, *Fos*, and *Jun* at 48 h after irradiation (**Figures 3E,F**). The apoptosis-related genes, such as *Caspase-3* and *Bax*, in the irradiated intestinal organoids were remarkably downregulated by TT-2 (**Figure 3G**). These

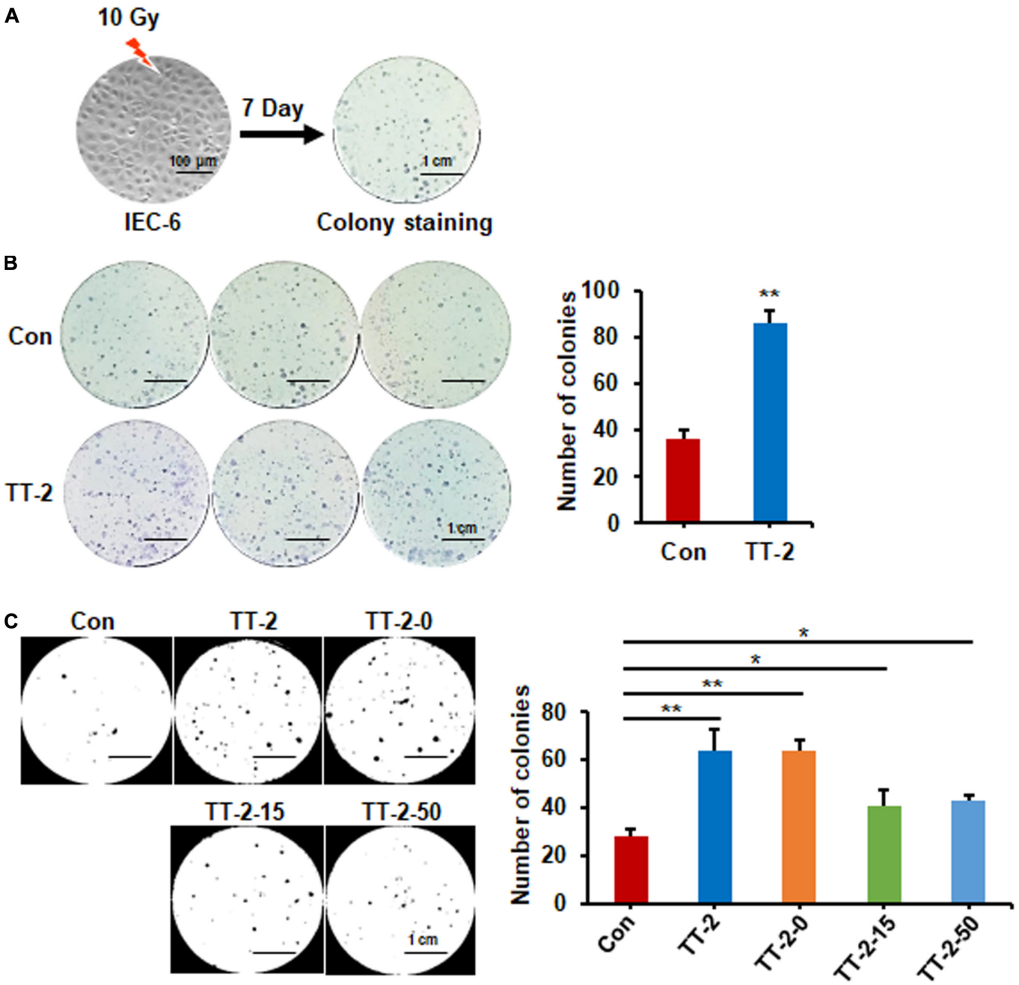

FIGURE 1 | Active fraction of *Trillium tschonoskii* (TT) promoted colony formation of rat intestinal epithelial cell line 6 (IEC-6) cells. **(A)** Schematic diagram of colony formation by IEC-6 cells after 10 Gy irradiation. **(B)** Representative colony image and colony numbers formed by IEC-6 cells after 10 Gy irradiation and addition of H_2O, or TT-2 to the culture medium (**$p < 0.01$, scale bar = 1 cm). **(C)** Representative colony staining image and colony numbers formed by IEC-6 cells after 10 Gy irradiation and addition of TT-2 or samples isolated after elution with different concentrations of ethanol (TT-2-0, TT-2-15, and TT-2-50) (*$p < 0.05$, **$p < 0.01$, scale bar = 1 cm).

observations indicated that TT-2 promoted intestinal organoid growth and ISC proliferation *in vitro*.

Trillium tschonoskii-2 Enhances Repair of Intestinal Epithelium in Mice After Abdominal Irradiation

Acute and lethal intestinal crypt injury is triggered upon exposure to high doses of radiation (>12 Gy) (Kuhnert et al., 2004; Chen et al., 2014). To evaluate the beneficial effects of TT-2 on radiation-induced intestinal tissue damage, C57BL/6 mice were exposed to 14 Gy ABI on day 0, and were gavaged TT-2 or H_2O every day from day −2–4 (**Figure 4A**). It has been reported that ISCs in the crypt base are initially inactive, are activated within several hours to 4 days after irradiation, and are mainly responsible for crypt regeneration (Booth et al., 2012; Yan et al., 2012). Therefore, we collected intestinal tissue 4 days after ABI. Notably, oral administration of TT-2 improved intestinal tissue morphology (**Figure 4B**). Histological analysis of H&E-stained intestinal sections showed that TT-2 administration significantly increased intestinal villus and crypt lengths compared to those in the control group (**Figure 4B**). The villus and crypt length in the TT-2 group was remarkably higher than in the control group, 4 days after irradiation (**Figure 4B**). After treatment with TT-2, the number of apoptotic cells in the villus and crypt was significantly decreased (**Figure 4C**). To gain insight into the proliferative status of the intestinal crypts upon irradiation and TT-2 treatment, we performed a 12 h bromodeoxyuridine (BrdU) tracer experiment. We observed a 2.1-fold increase in the percentage of $BrdU^+$ cells in the small intestine section of TT-2-treated mice than that in the controls 4 days after irradiation (**Figure 4D**). The immunohistochemical staining results demonstrated significant increases in the positive cell number of Ki67 and Cyclin D1 in the crypt of TT-2-treated

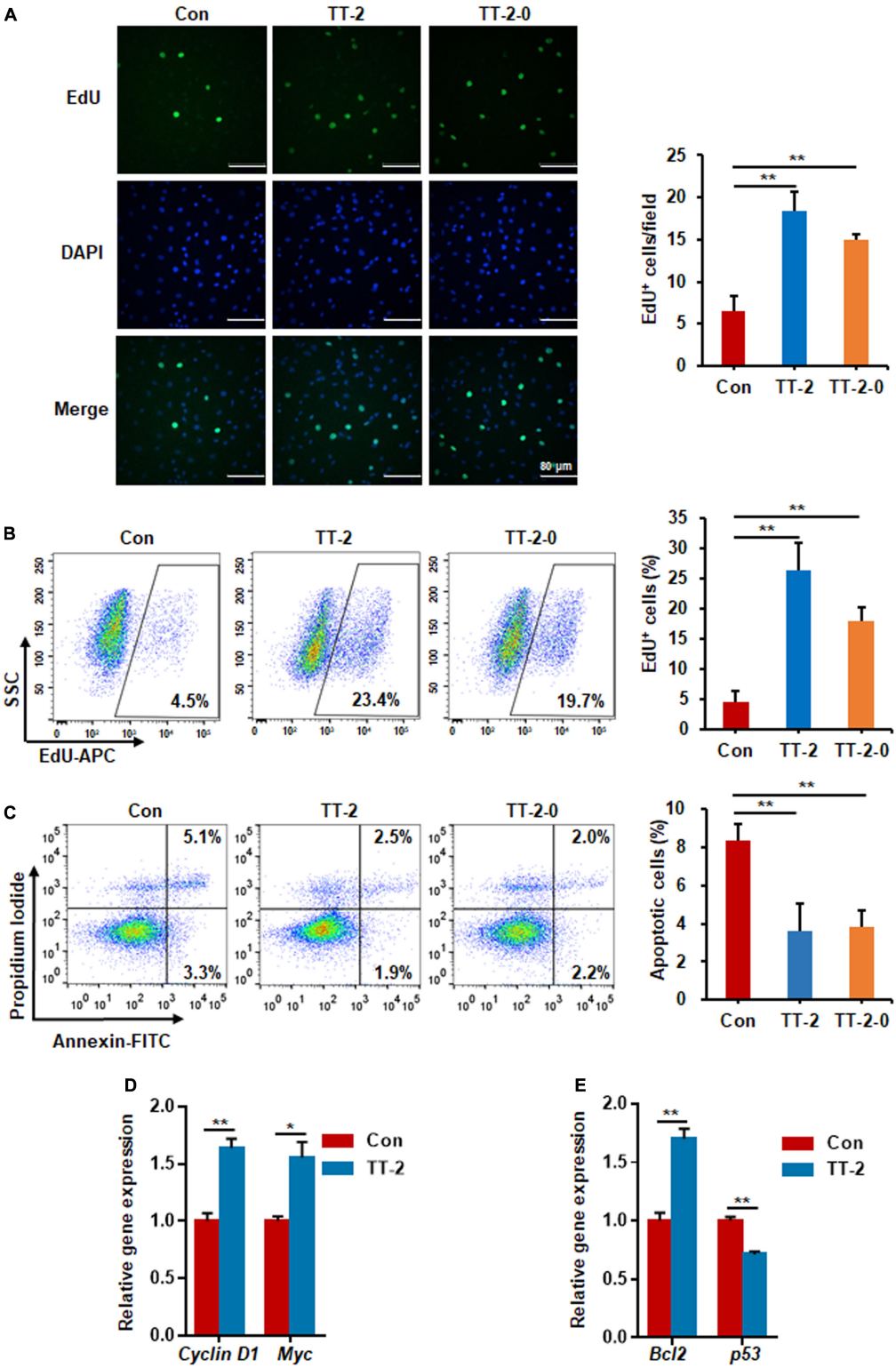

FIGURE 2 | Active fraction of *Trillium tschonoskii* (TT) promoted proliferation and inhibited apoptosis of IEC-6 cells after irradiation. **(A)** Immunostaining analysis of EdU in IEC-6 cells after irradiation with or without TT-2 or TT-2-0 for 48 h (**$p < 0.01$, scale bar = 80 μm). **(B)** Percentage analysis of EdU incorporation for 4 h in IEC-6 cells after 10 Gy irradiation with or without TT-2 or TT-2-0 (**$p < 0.01$). **(C)** Percentage of apoptotic cells among IEC-6 cells after 10 Gy irradiation with or without TT-2 or TT-2-0 treatment for 48 h (**$p < 0.01$). **(D)** qPCR for proliferation-related gene expression in IEC-6 cells after 10 Gy irradiation with or without TT-2 treatment for 48 h (*$p < 0.05$, **$p < 0.01$). **(E)** qPCR for apoptosis-related gene expression in IEC-6 cells after 10 Gy irradiation with or without TT-2 treatment for 48 h (*$p < 0.05$, **$p < 0.01$).

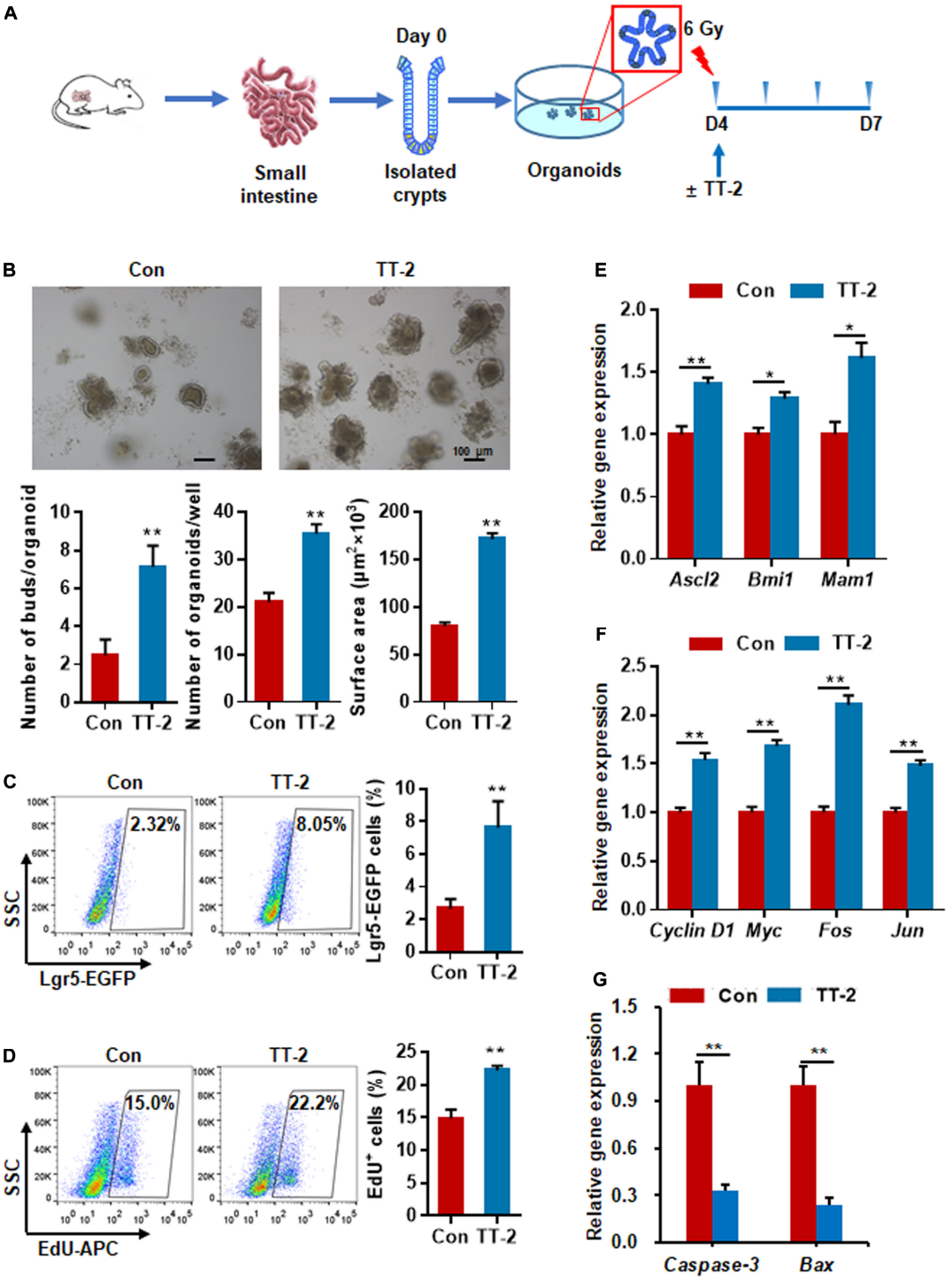

FIGURE 3 | Active fraction of *Trillium tschonoskii* (TT) promoted intestinal organoid growth after irradiation. **(A)** Schematic diagram of organoid isolation and irradiation. **(B)** Representative phase contrast microscopic images of intestinal organoids cultured in presence of TT-2, and quantification of organoid numbers per well, bud numbers, and surface area of each organoid (**$p < 0.01$, scale bar = 100 μm). **(C)** Representative dot plots and percentages of EGFP^{+} cells in the intestinal organoids with or without TT-2. The intestinal crypts were isolated from Lgr5-EGFP-IRES-creERT2 mice (**$p < 0.01$). **(D)** The percentage analysis of EdU incorporation for 4 h in organoids after 6 Gy irradiation with or without the addition of TT-2 to the medium for 48 h (**$p < 0.01$). **(E)** qPCR for ISC-related gene expression in organoids after 6 Gy irradiation with or without TT-2 treatment for 48 h (*$p < 0.05$, **$p < 0.01$). **(F)** qPCR for proliferation-related gene expression in organoids after 6 Gy irradiation with or without TT-2 treatment for 48 h (**$p < 0.01$). **(G)** qPCR for apoptosis-related gene expression in organoids after 6 Gy irradiation with or without TT-2 treatment for 48 h (**$p < 0.01$).

mice, as shown by the brown staining of the intestinal tissue sections (**Figures 4E,F**). On day 4 post ABI, TT-2- treated intestinal tissue sections showed significant increases in the numbers of $Ki67^+$ cells and Cyclin $D1^+$ cells by 2.8-fold and 1.1-fold, respectively (**Figures 4E,F**). We also detected the expression of Lgr5 mRNA and Sox9 protein in the small intestine sections, these are active ISC markers and are critical for crypt regeneration. Using an *in situ* hybridization assay, we found that TT-2 administration significantly improved the expression of Lgr5 mRNA in the intestinal crypts (**Figure 5A**). We also found that TT-2 administration significantly enhanced the percentage of $Sox9^+$ cells compared with that in the control group, 4 days after ABI (**Figure 5B**). The expression levels of the ISC-related genes, such as *Lgr5, Sox9, Dclk1, Hopx, Tert,* and *Prox1,* significantly increased after TT-2 treatment at 96 h after ABI (**Figure 5C**). To further evaluate the role of TT-2 in repairing intestinal epithelial cells after irradiation, we analyzed several types of intestinal epithelial cells after 14 Gy ABI, including enteroendocrine, Paneth, and goblet cells. Immunohistochemical staining results showed that TT-2 administration significantly increased the positivity rate of Chga for enteroendocrine cells, Lysozyme for Paneth cells, and Muc2 for goblet cells in the intestinal sections (**Figures 6A–C**). Gene expression analysis of the irradiated mice showed that TT-2 significantly upregulated the expression of *Chga*, *Lysozyme,* and *Muc2* genes at 48 h after irradiation (**Figure 6D**). We then employed FITC-Dextran assay to evaluate the effect of TT-2 on intestinal permeability in mice after irradiation. TT-2 administration significantly reduced the FITC-Dextran level in the serum of mice at day 4 after 14 Gy irradiation (**Figure 6E**). The result indicated that TT-2 administration decreased intestinal epithelial permeability and prevented gut leakiness to a greater extent in mice after irradiation. These data suggested that TT-2 promoted ISC differentiation and the repair of the intestinal epithelium of mice after high dosage of ABI.

DISCUSSION

In this study, we discovered a novel function of an active fraction of TT, TT-2, it promoted intestinal epithelial repair after irradiation. To the best of our knowledge, this is the first report on the mitigative function of this natural product on radiation-induced intestinal toxicity. TT-2 enhanced colony formation, promoted cell proliferation, and inhibited apoptosis of the irradiated intestinal crypt cell line, IEC-6. TT-2 also enhanced the growth of an irradiated intestinal organoid model. Results of *in vivo* experiments indicated that oral administration of TT-2 significantly improved the expression of ISC-related genes and enhanced crypt regeneration and epithelial repair of radiation-damaged intestinal tissue.

Radiotherapy is often used to kill residual tumor cells in clinics. However, abdominal or pelvic tumor radiotherapy is painful for patients with various symptoms, such as AGS, which limits the dosage of radiation. The lack of effective drugs with mitigative effects on AGS has stimulated efforts to find new and potential drugs to reduce radiation-induced intestinal damage and enhance intestinal epithelial repair. Primary screening of effective agents using intestinal cell lines or organoid models combined with special phenotype analysis will provide a clue to discover natural products or compounds with radiation countermeasure potential. China has abundant traditional herbs and several natural herbal products have been reported to play a beneficial role in tissue-injury repair (Meng et al., 2020). Hence, we established a screening system based on counting the numbers of colonies formed by irradiated IEC-6 cells treated with different constituents from a TCM library, which contains different extracts of TT. Some scientists are devoting to isolate and purify the chemical ingredients of TT and investigate the function of them. Accumulated evidence indicates that there are various constituents in TT with diverse function (Yan et al., 2016; Wang et al., 2018; Wang B. et al., 2020). The total saponins of TT showed the protective and repair-promoting effects on injured brain cells (Ludwig et al., 2018). However, a kind of chemical compounds, spirostanol saponins, showed an inhibitory role on the growth or/and metastasis of tumor cells (Huang et al., 2011). Interestingly, we found that a number of furostanol saponins isolated from TT promoted the expansion of hematopoietic stem and progenitor cells (Wang B. et al., 2020). Here, we also tested the effect of these saponin ingredients from TT on irradiated intestinal cell proliferation in primary screening step. TT-4 to TT-6, which mainly consist of steroidal saponins, showed less effect on enhancing the colony number of irradiated IEC-6 cells than TT-2 (data not shown). Thus, we further investigated the role of TT-2 on irradiated intestinal cells by using other proliferation-related detection criteria. The ingredients of TT-2 are different from TT-4 to TT-6, which mainly consists of oligosaccharide components according to our purification method and sample analysis results. It is difficult to further purify each oligosaccharide from TT-2 due to the limited oligosaccharide purification technique (Moravcova et al., 2021). We first found the novel function of TT-2 in improving irradiated intestinal epithelial regeneration by employing the colony-forming screening model. EdU incorporation detection and cell apoptosis analysis results indicated that TT-2 enhanced regeneration mainly by increasing cell proliferation and suppressing the apoptosis of irradiated IEC-6 cells. Results of gene expression analysis further supported these observations, indicating that TT-2 has a positive effect on the survival and proliferation of irradiated IEC-6 cells. We also confirmed the similar effect of TT-2 on human intestinal epithelial cell line HIEC-6. TT-2 significantly promoted the incorporation of EdU in the nucleus, increased the expression of proliferation-related genes and inhibited the expression of apoptosis-related genes in irradiated HIEC-6 (**Supplementary Figures 1A–C**). Notably, TT-2 showed no significant cytotoxic effect on unirradiated intestinal epithelial cells, and there was no obvious difference in the colony-forming number of unirradiated IEC-6 cells treated with different concentration of TT-2 (**Supplementary Figures 2A,B**).

To reduce the cost of research and development of new drugs and the risk of failure, many labs and pharmaceutical companies have focused on the development of predictive and reliable cell or tissue models for primary screening of drug-candidate efficacy *in vitro*. In recent years, several breakthroughs

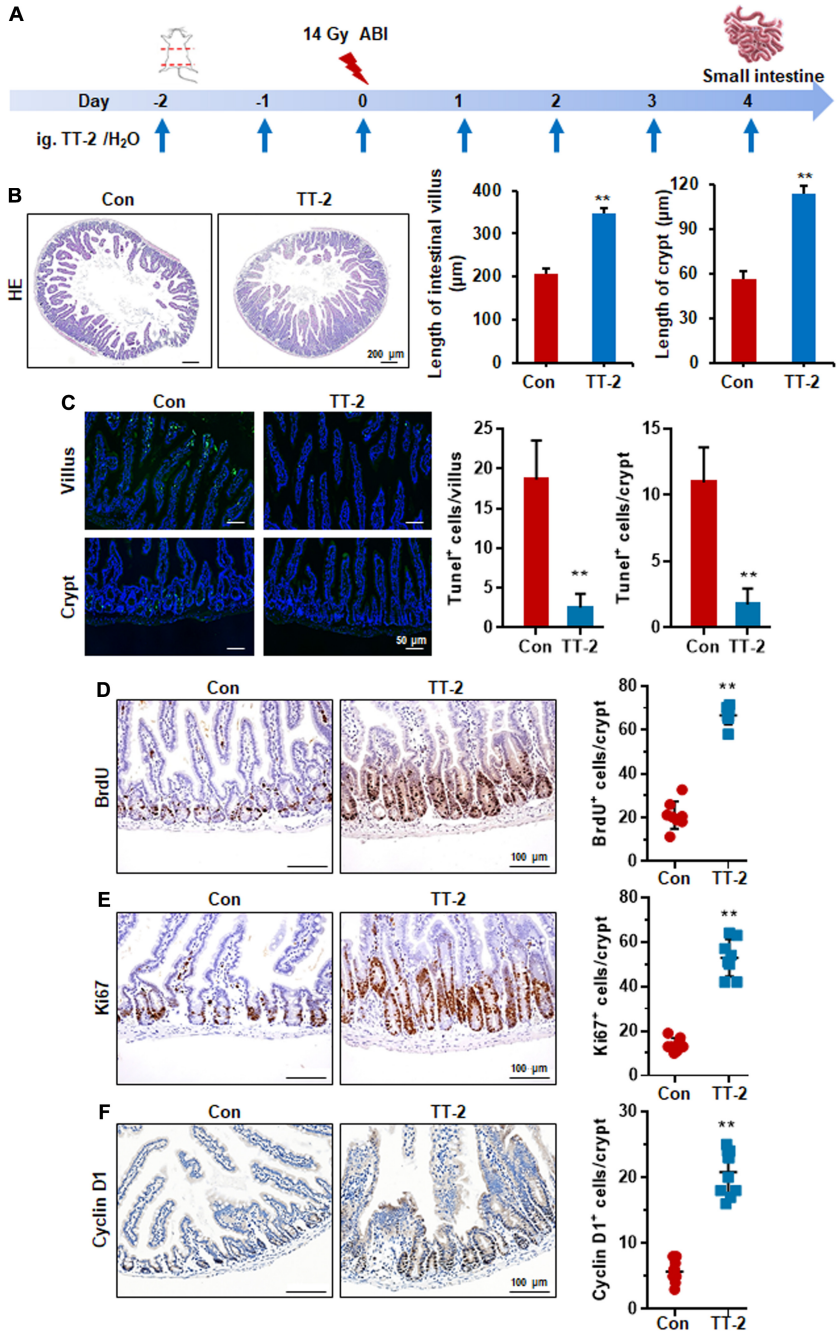

FIGURE 4 | TT-2 promoted proliferation of small intestinal epithelial cells. **(A)** Time schedule for TT-2/H_2O oral administration to mice after 14 Gy irradiation. **(B)** Representative H&E-stained sections and quantification of villus and crypt length 4 days after irradiation (**$p < 0.01$, scale bar = 200 μm). Three mice from each group were used. **(C)** Representative TUNEL-stained images and the quantification of the $TUNEL^+$ cells in the villus and crypt of the small intestine on day 4 after 14 Gy WBI and different treatments (**$p < 0.01$, Scale bar = 50 μm). **(D)** Representative BrdU-stained sections and quantification of $BrdU^+$ cells in crypt of small intestine after 14 Gy ABI and different treatments (**$p < 0.01$, scale bar = 100 μm). Three mice from each group were used. **(E)** Representative Ki67-stained sections and quantification of $Ki67^+$ cells in crypt of small intestine after 14 Gy ABI and different treatments (**$p < 0.01$, scale bar = 100 μm). Three mice from each group were used. **(F)** Representative Cyclin D1-stained sections and quantification of Cyclin $D1^+$ cells in crypt of small intestine after 14 Gy ABI and different treatments (**$p < 0.01$, scale bar = 100 μm). Three mice from each group were used.

have been achieved regarding the culture of ISC-derived intestinal organoids (Ootani et al., 2009; Sato et al., 2009; Jung et al., 2011; Mahe et al., 2013; Wang et al., 2013). Intestinal organoids have the epithelial architecture and physiological characteristics of the intestine, and are more effective and useful models for investigating factors that regulate ISC

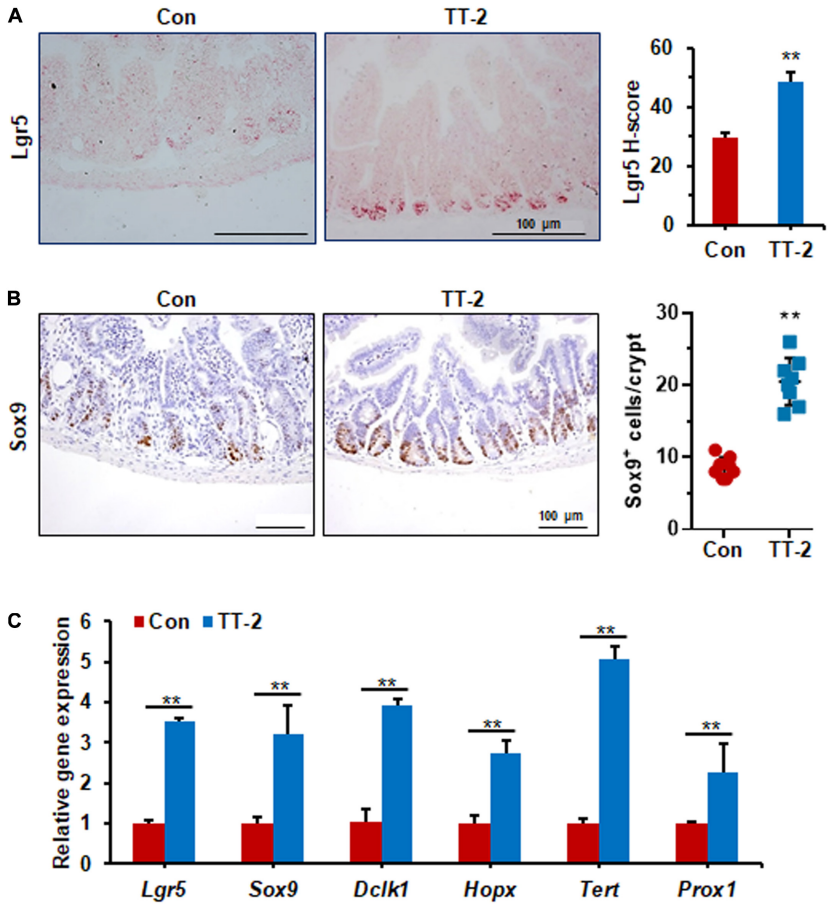

FIGURE 5 | TT-2 promoted intestinal stem cell proliferation of mice after 14 Gy ABI. **(A)** Representative images of *in situ* hybridization for Lgr5 mRNA in intestinal crypts after 14 Gy ABI and different treatments (**$p < 0.01$, scale bar = 100 μm). Three mice from each group were used. **(B)** Representative Sox9-stained sections and quantification of $Sox9^{+}$ cells in crypt of small intestine after 14 Gy ABI and different treatments (**$p < 0.01$, scale bar = 100 μm). Three mice from each group were used. **(C)** qPCR for *Lgr5, Sox9, Dclk1, Hopx, Tert,* and *Prox1* gene expression in mice after 14 Gy irradiation with or without TT-2 treatment for 96 h after ABI (**$p < 0.01$).

self-renewal, proliferation, and differentiation (Sato et al., 2011). Patient-derived organoids have proved to be a reliable model to test the treatment response of metastatic gastrointestinal cancer (Vlachogiannis et al., 2018). Here, we established an irradiated small intestinal organoid model to test the efficacy of primary-screened special active fractions of natural products. Utilizing the radiation-injured intestinal organoid model, we found that TT-2 significantly increased the total organoid numbers and budding rate of irradiated intestinal organoids, most likely by increasing proliferation-related gene expression and decreasing apoptosis-related gene expression in the irradiated organoids. These data provide compelling evidence for a novel role of TT-2 in promoting intestinal organoid growth after *in vitro* irradiation. TT-2 addition to the culture medium showed no significant effect on the growth of unirradiated intestinal organoids (**Supplementary Figures 3A,B**). There was no significant difference in the expression levels of the ISC-related genes, proliferation-related genes, and anti-apoptosis-related genes between Con- and TT-2-treated unirradiated organoids (**Supplementary Figures 3C–E**). These results indicated that TT-2 had no significant proliferation-enhancing role on normal intestinal epithelium. The beneficial influence of TT-2 on irradiated intestinal organoids prompted us to perform animal experiments to evaluate the effect of TT-2 on radiation-induced intestinal damage. We demonstrated that TT-2 is a potent radiation countermeasure, evidenced by the fact that oral administration of TT-2 into mice after lethal doses of ABI significantly increased the length of the intestinal crypts and villi by promoting intestinal cell and ISC proliferation. Several studies indicate that *in vivo* function of chemicals or biomaterials is complex and might involve in indirectly regulatory manner on tissue repairing (Bressan et al., 2019; Peng et al., 2020). Given that intestinal tissue contains multiple cell types and cytokines, it needs to do more work to investigate whether TT-2 can indirectly regulate intestinal cell regeneration *via* other type of cells or co-factors. In recent years, mesenchymal stem cells (MSCs) or their exosomes have demonstrated enhancing-repair function in injured tissue (Ballini et al., 2017; Soontararak et al., 2018). It is valuable to further evaluate the combination effect of MSC

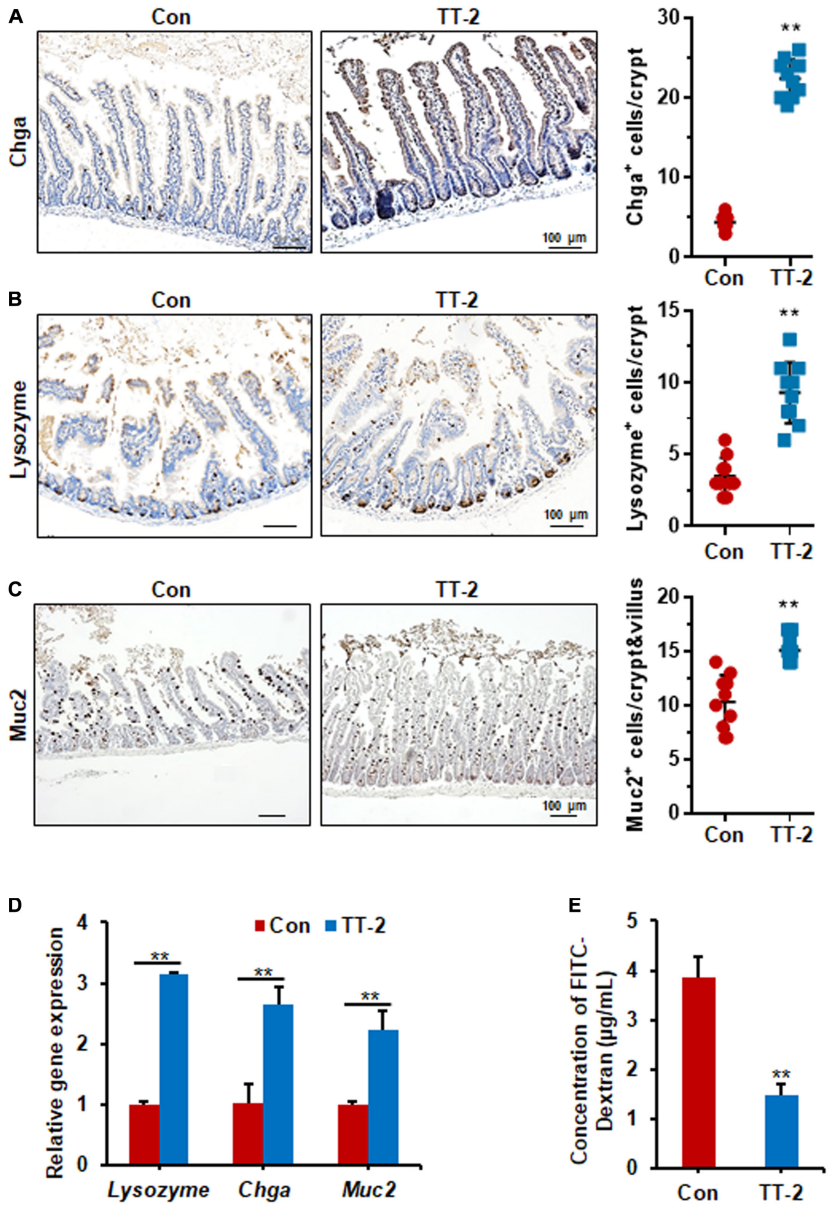

FIGURE 6 | TT-2 enhanced the integrity of intestinal epithelium of mice after 14 Gy ABI. **(A)** Representative Chga-stained sections and quantification of Chga$^+$ cells in crypt of small intestine after 14 Gy ABI and different treatments (**$p < 0.01$, scale bar = 100 μm). Three mice from each group were used. **(B)** Representative lysozyme-stained sections and quantification of lysozyme$^+$ cells in crypt of small intestine after 14 Gy ABI and different treatments (**$p < 0.01$, scale bar = 100 μm). Three mice from each group were used. **(C)** Representative Muc2-stained sections and quantification of Muc2$^+$ cells in crypt of small intestine after 14 Gy ABI and different treatments (**$p < 0.01$, scale bar = 100 μm). Three mice from each group were used. **(D)** qPCR for differentiation-related gene expression in mouse intestinal epithelial cells after 10 Gy irradiation with or without TT-2 treatment for 48 h (**$p < 0.01$). **(E)** The FITC-Dextran level in the serum of mice on day 4 after 14 Gy ABI and treatment with water with or without TT-2 from day −2 to 4 (**$p < 0.01$).

transplantation and TT-2 administration on radiation-injured animal model in the future.

CONCLUSION

Our data demonstrate a novel role for an active fraction of *Trillium tschonoskii*, TT-2, it enhanced the colony forming numbers and improved the proliferation of irradiated intestinal crypt cells. More importantly, TT-2 significantly accelerated intestinal organoid growth and increased Lgr5$^+$ ISC numbers after radiation exposure. TT-2 plays a beneficial role in irradiated intestinal crypt cells and organoids mainly by promoting the expression of proliferation-related genes and inhibiting the expression of apoptosis-related genes. *In vivo* animal experiments showed that TT-2 remarkably enhanced intestinal crypt cell proliferation and new crypt regeneration after irradiation damage. Notably, the administration of TT-2 significantly decreased intestinal epithelial permeability and reduced gut leakiness in irradiated mice. Overall, our data revealed that

this active fraction of TT has the potential to be further developed for use in clinics to treat patients with AGS by enhancing intestinal epithelium repair.

DATA AVAILABILITY STATEMENT

The original contributions presented in the study are included in the article/**Supplementary Material**, further inquiries can be directed to the corresponding author/s.

ETHICS STATEMENT

The animal study was reviewed and approved by the Institutional Animal Care and Use Committee of Laboratory Animal Center.

AUTHOR CONTRIBUTIONS

YL: conception and design, data analysis and interpretation, manuscript writing, and revising. XTP and BM: data analysis and interpretation. FS and SW: collection and assembly of data, and manuscript writing. XP, JZ, and XC: separation and extraction of fractions of Traditional Chinese Medicine. ZF and LH: helping in conducting *in vitro* cellular and molecular biology experiments. All authors contributed to the article and approved the submitted version.

FUNDING

This work was supported by the National Key Research and Development Program of China (2017YFA0103100, 2017YFA0103103, and 2017YFA0103104) and National Natural Science Foundation of China (No: 81872553).

SUPPLEMENTARY MATERIAL

The Supplementary Material for this article can be found online at: https://www.frontiersin.org/articles/10.3389/fcell.2021.745412/full#supplementary-material

REFERENCES

Ayehunie, S., Landry, T., Stevens, Z., Armento, A., Hayden, P., and Klausner, M. (2018). Human primary cell-based organotypic microtissues for modeling small intestinal drug absorption. *Pharm Res*. 35:72. doi: 10.1007/s11095-018-2362-0

Ballini, A., Boccaccio, A., Saini, R., Van Pham, P., and Tatullo, M. (2017). Dental-derived stem cells and their secretome and interactions with bioscaffolds/biomaterials in regenerative medicine: from the *in vitro* research to translational applications. *Stem Cells Int.* 2017:6975251. doi: 10.1155/2017/6975251

Berbee, M., and Hauer-Jensen, M. (2012). Novel drugs to ameliorate gastrointestinal normal tissue radiation toxicity in clinical practice: what is emerging from the laboratory? *Curr. Opin. Support Palliat. Care* 6, 54–59. doi: 10.1097/SPC.0b013e32834e3bd7

Booth, C., Tudor, G., Tudor, J., Katz, B. P., and MacVittie, T. J. (2012). Acute gastrointestinal syndrome in high-dose irradiated mice. *Health Phys.* 103, 383–399. doi: 10.1097/hp.0b013e318266ee13

Bressan, E., Ferroni, L., Gardin, C., Bellin, G., Sbricoli, L., Sivolella, S., et al. (2019). Metal nanoparticles released from dental implant surfaces: potential contribution to chronic inflammation and peri-implant bone loss. *Materials* 12:2036. doi: 10.3390/ma12122036

Chapel, A., Francois, S., Douay, L., Benderitter, M., and Voswinkel, J. (2013). New insights for pelvic radiation disease treatment: multipotent stromal cell is a promise mainstay treatment for the restoration of abdominopelvic severe chronic damages induced by radiotherapy. *World J. Stem Cells* 5, 106–111. doi: 10.4252/wjsc.v5.i4.106

Chen, H., Wang, S., Zhang, J., Ren, X., Zhang, R., Shi, W., et al. (2014). A novel molecule me6tren promotes angiogenesis *via* enhancing endothelial progenitor cell mobilization and recruitment. *Sci. Rep*. 4:6222. doi: 10.1038/srep06222

Choi, C., Lee, C., Shin, S. W., Kim, S. Y., Hong, S. N., and Park, H. C. (2019). Comparison of proton and photon beam irradiation in radiation-induced intestinal injury using a mouse model. *Int. J. Mol. Sci.* 20:1894. doi: 10.3390/ijms20081894

Dutta, A., Verma, S., Sankhwar, S., Flora, S. J., and Gupta, M. L. (2012). Bioavailability, antioxidant and non toxic properties of a radioprotective formulation prepared from isolated compounds of podophyllum hexandrum: a study in mouse model. *Cell. Mol. Biol.* 58(Suppl.), L1646–L1653.

Dutton, J. S., Hinman, S. S., Kim, R., Wang, Y., and Allbritton, N. L. (2019). Primary cell-derived intestinal models: recapitulating physiology. *Trends Biotechnol.* 37, 744–760. doi: 10.1016/j.tibtech.2018.12.001

Huang, W., Zou, K., and Xiong, B. (2011). The rhizome of trillium tschonoskii maxim. Extract induces apoptosis in human lung cancer cells. *Z. Naturforsch C J. Biosci*. 66, 477–484. doi: 10.1515/znc-2011-9-1007

Jung, P., Sato, T., Merlos-Suarez, A., Barriga, F. M., Iglesias, M., Rossell, D., et al. (2011). Isolation and *in vitro* expansion of human colonic stem cells. *Nat. Med.* 17, 1225–1227. doi: 10.1038/nm.2470

Kim, S. H., Lee, S. E., Oh, H., Kim, S. R., Yee, S. T., Yu, Y. B., et al. (2002). The radioprotective effects of bu-zhong-yi-qi-tang: a prescription of traditional chinese medicine. *Am. J. Chin. Med.* 30, 127–137. doi: 10.1142/S0192415X02000144

Kim, Y. H., Han, S. H., Kim, H., Lee, S. J., Joo, H. W., Kim, M. J., et al. (2020). Evaluation of the radiation response and regenerative effects of mesenchymal stem cell-conditioned medium in an intestinal organoid system. *Biotechnol. Bioeng.* 117, 3639–3650. doi: 10.1002/bit.27543

Kuhnert, F., Davis, C. R., Wang, H. T., Chu, P., Lee, M., Yuan, J., et al. (2004). Essential requirement for wnt signaling in proliferation of adult small intestine and colon revealed by adenoviral expression of dickkopf-1. *Proc. Natl. Acad. Sci. U.S.A*. 101, 266–271. doi: 10.1073/pnas.2536800100

Liu, W. C., Wang, S. C., Tsai, M. L., Chen, M. C., Wang, Y. C., Hong, J. H., et al. (2006). Protection against radiation-induced bone marrow and intestinal injuries by cordyceps sinensis, a chinese herbal medicine. *Radiat. Res.* 166, 900–907. doi: 10.1667/RR0670.1

Ludwig, P. E., Thankam, F. G., Patil, A. A., Chamczuk, A. J., and Agrawal, D. K. (2018). Brain injury and neural stem cells. *Neural Regen. Res.* 13, 7–18. doi: 10.4103/1673-5374.224361

Mahe, M. M., Aihara, E., Schumacher, M. A., Zavros, Y., Montrose, M. H., Helmrath, M. A., et al. (2013). Establishment of gastrointestinal epithelial organoids. *Curr. Protoc. Mouse Biol.* 3, 217–240. doi: 10.1002/9780470942390.mo130179

Martin, M. L., Adileh, M., Hsu, K. S., Hua, G., Lee, S. G., Li, C., et al. (2020). Organoids reveal that inherent radiosensitivity of small and large intestinal stem cells determines organ sensitivity. *Cancer Res.* 80, 1219–1227. doi: 10.1158/0008-5472.CAN-19-0312

Meng, J., Lv, Z., Sun, C., Qiao, X., and Chen, C. (2020). An extract oflycium barbarum mimics exercise to improve muscle endurance through increasing type iia oxidative muscle fibers by activating errγ. *FASEB J.* 34, 11460–11473. doi: 10.1096/fj.202000136R

Moravcova, D., Cmelik, R., and Krenkova, J. (2021). Separation of labeled isomeric oligosaccharides by hydrophilic interaction liquid chromatography - the role of organic solvent in manipulating separation selectivity of the amide stationary phase. *J. Chromatogr. A*. 1651, 462303. doi: 10.1016/j.chroma.2021.462303

Ootani, A., Li, X., Sangiorgi, E., Ho, Q. T., Ueno, H., Toda, S., et al. (2009). Sustained *in vitro* intestinal epithelial culture within a wnt-dependent stem cell niche. *Nat. Med.* 15, 701–706. doi: 10.1038/nm.1951

Peng, R., Zhang, W., Zuo, Z., Shan, Y., Liu, X., Tang, Y., et al. (2020). Dimethyl sulfoxide, a potent oral radioprotective agent, confers radioprotection of hematopoietic stem and progenitor cells independent of apoptosis. *Free Radic. Biol. Med*. 153, 1–11. doi: 10.1016/j.freeradbiomed.2020.03.021

Rahmani, S., Breyner, N. M., Su, H. M., Verdu, E. F., and Didar, T. F. (2019). Intestinal organoids: a new paradigm for engineering intestinal epithelium *in vitro*. *Biomaterials* 194, 195–214. doi: 10.1016/j.biomaterials.2018.12.006

Rizk, P., and Barker, N. (2012). Gut stem cells in tissue renewal and disease: methods, markers, and myths. *Wiley Interdiscip. Rev. Syst. Biol. Med.* 4, 475–496. doi: 10.1002/wsbm.1176

Roche, K. C., Gracz, A. D., Liu, X. F., Newton, V., Akiyama, H., and Magness, S. T. (2015). Sox9 maintains reserve stem cells and preserves radioresistance in mouse small intestine. *Gastroenterology* 149, 1553–1563.

Rockwell, S., Grove, T. A., Liu, Y., Cheng, Y. C., Higgins, S. A., and Booth, C. J. (2013). Preclinical studies of the chinese herbal medicine formulation phy906 (kd018) as a potential adjunct to radiation therapy. *Int. J. Radiat. Biol.* 89, 16–25. doi: 10.3109/09553002.2012.717733

Sato, T., and Clevers, H. (2013). Growing self-organizing mini-guts from a single intestinal stem cell: mechanism and applications. *Science* 340, 1190–1194. doi: 10.1126/science.1234852

Sato, T., Stange, D. E., Ferrante, M., Vries, R. G., Van Es, J. H., Van den Brink, S., et al. (2011). Long-term expansion of epithelial organoids from human colon, adenoma, adenocarcinoma, and barrett's epithelium. *Gastroenterology* 141, 1762–1772. doi: 10.1053/j.gastro.2011.07.050

Sato, T., Vries, R. G., Snippert, H. J., van de Wetering, M., Barker, N., Stange, D. E., et al. (2009). Single lgr5 stem cells build crypt-villus structures *in vitro* without a mesenchymal niche. *Nature* 459, 262–265. doi: 10.1038/nature07935

Shadad, A. K., Sullivan, F. J., Martin, J. D., and Egan, L. J. (2013). Gastrointestinal radiation injury: symptoms, risk factors and mechanisms. *World J. Gastroenterol.* 19, 185–198. doi: 10.3748/wjg.v19.i2.185

Soontararak, S., Chow, L., Johnson, V., Coy, J., Wheat, W., Regan, D., et al. (2018). Mesenchymal stem cells (msc) derived from induced pluripotent stem cells (ipsc) equivalent to adipose-derived msc in promoting intestinal healing and microbiome normalization in mouse inflammatory bowel disease model. *Stem Cells Transl. Med.* 7, 456–467. doi: 10.1002/sctm.17-0305

Sugimoto, S., and Sato, T. (2017). Establishment of 3d intestinal organoid cultures from intestinal stem cells. *Methods Mol. Biol.* 1612, 97–105. doi: 10.1007/978-1-4939-7021-6_7

Vlachogiannis, G., Hedayat, S., Vatsiou, A., Jamin, Y., Fernandez-Mateos, J., Khan, K., et al. (2018). Patient-derived organoids model treatment response of metastatic gastrointestinal cancers. *Science* 359, 920–926. doi: 10.1126/science.aao2774

Wallach, T. E., and Bayrer, J. R. (2017). Intestinal organoids: new frontiers in the study of intestinal disease and physiology. *J. Pediatr. Gastroenterol. Nutr.* 64, 180–185. doi: 10.1097/MPG.0000000000001411

Wang, B., Zhang, J., Pang, X., Yuan, J., Yang, J., Yang, Y., et al. (2020). Furostanol saponins from trillium tschonoskii promote the expansion of human cord blood hematopoietic stem and progenitor cells. *J. Nat. Prod.* 83, 2567–2577. doi: 10.1021/acs.jnatprod.9b01268

Wang, F., Scoville, D., He, X. C., Mahe, M. M., Box, A., Perry, J. M., et al. (2013). Isolation and characterization of intestinal stem cells based on surface marker combinations and colony-formation assay. *Gastroenterology* 145, 383–395. doi: 10.1053/j.gastro.2013.04.050

Wang, L., Du, J., Zhao, F., Chen, Z., Chang, J., Qin, F., et al. (2018). Trillium tschonoskii maxim saponin mitigates d-galactose-induced brain aging of rats through rescuing dysfunctional autophagy mediated by rheb-mtor signal pathway. *Biomed. Pharmacother.* 98, 516–522. doi: 10.1016/j.biopha.2017.12.046

Wang, S., Han, Y., Zhang, J., Yang, S., Fan, Z., Song, F., et al. (2020). Me6tren targets β-catenin signaling to stimulate intestinal stem cell regeneration after radiation. *Theranostics* 10, 10171–10185. doi: 10.7150/thno.46415

Yan, K. S., Chia, L. A., Li, X., Ootani, A., Su, J., Lee, J. Y., et al. (2012). The intestinal stem cell markers bmi1 and lgr5 identify two functionally distinct populations. *Proc. Natl. Acad. Sci. U.S.A.* 109, 466–471. doi: 10.1073/pnas.1118857109

Yan, T., Yu, X., Sun, X., Meng, D., and Jia, J. M. (2016). A new steroidal saponin, furotrilliumoside from trillium tschonoskii inhibits lipopolysaccharide-induced inflammation in raw264.7 cells by targeting pi3k/akt, mark and nrf2/ho-1 pathways. *Fitoterapia* 115, 37–45. doi: 10.1016/j.fitote.2016.09.012

Yang, J. B., Zhu, D. Q., Shao, M., Li, A. W., Liu, Z. R., Gao, R. J., et al. (2019). [effects of shengmai jianghuang san on intestinal flora in nude mice with radio resistant cells of nasopharyngeal carcinoma]. *Zhongguo Zhong Yao Za Zhi.* 44, 553–558. doi: 10.19540/j.cnki.cjcmm.20181203.001

Conflict of Interest: The authors declare that the research was conducted in the absence of any commercial or financial relationships that could be construed as a potential conflict of interest.

Publisher's Note: All claims expressed in this article are solely those of the authors and do not necessarily represent those of their affiliated organizations, or those of the publisher, the editors and the reviewers. Any product that may be evaluated in this article, or claim that may be made by its manufacturer, is not guaranteed or endorsed by the publisher.

frontiers in Cell and Developmental Biology

ORIGINAL RESEARCH
published: 09 November 2021
doi: 10.3389/fcell.2021.679866

Integrative Studies of Human Cord Blood Derived Mononuclear Cells and Umbilical Cord Derived Mesenchyme Stem Cells in Ameliorating Bronchopulmonary Dysplasia

Jia Chen[1,2,3,4†], Yuhan Chen[2,3,4†], Xue Du[2,3,4,5†], Guojun Liu[6], Xiaowei Fei[5,7], Jian Ru Peng[1,2,3,4], Xing Zhang[2,3,4], Fengjun Xiao[8], Xue Wang[9], Xiao Yang[2,3,4] and Zhichun Feng[1,2,3,4,5]*

[1] The Second School of Clinical Medicine, Southern Medical University, Guangzhou, China, [2] Department of Neonatology, Senior Department of Pediatrics, The Seventh Medical Center of PLA General Hospital, Beijing, China, [3] National Engineering Laboratory for Birth Defects Prevention and Control of Key Technology, Beijing, China, [4] Beijing Key Laboratory of Pediatric Organ Failure, Beijing, China, [5] The First Affiliated Hospital of Dalian Medical University, Dalian, China, [6] Shandong Qilu Stem Cell Engineering Co., Ltd., Jinan, China, [7] Department of Neurosurgery, Xijing Hospital, Air Force Military Medical University, Xi'an, China, [8] Department of Experimental Hematology and Biochemistry, Beijing Institute of Radiation Medicine, Beijing, China, [9] Experimental Research Center, China Academy of Chinese Medical Sciences, Beijing, China

OPEN ACCESS

Edited by:
Jianjun Zhou,
Tongji University, China

Reviewed by:
Songying Zhang,
Zhejiang University, China
Dilip Shah,
Cooper University Hospital,
United States

***Correspondence:**
Zhichun Feng
zhjfengzc@126.com

[†] These authors have contributed equally to this work

Specialty section:
This article was submitted to Stem Cell Research, a section of the journal Frontiers in Cell and Developmental Biology

Received: 12 March 2021
Accepted: 30 August 2021
Published: 09 November 2021

Citation:
Chen J, Chen Y, Du X, Liu G, Fei X, Peng JR, Zhang X, Xiao F, Wang X, Yang X and Feng Z (2021) Integrative Studies of Human Cord Blood Derived Mononuclear Cells and Umbilical Cord Derived Mesenchyme Stem Cells in Ameliorating Bronchopulmonary Dysplasia. Front. Cell Dev. Biol. 9:679866. doi: 10.3389/fcell.2021.679866

Bronchopulmonary dysplasia (BPD) is a common pulmonary complication observed in preterm infants that is composed of multifactorial pathogenesis. Current strategies, albeit successful in moderately reducing morbidity and mortality of BPD, failed to draw overall satisfactory conclusion. Here, using a typical mouse model mimicking hallmarks of BPD, we revealed that both cord blood-derived mononuclear cells (CB-MNCs) and umbilical cord-derived mesenchymal stem cells (UC-MSCs) are efficient in alleviating BPD. Notably, infusion of CB-MNCs has more prominent effects in preventing alveolar simplification and pulmonary vessel loss, restoring pulmonary respiratory functions and balancing inflammatory responses. To further elucidate the underlying mechanisms within the divergent therapeutic effects of UC-MSC and CB-MNC, we systematically investigated the long noncoding RNA (lncRNA)–microRNA (miRNA)–messenger RNA (mRNA) and circular RNA (circRNA)–miRNA–mRNA networks by whole-transcriptome sequencing. Importantly, pathway analysis integrating Gene Ontology (GO)/Kyoto Encyclopedia of Genes and Genomes (KEGG)/gene set enrichment analysis (GSEA) method indicates that the competing endogenous RNA (ceRNA) network is mainly related to the regulation of GTPase activity (GO: 0043087), extracellular signal-regulated kinase 1 (ERK1) and ERK2 signal cascade (GO: 0070371), chromosome regulation (GO: 0007059), and cell cycle control (GO: 0044770). Through rigorous selection of the lncRNA/circRNA-based ceRNA network, we demonstrated that the hub genes reside in UC-MSC- and CB-MNC-infused networks directed to the function of cell

adhesion, motor transportation (Cdk13, Lrrn2), immune homeostasis balance, and autophagy (Homer3, Prkcd) relatively. Our studies illustrate the first comprehensive mRNA–miRNA–lncRNA and mRNA–miRNA–circRNA networks in stem cell-infused BPD model, which will be valuable in identifying reliable biomarkers or therapeutic targets for BPD pathogenesis and shed new light in the priming and conditioning of UC-MSCs or CB-MNCs in the treatment of neonatal lung injury.

Keywords: bronchopulmonary dysplasia, cord blood mononuclear cell, umbilical cord mesenchymal stem cells, cytokines, whole transcriptome sequencing, noncoding RNA

INTRODUCTION

Bronchopulmonary dysplasia (BPD) is the most common complication associated with extremely preterm infants and is increasing in prevalence, most likely due to the increased survival of extremely low gestational age newborns (Thebaud et al., 2019). The pulmonary phenotypes of BPD are characterized by alveolar simplification, development retardation, impaired vascularization, progenitor cell reduction, as well as pulmonary function abnormality (Pasha et al., 2018). It was documented that 35% (18,000/50,000) of extremely preterm infants will develop BPD. Conventional therapies for BPD are symptom-targeted, whereas the mortality rate remains at high levels, with survivors displaying systematic adverse effects (Poets and Lorenz, 2018). Therefore, developing novel and efficient therapies to reduce overall morbidity and mortality in preterm infants with BPD is of great significance.

Stem cell-based therapies have been proven to alleviate various kinds of diseases, such as neurodegenerative diseases, heart malfunctions, as well as osteoporosis (Lou et al., 2021). Considering the self-renewal capacity, the multi-lineage differentiation, and site-directed mobilization, the broadly distributed mesenchymal stem cells (MSCs) have emerged as a key regulator in stem cell-based therapeutics for injuries (Thébaud, 2018). Recent data from allogeneic or autologous umbilical cord-derived MSC-based therapies have demonstrated promising results in studies based on animal models and early phase clinical studies of neonatal lung injury (Kang and Thébaud, 2018). Initially defined as adjuvant for human stem cell transplantation, mononuclear cells (MNCs) are another source of stem cell reservoir containing a high level of primitive multi-potent stem cells, progenitor cells, and regulatory T cells (Peters et al., 2015). MNCs consist of three categories, peripheral blood-derived mononuclear cells (PB-MNCs), bone marrow-derived mononuclear cells (BM-MNCs), and cord blood-derived mononuclear cells (CB-MNCs). Although a wide range of studies has revealed that MNCs with adult-appendage derivations are capable of presenting superior biological activity and regenerative efficacy in adult pulmonary conditions (Luan et al., 2012; Mills, 2017; Machado et al., 2018), conclusions on the effects of CB-MNCs toward treatment or pathogenesis of BPD remain vague. It is therefore worthwhile to determine the regulatory functions of human cord blood MNCs in an animal model. Furthermore, it is still hung in the balance whether a specific type of stem cell is the best candidate for a particular application in a certain disease model; comparison of the efficacies of UC-MSCs and CB-MNCs in preventing BPD is of great significance.

Noncoding RNAs (ncRNAs) are transcribed from more than 98% of human genome and regulate gene expression (Wright and Bruford, 2011), which can be subdivided into small noncoding RNAs [microRNAs (miRNAs)] and long noncoding RNAs (lncRNAs) as well as circular RNAs (circRNAs) by distinctive length and structure. Intriguingly, the reshaped expression profile of miRNA and lncRNA has been recently reported in the pathogenesis of a myriad of pathological and physiological conditions including BPD. For example, miR-206 (Duan et al., 2017) was boosted, whereas miRNA-489 (Olave et al., 2016) was shrunk in expression; the escalation of lncRNA–metastasis-associated lung adenocarcinoma transcript (MALAT)1 leads to the necrosis of type II alveolar epithelial cell (T2AEC), which ultimately induces lung injury (Cai et al., 2017). Strikingly, elevated levels of multiple miRNAs or lncRNAs have been found in preterm infants who later developed BPD (Syed et al., 2017; Chen J.H. et al., 2020), whereas most of the studies were conducted on cellular level or establishing a primitive correlation model in human specimens. Furthermore, circRNAs have attracted great research interest not only for its specific structure but also for its tissue- or developmental stage-specific expression features. Despite the accumulating knowledge obtained through studies from multiple human developmental diseases, reports about circRNA in the functional regulation of BPD are still poor.

Recently, the mechanisms of competing endogenous RNA (ceRNA) networks have been evidenced to explain a posttranscriptional layer of gene translation regulation. The classical ceRNA network is composed of various types of RNAs, such as lncRNAs, circRNAs, messenger RNAs (mRNAs), and pseudogenes. The potential regulatory lncRNA–miRNA–mRNA and circRNA–miRNA–mRNA pathways are therefore constructed on the basis of their shared bridge miRNAs imprinted with miRNA responsive elements (MREs). Although primitive studies have illustrated the putative circRNA-mediated ceRNA network in the pathogenesis of rat BPD model (Cheng et al., 2020), the comprehensive lncRNA–miRNA–mRNA and circRNA–miRNA–mRNA networks supported by physiological evidence are largely unknown. Moreover, priming and preconditioning of CB-MNCs or UC-MSCs with different cytokines or growth factors are of great importance in cell therapy-based treatment of BPD. Elucidation of the traceable biomarkers between stem cell implantation

and BPD would suggest new strategies for combating this life-threatening disease.

In the current research, with the aim of assessing the efficiency of CB-MNCs and UC-MSCs in restoring lung function and balancing inflammatory responses in hyperoxia-induced BPD, we adopted an experimental mouse model to systematically evaluate the most appropriate cell infusion of indicated stem cells. We also attempted to elucidate the relevant inflammatory responsive mechanisms underlying stem cell-based therapies. Moreover, we adopted whole-transcriptome RNA sequencing (RNA-seq) to identify differentially expressed mRNAs (DEmRNAs), lncRNAs, circRNAs, and miRNAs. Kyoto Encyclopedia of Genes and Genomes (KEGG) and Gene Ontology (GO) pathway analyses were performed for differentially expressed RNAs (DE-RNAs) with significantly different expressions in BPD. Then, the ceRNA networks of mRNAs, lncRNAs, circRNAs, and miRNAs were constructed on the basis of evidence obtained from integrative miRNA target databases combined with the Pearson correlation analysis. Taken together, our findings may provide new evidence for the underlying mechanisms of ncRNAs and related ceRNA networks in stem cell-infused BPD and uncover novel targets for better utilizing stem cells in the treatment of BPD.

MATERIALS AND METHODS

Study Approval and Ethics Statement

Animal procedures were reviewed and approved by the Animal Care and Ethics Committee of the Seventh Medical Center of PLA General Hospital (No. 2020-037). All animals were housed, cared for, and used in compliance with the guidelines regarding the humane use and care of laboratory animals for biomedical research published by the National Institutes of Health (No. 85-23, revised 1996).

Mouse Model

Experimental male mice maintained on a C57BL6/J background were obtained from Beijing Vital River Laboratory Animal Technology and housed under pathogen-free conditions. Typically, a minimum of six mice were included in each treatment group, and all experiments were repeated at least three times.

For constructing the hyperoxia-based BPD model, newborn pups with both genders from different litters were pooled and then randomly distributed to exposure to room air (21% O_2) and hyperoxia (85% O_2) for 14 days (PN1–PN14) starting between 12 and 24 h after birth (recognized as PN1, postnatal day 1). Nursing dams were rotated between room air and hyperoxia every 24 h. Oxygen exposure occurred in an airtight plexiglass chamber equipped with an in-line oxygen analyzer and controller system (Jian-de Xin'anjiang Analysis Instrument Second Factory) in the same room as room air control animals. Oxygen concentrations were monitored continuously and maintained at 85% in the chamber during the experiment. Hyperoxia-exposed pups at PN7 were further randomly assigned to receive stem cell infusion. Briefly, CB-MNCs or UC-MSCs (3×10^6 cells/kg, 0.03 ml) were delivered intravenously to pups through the great saphenous vein. Specifically, MSCs were transfected with green fluorescent protein (GFP)-tagged lentivirus to observe the distribution of cells. For blinding of the above experiments, mice were body-tagged with simple signs. The person who performed the experiments did not know the identity of the specific samples until data were collected and analyzed.

Extraction and Characterization of Human Cord Blood-Derived Mononuclear Cells and Umbilical Cord-Derived Mesenchymal Stem Cells

Briefly, CB-MNCs and UC-MSCs were provided by Shandong Cord Blood Hematopoietic Stem Cell Bank. Human umbilical cord was sourced from uncomplicated full-terms, while cord blood was collected and cryopreserved from the punctured umbilical vein postpartum. All human-derived samples were collected following approval by the ethics review board of the Seventh Medical Center of Chinese PLA General Hospital.

For extraction of CB-MNCs, the cryopreserved cord blood units were thawed immediately and gently shook in 37°C water. Cord blood was collected into 50-ml centrifuge tube thrice volume of premixed suspension buffer within 5 min and stored at room temperature (RT). Mononuclear cells were isolated by centrifugation over a Ficoll-Hypaque density gradient at 700 rpm for 20 min at 4°C in premixed suspension buffer. Cells at the interface were collected by adding premixed suspension buffer followed by centrifugation at 500 rpm for 5 min at 4°C. The collected cells were washed thrice with phosphate buffered saline (PBS) and subsequently resuspended in serum-free Dulbecco's modified Eagle's medium (DMEM). The morphology of resuspended mononuclear cells was determined by Wright Giemsa staining.

Umbilical cord-derived mesenchymal stem cells extraction and purification were as described. Briefly, freshly collected UCs were washed with PBS three times and cut into segments. After removing the two arteries and one vein, the cord segments were cut into small pieces of approximately 1 mm^3. The cord tissue blocks were cultivated in DMEM (Gibco, United States) supplemented with F12 and 10% fetal bovine serum (FBS; Gibco) in a humidified atmosphere at 37°C with 5% CO_2 (Bu et al., 2017). Cells were subcultured once they attained 80% confluence. Medium was replaced every 2 days, and UC-MSCs at passage 5 were used for these experiments. Flow cytometry, Wright–Giemsa staining, alizarin red S staining, and oil red O staining were used to analyze the stem cell phenotype as revealed in **Figure 2**.

Reagents and Antibodies

Antibodies were purchased from the following: primary antibodies subjected to immunohistochemistry including anti-vascular endothelial growth factor (VEGF)-α (Cat. #13034; 1:200), anti-matrix metalloproteinase (MMP)9 (Cat. #11132; 1:1,000), anti-transforming growth factor (TGF)-β (Cat. #11179; 1:1,000) were all purchased from Service Bio. Fluorescein

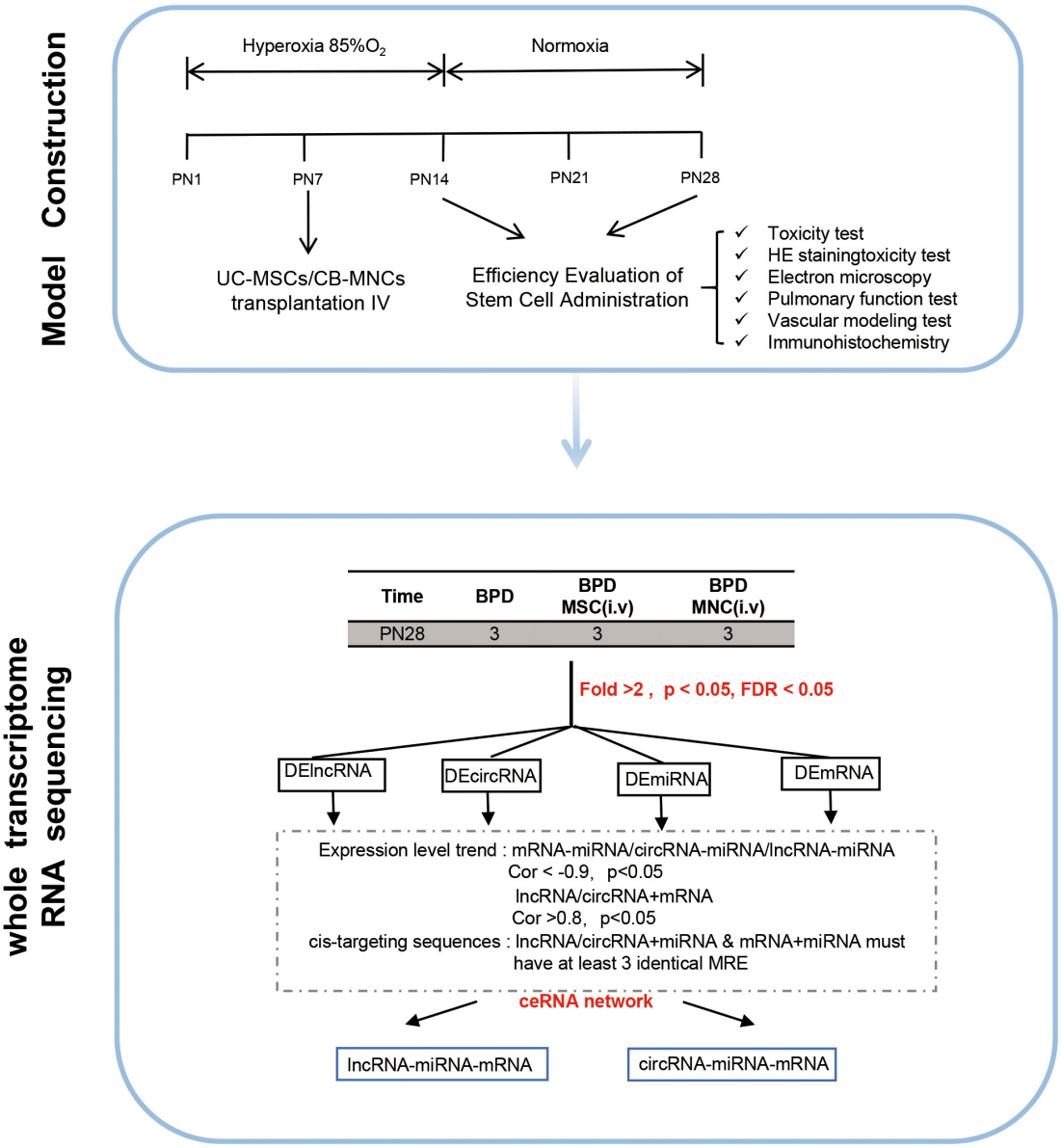

FIGURE 1 | Graphic overview of the study design. The overall scheme of the current research is displayed. Newborn mice (C57 BL/6J) were exposed to hyperoxia (85% O_2) for 14 days. Hyperoxia-exposed mice were compared with mice that remained in normoxic conditions (room air). Different indices and parameters evaluating the pulmonary–vascular functions were recorded and calculated. For better investigating the underlying mechanisms, whole-transcriptome sequencing was conducted in indicated groups. Details of the mRNA-seq, miRNA-seq, and circRNA-seq methods are described in the "Materials and Methods".

isothiocyanate (FITC)-CD44 (Cat. #347943; 1:100), FITC-CD45 (Cat. #347643; 1:100), phycoerythrin (PE)-CD34 (Cat. #652802; 1:100), PE-CD73 (Cat. #550257; 1:100), PE-CD90 (Cat. #555896; 1:100), PE-CD105 (Cat. #580839; 1:100), HLADR (Cat. #555561; 1:100), PE mouse IgG1 (Cat. #349043; 1:100), and FITC mouse IgG1 (#349041; 1:100) for flow cytometry were purchased from BD Biosciences. For immunofluorescence, anti-human-CD44 (Cat. #5640; 1:1,600) were commercially bought from CST. The gradients of the premixed suspension buffer for CB-MNC extractions are commercially obtained as follows: PBS (Beijing Solarbio Science & Technology Co., Ltd.), 2% human albumin (Baxter International Inc.), and 10 U/ml heparin (Changzhou Qianhong Bio-Pharma Co., Ltd.).

Immunofluorescence

Lung and brain tissue frozen sections were fixed in 4% paraformaldehyde 1 week post injection of indicated stem cells or sham controls. A standard immunofluorescence protocol was followed as previously described. Briefly, tissue was fixed in 1× zinc formaldehyde for 24 h at 4°C then rinsed with PBS. Tissue was dehydrated with a gradient of sucrose solution, cryo-sectioned, and rehydrated, followed by antigen retrieval. Blocking

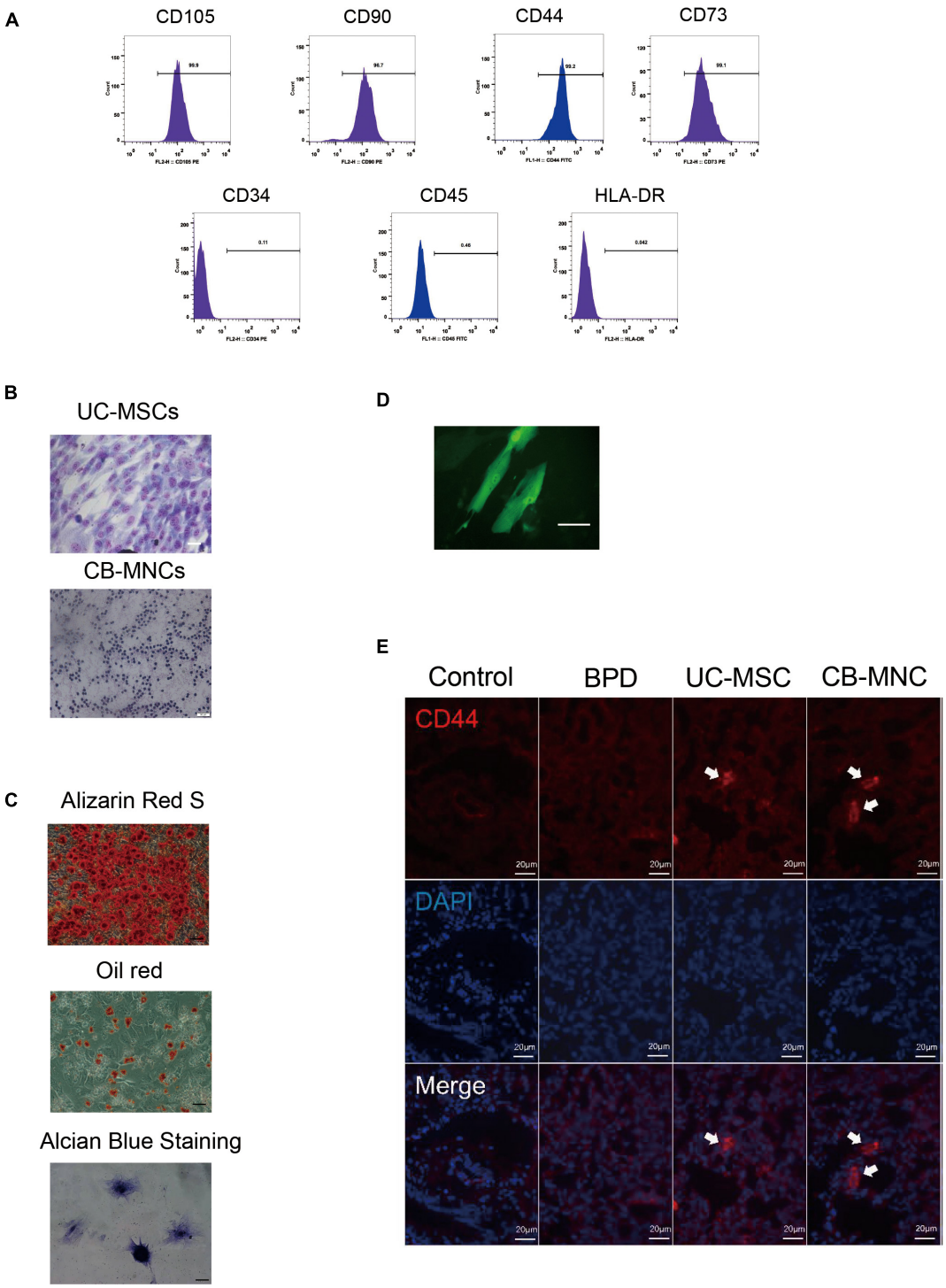

FIGURE 2 | Intravenous infusion of cord blood derived-mononuclear cell (CB-MNC) and umbilical cord derive-messenchymal stem cell (UC-MSC) through great saphenous vein injection. **(A)** Surface marker expression of umbilical cord-derived mesenchymal stem cells (UC-MSCs). Flow cytometry analysis indicated that UC-MSCs were positive for CD105, CD90, CD44, and CD73 but negative for CD34, CD45, and HLA-DR. **(B)** Wright–Giemsa staining illustrating the purity of UC-MSCs (upper panel, scale bar: 50 μm) and cord blood-derived mononuclear cells (CB-MNCs) (lower panel, scale bar: 50 μm). **(C)** The lineage differentiation capacity of UC-MSCs was revealed by induction of distinct reagents. Alizarin red S for osteogenic capacity, oil red O for adipogenic capacity, and Alcian blue for chondrogenic differentiation, scale bar: 50 μm. **(D)** Fluorescent image indicating the successful infection of green fluorescent protein (GFP)-lentivirus in MSC, scale bar: 20 μm. **(E)** Immunofluorescence analysis of lung tissues infused with indicated cells. CD44 antibodies were used to detect human-derived CD44 (red), blue staining shows cell nuclei [4′,6-diamidino-2-phenylindole (DAPI)]. Images are representative of three independent experiments, scale bar: 20 μm. Data are representative of three independent biological replicates.

and staining were performed in 1% bovine serum albumin (BSA) in PBS supplemented with 0.3% Triton X-100. Sections were incubated in primary antibodies including mouse anti-CD44 (Cell Signaling no. 5640, used at 1:1,600) overnight at 4°C (Chen et al., 2014). The corresponding secondary antibodies were incubated with tissue for 1–2 h at RT. The nuclei were stained with 4′,6-diamidino-2-phenylindole (DAPI; Sigma), and images were captured and processed using identical settings in the Zeiss LSM 510 Meta inverted Confocal Microscope.

Lung Morphology

Left-lobe lung sections (5 μm thick) were stained with H&E. For each morphometric analysis, 8–10 areas per slide were quantitated and averaged per slide. Images were acquired with a Nikon Eclipse TE300 inverted microscope, and quantification was performed using ImageJ. For radial alveolar count (RAC) measurement, the well-established method to quantify alveolarization (Hirsch et al., 2020), areas were randomly chosen and photographed at ×10 magnification. For each of six images, a perpendicular line was drawn from the center of a bronchial or bronchiolar airway to either the edge of the lung or the nearest connective tissue septum or airway. A minimum of 40 lines were drawn for each lung, and the number of septae intersected was counted for each line. Chord length (L_m) of the airspace was estimated, as previously described (Cooney and Thurlbeck, 1982). Briefly, the images were superimposed on parallel on a grid with parallel lines spaced at 58-μm intervals, and the mean length of each chord, defined as the distance between two sequential intersections of the alveolar surface with the test line, was measured. For measuring the radical alveolar area, the Analyze Particles function of ImageJ was used in conjunction with a custom written macro for the measurement of the lung architecture and alveolar area (Nold et al., 2013). To prevent inadvertent observer bias, an investigator blinded to the assigned groups performed image acquisition and analyses. Values were pooled for each individual animal for statistical analysis.

Transmission Electron Microscopy

Three slices of 2 mm × 2 mm × 2 mm were cut from three different segments of the left lung and fixed in 2.5% glutaraldehyde and phosphate buffer 0.1 M (pH = 7.4) for electron microscopy analysis. For each lung electron microscopy image (20/animal), the following alterations were analyzed as described previously (Buchacker et al., 2019) (a) alveolar-capillary membrane damage, (b) type II pneumocyte lesion, (c) type I pneumocyte infiltration, (d) elastic fiber breakdown, and (e) capillary and fibroblast deposition. Data were acquired using JEOL 1010 Transmission Electron Microscope, Tokyo, Japan.

Quantitative Real-Time PCR

RNAs of lung tissue samples from indicated groups were reverse-transcribed into complementary DNAs (cDNAs) using the ReverTra Ace qPCR RT Kit (TOYOBO, OSAKA, Japan, FSQ-101), according to the manufacturer's instructions. All primers used in the study are shown in **Table 1**. Real-time PCR was performed with THUNDERBIRD SYBR qPCR Mix (TOYOBO, OSAKA, Japan, QPS-201) on StepOnePlus™ Real-Time PCR System (Roche Diagnostics, CA, United States, lightcycler 480). The PCR conditions were as follows: an initial denaturation step at 95°C for 5 min, followed by 40 cycles of 95°C for 10 s, and 60°C for 30 s. The results were analyzed using $2^{-\Delta\Delta CT}$. $^{\Delta CT} = {}_{CT}$ (target gene) $- {}_{CT}$ (internal reference), $^{\Delta\Delta}{}_{CT} = {}^{\Delta}{}_{CT}$ (sample) $- {}^{\Delta}{}_{CT}$ (control). All experiments were performed in triplicate.

TABLE 1 | Hematological Indicators.

Index	Control group	CB-MNCs group	*p*
WBC	4.80 ± 1.63	5.70 ± 1.99	0.3709
HGB	146.75 ± 8.88	130.88 ± 6.88	0.0022*
PLT	827.75 ± 137.77	741.38 ± 149.69	0.2802
PCT	0.47 ± 0.08	0.44 ± 0.08	0.3994
NEU#	0.22 ± 0.12	1.21 ± 0.95	0.0167*
LYM#	4.30 ± 1.48	3.30 ± 2.19	0.3358
MON#	0.25 ± 0.24	0.70 ± 0.64	0.1046
BAS#	0.01 ± 0.02	0.00 ± 0.00	0.2117
MON%	4.78 ± 5.10	13.53 ± 14.57	0.1558

CB-MNC, cord blood-derived mononuclear cell; WBC, white blood cell (absolute numbers); HGB, hemoglobin; PLT, platelet (absolute numbers); PCT, Procalcitonin; NEU, neutrophils (absolute numbers); LYM, lymphocyte (absolute numbers); MON, monocyte (absolute numbers); MON%, percentage of monocyte; BAS, basophil (absolute numbers).
"#" means the absolute number of the index.
Values are mean ±SD of a minimum of six animals in each group.
**P < 0.05.*

Immunohistochemistry

Mice were anesthetized by intraperitoneal (i.p.) injection with 4% chloral hydrate (0.01 ml/g). Mouse lungs were collected after saline perfusion, and the tissue specimens were fixed overnight in 4% paraformaldehyde. After sequential steps of dehydration and embedding, 5-μm sections were rehydrated and stained with hematoxylin and eosin (Sigma-Aldrich) according to the manufacturer's instructions. For immunohistochemistry, tissue sections were deparaffinized and incubated in citrate buffer at 95°C for 40 min for antigen retrieval and then incubated overnight at 4°C with the primary antibodies including anti-VEGFα (1:100), anti-MMP (1:100), and anti-TGF-β (1:100). After washing three times, tissue sections were incubated with biotinylated anti-rabbit IgG (1:200 dilution) for 1 h at RT after washing three times. Then, streptavidin–horseradish peroxidase conjugates were added, and the slides were incubated for 45 min. Here, 3,3′-diaminobenzidine (DAB) solution was added post PBS washing, and the slides were counterstained with hematoxylin. Negative controls were treated in the same way except without adding the primary antibodies. All staining was evaluated by a quantitative imaging method (Xie et al., 2014). Briefly, the percentage of immunostaining was calculated by immunohistochemistry (IHC) profiler plug-ins of the ImageJ software, and the staining intensity (negative, score = 0; weak, score = 1; medium, score = 2; very strong, score = 3) was recorded. An H-score was further calculated using the following formula: H-score = Σ (PI × I) = (percentage of cells of weak intensity × 1) + (percentage of cells of moderate intensity × 2)

+ (percentage of cells of strong intensity × 3). PI indicates the percentage of positive cells vs. all cells, and I represents the staining intensity.

Pulmonary Function Assessment

For detection of respiratory motion function, mice were euthanized with 4% chloral hydrate (0.01 ml/g) i.p. followed by tracheostomy. Data were monitored and acquired by AcqKnowledge (Biopac Systems Inc., United States), a pulmonary maneuver system. During data collection, basic stable heart rate (HR) was recorded by ECG before tracheotomy operation. Mouse HR was maintained at proper level (<10% variation of basic HR) and breathing rate was maintained stable to ensure the reliability of the physiological data. Basic parameters included peak expiratory flow (PEF), peak inspiratory flow (PIF), breathing per minute (BPM), tidal volume (TV), and minute volume (MV).

For detection of pulmonary blood flow, all mice were subsequently transferred to evaluate pulmonary blood flow with laser Doppler flowmetry (LDF) using MoorFLPI (Moor Instruments, United Kingdom). Mice were ventilated (Alcott Biotech, China) with an average breathing frequency of 150 breaths/min, inspiratory/expiratory ratio 2.0, and tidal volume 1.0 ml/kg. The blood flow of bilateral lungs and heart were synchronizing measured after they were fully exposed. The pulmonary blood flow signal intensity was normalized to heart surface blood.

Blood Sampling and Hematology Test

With the aim of evaluating the safety of CB-MNC infusion, hematological indicators were enrolled to present the overall physiological status. Briefly, a 1.5-ml ethylene diamine tetraacetic acid (EDTA)-coated eppendorf® tube (EP tube) was used to collect approximately 200 μl of blood *via* the tail vein of the mice. The collected blood was placed at 4°C and transferred for analysis using BC-5180CRP (Mindray Instruments, Shenzhen, China).

RNA Extraction and Library Preparation

Total RNA was isolated using TRIzol reagent (Invitrogen), according to the manufacturer's instructions; RNA integrity was evaluated using the Agilent 2100 Bioanalyzer (Agilent Technologies, Santa Clara, CA, United States). The samples with RNA Integrity Number (RIN) R7 were subjected to the subsequent analysis of high-throughput sequencing. For small RNA-seq, a total of 1 μg of total RNA per sample was used for the small RNA library. Sequencing libraries were generated using NEBNext® Multiplex Small RNA Library Prep Set for IlluminaR (NEB, United States) following the manufacturer's recommendations. For mRNA+lncRNA sequencing, mRNA libraries were constructed using NEBNext® UltraTM II RNA Library Prep Kit for Illumina® (NEB Cat# E7770L/E7775L) following the manufacturer's instructions.

RNA Sequencing Analysis

mRNA–lncRNA seq reads were preprocessed as described previously (Chen W. et al., 2020). Briefly, the 150-nt paired-end retained reads were mapped to the reference genome (mice NCBI 37 assemblies) using STAR (version 2.5.3a) with the default parameters. The uniquely mapped reads with less than 2% mismatch were passed to StringTie (version 1.3.3b) for transcript assembly, and the fragments per kilobase of transcript per million mapped reads (FPKM) value was also generated for each gene. For the small RNA-seq reads, the clean reads with high quality were then aligned to the same reference genome using Tophat2 (version 2.0.13) with default parameters after FastQC assessment. miRNA reads were normalized with transcripts per million (TPM). Finally, the DEGs were called with limma and DEseq2 packages in R software with the criterion of an adjusted p-value < 0.1 as well as log2FC > 1. Notably, the p-values were attained by the Wald test and adjusted by BH method.

Gene Ontology and Kyoto Encyclopedia of Genes and Genomes Pathway Analysis

Gene ontology analysis functionally associates DEmRNAs with GO categories, which consist of biological process (BP), molecular function (MF), and cellular component (CC) networks that attribute the gene subsets to defined terms[1]. KEGG pathway analysis is optimal for analyzing DEmRNAs with defined signaling pathways based on the latest KEGG[2] database.

Gene Set Enrichment Analysis

The association between DEmRNAs and hallmark molecular signatures was analyzed using gene set enrichment analysis (GSEA v2.2) as previously described. We use default settings to calculate the enrichment score (ES), which estimates whether a certain term of gene set from the Molecular Signatures Database (MSigDB) (here refers to the term "hallmark") is enriched among the ordered predefined differently expressed gene sets or not. False discovery rate (FDR) < 0.05 was considered statistically significant.

Strategies in Identification of ceRNA Pairs

Based on the expression levels of mRNAs, lncRNAs, circRNAs, or miRNAs, Pearson's correlation coefficient and p-value were calculated for miRNA–target (mRNA/lncRNA/circRNA) or mRNA–lncRNA/circRNA coexpression networks. For miRNA–target, combining with evidence from miRNA–target-analyzing tools miRanda and Targetscan, negatively correlated pairs with Pearson's correlation coefficient value < −0.9 and p-value < 0.05 were subjected to further analysis. mRNA–lncRNA/circRNA coexpression pairs with Pearson's correlation coefficient value > 0.8 and p-value < 0.05 were retained. Subsequently, shared pairs from the predicted miRNA–target pairs from binding sites and the predicted pairs from the coexpression network were synergistically used for building ceRNA network. Finally, a hypergeometric test was introduced to filter the mRNA–miRNA–lncRNA/circRNA network of significance as previously described (Zhang et al., 2018).

[1]http://www.geneontology.org

[2]https://www.genome.jp/kegg

Network Building

Cytoscape software v.3.8.0 was utilized to construct and graph the corresponding networks (San Diego, CA, United States). In figures, distinct shapes of nodes define RNA types, and colors represent expression module. Patterns of edges define regulatory relationships. The size of the nodes represents the number of interactions (**Figure 1**).

Statistical Analysis

Data were all mean ± SD. Comparisons between different groups were performed by one-way ANOVA followed by Bonferroni's multiple comparison test or unpaired Student's *t*-test (GraphPad v7.03; GraphPad Software Inc.). Statistical significance was defined as a two-sided *p*-value less than 0.05. All statistical analyses were graphed by Prism software program (version 7.03; GraphPad Software, San Diego, CA, United States). Data are representative of three independent biological replicates.

Data Availability

Bioinformatics pipelines and scripts used for our analysis are available at https://github.com/mauve612/BPD-stem-cell-. All the datasets of RNA-seq included in this study have been uploaded to the Genome Sequence Archive at the National Genomics Data Center, Beijing Institute of Genomics (BIG), Chinese Academy of Sciences/China National Center for Bioinformation (GSA: CRA004720 with BioProject ID: PRJCA004041), and are publicly accessible at https://bigd.big.ac.cn/gsa/ after the release date of December 14, 2022.

RESULTS

Characterization and Distribution of Umbilical Cord-Derived Mesenchymal Stem Cells (UC-MSCs) and Cord Blood-Derived Mononuclear Cells

With the aim of testing our hypotheses that the infusion of fetus-derived stem cell can alleviate the phenotype of BPD, we set out to establish a BPD model that can phenocopy the features of severe BPD as previously discussed (Nardiello et al., 2017). In this model, newborn mice were exposed to 85% O_2 (hyperoxia) from postnatal day 1 (PN1) to PN14 and returned to room air at PN14 thereafter. Age-matched control litters were housed under standard room air conditions (normoxia) (**Figure 1**).

Before assessing the efficiency and safety of indicated stem cell infusion, purity of UC-MSCs and CB-MNCs was firstly characterized. Flow cytometry analysis of cell surface antigens revealed that UC-MSCs stained positive for the MSC markers CD73, CD44, CD90, and CD105 but negative for the hematopoietic lineage marker CD34, CD45, and the human leukocyte antigen HLA-DR (**Figure 2A**). Next, we observed the purities of UC-MSCs and CB-MNCs by Wright–Giemsa staining, as shown in **Figure 2B**. Randomly selected views have shown that the relative quantities of purified UC-MSCs (**Figure 2B**, upper panel) and resuspended CB-MNCs (**Figure 2B**, lower panel) are higher than 90%. Meanwhile, as shown by alizarin red S, oil red O, and Alcian blue staining, under specific culture conditions, UC-MSCs could differentiate into osteocytes and adipocytes *in vitro* (**Figure 2C**).

We went on to study the distribution of indicated stem cells after infusion. Initially, UC-MSCs were stably infected with GFP fluorescent virus, and intensive fluorescent signals were observed (**Figure 2D**). One day after stem cell infusion, GFP-labeled MSCs were found in the lung (**Figure 2D**), indicating the successful circulation of UC-MSCs. To further verify the residence of UC-MSCs and CB-MNCs, lung and brain sections of mice harvested at PN42 were stained with CD44, a human stem cell marker. UC-MSC- and CB-MNC-infused mice demonstrated strong immunofluorescent density, while tissue sections in BPD group can hardly detect any fluorescent signals in lung (**Figure 2F**). These results suggested that UC-MSCs and CB-MNCs were most prevalently residents in lung at indicated times post injection.

Intravenous Infusion of Cord Blood-Derived Mononuclear Cells and Umbilical Cord-Derived Mesenchymal Stem Cells Improves Hyperoxia-Induced Bronchopulmonary Dysplasia

To explore the potential impacts on stem cell-implanted hyperoxia-induced BPD, the body weights of mice following stem cell infusion were again traced and recorded based on the time point of intense acute lung injury and active tissue remodeling. Strikingly, the growth rate of mice in UC-MSC and CB-MNC groups was significantly enhanced compared to that of the mice in BPD group, rendering the mouse weights of UC-MSC group and CB-MNC group comparable to that of control group at the endpoint of the observation (**Figure 3A**). Importantly, integrating sex and gender considerations into basic experimental biomedical research can largely improve the reproducibility and fidelity of the conclusion (Freeman et al., 2017), which have been adopted in previous animal studies regarding BPD model (Leary et al., 2019). No striking differences were observed between male and female mice in corresponding groups (**Figure 3B**). Mouse lung histology analyses were performed on mice of indicated groups at PN28 after injections. As indicated in **Figure 3C**, male animals subjected to infusion with CB-MNCs and UC-MSCs presented with dramatically improved alveolarization and almost completely restored lung architecture compared with those of the BPD group at both monitoring time points, and the conclusion was consistent in age-matched female animals (**Supplementary Figure 1A**), as reflected by an increase in radical alveolar counts (RACs), shrunk MIL (mean chord length, Lm), and the radical alveolar area (RAR) compared with normoxia-control mice at both genders (**Figure 3D**, **Supplementary Figures 1B–D**).

We also utilized electron microscopy to observe ultrastructure changes by hyperoxia exposure; gradual degeneration of the alveolar capillary membrane and damage to type II pneumocytes, higher septal barrier (see blue arrows, compare the annotated distances) and lower septal surface density, and reduced density of storage organelles were shown in BPD group compared to those of the controls (**Figure 3G**, upper two lanes). Significantly, both CB-MNC- and UC-MSC-infused group

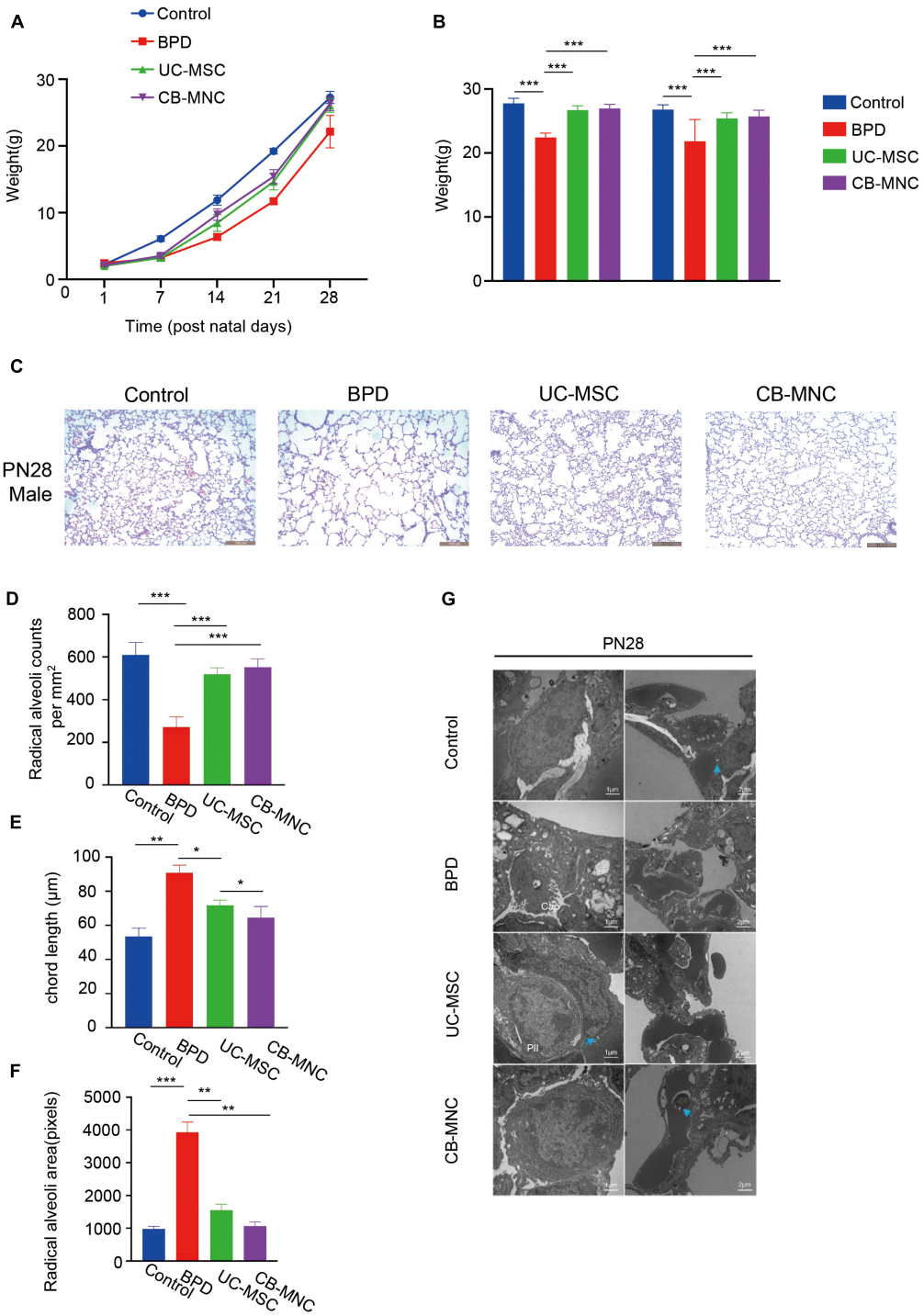

FIGURE 3 | Intravenous infusion of cord blood-derived mononuclear cells (CB-MNCs) and umbilical cord-derived mesenchymal stem cells (UC-MSCs) improves hyperoxia-induced bronchopulmonary dysplasia (BPD). **(A)** Line graph illustrating the changes of weight in mice with different treatments at indicated time points. **(B)** Bar graph illustrating the change of weight in male and female mice with different treatments at postnatal day (PN)28. **(C)** Representative H&E staining images of lung histology in hyperoxia-exposed male mice with indicated treatments at PN28. Scale bar: 100 μm. **(D–F)** Sections of whole lungs were analyzed for the number of alveoli per square millimeter **(D)**, the chord length **(E)**, the size of the alveoli **(F)**. **(G)** Electron microscopy presenting the distal lung architecture of hyperoxia-exposed preterm mice subjected to different treatments at indicated time points. Pictures in left orientation indicated the type II pneumocytes, scale bar: 1 μm, whereas pictures in right orientation indicated the capillaries, scale bar: 2 μm. Values are mean ± SD of a minimum of six animals in each group, *$p < 0.05$, **$p < 0.01$, ***$p < 0.001$, by one-way ANOVA test. Data are representative of three independent biological replicates.

displayed ameliorated lung morphology. Interestingly, CB-MNC and UC-MSC infusion contributes to proliferation in type II pneumocytes lamellar bodies resembling those of control groups and repairs of alveolar capillary disorganizations (**Figure 3G**; lanes 3,4). Taken together, both CB-MNCs and UC-MSCs are capable of restoring lung morphology and improving pulmonary development of BPD mouse lung.

Cord Blood-Derived Mononuclear Cells and Umbilical Cord-Derived Mesenchymal Stem Cells Attenuate Hyperoxia-Exposed Mouse Lung Inflammation Response

Given that inflammatory imbalance and abnormal growth are considered hallmarks of hyperoxia-induced BPD (Ryan et al., 2008), we examined the expression level of cytokines regarding vascular remodeling. As shown in **Figure 4A**, VEGF was significantly downregulated in BPD mice, which is consistent with the evidence that VEGF is decreased in infants dying with BPD and VEGF promotes lung angiogenesis and prevents alveolar damage in hyperoxia-exposed rats; injections of CB-MNCs restore their expression to the level comparable with the normoxia controls. TGF-β signaling plays a crucial role during lung development, and increased TGF-β levels negatively affect alveogenesis (Wu et al., 2020). Immunohistochemical staining analysis demonstrated that BPD mice had a marked increase in expression of the TGF-β and MMP-9 protein in the lung at 21 days of age compared to control group. Strikingly, there was significant abrogation in expression level of TGF-β1 and MMP-9 after CB-MNC infusion at both genders (**Figures 4A,B** and **Supplementary Figures 2A,B**). On the contrary, the expressions of TGF-β1 and MMP-9 were not significantly diminished post UC-MSC infusion compared to BPD mice among male mice. This might be due to a distinct mechanism of UC-MSCs and CB-MNCs that regulates the secretion of TGF-β1 and MMP-9 at different gender backgrounds of BPD. Subsequently, we adopted quantitative qPCR analysis to validate the expression levels of typical inflammatory factors and classical growth factors in lung tissue of hyperoxia-induced BPD mice, which were harvested 3 weeks post injection. We firstly examined the variations of the expression of indicated regulators in BPD model. Notably, there are folds of increase in expression of IL-6 and IL-1β concomitant with repression of IL-10, which is consistent with the long known evidence that elevated serum concentrations of pro-inflammatory cytokines IL-6 and IL-1β and declined anti-inflammatory IL-10 are markers of the pathogenesis of BPD in extremely low-birth weight infant (Yoon et al., 1997; Garingo et al., 2007). Infusion of UC-MSCs and CB-MNCs shrunk the expression of IL-6 and IL-1β, whereas it boosted the expression of IL-10 compared to BPD group (**Figures 4C–E**). In contrast to the sharp decline in BPD group, an increase of interleukin-2 (IL-2) was observed in the stem cell-infused groups (**Figure 4F**). IL-2 has been implied to play pivotal roles in T-cell activation and proliferation (Dhupkar and Gordon, 2017). We also observed that moderately decreased level of tumor necrosis factor-α (TNF-α) after UC-MSCs and CB-MNCs were infused (**Figure 4G**), which is supported by the evidence that preterm infants who went on to develop moderate or severe BPD showed significantly lower TNF-α levels at birth compared with no or mild BPD (Ehrhardt et al., 2016).

Intravenous Infusion of Cord Blood-Derived Mononuclear Cells and Umbilical Cord-Derived Mesenchymal Stem Cells Improved Pulmonary Respiratory Motion

To elucidate the impact of CB-MNCs and UC-MSCs on improvement of respiratory motion, we conducted pulmonary function test using integrative pulmonary respiratory analyzing system. Parameters including peak inspiratory flow (PIF), peak expiratory flow (PEF), tidal volume (TV), breaths per minute (BPM), and minute volume (MV) were monitored and assessed in different groups of both genders at PN28. In accordance with the alterations in lung morphology, BPD mice displayed shortest breath and highest respiratory rate upon hyperoxia exposure, evidenced by the square respiratory waveform compared to those in controls (**Figure 5A**, lane 2). Interestingly, infusion of stem cells greatly reshaped the respiratory wave by shifting from square-like to sinusoidal (**Figure 5A**, upper two panels). Mice in stem cell-infused groups resulted in a significant escalation in multiple indices of respiratory waveform and decline in BPM and MV compared to those of BPD mice (**Figures 5B–F**, **Supplementary Figures 4A–E**). Strikingly, infusion of CB-MNCs exhibited even stronger capacity in restoring the respiratory motion function compared to those in UC-MSC-infused group.

Intravenous Infusion of Cord Blood-Derived Mononuclear Cells and Umbilical Cord-Derived Mesenchymal Stem Cells Recovered Respiratory Blood Flow

With the aim of exploring the potential impact of UC-MSCs and CB-MNCs toward peripheral pulmonary vascular remodeling under hyperoxia exposure, lung perfusion with LDF was employed. Of note, left or right lung/heart blood flow ratio were recorded and calculated to analyze the pulmonary vascular resistance and pulmonary vascular areas. Notably, there was mild alteration of left lung/heart blood flow ratio after 3 weeks of infusion of UC-MSCs and CB-MNCs (**Figure 5G**, **Supplementary Figure 4G**), whereas the right lung/heart blood flow ratio were drastically escalated post UC-MSC and CB-MNC infusion (**Figure 5H**, **Supplementary Figure 4H**), compared to that of the BPD mice at both sex backgrounds. Collectively, these results suggested that stem cell injection, especially CB-MNC infusion, can improve the pulmonary vascular resistance and increased pulmonary vascular area upon hyperoxia stimulation.

Toxicity Test

Current reports on safety application of CB-MNC of preclinical animal level are inadequate. We therefore assessed the toxic impact of CB-MNC infusion in C57 mice. During the

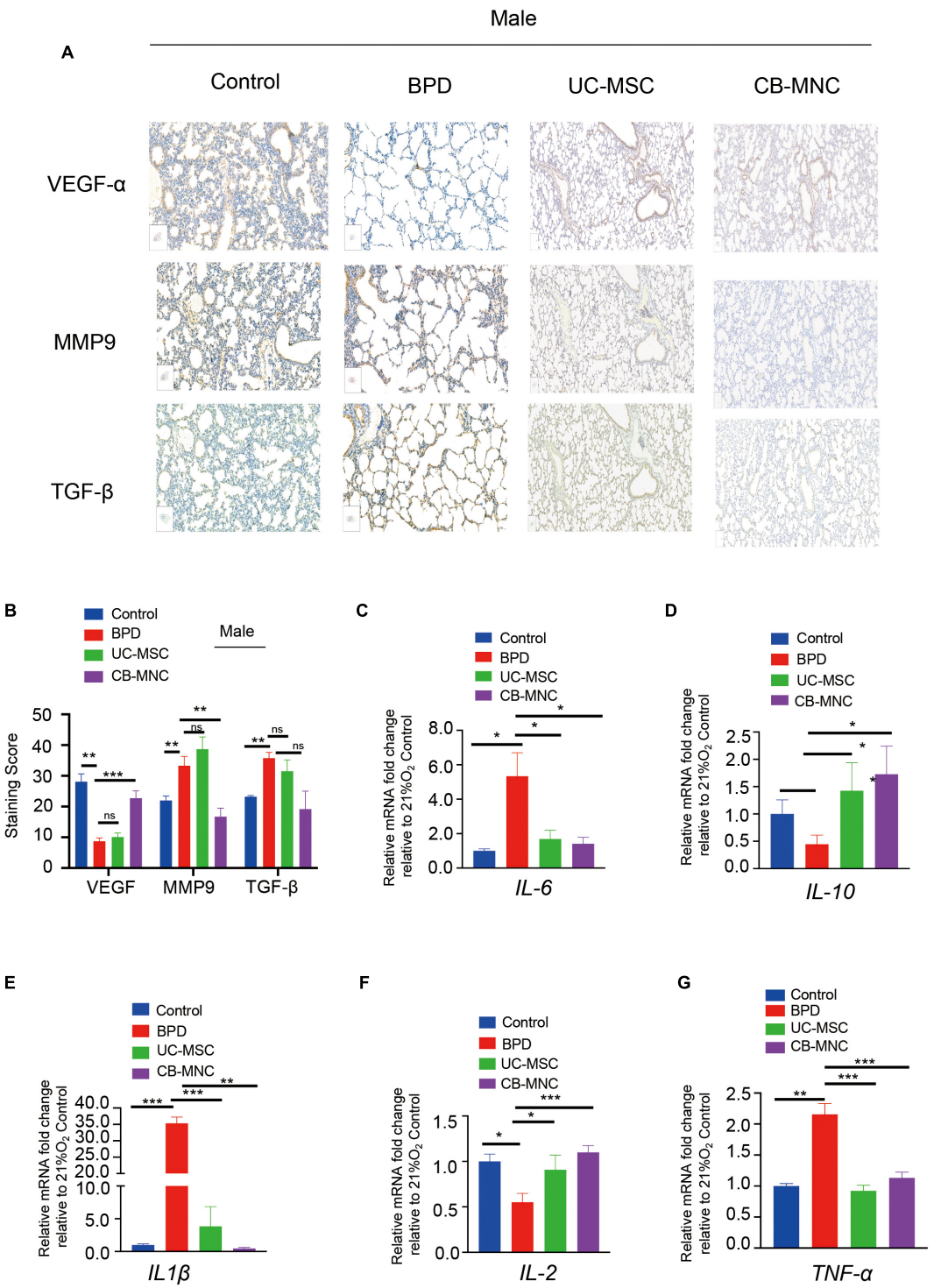

FIGURE 4 | Expression profiles of inflammatory factors and in lung of UC-MSC- and CB-MNC-infused mice. **(A)** Immunohistochemical staining of vascular endothelial growth factor (VEGF), transforming growth factor-β1 (TGF-β1), and matrix metalloproteinase-9 (MMP-9) in lung tissue of male mice. Positive staining of cytoplasm is yellow-brown and that of nuclei is blue. Scale bar: 100 μm. **(B)** Summary of the quantification of the immunohistochemical staining of the indicated factors in **(A)**. **(C–G)** Lung tissue was collected from mice in each group at postnatal day (PN)28. Transcriptional levels of cytokines and growth factors were determined by quantitative reverse transcription polymerase chain reaction analysis. **(C)** Interleukin (IL)-6, **(D)** IL-10, **(E)** IL1-β, **(F)** IL-2, **(G)** tumor necrosis factor (TNF)-α. p-values are based on two-sided Mann–Whitney *U*-tests. *$p < 0.05$, **$p < 0.01$, ***$p < 0.001$. Data are representative of three independent biological replicates.

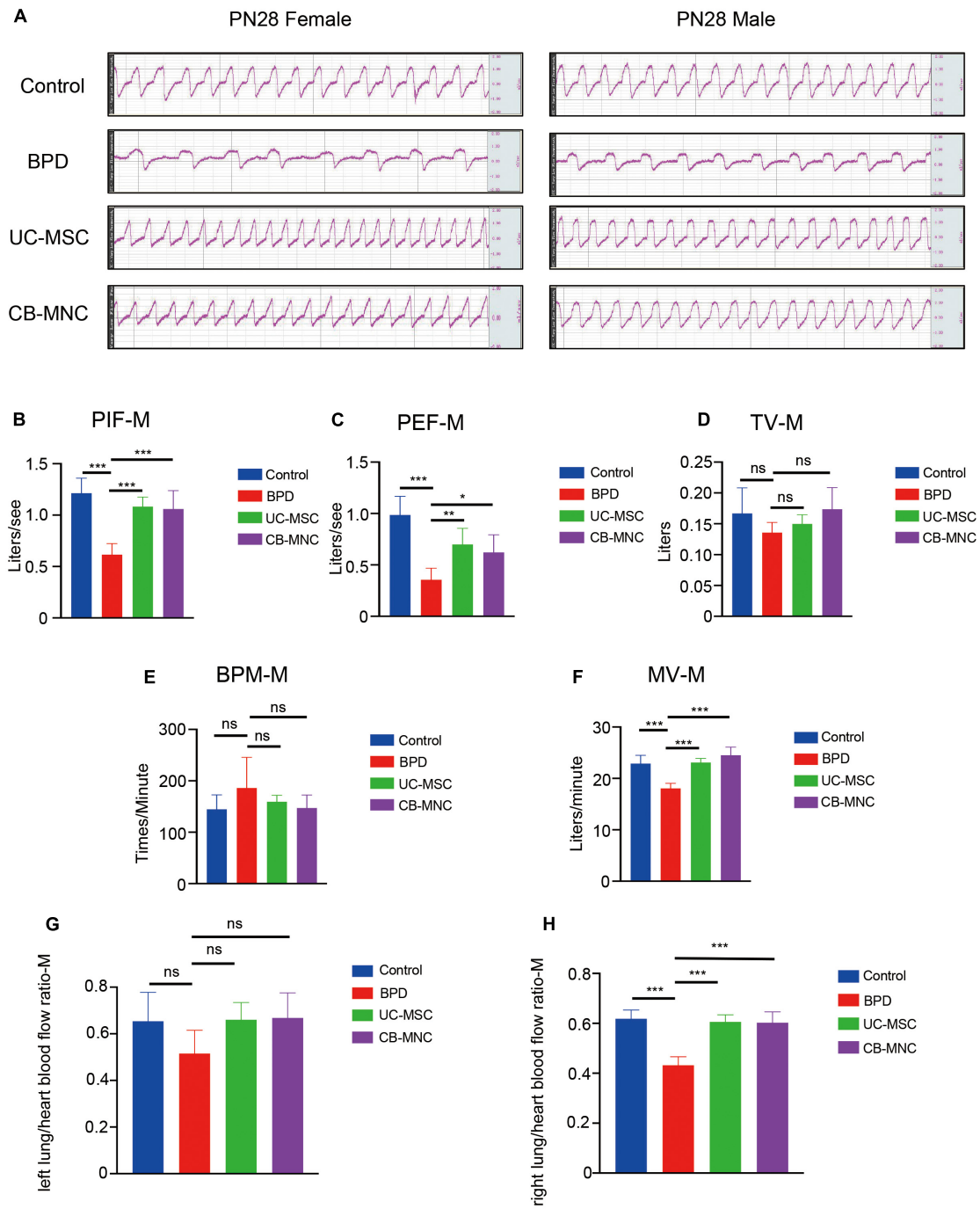

FIGURE 5 | Intravenous infusion of CB-MNCs and UC-MSCs improved pulmonary respiratory function and pulmonary vessel circulation. **(A)** Representative respiratory waveforms of male and female mice at postnatal day (PN)28 after indicated treatments. **(B–F)** Pulmonary function testing among male mouse groups. The indicators include peak inspiratory flow (PIF) **(B)**, peak expiratory flow (PEF) **(C)**, tidal volume (TV) **(D)**, breathing per minute (BPM) **(E)**, and minute volume (MV) **(F)**. Values are mean ± SD of a minimum of six animals in each group,*$p < 0.05$, **$p < 0.01$, ***$p < 0.001$, by one-way ANOVA test). **(G,H)** Bar graph showing lung/heart blood flow ratio analysis of pulmonary vascular function in different groups at indicated time points. **(G)** Left side, **(H)** right side. Values are mean ± SD of a minimum of six animals in each group, *$p < 0.05$, **$p < 0.01$, ***$p < 0.001$, by one-way ANOVA test.

experimental period, control group and BC-MNC group did not incur animal deaths. The body weight of animals in the CB-MNC group was not statistically different compared with that in the control group (**Figure 6A**). We also compared the hematological indicators in MNC-infused and control groups. Hematological indicators [hemoglobin (HGB) and lymphocytes

(%)] were statistically significant ($p < 0.05$). Other hematological indicators white blood cells (WBC), platelet (PLT), neutrophils (NEUT) ($\times 10^9$/L), lymphocytes ($\times 10^9$/L), monocyte (MONO) ($\times 10^9$/L), percentage of neutrophils [NEUT (%)], and percentage of monocyte [MONO (%)] were not statistically significant ($p > 0.05$) (**Table 1**). System autopsy at PN28 revealed no abnormal changes in the animals in indicated groups. There were no obvious pathological changes associated with the infusion of cells in the general and microscopic examinations, and representative histological images were shown in **Figures 6B–Q**. We observed unremarkable changes of corresponding parameters such as respiratory waveform, PIF, PEF, TV, BPM, and MV in CB-MNC group compared to those in control group at PN28 (**Supplementary Figures 4A–E**. The right or left lung/heart blood flow ratio of CB-MNC infusion was similar to those of the control group. Collectively, these results suggested that CB-MNC infusion will not influence the pulmonary vascular flow (**Supplementary Figures 4F,G**).

Differentially Expressed Gene Analysis Between Bronchopulmonary Dysplasia and Stem Cell-Infused Groups

As mentioned above, the therapeutic effects of CB-MNCs and UC-MSCs are divergent in trimming the imbalanced inflammatory network and restoring impaired structural remodeling. This phenomenon raised our attention to unravel the underlying molecular mechanisms with regard to the infusion of indicated stem cells. We therefore introduced whole-transcriptome sequencing, a highly popular and feasible approach, to analyze the differentially expressed (DE) ncRNAs (lncRNAs, circRNAs, miRNAs) and mRNAs in the compared groups. We adopted the value FPKMs to estimate the expression levels of mRNA transcripts. With cutoff of absolute Log2 fold changes ≥ 1 and adjusted p-value < 0.05, a total of 2,256 mRNA transcripts are significantly dysregulated, with 1,077 and 1,179 being, respectively, upregulated and downregulated in UC-MSC-transplanted mice relative to BPD mice (**Figure 7A** and **Supplementary Table 1**); 2,997 mRNAs were significantly dysregulated, with 1,595 and 1,402 being upregulated and downregulated in CB-MNC-infused mice relative to BPD mice (**Figure 7B**, **Supplementary Table 1**). After filtration of unannotated merged lncRNAs, we identified 1,065 significantly dysregulated lncRNA transcripts in UC-MSC-infused group relative to their levels in BPD mice group, within which 630 were upregulated and 435 downregulated (**Figure 7C** and **Supplementary Table 2**). As for CB-MNC-infused groups, 1,408 lncRNA transcripts were significantly dysregulated, 435 and 804 transcripts were upregulated and downregulated in CB-MNC-infused mice relative to BPD (**Figure 7D** and **Supplementary Table 2**). Next, based on TPM values, 42 miRNA transcripts were significantly dysregulated, with 21 and 21 being, respectively, upregulated and downregulated in UC-MSC-infused mice relative to BPD mice (**Figure 7E** and **Supplementary Table 3**); 69 miRNAs were significantly dysregulated, with 45 and 24 being, respectively, upregulated and downregulated in CB-MNC-transplanted mice relative to BPD mice (**Figure 7F** and **Supplementary Table 3**). Once again, differentially expressed circRNAs were revealed by spliced reads per billion mapping (SRPBM) value, and we mainly focus on the circbase-documented circRNAs for better validation of the functional markers. Here, 48 circRNA transcripts were significantly dysregulated, with 16 and 32 being, respectively, upregulated and downregulated, in UC-MSC-infused mice relative to BPD mice (**Figure 7G** and **Supplementary Table 4**); 58 circRNAs were significantly dysregulated, with 28 and 30 being, respectively, upregulated and downregulated in MNC-infused mice relative to BPD mice (**Figure 7H** and **Supplementary Table 4**). Detailed information on the number counts of the DEGs and the topmost DEGs was listed in **Table 2**; in UC-MSC-infused vs. BPD mice, the most upregulated mRNA was *Pcdhgb4* and the most downregulated mRNA was *Ucp2*. Besides, the most upregulated lncRNA, miRNA, and circRNA were NONMMUG041359.*2*, mmu-miR-5615-3p, and mmu_circ_0000628, respectively. The most downregulated lncRNA, miRNA, and circRNA were NONMMUG091403.1, mmu-miR-7650-5p, and mmu_circ_0000375, respectively. Whereas in groups between CB-MNC-infused and BPD mice, the most upregulated mRNA was *Nxt2* and the most downregulated mRNA was *Mknk2*. Besides, the most upregulated lncRNA, miRNA, and circRNA were NONMMUG017423.2, mmu-miR-6481, and mmu_circ_0001098, respectively. The most downregulated lncRNA, miRNA, and circRNA were NONMMUG046386.2, mmu-miR-6947-5p, and mmu_circ_0001879, respectively. We further analyzed the frequency distribution of the fold changes in different categories of DE-RNAs. As shown in **Table 3**, the 2–4-fold change (with Log_2FC 1∼2) was most common in all kinds of RNA transcripts between UC-MSC and CB-MNC injection group, while the percentages of differentially expressed mRNAs, lncRNAs, and circRNAs among Log_2FC ranging 2∼3 as well as 3∼4 were significantly higher in CB-MNC-infused group than that of the UC-MSC-infused group, which was in opposite trend with distribution of miRNA.

Pathway Analysis in Differentially Expressed ncRNAs and mRNAs

Considering that the complexities of the interactive pairs in lncRNA–miRNA–mRNA networks or the circRNA–miRNA–mRNA networks were both derived from the DEmRNAs in the indicated groups, we firstly performed the GO and KEGG pathway analysis upon DEmRNAs involved in the two different treatments. By conducting GO analysis, 274 GO terms were significantly enriched in DEmRNAs between the UC-MSC-infused and BPD mice, which are mainly related to regulation of GTPase activity (biological_process, GO: 0043087), fibrillar center (cellular_component, GO: 1901673), and nucleoside triphosphatase regulator activity (molecular_function, GO: 0060589). KEGG pathway analysis revealed the top 10 enriched pathways in these DEmRNAs. Of them, endocytosis, Axon guidance and protein processing in endoplasmic reticulum regulation of actin cytoskeleton, and phosphatidylinositol 3-kinase (PI3K)–Akt signaling pathway were the most significantly enriched (**Figure 8B**). Intriguingly,

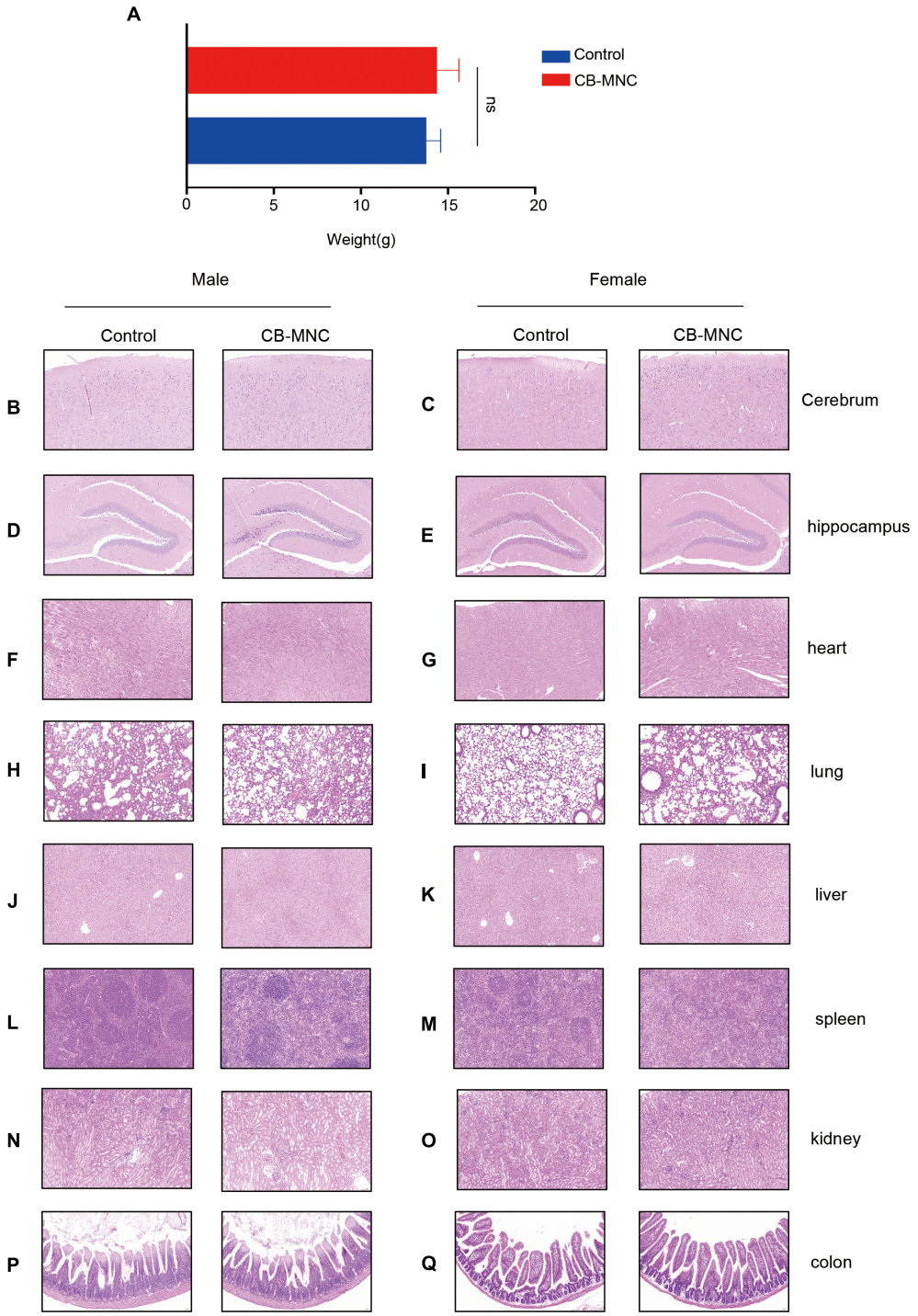

FIGURE 6 | General report of pathology regarding toxicity test. Mice in control group and mononuclear cell (MNC) group [intravenous infusion 3×10^6 cell/kg initiated at postnatal day (PN)7, twice in total] were sacrificed at PN28. Body weight was monitored **(A)**. At the end of the euthanasia infusion, neither cord blood-derived mononuclear cell (CB-MNC)-infused male nor female mice displayed significant abnormal changes in brain **(B–E)**, heart **(F,G)**, lung **(H,I)**, liver **(J,K)**, spleen **(L,M)**, kidney **(N,O)**, and colon tissues **(P,Q)**. Scale bar: 50 μm.

the introduction of CB-MNCs gives birth to quite different outcomes of pathway enrichment. Among the 823 significantly enriched GO terms between the CB-MNC-infused and BPD mice, the topmost enriched terms are regulation of chromosome segregation (biological_process, GO: 0007059), chromosome region (cellular_component, GO: 0098687), and microtube

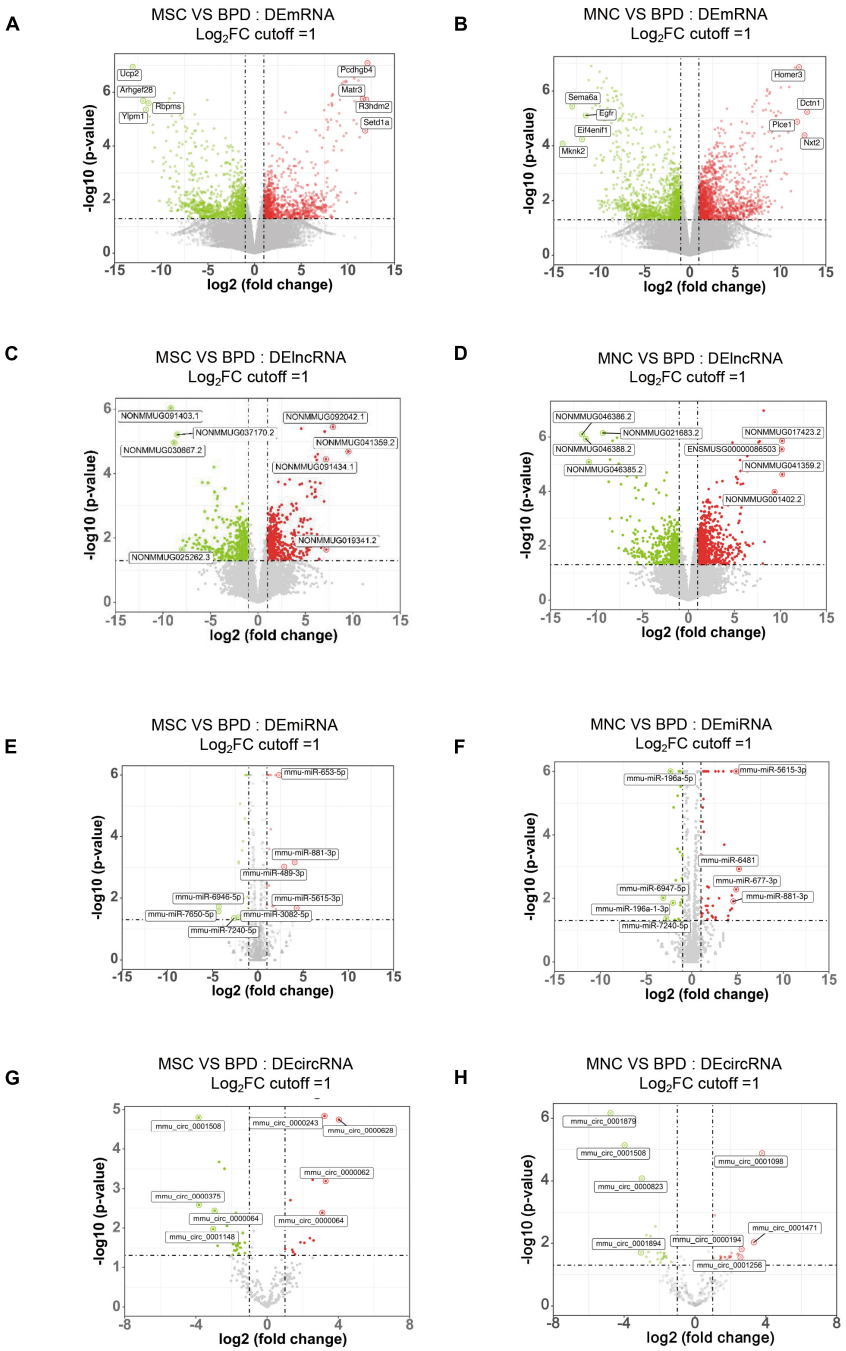

FIGURE 7 | Expression profiles of distinct RNAs. **(A,B)** Expression profiles of mRNAs. In the volcano plots, red, green, and black points represent mRNAs that were downregulated, upregulated, and not significantly different in UC-MSC-infused mice **(A)** and CB-MNC-infused mice **(B)** relative to bronchopulmonary dysplasia (BPD) mice, respectively. x axis: log2 ratio of mRNA expression levels between stem cell-infused BPD mice and BPD mice. y axis: false discovery rate values (−log10 transformed) of mRNAs. **(C,D)** Expression profiles of lncRNAs. In the volcano plots, red, green, and black points represent circRNAs that were downregulated, upregulated, and not significantly different in umbilical cord-derived mesenchymal stem cells (UC-MSC)-infused mice **(E)** and cord blood-derived mononuclear cell (CB-MNC)-transplanted mice **(F)** relative to BPD mice. x axis: log2 ratio of lncRNA expression levels between stem cell-infused BPD mice and BPD mice. y axis: false discovery rate values (-log10 transformed) of circRNAs. **(E,F)** Expression profiles of circRNAs. In the volcano plots, red, green, and black points represent circRNAs that were downregulated, upregulated, and not significantly different in UB-MSC-infused mice **(E)** and CB-MNC-infused mice **(F)** relative to BPD mice. x axis: log2 ratio of circRNA expression levels between stem cell-infused BPD mice and BPD mice. y axis: false discovery rate values (−log10 transformed) of circRNAs. **(G,H)** Expression profiles of miRNAs. In the volcano plots, red, green, and black points represent miRNAs that were downregulated, upregulated, and not significantly different in UB-MSC-infused mice **(G)** and CB-MNC-infused mice **(H)** relative to BPD mice. x-axis: log2 ratio of miRNA expression levels between stem cell-infused BPD mice and BPD mice. y axis: false discovery rate values (-log10 transformed) of miRNAs.

TABLE 2 | Statistical analysis of all of the differently expressed ncRNAs and mRNAs.

DE-RNAs	Total No.		Up No.		Down No.		The most upregulated (log2 Fold change)		The most downregulated (log2 Fold change)	
	MSC BPD	MNC BPD	MSC BPD	MNC BPD	MSC BPD	MNC BPD	MSC/BPD	MNC/BPD	MSC/BPD	MNC/BPD
mRNA	2,256	2,997	1,077	1,595	1,179	1,407	*Pcdhgb4 (11.85)*	*Nxt2 (10.87)*	*ucp2* (−13.07)	*Mknk2* (−14.17)
lncRNA	1,065	1,408	630	804	435	604	NONMMUG041359.2 (10.02)	NONMMUG017423.2 (10.20)	NONMMUG091403.1 (−9.18)	NONMMUG046386.2 (11.56)
miRNA	42	69	21	45	21	24	mmu-miR-5615-3p (4.28)	mmu-miR-6481 (3.44)	mmu-miR-7650-5p (−2.34)	mmu-miR-6947-5p (−4.32)
circRNA	48	58	16	28	32	30	mmu_circ_000628 (4.02)	mmu_circ_0001098 (3.87)	mmu_circ_0000375 (−3.85)	mmu9_circ_0001879 (−4.76)

binding (molecular_ function, GO: 0008017). KEGG pathway analysis revealed the top 10 enriched pathways in these DEmRNAs (**Figure 8D**). Of them, Epstein-barr virus infection, viral carcinogenesis, and cell cycle signaling pathway were the most significantly enriched.

We also conducted gene set enrichment analysis (GSEA) to better understand the signatures of these significantly changed genes. As shown in revised **Figures 8E–F**, the hallmarks of the top 2 significantly changed genes in UC-MSC group with p-value < 0.05 are interferon_alpha_response (NES = 1.49, $p = 0.0432$), Kras_signaling_DN (NES = 1.62, $p = 0.0345$). While the hallmarks of the significantly changed genes in CB-MNC group with p-value < 0.05 are G2M_checkpoint (NES = −1.67, $p = 0.0025$) and E2F targets (NES = −1.83, $p = 0.0026$). The opposite correlation value in the pivotal ways of UC-MSC- and CB-MNC-infused groups was a reflection of the distinct traits of the above two cells. Detailed gene enrichments are listed in **Supplementary Tables 5–7**. Normalized RNA-seq results of the topmost changed mRNAs, miRNAs, lncRNAs, and circRNAs and the key genes residing in the topmost enriched pathways regarding the divergence of CB-MNC and UC-MSC infusion were shown in **Supplementary Figure 6**.

Construction of DEmRNAs Mediating Protein–Protein Interaction Network in Stem Cell-Infused Bronchopulmonary Dysplasia Mice vs. Bronchopulmonary Dysplasia Mice

By converging the four common methods (DEseq2, edgeR, limma-voom, and limma-trend) in analyzing the DEmRNAs between BPD mice and the indicated stem cell-infused mice, 66 DEmRNAs coexist in all analyzed methods between UC-MSC-introduced mice and BPD mice (**Supplementary Figure 6A**), whereas 330 mRNAs were simultaneously contained in DEmRNAs between CB-MNC-introduced mice and BPD mice (**Supplementary Figure 6B**). We next constructed DEmRNAs mediating protein–protein interaction networks in indicated groups to reveal their complex interactions among each other using STRING system. Based on the filter parameters of the cytoHubba plug-ins, a total of 25 proteins and 41 edges were included in the network of UC-MSCs vs. BPD group (**Supplementary Figure 6C**), and a total of 168 proteins and 2,027 edges were included in the network of CB-MNCs vs. BPD group (**Supplementary Figure 6D**). Furthermore, a Cytoscape MCODE plug-in system was used to identify the key hubs of these PPI networks. The top key regulated genes mediating PPI networks of UC-MSC vs. BPD as well as CB-MNC vs. BPD were shown in **Supplementary Figures 6E,F**. Module 1 included five DEGs and 10 edges (**Supplementary Figure 6E**), and module 2 included 53 DEGs and 1,090 edges (**Supplementary Figure 6F**).

Construction and Analysis of the Dysregulated mRNA–lncRNA ceRNA Network and Dysregulated mRNA and circRNA ceRNA Network

In brief, firstly, we mapped all the DE-RNAs to the expression matrix in different categories and retrieved the expression profile, then we used miRanda as well as Targetscan to establish the putative miRNA–targets by screening the miRNA-binding sequence. As for the dysregulated mRNA–lncRNA ceRNA network (DMLCN), a candidate lncRNA–mRNA pair was generated if they competed for at least three common miRNAs. Furthermore, positive co-expression pairs between the differentially expressed lncRNA or circRNA and mRNA with coefficients > 0.8 and the negative regulatory relationships between the differentially expressed lncRNA or circRNA and miRNA with coefficients < -0.9 were retained. Finally, all

TABLE 3 | Summary of distribution of indicated DE-RNAs.

Log2 Fold Change (statistics)	mRNA		lncRNA		miRNA		circRNA	
	MSC	MNC	MSC	MNC	MSC	MNC	MSC	MNC
>4	36.25	37.85	15.86	15.79	9.00	11.54	2.08	2.72
1∼2	43.71	37.60	62.54	59.56	71.42	75	54.17	49
2–3	12.1	15.76	12.6	14.64	19.04	9.62	29.17	31.38
3∼4	7.93	8.79	8.64	10.01	0.00	3.85	14.58	16.90

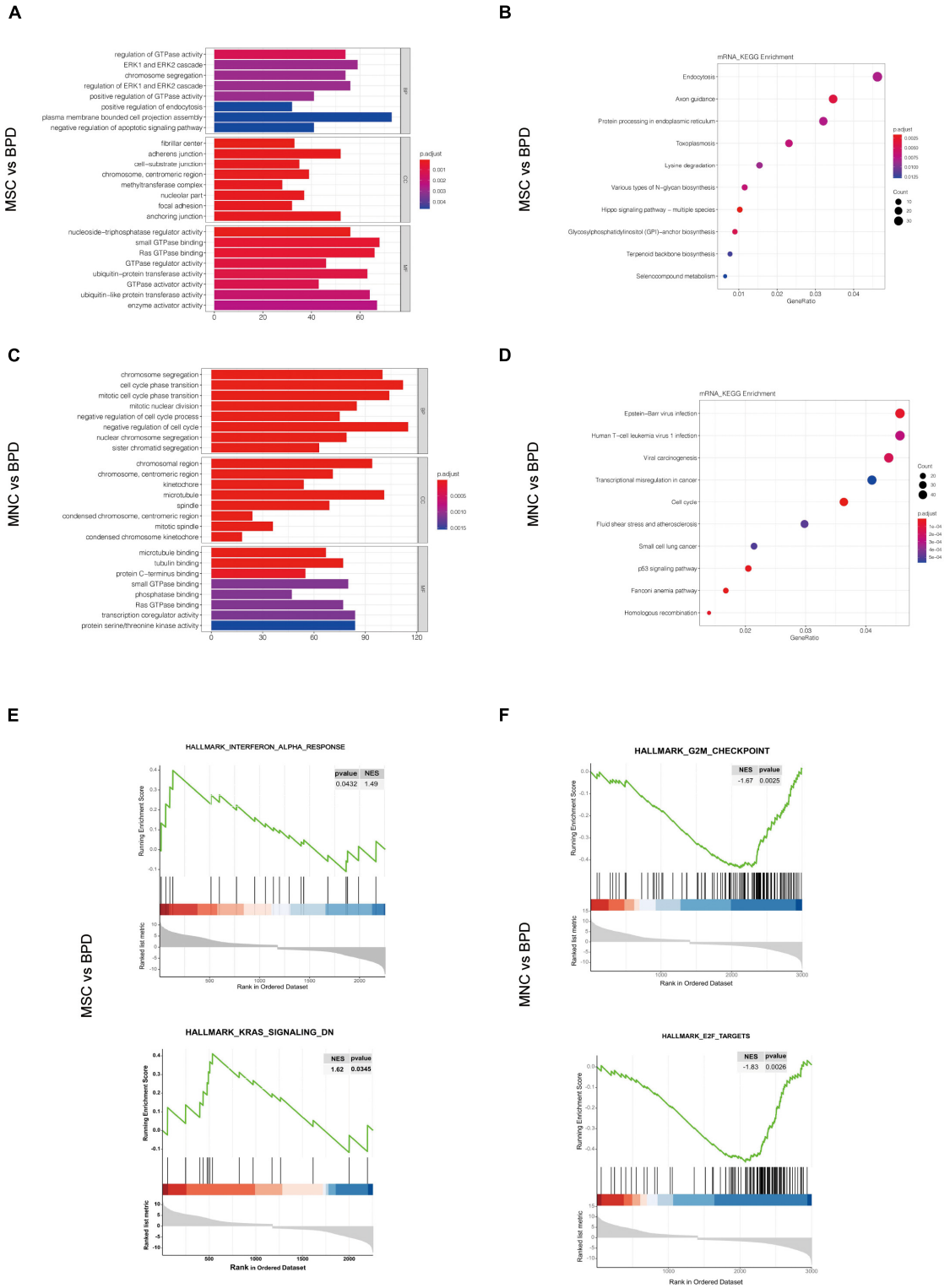

FIGURE 8 | Pathway analysis for the differentially expressed mRNAs (DEmRNAs). **(A,B)** Gene Ontology (GO) analysis of the significantly differently expressed mRNAs in umbilical cord-derived mesenchymal stem cell (UC-MSC)-infused **(A)** and cord blood-derived mononuclear cell (CB-MNC)-infused bronchopulmonary dysplasia (BPD) mice **(B)** relative to BPD mice. **(C,D)** Kyoto Encyclopedia of Genes and Genomes (KEGG) analysis significantly differently expressed mRNAs in UC-MSC-infused **(C)** and CB-MNC-infused BPD mice **(D)**. **(E,F)** Enrichment plots of gene expression signatures for topmost signaling hallmarks by gene set enrichment analysis (GSEA) of DEmRNAs in UC-MSC-infused group and CB-MNC-infused group.

the mRNA–miRNA–lncRNA ceRNA pairs were identified by performing hypergeometric test at the threshold of p-value < 0.05. As a result, DMLCN between MSC and BPD groups contained 60 lncRNA nodes (43 upregulated, 17 downregulated), 152 mRNA nodes (111 upregulated, 41 downregulated), 27 miRNA nodes (14 upregulated, 13 downregulated) in 602 pathway edges (**Figure 9A**). DMLCN between MNC and BPD groups contained 28 lncRNA nodes (25 upregulated, three downregulated), 211 mRNA nodes (193 upregulated, 18 downregulated), and 25 miRNA nodes (10 upregulated, 15 downregulated) in 2,138 pathway edges (**Figure 9B**). Thereafter, we constructed the dysregulated mRNA and circRNA ceRNA network (DMCCN) by above strategies. Notably, the estimated miRNA–circRNA interactions were obtained by mapping downloaded data in a combination of circBase and Starbase. DMCCN between MSC and BPD mice contained 30 circRNA nodes (eight upregulated, 22 downregulated), 111 mRNA nodes (42 upregulated, 69 downregulated), and 36 miRNA nodes (17 upregulated, 19 downregulated) in 1,326 pathway edges (**Figure 9C**). DMCCN between MNC and BPD groups contained 25 circRNA nodes (four upregulated, 21 downregulated), 105 mRNA nodes (96 upregulated, nine downregulated), and 52 miRNA nodes (33 upregulated, 19 downregulated) in 1,942 pathway edges (**Figure 9D**). All of the circRNA/lncRNA–miRNA–mRNA ceRNA pairs were provided in **Supplementary Table 6**. Importantly, the six DEmRNA nodes that presented in both the mRNA–miRNA–lncRNA and mRNA–miRNA–circRNA ceRNA networks in UC-MSC-implanted BPD group were *Cacnb1* (calcium voltage-gated channel auxiliary subunit beta 1, downregulated, modulator of G protein inhibition) (Lu et al., 2010); *Cacnb3* (calcium voltage-gated channel auxiliary subunit beta 3, upregulated, inducible responder of dendritic cells) (Bros et al., 2011); *Cdk13* (cyclin-dependent kinase 13, upregulated, regulator of global RNA polymerase) (Fan et al., 2021); *Lrrn2* (leucine-rich repeat protein 2, neuronal, upregulated, controller of cell adhesion and movement) (Haines et al., 2005); *R3hdm2* (R3H domain-containing protein 2, downregulated, independent risk factors of cardiovascular system) (Yang et al., 2010); and *RFX1* (regulatory factor RFX1, downregulated, transcriptional factor of FGF1) (Hsu et al., 2012; **Figure 9E**). On the other hand, five mRNA nodes that presented in both the mRNA–miRNA–lncRNA and mRNA–miRNA–circRNA ceRNA networks in CB-MNC-implanted BPD group were *Prkcd* [protein kinase C, delta, downregulated, suppressor of autophagy (Zhang et al., 2017)]; *Homer3* (Homer protein homolog 3, upregulated, scaffold of neutrophil polarity and involved in GTPase signaling) (Wu et al., 2015); *Eif2s3y* (eukaryotic translation initiation factor 2 subunit 3, Y-linked, downregulated, extracellular signal-regulated kinase (ERK) pathway-dependent regulators in proliferation of spermatogonial stem cells) (Zhang et al., 2021); *Uty* [ubiquitously transcribed tetratricopeptide repeat gene, Y chromosome (downregulated, site-specific histone demethylase (Shpargel et al., 2012)]; and *Ctnnd1* (cadherin-associated protein, delta 1, downregulated, promoters of proliferation in multiple cancers) (Castillo et al., 2010; **Figure 9F**). To sum up, the key hub DE protein-coding genes along with the ncRNA network can partially explain the therapeutic divergence upon UC-MSC and CB-MNC manipulation.

DISCUSSION

Hyperoxia causes direct injury to cells mainly through recruiting inflammatory cells to the residential organs, and human MSCs have been disclosed to show enhanced therapeutic effects *via* paracrine secretion or cell-to-cell contact that modulates inflammatory functions or differentiation capacities. Meanwhile, accumulating evidence has suggested that human MSCs can also possess the potential to facilitate tissue repair and stimulate lung maturation (Laube et al., 2016), while limited preclinical experiments have demonstrated that UC-MSCs can improve outcomes under hyperoxia-induced BPD. These might be due to the higher level of quality control and release criteria for UC-MSCs in neonatal manipulation than that of the utility in adulthood as well as the inadequate establishment of general standards in assessing ways of delivery. Considering the side effects of metastatic potential and EMT property raised by human MSC implantation in tumor treatment (Yan et al., 2021), MNCs are optimal alternatives in stem cell-based therapies, especially CB-MNCs, among which we have witnessed an increasing body of data (Yin et al., 2015; Shin et al., 2016). Additionally, the MNCs preferentially resided in the pulmonary concomitant with very low engraftment rate (O'Reilly and Thebaud, 2015). Moreover, unlike the frequently reported applications of UC-MSCs in managing pulmonary dysfunctions, few studies have examined the translational potential of CB-MNCs in neonatal BPD animal models to date, and conclusions remain staggering under different situations (Abreu et al., 2013; Monz et al., 2013; Mills, 2017). In our current research, we demonstrate that intravenous administration of CB-MNCs to hyperoxia-exposed mice had significant effects on stimulating alveolarization, promoting tissue repair, and alleviating pro-inflammatory responses with substantial evidence (**Figure 3** compares BPD group with CB-MNC group). Strikingly, CB-MNC transplantation exhibited strong capacity of enhancing the overall lung motion function and maintaining pulmonary–vascular flow homeostasis (**Figure 5**). Moreover, we also compared the efficiency between independent CB-MNC and UC-MSC infusion in all aspects. We observed generally better (albeit not consistent in all parameters or indices) effects of CB-MNC transplantation in balancing the inflammatory responses and restoring the lung morphogenesis compared to UC-MSC administrations (**Figures 3**–**5**).

Over the past few decades, the development of high-throughput sequencing has led to the identification of several lncRNAs and circRNAs in various tissues and cells (Hua et al., 2019; Wei et al., 2019). Increasing evidence has shown that these ncRNAs could participate in the regulation of multiple layers of the pathological and physiological event, including cell proliferation, migration, and metastasis (Zhou S.Y. et al., 2020) through regulating gene expression at the levels of pretranscription, transcription, and posttranscription (Zhang et al., 2019). Despite the combinative analysis integrating multiple datasets from public Gene Expression Omnibus (GEO)

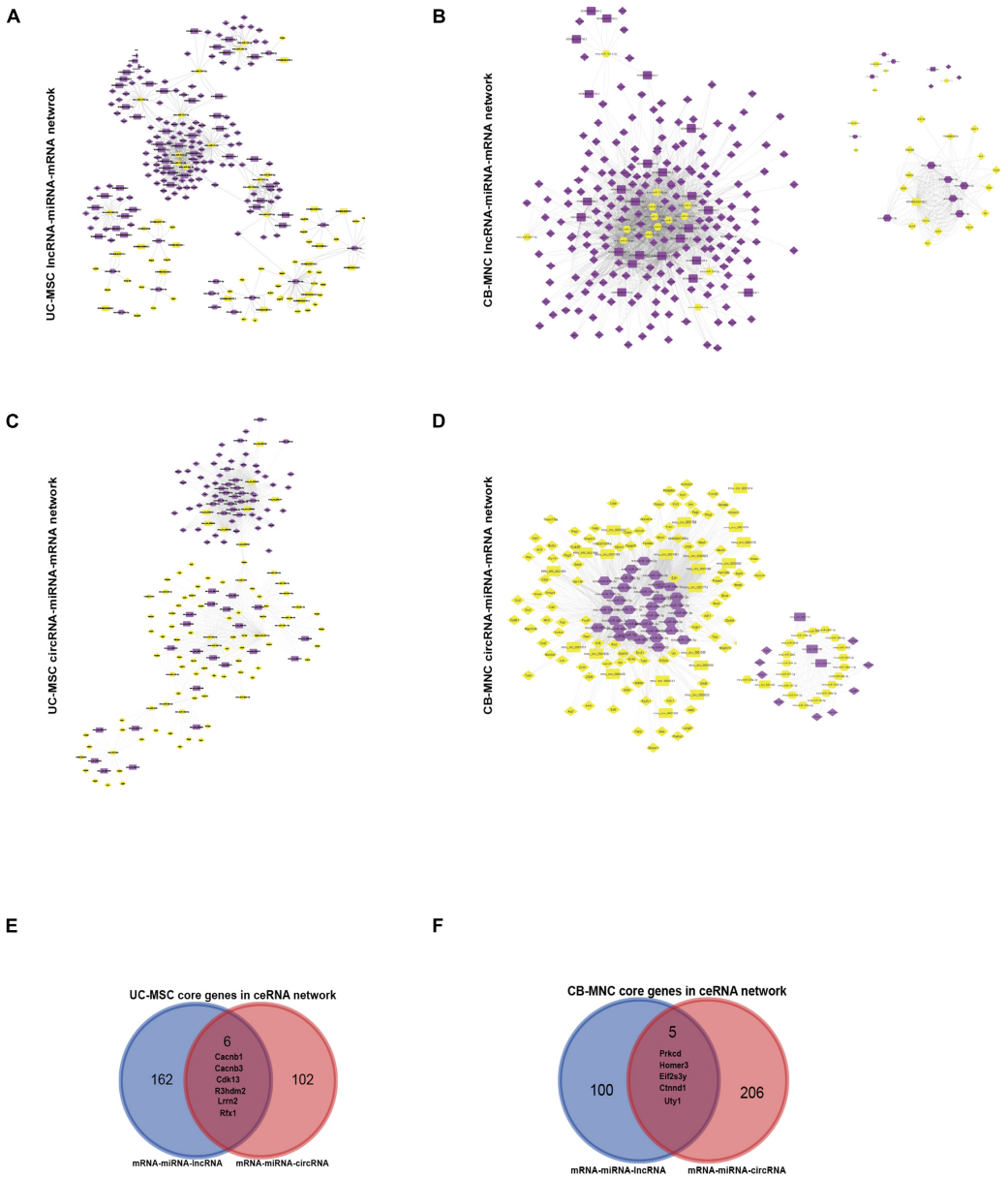

FIGURE 9 | Construction of dysregulated mRNA–lncRNA coexpression network (DMLCN) and the dysregulated mRNA–circRNA coexpression network (DMCCN) based on the correlation value. **(A,B)** The layout of dysregulated mRNA–lncRNA ceRNA network (DMLCN). A total of 239 nodes and 602 edges were identified in umbilical cord-derived mesenchymal stem cell (UC-MSC)-infused groups relative to bronchopulmonary dysplasia (BPD) mice, and a total of 264 nodes and 2,138 edges were identified in cord blood-derived mononuclear cell (CB-MNC)-infused groups relative to BPD mice. Purple diamond: upregulated mRNAs, yellow diamond: downregulated mRNAs; purple hexagon: upregulated miRNA, yellow hexagon: downregulated miRNA; purple round rectangle: upregulated lncRNAs, yellow round rectangle: downregulated lncRNAs. **(C,D)** The layout of dysregulated mRNA–circRNA ceRNA network (DMCCN). A total of 177 nodes and 1,326 edges were identified in UC-MSC-infused groups relative to BPD mice, and a total of 182 nodes and 1,942 edges were identified in CB-MNC-infused groups relative to BPD mice. Purple diamond: upregulated mRNAs, yellow diamond: downregulated mRNAs; purple round rectangle: upregulated circRNAs, yellow round rectangle: downregulated circRNAs. **(E)** The Venn diagram could demonstrate that six key genes were contained in the mRNA–miRNA–lncRNA and mRNA–miRNA–circRNA ceRNA network of UC-MSC-infused group simultaneously. **(F)** The Venn diagram could demonstrate that five genes were contained in the mRNA–miRNA–lncRNA and mRNA–miRNA–circRNA ceRNA network simultaneously.

database (Wang et al., 2019), comprehensive expression profile and analysis of mRNAs, miRNA, lncRNA, and circRNA with regard to mouse BPD model with or without intervention treatment are vague. To the best of our knowledge, this is the first comprehensive high-throughput sequencing analysis of circRNA, miRNA, lncRNA, and mRNA expression profiles in comparison between the MSC- or MNC-infused BPD mice and BPD mice. We found that there were 2,256 and 2,997

mRNAs, 1,065 and 1,408 lncRNAs, 48 and 58 circRNAs, and 42 and 69 miRNAs with significantly different variations (fold change > 2 and $p < 0.05$) in UC-MSC and CB-MNC infusions, respectively (**Figure 7**, **Table 2**, and **Supplementary Tables 1–4**). We further navigate to the comparison analysis on the biological pathways of GO (GO-BP) that features the functions of differentially expressed genes. Interestingly, the top GO-BPs in UC-MSC-infused groups are related to GTPase activity (i.e., *Rapgef3*/*Rapgef6*/*Rasgrp1*/*Rap1gap*), ERK1 and ERK2 cascade (i.e., *Fn1*, *Dab2*, *Fgfr2*, and *Fgf3*), and chromosome segregation (Nusap1, Bub1, Map10, and Cenpc1). On the other hand, the top GO-BPs in CB-MNC-infused groups are cohesively related to mitotic nuclear division (*Ccne2*, *Ccn*b1, *Cdc6*, and *Cdc27*), cell cycle phase transition (*Cdk4*, *Cdc25c*, *Aurkb*, and *Ccnd3*), and chromosome segregation (Bub1, Psrc1, Bub1, and Cenp1). Collectively, chromosome segregation a fundamental cell activity, were both drastically changed upon UC-MSC and CB-MNC infusion, which might be an explainable output owing to the strong capacity of stem cells with the key genes varied in different groups. Also, the divergent GO-BPs in the two groups are sense-making, since the stimulating and proliferation effects are robust in CB-MNC-infused BPD, while the widely accepted UC-MSC introduction in alleviating BPD can relieve the injured pulmonary microenvironment from stress suffering by refreshing the motor sensing (GTPase activity) and mitogen activation pathways (ERK1 and ERK2 cascade) (**Figure 8**).

The pathogenesis of BPD is a complex process characterized by fewer and larger simplified alveoli, influx of inflammatory cells, and endothelial and epithelial cell death (Choo-Wing et al., 2013) and regulated by signaling-regulatory networks (Zhao et al., 2014; Liu et al., 2020; Zhang et al., 2020), including growth factors, transcription factors, regulating enzymes, and ncRNAs, a number of which formed feedback loops controlling the process of damage repair, alveolarization revitalization, and angiogenesis restoration. By combining initial screening of DEmRNA with GO/KEGG analysis, multiple significantly dysregulated genes have drowned consistent conclusion with current studies. For instance, *Semaphorin* 4A is reported to regulate angiogenesis through modulating the VEGF pathway (Segarra et al., 2012), and *Ucp2* is a macrophage-specific inducer in response to pulmonary injury (Wang et al., 2016). Besides, many studies have indicated the important roles of an inflammatory response and immune response in cancers (Vilariño et al., 2020) and neurodevelopment (Tan et al., 2020). Among the gene lists of the top 10 most significantly upregulated and downregulated genes interfered by stem cell implantation, *NXT2* played pivotal roles in neurodevelopment, whereas *Mknk2*, *Sema6a*, and *PIR2* are frequently dysregulated molecules in the pathogenesis of multiple cancer types as evidenced by GeneRIF documented by PubMed. While implantation of UC-MSCs or CB-MNCs expectedly redirected the expression pattern (refer to **Table 1** and **Supplementary Tables 1–4**) of these candidates, further verifications are important for deepening the understanding of BPD and lay a good prediction ability for evaluating the treatment effects through single-factor model or multiple-factors model.

Despite their poor conservation and low levels of expression compared with protein-coding genes, lncRNAs are often regulated by transcription factors and are expressed in a cell- or tissue-specific manner. In this study, most of the lncRNAs in the co-expression network were not yet annotated. In addition, from DMLCN, the lncRNA–mRNA co-expression network, we found that *Rmi2* coexpressed with most numbers of lncRNAs (**Figure 8A**) and *Eif2s3y* coexpressed with most numbers of lncRNAs (**Figure 8B**), forming a complex network in UC-MSC-infused group or CB-MNC-infused group relative to BPD model, respectively. More importantly, recent studies have revealed that these hub genes played pivotal roles in pulmonary malfunctions (Ulke et al., 2019). It is therefore very much worth to perform further studies to reveal the underlying mechanisms of these lncRNAs and the interactions with the guiding hub genes.

Evidence is emerging that circRNAs can participate in the regulation of gene expression in various ways. It has been reported that circRNAs can function through their parental genes (Xu et al., 2020). Additionally, many more circRNAs have been reported to harbor multiple miRNA-binding sites, which seem to be a typical feature of this class of RNA molecules. This feature, together with covalently closed loop structure, suggests that circRNA can act as a sponge of miRNA to regulate a myriad of target genes. Interestingly, the DMCCN network we built exhibited a much concentrated network with highly centered distribution of the circRNA nodes in both UC-MSC- and CB-MNC-related groups compared with the scattered lncRNA distribution (**Figures 9C,D**). Intriguingly, much progress has been achieved in elucidating the roles of circRNA in lung cancer and multiple adult pulmonary malfunctions. For instance, a novel circular RNA, circXPO1, promotes lung adenocarcinoma progression by interacting with IGF2BP1 (Huang et al., 2020), and hot-star circRNA CDR1as and CircRNA0001859 are key players in balancing cardiovascular–pulmonary homeostasis (Chen S. et al., 2020; Ma et al., 2020). Linking the novel discovered circRNAs in alleviating BPD and stem cell-based therapy will make them optimal biomarkers.

Of note, we interpret the overall prior phenotype in CB-MNC group compared to UC-MSC group in two aspects: one is the same gene, same variation trend with different expression fold changes that impacts the regulation level and the other are distinct genes involved in the same pathway with divergent regulation modes. We focused on the significantly changed genes that reside in the hallmark pathways by GSEA analysis and BP term of GO analysis, among which *Clic3* (chloride intracellular channel protein 3), *Kdm4b* (lysine demethylase 4B), *Pxn* (paxillin), *Sorbs2* (sorbin and SH3 domain-containing protein 2), *Trafd1* (TRAF-type zinc finger domain containing 1), and *Tsku* (Tsukushi) coexisted in both CB-MNC and UC-MSC groups with larger extent variations in CB-MNC groups (**Supplementary Table 7**, sheet co_GSEA). As typical examples, their geneRIFs are closely related in the cellular hallmarks of BPD including epithelial transition, endothelial homeostasis, and inflammatory responses (Mashima et al., 2005; Zhou S. et al., 2020; Hurskainen et al., 2021). Tsku is a small leucine-rich proteoglycan that has been documented to be induced in proteomic profiling of a TGF-β1-induced *in vitro* model of

fibrosis in rat kidney fibroblasts (Zhou S. et al., 2020). When we reviewed our data, MSC group: downregulated log_2FC −4.99, MNC group: −7.50, implying that introduction of the indicated stem cell can revert the induced Tsku level and the level of TGF-β expression with distinct extent. Meanwhile, in lung cancer cells, TSK expressed more highly than the other small leucine-rich repeat proteoglycan family members and regulates the epithelial–mesenchymal transition and cell proliferation (Yamada et al., 2019; Huang et al., 2021), indicating its pivotal functions in reverting the abrogated epithelium development and retarded EC proliferation. SORBS2 is another example of epithelial-regulating molecule, as a component of the acto-myosin ring at the apical junctional complex in epithelial cells (Fredriksson-Lidman et al., 2017) SORBS2 is a scaffolding protein associated with Abl/Arg non-receptor tyrosine kinase pathways and is known to interact with actin and several other cytoskeletal proteins in various cell types. The downregulated SORBS2 expression in both groups (CB-MNC: log_2FC −6.25, UC-MSC: log_2FC −6.52) implies that the rebalancing of the epithelial junction complex greatly contributes to the integrity of the pulmonary development. Another interesting example is Pxn (paxillin), whose knockdown has been proven to enhance endothelial cell migration *in vitro* and stimulate angiogenesis during normal development and in response to tumor angiogenic factors *in vivo* (German et al., 2014). In our data, MNC group pxn attenuated at Log_2FC −9.88 while MSC group pxn reduced at log_2FC −5.50, indicating the angiogenesis promoting functions of this gene in rescuing histopathological phenotype of abnormal growth and development. We also found that Clic3 is a chloride intracellular channel protein. It has been reported that its homologous family member, Clic1, has been significantly reduced in severe BPD compared to the moderate BPD (Magagnotti et al., 2013). Infusion of CB-MNC robustly enhanced the expression level of Clic3, with log_2FC 5.06 in UC-MSC group while log_2FC 9.88 in CB-MNC group. The calcium-related channel protein might participate in the reescalating effect of CB-MNC and UC-MSC in alleviating BPD.

We have thoroughly detected the factors regarding inflammatory regulation, tissue repair, and vascular remodeling (**Figure 4**). Interestingly, the classical pro-inflammatory factors (i.e., IL-6 and IL-1β) and classical anti-inflammatory factors (i.e., IL-10 and IL-2) exhibited a Yin–Yang balance expression module in response to experimental BPD model expectedly (**Figures 4A–E**). Inflammation is generally considered to be detrimental in recovery from hyperoxia-induced lung injuries, while single use of anti-inflammatory treatments targeting specific inflammatory mediators has yet been ineffective to date. It has been proven that Toll-like receptor (TLR)-mediated regulation of inflammasomes is a significant prognostic marker of BPD with different severities (Liao et al., 2015; Syed et al., 2019). Furthermore, cell-extrinsic responses induced by TLR signaling consist of inflammation (TNF-α) and tissue repair (IL-10). In the GSEA-enriched core genes, Trafd1, also named FLN29, is a novel interferon- and lipopolysaccharide (LPS)-inducible gene acting as a negative regulator of TLR signaling. As shown in **Figures 4A–E**, restraint levels of inflammatory marker IL-1β and IL-6 were concomitant with augmenting secretion of IL-10 and TGF-β. The reversion effect was more significant in CB-MNC group than in UC-MSC group (with log_2FC in CB-MNC 6.72 and log_2FC in UC-MSC 1.52). The unveiled functions of Trafad1 might provide another great example in illustrating the conversion of the inflammatory network.

The slightly declined TGF-β signaling and MMP-9 expression along with escalated VEGF expression after CB-MNC infusion (**Figures 4F,G**) implied the prevalence of adopting MNC in both balancing the delicate and intertwining feature of inflammatory networks and rescuing the devastative developing lung in experimental BPD model caused by hyperoxia exposure. The recovery of an intact epithelium following lung injury is critical for restoration of lung homeostasis, which includes an acute inflammatory response, recruitment of immune cells, and epithelial cell spreading and migration upon an autologously secreted provisional matrix. MMP-9 involves the breakdown of extracellular matrix in normal physiological and pathological processes regarding pulmonary homeostasis. Several key signaling pathways are important in regulating these processes, including sonic hedgehog, Rho GTPases, MAP kinase pathways, STAT3, and Wnt (Crosby and Waters, 2010), within which the uniquely differently expressed hub genes reside in the pathways (**Supplementary Table 7**). Previous studies have established the functional links between oxidative stress, apoptosis, autophagy, and endoplasmic reticulum (ER) stress through the nuclear factor erythroid-like 2 (Nrf2)/antioxidant response element (ARE) signaling pathways (Chen Y. et al., 2020; Zhang et al., 2020), and it has been reported that mesenchymal stem cells attenuate diabetic lung fibrosis *via* adjusting Sirt3-mediated stress responses in rats. In our data, in CB-MNC vs. BPD group, Sirt3 was among the significantly changed genes (log_2FC 6.93, sheet CB-MNC vs. BPD group), while in UC-MSC, the changed Sirt family members were sirt2, and the expression level was downregulated (Chen Y. et al., 2020). Aberrant pulmonary vascular growth and remodeling are frequently seen in bronchopulmonary dysplasia (Alvira, 2016), and the fibroblast growth factor (FGF)-2 and VEGF are promising targets in the treatment of respiratory disorders (Laddha and Kulkarni, 2019). In CB-MNC group, the FGF-2 was slightly decreased (log_2FC −1.68), and the FGFR (log_2FC 1.27) was slightly increased (see sheet UC-MSC vs. BPD). This might partly explain the moderately mitigated VEGF level in MSC-introduced groups while the escalating of VEGF in CB-MNC group was largely due to the role of FoxM1, a transcriptional regulator of G1/S and G2/M transition and M phase progression in the cell cycle and a multifaced regulator in pulmonary disease. It can significantly activate adherens junctions, vascular formation, and pulmonary inflammation through multiple direct targets. In our data, the CB-MNC infusion can largely increase the level of Foxm1 (log_2FC 2.46). Therefore, the robust enhancement of VEGF in CB-MNC group can be explained, which accounts for the second way of understanding the links between key genes in the pathways. Collectively, the concentrated molecules and hub genes are interpretable in understanding the divergence of UC-MSC and CB-MNC in alleviating BPD, especially the phenotypes related with VEGF, MMP-9, TGF-β.

Interestingly, the hub DEmRNAs within ceRNA pairs between UC-MSC and BPD groups are closely related with cell cycle

integrity, cell adhesion, cell proliferation, and transcriptional homeostasis. The hub DEmRNAs within ceRNA pairs between CB-MNC and BPD groups are closely related with autophagy, neutrophil polarity, cell proliferation, and histone methylation, which is consistent with the result of global DEmRNA GO analysis. Taken together, our findings may provide new evidence for the underlying mechanisms of mRNA/ncRNAs and related ceRNA networks in stem cell-infused BPD and uncover novel targets for better utilizing stem cells in the treatment of BPD (**Figure 1**).

DATA AVAILABILITY STATEMENT

The datasets presented in this study can be found in online repositories. All the datasets of RNA-seq included in this study have been uploaded to the GSA system with GSA ID: CRA004720 and BioProject ID: PRJCA004041 and are publicly accessible at https://ngdc.cncb.ac.cn/gsa/browse/CRA004720 after the release date of December 14, 2022.

ETHICS STATEMENT

Animal procedures were reviewed and approved by the Animal Care and Ethics Committee of the Seventh Medical Center of PLA general Hospital (No. 2020-037).

AUTHOR CONTRIBUTIONS

JC, YC, and ZF conceptualized the study and wrote the manuscript. JC, YC, and XD conceived and designed the study. XD and JP contributed to the performance of the mice husbandry, BPD animal model, and pulmonary function test. GL, XZ, XF, and FX participated in stem cell purification and injection. YC, JC, and XD performed gene expression analysis and immunohistochemistry. YC and XD performed the computational analysis of the data. XY and XW contributed to the discussion and polish of the manuscript. All authors read and approved the manuscript.

FUNDING

This research was jointly granted funds by the National Key R&D Program of China (2018YFC1002701) and Chinese National Natural Science Foundation Projects (81901518).

ACKNOWLEDGMENTS

We thank Xiaolu Shi (Experimental Research Center, China Academy of Chinese Medical Sciences, Beijing, China) for kindly helping them with pulmonary function tests and Guosheng Xing (Department of Hematology, the Seventh Medical Center of PLA General Hospital, Beijing, China) for contributions in FACS analysis.

SUPPLEMENTARY MATERIAL

The Supplementary Material for this article can be found online at: https://www.frontiersin.org/articles/10.3389/fcell.2021.679866/full#supplementary-material

REFERENCES

Abreu, S. C., Antunes, M. A., de Castro, J. C., de Oliveira, M. V., Bandeira, E., Ornellas, D. S., et al. (2013). Bone marrow-derived mononuclear cells vs. mesenchymal stromal cells in experimental allergic asthma. *Respir. Physiol. Neurobiol.* 187, 190–198. doi: 10.1016/j.resp.2013.03.014

Alvira, C. M. (2016). Aberrant pulmonary vascular growth and remodeling in bronchopulmonary dysplasia. *Front. Med.* 3:21. doi: 10.3389/fmed.2016.00021

Bros, M., Dexheimer, N., Ross, R., Trojandt, S., Höhn, Y., Tampe, J., et al. (2011). Differential gene expression analysis identifies murine Cacnb3 as strongly upregulated in distinct dendritic cell populations upon stimulation. *Gene* 472, 18–27. doi: 10.1016/j.gene.2010.10.013

Bu, Z. Y., Wu, L. M., Yu, X. H., Zhong, J. B., Yang, P., and Chen, J. (2017). Isolation and characterization of in vitro culture of hair follicle cells differentiated from umbilical cord blood mesenchymal stem cells. *Exp. Ther. Med.* 14, 303–307. doi: 10.3892/etm.2017.4456

Buchacker, T., Mühlfeld, C., Wrede, C., Wagner, W. L., Beare, R., McCormick, M., et al. (2019). Assessment of the alveolar capillary network in the postnatal mouse lung in 3d using serial block-face scanning electron microscopy. *Front. Physiol.* 10:1357. doi: 10.3389/fphys.2019.01357

Cai, C., Qiu, J., Qiu, G., Chen, Y., Song, Z., Li, J., et al. (2017). Long non-coding RNA MALAT1 protects preterm infants with bronchopulmonary dysplasia by inhibiting cell apoptosis. *BMC Pulm. Med.* 17:199. doi: 10.1186/s12890-017-0524-1

Castillo, S. D., Angulo, B., Suarez-Gauthier, A., Melchor, L., Medina, P. P., Sanchez-Verde, L., et al. (2010). Gene amplification of the transcription factor DP1 and CTNND1 in human lung cancer. *J. Pathol.* 222, 89–98. doi: 10.1002/path.2732

Chen, J. H., Feng, D. D., Chen, Y. F., Yang, C. X., Juan, C. X., Cao, Q., et al. (2020). Long non-coding RNA MALAT1 targeting STING transcription promotes bronchopulmonary dysplasia through regulation of CREB. *J. Cell. Mol. Med.* 24, 10478–10492. doi: 10.1111/jcmm.15661

Chen, S., Yao, Y., Lu, S., Chen, J., Yang, G., Tu, L., et al. (2020). CircRNA0001859, a new diagnostic and prognostic biomarkers for COPD and AECOPD. *BMC Pulm. Med.* 20:311. doi: 10.1186/s12890-020-01333-1

Chen, W. J., Ho, C. C., Chang, Y. L., Chen, H. Y., Lin, C. A., Ling, T. Y., et al. (2014). Cancer-associated fibroblasts regulate the plasticity of lung cancer stemness via paracrine signalling. *Nat. Commun.* 5:3472. doi: 10.1038/ncomms4472

Chen, W., Peng, Y., Ma, X., Kong, S., Tan, S., Wei, Y., et al. (2020). Integrated multi-omics reveal epigenomic disturbance of assisted reproductive technologies in human offspring. *EBioMedicine* 61:103076. doi: 10.1016/j.ebiom.2020.103076

Chen, Y., Zhang, F., Wang, D., Li, L., Si, H., Wang, C., et al. (2020). Mesenchymal stem cells attenuate diabetic lung fibrosis via adjusting sirt3-mediated stress responses in rats. *Oxid. Med. Cell Longev.* 2020:8076105. doi: 10.1155/2020/8076105

Cheng, H., Wu, B., Wang, L., Hu, T., Deng, Z., and Li, D. (2020). Insights into the expression profiles and functions of circRNAs in a newborn hyperoxia-induced rat bronchopulmonary dysplasia model. *J. Gene Med.* 22:e3163. doi: 10.1002/jgm.3163

Choo-Wing, R., Syed, M. A., Harijith, A., Bowen, B., Pryhuber, G., Janer, C., et al. (2013). Hyperoxia and interferon-gamma-induced injury in developing lungs occur via cyclooxygenase-2 and the endoplasmic reticulum stress-dependent

pathway. *Am. J. Respir. Cell Mol. Biol.* 48, 749–757. doi: 10.1165/rcmb.2012-0381OC

Cooney, T. P., and Thurlbeck, W. M. (1982). The radial alveolar count method of Emery and Mithal: a reappraisal 1–postnatal lung growth. *Thorax* 37, 572–579. doi: 10.1136/thx.37.8.572

Crosby, L. M., and Waters, C. M. (2010). Epithelial repair mechanisms in the lung. *Am. J. Physiol. Lung Cell Mol. Physiol.* 298, L715–L731. doi: 10.1152/ajplung.00361.2009

Dhupkar, P., and Gordon, N. (2017). Interleukin-2: old and new approaches to enhance immune-therapeutic efficacy. *Adv. Exp. Med. Biol.* 995, 33–51. doi: 10.1007/978-3-319-53156-4_2

Duan, J., Zhang, X., Zhang, S., Hua, S., and Feng, Z. (2017). miR-206 inhibits FN1 expression and proliferation and promotes apoptosis of rat type II alveolar epithelial cells. *Exp. Ther. Med.* 13, 3203–3208. doi: 10.3892/etm.2017.4430

Ehrhardt, H., Pritzke, T., Oak, P., Kossert, M., Biebach, L., Förster, K., et al. (2016). Absence of TNF-α enhances inflammatory response in the newborn lung undergoing mechanical ventilation. *Am. J. Physiol. Lung Cell. Mol. Physiol.* 310, L909–L918. doi: 10.1152/ajplung.00367.2015

Fan, Z. A.-O., Devlin, J. A.-O., Hogg, S. A.-O. X., Doyle, M. A., Harrison, P. A.-O. X., Todorovski, I., et al. (2021). CDK13 cooperates with CDK12 to control global RNA polymerase II processivity. *Sci. Adv.* 6:eaaz5041. doi: 10.1126/sciadv.aaz5041

Fredriksson-Lidman, K. A.-O., Van Itallie, C. M., Tietgens, A. J., and Anderson, J. M. (2017). Sorbin and SH3 domain-containing protein 2 (SORBS2) is a component of the acto-myosin ring at the apical junctional complex in epithelial cells. *PLoS One* 2:e0185448. doi: 10.1371/journal.pone.0185448

Freeman, A., Stanko, P., Berkowitz, L. N., Parnell, N., Zuppe, A., Bale, T. L., et al. (2017). Inclusion of sex and gender in biomedical research: survey of clinical research proposed at the University of Pennsylvania. *Biol. Sex Diff.* 8:22. doi: 10.1186/s13293-017-0139-5

Garingo, A., Tesoriero, L., Cayabyab, R., Durand, M., Blahnik, M., Sardesai, S., et al. (2007). Constitutive IL-10 expression by lung inflammatory cells and risk for bronchopulmonary dysplasia. *Pediatr. Res.* 61, 197–202. doi: 10.1203/pdr.0b013e31802d8a1c

German, A. E., Mammoto, T., Jiang, E., Ingber, D. E., and Mammoto, A. (2014). Paxillin controls endothelial cell migration and tumor angiogenesis by altering neuropilin 2 expression. *J. Cell Sci.* 127(Pt 8), 1672–1683. doi: 10.1242/jcs.132316

Haines, B. P., Gupta, R., Jones, C. M., Summerbell, D., and Rigby, P. W. (2005). The NLRR gene family and mouse development: modified differential display PCR identifies NLRR-1 as a gene expressed in early somitic myoblasts. *Dev. Biol.* 281, 145–159. doi: 10.1016/j.ydbio.2005.01.030

Hirsch, K., Taglauer, E., Seedorf, G., Callahan, C., Mandell, E., White, C. W., et al. (2020). Perinatal hypoxia-inducible factor stabilization preserves lung alveolar and vascular growth in experimental bronchopulmonary dysplasia. *Am. J. Respir. Crit. Care Med.* 202, 1146–1158. doi: 10.1164/rccm.202003-0601OC

Hsu, Y. C., Kao, C. Y., Chung, Y. F., Chen, M. S., and Chiu, I. M. (2012). Ciliogenic RFX transcription factors regulate FGF1 gene promoter. *J. Cell Biochem.* 113, 2511–2522. doi: 10.1002/jcb.24127

Hua, J. T., Chen, S., and He, H. H. (2019). Landscape of Noncoding RNA in prostate cancer. *Trends Genet. TIG* 35, 840–851. doi: 10.1016/j.tig.2019.08.004

Huang, H., Zhang, D., Fu, J., Zhao, L., Li, D., Sun, H., et al. (2021). Tsukushi is a novel prognostic biomarker and correlates with tumor-infiltrating B cells in non-small cell lung cancer. *Aging (Albany NY)* 13, 4428–4451. doi: 10.18632/aging.202403

Huang, Q., Guo, H., Wang, S., Ma, Y., Chen, H., Li, H., et al. (2020). A novel circular RNA, circXPO1, promotes lung adenocarcinoma progression by interacting with IGF2BP1. *Cell Death Dis.* 11:1031. doi: 10.1038/s41419-020-03237-8

Hurskainen, M., Mizikova, I., Cook, D. P., Andersson, N., Cyr-Depauw, C., Lesage, F., et al. (2021). Single cell transcriptomic analysis of murine lung development on hyperoxia-induced damage. *Nat. Commun.* 12:1565. doi: 10.1038/s41467-021-21865-2

Kang, M., and Thébaud, B. (2018). Stem cell biology and regenerative medicine for neonatal lung diseases. *Pediatr. Res.* 83, 291–297. doi: 10.1038/pr.2017.232

Laddha, A. P., and Kulkarni, Y. A. (2019). VEGF and FGF-2: promising targets for the treatment of respiratory disorders. *Respir. Med.* 156, 33–46. doi: 10.1016/j.rmed.2019.08.003

Laube, M., Stolzing, A., Thome, U. H., and Fabian, C. (2016). Therapeutic potential of mesenchymal stem cells for pulmonary complications associated with preterm birth. *Int. J. Biochem. Cell Biol.* 74, 18–32. doi: 10.1016/j.biocel.2016.02.023

Leary, S., Das, P., Ponnalagu, D., Singh, H., and Bhandari, V. (2019). Genetic strain and sex differences in a hyperoxia-induced mouse model of varying severity of bronchopulmonary dysplasia. *Am. J. Pathol.* 189, 999–1014. doi: 10.1016/j.ajpath.2019.01.014

Liao, J., Kapadia, V. S., Brown, L. S., Cheong, N., Longoria, C., Mija, D., et al. (2015). The NLRP3 inflammasome is critically involved in the development of bronchopulmonary dysplasia. *Nat. Commun.* 6:8977. doi: 10.1038/ncomms9977

Liu, H., Lin, Z., and Ma, Y. (2020). Suppression of Fpr2 expression protects against endotoxin-induced acute lung injury by interacting with Nrf2-regulated TAK1 activation. *Biomed. Pharmacother.* 125:109943. doi: 10.1016/j.biopha.2020.109943

Lou, S., Duan, Y., Nie, H., Cui, X., Du, J., and Yao, Y. (2021). Mesenchymal stem cells: biological characteristics and application in disease therapy. *Biochimie* 185, 9–21. doi: 10.1016/j.biochi.2021.03.003

Lu, Y., Zhang, Y., Wang, N., Pan, Z., Gao, X., Zhang, F., et al. (2010). MicroRNA-328 contributes to adverse electrical remodeling in atrial fibrillation. *Circulation* 122, 2378–2387. doi: 10.1161/CIRCULATIONAHA.110.958967

Luan, Y., Zhang, Z. H., Wei, D. E., Lu, Y., and Wang, Y. B. (2012). Effects of autologous bone marrow mononuclear cells implantation in canine model of pulmonary hypertension. *Circ. J.* 76, 977–985. doi: 10.1253/circj.CJ-11-1175

Ma, C., Gu, R., Wang, X., He, S., Bai, J., Zhang, L., et al. (2020). circRNA CDR1as promotes pulmonary artery smooth muscle cell calcification by upregulating CAMK2D and CNN3 via sponging miR-7-5p. *Mol. Ther. Nucleic Acids* 22, 530–541. doi: 10.1016/j.omtn.2020.09.018

Machado, M. N., Mazzoli-Rocha, F., Casquilho, N. V., Maron-Gutierrez, T., Ortenzi, V. H., Morales, M. M., et al. (2018). Bone marrow-derived mononuclear cell therapy in papain-induced experimental pulmonary emphysema. *Front. Physiol.* 9:121. doi: 10.3389/fphys.2018.00121

Magagnotti, C., Matassa, P. G., Bachi, A., Vendettuoli, V., Fermo, I., Colnaghi, M. R., et al. (2013). Calcium signaling-related proteins are associated with broncho-pulmonary dysplasia progression. *J. Proteomics* 94, 401–412. doi: 10.1016/j.jprot.2013.10.007

Mashima, R., Saeki, K., Aki, D., Minoda, Y., Takaki, H., Sanada, T., et al. (2005). FLN29, a novel interferon- and LPS-inducible gene acting as a negative regulator of toll-like receptor signaling. *J. Biol. Chem.* 280, 41289–41297. doi: 10.1074/jbc.M508221200

Mills, D. R. (2017). Effects of human umbilical cord blood mononuclear cells on respiratory system mechanics in a murine model of neonatal lung injury. *Exp. Lung Res.* 43, 66–81. doi: 10.1080/01902148.2017.1300713

Monz, D., Tutdibi, E., Mildau, C., Shen, J., Kasoha, M., Laschke, M. W., et al. (2013). Human umbilical cord blood mononuclear cells in a double-hit model of bronchopulmonary dysplasia in neonatal mice. *PLoS One* 8:e74740. doi: 10.1371/journal.pone.0074740

Nardiello, C., Mižíková, I., Silva, D. M., Ruiz-Camp, J., Mayer, K., Vadász, I., et al. (2017). Standardisation of oxygen exposure in the development of mouse models for bronchopulmonary dysplasia. *Dis. Models Mech.* 10, 185–196. doi: 10.1242/dmm.027086

Nold, M. F., Mangan, N. E., Rudloff, I., Cho, S. X., Shariatian, N., Samarasinghe, T. D., et al. (2013). Interleukin-1 receptor antagonist prevents murine bronchopulmonary dysplasia induced by perinatal inflammation and hyperoxia. *Proc. Natl. Acad. Sci. U.S.A.* 110, 14384–14389. doi: 10.1073/pnas.1306859110

Olave, N., Lal, C. V., Halloran, B., Pandit, K., Cuna, A. C., Faye-Petersen, O. M., et al. (2016). Regulation of alveolar septation by microRNA-489. *Nat. Commun.* 310, L476–L487. doi: 10.1152/ajplung.00145.2015

O'Reilly, M., and Thebaud, B. (2015). Stem cells for the prevention of neonatal lung disease. *Neonatology* 107, 360–364. doi: 10.1159/000381135

Pasha, A. B., Chen, X. Q., and Zhou, G. P. (2018). Bronchopulmonary dysplasia: pathogenesis and treatment. *Exp. Ther. Med.* 16, 4315–4321. doi: 10.3892/etm.2018.6780

Peters, E. B., Liu, B., Christoforou, N., West, J. L., and Truskey, G. A. (2015). Umbilical cord blood-derived mononuclear cells exhibit pericyte-like phenotype and support network formation of endothelial progenitor cells in vitro. *Ann. Biomed. Eng.* 43, 2552–2568. doi: 10.1007/s10439-015-1301-z

Poets, C. F., and Lorenz, L. (2018). Prevention of bronchopulmonary dysplasia in extremely low gestational age neonates: current evidence. *Arch. Dis.*

Child. Fetal Neonatal Ed. 103, F285–F291. doi: 10.1136/archdischild-2017-314264

Ryan, R. M., Ahmed, Q., and Lakshminrusimha, S. (2008). Inflammatory mediators in the immunobiology of bronchopulmonary dysplasia. *Clin. Rev. Allergy Immunol.* 34, 174–190. doi: 10.1007/s12016-007-8031-4

Segarra, M., Ohnuki, H., Maric, D., Salvucci, O., Hou, X., Kumar, A., et al. (2012). Semaphorin 6A regulates angiogenesis by modulating VEGF signaling. *Blood* 120, 4104–4115. doi: 10.1182/blood-2012-02-410076

Shin, T.-H., Kim, H.-S., Kang, T.-W., Lee, B.-C., Lee, H.-Y., Kim, Y.-J., et al. (2016). Human umbilical cord blood-stem cells direct macrophage polarization and block inflammasome activation to alleviate rheumatoid arthritis. *Cell Death Dis.* 7:e2524. doi: 10.1038/cddis.2016.442

Shpargel, K. B., Sengoku, T., Yokoyama, S., and Magnuson, T. (2012). UTX and UTY demonstrate histone demethylase-independent function in mouse embryonic development. *PLoS Genet.* 8:e1002964. doi: 10.1371/journal.pgen.1002964

Syed, M. A., Shah, D., Das, P., Andersson, S., Pryhuber, G., and Bhandari, V. (2019). TREM-1 attenuates RIPK3-mediated necroptosis in hyperoxia-induced lung injury in neonatal mice. *Am. J. Respir. Cell Mol. Biol.* 60, 308–322. doi: 10.1165/rcmb.2018-0219OC

Syed, M., Das, P., Pawar, A., Aghai, Z. H., Kaskinen, A., Zhuang, Z. W., et al. (2017). Hyperoxia causes miR-34a-mediated injury via angiopoietin-1 in neonatal lungs. *Nat. Commun.* 8:1173. doi: 10.1038/s41467-017-01349-y

Tan, E. K., Chao, Y. X., West, A., Chan, L. L., Poewe, W., and Jankovic, J. (2020). Parkinson disease and the immune system – associations, mechanisms and therapeutics. *Nat. Rev. Neurol.* 16, 303–318. doi: 10.1038/s41582-020-0344-4

Thébaud, B. (2018). Mesenchymal stromal cell therapy for respiratory complications of extreme prematurity. *Am. J. Perinatol.* 35, 566–569. doi: 10.1055/s-0038-1639371

Thebaud, B., Goss, K. N., Laughon, M., Whitsett, J. A., Abman, S. H., Steinhorn, R. H., et al. (2019). Bronchopulmonary dysplasia. *Nat. Rev. Dis. Primers* 5:78. doi: 10.1038/s41572-019-0127-7

Ulke, H. M., Mutze, K., Lehmann, M., Wagner, D. E., Heinzelmann, K., Gunther, A., et al. (2019). The oncogene ECT2 contributes to a hyperplastic, proliferative lung epithelial cell phenotype in idiopathic pulmonary fibrosis. *Am. J. Respir. Cell Mol. Biol.* 61, 713–726. doi: 10.1165/rcmb.2019-0047OC

Vilariño, N., Bruna, J., Kalofonou, F., Anastopoulou, G. G., and Argyriou, A. A. (2020). Immune-driven pathogenesis of neurotoxicity after exposure of cancer patients to immune checkpoint inhibitors. *Int. J. Mol. Sci.* 21:5774. doi: 10.3390/ijms21165774

Wang, J., Yin, J., Wang, X., Liu, H., Hu, Y., Yan, X., et al. (2019). Changing expression profiles of mRNA, lncRNA, circRNA, and miRNA in lung tissue reveal the pathophysiological of bronchopulmonary dysplasia (BPD) in mouse model. *J. Cell. Biochem.* 120, 9369–9380. doi: 10.1002/jcb.28212

Wang, Q., Wang, J., Hu, M., Yang, Y., Guo, L., Xu, J., et al. (2016). Uncoupling protein 2 increases susceptibility to lipopolysaccharide-induced acute lung injury in mice. *Med. Inflamm.* 2016:9154230. doi: 10.1155/2016/9154230

Wei, L., Wang, X., Lv, L., Liu, J., Xing, H., Song, Y., et al. (2019). The emerging role of microRNAs and long noncoding RNAs in drug resistance of hepatocellular carcinoma. *Mol. Cancer* 18:147. doi: 10.1186/s12943-019-1086-z

Wright, M. W., and Bruford, E. A. (2011). Naming 'junk': human non-protein coding RNA (ncRNA) gene nomenclature. *Hum. Genomics* 5, 90–98. doi: 10.1186/1479-7364-5-2-90

Wu, J., Pipathsouk, A., Keizer-Gunnink, A., Fusetti, F., Alkema, W., Liu, S., et al. (2015). Homer3 regulates the establishment of neutrophil polarity. *Mol. Biol. Cell.* 26, 1629–1639. doi: 10.1091/mbc.E14-07-1197

Wu, X., Zheng, X., Cheng, J., Zhang, K., and Ma, C. (2020). LncRNA TUG1 regulates proliferation and apoptosis by regulating miR-148b/IGF2 axis in ox-LDL-stimulated VSMC and HUVEC. *Life Sci.* 243, 117287–117287. doi: 10.1016/j.lfs.2020.117287

Xie, P., Zhang, M., He, S., Lu, K., Chen, Y., Xing, G., et al. (2014). The covalent modifier Nedd8 is critical for the activation of Smurf1 ubiquitin ligase in tumorigenesis. *Nat. Commun.* 5:3733. doi: 10.1038/ncomms4733

Xu, X., Zhang, J., Tian, Y., Gao, Y., Dong, X., Chen, W., et al. (2020). CircRNA inhibits DNA damage repair by interacting with host gene. *Mol. Cancer* 19:128. doi: 10.1186/s12943-020-01246-x

Yamada, T., Ohta, K., Motooka, Y., Fujino, K., Kudoh, S., Tenjin, Y., et al. (2019). Significance of Tsukushi in lung cancer. *Lung Cancer* 131, 104–111. doi: 10.1016/j.lungcan.2019.03.024

Yan, C., Chang, J., Song, X., Qi, Y., Ji, Z., Liu, T., et al. (2021). Lung cancer-associated mesenchymal stem cells promote tumor metastasis and tumorigenesis by induction of epithelial-mesenchymal transition and stem-like reprogram. *Aging (Albany NY)* 13, 9780–9800. doi: 10.18632/aging.202732

Yang, Q., Köttgen, A., Dehghan, A., Smith, A. V., Glazer, N. L., Chen, M. H., et al. (2010). Multiple genetic loci influence serum urate levels and their relationship with gout and cardiovascular disease risk factors. *Circ. Cardiovasc. Genet.* 3, 523–530. doi: 10.1161/CIRCGENETICS.109.934455

Yin, Y., Liu, H., Wang, F., Li, L., Deng, M., Huang, L., et al. (2015). Transplantation of cryopreserved human umbilical cord blood-derived endothelial progenitor cells induces recovery of carotid artery injury in nude rats. *Stem Cell Res. Ther.* 6, 37–37. doi: 10.1186/s13287-015-0022-4

Yoon, B. H., Romero, R., Jun, J. K., Park, K. H., Park, J. D., Ghezzi, F., et al. (1997). Amniotic fluid cytokines (interleukin-6, tumor necrosis factor-alpha, interleukin-1 beta, and interleukin-8) and the risk for the development of bronchopulmonary dysplasia. *Am. J. Obstet. Gynecol.* 177, 825–830. doi: 10.1016/S0002-9378(97)70276-X

Zhang, D., Xu, X., and Dong, Z. (2017). PRKCD/PKCdelta contributes to nephrotoxicity during cisplatin chemotherapy by suppressing autophagy. *Autophagy* 13, 631–632. doi: 10.1080/15548627.2016.1269990

Zhang, F., Zhang, R., Zhang, X., Wu, Y., Li, X., Zhang, S., et al. (2018). Comprehensive analysis of circRNA expression pattern and circRNA-miRNA-mRNA network in the pathogenesis of atherosclerosis in rabbits. *Aging (Albany NY)* 10, 2266–2283. doi: 10.18632/aging.101541

Zhang, M., Li, N., Liu, W., Du, X., Wei, Y., Yang, D., et al. (2021). Eif2s3y promotes the proliferation of spermatogonial stem cells by activating ERK signaling. *Stem Cells Int.* 2021:6668658. doi: 10.1155/2021/6668658

Zhang, X., Chu, X., Gong, X., Zhou, H., and Cai, C. (2020). The expression of miR-125b in Nrf2-silenced A549 cells exposed to hyperoxia and its relationship with apoptosis. *J. Cell Mol. Med.* 24, 965–972. doi: 10.1111/jcmm.14808

Zhang, X., Hong, R., Chen, W., Xu, M., and Wang, L. (2019). The role of long noncoding RNA in major human disease. *Bioorg. Chem.* 92:103214. doi: 10.1016/j.bioorg.2019.103214

Zhao, T., Liu, M., Gu, C., Wang, X., and Wang, Y. (2014). Activation of c-Src tyrosine kinase mediated the degradation of occludin in ventilator-induced lung injury. *Respir. Res.* 15:158. doi: 10.1186/s12931-014-0158-2

Zhou, S. Y., Chen, W., Yang, S. J., Li, J., Zhang, J. Y., Zhang, H. D., et al. (2020). Circular RNA circVAPA regulates breast cancer cell migration and invasion via sponging miR-130a-5p. *Cancer Cell Int.* 12, 303–317. doi: 10.2217/epi-2019-0124

Zhou, S., Yin, X., Mayr, M., Noor, M., Hylands, P. J., and Xu, Q. (2020). Proteomic landscape of TGF-β1-induced fibrogenesis in renal fibroblasts. *Sci. Rep.* 10:19054. doi: 10.1038/s41598-020-75989-4

Conflict of Interest: GL was employed by the company Shandong Qilu Stem Cell Engineering Co., Ltd.

The remaining authors declare that the research was conducted in the absence of any commercial or financial relationships that could be construed as a potential conflict of interest.

Publisher's Note: All claims expressed in this article are solely those of the authors and do not necessarily represent those of their affiliated organizations, or those of the publisher, the editors and the reviewers. Any product that may be evaluated in this article, or claim that may be made by its manufacturer, is not guaranteed or endorsed by the publisher.

frontiers in Cell and Developmental Biology

REVIEW
published: 26 November 2021
doi: 10.3389/fcell.2021.765980

Induction and Maturation of Hepatocyte-Like Cells *In Vitro*: Focus on Technological Advances and Challenges

Ye Xie[1], *Jia Yao*[1,2], *Weilin Jin*[1,3,4], *Longfei Ren*[1,5] *and Xun Li*[1,2,4,5,6]*

[1]The First Clinical Medical College, Lanzhou University, Lanzhou, China, [2]Key Laboratory of Biotherapy and Regenerative Medicine of Gansu Province, Lanzhou, China, [3]Institute of Cancer Neuroscience, The First Hospital of Lanzhou University, Lanzhou, China, [4]The Medical Frontier Innovation Research Center, The First Hospital of Lanzhou University, Lanzhou, China, [5]The Department of General Surgery, The First Hospital of Lanzhou University, Lanzhou, China, [6]Hepatopancreatobiliary Surgery Institute of Gansu Province, Lanzhou, China

Limited by the poor proliferation and restricted sources of adult hepatocytes, there is an urgent need to find substitutes for proliferation and cultivation of mature hepatocytes *in vitro* for use in disease treatment, drug approval, and toxicity testing. Hepatocyte-like cells (HLCs), which originate from undifferentiated stem cells or modified adult cells, are considered good candidates because of their advantages in terms of cell source and *in vitro* expansion ability. However, the majority of induced HLCs are in an immature state, and their degree of differentiation is heterogeneous, diminishing their usability in basic research and limiting their clinical application. Therefore, various methods have been developed to promote the maturation of HLCs, including chemical approaches, alteration of cell culture systems, and genetic manipulation, to meet the needs of *in vivo* transplantation and *in vitro* model establishment. This review proposes different cell types for the induction of HLCs, and provide a comprehensive overview of various techniques to promote the generation and maturation of HLCs *in vitro*.

Keywords: hepatocyte-like cells, hepatocyte induction, chemical approach, culture system, genetic manipulation

OPEN ACCESS

Edited by:
Wencheng Zhang,
Tongji University, China

Reviewed by:
Ken-ichiro Kamei,
Kyoto University, Japan
Kazuo Takayama,
Kyoto University, Japan

***Correspondence:**
Xun Li
lxdr21@126.com

Specialty section:
This article was submitted to Stem Cell Research, a section of the journal Frontiers in Cell and Developmental Biology

Received: *28 August 2021*
Accepted: *08 November 2021*
Published: *26 November 2021*

Citation:
Xie Y, Yao J, Jin W, Ren L and Li X (2021) Induction and Maturation of Hepatocyte-Like Cells In Vitro: Focus on Technological Advances and Challenges. Front. Cell Dev. Biol. 9:765980. doi: 10.3389/fcell.2021.765980

1 INTRODUCTION

Liver transplantation is the only therapeutic modality for curing end-stage liver disease. However, the chronic shortage of donors has compelled researchers to develop alternative treatments. Clinical studies have demonstrated that transplanted hepatocytes can relieve patient symptoms, prolong their survival (Hansel et al., 2014), and provide a "bridge" therapy until patients are matched with an appropriate liver for transplantation (Nguyen et al., 2020). However, there are problems associated with human hepatocyte transplantation. First, human primary hepatocytes have higher cell quality requirements, and isolated hepatocytes lose their functionality after prolonged periods of culture *in vitro*. In addition, long-term oral immunosuppressive drugs are needed after allogeneic hepatocyte transplantation which has arisen adverse effect and given negative impact of patient's life quality. (Zeilinger et al., 2016; Miki, 2019; Ruoss et al., 2020).

In theory, undifferentiated stem cells can be induced into hepatocytes along the development track of hepatocytes under external intervention. The final induced cells were shown to adopt the phenotypes of hepatocytes, express hepatocyte-specific genes, perform glycogen storage and albumin synthesis functions. However, when compared with human hepatocytes (HHs), most

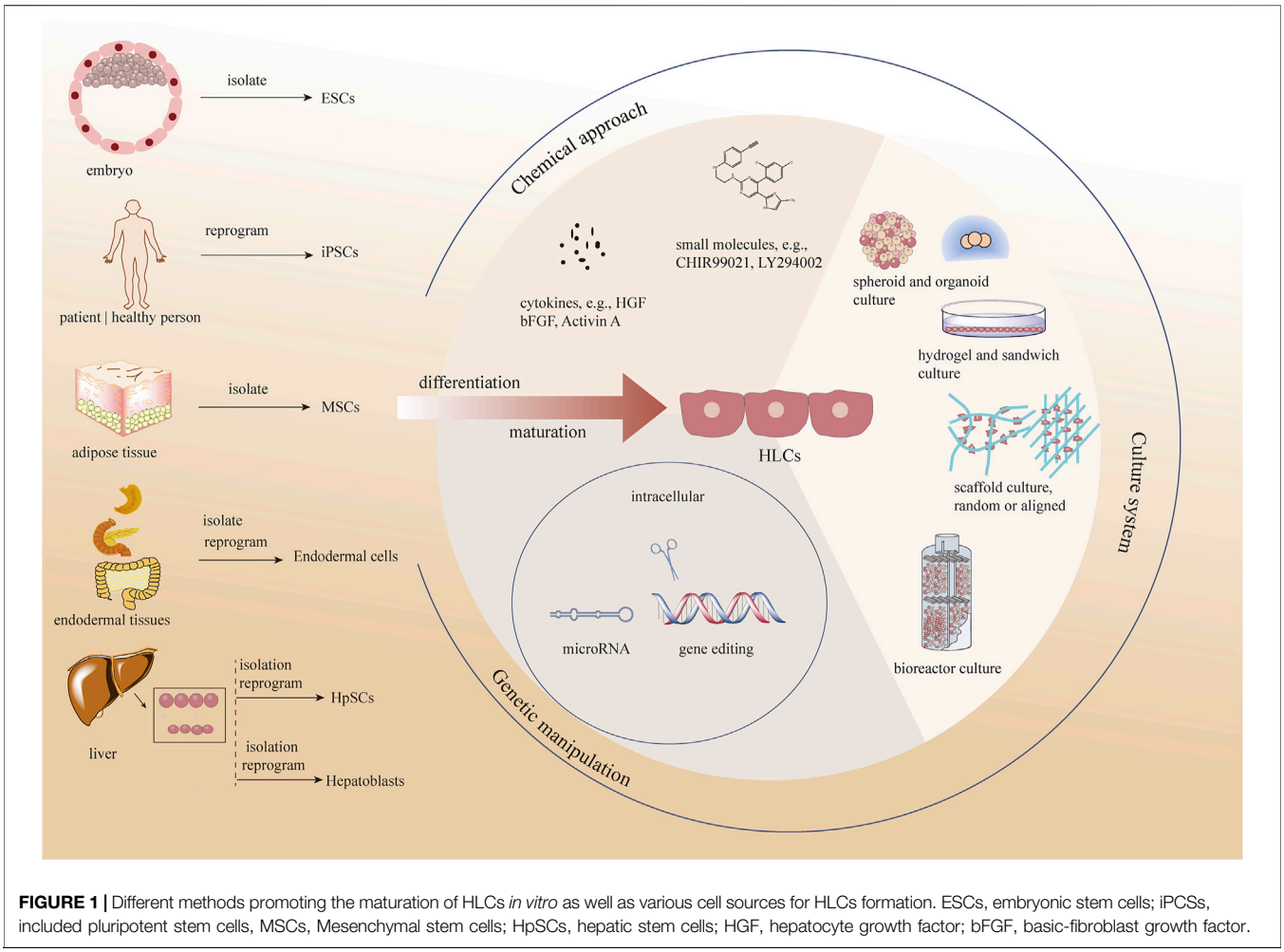

FIGURE 1 | Different methods promoting the maturation of HLCs *in vitro* as well as various cell sources for HLCs formation. ESCs, embryonic stem cells; iPCSs, included pluripotent stem cells, MSCs, Mesenchymal stem cells; HpSCs, hepatic stem cells; HGF, hepatocyte growth factor; bFGF, basic-fibroblast growth factor.

of these cells express higher level of alpha-fetoprotein (AFP) and, perform insufficient detoxification functions, so called hepatocyte-like cells (HLCs). (Bell et al., 2017; Roy-Chowdhury et al., 2017; Cotovio and Fernandes, 2020). Nevertheless, even with this immature state, HLCs show an ideal effect in treating animal models of liver diseases and, are used for generating *in vitro* organoid models for predicting the hepatotoxicity of new drug (Corbett and Duncan, 2019). Unfortunately, immature phenotypes and the inconsistent differentiation of HLCs in the same batch, especially those derived from stem cells, pose a risk of tumorigenesis after transplantation into humans (Xu et al., 2018). All of these obstacles block the transformation of HLCs as an alternative to HHs in clinical applications, and greatly discount the authenticity of drug prediction results in some basic experiments, because HLCs cannot fully express the function of mature hepatocytes.

Thus, the question arises as to how HLCs can be generated with similarities to HHs both for *ex vivo* use and towards eventual clinical programs. Researchers have developed several methods to promote hepatocyte maturation by attempting to simulate hepatocytes *in vivo* for liver progenitors to induce mature and stable HLCs *in vitro* (Berger et al., 2015; Touboul et al., 2016). Actually, these methods can be divided into three types, chemical approaches, changing the culture system, and genetic manipulation. In this review, we discuss various cell sources for HLCs formation and methods promoting the maturation of HLCs *in vitro* (**Figure 1**).

2 CELL SOURCES FOR GENERATING HEPATOCYTE-LIKE CELLS *IN VITRO*

HHs are considered the "gold standard" for functional cells used for drug screening and for cell transplantation. It is noteworthy that neonatal hepatocytes, compared with adult hepatocytes, have higher viability with better treatment outcomes in clinical settings, even after cellular cryopreservation (Tolosa et al., 2014; Lee et al., 2018). However, owing to a chronic, global shortage of donors, and ethical issues, alternative cell sources are needed (Zeilinger et al., 2016; Ruoss et al., 2020). Studies shows that HLCs can be derived from embryonic stem cells (ESCs), induced pluripotent stem cells (iPSCs), mesenchymal stem cells (MSCs), endodermal cells and hepatic stem/progenitor cells.

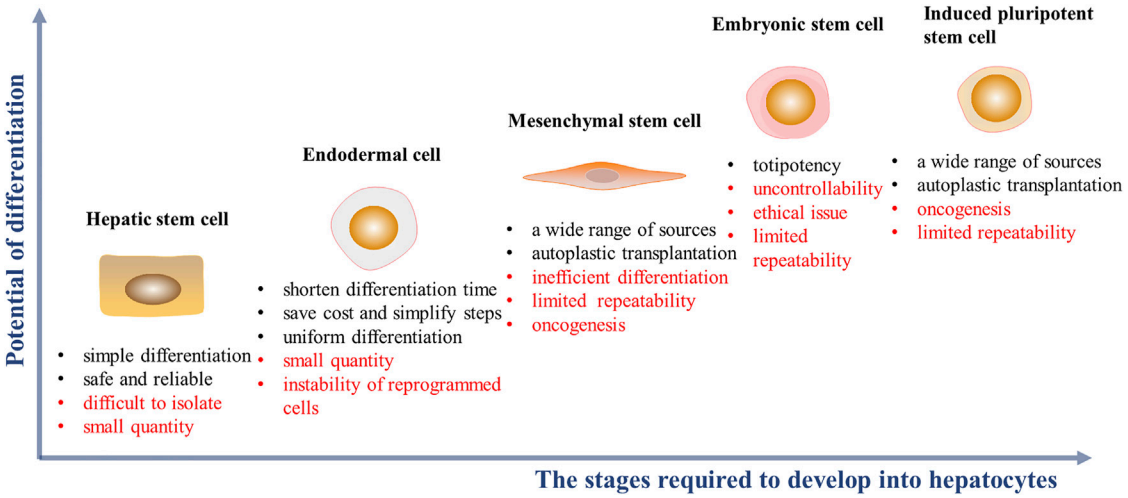

FIGURE 2 | Cell sources of HLCs induction *in vitro* and their advantages (black font) and disadvantages (red font). The abscissa represents the complexity of the stages required during hepatic differentitation. The ordinate represents the potential of cell differentiation into other cell types.

HLCs, performing some characteristics of hepatocytes, can be a promising alternative of hepatocytes to be tested in some preclinical researches which need to consume sufficient number of cells (Zhou et al., 2017; Wang et al., 2018; Mun et al., 2019) (**Figure 2**). Some key features of ideal HLCs cell source scientific research and clinical application are sufficient, accessible, and restricted differentiation into hepatic lines with complete phenotype and function in scientific research and clinical application.

2.1 Embryonic Stem Cells

Embryonic stem cells (ESCs) feature the pluripotency to differentiate into endoderm, mesoderm and ectoderm. ESC lineages may be restricted to cells with hepatocyte-like features under induction conditions (Mun et al., 2019). ESCs with a comprehensive spectrum are more likely to differentiate into other lineages, which leads to heterogeneous differentiation of HLCs. Before differentiation, if ESCs are transformed into definitive endoderm for narrow-spectrum differentiation, the differentiation efficiency can be improved. However, this may increase the number of steps and duration of differentiation. In addition, it is necessary to provide an appropriate environment for stem cells to support their pluripotency when cultured *in vitro*. Generally, according to the materials of substratum on the dish, the culture methods are divided into feeder-dependent culture (e.g., mouse embryonic fibroblasts and skin fibroblasts) and feeder-free culture (e.g., Matrigel, collagen, human recombinant laminin and its subtypes) (Hoffman and Carpenter, 2005; Dakhore et al., 2018). It has been found that some cytokines and extracellular matrix components secreted by the feeder layer into the culture medium can form a benefit environment for growth of stem cells. For example, basic fibroblast growth factor (bFGF), transforming growth factor-β (TGF-β), and Laminin-511 secreted by fibroblast feeder layer is associated with the cell self-renewal and pluripotency maintenance of human ESCs (Stacey et al., 2006; Hongisto et al., 2012; Lim et al., 2019). Limited by the potential of unidentified pathogens from feeder cells, feeder-free culture represents a greater prospect (Llames et al., 2015). At present, some fully defined commercial media for feeder-free culture, such as E8 and TeSR, optimizes the passage and maintenance of stem cells (Lim et al., 2019). Compared with TeSR medium, the development of E8 medium rejects the animal derived bovine serum albumin and some non-essential additions, simplifying the medium components, maintaining the undifferentiated proliferation of ESCs, and further reducing the culture cost (Ludwig et al., 2006; Chen et al., 2011).

2.2 Induced Pluripotent Stem Cells

Induced pluripotent stem cells (iPSCs), which represent a promising source of HLCs, can be reprogrammed from different adult cells (Wang et al., 2016; Roy-Chowdhury et al., 2017). The classic reprogramming technique involves introducing Oct4/Sox2/KLF4/c-MYC genes into candidate cells to reverse cells from a differentiated state to the ground state with the ability to re-differentiate (Takahashi and Yamanaka, 2006). However, the reprogramming efficiency is affected by the expression level of the four transcription factors, and the method poses a potential risk of insertion mutation; furthermore, the continuous expression of *c-MYC* may pose a risk of tumorigenesis *in vivo* (Xu et al., 2018; Haridhasapavalan et al., 2020). Based on efficiency and safety considerations, reprogramming methods have been explored and optimized, such as reducing or replacing the application of c-MYC (Huang et al., 2018; Nakagawa et al., 2008), shifting from genetic integration to integration-free methods, or using small-molecule cocktails for direct reprogramming (Fusaki et al., 2009; Okita et al., 2011; Ma et al., 2017). The culture and induction methods of iPSCs *in vitro* are very similar to those of ESCs. iPSCs

are differentiated into HLCs through three stages: endoderm formation, hepatic specification, and maturation (Li et al., 2019). In addition, transcription factor-based reprogramming retains the epigenetic memory of donor cells, which may favor iPSC differentiation along the original tissue and limit the efficiency of differentiation into other lineages, without contributing to performance of the complete phenotype of HLCs induced from liver-derived iPSCs (Kim et al., 2010; Calabrese et al., 2019). The emergence of iPSCs provides a sustainable concept for high-value precision medicine; the use of patient-specific recombinant iPSCs can not only solve the problem of cell source but also avoid various risks related to inhibition and rejection in *in vivo* applications; however, the reprogramming efficiency and culture mode of iPSCs need to be further optimized.

2.3 Mesenchymal Stem Cells

Mesenchymal stem cells (MSCs) are a type of non-hematopoietic stem cells that exist in a wide range of tissues such as bone marrow, adipose tissue, menstrual blood and umbilical cord (Raoufil et al., 2015; Farnaz Sani et al., 2016; Xing et al., 2016; Cipriano et al., 2017; Xu et al., 2017). Among them, umbilical cord mesenchymal stem cells are widely studied as the candidate for the treatment of end-stage liver disease and HLCs differentiation (Talaei-Khozani et al., 2015; Varaa et al., 2019). Typically, liver-specific induction and maturation stages are required to obtain HLCs, which are unstable and inefficient due to the need to transition from mesoderm to endoderm (Vojdani et al., 2015; Huang et al., 2017). There is a type of stem cell localized in the liver with a phenotype similar to that of MSCs, can be successfully differentiated into HLCs (Najimi et al., 2007; Lee et al., 2020). Even that being of hepatic origin, these cells are not more mature in hepatic differentiation compared with extrahepatic MSCs (Chinnici et al., 2019). Of course, as an accessible cell source of HLCs *in vitro*, MSCs have the advantages of their low immunogenicity *in vivo*, strong proliferation ability *in vitro*, and unaffected cell vitality and differentiation ability after cryopreservation. However, it is noteworthy that adult stem cell actually accounts for only a small part of the tissue, and the number and proliferation ability of MSCs will decrease along with donor age.

2.4 Endodermal Cells

Organs from endodermal origins, including the gallbladder, pancreas and intestine, which are of the same germ layer origins as the liver, also contain endodermal stem cells (Carpino et al., 2014; Lanzoni et al., 2016). These cells can differentiate into HLCs with a shorter differentiation path. Isolation of tissue-derived endodermal stem cells cost far less than that the pluripotent stem cell-derived. The issue with the tissue-derived endodermal stem cells is their *ex vivo* expansion limitation due to the underdeveloped expansion condition. Therefore, pluripotent stem cells are recombined into stable and expandable endodermal progenitor cells as a new cell-type source of HLCs *in vitro* (Cheng et al., 2013; Sambathkumar et al., 2018). This approach represents a more simple and safe method than other strategies that require endodermal differentiation because endoderm formation has already occurred by the time of isolation. Furthermore, selecting an endodermal source (e.g., intestine) with a close lineage relationship is logical since one is not trying to reprogram cells from ectoderm or mesoderm to endoderm (Wang et al., 2016). The transformation of digestive tract epithelial cells into endoderm cells using a small molecule cocktail has already been achieved and such cells are genetically stable (Wang et al., 2016). The strategy of using endodermal cells as initiators for differentiation can be less fraught, with greater chance of success and at far lower cost. This has been an increasingly interesting and promising strategy, but additional investigations are necessary to validate these early findings.

2.5 Hepatic Stem/Progenitor Cells

There are two types of multipotent cells in the liver: hepaoblasts and hepatic stem cells (HpSCs). Hepatoblasts are diploid bipotent cells with hepatocytes and cholangiocytes differentiation, locating in the canals of Hering in the adult liver. As the precursors of hepatoblasts, HpSCs are multipotent and can give rise to pancreatic islets cells except for hepatocytes and cholangiocytes. These cells can be found in the ductal plates of fetal and neonatal livers, and the canals of Hering in pediatric and adult livers. These two kinds of cells have very similar antigenic profiles, only with and without AFP expression, respectively (Chen et al., 2017; Schmelzer et al., 2007; Turner et al., 2011; Zhang, et al., 2008). These cells can be lineage-restricted into hepatocytes under different condition, which indicates that they are safe for use in transplantation *in vivo* (Cardinale et al., 2011; Turner et al., 2011). However, the extraction and separation of HpSCs or hepatoblasts presents a challenge due to the scant numbers of HpSCs (0.5–2.5% of liver parenchyma of all donor ages) and hepatoblasts (<0.01% in adult livers) (Turner et al., 2011; Liu et al., 2019). Although it is possible to obtain proliferative hepatoblasts by transferring both stem maintaining genes and liver specific genes, the final differentiation efficiency seems to be dissatisfactory (only 56.7%) (Yu et al., 2013; Park et al., 2019). Some scientists tried to change the composition of the culture medium and add some growth factors to transform mature hepatocytes into proliferative hepatoblasts, which have been realized in both mouse and human cells (Katsuda et al., 2017; Wu et al., 2017; Fu et al., 2019; Katsuda et al., 2019; Katsuda and Ochiya, 2019). Such chemically-induced hepatoblasts can stably expand *in vitro* and differentiate into mature hepatocytes under appropriate conditions and without gene mutations (Katsuda et al., 2017). The degree of differentiation of initial cells is close to the terminal state, and the inertia of cells makes it less steps to differentiate into HLCs.

3 INDUCTION AND MATURATION OF HEPATOCYTE-LIKE CELLS *IN VITRO*

Reviewing the development history of the whole liver, it is not difficult to find that process is committed and complex. Immature stem cells develop into polarity and functional maturation hepatocytes, initiated by exogenous signals, cell localization clues and accumulated transcription factors, which is inseparable from the transduction and regulation of chemical and mechanical signals

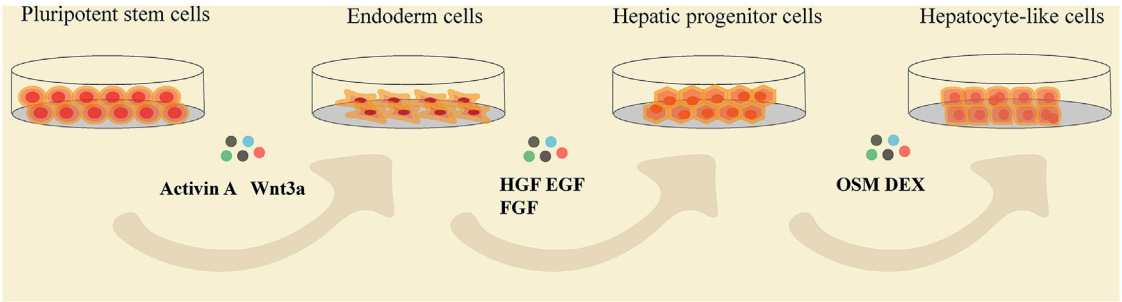

FIGURE 3 | The flow chat showing the stages of pluripotent stem cells differentiating into HLCs and the common cytokines added at each differentiation stage. HGF, hepatocyte growth factor; EGF, epidermal growth factor; FGF, fibroblast growth factor; OSM, oncostatin M; DEX, dexamethasone.

TABLE 1 | Hepatocyte-like cells formation by cytokines and growth factors.

Cell source	Endoderm formation	Hepatic specification	Maturation	Days	Ref.
Foreskin fibroblast-derived iPSCs	100 ng/ml Activin A 50 ng/ml Wnt3a	1% DMSO	30 ng/ml OSM 50 ng/ml HGF 10 μmol DEX	19	Wang et al. (2016)
iPSCs	10 ng/ml BMP4 10 ng/ml VEGF 10 ng/ml FGF2	50 ng/ml BMP4 10 ng/ml FGF2 10 ng/ml VEGF 10 ng/ml EGF 20 ng/ml TGF-α 100 ng/ml HGF 100 nmol/L DEX	100 ng/ml HGF 20 ng/ml OSM 6 μmol Vk 100 nmol DEX	25	Kaserman and Wilson (2017)
iPSCs	100 ng/ml Activin A	20 ng/ml BMP4 10 ng/ml FGF-2	20 ng/ml HGF 20 ng/ml OSM DEX	15	Kehtari et al. (2018)
ESCs	100 ng/ml Activin A	20 ng/ml BMP2 30 ng/ml FGF4 2 μmol/L RA 10 nmol nicotinamide 1 ng/ml b-FGF 100 μmol/L Vc	ITS 10 ng/ml OSM DEX 20 ng/ml HGF	22	Kim et al. (2015)
ESCs/iPSCs	100 ng/ml Activin A	20 ng/ml BMP4 10 ng/ml FGF2 20 ng/ml HGF	20 ng/ml OSM	20	Si-Tayeb et al. (2010)

Cell source	Hepatic specification	Maturation	Days	Ref.
WJ-MSCs	10 ng/ml FGF4 20 ng/ml HGF 20 ng/ml IGF 100 nmol/L DEX	20 ng/ml HGF 20 ng/ml IGF 100 nmol/L DEX 10 ng/ml OSM	21	Vojdani et al. (2015)
UV-MSCs	500 nmol DEX 1 × ITS 50 ng/ml HGF 10 ng/ml EGF 20 ng/ml b-FGF	10 ng/ml EGF 20 ng/ml b-FGF 1 × ITS 50 ng/ml OSM	28	Raoufil et al. (2015)
AD-MSCs	20 ng/ml HGF DEX 20 ng/ml IGF-I 10 ng/ml OSM	20 ng/ml HGF DEX 20 ng/ml IGF-I	21	Shabani Azandaryani et al. (2019)

Abbreviation: FGF, 4, fibroblast growth factor 4; HGF, hepatocyte growth factor; IGF, insulin like growth factor; DEX, dexamethasone; OSM, oncostatin M; ITS, insulin/transferrin/selenium; EGF, epidermal growth factor; b-FGF, basic-fibroblast growth factor; DMSO, dimethyl sulfoxide; BMP4, bone morphogenetic protein 4; VEGF, vascular endothelial growth factor; TGF-α, transforming growth factor-α; Vk, vitamin K; RA, retinoic acid; Vc, ascorbic acid.

TABLE 2 | Small molecules and possible mechanisms in HLCs formation.

Effect	Small molecules	Mechanism	Cell application	Ref.
Endoderm induction	IDE1	similar to activin A, induces Smad2 phosphorylation and drives AD-MSCs to endoderm formation	AD-MSCs	Xu et al. (2015)
	CHIR99021	a specific chemical inhibitor of GSK-3, can induce a rapid increase in the expression of the endoderm makers	AD-MSCs ESCs iPSCs	Xu et al. (2015) Siller et al. (2015) Du et al. (2018)
	6-bromo-indirubin-3′-oxime (BIO)	a GSK-3 inhibitor, mimics activation of Wnt signaling	ESCs	Tasnim et al. (2015)
	LY294002	inhibits maintenance of pluripotency and promotes differentiation to endoderm	ESCs	Tasnim et al. (2015)
Promotion of liver-specific induction and maturation	SJA710-6	a novel small molecule, can improve the process of hepatic differentiation by regulating the high expression of FOXH1 (FAST1/2)	MSCs	Ouyang et al. (2012)
	dimethyl sulfoxide (DMSO)	drives endoderm toward a hepatic fate and promotes maturation	ESCs iPSCs NMSCs	Tasnim et al. (2015) Cipriano et al. (2017) Du et al. (2018) Siller et al. (2015)
	Ile-(6) aminohexanoic amide (Dihexa)	an HGF receptor agonist, can promote hepatic maturation	ESCs iPSCs	Siller et al. (2015)
	sodium butyrate (SB)	a histone deacetylase inhibitor, results in high levels of hepatic marker expression and reduces cell death	ESCs WJ-MSCs	Tasnim et al. (2015) Du et al. (2018) Panta et al. (2019)
	SB431542	a TGF-β inhibitor, is used for the differentiation of progenitors to HLCs	ESCs	Tasnim et al. (2015)
	5-Azacytidine (5-aza)	a DNA methyltransferase inhibitor, epigenetic changes support the hepatic differentiation	NMSCs	Cipriano et al. (2017)
	Trichostatin A	a histone deacetylase inhibitor, improves hepatocyte phenotype	NMSCs AD-MSC	Cipriano et al. (2017)
	A83-01	a TGF-β inhibitor, is continuously used to promote hepatocyte differentiation	ESCs iPSCs	Du et al. (2018)
	FH1 and FPH1	are used to replace HGF and OSM to promote hepatocyte generation	ESCs iPSCs	Du et al. (2018)

Abbreviations: AD-MSC, adipose-derived mesenchymal stem cells; ESCs, embryonic stem cells; iPSCs, induced pluripotent stem cells; MSCs, mesenchymal stem cells; NMSCs, neonatal mesenchymal stromal cell; WJ-MSCs, Wharton's Jelly-derived mesenchymal stem cells; GSK-3, glycogen synthase kinase 3; TGF-β, transforming growth factor-β; OSM, oncostatin M.

(Trefts et al., 2017; Ober and Lemaigre, 2018). Therefore, in the induction of HLCs *in vitro*, from the initial attempt to stimulate cell differentiation by adding a certain proportion of xenobiotics, in recent years, increasing researches also take into account the interaction between cells and cells and the extracellular matrix. The development from monolayer to multilayer differentiation and even multicellular culture has promoted the maturation of HLCs *in vitro* significantly (Kaserman and Wilson, 2017; Tomizawa et al., 2017; Blau and Miki, 2019; Mun et al., 2019).

3.1 Chemical Approach, Adding Exogenous Substances

Using different proportions of cytokines and growth factors based on activation or inhibition of signals on a regular basis is the basic induction method of generating HLCs *in vitro* (**Figure 3**). Generally, totipotent cells need to go through three stages to differentiate into HLCs in natural state (**Table 1**). Activin A acts via BMP signaling pathway, which often is coupled with Wnt3a during the highly efficient induction of definitive endoderm from pluripotent stem cells (Hay et al., 2008; Mitani et al., 2017; Si-Tayeb et al., 2010). And this process is considered to be the premise of formation of available HLCs *in vitro*. Hepatic nuclear factor (HGF), epidermal growth factor (EGF), FGF, and other growth factors are commonly used, which mainly promote the differentiation of endodermal cells into hepatocytes and inhibit the differentiation of non-hepatocyte cells (Raoufil et al., 2015; Vojdani et al., 2015; Kaserman and Wilson, 2017). In the process of HLCs generation, the key is to promote and induce the mature phenotype of cells, which determines the authenticity and safety of the experiments based on it. Generally, dexamethasone (DEX), oncostatin M (OSM) are often added at the mature stage to increase the expression of maturation HLCs genes and enhance their functions (Tomizawa et al., 2017). OSM is a key factor involved in the development and maturation of fetal liver, and OSM can also promote hepatic progenitor cells to hepatocyte

maturation when adult liver injured (Kamiya et al., 1999; Okaya et al., 2005). *In vitro* culture, the addition of OSM combined with DEX which is prominent in inducing the expression of cytochrome enzyme in hepatocytes, can significantly increase hepatic protein synthesis was demonstrated (Lindley et al., 2002; Chivu et al., 2009; Zhang et al., 2012). The use of cytokines to induce hepatocyte formation is a classic method with high success rates, but this technique is often accompanied by the high costs and poor efficiency, and cannot meet clinical needs. Obviously, the induction of HLCs only with growth factors is no longer a routinely induction pathway because of its high cost and long time (about 15–28 days). However, this method is still as the basic idea to combined with other improved methods for yielding HLCs.

Small molecules, economic and effective substitutes for cytokines, can modulate gene expression and epigenetic modifications, accelerate the differentiation process, and promote maturation in hepatocytes (Du et al., 2018; (Qin et al., 2018; Tasnim et al., 2015) (**Table 2**). The chemical inhibitors GSK-3β, CHIR99021 and 6-bromo-indirubin-3′-oxime can activate Wnt signaling, regulate SOX17 expression, and promote dedifferentiation (Tasnim et al., 2015; Xu et al., 2015; Huang et al., 2017). The use of CHIR99021 reduce concentrations of activin A without affecting the differentiation rate of endoderm (Farzaneh et al., 2018). Sodium butyrate and valproic acid are histone deacetylation inhibitors that can promote the differentiation of definitive entoderm into liver-specific cells (Kondo et al., 2014; Panta et al., 2019). Trichostatin A, 5-aza, and nanomycin A, all of which are epigenetic modifiers, can be employed to induce differentiation of HLCs (Seeliger et al., 2013; Cipriano et al., 2017; Nakamae et al., 2018). FH1 and FPH1 have been used to replace HGF and OSM, respectively, to promote hepatocyte maturation. When used in conjunction with A83-01, dexamethasone, and hydrocortisone, the rate of cell differentiation was increased to 67.7% (37.1% in the cytokines cocktail group) (Shan et al., 2013; Du et al., 2018).

Much controversy exists regarding the use of dimethyl sulfoxide (DMSO); in particular, its dose may affect the differentiation results. Indeed, studies have shown that 0.1% DMSO can accelerate the morphological differentiation of stem cells, whereas 1% or 0.5% DMSO can enhance the differentiation of liver specificity (Siller et al., 2015; Alizadeh et al., 2016). Contrary to this conclusion, Wang et al. pointed out that the differentiation efficiency of cells was not affected with the use of DMSO (Wang et al., 2019). Nevertheless, as a sulfur-containing organic compound, DMSO can interact with protein hydrophobic groups, resulting in protein denaturation, affecting cell metabolism and free radical scavenging, which also contribute to its controversial use.

In brief, exogenous substances are added to simulate cytochemical signals and the paracrine mechanism of cell development *in vivo*. The application of classical cytokines to small molecules is not only an innovative, simplified induction method but also the embodiment of deep insight into cell development and differentiation. Although the induction method involving small molecules is simple and cost-effective and can even be used to replace growth factors, screening an effective small molecule is a time- and money-intensive process (Siller et al., 2015). Generally, a mixture of growth factors and small molecules has been shown to effectively induce directional hepatic differentiation from stem cells. However, this approach still suffers from challenges in finding the most appropriate mixture proportion once the culture system becomes complex, such as the need to regulate the fate of different cell types at the same time.

3.2 Culture System

It is also important to provide appropriate mechanical stimulation and growth space for cells to further promote differentiation and maturation. Therefore, a number of studies have sought to change the physical environment of cell growth, including the matrix, oxygen concentration, and flow effect, using different culture systems.

3.2.1 Spheroid Culture

Spheroid cultures involve the self-aggregation of cells in static culture systems, such as low-adhesion culture plates or suspension cultures, resulting in the formation of cell spheres. The spatial distribution formed by the cells in the sphere is conducive to the extension of the three-dimensional (3D) structure of the cells that can show the function of the cells better. Meanwhile, the cells separated from the single mode of monolayer growth in the dish can be more beneficial for absorption and exchange of nutrients and promote the maturation of HLCs *in vitro* (Lauschke et al., 2016; Choi et al., 2018). Studies have shown that HLCs in spheroid culture show increased expression levels of liver-specific genes, cytochrome enzymes, and esterase, with the appearance of bile canaliculi (Kim et al., 2015; Choi et al., 2018). However, the size of the aggregates formed by HLCs affects nutrient exchange and signal reception by cells in the sphere, thus affecting their subsequent differentiation (Meier et al., 2017). Extremely small spheroids result in the loss of cells if there is fluid shear stress in the culture. Large-sized spheroids may exhibit issues regarding the diffusion of oxygen and metabolism of substances in cells within the spheroids, resulting in inconsistent differentiation of the whole spheroid (Farzaneh et al., 2018). Recently, Zeinab et al. placed particles containing growth factors in the center of such spheres to ensure an evenly distributed release of growth factors, thereby reducing the otherwise uneven absorption of nutrients at the center of the sphere (Heidariyan et al., 2018).

3.2.2 Organoid Culture

Organoid cultures, comprising parenchymal cells along with one (or more) mesenchymal cell types, reproduce primary tissues more accurately and incorporate more of the original developmental processes of cells (Koike et al., 2019). Compared with spheroid cultures, liver organoids are superior in terms of cell diversity and long-term culture *in vitro* (Mun et al., 2019). The effective microvascular structure formed by organoids can provide oxygen and nutrients to the cells in the center, thus improving the maturity of organoids and prolonging

the culture time *in vitro*. Organoids with microstructures and microvasculature show irreplaceable advantages in recapitulating organogenesis and as the alternative treatment for organ failure (Takebe et al., 2017; Koike et al., 2019). At present, the use of organoids is the most widespread method to implant cells in Matrigel domes along with different cytokines to promote differentiation. However, the need for an extracellular matrix (e.g., Matrigel) to maintain long-term culture introduces undefined components, making it difficult to reproduce appropriate culture conditions. In addition, the size of organoids formed by this method is limited, and it is still a simplified organ compared to the native tissue with complex architecture and cellular diversity (Brassard et al., 2021). Although the continuous constructional improvements of organoid platforms are gaining momentum and result in improved physiological interactions between different systems (e.g., immune system and vascular system), cultivating multiple cell types on a single platform is still a challenge. Furthermore, effective replication of the cellular diversity of the liver is a time- and money-consuming process (Harrison SP et al., 2021; Shiota et al., 2021).

3.2.3 Culture Based on Hydrogel

Hydrogels are a type of polymer that can swell in water, providing an extracellular matrix by coating culture dishes, there by simulating the physiological growth of cells and promoting the diffusion of nutrients and cellular growth factors. As a biomaterial, hydrogels also play a non-negligible role in regulating cell proliferation, activity, and differentiation when they become part of the microenvironment of culture systems (Lutolf and Hubbell, 2005; Biggs et al., 2010). Hydrogels possess beneficial inherent chemical properties, as well as ideal wettability, roughness, and stiffness, which may affect cell growth, adhesion, migration, and apoptosis (Gentile et al., 2010; Slepicka et al., 2015). Hydrogels are classified into natural and synthetic polymer hydrogels, depending on their source. Natural hydrogels include alginate, collagen, and gelatin, while synthetic polymers include polyacrylamide (Toivonen et al., 2016; Luo et al., 2018; Ma and Huang, 2020).

A natural hydrogel derived from the decellularized extracellular matrix (ECM) of animal liver tissue not only provides a complex scaffold structure but also preserves the active substances present in it, including collagen, fibronectin, and glycosaminoglycans, as well as HGF, bFGF and other growth factors, in the cell growth microenvironment (Wang et al., 2016; Lorvellec et al., 2017; Wang et al., 2018). Spheroids formed by stem cells in liver ECM hydrogels have a smooth surface and are homogeneous in size (Toivonen et al., 2016). This method promotes the expression of maturation genes, such as *ALB* and *CYP3A4*, in HLCs, while effectively reducing the expression of *AFP* (Wang et al., 2016). However, polypeptides in natural hydrogels (e.g., collagen type I) contain animal-sourced antigens; this characteristic reduces their biological safety and thus limits their clinical applications. Recyclable mixed hydrogels with stable chemical properties and the plant-derived biomaterials known as cellulose nanofibrils, which are nontoxic, biocompatible, and biodegradable, have gained attention recently (Chitrangi et al., 2017; Poorna et al., 2021).

Polymeric synthetic hydrogels have similar structures and properties to natural ECM, providing suitable mechanical simulation and adhesion sites for the formation and maturation of HLCs (Yamazoe et al., 2013; Mahmoodinia Maymand et al., 2017). Common scaffold materials include poly L-lactic acid, polyether sulfone, and polycaprolactone. Because of the difference in the synthesis process and material source, cell adhesion, growth, and differentiation are affected (Biggs et al., 2010). Thus, aligned polyethersulfone synthesized by electrospinning technology is more conducive to the differentiation of HLCs and increases the expression of CYPs than random polyethersulfone (Mahmoodinia Maymand et al., 2018); this difference may be attributed to the fact that orderly arrangement of materials is beneficial for the formation of highly ordered tissue assemblies. Furthermore, compared with single polymers, hybrid scaffolds have better biocompatibility and material properties and can effectively improve the phenotype of HLCs and maintain phenotype stability *in vitro* (Mahmoodinia Maymand et al., 2017; Mobarra et al., 2019). For example, mixed scaffolds comprising poly L-lactic acid and collagen-I have a clear fiber structure, which can improve the maturation of hepatocytes and simplify the differentiation process (Wang et al., 2016).

Hydrogels can be used for single-layer cultures or covered with the same or different matrices to form a so-called sandwich culture (Bi et al., 2006). Sandwich culture promotes cell growth by maintaining material exchange on top of the substrate and a stable cell culture *in vitro,* providing an effective hepatotoxicity prediction model (Bi et al., 2006; Sakai et al., 2019). Unfortunately, this method is limited by the inability to remove apoptotic cells. Furthermore, an obvious shortcoming is that the extract of proteins from cells always mixes with exogenous proteins present in polypeptide-based hydrogels, leading to experimental difficulties.

3.2.4 Hydrogels in 3D Bioprinting

The controllable viscosity and water storage ability of hydrogels, as well as excellent cytocompatibility, make then the ideal choice for 3D bioprinting technology (Irvine and Venkatraman, 2016). Bio-inks composed of hydrogels and cells allow the replication of functional organs with tissue structure during printing; moreover, the location of cells can be preset in order to simulate natural tissues more accurately and show better therapeutic effects in disease treatment (Wust et al., 2011; Brassard et al., 2021). It is expected that HLCs are more mature both in liver phenotype and function after incubation on 3D-printing scaffolds (Kang et al., 2018). As a vital part of 3D printing, hydrogels can not only provide temporary residence for the isolated cells but also stabilize cells in the printing process to avoid thermal and mechanical damage and ensure the survival rate of cells (Belk et al., 2020). Indeed, potential pollution in the process of *in vitro* printing and the product damage owing to toxic particles produced by the materials, cannot be ignored. Notably, the

effects of material factors on cell differentiation should also be controlled.

3.2.5 Bioreactor

Bioreactors can comprehensively simulate microenvironments suitable for hepatocyte growth *in vivo* and enable scaling-up of the cell culture system (Ardalani et al., 2019; Yamashita, et al., 2018). The bioreactor is equipped with parameter setting systems, which can realize the real-time monitoring and adjustment of temperature, oxygen concentration and shear force in the incubator. By enabling fluid flow in the culture medium, simulating the flow in peripheral blood vessels experienced by hepatocytes *in vivo*, the cells are always exposed to consistent concentrations of nutrients and oxygen (Yen et al., 2016; Kehtari et al., 2018). Such dynamic culture systems can remove unhealthy cells with weak adhesion and dispose of cellular metabolites. For example, microfluidic-based biochips provide cells with a stable fluid-flow environment (Jang et al., 2019). The presence of a flow effect is expected to not only to improve the maturation of HLCs, but also to increase the levels of CYP1A2 activity. Furthermore, the effect of two-sided flow on cells is greater than that of one-sided flow set-ups. HLCs express increased levels of phase I and II enzymes, as well as undergo bile duct formation (Jang et al., 2019). Compared with static cell culture, ESCs cultured in stirred bioreactors can function as more mature HLCs, exhibiting upregulated liver gene mRNA transcripts and enhanced liver functionality (Park et al., 2014). In addition, bioreactors can maintain a relatively constant oxygen concentration in long-term culture. Research has demonstrated that the concentration of oxygen around cells can have a large impact on the state of cells (van Wenum et al., 2018; Kimura et al., 2019). IPSCs cultured under high oxygen levels differentiate into definitive endoderm more efficiently, and the expression of albumin and cytochrome enzymes in HLCs is significantly improved (Kimura et al., 2019). High oxygen (40%) conditions also promote the maturation of HLCs (van Wenum et al., 2018). However, Zhi found that the effects of hypoxia on liver differentiation depend on the duration of treatment, because short-term (24 h) hypoxic (10% O_2) pretreatment can also increase hepatic gene expression and glycogen storage (Zhi et al., 2018).

Bioreactors enable simultaneous co-culture of various cell types. It is well known that nonparenchymal liver cells, such as endothelial sinus, Kupffer, hepatic stellate, and bile duct cells, play important roles in the process of liver development by secreting cytokines or contacting hepatocytes directly (Kitade et al., 2016). Co-culture with non-liver cells can prolong the culture time of hepatocytes *in vitro* and maintain the function of HLCs when cultured together with MSCs (Rebelo et al., 2017). MSCs not only provide signal transduction for HLCs, but also protect the spheroid from shear stress.

Microbioreactor represented by microfluidic biochips require low cost but high precision; therefore, they are usually used for high-throughput drug screening but not for large-scale cell preparation. Large bioreactors can increase cell production, especially when producing clinical quantities of cells (Tandon et al., 2013; Samal et al., 2019). However, because cells adhere to capillaries filled with nutrients and oxygen, the rate of perfusion and the properties of substances affect the efficiency of cellular metabolite exchange (Meier et al., 2017). Therefore, adjusting parameter variation to achieve the ideal differentiation effect *in vitro* has become one of the challenges in the popularization and application of bioreactors. Nevertheless, the use of bioreactors is still anticipated to become widespread owing to the quantitative advantage of cell culture.

3.3 Blastocyst Complementation

Although, to some extent, *in vitro* differentiation has been mimicking all the induction cues required for liver development *in vivo*, the immature and complex production processes are incompatible, resulting in a lag in clinical transplantation applications. Differentiation is optimally induced *in vivo*, where the host can provide all factors and conditions for cell development. Therefore, blastocyst complementation technology is used to confer a vacant developmental niche in the host via gene knockout, so as to provide a suitable growth environment for stem cells. Finally, the stem cells can compensate for the developmental vacancies and produce derived organs from donor cells (Wu et al., 2017; De Los Angeles et al., 2018; Crane et al., 2019). Using this strategy, human organs such as the pancreas, kidney, skeletal muscle, and liver, have been successfully derived from rodents and large non-rodents (Goncalves et al., 2008; Kobayashi et al., 2010; Usui et al., 2012; Matsunari et al., 2013). Recently, it was found that in the animal model of liver development disorder caused by deletion of the *HHEX* gene, normal liver could develop after blastomere supplementation in the embryonic stage; this result suggests that patient-derived iPSCs can be used to derive the mature liver tissue in some large animals suitable for *in vivo* transplantation (Matsunari et al., 2020).

3.4 Genetic Manipulation

Changing the expression of specific genes and introducing exogenous ones represent direct and effective strategies to regulate the function of differentiated HLCs *in vitro* (**Table 3**). The specific expression of target genes in host cells can be realized through a virus delivery system. For example, overexpression of liver-enriched transcription factors (*HNF4α* and *HNF1α*) and forkhead box (*FOXa2* and *FOXa3*) was found to shorten stem cell differentiation time, improve differentiation efficiency, and promote HLC maturation (Takayama et al., 2012; Hu et al., 2016; Hanawa et al., 2017). In addition, the use of adenovirus as a vector to transduce *ATF5*, *c/EBPα*, and *Prox1*, the three important mature hepatocyte transcription factors, into HLCs induced by traditional growth factors for 25 days, led to upregulated expression levels of liver markers, such as drug-metabolizing enzymes and liver cell metabolite transporters (Nakamori et al., 2016). Indeed, this genomic non-integration method has advantages for adjusting the poor metabolic function of HLCs, because it exhibits high transfection efficiency without the risk of insertion mutation.

Another approach is represented in the hepatic direct reprogramming, that is, human somatic cells bypass the induced pluripotent stage and directly reprogram into

TABLE 3 | Application of gene editing technology in human HLCs formation.

Method of modification	Aim	HLCs generation (%)	Advantages	Limits	Example of cell types	Ref.
Lentivirus	overexpression of *HNF4α*	~28%	induces HLCs directly and saves time and materials	genomic integration poor transfection efficiency	immortalized BM-MSCs	Hu et al. (2016)
	overexpression of *HNF4α-1D*	N.D.	promotes definitive endoderm differentiation	genomic integration poor transfection efficiency	iPSCs	Hanawa et al. (2017)
	overexpression of *FOXa3, HNF1a,* and *HNF4a*	~20%	shows the function of mature hepatocytes	genomic integration proliferation arrest	HFF1	Huang et al. (2014)
	overexpression of *FOXa3, HNF1a, HNF4a, ATF5, PROX1,* and *c/EBPα*	~90%	generates functional HLCs efficiently and reproducibly	genomic integration poor transfection efficiency	HEFs	Du et al. (2014)
	overexpression of *FOXa3, HNF1a,* and *GATA4*	N.D.	a non-invasive way as seed cells for reprogramming	genomic integration poor transfection efficiency	UCs	Wu et al. (2020)
Adenovirus	overexpression of *FOXa2* and *HNF1α*	N.D.	promotes definitive endoderm differentiation and improves functionality of HLCs	instability of transgene expression	iPSCs and ESCs	Takayama et al. (2012)
	overexpression of *ATF5, c/EBPα,* and *PROX1*	N.D.	enhances the hepatic functions of HLCs	instability of transgene expression	iPSCs	Nakamori et al. (2016)
Transfect microRNA mimics	overexpression of miR-122, miR148a, miR-424, miR-542-5p and miR-1246	N.D.	induces HLCs directly and saves time and materials	long-term effect undefined	UC-MSCs	Zhou et al. (2017)
Electroporation	overexpression of miR-106a, miR-574-3p and miR-45	N.D.	induces HLCs directly and save times and materials	cell damage	UC-MSCs	Khosravi et al. (2018)
CRISPR/Cas9 system	PXR-mCherry	N.D.	can be used for identifying factors that increase PXR-mediated drug metabolism and hepatocyte proliferation	hard technique	iPSCs	Kim et al. (2018)
	target to *CYP3A4* locus	N.D.	realizes enrichment of high-functioning human iPSC-derived HLCs	hard technique	iPSCs	Takayama et al. (2018)

Abbreviations: BM-MSCs, bone marrow-derived mesenchymal stem cells; ESCs, embryonic stem cells; iPSCs, induced pluripotent stem cells; UC-MSCs, umbilical cord-derived mesenchymal stem cells; HEFs, human embryonic fibroblasts; HFF1, human fetal limb fibroblasts, UCs, urinary epithelial cells; N.D., no data.

functional HLCs (Du et al., 2014; Huang et al., 2014; Wu et al., 2020) (**Table 3**). At present, induced functional HLCs have been successfully generated, by introducing a combination of some liver fate determined factors (e.g., *FOXa3, HNF1a, HNF4a,* and *GATA4*), from fibroblasts and urine epithelial cells (Huang et al., 2014; Wu et al., 2020). In addition, for further promoting the maturation of HLCs and their application in drug development, the overexpression of maturation factors (*ATF5, PROX1,* and *c/EBPα*) can greatly improve the level of drug metabolism enzymes, even comparable to human hepatocytes (Du et al., 2014). Although this approach is beneficial for the short-term induction of a large number of HLCs, it is known that liver development is a continuous change process, indicating that its network of expression regulation is continuous and complex (Ober and Lemaigre, 2018). Therefore, it is difficult to prove whether the constant expression of some genes can truly represent the differentiation of hepatocytes.

MicroRNAs (miRNAs), which regulate gene expression at the post-transcriptional level during cell development and growth, play significant roles during HLC induction. Zhou et al. found that a combination of five miRNAs (miR-122, miR148a, miR-424, miR-542-5p, and miR-1246) in cord mesenchymal stem cells could induce functional hepatocytes within 7 days without the addition of cytokines, providing a new strategy for *in vitro* induction of HLCs (Zhou et al., 2017). Among them, mir-122, as a liver-specific miRNA, exhibits the highest expression in the adult liver, accounting for approximately 70% of all cloned miRNAs. It plays an important role in the regulation of liver function and pathological development (Girard et al., 2008; Hu et al., 2012). Studies have shown that miR-122 can stimulate the expression of hepatocyte-specific genes and most hepatocyte-enriched transcription factors to form a positive feedback loop and induce hepatocyte differentiation *in vitro* (Laudadio et al.,

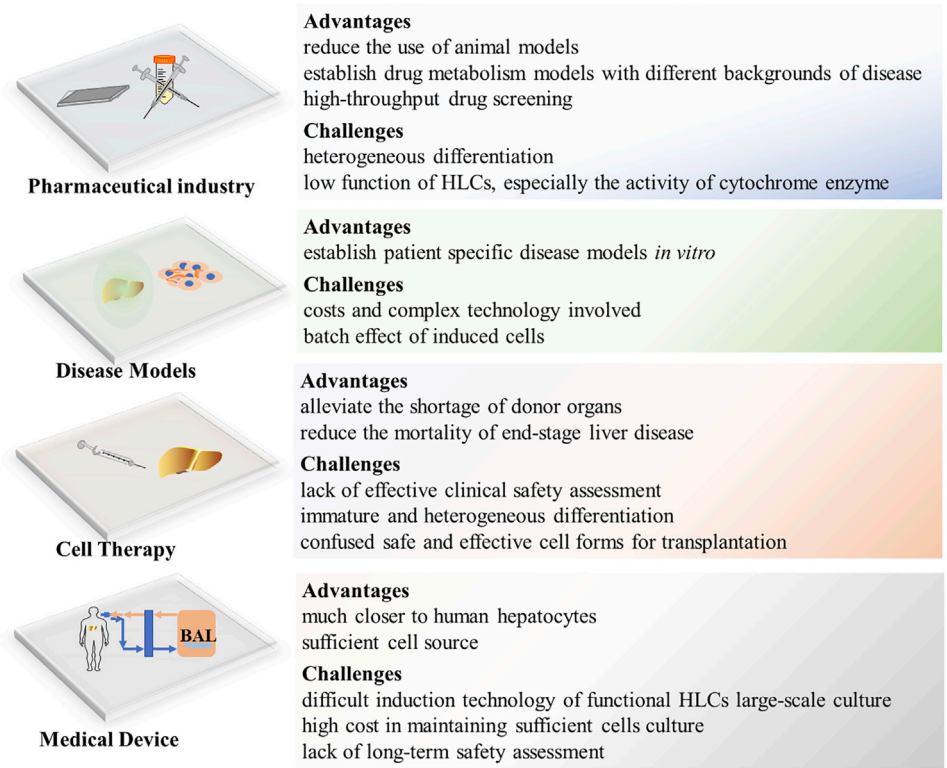

FIGURE 4 | Applicaton and Challenges of HLCs, BAL, bioartificial liver.

2012). Overexpression of miR-106a, miR-574-3p, and miR-451 in cells resulted in formation of HLCs in 28 days; these HLCs expressed higher levels of ALB, cytokeratin (CK18), and HNF4α compared with cells induced by traditional cytokines (Khosravi et al., 2018). Moreover, the overexpression of miR-382 in rat hepatocyte progenitor cells promoted the maturation of HLCs (Zheng et al., 2018). In addition, miRNA induction methods usually require a combination of a variety of miRNAs; however, the network of miRNAs regulating gene expression is very complex. This characteristic increases the cost of the experiment because of the need for constant testing of new combinations to find an ideal one.

Overexpression of certain maturation genes in immature HLCs can optimize their liver-specific functions. Studies have shown that iPSC genome editing can be used to improve the expression of cytochrome enzymes and obtain high-purity CYP3A4-like hepatocytes that are needed to evaluate the risks of candidate drugs (Takayama et al., 2018). The CRISPR/Cas9 system has been used to establish a hepatocyte line with high *PXR* expression, which could promote the expression of iPSC-derived hepatocyte cytochrome enzymes and enhance cell proliferation capacity (Kim et al., 2018).

As mentioned earlier, compared with the traditional method of inducing cells from an undifferentiated state into appointed cells step by step, direct transdifferentiation based on genetic operation and epigenetic regulation has a higher efficiency and shorter cycle. However, the expression instability and tumorigenicity caused by the inherent defects of virus transfection may lead to inconsistent differentiation, which manifests itself in the mixed expression of immature hepatocyte progenitor cells and mature hepatocytes (Orge et al., 2020). While it is easy to induce epithelial stromal transformation in long-term *in vitro* culture, phenotypic instability can lead to poor transplantation outcomes *in vivo* (Xue et al., 2016). Although this drawback may lead to the limited application of this method *in vivo*, its application in drug screening and disease modeling cannot be ignored.

4 APPLICATIONS AND CHALLENGES

4.1 Pharmaceutical Industry

Monolayer HLCs and organoid-derived HLCs provide high-throughput predictive models for drug screening and toxicity prediction and can become important drug research tools (Cayo et al., 2017; Shinozawa et al., 2021). In particular, HLCs in 3D culture show higher cytochrome enzyme activity and sensitivity to hepatotoxicants than those in 2D culture, as well as provide suitable platforms for drug screening (Lee et al., 2021). Meanwhile, special gene expression cell lines for scientific research can be established in combination with genetic manipulation technology. For example, *CYP2C19*-knockout human iPSC-derived HLCs can be used as a new

CYP2C19-deficient metabolism model for drug research (Deguchi et al., 2019). The use of HLCs as a drug-screening model *in vitro* has been reported to be efficient, safe, and ethical (Williams, 2018). At present, the immature function of HLCs poses a significant challenge in toxicology studies. Although genetic editing can enhance the expression of some cytochrome enzymes, it is impossible to fully cover the CYP450 system containing all phase I and phase II enzymes. Therefore, HLCs cannot fully reproduce the oxidation–reduction reaction during drug metabolism (**Figure 4**).

4.2 Disease Models

Disease modeling from HLCs is not limited by the ethical issues of cell origin, because the current reprogramming technology of iPSCs can be applied to most adult cells in the human body, including the easily available urine epithelial cells and hair follicle epithelial cells (Zhou et al., 2011; Xu et al., 2018). In addition, HLCs can be used to establish disease models based on genetic backgrounds (e.g., autosomal recessive hypercholesterolemia) or specific disease models, such as *in vitro* HBV, HCV infection, and CYP2C19-deficient metabolism models (Schwartz et al., 2012; Sakurai et al., 2017; Deguchi et al., 2019; Nikasa et al., 2021). Additionally, expandable liver organoids provide a more favorable research tool for further exploring the etiology and pathophysiology of disease as a whole, not only from damaged cells but also from changes in the microenvironment (Gomez-Mariano et al., 2020; Ramli et al., 2020; Shinozawa et al., 2021). Considering that the occurrence and development of disease involve crosstalk and interaction between various cells and multiple systems, recent research has established a steatohepatitis model using multicellular cultured organoids, which presented a continuous pathological process of steatohepatitis from inflammation to fibrosis *in vitro* (Kisseleva and Brenner, 2019; Ouchi et al., 2019). As an *in vitro* research tool, organoids are not only highly physiologically related but also maintain genetic stability during long-term culture (Fiorotto et al., 2019). However, the costs and complex technology involved in establishing and maintaining organoid cultures are causes of the limited research. In addition, the batch effect caused by varying environments and culture durations affect the experimental results (Luce et al., 2021) (**Figure 4**).

4.3 Cell Therapy

HLCs are considered the most promising cells for liver regeneration and tissue engineering. Animal experiments have demonstrated that HLC transplantation in mice with liver injury significantly improves liver function and promotes liver regeneration (Park et al., 2019) and human iPSC combined with gene correction can induce normal hepatocytes to realize autologous cell therapy for patients with metabolic diseases (Yusa et al., 2011). Exploratory applications of HLCs in clinical treatments have shown satisfactory results (Mohamadnejad et al., 2010; Amer et al., 2011). Recently, liver organoid transplantation and cell sheet technology provide advanced methods to solve the loss in cell transplantation and improves therapeutic effects (Nagamoto et al., 2016; Tsuchida et al., 2020; Imashiro and Shimizu, 2021). However, cell therapy requires sufficient number of HLCs (2×10^8/per injection) (Amer et al., 2011), which takes a certain time to extend such number of HLCs *in vitro*. But for patients with acute liver failure, 1 min less waiting will give them more chance to live. Therefore, it is very important to establish HLCs cell bank to store HLCs. Before that, we still need to solve the problems of low activity after long-term culture and cryopreservation of HLCs (**Figure 4**).

4.4 Medical Device

In bioartificial liver (BAL) research, there are mainly two cell lines employed; hepatoma cell lines and porcine hepatocytes, which have achieved ideal results. However, expandable PHHs may be more in accord with the characteristics of human liver metabolism and with ethical requirements. Compared with hepatoma cell lines, HLCs exhibit similarities to PHHs and show very substantial curative effects in treatment of a porcine acute liver failure (ALF) model (Shi et al., 2016). Recently, Li et al. developed a new BAL embedded with expandable liver progenitor-like cells from human primary hepatocytes for the treatment of an ALF porcine model, and the results showed that BAL attenuates liver damage, ameliorates inflammation, and enhances liver regeneration (Wei-Jian Li et al., 2020). Although stem cell-derived HLCs are considered the ideal cell source second to primary hepatocytes, their translation from laboratory to clinical application is limited by the difficult induction technology of functional HLCs large-scale culture and the high cost involved. In addition, whether BAL can be reused is still unclear because there is a lack of evaluation of the functional changes of HLCs before and after exposure to patient serum.

5 CONCLUSION

In conclusion, great progress has been made to improve the induction and culture of HLCs *in vitro* and enhance their potential applications. The increasing experiments suggest that cell fate is not only related to chemical signal, but also the mechanical signals and structural support provided by the extracellular environment are the key points to promote functional cells. Organ is a 3D architecture composed of cells, which means that co-culture of multiple cells and reasonable spatial distribution of cells are conducive to maturation of organ. Admittedly, that the maturity of HLCs has been improved to a certain extent, but the operation steps and culture system inevitably become complex, and there is no standard induction scheme to produce uniformly differentiated HLCs, which confuses the choice of induction protocol and rare replication of the same results. Although this review discussed fundamental and advanced methods in culturing HLCs, it inevitably puts too much focus on *ex vivo* research. Exploring the process of culturing functional hepatocytes *in vitro* will contribute to uncover the regulatory mechanism of cell fate and the interaction between microenvironment and cells, which is basic clues for disease modeling and personalized medicine. However, before the widespread application of HLCs in clinical treatment, there is still

much research and investigation required, especially in terms of the safety of *in vivo* treatment.

AUTHOR CONTRIBUTIONS

YX, Original draft preparation. XL, Conceptualization, Funding acquisition. JY and W-LJ Review and Editing. L-FR, Data curation. All authors have approved the final article.

FUNDING

This work was supported by Major Science and Technology Projects of Gansu Province (No. 1602FKDA001), the Health Industry Research Program (No. GSWSKY-2015-49), Gansu Science and Technology Program (No. 18JR2TA018) and the National Natural Science Foundation of China (Nos. 82060119 and 32160230).

REFERENCES

Alizadeh, E., Zarghami, N., Eslaminejad, M. B., Akbarzadeh, A., Barzegar, A., and Mohammadi, S. A. (2016). The Effect of Dimethyl Sulfoxide on Hepatic Differentiation of Mesenchymal Stem Cells. *Artif. Cell Nanomedicine, Biotechnol.* 44 (1), 157–164. doi:10.3109/21691401.2014.928778

Amer, M.-E. M., El-Sayed, S. Z., El-Kheir, W. A., Gabr, H., Gomaa, A. A., El-Noomani, N., et al. (2011). Clinical and Laboratory Evaluation of Patients with End-Stage Liver Cell Failure Injected with Bone Marrow-Derived Hepatocyte-like Cells. *Eur. J. Gastroenterol. Hepatol.* 23 (10), 936–941. doi:10.1097/MEG.0b013e3283488b00

Ardalani, H., Sengupta, S., Harms, V., Vickerman, V., Thomson, J. A., and Murphy, W. L. (2019). 3-D Culture and Endothelial Cells Improve Maturity of Human Pluripotent Stem Cell-Derived Hepatocytes. *Acta Biomater.* 95, 371–381. doi:10.1016/j.actbio.2019.07.047

Belk, L., Tellisi, N., Macdonald, H., Erdem, A., Ashammakhi, N., and Pountos, I. (2020). Safety Considerations in 3D Bioprinting Using Mesenchymal Stromal Cells. *Front. Bioeng. Biotechnol.* 8, 924. doi:10.3389/fbioe.2020.00924

Bell, C. C., Lauschke, V. M., Vorrink, S. U., Palmgren, H., Duffin, R., Andersson, T. B., et al. (2017). Transcriptional, Functional, and Mechanistic Comparisons of Stem Cell-Derived Hepatocytes, HepaRG Cells, and Three-Dimensional Human Hepatocyte Spheroids as Predictive *In Vitro* Systems for Drug-Induced Liver Injury. *Drug Metab. Dispos* 45 (4), 419–429. doi:10.1124/dmd.116.074369

Berger, D. R., Ware, B. R., Davidson, M. D., Allsup, S. R., and Khetani, S. R. (2015). Enhancing the Functional Maturity of Induced Pluripotent Stem Cell-Derived Human Hepatocytes by Controlled Presentation of Cell-Cell Interactionsin Vitro. *Hepatology* 61 (4), 1370–1381. doi:10.1002/hep.27621

Bi, Y.-a., Kazolias, D., and Duignan, D. B. (2006). Use of Cryopreserved Human Hepatocytes in sandwich Culture to Measure Hepatobiliary Transport. *Drug Metab. Dispos* 34 (9), 1658–1665. doi:10.1124/dmd.105.009118

Biggs, M. J. P., Richards, R. G., and Dalby, M. J. (2010). Nanotopographical Modification: a Regulator of Cellular Function through Focal Adhesions. *Nanomedicine: Nanotechnology, Biol. Med.* 6 (5), 619–633. doi:10.1016/j.nano.2010.01.009

Blau, B. J., and Miki, T. (2019). The Role of Cellular Interactions in the Induction of Hepatocyte Polarity and Functional Maturation in Stem Cell-Derived Hepatic Cells. *Differentiation* 106, 42–48. doi:10.1016/j.diff.2019.02.006

Brassard, J. A., Nikolaev, M., Hübscher, T., Hofer, M., and Lutolf, M. P. (2021). Recapitulating Macro-Scale Tissue Self-Organization through Organoid Bioprinting. *Nat. Mater.* 20 (1), 22–29. doi:10.1038/s41563-020-00803-5

Calabrese, D., Roma, G., Bergling, S., Carbone, W., Mele, V., Nuciforo, S., et al. (2019). Liver Biopsy Derived Induced Pluripotent Stem Cells Provide Unlimited Supply for the Generation of Hepatocyte-like Cells. *PLoS One* 14 (8), e0221762. doi:10.1371/journal.pone.0221762

Cardinale, V., Wang, Y., Carpino, G., Cui, C.-B., Gatto, M., Rossi, M., et al. (2011). Multipotent Stem/progenitor Cells in Human Biliary Tree Give Rise to Hepatocytes, Cholangiocytes, and Pancreatic Islets. *Hepatology* 54 (6), 2159–2172. doi:10.1002/hep.24590

Carpino, G., Cardinale, V., Gentile, R., Onori, P., Semeraro, R., Franchitto, A., et al. (2014). Evidence for Multipotent Endodermal Stem/progenitor Cell Populations in Human Gallbladder. *J. Hepatol.* 60 (6), 1194–1202. doi:10.1016/j.jhep.2014.01.026

Cayo, M. A., Mallanna, S. K., Di Furio, F., Jing, R., Tolliver, L. B., Bures, M., et al. (2017). A Drug Screen Using Human iPSC-Derived Hepatocyte-like Cells Reveals Cardiac Glycosides as a Potential Treatment for Hypercholesterolemia. *Cell Stem Cell* 20 (4), 478–489. doi:10.1016/j.stem.2017.01.011

Chen, G., Gulbranson, D. R., Hou, Z., Bolin, J. M., Ruotti, V., Probasco, M. D., et al. (2011). Chemically Defined Conditions for Human iPSC Derivation and Culture. *Nat. Methods* 8 (5), 424–429. doi:10.1038/nmeth.1593

Chen, J., Chen, L., Zern, M. A., Theise, N. D., Diehl, A. M., Liu, P., et al. (2017). The Diversity and Plasticity of Adult Hepatic Progenitor Cells and Their Niche. *Liver Int.* 37 (9), 1260–1271. doi:10.1111/liv.13377

Cheng, X., Tiyaboonchai, A., and Gadue, P. (2013). Endodermal Stem Cell Populations Derived from Pluripotent Stem Cells. *Curr. Opin. Cel Biol.* 25 (2), 265–271. doi:10.1016/j.ceb.2013.01.006

Chinnici, C. M., Pietrosi, G., Iannolo, G., Amico, G., Cuscino, N., Pagano, V., et al. (2019). Mesenchymal Stromal Cells Isolated from Human Fetal Liver Release Soluble Factors with a Potential Role in Liver Tissue Repair. *Differentiation* 105, 14–26. doi:10.1016/j.diff.2018.12.001

Chitrangi, S., Nair, P., and Khanna, A. (2017). Three-dimensional Polymer Scaffolds for Enhanced Differentiation of Human Mesenchymal Stem Cells to Hepatocyte-like Cells: a Comparative Study. *J. Tissue Eng. Regen. Med.* 11 (8), 2359–2372. doi:10.1002/term.2136

Chivu, M., Dima, S. O., Stancu, C. I., Dobrea, C., Uscatescu, V., Necula, L. G., et al. (2009). *In Vitro* hepatic Differentiation of Human Bone Marrow Mesenchymal Stem Cells under Differential Exposure to Liver-specific Factors. *Translational Res.* 154 (3), 122–132. doi:10.1016/j.trsl.2009.05.007

Choi, Y.-J., Kim, H., Kim, J.-W., Yoon, S., and Park, H.-J. (2018). Hepatic Esterase Activity Is Increased in Hepatocyte-like Cells Derived from Human Embryonic Stem Cells Using a 3D Culture System. *Biotechnol. Lett.* 40 (5), 755–763. doi:10.1007/s10529-018-2528-1

Cipriano, M., Correia, J. C., Camões, S. P., Oliveira, N. G., Cruz, P., Cruz, H., et al. (2017). The Role of Epigenetic Modifiers in Extended Cultures of Functional Hepatocyte-like Cells Derived from Human Neonatal Mesenchymal Stem Cells. *Arch. Toxicol.* 91 (6), 2469–2489. doi:10.1007/s00204-016-1901-x

Corbett, J. L., and Duncan, S. A. (2019). iPSC-Derived Hepatocytes as a Platform for Disease Modeling and Drug Discovery. *Front. Med.* 6, 265. doi:10.3389/fmed.2019.00265

Cotovio, J. P., and Fernandes, T. G. (2020). Production of Human Pluripotent Stem Cell-Derived Hepatic Cell Lineages and Liver Organoids: Current Status and Potential Applications. *Bioengineering* 7 (2), 36. doi:10.3390/bioengineering7020036

Crane, A. T., Aravalli, R. N., Asakura, A., Grande, A. W., Krishna, V. D., Carlson, D. F., et al. (2019). Interspecies Organogenesis for Human Transplantation. *Cel Transpl.* 28 (9-10), 1091–1105. doi:10.1177/0963689719845351

Dakhore, S., Nayer, B., and Hasegawa, K. (20182018). Human Pluripotent Stem Cell Culture: Current Status, Challenges, and Advancement. *Stem Cell Int.* 2018, 1–17. doi:10.1155/2018/7396905

De Los Angeles, A., Pho, N., and Redmond, D. E., Jr (2018). Generating Human Organs via Interspecies Chimera Formation: Advances and Barriers. *Yale J. Biol. Med.* 91 (3), 333–342.

Deguchi, S., Yamashita, T., Igai, K., Harada, K., Toba, Y., Hirata, K., et al. (2019). Modeling of Hepatic Drug Metabolism and Responses in CYP2C19 Poor Metabolizer Using Genetically Manipulated Human iPS Cells. *Drug Metab. Dispos* 47 (6), 632–638. doi:10.1124/dmd.119.086322

Du, C., Feng, Y., Qiu, D., Xu, Y., Pang, M., Cai, N., et al. (2018). Highly Efficient and Expedited Hepatic Differentiation from Human Pluripotent Stem Cells by Pure Small-Molecule Cocktails. *Stem Cel Res Ther* 9 (1), 58. doi:10.1186/s13287-018-0794-4

Du, Y., Wang, J., Jia, J., Song, N., Xiang, C., Xu, J., et al. (2014). Human Hepatocytes with Drug Metabolic Function Induced from Fibroblasts by

Lineage Reprogramming. *Cell Stem Cell* 14 (3), 394–403. doi:10.1016/j.stem.2014.01.008

Farnaz Sani, G., Kazemnejad, Somayeh., Ebrahimi, Sepideh., Mohamadpour, Masoomeh., Khanjani, Sayeh., Latifi, Mona., et al. (2016). Differentiation of Menstrual Blood Derived Stem Cell (MensSCs) to Hepatocyte-Liked Cell on Three Dimensional Nanofiber Scaffold: Poly Caprolacton (PCL). *J. Biomed. Sci. Eng.* 9 (9), 437–444. doi:10.4236/jbise.2016.9903910.4236/jbise.2016.94016

Farzaneh, Z., Najarasl, M., Abbasalizadeh, S., Vosough, M., and Baharvand, H. (2018). Developing a Cost-Effective and Scalable Production of Human Hepatic Competent Endoderm from Size-Controlled Pluripotent Stem Cell Aggregates. *Stem Cell Dev.* 27 (4), 262–274. doi:10.1089/scd.2017.0074

Fiorotto, R., Amenduni, M., Mariotti, V., Fabris, L., Spirli, C., and Strazzabosco, M. (2019). Liver Diseases in the Dish: iPSC and Organoids as a New Approach to Modeling Liver Diseases. *Biochim. Biophys. Acta (Bba) - Mol. Basis Dis.* 1865 (5), 920–928. doi:10.1016/j.bbadis.2018.08.038

Fu, G.-B., Huang, W.-J., Zeng, M., Zhou, X., Wu, H.-P., Liu, C.-C., et al. (2019). Expansion and Differentiation of Human Hepatocyte-Derived Liver Progenitor-like Cells and Their Use for the Study of Hepatotropic Pathogens. *Cell Res* 29 (1), 8–22. doi:10.1038/s41422-018-0103-x

Fusaki, N., Ban, H., Nishiyama, A., Saeki, K., and Hasegawa, M. (2009). Efficient Induction of Transgene-free Human Pluripotent Stem Cells Using a Vector Based on Sendai Virus, an RNA Virus that Does Not Integrate into the Host Genome. *Proc. Jpn. Acad. Ser. B Phys. Biol.* doi:10.2183/pjab.85.348

Gentile, F., Tirinato, L., Battista, E., Causa, F., Liberale, C., di Fabrizio, E. M., et al. (2010). Cells Preferentially Grow on Rough Substrates. *Biomaterials* 31 (28), 7205–7212. doi:10.1016/j.biomaterials.2010.06.016

Girard, M., Jacquemin, E., Munnich, A., Lyonnet, S., and Henrion-Caude, A. (2008). miR-122, a Paradigm for the Role of microRNAs in the Liver. *J. Hepatol.* 48 (4), 648–656. doi:10.1016/j.jhep.2008.01.019

Gómez-Mariano, G., Matamala, N., Martínez, S., Justo, I., Marcacuzco, A., Jimenez, C., et al. (2020). Liver Organoids Reproduce Alpha-1 Antitrypsin Deficiency-Related Liver Disease. *Hepatol. Int.* 14 (1), 127–137. doi:10.1007/s12072-019-10007-y

Gonçalves, M. A., Swildens, J., Holkers, M., Narain, A., van Nierop, G. P., van de Watering, M. J., et al. (2008). Genetic Complementation of Human Muscle Cells via Directed Stem Cell Fusion. *Mol. Ther.* 16 (4), 741–748. doi:10.1038/mt.2008.16

Hanawa, M., Takayama, K., Sakurai, F., Tachibana, M., and Mizuguchi, H. (2017). Hepatocyte Nuclear Factor 4 Alpha Promotes Definitive Endoderm Differentiation from Human Induced Pluripotent Stem Cells. *Stem Cel Rev Rep* 13 (4), 542–551. doi:10.1007/s12015-016-9709-x

Hansel, M. C., Gramignoli, R., Skvorak, K. J., Dorko, K., Marongiu, F., Blake, W., et al. (2014). The History and Use of Human Hepatocytes for the Treatment of Liver Diseases: the First 100 Patients. *Curr. Protoc. Toxicol.* 62, 14–1123. doi:10.1002/0471140856.tx1412s62 12

Haridhasapavalan, K. K., Raina, K., Dey, C., Adhikari, P., and Thummer, R. P. (2020). An Insight into Reprogramming Barriers to iPSC Generation. *Stem Cel Rev Rep* 16 (1), 56–81. doi:10.1007/s12015-019-09931-1

Harrison, S. P., Baumgarten, S. F., Verma, R., Lunov, O., Dejneka, A., and Sullivan, G. J. (2021). Liver Organoids: Recent Developments, Limitations and Potential. *Front. Med.* 8, 574047. doi:10.3389/fmed.2021.574047

Hay, D. C., Fletcher, J. F. J., Payne, C., Terrace, J. D., Gallagher, R. C. J., Snoeys, J., et al. (2008). Highly Efficient Differentiation of hESCs to Functional Hepatic Endoderm Requires ActivinA and Wnt3a Signaling. *Proc. Natl. Acad. Sci.* 105 (34), 12301–12306. doi:10.1073/pnas.0806522105

Heidariyan, Z., Ghanian, M. H., Ashjari, M., Farzaneh, Z., Najarasl, M., Rezaei Larijani, M., et al. (2018). Efficient and Cost-Effective Generation of Hepatocyte-like Cells through Microparticle-Mediated Delivery of Growth Factors in a 3D Culture of Human Pluripotent Stem Cells. *Biomaterials* 159, 174–188. doi:10.1016/j.biomaterials.2018.01.005

Hoffman, L. M., and Carpenter, M. K. (2005). Characterization and Culture of Human Embryonic Stem Cells. *Nat. Biotechnol.* 23 (6), 699–708. doi:10.1038/nbt1102

Hongisto, H., Vuoristo, S., Mikhailova, A., Suuronen, R., Virtanen, I., Otonkoski, T., et al. (2012). Laminin-511 Expression Is Associated with the Functionality of Feeder Cells in Human Embryonic Stem Cell Culture. *Stem Cel Res.* 8 (1), 97–108. doi:10.1016/j.scr.2011.08.005

Hu, J., Xu, Y., Hao, J., Wang, S., Li, C., and Meng, S. (2012). MiR-122 in Hepatic Function and Liver Diseases. *Protein Cell* 3 (5), 364–371. doi:10.1007/s13238-012-2036-3

Hu, X., Xie, P., Li, W., Li, Z., and Shan, H. (2016). Direct Induction of Hepatocyte-like Cells from Immortalized Human Bone Marrow Mesenchymal Stem Cells by Overexpression of HNF4α. *Biochem. Biophysical Res. Commun.* 478 (2), 791–797. doi:10.1016/j.bbrc.2016.08.026

Huang, C.-S., Lin, H.-C., Lu, K.-H., Wu, W.-W., Yang, Y.-C., Yang, Y.-P., et al. (2018). Generation of High Quality of Hepatocyte-like Cells from Induced Pluripotent Stem Cells with Parp1 but Lacking C-Myc. *J. Chin. Med. Assoc.* 81 (10), 871–877. doi:10.1016/j.jcma.2018.06.002

Huang, J., Guo, X., Li, W., and Zhang, H. (2017). Activation of Wnt/β-Catenin Signalling via GSK3 Inhibitors Direct Differentiation of Human Adipose Stem Cells into Functional Hepatocytes. *Sci. Rep.* 7, 40716. doi:10.1038/srep40716

Huang, P., Zhang, L., Gao, Y., He, Z., Yao, D., Wu, Z., et al. (2014). Direct Reprogramming of Human Fibroblasts to Functional and Expandable Hepatocytes. *Cell Stem Cell* 14 (3), 370–384. doi:10.1016/j.stem.2014.01.003

Imashiro, C., and Shimizu, T. (2021). Fundamental Technologies and Recent Advances of Cell-Sheet-Based Tissue Engineering. *Ijms* 22 (1), 425. doi:10.3390/ijms22010425

Irvine, S., and Venkatraman, S. (2016). Bioprinting and Differentiation of Stem Cells. *Molecules* 21 (9), 1188. doi:10.3390/molecules21091188

Jang, M., Kleber, A., Ruckelshausen, T., Betzholz, R., and Manz, A. (2019). Differentiation of the Human Liver Progenitor Cell Line (HepaRG) on a Microfluidic-based Biochip. *J. Tissue Eng. Regen. Med.* 13 (3), 482–494. doi:10.1002/term.2802

Kamiya, A., Kinoshita, T., Ito, Y., Matsui, T., Morikawa, Y., Senba, E., et al. (1999). Fetal Liver Development Requires a Paracrine Action of Oncostatin M through the Gp130 Signal Transducer. *EMBO J.* 18 (8), 2127–2136. doi:10.1093/emboj/18.8.2127

Kang, K., Kim, Y., Jeon, H., Lee, S. B., Kim, J. S., Park, S. A., et al. (2018). Three-Dimensional Bioprinting of Hepatic Structures with Directly Converted Hepatocyte-like Cells. *Tissue Eng. A* 24 (7-8), 576–583. doi:10.1089/ten.TEA.2017.0161

Kaserman, J. E., and Wilson, A. A. (2017). Protocol for Directed Differentiation of Human Induced Pluripotent Stem Cells (iPSCs) to a Hepatic Lineage. *Methods Mol. Biol.* 1639, 151–160. doi:10.1007/978-1-4939-7163-3_15

Katsuda, T., Kawamata, M., Hagiwara, K., Takahashi, R.-u., Yamamoto, Y., Camargo, F. D., et al. (2017). Conversion of Terminally Committed Hepatocytes to Culturable Bipotent Progenitor Cells with Regenerative Capacity. *Cell Stem Cell* 20 (1), 41–55. doi:10.1016/j.stem.2016.10.007

Katsuda, T., Matsuzaki, J., Yamaguchi, T., Yamada, Y., Prieto-Vila, M., Hosaka, K., et al. (2019). Generation of Human Hepatic Progenitor Cells with Regenerative and Metabolic Capacities from Primary Hepatocytes. *Elife* 8. doi:10.7554/eLife.47313

Katsuda, T., and Ochiya, T. (20191905). Chemically Induced Liver Progenitors (CLiPs): A Novel Cell Source for Hepatocytes and Biliary Epithelial Cells. *Methods Mol. Biol.*, 117–130. doi:10.1007/978-1-4939-8961-4_11

Kehtari, M., Zeynali, B., Soleimani, M., Kabiri, M., and Seyedjafari, E. (2018). Fabrication of a Co-culture Micro-bioreactor Device for Efficient Hepatic Differentiation of Human Induced Pluripotent Stem Cells (hiPSCs). *Artif. Cell Nanomedicine, Biotechnol.* 46 (Suppl. 2), 161–170. doi:10.1080/21691401.2018.1452753

Khosravi, M., Azarpira, N., Shamdani, S., Hojjat-Assari, S., Naserian, S., and Karimi, M. H. (2018). Differentiation of Umbilical Cord Derived Mesenchymal Stem Cells to Hepatocyte Cells by Transfection of miR-106a, miR-574-3p, and miR-451. *Gene* 667, 1–9. doi:10.1016/j.gene.2018.05.028

Kim, H., Kim, J.-W., Kim, S.-J., Choi, Y.-J., Kim, D.-S., and Park, H.-J. (2018). Generation of a PXR Reporter Human Induced Pluripotent Stem Cell Line (PXR-mCherry hiPSC) Using the CRISPR/Cas9 System. *Stem Cel Res.* 26, 72–75. doi:10.1016/j.scr.2017.12.001

Kim, J. H., Jang, Y. J., An, S. Y., Son, J., Lee, J., Lee, G., et al. (2015). Enhanced Metabolizing Activity of Human ES Cell-Derived Hepatocytes Using a 3D Culture System with Repeated Exposures to Xenobiotics. *Toxicol. Sci.* 147 (1), 190–206. doi:10.1093/toxsci/kfv121

Kim, K., Doi, A., Wen, B., Ng, K., Zhao, R., Cahan, P., et al. (2010). Epigenetic Memory in Induced Pluripotent Stem Cells. *Nature* 467 (7313), 285–290. doi:10.1038/nature09342

Kimura, K., Horiguchi, I., Kido, T., Miyajima, A., and Sakai, Y. (2019). Enhanced Hepatic Differentiation of Human Induced Pluripotent Stem Cells Using Gas-Permeable Membrane. *Tissue Eng. Part A* 25 (5-6), 457–467. doi:10.1089/ten.TEA.2018.0084

Kisseleva, T., and Brenner, D. A. (2019). The Crosstalk between Hepatocytes, Hepatic Macrophages, and Hepatic Stellate Cells Facilitates Alcoholic Liver Disease. *Cel Metab*. 30 (5), 850–852. doi:10.1016/j.cmet.2019.10.010

Kitade, M., Kaji, K., and Yoshiji, H. (2016). Relationship between Hepatic Progenitor Cell-Mediated Liver Regeneration and Non-parenchymal Cells. *Hepatol. Res.* 46 (12), 1187–1193. doi:10.1111/hepr.12682

Kobayashi, T., Yamaguchi, T., Hamanaka, S., Kato-Itoh, M., Yamazaki, Y., Ibata, M., et al. (2010). Generation of Rat Pancreas in Mouse by Interspecific Blastocyst Injection of Pluripotent Stem Cells. *Cell* 142 (5), 787–799. doi:10.1016/j.cell.2010.07.039

Koike, H., Iwasawa, K., Ouchi, R., Maezawa, M., Giesbrecht, K., Saiki, N., et al. (2019). Modelling Human Hepato-Biliary-Pancreatic Organogenesis from the Foregut-Midgut Boundary. *Nature* 574 (7776), 112–116. doi:10.1038/s41586-019-1598-0

Kondo, Y., Iwao, T., Yoshihashi, S., Mimori, K., Ogihara, R., Nagata, K., et al. (2014). Histone Deacetylase Inhibitor Valproic Acid Promotes the Differentiation of Human Induced Pluripotent Stem Cells into Hepatocyte-like Cells. *PLoS One* 9 (8), e104010. doi:10.1371/journal.pone.0104010

Lanzoni, G., Cardinale, V., and Carpino, G. (2016). The Hepatic, Biliary, and Pancreatic Network of Stem/progenitor Cell Niches in Humans: A New Reference Frame for Disease and Regeneration. *Hepatology* 64 (1), 277–286. doi:10.1002/hep.28326

Laudadio, I., Manfroid, I., Achouri, Y., Schmidt, D., Wilson, M. D., Cordi, S., et al. (2012). A Feedback Loop between the Liver-Enriched Transcription Factor Network and miR-122 Controls Hepatocyte Differentiation. *Gastroenterology* 142 (1), 119–129. doi:10.1053/j.gastro.2011.09.001

Lauschke, V. M., Hendriks, D. F. G., Bell, C. C., Andersson, T. B., and Ingelman-Sundberg, M. (2016). Novel 3D Culture Systems for Studies of Human Liver Function and Assessments of the Hepatotoxicity of Drugs and Drug Candidates. *Chem. Res. Toxicol.* 29 (12), 1936–1955. doi:10.1021/acs.chemrestox.6b00150

Lee, C. A., Dhawan, A., Iansante, V., Lehec, S., Khorsandi, S. E., Filippi, C., et al. (2018). Cryopreserved Neonatal Hepatocytes May Be a Source for Transplantation: Evaluation of Functionality toward Clinical Use. *Liver Transpl.* 24 (3), 394–406. doi:10.1002/lt.25015

Lee, G., Kim, H., Park, J. Y., Kim, G., Han, J., Chung, S., et al. (2021). Generation of Uniform Liver Spheroids from Human Pluripotent Stem Cells for Imaging-Based Drug Toxicity Analysis. *Biomaterials* 269, 120529. doi:10.1016/j.biomaterials.2020.120529

Lee, J., Choi, J., Kang, S., Kim, J., Lee, R., So, S., et al. (2020). Hepatogenic Potential and Liver Regeneration Effect of Human Liver-Derived Mesenchymal-like Stem Cells. *Cells* 9 (6), 1521. doi:10.3390/cells9061521

Li, S., Huang, S.-Q., Zhao, Y.-X., Ding, Y.-J., Ma, D.-J., and Ding, Q.-R. (2019). Derivation and Applications of Human Hepatocyte-like Cells. *Wjsc* 11 (8), 535–547. doi:10.4252/wjsc.v11.i8.535

Li, W. J., Zhu, X. J., Yuan, T. J., Wang, Z. Y., Bian, Z. Q., Jing, H. S., et al. (2020). An Extracorporeal Bioartificial Liver Embedded with 3D-Layered Human Liver Progenitor-like Cells Relieves Acute Liver Failure in Pigs. *Sci. Transl Med.* 12, 1–15. doi:10.1126/scitranslmed.aba5146

Lim, J. J., Kim, H. J., Rhie, B.-h., Lee, M. R., Choi, M. J., Hong, S.-H., et al. (2019). Maintenance of hPSCs under Xeno-free and Chemically Defined Culture Conditions. *Ijsc* 12 (3), 484–496. doi:10.15283/ijsc19090

Lindley, C., Hamilton, G., McCune, J. S., Faucette, S., Shord, S. S., Hawke, R. L., et al. (2002). The Effect of Cyclophosphamide with and without Dexamethasone on Cytochrome P450 3A4 and 2B6 in Human Hepatocytes. *Drug Metab. Dispos* 30 (7), 814–822. doi:10.1124/dmd.30.7.814

Liu, W., Wang, Y., Sun, Y., Wu, Y., Ma, Q., Shi, Y., et al. (2019). Clonal Expansion of Hepatic Progenitor Cells and Differentiation into Hepatocyte-like Cells. *Develop. Growth Differ.* 61 (3), 203–211. doi:10.1111/dgd.12596

Llames, S., García-Pérez, E., Meana, Á., Larcher, F., and del Río, M. (2015). Feeder Layer Cell Actions and Applications. *Tissue Eng. B: Rev.* 21 (4), 345–353. doi:10.1089/ten.TEB.2014.0547

Lorvellec, M., Scottoni, F., Crowley, C., Fiadeiro, R., Maghsoudlou, P., Pellegata, A. F., et al. (2017). Mouse Decellularised Liver Scaffold Improves Human Embryonic and Induced Pluripotent Stem Cells Differentiation into Hepatocyte-like Cells. *PLoS One* 12 (12), e0189586. doi:10.1371/journal.pone.0189586

Luce, E., Messina, A., Duclos-Vallée, J. C., and Dubart-Kupperschmitt, A. (2021). Advanced Techniques and Awaited Clinical Applications for Human Pluripotent Stem Cell Differentiation into Hepatocytes. *Hepatology* 74, 1101–1116. doi:10.1002/hep.31705

Ludwig, T. E., Bergendahl, V., Levenstein, M. E., Yu, J., Probasco, M. D., and Thomson, J. A. (2006). Feeder-independent Culture of Human Embryonic Stem Cells. *Nat. Methods* 3 (8), 637–646. doi:10.1038/nmeth902

Luo, Y., Lou, C., Zhang, S., Zhu, Z., Xing, Q., Wang, P., et al. (2018). Three-dimensional Hydrogel Culture Conditions Promote the Differentiation of Human Induced Pluripotent Stem Cells into Hepatocytes. *Cytotherapy* 20 (1), 95–107. doi:10.1016/j.jcyt.2017.08.008

Lutolf, M. P., and Hubbell, J. A. (2005). Synthetic Biomaterials as Instructive Extracellular Microenvironments for Morphogenesis in Tissue Engineering. *Nat. Biotechnol.* 23 (1), 47–55. doi:10.1038/nbt1055

Ma, J., and Huang, C. (2020). Composition and Mechanism of Three-Dimensional Hydrogel System in Regulating Stem Cell Fate. *Tissue Eng. Part B: Rev.* 26, 498–518. doi:10.1089/ten.TEB.2020.0021

Ma, X., Kong, L., and Zhu, S. (2017). Reprogramming Cell Fates by Small Molecules. *Protein Cell* 8 (5), 328–348. doi:10.1007/s13238-016-0362-6

Mahmoodinia Maymand, M., Soleimanpour-Lichaei, H. R., Ardeshirylajimi, A., Soleimani, M., Enderami, S. E., Nojehdehi, S., et al. (2018). Improvement of Hepatogenic Differentiation of iPS Cells on an Aligned Polyethersulfone Compared to Random Nanofibers. *Artif. Cell Nanomedicine, Biotechnol.* 46 (4), 853–860. doi:10.1080/21691401.2017.1345929

Mahmoodinia Maymand, M., Soleimanpour-Lichaei, H. R., Ardeshirylajimi, A., Soleimani, M., Mirzaei, S., Hajarizadeh, A., et al. (2017). Hepatogenic Differentiation of Human Induced Pluripotent Stem Cells on Collagen-Coated Polyethersulfone Nanofibers. *ASAIO J.* 63 (3), 316–323. doi:10.1097/MAT.0000000000000469

Matsunari, H., Nagashima, H., Watanabe, M., Umeyama, K., Nakano, K., Nagaya, M., et al. (2013). Blastocyst Complementation Generates Exogenic Pancreas *In Vivo* in Apancreatic Cloned Pigs. *Proc. Natl. Acad. Sci.* 110 (12), 4557–4562. doi:10.1073/pnas.1222902110

Matsunari, H., Watanabe, M., Hasegawa, K., Uchikura, A., Nakano, K., Umeyama, K., et al. (2020). Compensation of Disabled Organogeneses in Genetically Modified Pig Fetuses by Blastocyst Complementation. *Stem Cel Rep.* 14 (1), 21–33. doi:10.1016/j.stemcr.2019.11.008

Meier, F., Freyer, N., Brzeszczynska, J., Knï¿½spel, F., Armstrong, L., Lako, M., et al. (2017). Hepatic Differentiation of Human iPSCs in Different 3D Models: A Comparative Study. *Int. J. Mol. Med.* 40 (6), 1759–1771. doi:10.3892/ijmm.2017.3190

Miki, T. (2019). Clinical Hepatocyte Transplantation. *Gastroenterología y Hepatología* 42 (3), 202–208. doi:10.1016/j.gastrohep.2018.10.007

Mitani, S., Takayama, K., Nagamoto, Y., Imagawa, K., Sakurai, F., Tachibana, M., et al. (2017). Human ESC/iPSC-Derived Hepatocyte-like Cells Achieve Zone-specific Hepatic Properties by Modulation of WNT Signaling. *Mol. Ther.* 25 (6), 1420–1433. doi:10.1016/j.ymthe.2017.04.006

Mobarra, N., Soleimani, M., Ghayour-Mobarhan, M., Safarpour, S., Ferns, G. A., Pakzad, R., et al. (2019). Hybrid Poly- L -lactic Acid/poly(ε-caprolactone) Nanofibrous Scaffold Can Improve Biochemical and Molecular Markers of Human Induced Pluripotent Stem Cell-derived Hepatocyte-like Cells. *J. Cel Physiol* 234 (7), 11247–11255. doi:10.1002/jcp.27779

Mohamadnejad, M., Pournasr, B., Bagheri, M., Aghdami, N., Shahsavani, M., Hosseini, L. A., et al. (2010). Transplantation of Allogeneic Bone Marrow Mesenchymal Stromal Cell-Derived Hepatocyte-like Cells in Homozygous Familial Hypercholesterolemia. *Cytotherapy* 12 (4), 566–568. doi:10.3109/14653240903511143

Mun, S. J., Ryu, J.-S., Lee, M.-O., Son, Y. S., Oh, S. J., Cho, H.-S., et al. (2019). Generation of Expandable Human Pluripotent Stem Cell-Derived Hepatocyte-like Liver Organoids. *J. Hepatol.* 71 (5), 970–985. doi:10.1016/j.jhep.2019.06.030

Nagamoto, Y., Takayama, K., Ohashi, K., Okamoto, R., Sakurai, F., Tachibana, M., et al. (2016). Transplantation of a Human iPSC-Derived Hepatocyte Sheet

Increases Survival in Mice with Acute Liver Failure. *J. Hepatol.* 64 (5), 1068–1075. doi:10.1016/j.jhep.2016.01.004

Najimi, M., Khuu, D. N., Lysy, P. A., Jazouli, N., Abarca, J., Sempoux, C., et al. (2007). Adult-derived Human Liver Mesenchymal-like Cells as a Potential Progenitor Reservoir of Hepatocytes? *Cel Transpl.* 16 (7), 717–728. doi:10.3727/000000007783465154

Nakagawa, M., Koyanagi, M., Tanabe, K., Takahashi, K., Ichisaka, T., Aoi, T., et al. (2008). Generation of Induced Pluripotent Stem Cells without Myc from Mouse and Human Fibroblasts. *Nat. Biotechnol.* 26 (1), 101–106. doi:10.1038/nbt1374

Nakamae, S., Toba, Y., Takayama, K., Sakurai, F., and Mizuguchi, H. (2018). Nanaomycin A Treatment Promotes Hepatoblast Differentiation from Human iPS Cells. *Stem Cell Dev.* 27 (6), 405–414. doi:10.1089/scd.2017.0251

Nakamori, D., Takayama, K., Nagamoto, Y., Mitani, S., Sakurai, F., Tachibana, M., et al. (2016). Hepatic Maturation of Human iPS Cell-Derived Hepatocyte-like Cells by ATF5, c/EBPα, and PROX1 Transduction. *Biochem. Biophysical Res. Commun.* 469 (3), 424–429. doi:10.1016/j.bbrc.2015.12.007

Nguyen, M. P., Jain, V., Iansante, V., Mitry, R. R., Filippi, C., and Dhawan, A. (2020). Clinical Application of Hepatocyte Transplantation: Current Status, Applicability, Limitations, and Future Outlook. *Expert Rev. Gastroenterol. Hepatol.* 14 (3), 185–196. doi:10.1080/17474124.2020.1733975

Nikasa, P., Tricot, T., Mahdieh, N., Baharvand, H., Totonchi, M., Hejazi, M. S., et al. (2021). Patient-Specific Induced Pluripotent Stem Cell-Derived Hepatocyte-like Cells as a Model to Study Autosomal Recessive Hypercholesterolemia. *Stem Cell Dev.* 30, 714–724. doi:10.1089/scd.2020.0199

Ober, E. A., and Lemaigre, F. P. (2018). Development of the Liver: Insights into Organ and Tissue Morphogenesis. *J. Hepatol.* 68 (5), 1049–1062. doi:10.1016/j.jhep.2018.01.005

Okaya, A., Kitanaka, J., Kitanaka, N., Satake, M., Kim, Y., Terada, K., et al. (2005). Oncostatin M Inhibits Proliferation of Rat Oval Cells, OC15-5, Inducing Differentiation into Hepatocytes. *Am. J. Pathol.* 166 (3), 709–719. doi:10.1016/S0002-9440(10)62292-4

Okita, K. M. Y., Matsumura, Y., Sato, Y., Okada, A., Morizane, A., Okamoto, S., et al. (20112011). A More Efficient Method to Generate Integration-free Human iPS Cells. *Nat. Methods* 8 (5), 409–412. doi:10.1038/nmeth.1591

Orge, I. D., Gadd, V. L., Barouh, J. L., Rossi, E. A., Carvalho, R. H., Smith, I., et al. (2020). Phenotype Instability of Hepatocyte-like Cells Produced by Direct Reprogramming of Mesenchymal Stromal Cells. *Stem Cel Res Ther* 11 (1), 154. doi:10.1186/s13287-020-01665-z

Ouchi, R., Togo, S., Kimura, M., Shinozawa, T., Koido, M., Koike, H., et al. (2019). Modeling Steatohepatitis in Humans with Pluripotent Stem Cell-Derived Organoids. *Cel Metab.* 30 (2), 374–384. doi:10.1016/j.cmet.2019.05.007

Ouyang, J., Shao, J., Zou, H., Lou, Y., and Yu, Y. (2012). Hepatic Differentiation of Rat Mesenchymal Stem Cells by a Small Molecule. *ChemMedChem* 7 (8), 1447–1452. doi:10.1002/cmdc.201200162

Panta, W., Imsoonthornruksa, S., Yoisungnern, T., Suksaweang, S., Ketudat-Cairns, M., and Parnpai, R. (2019). Enhanced Hepatogenic Differentiation of Human Wharton's Jelly-Derived Mesenchymal Stem Cells by Using Three-step Protocol. *Ijms* 20 (12), 3016. doi:10.3390/ijms20123016

Park, M. R., Wong, M. S., Araúzo-Bravo, M. J., Lee, H., Nam, D., Park, S. Y., et al. (2019). Oct4 and Hnf4α-Induced Hepatic Stem Cells Ameliorate Chronic Liver Injury in Liver Fibrosis Model. *PLoS One* 14 (8), e0221085. doi:10.1371/journal.pone.0221085

Park, S., In Hwang, S., Kim, J., Hwang, S., Kang, S., Yang, S., et al. (2019). The Therapeutic Potential of Induced Hepatocyte-like Cells Generated by Direct Reprogramming on Hepatic Fibrosis. *Stem Cel Res Ther* 10 (1), 21. doi:10.1186/s13287-018-1127-3

Park, Y., Chen, Y., Ordovas, L., and Verfaillie, C. M. (2014). Hepatic Differentiation of Human Embryonic Stem Cells on Microcarriers. *J. Biotechnol.* 174, 39–48. doi:10.1016/j.jbiotec.2014.01.025

Poorna, M. R., Sudhindran, S., Thampi, M. V., and Mony, U. (2021). Differentiation of Induced Pluripotent Stem Cells to Hepatocyte-like Cells on Cellulose Nanofibril Substrate. *Colloids Surf. B: Biointerfaces* 198, 111466. doi:10.1016/j.colsurfb.2020.111466

Qin, H., Zhao, A., and Fu, X. (2018). Chemical Modulation of Cell Fates: *In Situ* Regeneration. *Sci. China Life Sci.* 61 (10), 1137–1150. doi:10.1007/s11427-018-9349-5

Ramli, M. N. B., Lim, Y. S., Koe, C. T., Demircioglu, D., Tng, W., Gonzales, K. A. U., et al. (2020). Human Pluripotent Stem Cell-Derived Organoids as Models of Liver Disease. *Gastroenterology* 159 (4), 1471–1486. doi:10.1053/j.gastro.2020.06.010

Raoufil, A., Aminil, A., Azadbakht, M., Farhadifar, F., and Rahram Nikhn Frrfin Fthi, N. F. (2015). Production of Hepatocyte-like Cells from Human Umbilical Vein Mesenchymal Stem Cells. *Ital. J. Anat. Embryol.* 120 (3), 150–161.

Rebelo, S. P., Costa, R., Silva, M. M., Marcelino, P., Brito, C., and Alves, P. M. (2017). Three-dimensional Co-culture of Human Hepatocytes and Mesenchymal Stem Cells: Improved Functionality in Long-Term Bioreactor Cultures. *J. Tissue Eng. Regen. Med.* 11 (7), 2034–2045. doi:10.1002/term.2099

Roy-Chowdhury, N., Wang, X., Guha, C., and Roy-Chowdhury, J. (2017). Hepatocyte-like Cells Derived from Induced Pluripotent Stem Cells. *Hepatol. Int.* 11 (1), 54–69. doi:10.1007/s12072-016-9757-y

Ruoss, M., Vosough, M., Königsrainer, A., Nadalin, S., Wagner, S., Sajadian, S., et al. (2020). Towards Improved Hepatocyte Cultures: Progress and Limitations. *Food Chem. Toxicol.* 138, 111188. doi:10.1016/j.fct.2020.111188

Sakai, Y., Iwao, T., Susukida, T., Nukaga, T., Takemura, A., Sekine, S., et al. (2019). *In Vitro* bile Acid-dependent Hepatocyte Toxicity Assay System Using Human Induced Pluripotent Stem Cell-Derived Hepatocytes: Current Status and Disadvantages to Overcome. *Drug Metab. Pharmacokinet.* 34 (4), 264–271. doi:10.1016/j.dmpk.2019.04.004

Sakurai, F., Mitani, S., Yamamoto, T., Takayama, K., Tachibana, M., Watashi, K., et al. (2017). Human Induced-Pluripotent Stem Cell-Derived Hepatocyte-like Cells as an *In Vitro* Model of Human Hepatitis B Virus Infection. *Sci. Rep.* 7, 45698. doi:10.1038/srep45698

Samal, P., van Blitterswijk, C., Truckenmüller, R., and Giselbrecht, S. (2019). Grow with the Flow: When Morphogenesis Meets Microfluidics. *Adv. Mater.* 31 (17), 1805764. doi:10.1002/adma.201805764

Sambathkumar, R., Akkerman, R., Dastidar, S., Roelandt, P., Kumar, M., Bajaj, M., et al. (2018). Generation of Hepatocyte- and Endocrine Pancreatic-like Cells from Human Induced Endodermal Progenitor Cells. *PLoS One* 13 (5), e0197046. doi:10.1371/journal.pone.0197046

Schmelzer, E., Zhang, L., Bruce, A., Wauthier, E., Ludlow, J., Yao, H.-l., et al. (2007). Human Hepatic Stem Cells from Fetal and Postnatal Donors. *J. Exp. Med.* 204 (8), 1973–1987. doi:10.1084/jem.20061603

Schwartz, R. E., Trehan, K., Andrus, L., Sheahan, T. P., Ploss, A., Duncan, S. A., et al. (2012). Modeling Hepatitis C Virus Infection Using Human Induced Pluripotent Stem Cells. *Proc. Natl. Acad. Sci.* 109 (7), 2544–2548. doi:10.1073/pnas.1121400109

Seeliger, C., Culmes, M., Schyschka, L., Yan, X., Damm, G., Wang, Z., et al. (2013). Decrease of Global Methylation Improves Significantly Hepatic Differentiation of Ad-MSCs: Possible Future Application for Urea Detoxification. *Cel Transpl.* 22 (1), 119–131. doi:10.3727/096368912x638946

Shabani Azandaryani, Z., Davoodian, N., Samiei, A., and Rouzbehan, S. (2019). Insulin-like Growth factor-I Promotes Hepatic Differentiation of Human Adipose Tissue-derived Stem Cells. *Cell Biol Int* 43 (5), 476–485. doi:10.1002/cbin.11113

Shan, J., Schwartz, R. E., Ross, N. T., Logan, D. J., Thomas, D., Duncan, S. A., et al. (2013). Identification of Small Molecules for Human Hepatocyte Expansion and iPS Differentiation. *Nat. Chem. Biol.* 9 (8), 514–520. doi:10.1038/nchembio.1270

Shi, X.-L., Gao, Y., Yan, Y., Ma, H., Sun, L., Huang, P., et al. (2016). Improved Survival of Porcine Acute Liver Failure by a Bioartificial Liver Device Implanted with Induced Human Functional Hepatocytes. *Cel Res* 26 (2), 206–216. doi:10.1038/cr.2016.6

Shinozawa, T., Kimura, M., Cai, Y., Saiki, N., Yoneyama, Y., Ouchi, R., et al. (2021). High-Fidelity Drug-Induced Liver Injury Screen Using Human Pluripotent Stem Cell-Derived Organoids. *Gastroenterology* 160 (3), 831–846. doi:10.1053/j.gastro.2020.10.002

Shiota, J., Samuelson, L. C., and Razumilava, N. (2021). Hepatobiliary Organoids and Their Applications for Studies of Liver Health and Disease: Are We There yet? *Hepatology* 74, 2251–2263. doi:10.1002/hep.31772

Si-Tayeb, K., Noto, F. K., Nagaoka, M., Li, J., Battle, M. A., Duris, C., et al. (2010). Highly Efficient Generation of Human Hepatocyte-like Cells from Induced Pluripotent Stem Cells. *Hepatology* 51 (1), 297–305. doi:10.1002/hep.23354

Siller, R., Greenhough, S., Naumovska, E., and Sullivan, G. J. (2015). Small-molecule-driven Hepatocyte Differentiation of Human Pluripotent Stem Cells. *Stem Cel Rep.* 4 (5), 939–952. doi:10.1016/j.stemcr.2015.04.001

Slepicka, P., Kasalkova, N. S., Siegel, J., Kolska, Z., Bacakova, L., and Svorcik, V. (2015). Nano-structured and Functionalized Surfaces for Cytocompatibility

Improvement and Bactericidal Action. *Biotechnol. Adv.* 33 (6 Pt 2), 1120–1129. doi:10.1016/j.biotechadv.2015.01.001

Stacey, G. N., Cobo, F., Nieto, A., Talavera, P., Healy, L., and Concha, Á. (2006). The Development of 'feeder' Cells for the Preparation of Clinical Grade hES Cell Lines: Challenges and Solutions. *J. Biotechnol.* 125 (4), 583–588. doi:10.1016/j.jbiotec.2006.03.011

Takahashi, K., and Yamanaka, S. (2006). Induction of Pluripotent Stem Cells from Mouse Embryonic and Adult Fibroblast Cultures by Defined Factors. *Cell* 126 (4), 663–676. doi:10.1016/j.cell.2006.07.024

Takayama, K., Hagihara, Y., Toba, Y., Sekiguchi, K., Sakurai, F., and Mizuguchi, H. (2018). Enrichment of High-Functioning Human iPS Cell-Derived Hepatocyte-like Cells for Pharmaceutical Research. *Biomaterials* 161, 24–32. doi:10.1016/j.biomaterials.2018.01.019

Takayama, K., Inamura, M., Kawabata, K., Sugawara, M., Kikuchi, K., Higuchi, M., et al. (2012). Generation of Metabolically Functioning Hepatocytes from Human Pluripotent Stem Cells by FOXA2 and HNF1α Transduction. *J. Hepatol.* 57 (3), 628–636. doi:10.1016/j.jhep.2012.04.038

Takebe, T., Sekine, K., Kimura, M., Yoshizawa, E., Ayano, S., Koido, M., et al. (2017). Massive and Reproducible Production of Liver Buds Entirely from Human Pluripotent Stem Cells. *Cel Rep.* 21 (10), 2661–2670. doi:10.1016/j.celrep.2017.11.005

Talaei-Khozani, T., Borhani-Haghighi, M., Ayatollahi, M., and Vojdani, Z. (2015). An *In Vitro* Model for Hepatocyte-like Cell Differentiation from Wharton's Jelly Derived-Mesenchymal Stem Cells by Cell-Base Aggregates. *Gastroenterol. Hepatol. Bed Bench* 8 (3), 188–199.

Tandon, N., Marolt, D., Cimetta, E., and Vunjak-Novakovic, G. (2013). Bioreactor Engineering of Stem Cell Environments. *Biotechnol. Adv.* 31 (7), 1020–1031. doi:10.1016/j.biotechadv.2013.03.007

Tasnim, F., Phan, D., Toh, Y.-C., and Yu, H. (2015). Cost-effective Differentiation of Hepatocyte-like Cells from Human Pluripotent Stem Cells Using Small Molecules. *Biomaterials* 70, 115–125. doi:10.1016/j.biomaterials.2015.08.002

Toivonen, S., Malinen, M. M., Küblbeck, J., Petsalo, A., Urtti, A., Honkakoski, P., et al. (2016). Regulation of Human Pluripotent Stem Cell-Derived Hepatic Cell Phenotype by Three-Dimensional Hydrogel Models. *Tissue Eng. Part A* 22 (13-14), 971–984. doi:10.1089/ten.TEA.2016.0127

Tolosa, L., Pareja-Ibars, E., Donato, M. T., Cortés, M., López, S., Jiménez, N., et al. (2014). Neonatal Livers: a Source for the Isolation of Good-Performing Hepatocytes for Cell Transplantation. *Cel Transpl.* 23 (10), 1229–1242. doi:10.3727/096368913X669743

Tomizawa, M., Shinozaki, F., Motoyoshi, Y., Sugiyama, T., Yamamoto, S., and Ishige, N. (2017). Oncostatin M in William's E Medium Is Suitable for Initiation of Hepatocyte Differentiation in Human Induced Pluripotent Stem Cells. *Mol. Med. Rep.* 15 (5), 3088–3092. doi:10.3892/mmr.2017.6406

Touboul, T., Chen, S., To, C. C., Mora-Castilla, S., Sabatini, K., Tukey, R. H., et al. (2016). Stage-specific Regulation of the WNT/β-catenin Pathway Enhances Differentiation of hESCs into Hepatocytes. *J. Hepatol.* 64 (6), 1315–1326. doi:10.1016/j.jhep.2016.02.028

Trefts, E., Gannon, M., and Wasserman, D. H. (2017). The Liver. *Curr. Biol.* 27 (21), R1147–R1151. doi:10.1016/j.cub.2017.09.019

Tsuchida, T., Murata, S., Hasegawa, S., Mikami, S., Enosawa, S., Hsu, H.-C., et al. (2020). Investigation of Clinical Safety of Human iPS Cell-Derived Liver Organoid Transplantation to Infantile Patients in Porcine Model. *Cel Transpl.* 29, 096368972096438. doi:10.1177/0963689720964384

Turner, R., Lozoya, O., Wang, Y., Cardinale, V., Gaudio, E., Alpini, G., et al. (2011). Human Hepatic Stem Cell and Maturational Liver Lineage Biology. *Hepatology* 53 (3), 1035–1045. doi:10.1002/hep.24157

Usui, J.-i., Kobayashi, T., Yamaguchi, T., Knisely, A. S., Nishinakamura, R., and Nakauchi, H. (2012). Generation of Kidney from Pluripotent Stem Cells via Blastocyst Complementation. *Am. J. Pathol.* 180 (6), 2417–2426. doi:10.1016/j.ajpath.2012.03.007

van Wenum, M., Adam, A. A. A., van der Mark, V. A., Chang, J.-C., Wildenberg, M. E., Hendriks, E. J., et al. (2018). Oxygen Drives Hepatocyte Differentiation and Phenotype Stability in Liver Cell Lines. *J. Cel Commun. Signal.* 12 (3), 575–588. doi:10.1007/s12079-018-0456-4

Varaa, N., Azandeh, S., Khodabandeh, Z., and Gharravi, A. M. (2019). Wharton's Jelly Mesenchymal Stem Cell: Various Protocols for Isolation and Differentiation of Hepatocyte-like Cells; Narrative Review. *Iran J. Med. Sci.* 44 (6), 437–448. doi:10.30476/ijms.2019.44952

Vojdani, Z., Khodabandeh, Z., Jaberipour, M., Hosseini, A., Bahmanpour, S., and Talaei-Khozani, T. (2015). The Influence of Fibroblast Growth Factor 4 on Hepatogenic Capacity of Wharton's Jelly Mesenchymal Stromal Cells. *Rom. J. Morphol. Embryol.* 56 (3), 1043–1050.

Wang, B., Jakus, A. E., Baptista, P. M., Soker, S., Soto-Gutierrez, A., Abecassis, M. M., et al. (2016). Functional Maturation of Induced Pluripotent Stem Cell Hepatocytes in Extracellular Matrix-A Comparative Analysis of Bioartificial Liver Microenvironments. *STEM CELLS Translational Med.* 5 (9), 1257–1267. doi:10.5966/sctm.2015-0235

Wang, B., Li, W., Dean, D., Mishra, M. K., and Wekesa, K. S. (2018). Enhanced Hepatogenic Differentiation of Bone Marrow Derived Mesenchymal Stem Cells on Liver ECM Hydrogel. *J. Biomed. Mater. Res.* 106 (3), 829–838. doi:10.1002/jbm.a.36278

Wang, J., Zhao, P., Wan, Z., Jin, X., Cheng, Y., Yan, T., et al. (2016). Differentiation of Human Foreskin Fibroblast-Derived Induced Pluripotent Stem Cells into Hepatocyte-like Cells. *Cell Biochem Funct* 34 (7), 475–482. doi:10.1002/cbf.3210

Wang, Y., Qin, J., Wang, S., Zhang, W., Duan, J., Zhang, J., et al. (2016). Conversion of Human Gastric Epithelial Cells to Multipotent Endodermal Progenitors Using Defined Small Molecules. *Cell Stem Cell* 19 (4), 449–461. doi:10.1016/j.stem.2016.06.006

Wang, Z.-Y., Li, W.-J., Li, Q.-G., Jing, H.-S., Yuan, T.-J., Fu, G.-B., et al. (2019). A DMSO-free Hepatocyte Maturation Medium Accelerates Hepatic Differentiation of HepaRG Cells *In Vitro*. *Biomed. Pharmacother.* 116, 109010. doi:10.1016/j.biopha.2019.109010

Williams, D. P. (2018). Application of Hepatocyte-like Cells to Enhance Hepatic Safety Risk Assessment in Drug Discovery. *Phil. Trans. R. Soc. B* 373 (1750), 20170228. doi:10.1098/rstb.2017.0228

Wu, H., Du, C., Yang, F., Zheng, X., Qiu, D., Zhang, Q., et al. (2020). Generation of Hepatocyte-like Cells from Human Urinary Epithelial Cells and the Role of Autophagy during Direct Reprogramming. *Biochem. Biophysical Res. Commun.* 527 (3), 723–729. doi:10.1016/j.bbrc.2020.03.119

Wu, H., Zhou, X., Fu, G.-B., He, Z.-Y., Wu, H.-P., You, P., et al. (2017). Reversible Transition between Hepatocytes and Liver Progenitors for *In Vitro* Hepatocyte Expansion. *Cel Res* 27 (5), 709–712. doi:10.1038/cr.2017.47

Wu, J., Platero-Luengo, A., Sakurai, M., Sugawara, A., Gil, M. A., Yamauchi, T., et al. (2017). Interspecies Chimerism with Mammalian Pluripotent Stem Cells. *Cell* 168 (3), 473–486. doi:10.1016/j.cell.2016.12.036

Wüst, S., Müller, R., and Hofmann, S. (2011). Controlled Positioning of Cells in Biomaterials-Approaches towards 3D Tissue Printing. *Jfb* 2 (3), 119–154. doi:10.3390/jfb2030119

Xing, X. K., Feng, H. G., and Yuan, Z. Q. (2016). Differentiation of Bone Mesenchymal Stem Cells into Hepatocyte-like Cells Induced by Liver Tissue Homogenate. *Genet. Mol. Res.* 15 (3). doi:10.4238/gmr.15038550

Xu, F., Liu, J., Deng, J., Chen, X., Wang, Y., Xu, P., et al. (2015). Rapid and High-Efficiency Generation of Mature Functional Hepatocyte-like Cells from Adipose-Derived Stem Cells by a Three-step Protocol. *Stem Cel Res Ther* 6, 193. doi:10.1186/s13287-015-0181-3

Xu, L.-J., Wang, S.-F., Wang, D.-Q., Ma, L.-J., Chen, Z., Chen, Q.-Q., et al. (2017). Adipose-derived Stromal Cells Resemble Bone Marrow Stromal Cells in Hepatocyte Differentiation Potential *In Vitro* and *In Vivo*. *Wjg* 23 (38), 6973–6982. doi:10.3748/wjg.v23.i38.6973

Xu, Z., He, X., Shi, X., Xia, Y., Liu, X., Wu, H., et al. (2018). Analysis of Differentially Expressed Genes Among Human Hair Follicle-Derived iPSCs, Induced Hepatocyte-like Cells, and Primary Hepatocytes. *Stem Cel Res Ther* 9 (1), 211. doi:10.1186/s13287-018-0940-z

Xue, G., Han, X., Ma, X., Wu, H., Qin, Y., Liu, J., et al. (20162016). Effect of Microenvironment on Differentiation of Human Umbilical Cord Mesenchymal Stem Cells into HepatocytesIn VitroandIn Vivo. *Biomed. Res. Int.* 2016, 1–13. doi:10.1155/2016/8916534

Yamashita, T., Takayama, K., Sakurai, F., and Mizuguchi, H. (2018). Billion-scale Production of Hepatocyte-like Cells from Human Induced Pluripotent Stem Cells. *Biochem. Biophysical Res. Commun.* 496 (4), 1269–1275. doi:10.1016/j.bbrc.2018.01.186

Yamazoe, T., Shiraki, N., Toyoda, M., Kiyokawa, N., Okita, H., Miyagawa, Y., et al. (2013). A Synthetic Nanofibrillar Matrix Promotes *In Vitro* Hepatic Differentiation of Embryonic Stem Cells and Induced Pluripotent Stem Cells. *J. Cel Sci* 126 (Pt 23), 5391–5399. doi:10.1242/jcs.129767

Yen, M.-H., Wu, Y.-Y., Liu, Y.-S., Rimando, M., Ho, J. H.-C., and Lee, O. K.-S. (2016). Efficient Generation of Hepatic Cells from Mesenchymal Stromal Cells by an Innovative Bio-Microfluidic Cell Culture Device. *Stem Cel Res Ther* 7 (1), 120. doi:10.1186/s13287-016-0371-7

Yu, B., He, Z.-Y., You, P., Han, Q.-W., Xiang, D., Chen, F., et al. (2013). Reprogramming Fibroblasts into Bipotential Hepatic Stem Cells by Defined Factors. *Cell Stem Cell* 13 (3), 328–340. doi:10.1016/j.stem.2013.06.017

Yusa, K., Rashid, S. T., Strick-Marchand, H., Varela, I., Liu, P.-Q., Paschon, D. E., et al. (2011). Targeted Gene Correction of α1-antitrypsin Deficiency in Induced Pluripotent Stem Cells. *Nature* 478 (7369), 391–394. doi:10.1038/nature10424

Zeilinger, K., Freyer, N., Damm, G., Seehofer, D., and Knöspel, F. (2016). Cell Sources for *In Vitro* Human Liver Cell Culture Models. *Exp. Biol. Med. (Maywood)* 241 (15), 1684–1698. doi:10.1177/1535370216657448

Zhang, L., Theise, N., Chua, M., and Reid, L. M. (2008). The Stem Cell Niche of Human Livers: Symmetry between Development and Regeneration. *Hepatology* 48 (5), 1598–1607. doi:10.1002/hep.22516

Zhang, W., Li, W., Liu, B., Wang, P., Li, W., and Zhang, H. (2012). Efficient Generation of Functional Hepatocyte-like Cells from Human Fetal Hepatic Progenitor Cells *In Vitro*. *J. Cel. Physiol.* 227 (5), 2051–2058. doi:10.1002/jcp.22934

Zheng, Y., Zhou, J., Li, X., Xu, G., Jin, M., Shen, R., et al. (2018). Mir-382 Promotes Differentiation of Rat Liver Progenitor Cell WB-F344 by Targeting Ezh2. *Cell Physiol Biochem* 48 (6), 2389–2398. doi:10.1159/000492654

Zhi, X., Xiong, J., Wang, M., Zhang, H., Huang, G., Zhao, J., et al. (20182018). Physiological Hypoxia Enhances Stemness Preservation, Proliferation, and Bidifferentiation of Induced Hepatic Stem Cells. *Oxidative Med. Cell Longevity* 2018, 1–10. doi:10.1155/2018/7618704

Zhou, T., Benda, C., Duzinger, S., Huang, Y., Li, X., Li, Y., et al. (2011). Generation of Induced Pluripotent Stem Cells from Urine. *Jasn* 22 (7), 1221–1228. doi:10.1681/ASN.2011010106

Zhou, X., Cui, L., Zhou, X., Yang, Q., Wang, L., Guo, G., et al. (2017). Induction of Hepatocyte-like Cells from Human Umbilical Cord-Derived Mesenchymal Stem Cells by Defined microRNAs. *J. Cel. Mol. Med.* 21 (5), 881–893. doi:10.1111/jcmm.130210.1111/jcmm.13027

Conflict of Interest: The authors declare that the research was conducted in the absence of any commercial or financial relationships that could be construed as a potential conflict of interest.

Publisher's Note: All claims expressed in this article are solely those of the authors and do not necessarily represent those of their affiliated organizations, or those of the publisher, the editors and the reviewers. Any product that may be evaluated in this article, or claim that may be made by its manufacturer, is not guaranteed or endorsed by the publisher.

frontiers in Cell and Developmental Biology

ORIGINAL RESEARCH
published: 20 January 2022
doi: 10.3389/fcell.2021.808905

Human Umbilical Cord Mesenchymal Stem Cells Improve Locomotor Function in Parkinson's Disease Mouse Model Through Regulating Intestinal Microorganisms

Zhengqin Sun[1,2], Ping Gu[1], Hongjun Xu[2,3,4], Wei Zhao[2,3,4,5], Yongjie Zhou[2,3,4], Luyang Zhou[2,3,4], Zhongxia Zhang[1,2], Wenting Wang[1], Rui Han[1], Xiqing Chai[1] and Shengjun An[2,3,4]**

[1]Department of Neurology, The First Hospital of Hebei Medical University, Shijiazhuang, China, [2]Hebei Provincial Engineering Laboratory of Plant Bioreactor Preparation Technology, Shijiazhuang, China, [3]Research Center, Hebei University of Chinese Medicine, Shijiazhuang, China, [4]College of Integrated Chinese and Western Medicine, Hebei University of Chinese Medicine, Shijiazhuang, China, [5]Affiliated Hospital of Hebei University of Engineering, Handan, China

OPEN ACCESS

Edited by:
Wencheng Zhang, Tongji University, China

Reviewed by:
Tokiko Nagamura-Inoiue, Takeo Mukai, The University of Tokyo, Japan

***Correspondence:**
Xiqing Chai
sunhbykdx@126.com
Shengjun An
sjsjan@126.com

Specialty section:
This article was submitted to Stem Cell Research, a section of the journal Frontiers in Cell and Developmental Biology

Received: *04 November 2021*
Accepted: *10 December 2021*
Published: *20 January 2022*

Citation:
Sun Z, Gu P, Xu H, Zhao W, Zhou Y, Zhou L, Zhang Z, Wang W, Han R, Chai X and An S (2022) Human Umbilical Cord Mesenchymal Stem Cells Improve Locomotor Function in Parkinson's Disease Mouse Model Through Regulating Intestinal Microorganisms. Front. Cell Dev. Biol. 9:808905. doi: 10.3389/fcell.2021.808905

Parkinson's disease (PD) is a progressive neurological disorder characterized by loss of neurons that synthesize dopamine, and subsequent impaired movement. Umbilical cord mesenchymal stem cells (UC-MSCs) exerted neuroprotection effects in a rodent model of PD. However, the mechanism underlying UC-MSC-generated neuroprotection was not fully elucidated. In the present study, we found that intranasal administration of UC-MSCs significantly alleviated locomotor deficits and rescued dopaminergic neurons by inhibiting neuroinflammation in a PD mouse model induced by 1-methyl-4-phenyl-1,2,3,6-tetrahydropyridine (MPTP, a toxic agent which selectively destroys nigrostriatal neurons but does not affect dopaminergic neurons elsewhere). Furthermore, UC-MSC treatment altered gut microbiota composition characterized by decreased phylum Proteobacteria, class Gammaproteobacteria, family Enterobacteriaceae, and genus *Escherichia-Shigella*. In addition, the neurotransmitter dopamine in the striatum and 5-hydroxytryptamine in the colon were also modulated by UC-MSCs. Meanwhile, UC-MSCs significantly maintained intestinal goblet cells, which secrete mucus as a mechanical barrier against pathogens. Furthermore, UC-MSCs alleviate the level of TNF-α and IL-6 as well as the conversion of NF-κB expression in the colon, indicating that inflammatory responses were blocked by UC-MSCs. PICRUSt showed that some pathways including bacterial invasion of epithelial cells, fluorobenzoate degradation, and pathogenic *Escherichia coli* infection were significantly reversed by UC-MSCs. These data suggest that the beneficial effects were detected following UC-MSC intranasal transplantation in MPTP-treated mice. There is a possible neuroprotective role of UC-MSCs in MPTP-induced PD mice by cross talk between the brain and gut.

Keywords: human umbilical cord mesenchymal stem cells, Parkinson's disease (PD), gut microbiota, inflammation, neurotransmitter, goblet cells

Abbreviations: DA, dopamine; ELISA, enzyme-linked immunosorbent assay; GFAP, glial fibrillary acid protein; 5-HIAA, 5-hydroxyindoleacetic; 5-HT, 5-hydroxytryptamine; Iba-1, ionized calcium-binding adaptor molecule 1; LPS, lipopolysaccharide; MSCs, mesenchymal stem cells; PD, Parkinson's disease; SN, substantia nigra; ST, striatum.

INTRODUCTION

Parkinson's disease (PD) is a common neurodegenerative disorder which occurs due to the loss of dopaminergic neurons. The global prevalence of PD is predicted to be doubled by the year 2040 (Dorsey and Bloem, 2018), making it a faster growing neurodegenerative disorder than Alzheimer's disease (Group, 2017). It has been shown that pathological mechanisms of PD include α-synuclein aggregation, mitochondrial dysfunction, oxidative stress, autophagy, and neuroinflammation (Charvin et al., 2018). Recent studies have revealed that dysfunction and alteration intestinal barrier in the microbial composition are related to the etiology of PD. In addition, the common non-motor symptoms of PD patients such as constipation begin years before the onset of motor dysfunction (Visanji et al., 2013). The PD mouse model disrupts the intestinal barrier, suggesting that gut–brain interaction plays an important role in PD pathology (Perez-Pardo et al., 2019). In addition, microbiome normalization can improve impaired motor function in MPTP-induced PD mice (Zhou et al., 2019; Sun et al., 2021). These findings indicate that targeting the gut–brain axis is a promising strategy to treat PD.

Mesenchymal stem cells (MSCs) are an important source for tissue repair due to their multifunctional differentiation, easy sampling, rapid expansion, and low immunogenicity, and are also free from ethical issues. MSCs have been used in clinical trials to treat neuropsychiatric disorders such as autism spectrum disorder and multiple sclerosis (Riordan et al., 2018; Riordan et al., 2019). Evidence shows that MSCs have been used to improve intestinal functions and inflammation in inflammatory bowel disease (Soontararak et al., 2018) and to restore gut microbial dysbiosis in various refractory diseases, such as acute liver injury (Dong et al., 2019), rheumatoid arthritis (Li et al., 2020), type 1 diabetes (Lv et al., 2020), and acute lung injury (Sun et al., 2020). Previous studies had reported that administration of MSCs improves motor function and rescues dopaminergic neurons in PD animal models by reducing oxidative stress (Chi et al., 2019), modulating autophagy (Park et al., 2014), and inhibiting neuroinflammation (Kim et al., 2009). However, the molecular mechanisms and interactions between MSCs and gut microbiota in PD remain unknown. What is more, studies demonstrate similar trends in the microbial composition of PD subjects, while pathogenic Gram-negative bacteria (Proteobacteria, Enterobacteriaceae, and *Escherichia-Shigella*) and mucin-degrading Verrucomicrobiaceae are increased (Gorecki et al., 2019). MSC treatment can reduce the proportion of Proteobacteria (Lv et al., 2020) and *Escherichia-Shigella* (Sun et al., 2020). Taken together, we assume that the intestinal microbes of PD were also regulated by MSCs.

MSCs are mainly derived from the bone marrow (BM), adipose (AD), and umbilical cord (UC). Compared with BM and AD, UC-MSC harvesting is non-invasive, and cell proliferation is fastest *in vitro* (Li et al., 2015; Fričová et al., 2020). UC-MSCs are not affected by cell contact inhibition, and they are still in a state of proliferation after confluence (Choudhery et al., 2013). These studies indicate that UC-MSCs may be ideal for PD therapy. However, previous studies had reported that UC-MSC transplantation methods mainly focus on stereotactic and intravenous injection in PD animal models (Wang et al., 2016; Chi et al., 2019). There is still a lack of research on the intranasal instillation of UC-MSCs. The advantage of intranasal delivery is brain-targeting; BM-MSCs can be found in multiple brain regions and last up to 4.5 months by intranasal delivery in the PD animal model (Danielyan et al., 2014). Therefore, the present study will further explore the neuroprotective effect of nasal drip transplantation UC-MSCs on PD model mice.

In the present study, we discovered the neuroprotective effects of UC-MSC administration in PD mice. UC-MSCs inhibited reactive gliosis and neuroinflammation and facilitated motor functional recovery in MPTP-treated mice. The neurotransmitter dopamine (DA) in the striatum (ST) and 5-hydroxytryptamine (5-HT) in the colon were also modulated by UC-MSCs. In the same animal, we found that UC-MSCs corrected microbial composition, maintained colonic goblet cells, suppressed colonic pro-inflammatory response, and the activation of the NF-κB pathway in MPTP-treated mice. Our findings provide insights into the effects of UC-MSCs on the brain–gut axis in the PD mouse model.

MATERIALS AND METHODS

Cell Culture and Phenotype Identification

Fresh umbilical cord samples were obtained from normal spontaneous full-term delivery mothers with written informed consent and reserved in a sterilized phosphate-buffered saline (PBS) solution processed within 3 h. The cord was rinsed three times to remove the residue blood and clots, cut into 3-cm-long pieces, and rinsed again in a petri dish until the solution became clear. After blood vessels were removed, Wharton's jelly was dissected into pieces approximately 0.3 cm^3 in size and then transferred into culture vessels, with 10 ml mesenchymal stem cell complete medium (Beijing Yocon Biology Co., Ltd.) at 37°C in a 5% CO_2 incubator. The medium was replaced with fresh medium every 3 days after the initial plating. The cultured cells were passaged when cell confluency reached 80%.

Cells at passage 3 were seeded into 12-well plates at a density of 1.3×10^4 cells per well and observed for 5 days for proliferation measurement. At passage 3, the cells were harvested for phenotype identification through staining with antibodies against CD34, CD45, HLA-DR, CD73, CD90, and CD105 (Sino Biological, Beijing, China) and analyzed using a flow cytometer (Celula, Sichuan, China). An MSC three-line differentiation kit was purchased from Guangzhou Cyagen Biological Co., Ltd. The adipogenic, osteogenic, and chondrogenic differentiation were carried out in accordance with the product instructions. Oil red O, Alizarin Red, and Alcian Blue staining were used to observe the abilities of adipogenesis, osteogenic, and chondrogenic differentiation. UC-MSCs from passages 2 to 5 were used for the experiments.

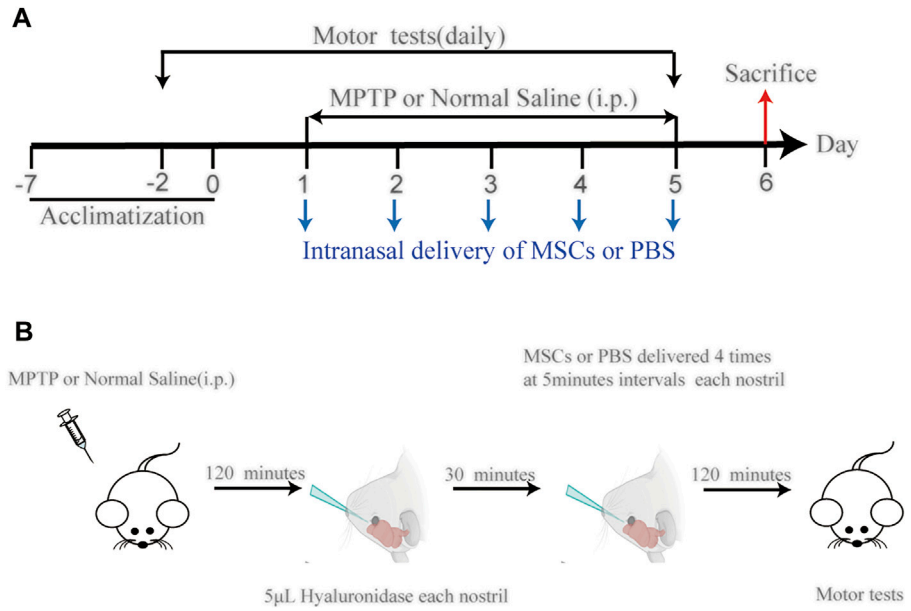

FIGURE 1 | (A) Schematic diagram of the experimental design. **(B)** Diagram of the experimental process before sample collection, among which intranasal delivery schema can be found in Rhea EM et al. (2020). DOI:10.3390/pharmaceutics12111120.

MPTP Injury Mouse Model and UC-MSC Treatment

Sixty male C57BL/6 mice (8 weeks old, body weight 22–25 g) were purchased from Vital River Laboratory Animal Technology Co., Ltd. (Beijing, China). The mice were housed in a specific pathogen-free laboratory under a controlled environment with a temperature of 22 ± 3°C and humidity 60 ± 5% at 12-h light/12-h dark cycle. All mice were given free access to food and tap water. The experimental protocols and animal care were strictly in accordance with the approval of the Animal Care and Management Committee of Hebei Medical University.

The mice were randomly assigned to receive either intraperitoneal injection of MPTP or normal saline. The MPTP-induced PD mouse model was conducted as previously described (Xu et al., 2019a). MPTP (30 mg/kg, M0896; Sigma-Aldrich) was injected intraperitoneally once a day for 5 days to produce an experimental PD model.

The method of UC-MSC administration is modified according to previously published (Long et al., 2017; Narbute et al., 2019; Simon et al., 2019). Intranasal application of UC-MSCs or PBS into MPTP-or vehicle-treated mice was performed 5 days after MPTP injection. Two hours after MPTP injection, each nostril was treated with 5.0 μl of hyaluronidase (100 U; H3506; Sigma-Aldrich) in sterile PBS solution to enhance the permeability of the nasal mucous membrane. Thirty minutes later, 5.0 μl cell suspension was instilled in the nasal cavity with a pipette in a 5-min interval. The daily dose contained 1×10^6 cells/40 μl (**Figure 1B**).

Behavioral Test

The motor function was evaluated by two modified pole tests and a traction test (Sun et al., 2018). Behavior training was conducted once a day for three consecutive days, and a behavior test was conducted on the day after the last treatment. The two neurobehavioral tests were performed by investigators blinded to other treatment and group assignment information.

Immunohistochemistry and Immunofluorescence Staining

Mice were anesthetized with isoflurane, and their brains were gently and quickly removed and post-fixed for 24 h in 4% paraformaldehyde. After being embedded in paraffin, the brains were cut into 3-μm coronal sections by using a microtome (Leica). Sections containing the substantia nigra (SN) were subjected to immunostaining. Briefly, the sections were dewaxed by xylene (I, II, III) for 15 min and rehydrated in alcohol (100, 100, 85, and 75%) for 5 min. The tissue sections are placed in citric acid antigen retrieval buffer (pH 6.0) for antigen retrieval. Endogenous peroxidase activity was inhibited by incubation with 3% hydrogen peroxide for 25 min. Then sections were blocked with 3% BSA for 30 min at room temperature and overnight at 4°C with rabbit anti-tyrosine hydroxylase (TH, dilution 1:1000 for immunohistochemistry and 1:2000 for immunofluorescence staining, GB11181, Servicebio). Subsequently, the sections were incubated with horseradish–peroxidase-labeled goat anti-rabbit IgG antibody (dilution 1:200, GB23303; Servicebio) for 50 min

at room temperature. The sections then were transferred to fresh 3, 3′-diaminobenzidine for coloration and rinsed with tap water to stop staining. Results were expressed as TH-positive neuron numbers in SN. For immunofluorescence staining, antigen retrieval was performed after the sections were treated with FITC reagent, rabbit-anti-Iba-1 (dilution 1: 200, 01919741; Wako), and its corresponding secondary antibody CY3-conjugated goat anti-rabbit IgG (1:300, GB21303; Servicebio) were incubated. For co-expression of TH and GFAP, the mice brain sections were co-incubated with rabbit anti-TH (dilution 1:200, GB11181; Servicebio) and mouse anti-glial fibrillary acid protein (dilution 1:800, GB12096; Servicebio) overnight at 4°C. After being washed in PBS, secondary antibody (488)–conjugated goat anti-rabbit IgG (1:400, GB25303; Servicebio) and CY3-conjugated goat anti-mouse IgG (1:300, GB21301; Servicebio) were incubated. Immunofluorescence images were observed under a fluorescent microscope, and areas of interest were captured and analyzed by ImageJ software.

Neurotransmitter Measurement by HPLC-MS

The distal colon tissues were collected following previous methods (Li et al., 2019). Striatal DA and colonic DA, 5-HT, 5-hydroxyindoleacetic (5-HIAA) were determined by high-performance liquid chromatography–mass spectrometry (HPLC-MS). The chromatogram collection and integration of each analyte were processed by software Xcalibur 4.0 (Thermo Fisher), and linear regression was performed with weighting coefficients.

16S rRNA Sequencing

The fresh feces from mice were collected in sterile tubes and immediately flash-frozen in liquid nitrogen and stored at −80°C until analysis, as previously described (Jiang et al., 2019). The feces samples were transported to OE Biotech Co., Ltd (Shanghai, China) and analyzed on the Illumina MiSeq PE300. After the sequencing data are preprocessed to generate high-quality sequences, Vsearch software is used to classify the sequences into multiple OTUs based on the similarity of the sequences. Then, QIIME software was used to select the representative sequence of each OTU and compare all representative sequences with the Greengenes or Silva database (v. 123) database. Species comparison annotation uses an RDP classifier, and the confidence threshold was 70%.

Measurement of Cytokines in Serum and Colon

Blood was collected *via* the orbital venous plexus with anticoagulant-free tubes. Blood was centrifuged at 4500 g for 10 min at 15°C, and serum was isolated and stored at −80°C until it was used. The contents of tumor necrosis factor-alpha (TNF-α) and interleukin 6 (IL-6) in serum and the colon were measured using ELISA kits (Proteintech, Wuhan, China) according to the protocol of the manufacturer. The contents of lipopolysaccharides (LPSs) in serum were measured with commercial kits (Nanjing Jiancheng Bioengineering Institute, Nanjing, China) according to the manufacturer's instructions.

Periodic Acid–Schiff (PAS) Staining

The colon was fixed in 4% paraformaldehyde, embedded, and cut to 3-μm-thick sections. The sections of the colon were stained with periodic acid–Schiff (PAS) according to a standard procedure. The colonic goblet cells/crypts were analyzed using ImageJ software.

Western Blot

Colon samples were collected and stored at −80°C. RIPA and PMSF buffer (Solarbio, Beijing, China) was added to extract the protein in the tissue. Protein concentrations were determined using a BCA kit (Solarbio, Beijing, China). Primary antibodies against NF-κB (Cell Signaling Technology, 8242S, 1:1000 dilution), GAPDH (Proteintech, 60004-1-lg, 1:20000 dilution) were incubated at 4°C overnight. The membranes were incubated with horseradish peroxidase (HRP)–conjugated secondary antibodies (Abcam, ab205718, 1:2000 dilution; Proteintech, SA00001-1, 1:2000 dilution) for 1.5 h. The protein bands were visualized by a chemiluminescent substrate (EpiZyme, shanghai, China) and quantitated using ImageJ software.

Statistical Analyses

Statistical analysis was performed using SPSS 26 software (IBM, United States), and the data were presented as mean ± standard error. Statistical significance between four groups was determined by one-way analysis of variance (ANOVA) with the LSD assay. Bacteria relative abundance differences were performed by Tukey's honest significant difference (HSD) tests. A $p < 0.05$ was considered statistically significant.

RESULTS

Identification of Human Umbilical Cord Mesenchymal Stem Cells (UC-MSCs)

We were able to successfully isolate and culture UC-MSCs from the fresh umbilical cord (Zheng et al., 2020; Yang et al., 2021). The UC-MSCs displayed as spindle-shaped cells crawled out of the tissue pieces when the tissue blocks adhered to the bottom of the culture flask within the medium for 7–10 days (**Figure 2A**). After culture for 10–14 days, the UC-MSCs were harvested for subculturing. As shown in the third passage, the cell cluster resembled a shoal and small balls in the middle of the cells can be seen in the division phase (**Figure 2B**). The growth curve indicated that the UC-MSCs grew in an S-shaped curve (**Figure 2C**), and they continued to proliferate without being influenced by change medium, indicating that UC-MSCs had strong proliferation and self-renewal capabilities. UC-MSCs were identified by harvesting cells at the third passage and analyzed by flow cytometry. These MSCs were positive for CD73, CD105, and CD90 but negative for CD34, CD45, and HLA-DR (**Figure 2D**). Through induced differentiation of UC-MSCs, massive oil red O-positive lipid droplets and Alizarin Red-stained calcium nodules

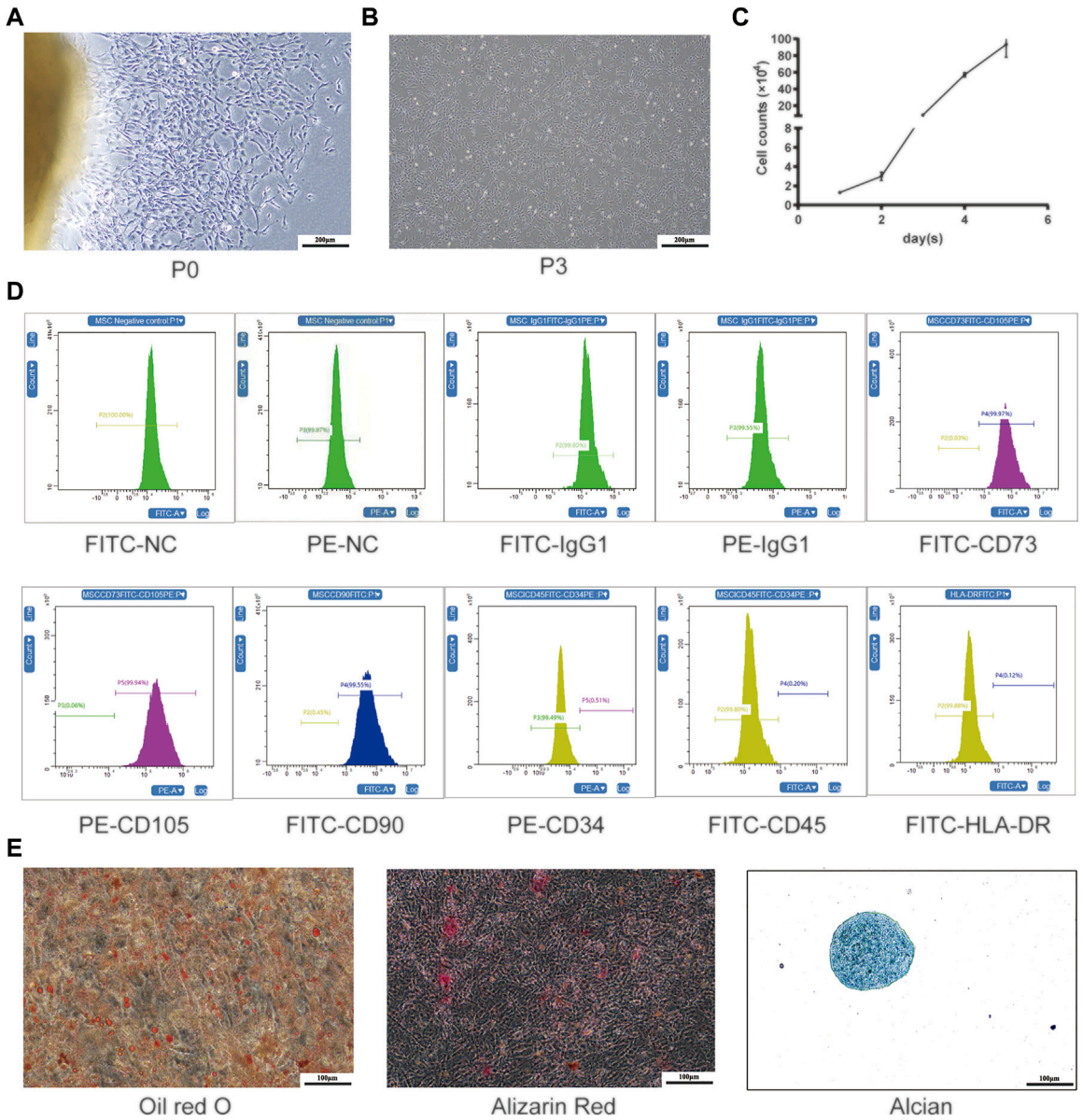

FIGURE 2 | Isolation and production of UC-MSCs. **(A)** Primary cultured UC-MSCs; **(B)** morphological feature and **(C)** growth curve of UC-MSCs at the third passage; **(D)** surface antigen labels of UC-MSCs; **(E)** induced differentiation of UC-MSCs was stained by oil red O, Alizarin Red, and Alcian Blue.

were formed. Alcian Blue staining shows acid mucopolysaccharides in cartilage tissue (**Figure 2E**).

UC-MSCs Improve Motor Function, Restore Dopaminergic Neurons, and Mitigate Microglia-Mediated Neuroinflammation in PD Mice

To assess the effects of UC-MSCs on motor function in MPTP-induced PD mice, we used the pole test to determine bradykinesia by measuring the total descent time (**Figure 3A**) and the traction test to evaluate the muscle strength and equilibrium by measuring the traction scores (**Figure 3B**). Compared with saline-treated mice, MPTP-treated mice exhibited prolonged pole descent time (9.19 ± 0.32) and lower scores (2.08 ± 0.08) in the traction test. MPTP-treated mice that received UC-MSC treatment had shortened pole descent time (6.11 ± 0.16) in the pole test and increased traction test scores (3.08 ± 0.23). Intriguingly, there was no obvious difference in

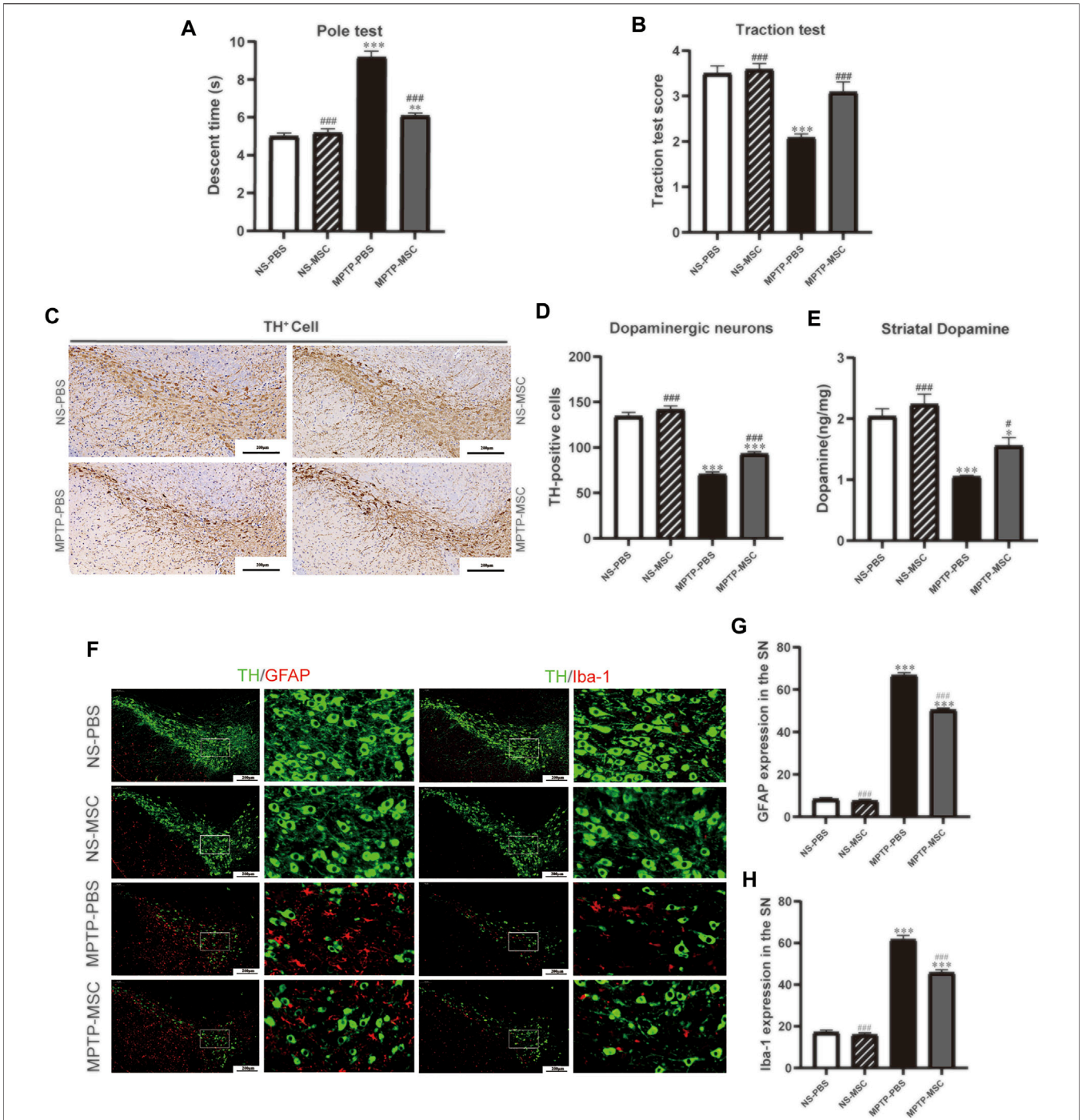

FIGURE 3 | UC-MSCs improved motor function, protected dopaminergic neurons in the substantia nigra and striatum, and alleviated microglia-mediated neuroinflammation in MPTP-induced PD mice. **(A)** Pole test; **(B)** traction test; **(C)** Immunohistostaining for tyrosine hydroxylase (TH) in the SN; **(D)** quantitative analysis of the number of TH-positive cells in the SN; **(E)** content of dopamine was measured by HPLC-MS in the ST. Data of **(A**,**B)** (n = 12 per group) are expressed as mean ± SE. Data of **(C**,**D)** (n = 3–4 per group) are expressed as mean ± SE. Scale bar: 100 μm (SN). **(F)** Double immunofluorescence staining for TH (green), GFAP (red), and Iba-1 (red) in the SN; **(G)** Quantitative analysis of the number of GFAP positive cells in each group; **(H)** Quantitative analysis of the number of microglia in each group; Data of **(F**–**H)** (n = 4 per group) are expressed as mean ± SE. Scale bar: 100 μm (SN). $^{*}p < 0.05$, $^{**}p < 0.01$, $^{***}p < 0.001$ compared with NS-PBS group, $^{\#\#}p < 0.01$, $^{\#\#\#}p < 0.001$ compared with MPTP-PBS group by one-way ANOVA.

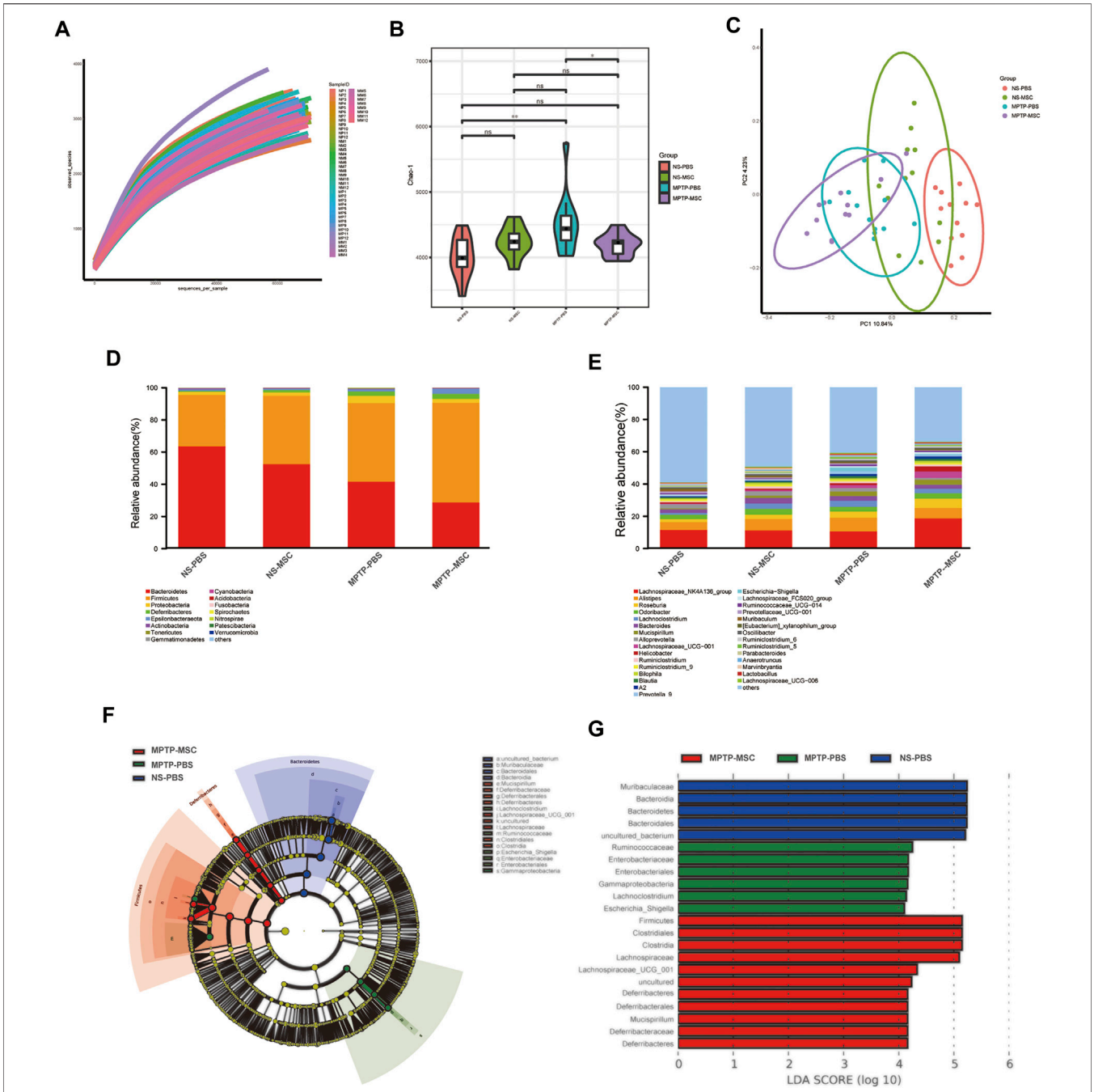

FIGURE 4 | UC-MSCs modulated the composition of gut microbiota in MPTP-induced PD mice. **(A)** Rarefaction curves of samples; **(B)** alpha diversity presented by Chao-1 index; **(C)** PCoA analysis of samples; **(D)** histogram based on relative abundance at phylum level; **(E)** average relative abundance of the microbial community for each group at the genus level. **(F,G)** Comparison of gut microbiota using LES among the NS-PBS, NS-MSC, MPTP-PBS, and MPTP-MSC groups at the OUT level. Cladogram **(F)** and histogram **(G)** of bacterial taxa that significantly differed among the three groups (LDA >4.0 and $p < 0.05$). Blue, green, red, or shading in the cladogram depicts bacterial taxa that were significantly higher in the NS-PBS, MPTP-PBS, or MPTP-MSC groups, $n = 12$ per group. *$p < 0.05$, **$p < 0.01$ compared with the MPTP-PBS group.

motor performance between UC-MSC-treated and PBS-treated mice. Therefore, UC-MSC treatment appears to selectively prevent motor dysfunction in PD mice.

To determine the effects of UC-MSCs on the survival of dopaminergic neurons in the SN and DA levels in the ST, we characterized TH expression by immunohistochemistry staining in the SN and HPLC-MS detection in the ST. Immunohistochemistry staining in the tyrosine hydroxylase revealed a significant loss of TH-positive cells in MPTP-PBS mice compared with NS-PBS mice (70.58 ± 2.56 vs 134.46 ± 4.28, $p < 0.001$). MPTP-treated mice

received UC-MSCs displayed more TH-positive cells than MPTP-mice received PBS in the SN (70.58 ± 2.56 vs 93.08 ± 2.41, $p < 0.001$). TH-positive cells in the SN did not differ between PBS-treated mice and UC-MSC-treated mice (134.46 ± 4.28 vs 141.71 ± 4.02, $p < 0.001$, **Figures 3C,D**). HPLC-MS detection showed that the DA levels in the ST dramatically decreased in MPTP-PBS mice compared with NS-PBS mice (1.05 ± 0.02 vs 2.04 ± 0.12, $p < 0.001$). MPTP-treated mice received UC-MSC treatment displayed higher DA levels than MPTP-treated mice thhat received PBS (1.56 ± 0.14 vs 1.05 ± 0.02, **Figure 3E**). These data confirmed the loss of dopaminergic neurons in the SN and decreased DA levels in the ST induced by MPTP and rescued by UC-MSCs.

To explore the effects of UC-MSCs on microglial phenotype, we analyzed microglia marker Iba-1 and GFAP by immunofluorescence. Double immunofluorescence staining for TH (dopaminergic neuron marker) and GFAP (astrocyte marker) revealed the presence of a higher number of astrocytes in MPTP-PBS mice than NS-PBS mice in the SN (66.67 ± 1.33 vs 8.33 ± 0.80, $p < 0.001$). UC-MSCs significantly decreased the number of astrocytes around dopaminergic neurons compared with MPTP-PBS mice (50.44 ± 0.84 vs 66.67 ± 1.33, $p < 0.001$, **Figures 3F,G**). Similarly, co-expression of TH with Iba-1 (microglia marker) showed that the microglia number in the SN increased in MPTP-PBS mice compared with NS-PBS mice (61.56 ± 2.08 vs 17.11 ± 1.05, $p < 0.001$), and in MPTP-MSC mice, the microglia number decreased by compared with MPTP-PBS mice (45.67 ± 1.47 vs 61.56 ± 2.08, $p < 0.001$, **Figures 3F,H**).

UC-MSCs Modulate Gut Microbiota in PD Mice

To identify the intestinal microbe phenotypes in responding to UC-MSC treatment, we analyzed the species complexity and difference of bacterial community between groups based on the OTUs and species annotation results. A flat curve was observed as the sequencing quantity increased based on the rarefaction curve, indicating that the sequencing was sufficient for data analysis (**Figure 4A**). The Chao-1 index, which illustrates the alpha diversity, was closer to the normal level in the MPTP-MSC group compared with the MPTP-PBS group (**Figure 4B**). The PCoA revealed distinct microbiota composition clustering among NS-PBS, NS-MSC, MPTP-PBS, and MPTP-MSC groups ($p < 0.001$), indicating that MPTP altered the gut microbiota, and UC-MSC administration influences the microbiota composition significantly (**Figure 4C**). As shown in the histogram at the phylum level, proteobacteria in the MPTP-PBS group were more abundant than the other three groups (**Figure 4D**). Differential abundance analyses at the genus level revealed that the relative abundance of *Escherichia-Shigella* was significantly increased in the MPTP-PBS group, and the trend was significantly reversed by UC-MSCs treatment (**Figure 4E**). Furthermore, LEfSe analyses were performed to identify the bacterial taxa that significantly differed after UC-MSC treatment. A significant shift in the microbiota based on relative abundance is shown in the cladogram (**Figure 4F**). These LEfSe comparisons identified 20 taxa (three phyla, four class, four order, five families, four genera) that were differentially abundant among the three groups (**Figure 4F**). Significant enrichments in class Gammaproteobacteria, order Enterobacteriales, families Ruminococcaceae and Enterobacteriaceae, and genera *Lachnoclostridium* and *Escherichia-Shigella* were identified in MPTP-PBS mice, while the phylum Bacteroidetes, class Bacteroidia, order Bacteroidales, and families Muribaculaceae were significantly more abundant in fecal samples from NS-PBS mice. Phylum Firmicutes and Deferribacteres, class Clostridia and Deferribacteres, order Clostridiales and Deferribacterales, families Lachnospiraceae and Deferribacteraceae, and genera Mucispirillum and Lachnospiraceae_UCG_001 were significantly enriched following UC-MSC treatment (**Figure 4G**).

UC-MSC Treatment Affects the Abundance of Certain Bacteria in MPTP-Induced PD Mice

Further analysis was performed to compare the relative abundance of certain bacteria in these four groups. At the phylum and class levels, MPTP-PBS significantly increased the relative abundance of Proteobacteria and Gammaproteobacteria compared with the NS-PBS group, and UC-MSC treatment decreased the relative abundance of Proteobacteria and Gammaproteobacteria in MPTP-PBS mice. At the order and family levels, the relative abundance of Enterobacteriales, Lactobacillales, Enterobacteriaceae, and Lactobacillaceae was significantly increased in the MPTP-PBS group compared with the NS-PBS group. UC-MSC treatment decreased the relative abundance of Enterobacteriales and Enterobacteriaceae while did not change significantly in the relative abundance of Lactobacillales and Lactobacillaceae in MPTP-PBS mice. At the genus level, the relative abundance of *Escherichia-Shigella*, Alistipes, Lachnoclostridium, and Prevotella 9 significantly increased in the MPTP-PBS group compared with the NS-PBS group. UC-MSC treatment decreased the relative abundance of *Escherichia-Shigella* and Prevotella 9, while did not alter the relative abundance of Alistipes and Lachnoclostridium in MPTP-PBS mice (**Table 1**).

UC-MSCs Modulate the Function of Gut Microbiota in MPTP-Induced PD Mice

We analyzed the correlation between the neurobehavioral parameters and relative abundance of gut microbiota by Spearman's correlation. Gammaproteobacteria, Enterobacteriaceae, Lactobacillaceae, Enterobacteriales, Lactobacillales, *Escherichia-Shigella*, Alistipes, Lachnoclostridium, and Prevotella 9 were negatively associated with the traction test scores. Proteobacteria, Gammaproteobacteria, Enterobacteriaceae, Lactobacillaceae, Enterobacterales, Lactobacillales, *Escherichia-Shigella*, and Prevotella_9 were positively associated with descent time (**Figure 5A**). PIRCUSt analysis indicated that the MPTP-PBS group had lower heatmap scores in colorectal cancer, influenza A, lysosome, small-cell lung cancer, toxoplasmosis, viral myocarditis, and p53 signaling pathway and higher scores in arachidonic acid metabolism, bacterial invasion of epithelial cells, basal transcription factors, biosynthesis of siderophore group non-ribosomal peptides, caprolactam degradation, carbohydrate digestion and absorption, circadian rhythm plant, drug metabolism-cytochrome P450, ether lipid metabolism, fluorobenzoate degradation, geraniol degradation, metabolism of xenobiotics by cytochrome P450, non-homologous end-joining, pathogenic *Escherichia coli* infection, *Staphylococcus*

TABLE 1 | Top 10 bacteria at differential levels in the four groups.

Relative abundance (%)	Group				*p*-value	
	NP	NM	MP	MM	NP vs MP	MP vs MM
p_proteobacteria	1.91 ± 0.20	2.08 ± 0.24	4.51 ± 1.20	2.40 ± 0.43	0.007	0.027
c_Gammaproteobacteria	0.69 ± 0.14	0.69 ± 0.22	3.29 ± 1.15	0.95 ± 0.39	0.005	0.011
o_Enterobacteriales	0.19 ± 0.05	0.27 ± 0.19	2.87 ± 1.14	0.64 ± 0.35	0.003	0.013
o_Lactobacillales	0.46 ± 0.49	0.38 ± 0.35	0.76 ± 0.57	0.71 ± 0.12	0.005	0.654
f_Enterobacteriaceae	0.19 ± 0.05	0.27 ± 0.19	2.87 ± 1.14	0.64 ± 0.35	0.003	0.013
f_Lactobacillaceae	0.37 ± 0.03	0.35 ± 0.03	0.66 ± 0.04	0.63 ± 0.10	0.001	0.689
g_*Escherichia-Shigella*	0.10 ± 0.03	0.12 ± 0.07	2.42 ± 1.07	0.39 ± 0.17	0.004	0.012
g_Alistipes	4.85 ± 0.68	7.05 ± 0.86	8.55 ± 0.81	6.48 ± 0.89	0.002	0.080
g_Lachnoclostridum	1.15 ± 0.12	3.36 ± 0.42	3.73 ± 0.61	2.83 ± 0.42	0.000	0.146
g_Prevotella_9	0.64 ± 0.03	0.41 ± 0.06	1.64 ± 0.11	1.06 ± 0.06	0.000	0.000

Significant changes of bacteria relative abundance in the four groups. "NP" represents the NS-PBS group, "NM" represents the NS-MSC group, "MP" represents the MPTP-PBS group, and "MM" represents the MPTP-MSC group. Statistical comparison by one-way ANOVA with post hoc comparisons of LSD. Data represent the mean ± SE, n = *12.*

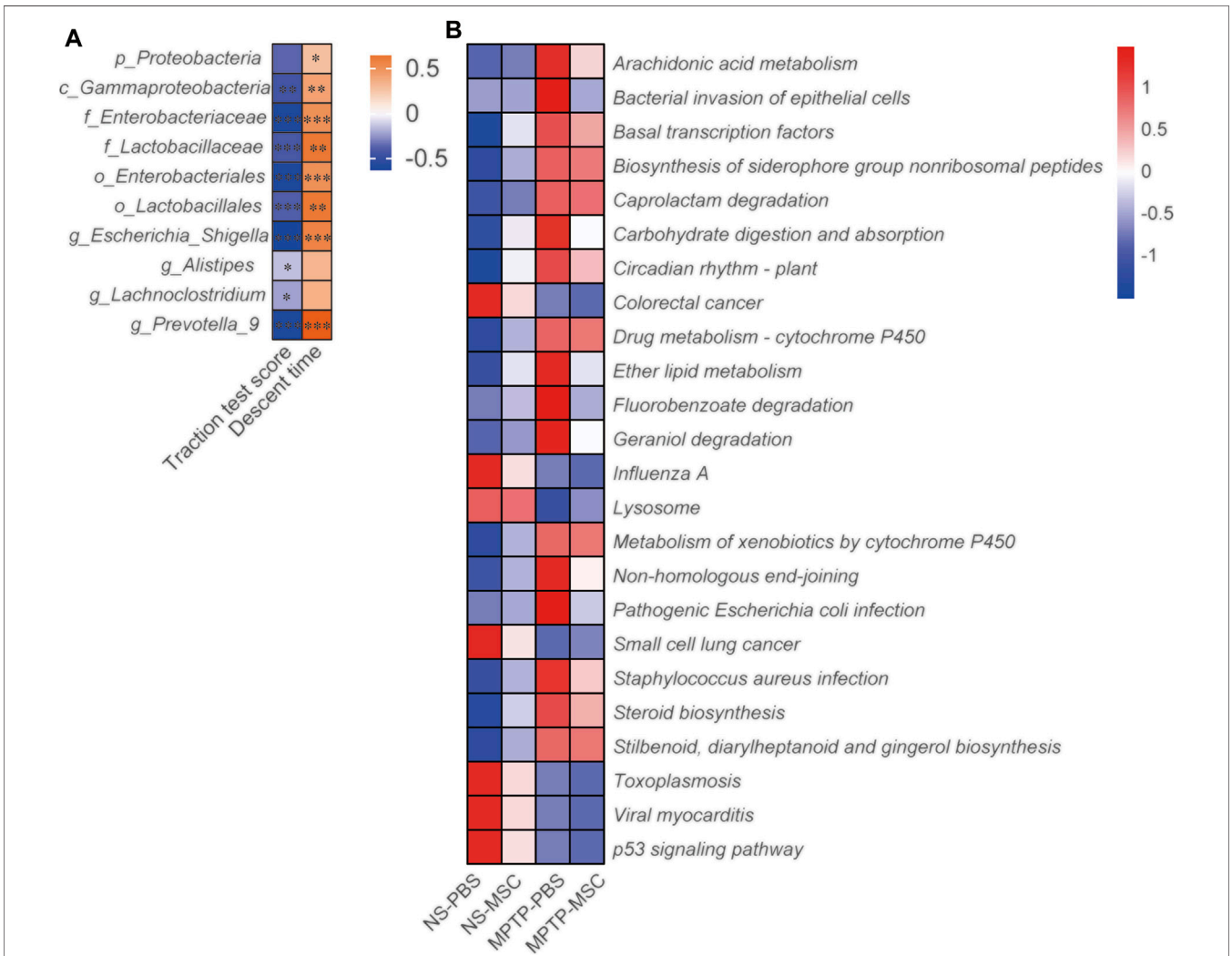

FIGURE 5 | UC-MSCs regulated the effects of gut microbiota in MPTP-induced PD mice. **(A)** The motor function score and relative abundance of gut microbiota were analyzed by Spearman correlation analyses. The association coefficient was performed on the legend of the heatmap. *, **, *** represent the correlation significant ($p < 0.05$, $p < 0.01$, $p < 0.001$, respectively); **(B)** PICRUSt analyses between the four groups. $n = 12$.

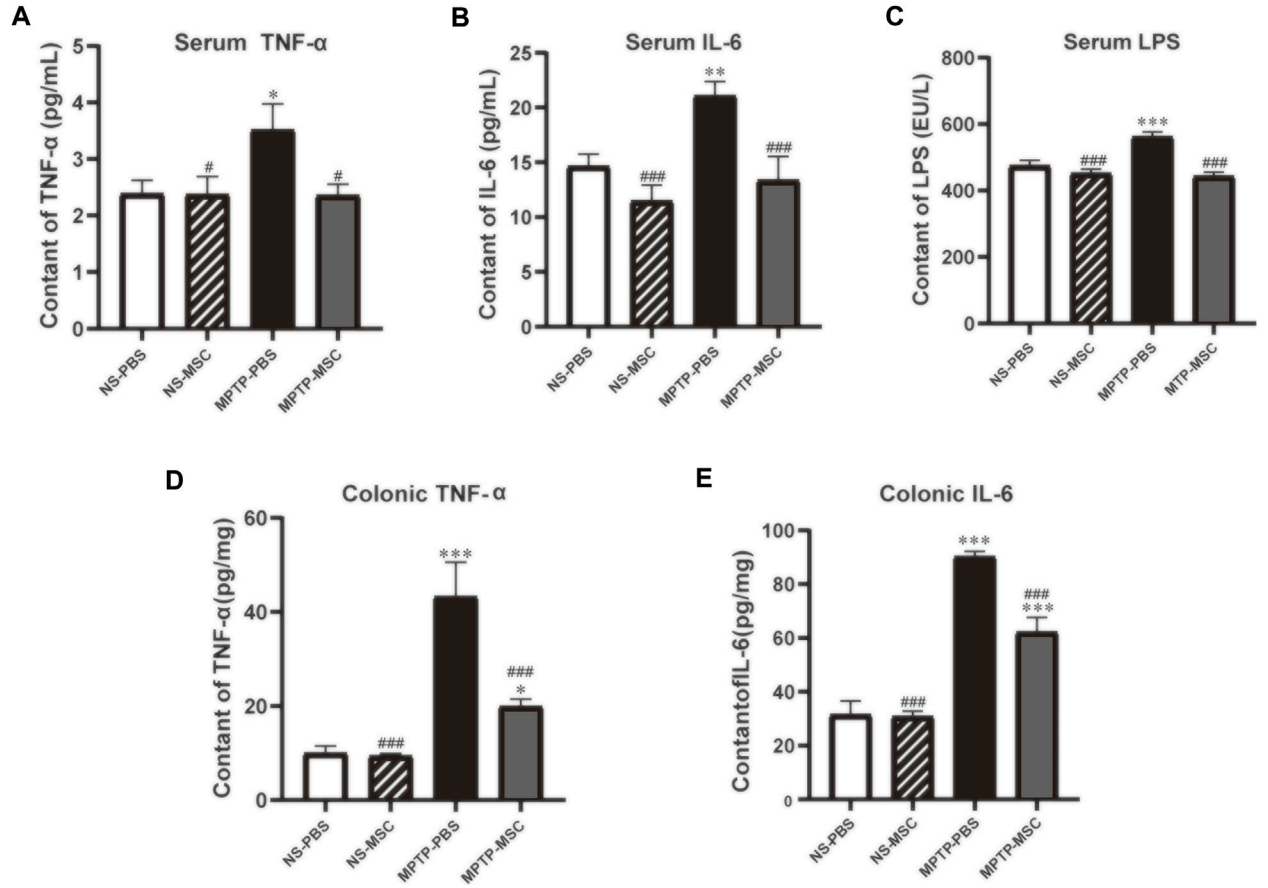

FIGURE 6 | UC-MSCs alleviated serum and colonic inflammatory cytokines in PD mice. Serum levels (pg/ml) of TNF-α **(A)**, IL-6 **(B)**, and LPS **(C)** in mice; colonic levels (pg/mg) of TNF-α **(D)** and IL-6 **(E)** in mice. Data of **(A–E)** (n = 5–6 per group) are expressed as mean ± SE. $^{*}p < 0.05$, $^{**}p < 0.01$, $^{***}p < 0.001$ compared with NS-PBS group, $^{\#}p < 0.05$, $^{\#\#\#}p < 0.001$ compared with MPTP-PBS group by one-way ANOVA.

aureus infection, steroid biosynthesis, stilbenoid, diarylheptanoid, and gingerol biosynthesis compared with mice in the NS-PBS group. UC-MSC treatment altered the bacterial invasion of epithelial cells, fluorobenzoate degradation, and pathogenic *Escherichia coli* infection compared with the MPTP-PBS group (**Figure 5B**).

Effects of UC-MSCs on Pro-Inflammatory Cytokines in Serum and Colon

The serum and colon levels of pro-inflammatory cytokines are shown in **Figure 6**. Serum TNF-α, IL-6, and LPS levels were similar between NS-PBS and NS-MSC groups, but PD model mice had higher serum levels of all pro-inflammatory cytokines. After treatment with UC-MSCs, the status of pro-inflammatory was lower than that of the MPTP-PBS group and similar to that of the NS-PBS group (**Figures 6A–C**). In addition, the effects of UC-MSCs on MPTP-induced pro-inflammatory cytokines in the colon were next explored. Compared with NS-PBS mice, the level of TNF-α and IL-6 in the colon was upregulated in MPTP-induced mice, while the mice treated with UC-MSCs showed lower levels of TNF-α and IL-6 (**Figures 6D,E**). Generally, UC-MSCs alleviated the levels of pro-inflammatory cytokines in serum and the colon in PD mice.

Effects of UC-MSC Transplantation on the Level of Neurotransmitter, the Number of Goblet Cells, and the Expression of NF-κB in Colon

We used HPLC-MS to detect the DA, 5-HT, and 5-HIAA in the colon of each group of mice. The content of DA, 5-HT, and 5-HIAA in the MPTP-PBS group was reduced compared to that in the NS-PBS group, and the intervention of UC-MSCs increased the content of 5-HT and 5-HIAA in the colon of PD mice. There is also a growing trend toward the content of DA in the MPTP-MSC group, although it has not reached statistical significance (**Figures 7A–D**). The goblet cells of the colon are closely related to the function of the intestine. Next, the goblet cells of the colon in every group were detected. As shown in **Figures 7E,F**, compared with the NS-PBS group, the goblet cells in the MPTP-PBS group were decreased, while UC-MSC treatment significantly attenuated these reductions in MPTP-injury mice, as compared to the MPTP-PBS group. There was no significant difference in the number of colonic goblet cells between the NS-PBS group and the NS-MSC group. Therefore, UC-MSC transplantation can repair the goblet cells in the colon of PD mice. To explore the pathway between the

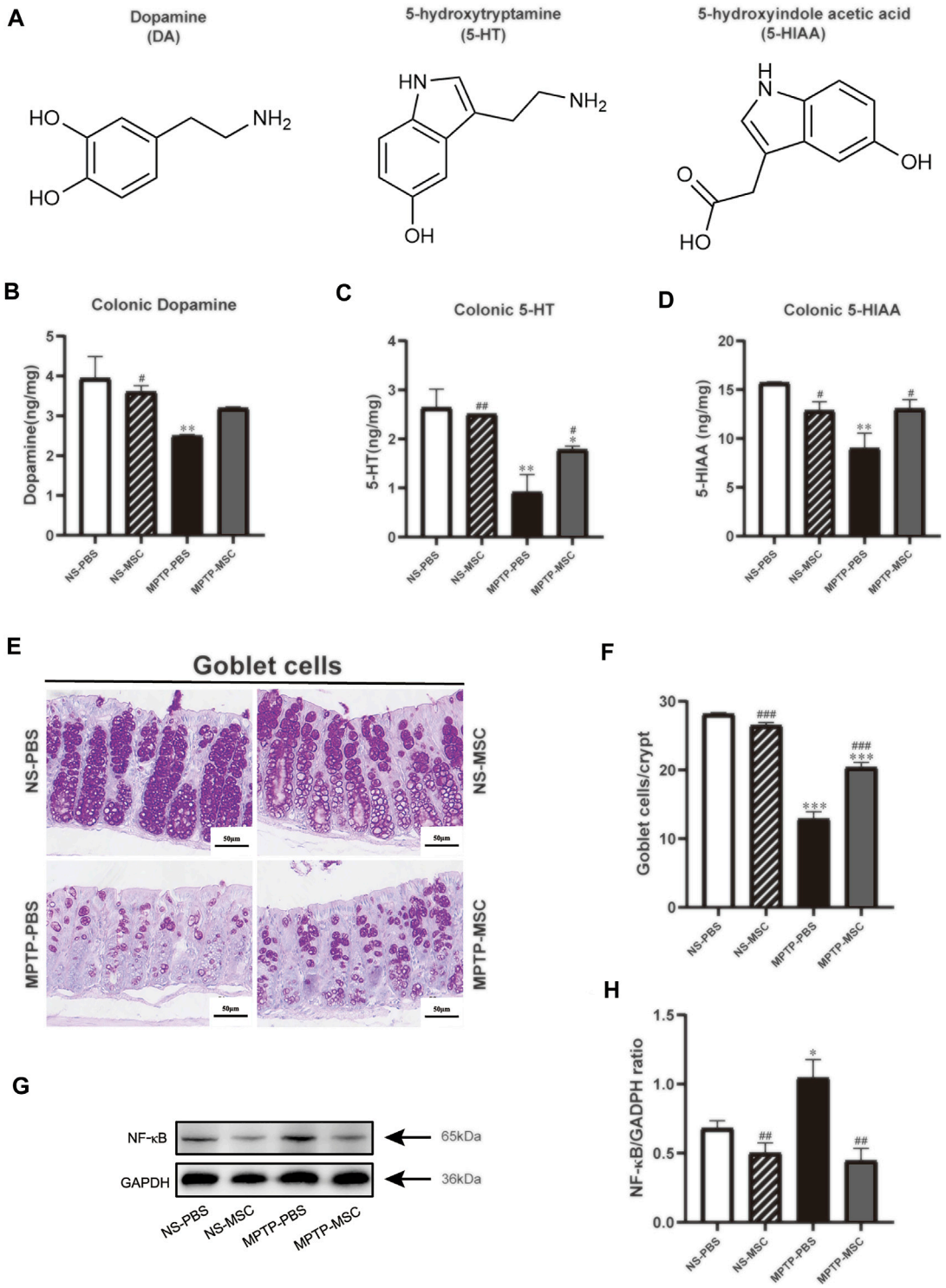

FIGURE 7 | Effects of UC-MSC treatment on the neurotransmitters, goblet cells, and the expression of NF-κB in the colon of MPTP-treated PD mice. **(A)** Chemical structures of the neurotransmitters; **(B–D)** DA, 5-HT, and 5-HIAA were analyzed by HPLC; **(E)** PAS staining of the colon (scale bar, 50 μm); **(F)** goblet cells/crypt of colon; **(G,H)** Western blot and quantitation of NF-κB protein expression in the colon. Data of **(A–H)** ($n = 3$ per group) are expressed as mean ± SE. $^{*}p < 0.05$, $^{**}p < 0.01$, $^{***}p < 0.001$ compared with the NS-PBS group, $^{\#}p < 0.05$, $^{\#\#}p < 0.01$, $^{\#\#\#}p < 0.001$ compared with the MPTP-PBS group by one-way ANOVA.

intestinal flora of disbalance and inflammation in the colon, we performed NF-κB by Western blotting. Our results indicated that UC-MSC treatment partially inhibited the expression of NF-κB following MPTP injury (**Figures 7G,H**).

DISCUSSION

To our knowledge, this is the first study to determine the effect of UC-MSCs on microbial composition in MPTP-induced PD mouse model. We found that administration of UC-MSCs through intranasal instillation ameliorated motor dysfunction in MPTP-induced PD mice. Furthermore, treatment with UC-MSCs attenuated degeneration of dopamine neurons by inhibiting glial cell activation and decreasing pro-inflammatory cytokine release. In addition, we found that nasal instillation of UC-MSCs changed gut microbiota components, maintained moral mucous barrier, and restrained NF-κB expression. These findings suggest that the brain–gut axis may mediate the beneficial effect of UC-MSCs on motor dysfunction and the protective effect on dopaminergic neurons in PD mice.

A previous study has shown that human umbilical cord blood plasma is beneficial to MPTP-treated rats by reducing pro-inflammatory cytokines in both the SNpc and intestinal mucosa and dampening inflammation-associated gut microbiota (Lee et al., 2019). In addition, altering the composition of the gut microbiota ameliorates the neurotoxicity in PD animal models (Dong et al., 2020; Koutzoumis et al., 2020). Our findings in this study provided proof-of-concept evidence that MPTP-treated mice displayed intestinal dysbiosis including impaired goblet cells and subsequently triggered SN neuroinflammation. UC-MSCs administration markedly inhibited the neuroinflammation in the SN and normalized gut microbial dysbiosis, indicating that UC-MSCs play an important role in regulating intestinal disorders in the PD.

In animal studies, intravenous injection of 5×10^5 UC-MSCs to a 6-OHDA–induced PD rat model for 3 days causes significant improvement in motor deficits, and substantia nigra TH^+ cells significantly increased compared to the vehicle group ($p < 0.05$) (Chi et al., 2019). Another study has shown that in intranasal administration of BM-MSCs to rotenone-induced PD model mice, dopaminergic cellular density in striatum dramatically increased after 10-day transplantation (Salama et al., 2017). However, the therapeutic effect was observed approximately for 5–7 days in the MPTP-induced PD model (Feng et al., 2018; Xu et al., 2019a; Rinaldi et al., 2019). Therefore, the current study explored the effect of intranasal transplantation of UC-MSCs for 5 days on the motor function and dopamine neurons of MPTP-induced PD model mice. We found that intranasal administration of UC-MSCs improved behavioral performance and protected the damaged dopaminergic neurons in the substantia nigra and striatum of PD model mice.

Dysfunction of astrocytic and microglia is involved in the pathogenesis and progression of PD because activated microglia and astrocytes by pathologic α-synuclein (α-Syn) release pro-inflammatory mediators such as TNF-α and IL-1β to promote dopaminergic neuron degeneration (Kam et al., 2020). It has been indicated that MSCs may directly impact glial cells through paracrine (Gharbi et al., 2020), the release of neurotrophic factors (Ko et al., 2018), and macrophage polarization (Lu et al., 2020). Our data showed that intranasal administration of UC-MSCs retained a normal number of astrocyte and microglial cells in the substantia nigra and decreased the level of TNF-α and IL-6 in MPTP-PD mice.

The most salient finding of our study is that UC-MSC administration decreased the relative abundance of *Proteobacteria* in MPTP-induced PD mice. Our results also demonstrated that gut microbial dysbiosis in PD mice is characterized as increases in class Gammaproteobacteria, order Enterobacteriales and Lactobacillales, family Enterobacteriaceae and Lactobacillaceae, and genus *Escherichia_shigella*. It is well known that (Ling et al., 2020) the growth of Gammaproteobacteria, Enterobacteriales, and Enterobacteriaceae of Proteobacteria could trigger the secretion of pro-inflammatory cytokines, which are induced by LPS (Dinh et al., 2015; Shin et al., 2015), and subsequently contribute to the disruption of the intestinal barrier (Litvak et al., 2017). Previous studies have reported that compared with healthy subjects, bacteria in feces from PD patients were higher in Lactobacillaceae, Enterobacteriaceae, and Enterococcaceae, while a reduction in Lachnospiraceae and an increase in Enterobacteriaceae were correlated with motor impairment and disease severity (Pietrucci et al., 2019). Another clinical study has shown that (Xu et al., 2019b) the abundance of Enterobacteriales and Enterobacteriaceae in patients during the first week in the neurological intensive care unit increases the risk of 180-day mortality, whereas a low level of Lachnospiraceae and the enrichment of Lactobacillaceae were associated with postural instability and gait disturbances (Barichella et al., 2019). The facultative anaerobes belonging to the phylum Proteobacteria, such as *Escherichia*, have been reported to be related to colitis (Hu et al., 2020). In addition, we found that UC-MSC treatment decreased the relative abundance of *Escherichia-Shigella*. It has been shown that *Escherichia-Shigella* can secrete amyloid protein to activate microglia (Chen et al., 2020), induce oxidative stress, and release inflammatory factors such as TNF-α, IL-1β, and IL-6 (Harach et al., 2017; Van Gerven et al., 2018). These inflammatory factors may increase the permeability of the intestinal epithelial and blood–brain barrier and subsequently damage the cell in the brain (Lee and Tesh, 2019). Thus, UC-MSC treatment improved gut microbial dysbiosis in the PD mouse model.

The functional pathways involved in the effect of UC-MSCs on the MPTP-induced PD model were assessed by PICRUSt Kyoto Encyclopedia of Genes and Genomes (KEGG) pathway analysis. UC-MSC treatment rescued epithelial cells by preventing bacterial invasion. Interestingly, the number of *Escherichia coli* is increased in inflammatory bowel disease (IBD) patients' fecal samples as revealed by bacteriological analysis (Mirsepasi-Lauridsen et al., 2019), and MSC therapy enhances *Escherichia coli* clearance in a mice model of bacterial pneumonia (Gupta et al., 2012). Furthermore, a recent study suggested that

colonization of Curli-producing *Escherichia coli* accelerates a-Syn pathology in the gut and brain. *Escherichia coli* needs Curli expression to exacerbate a-Syn–induced intestinal and motor disorders (Sampson et al., 2020). Our results showed that UC-MSCs reduced the expression of pathogenic *Escherichia coli* infection, indicating that UC-MSCs play a vital role in intestinal flora modulation. It has been shown that the fluorobenzoate degradation pathway is related to the severity of intestinal inflammation (Montassier et al., 2015). Furthermore, the disappearance of Proteobacteria and the subsequent decreased level of fluorobenzoate degradation improve intestinal *C. difficile* infection (Fujimoto et al., 2021). Strikingly, we found that UC-MSC administration decreased lower heatmap scores involved in fluorobenzoate degradation. This is a promising index to evaluate UC-MSC efficacy. Previous studies have verified the protective effect of geraniol on PD animal models by alleviating a-Syn aggregation, maintaining the mitochondrial function, enhancing antioxidant, and restoring the generation of BDNF and GDNF (Rekha et al., 2013a; Rekha et al., 2013b; Rekha and Inmozhi Sivakamasundari, 2018). Geraniol also targets systemic and local inflammation, dysbiosis, and mucosal damage to alleviate the dextran sulfate sodium (DSS)–induced colitis mouse model. These effects were speculated to be related to Lactobacillaceae (De Fazio et al., 2016). We observed that UC-MSC treatment slightly alleviated geraniol degradation without reaching statistical significance. Thus, future studies are warranted to assess the effect of UC-MSCs on geraniol degradation.

Dopamine and serotonin are major neurotransmitters in the gut in the regulation of nutrient absorption, blood flow, gut microbiome, local immune system, and overall gut motility (Mittal et al., 2017). A decrease in dopamine in mucus in colitis patients is a marker for impaired intestinal mucosal barrier (Magro et al., 2002; Dorofeyev et al., 2013). Furthermore, the level of 5-HT is a key player in regulating mood, sleep, and behavior disorders and is linked to imbalanced 5-HT in the gut (Delgado et al., 1990; Berger et al., 2009). We found that UC-MSC treatment significantly elevated the reduced colonic dopamine, 5-HT, and 5-HIAA levels in MPTP-treated mice. Furthermore, the observed effects of UC-MSCs on colonic neurotransmitters are consistent with the degree of colonic injury. Consistent with a recent study showing that MSCs increase goblets, where the mucus is mainly synthesized, stored, and released in experimental colitis (Alves et al., 2019), we found that UC-MSCs recovered the reduced number of goblets in the MPTP-treated mice. It has been shown that the intestinal microbiota can influence the properties of the colonic mucus layer, and mice with a penetrable mucus layer had higher levels of *Proteobacteria* in the distal colon mucus (Jakobsson et al., 2015). Thus, further investigation is needed to elucidate the precise mechanism through which other bacteria interact with mucus production.

It has been shown that the expression of α-Syn in the brain positively correlated with the degree of α-Syn in the intestinal wall since injection of Lewy bodies into the striatum induces enteric synucleinopathy in baboon monkeys (Stolzenberg et al., 2017). In addition, microbial dysbiosis can lead to increased gut mucosal permeability and inflammation, which in turn trigger α-synuclein aggregation [77]. Previous studies have shown that MSC intervention reduces the expression of α-Syn aggregates through the secretion of metal matrix protease (MMP2) (Oh et al., 2017) and induction of autophagy (Park et al., 2014). UC-MSCs may also reduce the increase in Lewy bodies in the brain and subsequently reduce the abnormal accumulation of α-Syn in the intestine, which further alleviates the inflammation of the gut. Microbial dysbiosis can lead to increased gut mucosal permeability and inflammation, which in turn trigger α-synuclein aggregation (Dalile et al., 2019). Consistently, we found that the level of TNF-α and IL-6 and the expression of NF-κB were decreased in the colon, indicating that UC-MSCs exert anti-inflammatory effects in the colon in MPTP-treated mice.

In summary, we found that UC-MSCs modulated microbial composition in an MPTP-induced PD mouse model. UC-MSCs ameliorate motor dysfunction and repair degeneration of dopamine neurons through inhibiting activated glial cells, decreasing the release of pro-inflammatory cytokines, maintaining the normal mucous barrier, and restraining the expression of NF-κB. Our findings suggest that the brain–gut axis may be a potential mechanism underlying the beneficial effect of UC-MSCs on PD mice.

DATA AVAILABILITY STATEMENT

The original contributions presented in the study are publicly available. This data can be found here: https://www.ncbi.nlm.nih.gov/sra/PRJNA784361.

ETHICS STATEMENT

The animal study was reviewed and approved by the Animal Care and Management Committee of Hebei Medical University.

AUTHOR CONTRIBUTIONS

ZS, PG, XC, and SA designed the study, analyzed and interpreted the data, and drafted the manuscript. HX, WZ, YZ, LZ, ZZ, WW, and RH conducted the experiments and analyzed the data. All authors have read and approved the final version of the manuscript.

FUNDING

This work was supported by grants from the Natural Science Foundation of Hebei Province (18967728D) and the National Natural Science Foundation of China (81273983).

REFERENCES

Alves, V. B. F., de Sousa, B. C., Fonseca, M. T. C., Ogata, H., Caliári-Oliveira, C., Yaochite, J. N. U., et al. (2019). A Single Administration of Human Adipose Tissue-Derived Mesenchymal Stromal Cells (MSC) Induces Durable and Sustained Long-Term Regulation of Inflammatory Response in Experimental Colitis. *Clin. Exp. Immunol.* 196 (2), 139–154. doi:10.1111/cei.13262

Barichella, M., Severgnini, M., Cilia, R., Cassani, E., Bolliri, C., Caronni, S., et al. (2019). Unraveling Gut Microbiota in Parkinson's Disease and Atypical Parkinsonism. *Mov. Disord.* 34 (3), 396–405. doi:10.1002/mds.27581

Berger, M., Gray, J. A., and Roth, B. L. (2009). The Expanded Biology of Serotonin. *Annu. Rev. Med.* 60, 355–366. doi:10.1146/annurev.med.60.042307.110802

Charvin, D., Medori, R., Hauser, R. A., and Rascol, O. (2018). Therapeutic Strategies for Parkinson Disease: Beyond Dopaminergic Drugs. *Nat. Rev. Drug Discov.* 17 (11), 804–822. doi:10.1038/nrd.2018.136

Chen, T.-J., Feng, Y., Liu, T., Wu, T.-T., Chen, Y.-J., Li, X., et al. (2020). Fisetin Regulates Gut Microbiota and Exerts Neuroprotective Effect on Mouse Model of Parkinson's Disease. *Front. Neurosci.* 14, 549037. doi:10.3389/fnins.2020.549037

Chi, H., Guan, Y., Li, F., and Chen, Z. (2019). The Effect of Human Umbilical Cord Mesenchymal Stromal Cells in Protection of Dopaminergic Neurons from Apoptosis by Reducing Oxidative Stress in the Early Stage of a 6-OHDA-Induced Parkinson's Disease Model. *Cel. Transpl.* 28 (1_Suppl. l), 87S–99S. doi:10.1177/0963689719891134

Choudhery, M. S., Badowski, M., Muise, A., and Harris, D. T. (2013). Comparison of Human Mesenchymal Stem Cells Derived from Adipose and Cord Tissue. *Cytotherapy* 15 (3), 330–343. doi:10.1016/j.jcyt.2012.11.010

Dalile, B., Van Oudenhove, L., Vervliet, B., and Verbeke, K. (2019). The Role of Short-Chain Fatty Acids in Microbiota-Gut-Brain Communication. *Nat. Rev. Gastroenterol. Hepatol.* 16 (8), 461–478. doi:10.1038/s41575-019-0157-3

Danielyan, L., Beer-Hammer, S., Stolzing, A., Schäfer, R., Siegel, G., Fabian, C., et al. (2014). Intranasal Delivery of Bone Marrow-Derived Mesenchymal Stem Cells, Macrophages, and Microglia to the Brain in Mouse Models of Alzheimer's and Parkinson's Disease. *Cel. Transpl.* 23 (Suppl. 1), 123–139. doi:10.3727/096368914x684970

De Fazio, L., Spisni, E., Cavazza, E., Strillacci, A., Candela, M., Centanni, M., et al. (2016). Dietary Geraniol by Oral or Enema Administration Strongly Reduces Dysbiosis and Systemic Inflammation in Dextran Sulfate Sodium-Treated Mice. *Front. Pharmacol.* 7, 38. doi:10.3389/fphar.2016.00038

Delgado, P. L., Charney, D., Price, L., Aghajanian, G., Landis, H., and Heninger, G. (1990). Serotonin Function and the Mechanism of Antidepressant Action. *Arch. Gen. Psychiatry* 47 (5), 411–418. doi:10.1001/archpsyc.1990.01810170011002

Dinh, D. M., Volpe, G. E., Duffalo, C., Bhalchandra, S., Tai, A. K., Kane, A. V., et al. (2015). Intestinal Microbiota, Microbial Translocation, and Systemic Inflammation in Chronic HIV Infection. *J. Infect. Dis.* 211 (1), 19–27. doi:10.1093/infdis/jiu409

Dong, X.-L., Wang, X., Liu, F., Liu, X., Du, Z.-R., Li, R. W., et al. (2020). Polymannuronic Acid Prevents Dopaminergic Neuronal Loss via Brain-Gut-Microbiota Axis in Parkinson's Disease Model. *Int. J. Biol. Macromolecules* 164, 994–1005. doi:10.1016/j.ijbiomac.2020.07.180

Dong, X., Feng, X., Liu, J., Xu, Y., Pan, Q., Ling, Z., et al. (2019). Characteristics of Intestinal Microecology During Mesenchymal Stem Cell-Based Therapy for Mouse Acute Liver Injury. *Stem Cell Int.* 2019, 1–14. doi:10.1155/2019/2403793

Dorofeyev, A. E., Vasilenko, I. V., Rassokhina, O. A., and Kondratiuk, R. B. (2013). Mucosal Barrier in Ulcerative Colitis and Crohn's Disease. *Gastroenterol. Res. Pract.* 2013, 1–9. doi:10.1155/2013/431231

Dorsey, E. R., and Bloem, B. R. (2018). The Parkinson Pandemic-A Call to Action. *JAMA Neurol.* 75 (1), 9–10. doi:10.1001/jamaneurol.2017.3299

Feng, P., Zhang, X., Li, D., Ji, C., Yuan, Z., Wang, R., et al. (2018). Two Novel Dual GLP-1/GIP Receptor Agonists Are Neuroprotective in the MPTP Mouse Model of Parkinson's Disease. *Neuropharmacology* 133, 385–394. doi:10.1016/j.neuropharm.2018.02.012

Fričová, D., Korchak, J. A., and Zubair, A. C. (2020). Challenges and Translational Considerations of Mesenchymal Stem/stromal Cell Therapy for Parkinson's Disease. *Npj Regen. Med.* 5 (1), 20. doi:10.1038/s41536-020-00106-y

Fujimoto, K., Kimura, Y., Allegretti, J. R., Yamamoto, M., Zhang, Y.-z., Katayama, K., et al. (2021). Functional Restoration of Bacteriomes and Viromes by Fecal Microbiota Transplantation. *Gastroenterology* 160 (6), 2089–2102. doi:10.1053/j.gastro.2021.02.013

Gharbi, T., Zhang, Z., and Yang, G.-Y. (2020). The Function of Astrocyte Mediated Extracellular Vesicles in Central Nervous System Diseases. *Front. Cel. Dev. Biol.* 8, 568889. doi:10.3389/fcell.2020.568889

Gorecki, A. M., Preskey, L., Bakeberg, M. C., Kenna, J. E., Gildenhuys, C., MacDougall, G., et al. (2019). Altered Gut Microbiome in Parkinson's Disease and the Influence of Lipopolysaccharide in a Human α-Synuclein Over-expressing Mouse Model. *Front. Neurosci.* 13, 839. doi:10.3389/fnins.2019.00839

Group, G. B. D. N. D. C. (2017). Global, Regional, and National Burden of Neurological Disorders During 1990-2015: A Systematic Analysis for the Global Burden of Disease Study 2015. *Lancet Neurol.* 16 (11), 877–897. doi:10.1016/S1474-4422(17)30299-5

Gupta, N., Krasnodembskaya, A., Kapetanaki, M., Mouded, M., Tan, X., Serikov, V., et al. (2012). Mesenchymal Stem Cells Enhance Survival and Bacterial Clearance in Murine Escherichia Coli Pneumonia. *Thorax* 67 (6), 533–539. doi:10.1136/thoraxjnl-2011-201176

Harach, T., Marungruang, N., Duthilleul, N., Cheatham, V., Mc Coy, K. D., Frisoni, G., et al. (2017). Reduction of Abeta Amyloid Pathology in APPPS1 Transgenic Mice in the Absence of Gut Microbiota. *Sci. Rep.* 7, 41802. doi:10.1038/srep41802

Hu, B., Yu, S., Shi, C., Gu, J., Shao, Y., Chen, Q., et al. (2020). Amyloid-Polyphenol Hybrid Nanofilaments Mitigate Colitis and Regulate Gut Microbial Dysbiosis. *ACS Nano* 14 (3), 2760–2776. doi:10.1021/acsnano.9b09125

Jakobsson, H. E., Rodríguez-Piñeiro, A. M., Schütte, A., Ermund, A., Boysen, P., Bemark, M., et al. (2015). The Composition of the Gut Microbiota Shapes the Colon Mucus Barrier. *EMBO Rep.* 16 (2), 164–177. doi:10.15252/embr.201439263

Jiang, X. L., Gu, X. Y., Zhou, X. X., Chen, X. M., Zhang, X., Yang, Y. T., et al. (2019). Intestinal Dysbacteriosis Mediates the Reference Memory Deficit Induced by Anaesthesia/surgery in Aged Mice. *Brain Behav. Immun.* 80, 605–615. doi:10.1016/j.bbi.2019.05.006

Kam, T.-I., Hinkle, J. T., Dawson, T. M., and Dawson, V. L. (2020). Microglia and Astrocyte Dysfunction in Parkinson's Disease. *Neurobiol. Dis.* 144, 105028. doi:10.1016/j.nbd.2020.105028

Kim, Y.-J., Park, H.-J., Lee, G., Bang, O. Y., Ahn, Y. H., Joe, E., et al. (2009). Neuroprotective Effects of Human Mesenchymal Stem Cells on Dopaminergic Neurons Through Anti-inflammatory Action. *Glia* 57 (1), 13–23. doi:10.1002/glia.20731

Ko, H. R., Ahn, S. Y., Chang, Y. S., Hwang, I., Yun, T., Sung, D. K., et al. (2018). Human UCB-MSCs Treatment Upon Intraventricular Hemorrhage Contributes to Attenuate Hippocampal Neuron Loss and Circuit Damage Through BDNF-CREB Signaling. *Stem Cel. Res. Ther.* 9 (1), 326. doi:10.1186/s13287-018-1052-5

Koutzoumis, D. N., Vergara, M., Pino, J., Buddendorff, J., Khoshbouei, H., Mandel, R. J., et al. (2020). Alterations of the Gut Microbiota with Antibiotics Protects Dopamine Neuron Loss and Improve Motor Deficits in a Pharmacological Rodent Model of Parkinson's Disease. *Exp. Neurol.* 325, 113159. doi:10.1016/j.expneurol.2019.113159

Lee, J. Y., Tuazon, J. P., Ehrhart, J., Sanberg, P. R., and Borlongan, C. V. (2019). Gutting the Brain of Inflammation: A Key Role of Gut Microbiome in Human Umbilical Cord Blood Plasma Therapy in Parkinson's Disease Model. *J. Cel. Mol. Med.* 23 (8), 5466–5474. doi:10.1111/jcmm.14429

Lee, M.-S., and Tesh, V. (2019). Roles of Shiga Toxins in Immunopathology. *Toxins* 11 (4), 212. doi:10.3390/toxins11040212

Li, C.-y., Wu, X.-y., Tong, J.-b., Yang, X.-x., Zhao, J.-l., Zheng, Q.-f., et al. (2015). Comparative Analysis of Human Mesenchymal Stem Cells from Bone Marrow and Adipose Tissue Under Xeno-free Conditions for Cell Therapy. *Stem Cel. Res. Ther.* 6, 55. doi:10.1186/s13287-015-0066-5

Li, X., Lu, C., Fan, D., Lu, X., Xia, Y., Zhao, H., et al. (2020). Human Umbilical Mesenchymal Stem Cells Display Therapeutic Potential in Rheumatoid Arthritis by Regulating Interactions Between Immunity and Gut Microbiota via the Aryl Hydrocarbon Receptor. *Front. Cel Dev. Biol.* 8, 131. doi:10.3389/fcell.2020.00131

Li, Y., Zhang, Y., Zhang, X.-L., Feng, X.-Y., Liu, C.-Z., Zhang, X.-N., et al. (2019). Dopamine Promotes Colonic Mucus Secretion Through Dopamine D5 Receptor in Rats. *Am. J. Physiology-Cell Physiol.* 316 (3), C393–C403. doi:10.1152/ajpcell.00261.2017

Ling, Y., Gu, Q., Zhang, J., Gong, T., Weng, X., Liu, J., et al. (2020). Structural Change of Gut Microbiota in Patients with Post-Stroke Comorbid Cognitive Impairment and Depression and its Correlation with Clinical Features. *J. Alzheimers Dis.* 77 (4), 1595–1608. doi:10.3233/jad-200315

Litvak, Y., Byndloss, M. X., Tsolis, R. M., and Bäumler, A. J. (2017). Dysbiotic Proteobacteria Expansion: A Microbial Signature of Epithelial Dysfunction. *Curr. Opin. Microbiol.* 39, 1–6. doi:10.1016/j.mib.2017.07.003

Long, Q., Upadhya, D., Hattiangady, B., Kim, D.-K., An, S. Y., Shuai, B., et al. (2017). Intranasal MSC-Derived A1-Exosomes Ease Inflammation, and Prevent Abnormal Neurogenesis and Memory Dysfunction after Status Epilepticus. *Proc. Natl. Acad. Sci. USA* 114 (17), E3536–E3545. doi:10.1073/pnas.1703920114

Lu, X., Li, N., Zhao, L., Guo, D., Yi, H., Yang, L., et al. (2020). Human Umbilical Cord Mesenchymal Stem Cells Alleviate Ongoing Autoimmune Dacryoadenitis in Rabbits via Polarizing Macrophages into an Anti-inflammatory Phenotype. *Exp. Eye Res.* 191, 107905. doi:10.1016/j.exer.2019.107905

Lv, W., Graves, D. T., He, L., Shi, Y., Deng, X., Zhao, Y., et al. (2020). Depletion of the Diabetic Gut Microbiota Resistance Enhances Stem Cells Therapy in Type 1 Diabetes Mellitus. *Theranostics* 10 (14), 6500–6516. doi:10.7150/thno.44113

Magro, F., Vieira-Coelho, M. A., Fraga, S., Serräo, M. P., Veloso, F. T., Ribeiro, T., et al. (2002). Impaired Synthesis or Cellular Storage of Norepinephrine, Dopamine, and 5-hydroxytryptamine in Human Inflammatory Bowel Disease. *Dig. Dis. Sci.* 47 (1), 216–224. doi:10.1023/a:1013256629600

Mirsepasi-Lauridsen, H. C., Vallance, B. A., Krogfelt, K. A., and Petersen, A. M. (2019). *Escherichia coli* Pathobionts Associated with Inflammatory Bowel Disease. *Clin. Microbiol. Rev.* 32 (2), e00060. doi:10.1128/cmr.00060-18

Mittal, R., Debs, L. H., Patel, A. P., Nguyen, D., Patel, K., O'Connor, G., et al. (2017). Neurotransmitters: The Critical Modulators Regulating Gut-Brain Axis. *J. Cel. Physiol.* 232 (9), 2359–2372. doi:10.1002/jcp.25518

Montassier, E., Gastinne, T., Vangay, P., Al-Ghalith, G. A., Bruley des Varannes, S., Massart, S., et al. (2015). Chemotherapy-driven Dysbiosis in the Intestinal Microbiome. *Aliment. Pharmacol. Ther.* 42 (5), 515–528. doi:10.1111/apt.13302

Narbute, K., Piļipenko, V., Pupure, J., Dzirkale, Z., Jonavičė, U., Tunaitis, V., et al. (2019). Intranasal Administration of Extracellular Vesicles Derived from Human Teeth Stem Cells Improves Motor Symptoms and Normalizes Tyrosine Hydroxylase Expression in the Substantia Nigra and Striatum of the 6-Hydroxydopamine-Treated Rats. *Stem Cell Translational Med.* 8 (5), 490–499. doi:10.1002/sctm.18-0162

Oh, S. H., Kim, H. N., Park, H. J., Shin, J. Y., Kim, D. Y., and Lee, P. H. (2017). The Cleavage Effect of Mesenchymal Stem Cell and its Derived Matrix Metalloproteinase-2 on Extracellular α-Synuclein Aggregates in Parkinsonian Models. *Stem Cell Translational Med.* 6 (3), 949–961. doi:10.5966/sctm.2016-0111

Park, H. J., Shin, J. Y., Kim, H. N., Oh, S. H., and Lee, P. H. (2014). Neuroprotective Effects of Mesenchymal Stem Cells Through Autophagy Modulation in a Parkinsonian Model. *Neurobiol. Aging* 35 (8), 1920–1928. doi:10.1016/j.neurobiolaging.2014.01.028

Perez-Pardo, P., Dodiya, H. B., Engen, P. A., Forsyth, C. B., Huschens, A. M., Shaikh, M., et al. (2019). Role of TLR4 in the Gut-Brain Axis in Parkinson's Disease: A Translational Study from Men to Mice. *Gut* 68 (5), 829–843. doi:10.1136/gutjnl-2018-316844

Pietrucci, D., Cerroni, R., Unida, V., Farcomeni, A., Pierantozzi, M., Mercuri, N. B., et al. (2019). Dysbiosis of Gut Microbiota in a Selected Population of Parkinson's Patients. *Parkinsonism Relat. Disord.* 65, 124–130. doi:10.1016/j.parkreldis.2019.06.003

Rekha, K. R., and Inmozhi Sivakamasundari, R. (2018). Geraniol Protects Against the Protein and Oxidative Stress Induced by Rotenone in an In Vitro Model of Parkinson's Disease. *Neurochem. Res.* 43 (10), 1947–1962. doi:10.1007/s11064-018-2617-5

Rekha, K. R., Selvakumar, G. P., Santha, K., and Inmozhi Sivakamasundari, R. (2013). Geraniol Attenuates α-synuclein Expression and Neuromuscular Impairment Through Increase Dopamine Content in MPTP Intoxicated Mice by Dose Dependent Manner. *Biochem. Biophysical Res. Commun.* 440 (4), 664–670. doi:10.1016/j.bbrc.2013.09.122

Rekha, K. R., Selvakumar, G. P., Sethupathy, S., Santha, K., and Sivakamasundari, R. I. (2013). Geraniol Ameliorates the Motor Behavior and Neurotrophic Factors Inadequacy in MPTP-Induced Mice Model of Parkinson's Disease. *J. Mol. Neurosci.* 51 (3), 851–862. doi:10.1007/s12031-013-0074-9

Rinaldi, F., Seguella, L., Gigli, S., Hanieh, P. N., Del Favero, E., Cantù, L., et al. (2019). inPentasomes: An Innovative Nose-To-Brain Pentamidine Delivery Blunts MPTP Parkinsonism in Mice. *J. Controlled Release* 294, 17–26. doi:10.1016/j.jconrel.2018.12.007

Riordan, N. H., Hincapié, M. L., Morales, I., Fernández, G., Allen, N., Leu, C., et al. (2019). Retracted: Allogeneic Human Umbilical Cord Mesenchymal Stem Cells for the Treatment of Autism Spectrum Disorder in Children: Safety Profile and Effect on Cytokine Levels. *Stem Cell translational Med.* 8 (10), 1008–1016. doi:10.1002/sctm.19-0010

Riordan, N. H., Morales, I., Fernández, G., Allen, N., Fearnot, N. E., Leckrone, M. E., et al. (2018). Clinical Feasibility of Umbilical Cord Tissue-Derived Mesenchymal Stem Cells in the Treatment of Multiple Sclerosis. *J. Transl Med.* 16 (1), 57. doi:10.1186/s12967-018-1433-7

Salama, M., Sobh, M., Emam, M., Abdalla, A., Sabry, D., El-Gamal, M., et al. (2017). Effect of Intranasal Stem Cell Administration on the Nigrostriatal System in a Mouse Model of Parkinson's Disease. *Exp. Ther. Med.* 13 (3), 976–982. doi:10.3892/etm.2017.4073

Sampson, T. R., Challis, C., Jain, N., Moiseyenko, A., Ladinsky, M. S., Shastri, G. G., et al. (2020). A Gut Bacterial Amyloid Promotes α-synuclein Aggregation and Motor Impairment in Mice. *eLife* 9, e53111. doi:10.7554/eLife.53111

Shin, N.-R., Whon, T. W., and Bae, J.-W. (2015). Proteobacteria: Microbial Signature of Dysbiosis in Gut Microbiota. *Trends Biotechnology* 33 (9), 496–503. doi:10.1016/j.tibtech.2015.06.011

Simon, C., Gan, Q., Kathivaloo, P., Mohamad, N., Dhamodharan, J., Krishnan, A., et al. (2019). Deciduous DPSCs Ameliorate MPTP-Mediated Neurotoxicity, Sensorimotor Coordination and Olfactory Function in Parkinsonian Mice. *Int. J. Mol. Sci.* 20 (3), 568. doi:10.3390/ijms20030568

Soontararak, S., Chow, L., Johnson, V., Coy, J., Wheat, W., Regan, D., et al. (2018). Mesenchymal Stem Cells (MSC) Derived from Induced Pluripotent Stem Cells (iPSC) Equivalent to Adipose-Derived MSC in Promoting Intestinal Healing and Microbiome Normalization in Mouse Inflammatory Bowel Disease Model. *Stem Cell translational Med.* 7 (6), 456–467. doi:10.1002/sctm.17-0305

Stolzenberg, E., Berry, D., Yang, D., Lee, E. Y., Kroemer, A., Kaufman, S., et al. (2017). A Role for Neuronal Alpha-Synuclein in Gastrointestinal Immunity. *J. Innate Immun.* 9 (5), 456–463. doi:10.1159/000477990

Sun, J., Ding, X., Liu, S., Duan, X., Liang, H., and Sun, T. (2020). Adipose-derived Mesenchymal Stem Cells Attenuate Acute Lung Injury and Improve the Gut Microbiota in Septic Rats. *Stem Cel. Res. Ther.* 11 (1), 384. doi:10.1186/s13287-020-01902-5

Sun, J., Li, H., Jin, Y., Yu, J., Mao, S., Su, K.-P., et al. (2021). Probiotic Clostridium Butyricum Ameliorated Motor Deficits in a Mouse Model of Parkinson's Disease via Gut Microbiota-GLP-1 Pathway. *Brain Behav. Immun.* 91, 703–715. doi:10.1016/j.bbi.2020.10.014

Sun, M.-F., Zhu, Y.-L., Zhou, Z.-L., Jia, X.-B., Xu, Y.-D., Yang, Q., et al. (2018). Neuroprotective Effects of Fecal Microbiota Transplantation on MPTP-Induced Parkinson's Disease Mice: Gut Microbiota, Glial Reaction and TLR4/TNF-α Signaling Pathway. *Brain Behav. Immun.* 70, 48–60. doi:10.1016/j.bbi.2018.02.005

Van Gerven, N., Van der Verren, S. E., Reiter, D. M., and Remaut, H. (2018). The Role of Functional Amyloids in Bacterial Virulence. *J. Mol. Biol.* 430 (20), 3657–3684. doi:10.1016/j.jmb.2018.07.010

Visanji, N. P., Brooks, P. L., Hazrati, L.-N., and Lang, A. E. (2013). The Prion Hypothesis in Parkinson's Disease: Braak to the Future. *Acta Neuropathol. Commun.* 1, 2. doi:10.1186/2051-5960-1-2

Wang, Z., Chen, A., Yan, S., and Li, C. (2016). Study of Differentiated Human Umbilical Cord-Derived Mesenchymal Stem Cells Transplantation on Rat Model of Advanced Parkinsonism. *Cell Biochem. Funct.* 34 (6), 387–393. doi:10.1002/cbf.3204

Xu, R., Tan, C., Zhu, J., Zeng, X., Gao, X., Wu, Q., et al. (2019). Dysbiosis of the Intestinal Microbiota in Neurocritically Ill Patients and the Risk for Death. *Crit. Care* 23 (1), 195. doi:10.1186/s13054-019-2488-4

Xu, S.-F., Zhang, Y.-H., Wang, S., Pang, Z.-Q., Fan, Y.-G., Li, J.-Y., et al. (2019). Lactoferrin Ameliorates Dopaminergic Neurodegeneration and Motor Deficits in MPTP-Treated Mice. *Redox. Biol.* 21, 101090. doi:10.1016/j.redox.2018.101090

Yang, S., Liang, X., Song, J., Li, C., Liu, A., Luo, Y., et al. (2021). A Novel Therapeutic Approach for Inflammatory Bowel Disease by Exosomes Derived from Human Umbilical Cord Mesenchymal Stem Cells to Repair Intestinal Barrier via TSG-6. *Stem Cel. Res. Ther.* 12 (1), 315. doi:10.1186/s13287-021-02404-8

Zheng, J.-H., Zhang, J.-K., Kong, D.-S., Song, Y.-B., Zhao, S.-D., Qi, W.-B., et al. (2020). Quantification of the CM-Dil-Labeled Human Umbilical Cord Mesenchymal Stem Cells Migrated to the Dual Injured Uterus in SD Rat. *Stem Cel. Res. Ther.* 11 (1), 280. doi:10.1186/s13287-020-01806-4

Zhou, Z.-L., Jia, X.-B., Sun, M.-F., Zhu, Y.-L., Qiao, C.-M., Zhang, B.-P., et al. (2019). Neuroprotection of Fasting Mimicking Diet on MPTP-Induced Parkinson's Disease Mice via Gut Microbiota and Metabolites. *Neurotherapeutics* 16 (3), 741–760. doi:10.1007/s13311-019-00719-2

Conflict of Interest: The authors declare that the research was conducted in the absence of any commercial or financial relationships that could be construed as a potential conflict of interest.

Publisher's Note: All claims expressed in this article are solely those of the authors and do not necessarily represent those of their affiliated organizations, or those of the publisher, the editors, and the reviewers. Any product that may be evaluated in this article, or claim that may be made by its manufacturer, is not guaranteed or endorsed by the publisher.

frontiers in Cell and Developmental Biology

ORIGINAL RESEARCH
published: 03 February 2022
doi: 10.3389/fcell.2021.752053

Human Amniotic Epithelial Cells and Their Derived Exosomes Protect Against Cisplatin-Induced Acute Kidney Injury Without Compromising Its Antitumor Activity in Mice

Xin Kang[1,2,3†], *Ying Chen*[1,2,3,4,5†], *Xiaohong Xin*[1,2,3], *Menghan Liu*[1,2,3], *Yuan Ma*[1,2,3], *Yifei Ren*[1,2,3], *Jing Ji*[1,2,3], *Qi Yu*[1,2,3], *Lei Qu*[1,2,3], *Suxia Wang*[6], *Gang Liu*[1,2,3,4,5], *Chengang Xiang*[1,2,3,4,5*] *and Li Yang*[1,2,3,4,5*]

[1]*Renal Division, Renal Pathology Center, Peking University First Hospital, Beijing, China,* [2]*Institute of Nephrology, Peking University, Beijing, China,* [3]*Key Laboratory of Renal Disease, Ministry of Health of China, Beijing, China,* [4]*Key Laboratory of CKD Prevention and Treatment, Ministry of Education of China, Peking University, Beijing, China,* [5]*Research Units of Diagnosis and Treatment of Immune-mediated Kidney Diseases, Chinese Academy of Medical Sciences, Beijing, China,* [6]*Laboratory of Electron Microscopy, Pathological Center, Peking University First Hospital, Beijing, China*

OPEN ACCESS

Edited by:
Jianjun Zhou,
Tongji University, China

Reviewed by:
Zheng Dong,
Augusta University, United States
Chuanming Hao,
Fudan University, China
Aihua Zhang,
Nanjing Children's Hospital, China

***Correspondence:**
Li Yang
li.yang@bjmu.edu.cn
Chengang Xiang
chengangxiang@bjmu.edu.cn

†These authors have contributed equally to this work and share first authorship

Specialty section:
This article was submitted to Stem Cell Research, a section of the journal Frontiers in Cell and Developmental Biology

Received: *02 August 2021*
Accepted: *08 December 2021*
Published: *03 February 2022*

Citation:
Kang X, Chen Y, Xin X, Liu M, Ma Y, Ren Y, Ji J, Yu Q, Qu L, Wang S, Liu G, Xiang C and Yang L (2022) Human Amniotic Epithelial Cells and Their Derived Exosomes Protect Against Cisplatin-Induced Acute Kidney Injury Without Compromising Its Antitumor Activity in Mice. Front. Cell Dev. Biol. 9:752053. doi: 10.3389/fcell.2021.752053

Background: Cisplatin is a widely used chemotherapeutic drug, whereas the clinical application is greatly limited by its nephrotoxic side effect. Currently, there has been no effective treatment to prevent cisplatin-induced acute kidney injury (cisplatin-AKI). Human amniotic epithelial cells (hAECs) and their derived exosomes (EXOs) have been proven to effectively protect against ischemia reperfusion-induced AKI, yet their roles in cisplatin-AKI are still unknown.

Methods: C57BL/6J mice were given two doses of cisplatin at 20 or 15 mg/kg of body weight to induce AKI with or without mortality. hAECs or EXOs were injected via tail vein 1 day after cisplatin administration. Serum and kidney tissues were collected on the fourth day after 15 mg/kg cisplatin treatment to explore the nephro-protective effects of hAECs and EXOs on cisplatin-AKI. Lung cancer xenograft model was built by subcutaneous injection of A549 cells into BALB/c nude mice to evaluate the effect of hAECs or EXOs on cisplatin chemotherapy.

Results: Cisplatin nephrotoxicity was significantly attenuated by hAECs and EXOs as evidenced by reduced mortality rate and decreased serum creatinine (sCr) and reduced tubular injury score. hAECs or EXOs exerted the nephro-protective effects via suppression of TNF-α/MAPK and caspase signaling pathways. In the A549 lung cancer xenograft mouse model, administration of hAECs or EXOs did not promote tumor growth or compromise the therapeutic effects of cisplatin on tumors.

Conclusion: This study is the first to demonstrate that hAECs and their derived exosomes have nephro-protective effects in cisplatin-AKI *in vivo*. Importantly, neither hAECs nor EXOs compromise the antitumor activity of cisplatin. These results potentially support the use of hAECs and their derived EXOs as nephro-protectors against cisplatin-induced nephrotoxicity clinically.

Keywords: human amniotic epithelial cells (hAECs), exosomes, cisplatin, acute kidney injury, chemotherapy

INTRODUCTION

Acute kidney injury (AKI) is defined as an abrupt decrease in kidney function within hours, which encompasses structural damage of the kidney and loss of renal function (Makris and Spanou, 2016). It is a common clinical syndrome that complicates the course and worsens the outcome in a significant number of hospitalized patients including patients with tumors (Sanchez and Francoz, 2021). Cis-diamminedichloroplatinum (II) (cisplatin), is one of the most effective chemotherapeutic drugs for a variety of malignant tumors, such as non-small cell lung cancer (NSCLC), head and neck malignancies, bladder cancer, advanced gastric cancer, metastatic triple-negative breast cancer, etc., (Dasari and Tchounwou, 2014). However, the nephrotoxic side effects of cisplatin greatly restrict its clinical application (Volarevic et al., 2019). Cisplatin is mainly taken up and excreted through proximal tubule-localized transporters, such as OCT2 and MATE1 (Ciarimboli, 2014). Consequently, cisplatin accumulates in renal proximal tubular cells, resulting in inflammation, injury, and cell death (Holditch et al., 2019). It is reported that the incidence of AKI in cancer patients after receiving cisplatin chemotherapy reaches about 20%–40% (Arany and Safirstein, 2003; dos Santos et al., 2012), of which about 13% of patients develop AKI after the first course of cisplatin chemotherapy. Therefore, there is an urgent need for the clinical application of safe and efficacious nephro-protective therapy for cisplatin-treated patients (Motwani et al., 2018).

In recent years, stem cell therapy has shown great potential in the treatment of AKI (Barnes et al., 2016; Sávio-Silva et al., 2020). Allogeneic or xenotransplantation of mesenchymal stem cells (MSCs) from different sources (such as bone marrow, fat, cord blood, etc.,) has been reported to have beneficial therapeutic effects on cisplatin induced AKI (cisplatin-AKI) (Sávio-Silva et al., 2020). Despite the supportive results, the use of MSCs in cisplatin-AKI still encounters the risks of tumorigenicity and promotion of tumor cell proliferation. Human amniotic epithelial cells (hAECs) are epithelial cells isolated from the amniotic membrane tissue on the side of the placenta near the fetus. hAECs have the ability to differentiate into cells of all three germ layers, namely, ectoderm, mesoderm, and endoderm (Miki et al., 2005). Studies have shown that hAECs have the advantages of low mutation frequency, low immunogenicity, lack of telomerase leading to non-tumorigenicity, abundant cell sources, no ethical risks, etc., which have attracted widespread attention in regenerative medicine (Miki, 2018).

Recent studies have shown that the application of hAECs in animal models of many diseases has achieved good therapeutic effects, including lung injury and liver fibrosis (Cargnoni et al., 2018; Tan et al., 2018). It has been reported that in chemotherapy-induced premature ovarian failure, exosomes (EXOs) derived from hAECs can inhibit apoptosis by transferring miRNAs and restore ovarian function (Zhang et al., 2019). Combining the limitations of previous stem cell therapy on cisplatin-AKI and the advantages of hAECs, this study aims to explore the therapeutic effects of hAECs and EXOs on cisplatin induced acute nephrotoxicity, and to systematically evaluate the safety of hAECs or EXOs on tumor proliferation and on the effect of cisplatin chemotherapy in NSCLC xenograft mouse model.

METHODS

Experimental Animals

Male C57BL/6J mice (7 weeks old) and BALB/c nude mice (4 weeks old) were purchased from Vital River Laboratory Animal Technology (Beijing, China) [License No. SCXK (Jing) 2016–0011]. All mice were maintained in animal facilities under specific pathogen-free (SPF) conditions. All animal experiments were performed with the approval of the Institutional Animal Care and Use Committee of Peking University First Hospital (Approval Number: J202065).

Isolation and Culture of hAECs

hAECs were provided by Shanghai iCELL Biotechnology Co., Ltd. (Shanghai, China). The isolation and culture of hAECs had been described in our previous study (Ren et al., 2020). Briefly, hAECs were isolated from fresh amnion membranes collected from healthy mothers after cesarean deliveries with written and informed consent. The procedure was approved by the Institutional Ethics Committee of the International Peace Maternity and Child Health Hospital, School of Medicine, Shanghai Jiao Tong University (Approval Number: [2014] 11). hAECs were cultured by complete culture medium (DMEM/F12 supplemented with 10% FBS, 2 mM glutamine, 1% streptomycin-penicillin, and 10 ng/ml recombinant human epidermal growth factor) in 5% CO2 incubated at 37°C. The P1 hAECs resuspended in PBS at 1×10^7/ml were used in the follow-up experiments.

Isolation and Identification of EXOs

The isolation and identification of hAECs derived EXOs have been described in our previous study (Ren et al., 2020). Briefly, when cultured hAECs were 80%–90% confluent, the complete culture medium was replaced with serum-free DMEM/F12 medium. After 24 h, the conditioned culture medium was collected and experienced serial centrifugation at $2,000 \times g$ for 30 min at 4°C, and $20,000 \times g$ (Beckman Coulter, USA) for 30 min at 4°C and $150,000 \times g$ for 70 min at 4°C twice to obtain EXOs. The ultrastructure of the EXOs was analyzed under a transmission electron microscope (Zeiss, Oberkochen, Germany). The protein levels of exosome markers CD63, TSG101, Alix, and Flotllin were detected using Western blots. Nanoparticle tracking analysis (NTA) was performed to determine the size and concentration of the purified vesicles (Particle Metrix, Meerbusch, Germany).

Cisplatin-AKI in C57BL/6J Mice

After adaptive feeding for 1 week, 7-week-old male C57BL/6J mice were randomly divided into four groups: PBS group, cisplatin group, cisplatin + hAECs group, and cisplatin + EXOs group. Each group contained 9 or 10 mice. A single intraperitoneal injection of cisplatin (Cat# P4394, Sigma Aldrich, USA) was used to induce AKI. Cisplatin at 20 mg/kg of body weight was used to induce severe AKI with mortality after 3 days post cisplatin injection (Holditch et al., 2019). Cisplatin at 15 mg/kg of body weight was used to induce moderate AKI without mortality. The normal control mice were

administered the same volume of PBS. At 24 h after cisplatin injection, 100 μl of PBS, hAECs (1×10^6), or EXOs (1×10^8) resuspended in PBS was injected into the mice intravenously. The dosages of hAECs and EXOs in the treatment groups were determined according to our previous study (Ren et al., 2020). Blood and kidney samples were collected from moderate cisplatin-AKI mice 4 days after cisplatin injection. Serum creatinine (sCr) levels were measured by the creatinine assay kit (Cat# DICT-500, BioAssay Systems, USA) according to the improved Jaffe method.

Renal Histology

Kidney tissue sections were fixed with 10% buffered formalin followed by paraffin embedding and stained with periodic acid-Schiff (PAS). The degree of tubulointerstitial damage was scored semi-quantitatively by two renal pathologists who were blinded to the experimental groups. The scores were based on a 0 to 4 + scale, according to the percentage of the cortex and outer medullar region affected by loss of brush border, tubular necrosis, and renal tubular cell cast (0 = no lesion, 1+ = < 25%, 2+ = >25%–50%, 3+ = >50%–75%, 4+ = >75% to <100%).

NSCLC Tumor Model in Nude Mice

A549, a cell line of non-small cell lung cancer (NSCLC), was purchased from the American Type Culture Collection. A549 was cultured in high-glucose DMEM with 10% FBS and 1% penicillin–streptomycin. To establish NSCLC xenografts, 1×10^6 A549 suspended in 50 μl of PBS added with 50 μl of Matrigel (Cat#356234, BD, USA) was subcutaneously injected at the right flank of male BALB/c nude mice to grow tumor for about 1 month. Measurements of tumor volume were calculated using the following formula: volume (mm^3) = [the longer diameter × (the shorter diameter)^2]/2. When the volume of the NSCLC xenografts reached to about 80 mm^3, tumor-bearing nude mice were randomly assigned to six groups to receive PBS, hAECs, EXOs, cisplatin, cisplatin + hAECs, or cisplatin + EXOs. A single intraperitoneal injection of cisplatin was conducted on nude mice at a dose of 10 mg/kg; 24 h after cisplatin injection, hAECs (1×10^6/100 μl) or EXOs (1×10^8/100 μl) resuspended in PBS were injected into the mice intravenously. Tumor volumes were measured every 4 days *in situ*. Nude mice were sacrificed on day 12 after cisplatin injection to collect NSCLC tumors and mouse kidneys.

RNA Sequencing

On day 4 after cisplatin treatment, kidney samples of two randomly selected C57BL/6J mice in each group and tumor samples from two randomly selected nude mice with NSCLC in each group, including PBS group, cisplatin group, cisplatin + hAECs group, and cisplatin + EXOs group, were extracted for RNA sequencing. Briefly, total RNA of tissues was extracted, the integrity and purity of RNA were detected by an Agilent 2,100 Bioanalyzer system, and the cDNA libraries constructed by polymerase chain reaction amplification were sequenced by Novaseq, the Illumina High-Throughput Sequencing Platform. Cutadapt (v1.10) was used to filter low-quality reads. When the N content of any sequencing read was more than 10% of the number of bases of the read, these paired reads were removed. When the number of low quality (Qphred≤5) bases in any of the sequencing reads was more than 50% of the number of bases in the read, these paired reads were removed. The clean reads were aligned to the UCSC mm10 (the kidneys of C57BL/J mice) or hg19 genome (the tumors of mice with A549 NSCLC) by the HISAT2 program. The edgeRSeq algorithms were applied to recognize significantly differentially expressed genes with the following criteria: log2 fold-change > 2 or < −2.

Gene Ontology (GO) (http://www.geneontology.org) analysis was conducted to construct the main function of the differentially expressed mRNAs (p-value <0.05). The −log 10 (p-value) value with the enrichment score represents the significance of the GO term. The Kyoto Encyclopedia of Genes and Genomes (KEGG) pathway analysis (http://www.genome.jp/kegg/) was performed to harvest pathway clusters covering differentially regulated mRNA profiles in the molecular interaction networks. The −log 10 (p-value) value with the enrichment score indicates the significance of correlation in the pathway.

Cell Counting kit-8 Assay

HK-2, the immortalized human proximal tubular cells, were cultured in DMEM with 10% FBS and 1% penicillin–streptomycin under a humidified atmosphere consisting of 5% CO_2 and 95% air at 37°C. When the degree of cell fusion reached about 70%, cisplatin injury was induced by treating the cells with 10 mM cisplatin for 48 h, and as for the treatment of EXOs, a concentration of 1×10^8/ml EXOs was added to DMEM culture medium after cisplatin treatment.

For cell growth assays, 5×10^3 cells per well were seeded into 96-well plates, with six wells used for each assayed group. After 48 h treatment of cisplatin and/or EXOs, cell numbers were evaluated using the cell counting kit-8 (CCK-8) (Cat# CK04, Dojindo, Japan). Ten microliters of CCK-8 reagent were added to each well, after which the plate was incubated at 37°C for 2 h. Subsequently, the absorbance at 450 nm was measured in each well by using a spectrophotometer (Bio-rad, USA).

Terminal Deoxynucleotidyl Transferase-Mediated dUTP Nick End-Labeling Assay

Apoptosis in kidney tissues and HK2 cells was detected by the *in situ* terminal deoxynucleotidyl transferase-mediated dUTP nick end-labeling (TUNEL) method following the standard protocol (Cat# C1088, Beyotime, China). Six to ten high-power fields were selected randomly from each slide and the number of TUNEL-positive cells was determined per field by Nikon 90i microscope.

Immunofluorescence Staining

Immunofluorescence staining of the kidneys was performed on paraffin sections. After fixation and antigen retrieval, nonspecific

binding was blocked with 3% BSA. Tissue sections were incubated with the mixed primary antibodies of rabbit anti-Ki67 (1:400, Cat# 9129, CST, USA) and mouse anti-Ecadherin (1:300, Cat# 14472, Abcam, USA) overnight at 4°C. After washed three times with PBS, the tissue sections were incubated with mixed secondary antibodies of Cy3-labeled goat anti-rabbit (1:500, Cat# A0516, Beyotime, China) and FITC-labeled goat anti-mouse (1:500, Cat# A0568, Beyotime, China). After another washing with PBS, the sections were coverslipped with fluorescent mounting medium with DAPI (4,6-diamidino-2-phenylindole) (Cat# ZLI-9557, ZSGB-BIO, China). The staining was examined using fluorescence microscope (Leica, Germany). All images were acquired using the same microscope and camera set. Six to ten high-power fields from the outer medulla and cortex in each kidney examined were captured, then the number of Ki67-positive cells was counted, and the fluorescence intensity of Ecadherin was measured by Image Pro Plus (Media Cybernetics, USA).

Immunohistochemistry Staining

Immunohistochemistry staining of the kidney was performed on paraffin sections. The primary antibodies included rabbit anti-Ly6G (1:2000, Cat# 238132, Abcam, USA) and rabbit anti-F4/80 (1:200, Cat# 70076, CST, USA). The slides were then exposed to DAB-labeled secondary antibodies. Six to ten fields (×400) were selected randomly from each section, and the staining was examined using a microscope (Leica, Germany).

Western Blots

Total protein from kidney samples of C57BL/6J mice or HK2 cells was extracted on ice with RIPA buffer (Cat# P0013B, Beyotime, China) supplemented with protease and phosphatase inhibitor cocktail (Cat# P1046, Beyotime, China) following standard protocols. Protein concentration was measured using a Pierce BCA Protein Assay kit (Cat# 23227, Thermo Fisher Scientific, USA). Next, denatured proteins were separated in sodium dodecyl sulfate-polyacrylamide gels and then were electrically transferred onto polyvinylidene difluoride membranes. The membranes were blocked with 5% BSA in Tris-buffer saline with 0.1% Tween 20 (TBST) for 1 h at room temperature and incubated with primary antibodies at 4°C overnight. The following primary antibodies and dilutions were used: anti-kidney injury molecule 1 (KIM-1) (1:1000, Cat# 233720, Abcam, USA), anti-TNF-α (1:1000, Cat# 11948, CST, USA), anti-p-ERK (1:1000, Cat# 4370, CST, USA), anti-ERK (1:1000, Cat# 4695, CST, USA), anti-p-p38 (1:1000, Cat# 4511, CST, USA), anti-p38 (1:1000, Cat# 8690, CST, USA), anti-p-JNK (1:1000, Cat# 4668, CST, USA), anti-JNK (1:1000, Cat# 9252, CST, USA), anti-cleaved caspase 3 (1:500, Cat# 9661, CST, USA), anti-caspase3 (1:1000, Cat# 9662, CST, USA), anti-β-actin (1:1000, Cat# 4970, CST, USA), and anti-GAPDH (1:10000, Cat# 181602, Abcam, USA). After washing three times with TBST, the membranes were incubated with horseradish peroxidase (HRP)-conjugated secondary antibodies for 1 h at room temperature. After three washes with TBST, the membranes were incubated in Immobilon® ECL Ultra Western HRP Substrate (Cat# WBULS0500, Millipore, USA), and images were captured by an ImageQuant LAS 4000 mini system (GE, Healthcare). The relative intensity of the protein bands was quantified by digital densitometry using ImageJ software (Media Cybernetics, USA). The level of GAPDH or β-actin was used as an internal standard.

RT-PCR

Kidney tissues were collected in RNase-free tubes, and total RNA was isolated using TRIzol® reagent following the instructions of the manufacturer (Cat# 15596026, Thermo Fisher, USA). RNA concentrations were determined by photometric measurements. cDNA was synthesized from 2 μg of total RNA using Fast King RT Enzyme (Cat# KR118, TIANGEN, China) for real-time RT-PCR. The mRNA expression levels of *Ccl2*, *Cxcl1*, *Cxcl2*, *IL-1β*, *IL-6*, and *Gapdh* were determined using SYBR Green PCR Master Mix (Cat# FP209, TIANGEN, China) based on the instructions of the manufacturer with the following primers. All PCR analyses were performed on an ABI Vii7 system. The comparative gene expression was calculated by the 2−ΔΔCt method.

Statistical Analysis

Statistical analysis was performed using SPSS 25.0 statistical software (SPSS, USA). Normally distributed variables are expressed as mean ± SEM and compared using a *t*-test. Non-normally distributed nonparametric variables are expressed as median and interquartile range and are compared between groups using the Mann–Whitney *U*-test. All *p*-values were two-tailed, and $p < 0.05$ was considered statistically significant. GraphPad Prism 8.0 was used to form the vector diagrams (GraphPad, USA).

RESULTS

hAECs and Their Derived EXOs Ameliorated Cisplatin-AKI in C57BL/6J Mice

To establish the roles of hAECs and their derived EXOs in cisplatin acute nephrotoxicity, we examined the mortality, renal function, and renal tissue damage in cisplatin-AKI mice with hAECs or EXOs administration 1 day post cisplatin injection. The 6-day mortality rate in high-dose cisplatin (20 mg/kg)-treated group reached to 100%, while hAECs or EXOs administration significantly decreased the 6-day mortality rate to 50% (**Figure 1A**). In the 15 mg/kg cisplatin-treated mice, renal function was evaluated on day 4 post cisplatin injection, and a significant high level of sCr was detected (146.7 ± 22.8 μmol/L vs. 41.1 ± 4.0 μmol/L in normal mice, $p = 0.006$). Administration of hAECs or EXOs substantially improved the renal function ($p < 0.05$) with sCr levels of 65.7 ± 12.0 μmol/L and 55.5 ± 9.4 μmol/L, respectively, ($p < 0.05$ vs. cisplatin group) (**Figure 1B**).

We next examined the renal histology. As shown in **Figure 1C**, PAS staining revealed severe tubular injury reflected by dilation, necrosis, cast formation, and loss of the brush border in the renal cortical region of mice treated with 15 mg/kg of cisplatin. hAEC- or EXO-treated mice showed significantly improved renal histology with decreased renal pathological scores compared with the cisplatin-AKI mice (2.4 ± 0.1 vs. 2.4 ± 0.1 vs. 4.6 ± 0.2,

Gene	Forward primers (5′-3′)	Reverse primers (5′-3′)
Ccl2	TTAAAAACCTGGATCGGAACCAA	GCATTAGCTTCAGATTTACGGGT
Cxcl1	CTGGGATTCACCTCAAGAACATC	CAGGGTCAAGGCAAGCCTC
Cxcl2	CCAACCACCAGGCTACAGG	GCGTCACACTCAAGCTCTG
Il-1β	GCAACTGTTCCTGAACTCAACT	ATCTTTTGGGGTCCGTCAACT
Il-6	TAGTCCTTCCTACCCCAATTTCC	TTGGTCCTTAGCCACTCCTTC
Gapdh	AGGTCGGTGTGAACGGATTTG	TGTAGACCATGTAGTTGAGGTCA

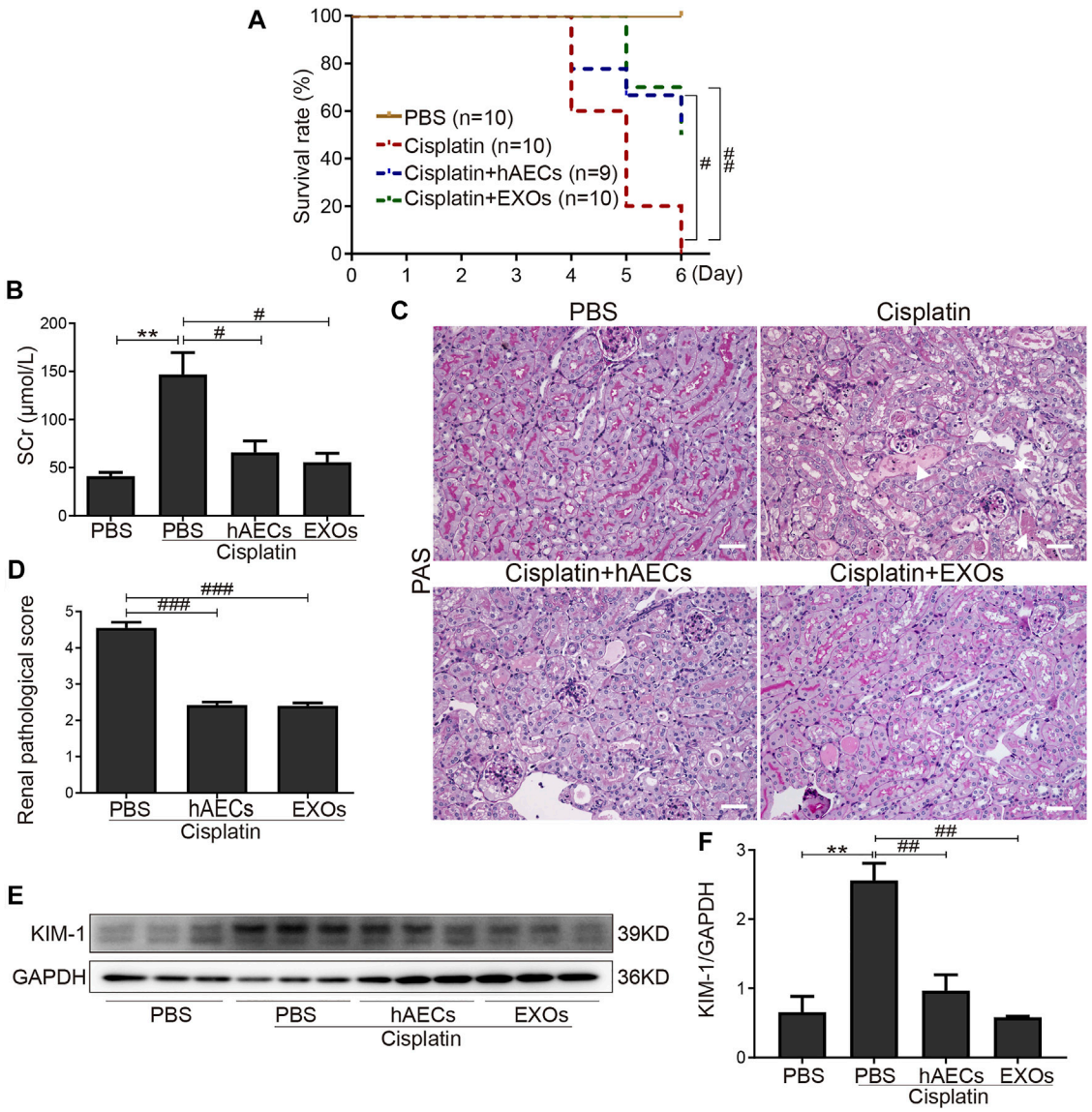

FIGURE 1 | Effects of hAECs or EXOs on C57BL/6J mice with cisplatin-AKI. **(A)** The 6-day mortality rate in mice treated with 20 mg/kg cisplatin (n = 9 or 10 mice in each group). **(B)** sCr levels of mice treated with 15 mg/kg cisplatin (n = 10). **(C)** Representative micrographs of PAS staining of kidneys from mice with 15 mg/kg cisplatin treatment. Triangle indicates renal tubular necrosis, pentagram indicates the shedding of the brush edge of renal tubules, and arrow indicates the formation of renal casts. Scale bar, 100 μm. **(D)** Semiquantitative renal pathological scores of mice treated with 15 mg/kg cisplatin (n = 3). **(E)** Representative Western blots showing protein expression of KIM-1 in kidneys from mice treated with 15 mg/kg cisplatin. **(F)** The relative protein expression of KIM-1 to GAPDH in different groups (n = 3). Data are shown as mean ± SEM. $^{**}p < 0.01$ vs. PBS group, $\#p < 0.05$, $\#\#p < 0.01$, and $\#\#\#p < 0.001$ vs. cisplatin group. hAECs, human amniotic epithelial cells; EXOs, exosomes; cisplatin-AKI, cisplatin induced acute kidney injury; sCr, serum creatinine; PAS, periodic acid-Schiff; KIM-1, anti-kidney injury molecule 1.

$p < 0.001$) (**Figure 1D**). Western blots showed that the protein level of KIM-1 in kidneys of cisplatin-treated mice were markedly reduced when treated with hAECs and EXOs (**Figures 1E, F**). All these data suggested that hAECs and EXOs could attenuate cisplatin-induced renal dysfunction and pathological damage, exhibiting the renal protective effects on cisplatin-AKI.

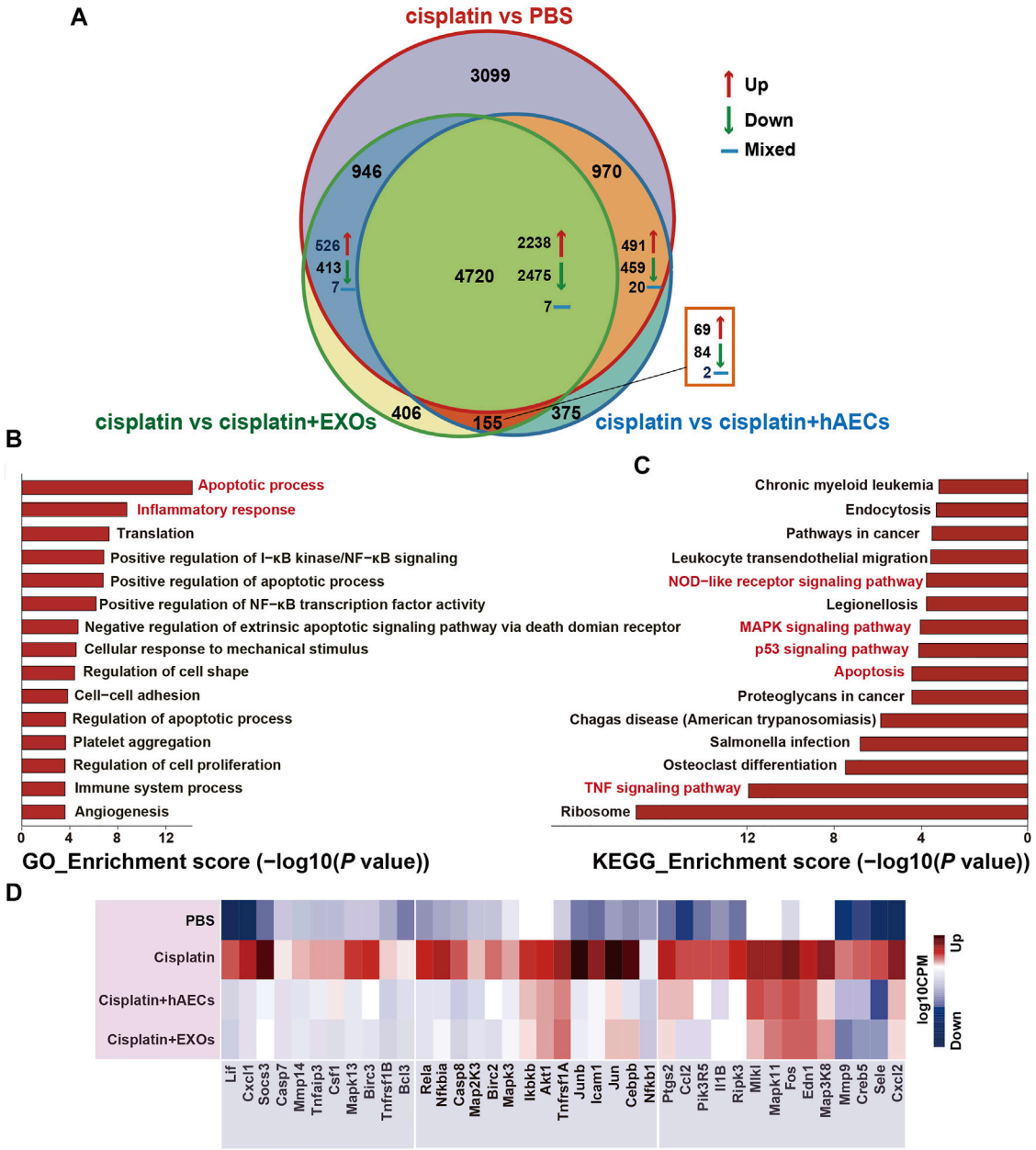

FIGURE 2 | RNA sequencing analysis of kidneys from C57BL/6J mice treated with 15 mg/kg cisplatin. **(A)** Venn diagram showing the numbers of significant DEGs across the four indicated groups. **(B,C)** The top 15 enriched GO terms and KEGG pathways of the 2,238 DEGs. **(D)** Heatmap showing the TNF pathway-related DEGs differentially expressed across the four groups. The colors indicate the value of log10 CPM. CPM, counts per million; cisplatin, Cis-diamminedichloroplatinum (II); DEGs, differentially expressed genes; GO, Gene Ontology; KEGG, Kyoto Encyclopedia of Genes and Genomes.

Molecular Modifications by hAECs and Their Derived EXOs in Cisplatin-injured Kidneys

To explore the mechanisms of hAECs and EXOs in protecting against cisplatin-AKI, we conducted a genome-wide transcriptomic sequencing of normal kidneys, cisplatin-injured kidneys, and cisplatin-injured kidneys treated with hAECs or EXOs. The log10 counts per million (CPM) value was used to quantify the mRNA expression. We analyzed the profiles of differentially expressed genes (DEGs) among the four groups. As shown in **Figure 2A**, compared with normal kidneys (PBS), totally 9,735 DEGs were found in cisplatin-AKI kidneys (cisplatin). Compared with the cisplatin group, a total of 6,220 DEGs were found in cisplatin-injured kidneys treated with hAECs (cisplatin + hAECs) and 6,227 DEGs in cisplatin-injured kidneys treated with EXOs (cisplatin + EXOs). Four thousand seven hundred twenty genes were found to be

significantly changed among the four groups, including 2,238 DEGs upregulated in cisplatin vs. PBS comparison while concomitantly downregulated in the comparison between cisplatin vs. cisplatin + hAECs or cisplatin + EXOs. These data indicated that the molecular regulation of hAECs and EXOs on cisplatin renal injury was very similar, and hAECs and EXOs could counteract on about half of the DEGs regulated by cisplatin injury.

The NIH Database for Annotation, Visualization, and Integrated Discovery (DAVID) was used to perform gene functional annotation clustering on the 2,238 identified DEGs. We focus on the GO terms of biological process since it is the most widely used subontology of GO to evaluate the functions of genes. Accordingly, we obtained 83 significant GO terms in the 2,238 DEGs. The top 15 GO terms of upregulated genes with an adjusted p-value <0.05 are shown in **Figure 2B**. Apoptotic process and inflammatory response were the most enriched GO terms of biological processes in these DEGs. The 2,238 DEGs were also analyzed by KEGG pathway analysis, and the top 15 significant KEGG pathways are shown in **Figure 2C**, including TNF signaling pathway, apoptosis, p53 signaling pathway, MAPK signaling pathway, and NOD-like receptor signaling pathway. TNF signaling pathway was reported to play a central role in cisplatin-induced renal inflammation (Holditch et al., 2019). We next explored TNF pathway-related DEGs with different expression directions between the cisplatin group and the cisplatin + hAECs or cisplatin + EXOs groups. As shown in **Figure 2D**, the TNF-associated DEGs including MAPK cascade compartments *Tnfaip3*, *Mapk3*, *Mapk13*, *Jun*, and the downstream effectors such as *Cxcl1*, *Cxcl2*, *Ccl2*, *Csf1*, *Socs3*, *Mmp9*, *Mmp14*, *Il1b* were upregulated in the cisplatin group compared with PBS control, but those genes were all downregulated in cisplatin + hAEC and cisplatin + EXO groups compared with the cisplatin group.

hAECs and Their Derived EXOs Alleviated Cisplatin-Induced Kidney Inflammation by Inhibiting TNF-α/MAPK Signaling Pathway

Multiple studies have shown that TNF-α-triggered MAPK cascades mediate various cellular responses to cisplatin-induced kidney injury (Jo et al., 2005; Ramesh and Reeves, 2005; Francescato et al., 2007). To further validate the results of RNA sequencing, Western blot was performed to detect TNF-α expression in the homogenates of normal kidneys, cisplatin-treated kidneys, and cisplatin-injured kidneys treated with hAECs or EXOs (**Figure 3A**). Compared with the PBS control, cisplatin treatment significantly increased the level of kidney TNF-α expression, which was greatly suppressed by hAECs or EXOs administration (**Figure 3B**). As shown in **Figure 3A**, the levels of phosphorylated ERK1/2 ($p < 0.001$), JNK ($p < 0.01$), and p38 ($p < 0.001$) were significantly increased in the cisplatin group compared with the PBS control group. As expected, the expression of these proteins was significantly reduced in hAEC- or EXO-treated groups (**Figures 3C–E**). These data indicated that hAECs or EXOs significantly prevented the activation of MAPK signaling cascade induced by cisplatin. Downstream expression of cytokines/chemokines was also detected. RT-PCR results showed that the expression of inflammatory factors including *Cxcl1*, *Cxcl2*, *Ccl2*, *Il-1β*, and *Il-6* was greatly induced by cisplatin, which was significantly decreased after hAECs or EXOs treatment (**Figure 3F**). Consequently, the infiltration of immune cells such as neutrophils (Ly6G) and macrophages (F4/80) were decreased in the cisplatin + hAECs and cisplatin + EXO-treated groups compared with the cisplatin group (**Figures 3G–J**).

hAECs and Their Derived EXOs Attenuated Cisplatin-Induced Apoptosis in Renal Tubular Epithelial Cells

We next evaluated the effects of hAECs and EXOs on the apoptosis and proliferation of kidney cells in cisplatin-AKI. TUNEL assay was performed in mouse kidney sections. As shown in **Figure 4A**, on the fourth day of cisplatin injection, a large number of TUNEL-positive cells was observed in the cisplatin group, and the number of TUNEL-positive cells were significantly reduced in hAEC- or EXO-treated groups (**Figure 4B**). Western blot analysis showed that the expression level of apoptosis-related marker cleaved caspase-3 in the cisplatin-treated group was significantly higher than that in the PBS control group, while hAEC and EXO treatment significantly suppressed cleaved caspase-3 expression in the kidneys (**Figures 4C, D**). We next examined the expression of Ecadherin, a marker for epithelial cell tight junctions, and Ki67 to evaluate the cell viability and proliferation states. As shown in **Figure 4E**, Ecadherin expression in renal tubular epithelial cells in the cisplatin group was significantly decreased compared with the PBS control group. However, the expression of Ecadherin and Ki67 in hAECs and EXOs treated groups increased significantly, and most of the Ki67 positive cells were located in the renal tubules, suggesting that hAECs and EXOs promoted the renal tubule repair and the proliferation of tubular epithelial cells post-cisplatin injury (**Figures 4F, G**).

We further cultured HK2 cells *in vitro* to observe whether EXOs could reduce the damage of cisplatin to renal tubular cells. We first assessed cell viability by the CCK8 assay. As shown in **Figure 4H**, after cisplatin stimulation for 48 h, the survival rate of cells in the EXOs group was significantly higher than that in the cisplatin group. The number of TUNEL positive cells was increased and the cleaved caspase-3 expression was upregulated in HK2 cells for cisplatin treated group. However, the apoptotic cell number and the enhanced protein levels of cleaved caspase-3 in cisplatin-treated HK2 cells were markedly decreased by EXOs treatment (**Figures 4I–L**). These findings suggested that hAEC and EXO treatment could prevent cisplatin-induced apoptosis and promote proliferation of renal tubular epithelial cells.

Effects of hAECs and Their Derived EXOs on the Antitumor Efficacy of Cisplatin in a Mouse NSCLC Xenograft Model

To clarify the effects of hAECs and EXOs on tumor proliferation and anti-tumor effects of cisplatin, we constructed an A549 lung cancer xenograft mouse model. On the 12th day of cisplatin injection, the subcutaneous tumors of A549 in nude mice were

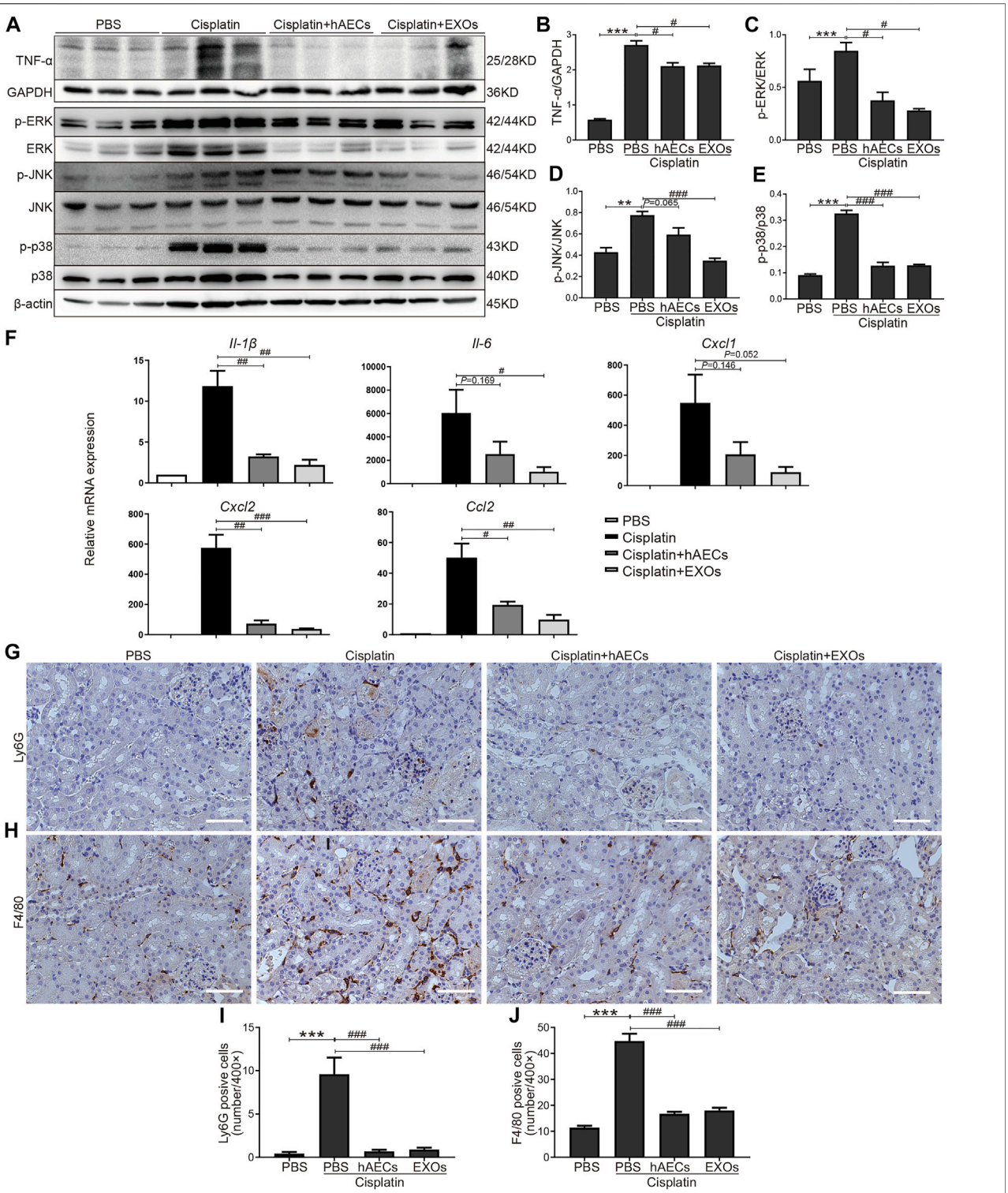

FIGURE 3 | Regulation of TNF-α/MAPK pathway by hAECs and EXOs in C57BL/6J mice treated with 15 mg/kg cisplatin. **(A)** Representative Western blots showing protein expression of TNF-α, p-ERK, ERK, p-JNK, JNK, p-p38, and p38 of kidneys in different groups as indicated. **(B–E)** The relative protein expression of TNF-α to GAPDH, p-ERK to ERK, p-JNK to JNK, and p-p38 to p38 in different groups ($n = 3$). **(F)** The relative mRNA expression of *Il-1β*, *Il-6*, *Cxcl1*, *Cxcl2*, and *Ccl2* determined by RT-PCR. **(G,I)** Representative micrographs and quantification of Ly6G positive staining on kidney sections of different groups as indicated. **(H,J)** Representative micrographs and quantification of F4/80 positive staining on kidney sections of different groups as indicated. Scale bar, 100 μm $n = 3$ for each group. Data are shown as mean ± SEM. $^{**}p < 0.01$ and $^{***}p < 0.001$ vs. PBS group, $\#p < 0.05$, $\#\#p < 0.01$, and $\#\#\#p < 0.001$ vs. cisplatin group.

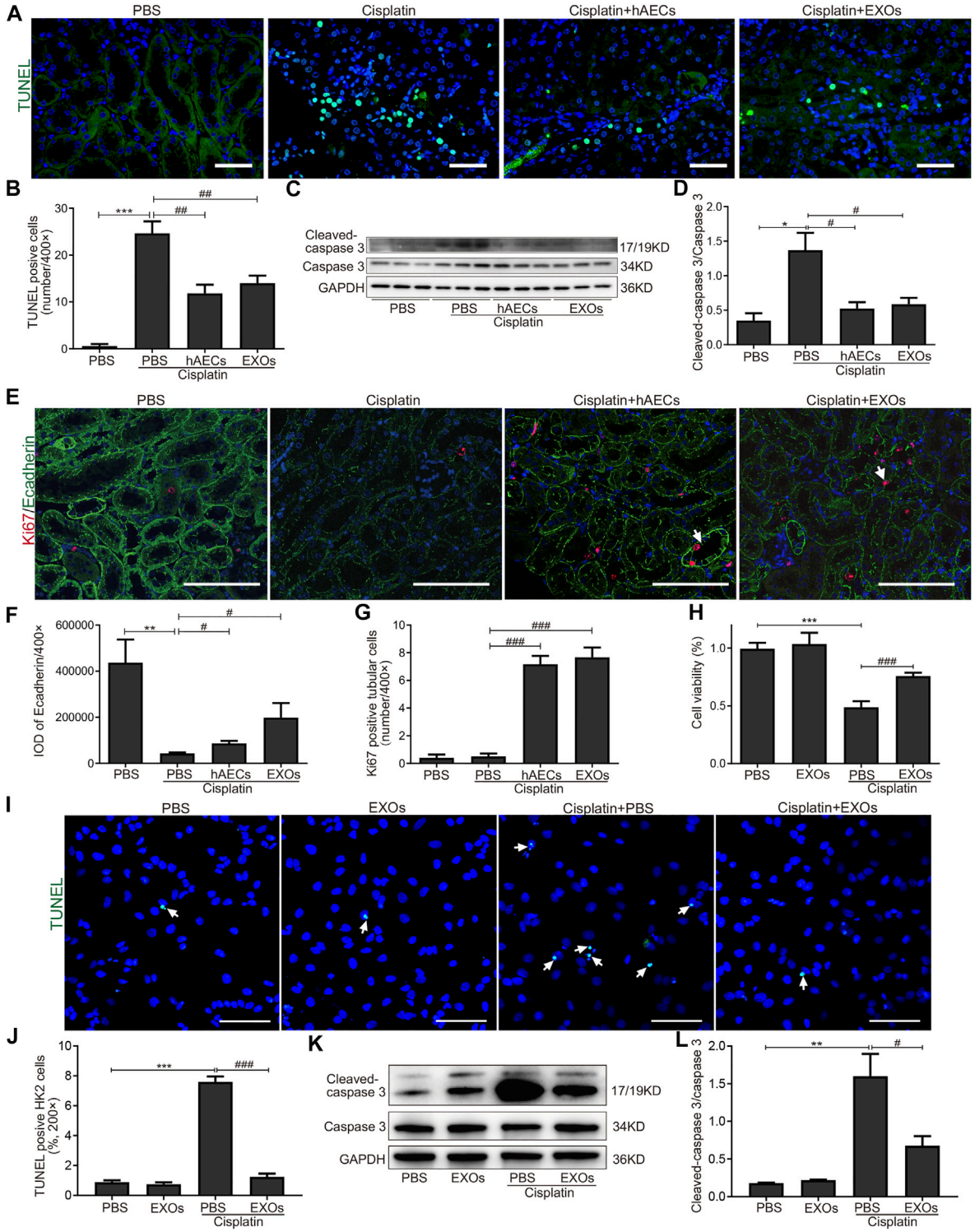

FIGURE 4 | Inhibition of cisplatin-induced apoptosis of renal tubular epithelial cells by hAECs and EXOs. **(A)** Representative micrographs of TUNEL (green) staining of kidneys from C57BL/6J mice treated with 15 mg/kg cisplatin. **(B)** Quantification of TUNEL-positive cells/400×. **(C)** Representative Western blots showing protein expressions of cleaved-caspase 3 and caspase 3 of kidneys from C57BL/6J mice treated with 15 mg/kg cisplatin. **(D)** The relative protein expression of cleaved-caspase 3 to caspase 3 in different groups. $n = 3$ for each group. **(E)** Representative micrographs of Ki67 (red) and Ecadherin (green) immunofluorescence staining of kidneys from C57BL/6J mice treated with 15 mg/kg cisplatin. **(F)** Semiquantitative analysis of intensity of Ecadherin immunofluorescence staining. IOD, integrated optical density. **(G)** Quantification of Ki67-positive tubular cells/400×. **(H)** CCK-8 assay showing the cell viability of HK2 cells with different treatments for 48 h. **(I)**

(*Continued*)

FIGURE 4 | Representative micrographs of TUNEL (green) staining of HK2 cells with different treatments for 24 h. **(J)** Percent of TUNEL-positive cells to all HK2 cells/200×. **(K)** Representative Western blots showing protein expressions of cleaved-caspase 3 and caspase 3 in HK2 cells with different treatments for 48 h. **(L)** The relative protein expression of cleaved-caspase 3 to caspase 3 in HK2 cells with different treatments for 48 h. Scale Bar, 100 μm $n = 3$ for each group. Data are shown as mean ± SEM. $^{*}p < 0.05$, $^{**}p < 0.01$, and $^{***}p < 0.001$ vs. PBS group, $\#p < 0.05$, $\#\#p < 0.01$, and $\#\#\#p < 0.001$ vs. cisplatin group. TUNEL, terminal deoxynucleotidyl transferase mediated dUTP nick end-labeling; CCK-8, cell counting kit-8.

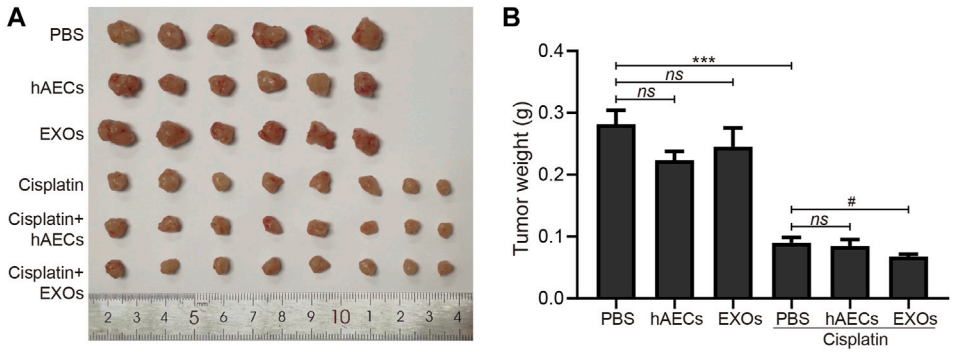

FIGURE 5 | Effects of hAECs and EXOs on the tumor growth in nude mice with A549 NSCLC. **(A)** The gross tumor images in different groups of nude mice with A549 NSCLC on day 12 after cisplatin injection. **(B)** Comparison of tumor weights in different groups of nude mice with A549 NSCLC on day 12 after cisplatin injection. Data are shown as mean ± SEM. $^{***}p < 0.05$ vs. PBS group, $\#p < 0.05$ vs. cisplatin group. NSCLC, non-small cell lung cancer.

collected, photographed, and weighed. As shown in **Figures 5A, B**, the tumor weight in the hAEC- and EXO-treated groups was similar to that in the PBS group, suggesting that hAECs and EXOs had no potential on promoting A549 lung tumor growth. Meanwhile, the tumor weight in the cisplatin group was significantly lower than that in the PBS group, indicating the treatment efficacy of cisplatin on tumor growth (0.090 ± 0.009 g vs. 0.282 ± 0.023 g, $p < 0.001$). Compared with the cisplatin group, the tumor weight in cisplatin + hAECs group (0.085 ± 0.010 g) was similar and in cisplatin + EXOs group was slightly lower (0.068 ± 0.004 g vs. cisplatin group: 0.090 ± 0.009 g, $p < 0.05$). These results suggested that hAECs and EXOs did not interfere with the tumor-suppressive effect of cisplatin.

RNA Sequencing Identified Signaling Pathways Specifically Regulated by hAECs and Their Derived EXOs in Cisplatin-Treated Lung Tumors

The RNA of PBS, cisplatin, cisplatin + hAECs, cisplatin + EXO-treated tumors on the fourth day after cisplatin injection was extracted and subjected to RNA sequencing for identification of differentially expressed genes and remarkably changed pathways. When using PBS treatment as the control (**Figure 6A**), 5,375 DEGs were considered as significantly changed for cisplatin vs. PBS, cisplatin + hAECs vs. PBS, and cisplatin + EXOs vs. PBS. The cisplatin, cisplatin + hAECs, and cisplatin + EXOs groups shared 226 DEGs. The functional associations of the 226 DEGs were implemented by the KEGG analysis (**Figure 6B**). The ECM–receptor interaction, p53 signaling pathway, estrogen signaling pathway, PI3K–AKT signaling pathway, regulation of actin cytoskeleton, and drug metabolism–cytochrome P450 were the most enriched pathways in the upregulated genes in the 226 DEGs, indicating a common regulation of tumor microenvironment, cell proliferation, cell division, and drug metabolism by cisplatin and hAECs or EXOs. However, when using cisplatin treatment as the control (**Figure 6C**), 4,228 DEGs were found significantly changed for cisplatin + hAECs vs. cisplatin and cisplatin + EXOs vs. cisplatin. Five hundred fifty DEGs were shared in cisplatin + hAECs and cisplatin + EXOs groups. KEGG analysis showed that TNF signaling pathway, RIG-I-like receptor signaling pathway, NOD-like receptor signaling pathway, and Toll-like receptor signaling pathway were the most enriched pathways in the upregulated 153 genes in the 550 DEGs (**Figure 6D**). We checked the functions of the 153 upregulated genes and found a serial of genes involved in cell cycle checkpoint control and DNA damage repair, including *Cbr1*, *Ccnb1*, *Cdc6*, *Cdk1*, *Ddias*, *Fignl*, *Mcm3*, *Nek6*, *Nupr1*, and *Psrc1* (**Table 1**).

DISCUSSION

In recent years, with the increase in the incidence of tumors, the progress of anti-tumor treatments, and the prolonged survival of cancer patients, chemotherapy-related AKI has become more and more common (Sahni et al., 2009; Troxell et al., 2016). Cisplatin, being an effective chemotherapeutic drug, is still widely used in a variety of solid tumors as the first-line chemotherapy. However, cisplatin induced nephrotoxicity greatly limits its clinical application and chemotherapeutic efficacy. According to European guidelines, the only recommended method of preventing cisplatin-AKI in clinic is to intravenously infuse

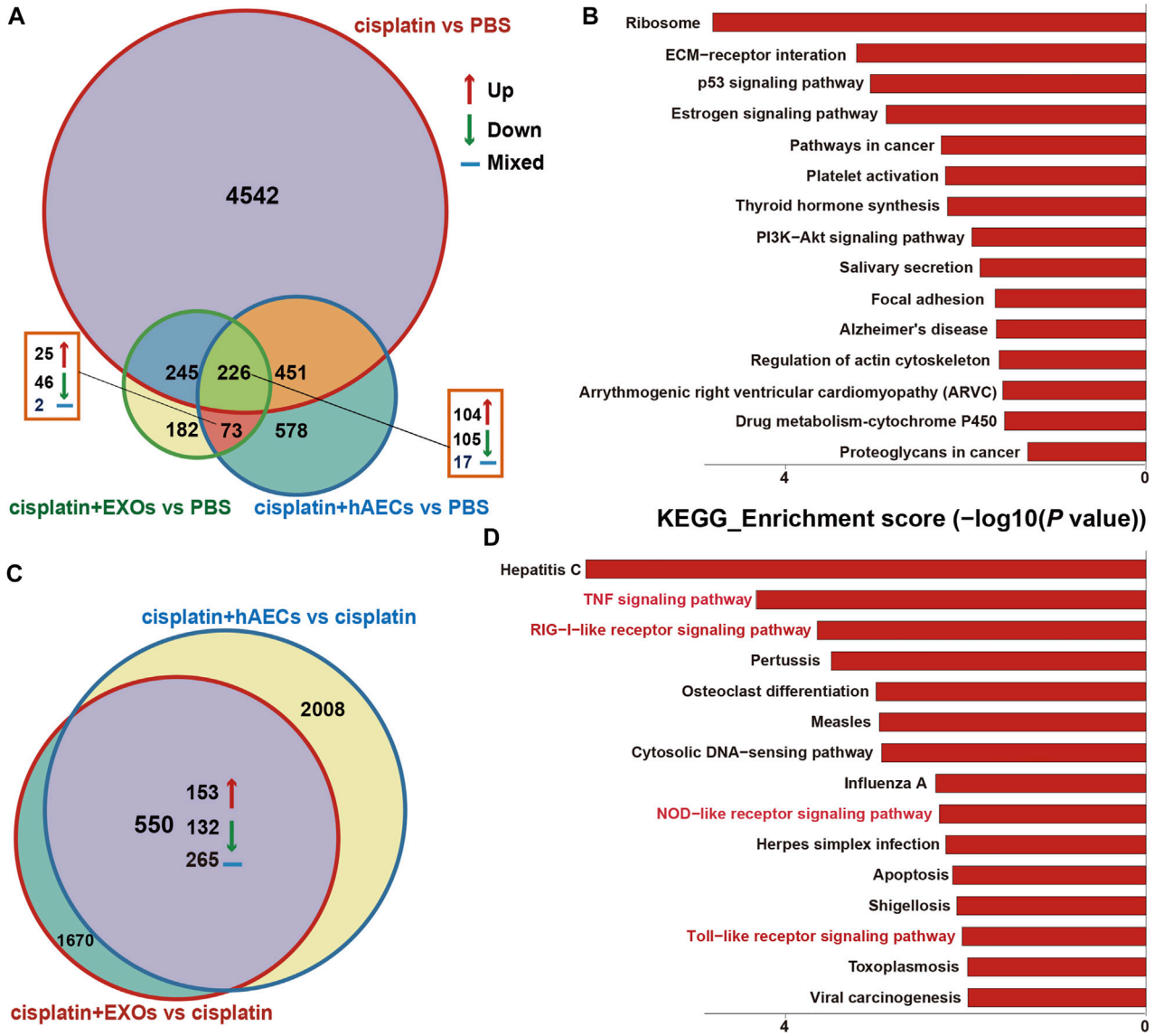

FIGURE 6 | RNA sequencing analysis on tumors from A549 NSCLC nude mice collected 4 days after cisplatin injection. **(A)** Venn diagram showing the numbers of significant DEGs across the four groups as indicated. **(B)** The top 15 enriched and upregulated KEGG pathways in the 226 DEGs across the four groups as indicated in **(A)**. **(C)** Venn diagram showing the numbers of significant DEGs across the two groups as indicated. **(D)** The top 15 enriched and upregulated KEGG pathways in the 550 DEGs across the four groups as indicated in **(C)**.

isotonic saline for hydration and supply with magnesium if necessary (Launay-Vacher et al., 2008). It is thus required to explore new methods for the treatment of cisplatin-AKI without interfering with its anti-cancer effects. The reparative therapeutic potential of hAECs have been assessed in a multitude of experimental animal models including lung injury, brain injury, hepatic fibrosis, and multiple sclerosis (Kakishita et al., 2000; McDonald et al., 2015; Cargnoni et al., 2018; Tan et al., 2018). To date, only a few applications of hAECs in renal injury have been reported. Previously our lab has proved that hAECs protected against ischemia–reperfusion AKI in mouse model (Ren et al., 2020). In the current study, we showed that hAECs or their derived EXOs administration in cisplatin-AKI mouse model could reduce mortality, improve renal function, and reduce renal tissue damage. Decreased inflammation and renal cell apoptosis, and increased renal tubular cell proliferation were also observed after hAECs or EXOs administration. Importantly, hAECs treatment did not compromise the antitumor activity of cisplatin in A549 tumor bearing nude mouse model.

More and more evidences indicate that renal tubular epithelial cell apoptosis and renal inflammation mainly determine the progression and outcome of cisplatin-AKI (Volarevic et al., 2019). TNF-α is a pleiotropic pro-inflammatory cytokine inducing a broad range of cellular responses, ranging from inflammatory cytokine production,

TABLE 1 | Representative DEGs identified by RNA sequencing in cisplatin + hAECs or cisplatin + EXOs compared with cisplatin-treated tumors.

Gene	Cisplatin + hAECs vs. cisplatin		Cisplatin + EXOs vs. cisplatin	
	Log2 FC	P_{adj}	Log2 FC	P_{adj}
Adam8	2.9686	3.31×10^{-9}	0.8359	3.31×10^{-9}
Bax	1.5060	3.78×10^{-16}	0.5605	3.78×10^{-18}
Bcl3	3.0509	1.27×10^{-32}	2.0370	1.27×10^{-32}
Brca1	1.9357	5.31×10^{-5}	1.7134	5.31×10^{-5}
Bzw2	0.5356	0.045483	0.5295	0.045483
Cbr1	1.9998	1.67×10^{-44}	0.5610	1.67×10^{-44}
Ccnb1	3.1586	0.017644	0.8020	0.017644
Cdc6	1.9437	0.021621	1.6689	0.021621
Cdca3	1.3727	0.015941	1.0782	0.015941
Cdca7	1.8503	0.014304	0.6242	0.014304
Cdk1	1.7407	0.000477	0.8007	0.000477
Cldn4	2.7803	9.10×10^{-38}	1.0485	9.14×10^{-38}
Clspn	2.5574	0.000734	1.7433	0.000734
Ddias	3.6595	3.69×10^{-22}	1.1992	3.69×10^{-22}
Dlgap5	2.5165	0.007954	0.9324	0.007954
Esco2	2.5888	0.000955	1.9327	0.000955
Fignl1	2.3678	0.001049	0.8020	0.001049
Gins2	1.5373	0.001835	1.3674	0.001835
Havcr1	9.3847	1.18×10^{-91}	1.8328	1.18×10^{-91}
Irf7	4.0488	4.41×10^{-162}	0.9286	4.41×10^{-162}
Lif	5.1139	3.86×10^{-24}	0.6457	3.86×10^{-24}
Mcm3	1.0524	0.001352	2.3359	0.001352
Nek6	1.5931	1.73×10^{-13}	0.7183	1.73×10^{-13}
Nupr1	1.0746	0.000120	0.9035	0.000120
Psrc1	5.6203	1.56×10^{-8}	1.6411	1.56×10^{-8}
Zbp1	2.6423	4.04×10^{-10}	2.5706	4.04×10^{-10}
Zmat3	1.4787	4.50×10^{-19}	1.5122	4.50×10^{-19}

Note. DEGs, differentially expressed genes; cisplatin, Cis-diamminedichloroplatinum (II); hAECs, human amniotic epithelial cells; EXOs, exosomes.

cell survival, cell proliferation, cell differentiation, and cell death (Chen and Goeddel, 2002). We performed RNA sequencing detection on the kidney tissue of C57BL/6J cisplatin-AKI mice, and found that after cisplatin injury and hAECs or EXOs treatment, the TNF pathway was enriched and upregulated in cisplatin-AKI group but downregulated in cisplatin-AKI mice treated with hAECs or EXOs. TNF-α expression was suppressed after hAECs or EXOs treatment in cisplatin-AKI as shown by Western blot analysis. Once TNF-α binds to the two cell surface receptors, TNFR1 and TNFR2, it can initiate multiple downstream signaling pathways, including NF-κB pathway, MAPK pathway, and exogenous apoptosis pathway (Chen and Goeddel, 2002). The MAPK family mainly includes three phosphorylated proteins, ERK, p38, and JNK (Yue and López, 2020). Our experimental results showed that the phosphorylation of ERK, p38, and JNK was decreased by hAECs or EXOs treatment in cisplatin-AKI, and the expression of apoptosis marker cleaved caspase-3 were also decreased in cisplatin injured HK2 cells treated with EXOs. Together, our data suggest that hAECs and EXOs may inhibit TNF-α production, downregulate the phosphorylation of MAPK signaling molecules, and ultimately inhibit TNF-α-induced inflammatory response and renal tubular cell apoptosis, thereby alleviating cisplatin-AKI.

Increasing studies have suggested that the protective effects of many stem cells, including hAECs, might not be achieved by homing to the injury site and differentiation (Wang et al., 2015; Grange et al., 2019; Lee et al., 2020). For example, in the previous IRI-AKI mouse model, we found that most of the hAECs were trapped in the lungs after tail vein injection, but not in the injured kidneys (Ren et al., 2020). Growing evidences have favored that the stem cell-secreted EXOs are potential carriers of DNA, microRNA, lipids, cell-surface proteins, cytosolic proteins, nucleic acids, amino acids, and metabolites to perform biological functions (He et al., 2018; Kalluri and LeBleu, 2020). In this study, we compared the therapeutic effects of hAECs derived EXOs and hAECs on cisplatin-AKI, and the results showed that EXOs have the same renal protective effects as hAECs. In addition, we found through cultured renal tubular epithelial cells *in vitro* that EXOs could significantly inhibit cisplatin-induced apoptosis and increase the survival rate of tubule cells after cisplatin injury. Our previous work has detected the abundance of extracellular matrix proteins and proteins involved in the IGF signaling, HIF signaling, integrin signaling, Wnt signaling, and TGFβ signaling in hAEC derived exosomes (Ren et al., 2020). EXOs are easy to extract, store, and transport, and have better biocompatibility (Gurunathan et al., 2019). Practically, the use of EXOs, that is, "cell-free" stem cell therapy, may have more advantages than direct infusion of its source stem cells for clinical transformation of cisplatin-AKI stem cell therapy.

The ideal cisplatin-AKI therapy is to protect the kidneys while not compromising the anti-tumor effect of cisplatin and the major concern of implementing MSCs therapy in cisplatin-AKI is their risks of tumorigenicity and the promotion of tumor cell proliferation (Belmar-Lopez et al., 2013; Večerić-Haler et al., 2017; Plava et al., 2020). In the current study, we used the A549 lung cancer cell xenograft mouse model to verify the safety of hAECs or EXOs on tumor growth. The data showed that the tumor weight after hAECs or EXOs administration alone were not significantly different from those in the PBS control group. The combined application of hAECs and cisplatin resulted in no significant change in tumor weight compared with tumors treated with cisplatin alone, while EXOs and cisplatin combination slightly decreased the tumor weight than cisplatin treatment alone. Previously, Kang et al. reported that in a breast cancer MDA-MB-231 cell xenograft mouse model, the application of hAECs resulted in a reduction in tumor volume (Kang et al., 2012). In another BALB/c nude mouse xenograft model, co-injection of hAECs and ovarian cancer cell SK-OV-3 has shown the inhibitory effect on tumor growth (Bu et al., 2017). There are also studies showing that hAECs are non-tumorigenic in immunodeficient mice and healthy volunteers (Akle et al., 1985; Yang et al., 2018). The results from the current study and the previous studies indicate that hAECs and EXOs themselves have no interference with tumor proliferation, and their combined use with cisplatin did not compromise the anti-tumor efficacy of cisplatin.

We then performed RNA sequencing analysis on the tumors to detect the transcriptome difference in the tumors treated with cisplatin combined with hAECs or EXOs with those treated with cisplatin alone. We found that TNF signaling pathway was

enriched and upregulated. Further analysis of the RNA-seq data showed that genes closely related to the DNA damage repair (*Bax*, *Bcl3*, *Brac1*, *Fignl1*), DNA replication (*Gins3*, *Mcm3*), and cell cycle progression (*Ccnb1*, *Cdk1*, *Cdc6*, and *Nek6*) were significantly changed with additional hAECs or EXOs treatment (**Table 1**). TNF-α has been reported to regulate cell cycle progression in different types of cancer cells (Pusztai et al., 1993; Zhang et al., 2018; Jacobson et al., 2019). Recently, studies have shown that combination with low-dose TNF-α could enhance therapeutic effects of chemotherapeutic drugs through the TNF-α/NFκB signaling cascade, driving quiescent cancer cells out of G0/G1 phase to enter treatment sensitive proliferating phases to be killed by chemotherapeutic drugs (Moon et al., 2010; Jayasooriya et al., 2013; Wu et al., 2017). The differential regulation of TNF signaling pathway by hAECs and EXOs in cisplatin injured kidney and in cisplatin treated tumors indicate the complexity of stem cell therapy. The mechanisms of these fine tunings require further investigations.

In the current study, we only tested the therapeutic effects of hAECs or EXOs by single dose injection 1 day after cisplatin administration. Although the results are promising, many challenges remain when translation to clinical application. Based on the significant progress in different types of stem cell therapy (Bagno et al., 2018; Tompkins et al., 2018; Zhang and Lai, 2020), we may achieve improvements on two aspects: one is to identify the beneficial factors carried by hAEC-derived exosomes and to precondition the hAECs to boost their release of therapeutic exosomes; another is to optimize the route of administration, the proper dose and the timing for treatment in order to achieve the goal of complete renal recovery after cisplatin chemotherapy.

CONCLUSION

Cisplatin nephrotoxicity is one of the major causes of chemotherapy-related AKI and severe cisplatin-AKI significantly increases the risk of hospital death in patients. Here, we demonstrate that hAECs and their derived EXOs could reduce the mortality rate and attenuate renal dysfunction and pathological damage in the cisplatin-AKI mouse model. The renal protective effects were exerted via inhibition of the TNF-α/MAPK and the caspase signaling pathways without compromising the antitumor activity of cisplatin. Our study may provide new insights for clinical treatment of cisplatin-AKI by stem cell therapy.

DATA AVAILABILITY STATEMENT

Data of RNA sequencing for all samples has been deposited in Sequence Read Archive (SRA) under accession code PRJNA751451. Other data that support the findings of this study are available from the corresponding author upon reasonable request.

ETHICS STATEMENT

The animal study was reviewed and approved by the Institutional Animal Care and Use Committee of Peking University First Hospital.

AUTHOR CONTRIBUTIONS

XK and YC performed the experiments, collected, analyzed, and interpreted the data. YC drafted the manuscript. XX analyzed the data of RNA sequencing. ML, YM, YR, JJ, and QY helped collect and assemble the data. LQ conducted the tissue embedding, sectioning, and PAS staining. SW and GL made the semi-quantitation of renal injury. CX helped assemble the data and revised the manuscript. LY conceived and supervised the study, interpreted the data, and revised the manuscript. All authors approved the final manuscript.

FUNDING

This study was supported by grants from the National Natural Science Foundation of China (No.91742205 and No.81625004), the Beijing Young Scientist Program (BJJWZYJH01201910001006), the Peking University Clinical Scientist Program by the Fundamental Research Funds for the Central Universities, CAMS innovation Fund for Medical Science (2019-I2M-5-046), and Innovation Team and Talents Cultivation Program of National Administration of Traditional Chinese Medicine (ZYYCXTD-C-202005).

REFERENCES

Akle, C., McColl, I., Dean, M., Adinolfi, M., Brown, S., Fensom, A. H., et al. (1985). Transplantation of Amniotic Epithelial Membranes in Patients with Mucopolysaccharidoses. *Exp. Clin. Immunogenet.* 2 (1), 43–48.

Arany, I., and Safirstein, R. L. (2003). Cisplatin Nephrotoxicity. *Semin. Nephrol.* 23 (5), 460–464. doi:10.1016/s0270-9295(03)00089-5

Bagno, L., Hatzistergos, K. E., Balkan, W., and Hare, J. M. (2018). Mesenchymal Stem Cell-Based Therapy for Cardiovascular Disease: Progress and Challenges. *Mol. Ther.* 26 (7), 1610–1623. doi:10.1016/j.ymthe.2018.05.009

Barnes, C. J., Distaso, C. T., Spitz, K. M., Verdun, V. A., and Haramati, A. (2016). Comparison of Stem Cell Therapies for Acute Kidney Injury. *Am. J. Stem Cell* 5 (1), 1–10.

Belmar-Lopez, C., Mendoza, G., Oberg, D., Burnet, J., Simon, C., Cervello, I., et al. (2013). Tissue-derived Mesenchymal Stromal Cells Used as Vehicles for Anti-tumor Therapy Exert Different in Vivoeffects on Migration Capacity and Tumor Growth. *BMC Med.* 11, 139. doi:10.1186/1741-7015-11-139

Bu, S., Zhang, Q., Wang, Q., and Lai, D. (2017). Human Amniotic Epithelial Cells Inhibit Growth of Epithelial Ovarian Cancer Cells via TGF-B1-Mediated Cell Cycle Arrest. *Int. J. Oncol.* 51 (5), 1405–1414. doi:10.3892/ijo.2017.4123

Cargnoni, A., Farigu, S., Cotti Piccinelli, E., Bonassi Signoroni, P., Romele, P., Vanosi, G., et al. (2018). Effect of Human Amniotic Epithelial Cells on Pro-fibrogenic Resident Hepatic Cells in a Rat Model of Liver Fibrosis. *J. Cel. Mol. Med.* 22 (2), 1202–1213. doi:10.1111/jcmm.13396

Chen, G., and Goeddel, D. V. (2002). TNF-R1 Signaling: a Beautiful Pathway. *Science* 296 (5573), 1634–1635. doi:10.1126/science.1071924

Kang, N. H., Yi, B. R., Lim, S. Y., Hwang, K. A., Baek, Y. S., Kang, K. S., et al. (2012). Human Amniotic Membrane-Derived Epithelial Stem Cells Display Anticancer Activity in BALB/c Female Nude Mice Bearing Disseminated Breast Cancer Xenografts. *Int. J. Oncol.* 40 (6), 2022–2028. doi:10.3892/ijo.2012.1372

Ciarimboli, G. (2014). Membrane Transporters as Mediators of Cisplatin Side-Effects. *Anticancer Res.* 34 (1), 547–550.

Dasari, S., and Tchounwou, P. B. (2014). Cisplatin in Cancer Therapy: Molecular Mechanisms of Action. *Eur. J. Pharmacol.* 740, 364–378. doi:10.1016/j.ejphar.2014.07.025

dos Santos, N. A. G., Carvalho Rodrigues, M. A., Martins, N. M., and dos Santos, A. C. (2012). Cisplatin-induced Nephrotoxicity and Targets of Nephroprotection: an Update. *Arch. Toxicol.* 86 (8), 1233–1250. doi:10.1007/s00204-012-0821-7

Francescato, H. D. C., Costa, R. S., Júnior, F. B., and Coimbra, T. M. (2007). Effect of JNK Inhibition on Cisplatin-Induced Renal Damage. *Nephrol. Dial. Transplant.* 22 (8), 2138–2148. doi:10.1093/ndt/gfm144

Grange, C., Skovronova, R., Marabese, F., and Bussolati, B. (2019). Stem Cell-Derived Extracellular Vesicles and Kidney Regeneration. *Cells* 8 (10), 1240. doi:10.3390/cells8101240

Gurunathan, S., Kang, M.-H., Jeyaraj, M., Qasim, M., and Kim, J.-H. (2019). Review of the Isolation, Characterization, Biological Function, and Multifarious Therapeutic Approaches of Exosomes. *Cells* 8 (4), 307. doi:10.3390/cells8040307

He, C., Zheng, S., Luo, Y., and Wang, B. (2018). Exosome Theranostics: Biology and Translational Medicine. *Theranostics* 8 (1), 237–255. doi:10.7150/thno.21945

Holditch, S. J., Brown, C. N., Lombardi, A. M., Nguyen, K. N., and Edelstein, C. L. (2019). Recent Advances in Models, Mechanisms, Biomarkers, and Interventions in Cisplatin-Induced Acute Kidney Injury. *Int. J. Mol. Sci.* 20 (12), 3011. doi:10.3390/ijms20123011

Jacobson, E. C., Jain, L., Vickers, M. H., Olins, A. L., Olins, D. E., Perry, J. K., et al. (2019). TNF-α Differentially Regulates Cell Cycle Genes in Promyelocytic and Granulocytic HL-60/S4 Cells. *G3 (Bethesda)* 9 (8), 2775–2786. doi:10.1534/g3.119.400361

Jayasooriya, R. G. P. T., Moon, D.-O., Park, S. R., Choi, Y. H., Asami, Y., Kim, M.-O., et al. (2013). Combined Treatment with Verrucarin A and Tumor Necrosis Factor-α Sensitizes Apoptosis by Overexpression of Nuclear Factor-kappaB-Mediated Fas. *Environ. Toxicol. Pharmacol.* 36 (2), 303–310. doi:10.1016/j.etap.2013.04.008

Jo, S.-K., Cho, W. Y., Sung, S. A., Kim, H. K., and Won, N. H. (2005). MEK Inhibitor, U0126, Attenuates Cisplatin-Induced Renal Injury by Decreasing Inflammation and Apoptosis. *Kidney Int.* 67 (2), 458–466. doi:10.1111/j.1523-1755.2005.67102.x

Kakishita, K., Elwan, M. A., Nakao, N., Itakura, T., and Sakuragawa, N. (2000). Human Amniotic Epithelial Cells Produce Dopamine and Survive after Implantation into the Striatum of a Rat Model of Parkinson's Disease: a Potential Source of Donor for Transplantation Therapy. *Exp. Neurol.* 165 (1), 27–34. doi:10.1006/exnr.2000.7449

Kalluri, R., and LeBleu, V. S. (2020). The Biology , Function , and Biomedical Applications of Exosomes. *Science* 367 (6478), eaau6977. doi:10.1126/science.aau6977

Launay-Vacher, V., Rey, J.-B., Isnard-Bagnis, C., Deray, G., and Daouphars, M. (2008). Prevention of Cisplatin Nephrotoxicity: State of the Art and Recommendations from the European Society of Clinical Pharmacy Special Interest Group on Cancer Care. *Cancer Chemother. Pharmacol.* 61 (6), 903–909. doi:10.1007/s00280-008-0711-0

Lee, J. H., Ha, D. H., Go, H.-k., Youn, J., Kim, H.-k., Jin, R. C., et al. (2020). Reproducible Large-Scale Isolation of Exosomes from Adipose Tissue-Derived Mesenchymal Stem/Stromal Cells and Their Application in Acute Kidney Injury. *Int. J. Mol. Sci.* 21 (13), 4774. doi:10.3390/ijms21134774

Makris, K., and Spanou, L. (2016). Acute Kidney Injury: Definition, Pathophysiology and Clinical Phenotypes. *Clin. Biochem. Rev.* 37 (2), 85–98.

McDonald, C. A., Payne, N. L., Sun, G., Moussa, L., Siatskas, C., Lim, R., et al. (2015). Immunosuppressive Potential of Human Amnion Epithelial Cells in the Treatment of Experimental Autoimmune Encephalomyelitis. *J. Neuroinflammation* 12, 112. doi:10.1186/s12974-015-0322-8

Miki, T. (2018). Stem Cell Characteristics and the Therapeutic Potential of Amniotic Epithelial Cells. *Am. J. Reprod. Immunol.* 80 (4), e13003. doi:10.1111/aji.13003

Miki, T., Lehmann, T., Cai, H., Stolz, D. B., and Strom, S. C. (2005). Stem Cell Characteristics of Amniotic Epithelial Cells. *Stem Cells* 23 (10), 1549–1559. doi:10.1634/stemcells.2004-0357

Moon, D.-O., Kim, M.-O., Lee, J.-D., Choi, Y. H., and Kim, G.-Y. (2010). Rosmarinic Acid Sensitizes Cell Death through Suppression of TNF-α-Induced NF-Kb Activation and ROS Generation in Human Leukemia U937 Cells. *Cancer Lett.* 288 (2), 183–191. doi:10.1016/j.canlet.2009.06.033

Motwani, S. S., McMahon, G. M., Humphreys, B. D., Partridge, A. H., Waikar, S. S., and Curhan, G. C. (2018). Development and Validation of a Risk Prediction Model for Acute Kidney Injury after the First Course of Cisplatin. *J. Clin. Oncol.* 36 (7), 682–688. doi:10.1200/jco.2017.75.7161

Plava, J., Cihova, M., Burikova, M., Bohac, M., Adamkov, M., Drahosova, S., et al. (2020). Permanent Pro-tumorigenic Shift in Adipose Tissue-Derived Mesenchymal Stromal Cells Induced by Breast Malignancy. *Cells* 9 (2), 480. doi:10.3390/cells9020480

Pusztai, L., Lewis, C., and McGee, J. D. (1993). Growth Arrest of the Breast Cancer Cell Line, T47D, by TNF α; Cell Cycle Specificity and Signal Transduction. *Br. J. Cancer* 67 (2), 290–296. doi:10.1038/bjc.1993.55

Ramesh, G., and Reeves, W. B. (2005). p38 MAP Kinase Inhibition Ameliorates Cisplatin Nephrotoxicity in Mice. *Am. J. Physiol. Renal Physiol.* 289 (1), F166–F174. doi:10.1152/ajprenal.00401.2004

Ren, Y., Chen, Y., Zheng, X., Wang, H., Kang, X., Tang, J., et al. (2020). Human Amniotic Epithelial Cells Ameliorate Kidney Damage in Ischemia-Reperfusion Mouse Model of Acute Kidney Injury. *Stem Cel Res. Ther.* 11 (1), 410. doi:10.1186/s13287-020-01917-y

Sahni, V., Choudhury, D., and Ahmed, Z. (2009). Chemotherapy-associated Renal Dysfunction. *Nat. Rev. Nephrol.* 5 (8), 450–462. doi:10.1038/nrneph.2009.97

Sanchez, L. O., and Francoz, C. (2021). Global Strategy for the Diagnosis and Management of Acute Kidney Injury in Patients with Liver Cirrhosis. *United Eur. Gastroenterol. J.* 9 (2), 220–228. doi:10.1177/2050640620980713

Sávio-Silva, C., Soinski-Sousa, P. E., Balby-Rocha, M. T. A., Lira, Á. d. O., and Rangel, É. B. (2020). Mesenchymal Stem Cell Therapy in Acute Kidney Injury (AKI): Review and Perspectives. *Rev. Assoc. Med. Bras (1992)* 66 (Suppl. 1), s45–s54. doi:10.1590/1806-9282.66.S1.45

Tan, J. L., Lau, S. N., Leaw, B., Nguyen, H. P. T., Salamonsen, L. A., Saad, M. I., et al. (2018). Amnion Epithelial Cell-Derived Exosomes Restrict Lung Injury and Enhance Endogenous Lung Repair. *Stem Cells Transl. Med.* 7 (2), 180–196. doi:10.1002/sctm.17-0185

Tompkins, B. A., Balkan, W., Winkler, J., Gyöngyösi, M., Goliasch, G., Fernández-Avilés, F., et al. (2018). Preclinical Studies of Stem Cell Therapy for Heart Disease. *Circ. Res.* 122 (7), 1006–1020. doi:10.1161/circresaha.117.312486

Troxell, M. L., Higgins, J. P., and Kambham, N. (2016). Antineoplastic Treatment and Renal Injury: An Update on Renal Pathology Due to Cytotoxic and Targeted Therapies. *Adv. Anat. Pathol.* 23 (5), 310–329. doi:10.1097/pap.0000000000000122

Večerić-Haler, Ž., Cerar, A., and Perše, M. (2017). (Mesenchymal) Stem Cell-Based Therapy in Cisplatin-Induced Acute Kidney Injury Animal Model: Risk of Immunogenicity and Tumorigenicity. *Stem Cell Int.* 2017, 1–17. doi:10.1155/2017/7304643

Volarevic, V., Djokovic, B., Jankovic, M. G., Harrell, C. R., Fellabaum, C., Djonov, V., et al. (2019). Molecular Mechanisms of Cisplatin-Induced Nephrotoxicity: a Balance on the Knife Edge between Renoprotection and Tumor Toxicity. *J. Biomed. Sci.* 26 (1), 25. doi:10.1186/s12929-019-0518-9

Wang, W.-W., Li, Z.-Z., Wang, W., Jiang, Y., Cheng, J., Lu, S., et al. (2015). Enhanced Renoprotective Effect of HIF-1α Modified Human Adipose-Derived Stem Cells on Cisplatin-Induced Acute Kidney Injury *In Vivo*. *Sci. Rep.* 5, 10851. doi:10.1038/srep10851

Wu, X., Wu, M.-Y., Jiang, M., Zhi, Q., Bian, X., Xu, M.-D., et al. (2017). TNF-α Sensitizes Chemotherapy and Radiotherapy against Breast Cancer Cells. *Cancer Cel Int.* 17, 13. doi:10.1186/s12935-017-0382-1

Yang, P.-j., Yuan, W.-x., Liu, J., Li, J.-y., Tan, B., Qiu, C., et al. (2018). Biological Characterization of Human Amniotic Epithelial Cells in a Serum-free System and Their Safety Evaluation. *Acta Pharmacol. Sin.* 39 (8), 1305–1316. doi:10.1038/aps.2018.22

Yue, J., and López, J. M. (2020). Understanding MAPK Signaling Pathways in Apoptosis. *Int. J. Mol. Sci.* 21 (7), 2346. doi:10.3390/ijms21072346

Zhang, C., Chen, B., Jiang, K., Lao, L., Shen, H., and Chen, Z. (2018). Activation of TNF-A/nf-Kb axis Enhances CRL4BDCAF 11 E3 Ligase Activity and Regulates Cell Cycle Progression in Human Osteosarcoma Cells. *Mol. Oncol.* 12 (4), 476–494. doi:10.1002/1878-0261.12176

Zhang, Q., and Lai, D. (2020). Application of Human Amniotic Epithelial Cells in Regenerative Medicine: a Systematic Review. *Stem Cel Res. Ther.* 11 (1), 439. doi:10.1186/s13287-020-01951-w

Zhang, Q., Sun, J., Huang, Y., Bu, S., Guo, Y., Gu, T., et al. (2019). Human Amniotic Epithelial Cell-Derived Exosomes Restore Ovarian Function by Transferring MicroRNAs against Apoptosis. *Mol. Ther. Nucleic Acids* 16, 407–418. doi:10.1016/j.omtn.2019.03.008

Conflict of Interest: LY, CX, YC, and XK have patents pending for the use of hAECs in repair of the injured kidney after AKI. The hAECs used in this study were provided by Shanghai iCELL Biotechnology Co., Ltd, (Shanghai, China). Shanghai iCELL Biotechnology Co., Ltd was not involved in the study design, collection, analysis, interpretation of data, the writing of this article or the decision to submit it for publication.

The remaining authors declare that the research was conducted in the absence of any commercial or financial relationships that could be construed as a potential conflict of interest.

Publisher's Note: All claims expressed in this article are solely those of the authors and do not necessarily represent those of their affiliated organizations, or those of the publisher, the editors and the reviewers. Any product that may be evaluated in this article, or claim that may be made by its manufacturer, is not guaranteed or endorsed by the publisher.

frontiers in Cell and Developmental Biology

BRIEF RESEARCH REPORT
published: 04 February 2022
doi: 10.3389/fcell.2022.814165

Islet Regeneration and Pancreatic Duct Glands in Human and Experimental Diabetes

Diletta Overi[1], Guido Carpino[2], Marta Moretti[3], Antonio Franchitto[1], Lorenzo Nevi[4], Paolo Onori[1], Enrico De Smaele[3], Luca Federici[5], Daniele Santorelli[6], Marella Maroder[7], Lola M. Reid[8], Vincenzo Cardinale[9], Domenico Alvaro[10] and Eugenio Gaudio[1]*

[1]Department of Anatomical, Histological, Forensic Medicine and Orthopedic Sciences, Sapienza University of Rome, Rome, Italy, [2]Department of Movement, Human and Health Sciences, Division of Health Sciences, University of Rome "Foro Italico", Rome, Italy, [3]Department of Experimental Medicine, Sapienza University of Rome, Rome, Italy, [4]Department of Biosciences, University of Milan, Milan, Italy, [5]CAST Center for Advanced Studies and Technology and Department of Innovative Technologies in Medicine and Odontoiatry, University "G. D'Annunzio" of Chieti-Pescara, Chieti, Italy, [6]Department of Biochemical Sciences "Rossi Fanelli", Sapienza University of Rome, Rome, Italy, [7]Department of Molecular Medicine, Sapienza University of Rome, Rome, Italy, [8]Departments of Cell Biology and Physiology, Program in Molecular Biology and Biotechnology, UNC School of Medicine, University of North Carolina, Chapel Hill, NC, United States, [9]Department of Medico-Surgical Sciences and Biotechnologies, Sapienza University of Rome, Latina, Italy, [10]Department of Translational and Precision Medicine, Sapienza University of Rome, Rome, Italy

OPEN ACCESS

Edited by:
Jianjun Zhou,
Tongji University, China

Reviewed by:
Fahd Qadir,
Tulane University, United States
Nashwa El-Tahawy,
Minia University, Egypt

***Correspondence:**
Guido Carpino
guido.carpino@uniroma1.it

Specialty section:
This article was submitted to Stem Cell Research, a section of the journal Frontiers in Cell and Developmental Biology

Received: *12 November 2021*
Accepted: *10 January 2022*
Published: *04 February 2022*

Citation:
Overi D, Carpino G, Moretti M, Franchitto A, Nevi L, Onori P, De Smaele E, Federici L, Santorelli D, Maroder M, Reid LM, Cardinale V, Alvaro D and Gaudio E (2022) Islet Regeneration and Pancreatic Duct Glands in Human and Experimental Diabetes. Front. Cell Dev. Biol. 10:814165. doi: 10.3389/fcell.2022.814165

Contrasting evidence is present regarding the contribution of stem/progenitor cell populations to pancreatic regeneration in diabetes. Interestingly, a cell compartment with stem/progenitor cell features has been identified in the pancreatic duct glands (PDGs). The aims of the present study were to evaluate pancreatic islet injury and regeneration, and the participation of the PDG compartment in type 2 diabetic mellitus (T2DM) and in an experimental model of diabetes. Human pancreata were obtained from normal (N = 5) or T2DM (N = 10) cadaveric organ donors. Experimental diabetes was generated in mice by intraperitoneal injection of 150 mg/kg of streptozotocin (STZ, N = 10); N = 10 STZ mice also received daily intraperitoneal injections of 100 µg of human recombinant PDX1 peptide (STZ + PDX1). Samples were examined by immunohistochemistry/immunofluorescence or RT-qPCR. Serum glucose and c-peptide levels were measured in mice. Islets in T2DM patients showed β-cell loss, signs of injury and proliferation, and a higher proportion of central islets. PDGs in T2DM patients had a higher percentage of proliferating and insulin$^+$ or glucagon$^+$ cells compared to controls; pancreatic islets could be observed within pancreatic duct walls of T2DM patients. STZ mice were characterized by reduced islet area compared to controls. PDX1 treatment increased islet area and the percentage of central islets compared to untreated STZ mice but did not revert diabetes. In conclusion, T2DM patients show signs of pancreatic islet regeneration and involvement of the PDG niche. PDX1 administration could support increased endocrine pancreatic regeneration in STZ. These findings contribute to defining the role and participation of stem/progenitor cell compartments within the pancreas.

Keywords: stem/progenitor cells, endocrine pancreas, streptozotocin, Pdx1, insulin

INTRODUCTION

Diabetes mellitus comprises metabolic diseases characterized by hyperglycemia. Type 1 diabetes mellitus (T1DM) is caused by an autoimmune destruction of pancreatic β-cells, while type 2 diabetes mellitus (T2DM) develops due to insulin resistance and can progress towards β-cell dysfunction (Mathieu et al., 2021). In these patients, regenerative processes can occur, attempting to compensate for the loss of β-cells (Yoneda et al., 2013). Therefore, the identification and characterization of regenerative trajectories within the pancreas could provide insight for the development of novel therapeutic strategies in diabetes treatment.

In the past years, evidence has emerged challenging the hypothesis of the presence of progenitor cell populations within the pancreas participating in islet regeneration; in particular, lineage tracing-based studies have indicated β-cell renewal to be sustained by mature cell replication more than progenitor cell commitment (Domínguez-Bendala et al., 2019). Interestingly, remnants of hepato-bilio-pancreatic precursors have been identified in the biliary tree and in the pancreatic duct system (Cardinale et al., 2012). In particular, the biliary tree stem/progenitor cells (BTSCs) have been identified within the peribiliary glands (PBGs) of the larger intrahepatic and extrahepatic bile ducts, and represent a multipotent stem/progenitor cell compartment. Their capabilities to differentiate towards mature endocrine pancreatic cells have been evaluated both *in vitro* and *in vivo* (Lanzoni et al., 2016). In particular, it has been shown how pancreatic and duodenal homeobox 1 (PDX1) can modulate the balanced differentiation of progenitor/stem cells towards endocrine pancreas commitment rather than towards the biliary fate (Cardinale et al., 2015). We have previously expressed human PDX1 sequence in *E. Coli* and tested *in vitro* the effects of the recombinant PDX1 protein on inducing differentiation toward pancreatic islet cells in BTSCs. We observed how PDX1 can trigger the expression of both intermediate and mature stage β-cell differentiation markers in BTSCs (Cardinale et al., 2015).

In parallel to the PBGs, the pancreatic duct system harbors similar glandular compartments: the pancreatic duct glands (PDGs) are tubulo-acinar glands located within the lamina propria of main pancreatic ducts and, occasionally, large interlobular ducts (Carpino et al., 2016a). PDGs have been shown to harbor a niche of committed precursors towards pancreatic fates (Carpino et al., 2016a). However, the response of this cellular compartment in diabetes has not been investigated yet.

Therefore, the aims of the present study were: 1) to evaluate pancreatic islet injury and phenotype in T2DM patients and in an experimental model of diabetes; 2) to describe the modifications of the PDG compartment in type 2 diabetic patients and in an experimental model of diabetes; 3) to test the possible effects of recombinant PDX1 administration on pancreatic islets and PDG in an experimental model of diabetes.

MATERIALS AND METHODS

Human Samples

Human pancreata were obtained from cadaveric donors (N = 15) from the surgical department of Policlinico Umberto I, Sapienza University of Rome, Italy. Based on anamnestic and serological data, samples were divided into normal (N = 5) or T2DM (N = 10). Informed consent was obtained from next of kin for use of the tissues for research purposes. Study protocols received Institutional Review Board approval from Policlinico Umberto I. Pancreas and duodenum were obtained *en bloc* from organ transplantation procedures. For each case, samples were taken at the level of the main pancreatic duct prior to merging with the choledocus, and at the different levels of the pancreatic body and tail.

Histomorphology, Immunohistochemistry, and Immunofluorescence

Specimens were fixed in 10% buffered formalin and embedded in paraffin, and 3–5 μm sections were obtained and processed for hematoxylin and eosin (H&E). For immunohistochemistry, endogenous peroxidase activity was blocked by a 30-min incubation in 2.5% hydrogen peroxide. Sections were incubated overnight at 4°C with primary antibodies (listed in **Supplementary Table S1**). Then, samples incubated for 20 min at room temperature with secondary biotinylated antibody, and then with streptavidin-horseradish peroxidase (LSAB+, Dako, Glostrup, Denmark, code: K0690). Diaminobenzidine (Dako, Glostrup, Denmark, code: K3468) was used as substrate, and sections were counterstained with hematoxylin. Sections were examined in a coded fashion by Leica Microsystems DM4500B Light and Fluorescence Microscopy (Weltzlar, Germany), equipped with a Jenoptik Prog Res C10 Plus Videocam (Jena, Germany).

For immunofluorescence (IF), non-specific protein binding was blocked by 5% normal goat serum. Specimens were incubated with primary antibodies overnight; then, samples were washed and incubated for 1 h with labeled isotype-specific secondary antibodies (AlexaFluor®, Invitrogen, Life Technologies Ltd., Paisley, United Kingdom) and counterstained with 4,6-diamidino-2-phenylindole (DAPI) for visualization of cell nuclei. To perform double immunostaining with two primary antibodies from the same host species, we followed a 3-step protocol: sections were incubated with the first primary antibody; then, a secondary fluorescent antibody was applied; finally, the second primary antibody was pre-labeled with a fluorophore using the APEX-594 labeling Kit (Invitrogen) and applied to the section.

For all immunoreactions, negative controls (the primary antibody was replaced with pre-immune serum) were also included.

Sections were examined in a coded fashion by Leica Microsystems DM4500B Light and Fluorescence Microscopy (Weltzlar, Germany), equipped with a Jenoptik Prog Res C10 Plus Videocam (Jena, Germany).

Immunofluorescence stains were also analyzed by Confocal Microscopy (Leica TCS-SP2). Slides were further scanned by a digital scanner (Aperio Scanscope CS and FL Systems, Aperio Digital Pathology, Leica Biosystems, Milan, Italy) and processed by ImageScope.

The area of pancreas occupied by the islets of Langerhans and islet's size were evaluated on H&E slides by ImageScope. Islets were considered as "central" or "peripheral" based on their position with respect to the pancreatic lobule and duct system: central islet are typically located close to interlobular septa, connected to a clearly-defined pancreatic inter/intralobular duct and in continuity with duct's surrounding stroma; peripheral islets are located in the middle of pancreatic lobule without connection with inter/intralobular duct stroma (Merkwitz et al., 2013). Islet composition was evaluated by counting positive cells within islets. Moreover, the expression of nuclear antigens was automatically calculated by a specific algorithm on selected areas and expressed as a percentage of positive cells.

Streptozotocin (STZ)-Induced Diabetic Mice and PDX1 Treatment

Male NOD/SCIDgamma (NSG) mice (N = 25) were purchased from Charles River (Calco, Milan, Italy). Mice were housed in a dedicated, pathogen-free barrier facility at the Sapienza University of Rome in compliance with Italian regulations. Mice were kept in a room with specific pathogen-free standards maintained at a temperature of 23 ± 1°C and 50 ± 10% relative humidity, with food and water available *ad libitum*. The animal room was on a 12:12 h light:dark cycle. Mice were individually identified by ear punching.

Type 1 diabetes mellitus was induced by a single intraperitoneal injection of a single dose of 150 mg/kg (N = 10) of STZ. Moreover, N = 10 additional STZ mice were treated with daily intraperitoneal injections of 100 µg of human recombinant PDX1 peptide (Cardinale et al., 2015). Mice in the STZ group were injected with saline solution. N = 5 mice were included as controls and did not receive STZ or PDX1. Animals that reached stable glucose levels >300 mg/dl were considered as diabetic (Leiter and Schile, 2013). The study was conducted on NSG mice in order to avoid a possible immune reaction of the host against the human PDX1.

Treatment with PDX1 was initiated 48 h after STZ injection and confirmation of stable serum glucose levels >300 mg/dl. To prevent mortality due to the hypoglycemia caused by massive insulin release after STZ-induced pancreatic islet damage, animals were treated with water supplemented with 10% sucrose for 48 h after STZ administration. Glucose levels were measured every 3 days by AlphaTRAK glucometer with strips (Abbott). Pancreatic tissue samples were obtained at sacrifice. Tissues were processed for histology, immunohistochemistry and immunofluorescence, or frozen for RT-qPCR analysis. All animal experiments were approved by the institutional animal care and use committee of Sapienza University of Rome and by the Italian Ministry of Health.

PDX1 Production and Purification

Recombinant PDX1 was obtained in the form of a fusion protein by linking 6His-tag to the N-terminus of the amino acid sequence. Full-length DNA coding sequence for human PDX1 (852 bp coding for 283 aa) adapted for heterologous expression in *E. Coli* was provided by GenScript United States Inc. (Piscataway, NJ). The sequence was amplified by PCR using primers 5′-TAT CATATGAACGGTGAAGAACAGTACTAC-3′ and 5′-ATA CTCGAGCTAACGTGGTTCTTGCGGACGGC-3'. After digestion with NdeI and BamHI, the amplicon was ligated into pET-28a expression vector (Novagen-Merck, Darmstadt, Germany), yielding pET-PDX1 plasmid. This construct was used to transform the BL21 (DE3) *E. Coli* strain (Invitrogen). BL 21 (DE3) cells were grown in Luria Bertani (LB) medium containing 34 µg/ml Kanamycin and at 37°C until the OD_{600} reached 0.6; then, protein expression was induced with 1 mM IPTG. After induction, cells were grown at 21°C overnight and then collected by centrifugation. For PDX1 purification, the cell pellet was resuspended in 20 mM Tris-HCl pH 8.0, 0.2 U/mL of Benzonase nuclease (Sigma-Aldrich), 5 mM MgCl2, protease inhibitor tablet (Complete EDTA-free, Roche), and glycerol 10%, sonicated and centrifuged. After addition of 500 mM NaCl and 25 mM imidazole, the soluble fraction was loaded on a 5 ml HisTrap FF (GE Healthcare) pre-equilibrated with resuspension buffer. The protein was eluted with an imidazole gradient (20 mM–1 M imidazole in buffered Tris-HCl (pH 8.0, NaCl 500 mM, glycerol 10%) and then fractions containing PDX1 protein were analyzed by SDS-PAGE. A Sephadex G-25 column (GE Heathcare) was employed to remove imidazole and to exchange buffer with PBS. Mass spectrometry analyses were performed after tryptic digestion of the band of 43 kDa isolated by Coomassie blue stained gel. Mass spectra were acquired by Ultraflex III MALDI-TOF-TOF instrument (Bruker-Daltonics, Bremen, Germany), and peptide sites were searched in the NCBI database by MASCOT search engine.

RT-qPCR Analysis and ELISA Assay

Total RNA was extracted by the procedures of Chomczynski and Sacchi (Chomczynski and Sacchi, 2006). RNA quality and quantity was evaluated with the Experion Automated Electrophoresis System. RNA equipped with the RNA StSens Analysis Chip (Bio-Rad Laboratories, Hercules, CA). RNA was extracted by TRIZOL reagent (Life Technologies, Rockville, MD; Cat# 15,596-026) according to manufacturer's instructions. One µg of RNA was retrotranscribed using High Capacity cDNA Reverse Transcription Kit (Applied Biosystems, Life Technologies, Paisley, United Kingdom: code 4368814), and cDNA was amplified using SensiMix SYBR kit (Bioline, London, United Kingdom: code QT605-05) according to manufacturer's instructions. The primers used are listed in **Supplementary Table S2**. The expression of the gene of interest was calculated by the ratio of the concentrations of the gene of interest and the reference gene 18 s.

Serum mouse C-peptide levels in response to glucose administration were measured by ELISA assay. Mice were fasted overnight, and 30% dextrose was injected intraperitoneally at 2 g/kg body weight. Sixty minutes after the

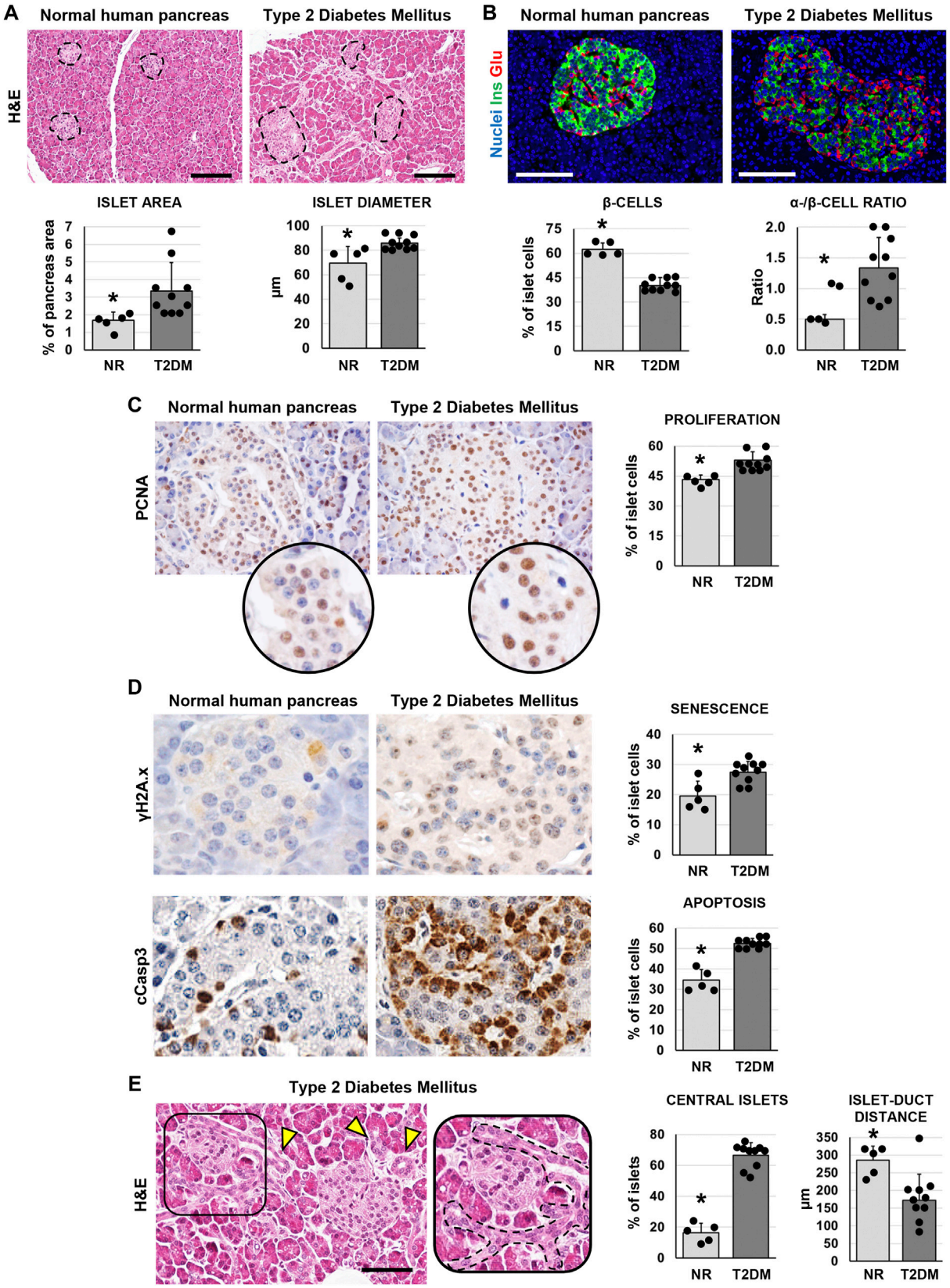

FIGURE 1 | Pancreatic islet histology and phenotype in normal (NR) human pancreas and in type 2 diabetes mellitus (T2DM) pancreas samples. **(A)** Hematoxylin

(*Continued*)

FIGURE 1 | and eosin (H&E) stain. T2DM patients showed higher islet area and islet size compared to normal samples. Dotted lines individuate pancreatic islets. Histograms show means and standard deviation (SD) for islet area and diameter. Scale bar: 150 μm. **(B)** Double immunofluorescence for insulin (green) and glucagon (red). Pancreatic islets in T2DM patients were characterized by a lower β-cell percentage and by a higher α-/β-cell ratio compared to normal pancreata. Histograms show means and SD for β-cell percentages and for the α-/β-cell ratio. Scale bar: 100 μm. Nuclei are displayed in blue (DAPI staining). **(C)** Immunohistochemistry for proliferating cell nuclear antigen (PCNA). T2DM patients showed increased percentage of proliferating PCNA + cells within islets compared to normal pancreata. Original magnification: 40x. Areas in the circle are magnifications of the images above. The histogram shows means and SD for the percentage of proliferating cells. **(D)** Immunohistochemistry for γH2A.x (upper panels) and cleaved caspase 3 (cCasp3, lower panels). Pancreatic islets in diabetic patients were characterized by a higher expression of senescence marker γH2A.x and apoptosis marker cCasp3 compared to normal pancreata. Histograms show means and standard deviation for the percentage of positive cells. Original magnification: 40x. **(E)** H&E stain on pancreata from T2DM patients. Pancreata from T2DM patients were characterized by a higher percentage of central islets compared to normal ones. Arrowheads indicate pancreatic ducts. The area in the box is magnified on the right; dotted line individuates a pancreatic duct branch surrounding an islet. Scale bar: 75 μm. The histogram shows means and SD for the percentage of central islets and the average distance between islets and neighboring ducts. * = p< 0.05 versus T2DM.

glucose injection, 80 μl of blood were collected into heparinized micro-hematocrit capillary tubes (Fisherbrand) and prepared serum samples were subjected to assays for mouse C-peptide. The Ultrasensitive Mouse C-peptide ELISA kit (ALPCO, Catalog Number 80-CPTMS-E01) was used according to manufacturer's instructions.

Statistical Analysis

Continuous data are presented as mean ± SD. Student's t-test or Mann–Whitney *U*-test were used to determine differences between groups for normally- or not normally-distributed data, respectively. A One-way ANOVA or Kruskal–Wallis H test were used to calculate differences between three groups. A p-value <0.05 was considered statistically significant. Analyses were performed using IBM SPSS software (SPSS Inc., United States).

RESULTS

Islet of Langerhans Modifications in Human Diabetes

In pancreata obtained from patients affected by T2DM, the area occupied by islets was significantly higher (3.3 ± 1.7%) compared to normal ones (1.8 ± 0.5%; $p < 0.05$; **Figure 1A**) In parallel, pancreatic islets in T2DM samples were larger (86.0 ± 4.4 μm) compared to the islets in normal pancreata (69.8 ± 13.5μm; $p < 0.05$; **Figure 1A**). However, when pancreatic islet composition was investigated (**Figure 1B**), islets in T2DM were characterized by a lower percentage of β-cells (40.2 ± 4.7%) and by a higher percentage of α-cells (55.0 ± 9.6%) compared to normal pancreata (62.2 ± 4.4% and 31.5 ± 6.1%, respectively; $p < 0.001$ and $p < 0.01$); therefore, T2DM was characterized by a higher α-/β-cell ratio (1.35 ± 0.49) compared to islets in normal pancreata (0.5 ± 0.08; $p < 0.01$).

We then performed immunohistochemical analysis to evaluate cell proliferation (by proliferating cell nuclear antigen—PCNA), senescence (by γH2A.x) and apoptosis (by cleaved caspase 3—cCasp3) in pancreatic islets. The percentage of PCNA + islet cells was higher in T2DM (52.9 ± 4.2%) compared to normal pancreata (43.2 ± 2.3%; $p < 0.01$; **Figure 1C**); however, cells within pancreatic islets in T2DM patients also showed an increase of γH2A.x (27.5 ± 3.5%) and cCasp3+ (52.6 ± 2.3%) expression compared to normal pancreatic islets (19.6 ± 4.9% and 34.4 ± 5.4%, respectively; $p < 0.05$ and $p < 0.001$; **Figure 1D**).

Interestingly, when we evaluated the localization of pancreatic islets, we observed a higher proportion of central islets in T2DM patient pancreata (66.7 ± 7.9%) compared to normal ones (16.4 ± 6.3%; $p < 0.001$; **Figure 1E**). Pancreatic islets were less distant from neighboring ducts in T2DM (172.0 ± 74.5 μm) compared to normal subject pancreata (285.4 ± 40.33 μm; $p < 0.01$).

Pancreatic Duct Glands (PDGs) in Human Type 2 Diabetes Mellitus

We investigated whether the PDG compartment could be modified in T2DM-affected pancreata. Interestingly, main pancreatic duct samples obtained from T2DM patients were characterized by a higher area occupied by PDGs in the duct wall (i.e. PDG mass; 3.6 ± 0.3%) compared to normal samples (1.6 ± 0.9%; $p < 0.01$; **Figure 2A**). Accordingly, an increased percentage of PCNA + cells was observed in PDGs of T2DM patients (80.7 ± 5.8%) compared to normal ones (53.4 ± 5.8%; $p < 0.001$; **Figure 2A**).

As in our previous study (Carpino et al., 2016a), cells within PDGs expressing insulin or glucagon could be observed (**Figure 2B**). Interestingly, PDGs in diabetic pancreata were characterized by a higher percentage of insulin+ (23.9 ± 8.9%) and glucagon+ (3.1 ± 0.2%) cells as compared to normal organs (7.2 ± 1.1% and 1.1 ± 0.2%, respectively; $p < 0.05$).

Uniquely, large islet-like structures could be found within main pancreatic duct walls in T2DM samples; these islets showed positivity for insulin and glucagon and were characterized by the presence of blood vessels within the islet (**Figure 2C**). Of note, main pancreatic duct in T2DM but not in normal samples, were also characterized by the presence of dysplastic lesions of the surface epithelium and PDGs (chi-squared test $p < 0.05$; **Figure 2C**).

Pancreatic Islet Injury and PDG Activation in Murine Streptozotocin-Induced Diabetes

We further investigated pancreatic islet morphology after injury in a murine model of diabetes, the STZ mice. We first examined the pathological modification of islets in mice, and we observed that the area of pancreatic islets was lower in STZ mice (0.19 ± 0.07%) compared to controls (0.57 ± 0.27%; $p < 0.05$; **Figure 3A**).

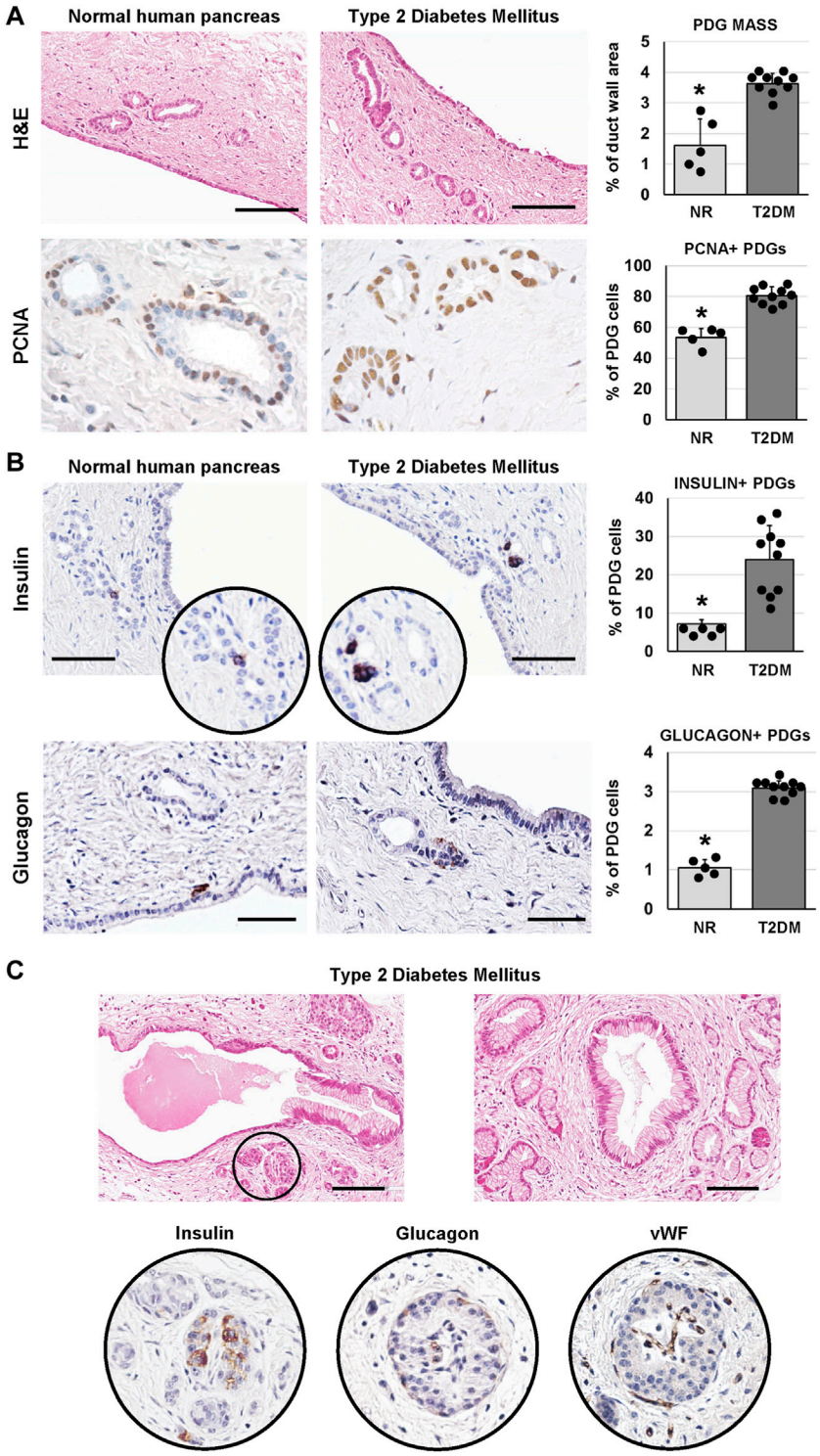

FIGURE 2 | Pancreatic duct glands (PDGs) in normal (NR) human pancreas and in type 2 diabetes mellitus (T2DM) pancreas samples. **(A)** Hematoxylin and eosin (H&E) stain (upper panels) and immunohistochemistry for proliferating cell nuclear antigen (PCNA, lower panels). Pancreatic ducts in T2DM patients were characterized by a higher PDG mass and by a higher expression of PCNA within PDGs compared to normal ducts. Histograms show means and standard deviation (SD) for the percentage of duct wall area occupied by PDGs and for the percentage of PCNA + PDG cells. Scale bar for H&E: 100 μm. Original magnification for PCNA: 40x. **(B)** Immunohistochemistry for insulin (upper panels) and glucagon (lower panels). T2DM patients showed a higher percentage of insulin+ and glucagon + cells within PDGs compared to normal ones. Histograms show means and SD for the percentage of positive cells. Scale bar: 75 μm (insulin) and 50 μm (glucagon). **(C)** H&E stain on T2DM samples shows pancreatic ducts with dysplastic lesions of surface epithelium and PDGs and the presence of pancreatic islets among PDGs (circle). Seriated sections of the same area show that islets in pancreatic ducts express insulin, glucagon and are vascularized. Scale bar: 100 μm * = $p < 0.05$ versus T2DM.

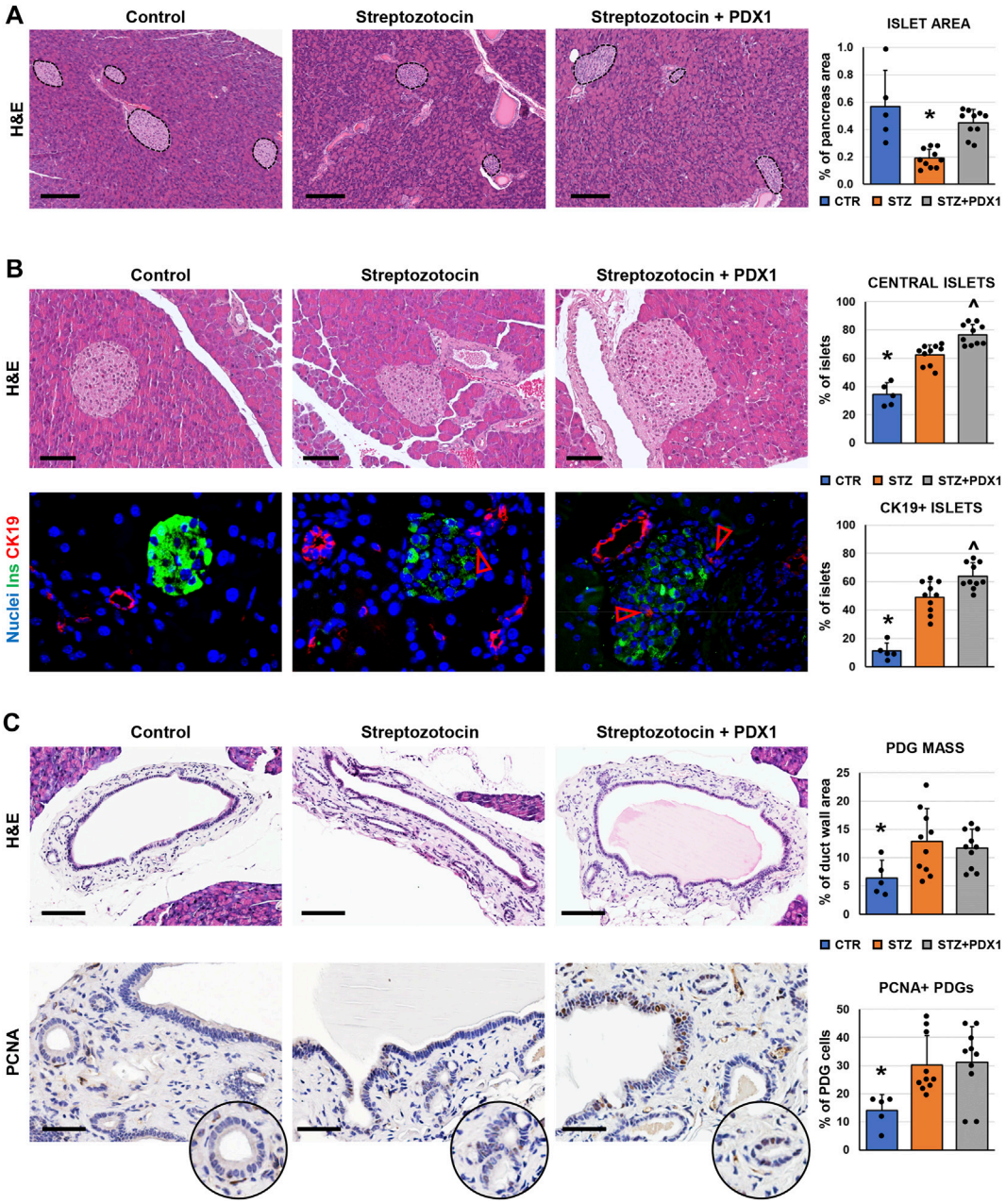

FIGURE 3 | Pancreatic islets and pancreatic duct glands (PDGs) in control mice, streptozotocin (STZ)-treated mice and STZ mice treated with PDX1. **(A)** Hematoxylin and eosin (H&E) stain on pancreas samples. STZ treated mice were characterized by a lower pancreatic islet area compared to controls; STZ + PDX1 mice showed a higher islet area compared to STZ, without significant differences compared to controls. Dotted lines individuate pancreatic islets. Histogram shows means and standard deviation (SD) for pancreatic area percentage. Scale bar: 150 μm. **(B)** H&E stain (upper panels) and double immunofluorescence for insulin (ins, in green) and cytokeratin 19 (CK19, in red) on pancreas samples. STZ-treated mice show a higher percentage of central islets compared to controls; moreover, STZ + PDX1 mice showed a significantly higher percentage of central islets compared to STZ and control mice. Scale bar in H&E: 75 μm. In immunofluorescence image, arrowheads indicate small CK19 + cells within islets. Nuclei are displayed in blue (DAPI staining). Original magnification: 40x. Histograms show means and SD for the percentage of central islets and islets containing CK19 + cells. **(C)** H&E stain and immunohistochemistry for proliferating cell nuclear antigen (PCNA) on pancreatic ducts. STZ- and STZ + PDX1-treated mice show a higher PDG mass and percentage of PCNA + cells within PDGs compared to controls. Histograms show means and SD for the percentage of duct wall area occupied by PDGs and for the percentage of PCNA + PDG cells. Scale bar: 100 μm (H&E) and 50 μm (PCNA). * = $p < 0.05$ versus other groups; ^ = $p < 0.05$ versus STZ group.

Moreover, pancreatic islets were smaller in STZ mice (diameter: 60.7 ± 15.6 μm) compared to control ones (88.6 ± 19.3μm; $p < 0.05$). Interestingly, the area of pancreatic islets was higher in STZ mice treated with PDX1 (0.45 ± 0.10%) than in untreated STZ mice ($p < 0.01$); no significant difference was observed between STZ + PDX1-treated and control mice.

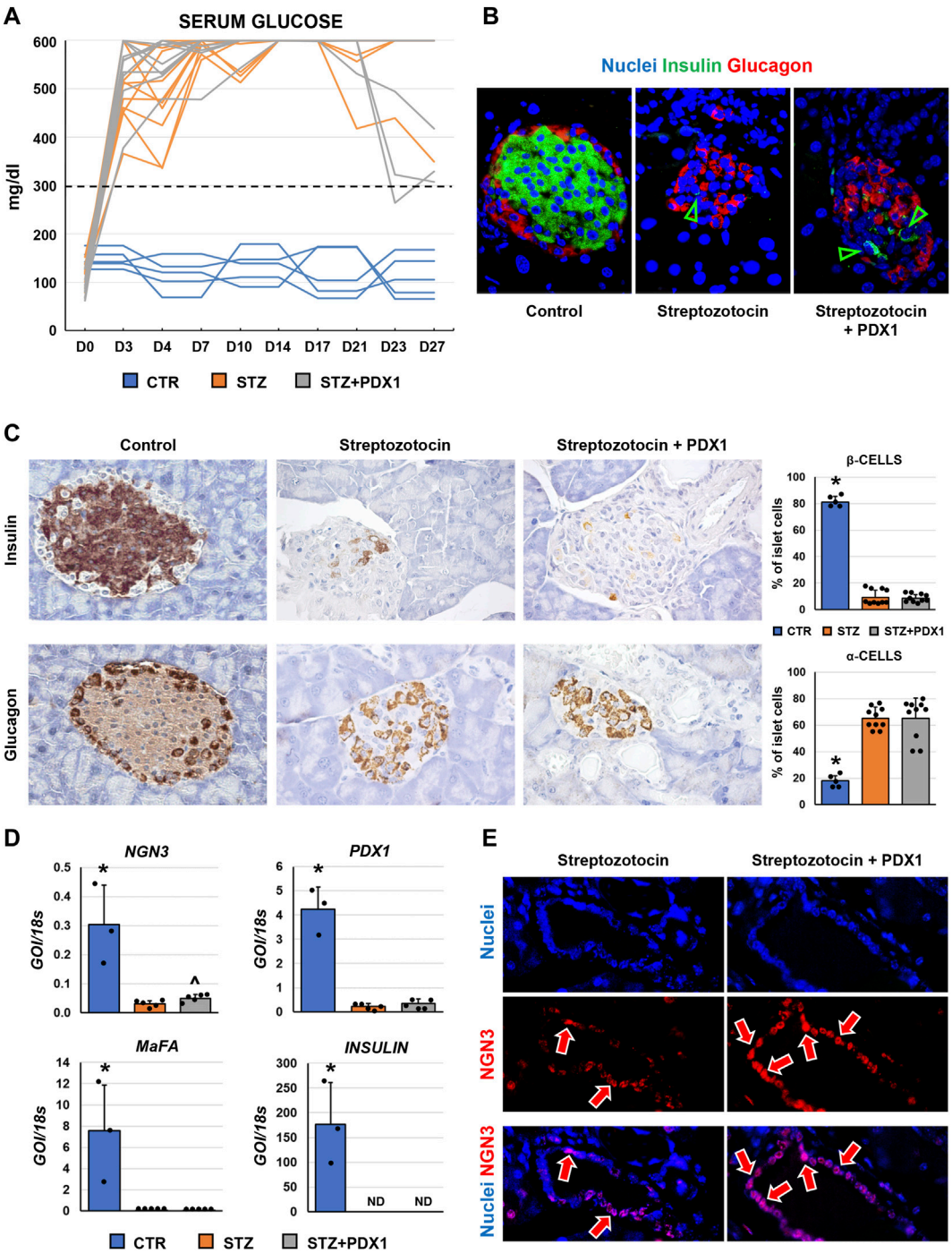

FIGURE 4 | Pancreatic islet phenotype and glycemic profile in control mice, streptozotocin (STZ)-treated mice and STZ mice treated with PDX1. **(A)** Graph shows individual values for serum glucose levels in STZ and STZ + PDX1 mice. Dotted line indicates the threshold for diabetes diagnosis (300 mg/dl). **(B)** Double immunofluorescence for insulin (ins, in green) and glucagon (glu, in red). **(C)** Immunohistochemistry for insulin (upper panels) and for glucagon (lower panels). STZ- and STZ + PDX1-treated mice showed a lower percentage of β-cells and a higher percentage of α-cells compared to controls. Histograms show means and standard deviation (SD) for the percentage of α-/β-cells. Original magnification: 40x. **(D)** Histograms show means and standard deviation for the RT-qPCR expression of *NGN3, PDX1, MaFA* and *Insulin* genes. Data are expressed as means and standard deviation (SD). GOI: gene of interest. ND: not detectable. (D) Immunofluorescence for NGN3 confirmed the higher expression of NGN3 in STZ + PDX1-treated mice compared to STZ group. NGN3 was mostly expressed by pancreatic duct cells (arrows). Separate channels were provided. Original Magnification: 40x. * = p< 0.05 versus other groups; ^ = p< 0.05 versus STZ group.

When the anatomical location of islets was studied (**Figure 3B**), the percentage of central islets was higher in mice treated with STZ (62.3 ± 7.1%) compared to control mice (34.5 ± 8.1%; $p < 0.001$). Furthermore, STZ + PDX1-treated mice were characterized by a higher percentage of central islets (76.5 ± 7.3%) compared to untreated STZ ($p = 0.03$) and control mice ($p < 0.001$). Islets in STZ + PDX1-treated mice showed a closer proximity to ducts (59.0 ± 13.5 μm) compared to STZ (79.3 ± 22.9 μm; $p < 0.05$) and control mice (154.8 ± 7.8 μm $p < 0.05$). Ductular CK19 + cells were found inside pancreatic islets (**Figure 3B**), and the percentage of islets with CK19 + cells was higher in STZ + PDX1 (63.7 ± 9.7) compared to STZ (49.0 ± 10.9; $p < 0.05$) and control mice (11.2 ± 5.5; $p < 0.05$).

We then investigated the modifications of the PDG cell compartment in STZ mice (**Figure 3C**). Interestingly, both STZ and STZ + PDX1 mice were characterized by a higher PDG mass (12.8 ± 5.8% and 11.7 ± 3.3%, respectively) compared to control ones (6.4 ± 3.1%; $p < 0.05$). Accordingly, PDG cells in STZ and STZ + PDX1 mice were characterized by a higher expression of PCNA (30.1 ± 10.5% and 31.2 ± 12.6%, respectively) compared to controls (14.1 ± 5.7%; $p < 0.05$). No significant differences were observed between STZ and STZ + PDX1 mice in term of PDG area and PCNA expression in PDG cells.

Islet Phenotype and Glycemic Profile in Murine Streptozotocin-Induced Diabetes

When glycemic profile was studied in mice (**Figure 4A**), serum glucose levels remained above the 300 mg/dl threshold in all animals, except for one mouse in the STZ + PDX1 group. At sacrifice, no STZ mice showed positivity for c-peptide at ELISA on serum. However, N = 2/10 STZ + PDX1 mice were positive for serum c-peptide (*chi-squared* test: $p < 0.001$).

When the phenotype of murine pancreatic islet cells was studied (**Figures 4B,C**), we observed that the percentage of β-cells within pancreatic islets was lower in STZ mice (9.1 ± 5.5%) and STZ + PDX1-treated mice (8.4 ± 2.6%) compared to control ones (81.2 ± 4.2%; $p < 0.001$). In parallel, the percentage of α-cells was higher in STZ mice (65.3 ± 8.3%) and STZ + PDX1-treated mice (65.1 ± 15.3%) compared to controls (17.9 ± 3.8%; $p = 0.004$ and $p < 0.001$, respectively). No differences were observed in the percentage of β-cells and α-cells in STZ + PDX1 mice compared to STZ mice.

Finally, when RT-qPCR analysis was performed on pancreatic tissues (**Figure 4D**), no significant differences were observed in terms of *Insulin*, *MaFA* and *PDX1* expression between STZ and STZ + PDX1 groups. However, we observed an increased gene expression of *NGN3* in STZ-PDX1 mice compared to STZ ones (N = 5, $p < 0.05$). The increased expression in STZ-PDX1 (56.1 ± 8.2%) compared to PDX1 mice (45.9 ± 10.1%; $p < 0.05$) was confirmed by immunofluorescence, which also showed that NGN3 expression was mainly located in ductal cells (**Figure 4E**).

DISCUSSION

The results obtained in the present study demonstrate that: 1) T2DM-affected pancreata are characterized by islet mass expansion and cell proliferation, accompanied by β-cell disruption and signs of pancreatic islet cell apoptosis and senescence; 2) PDG compartment proliferates in diabetic patients and shows sign of endocrine pancreas commitment (insulin/glucagon expression and neo-islet formation); 3) in STZ-treated mice, islet mass was impaired and associated to PDG proliferation and prevalence of central islets; 4) PDX1 administration in STZ-treated mice determined an increase in islet mass and in the percentage of central islets, but was not effective in restoring insulin production within the islets and in reverting the diabetic state in mice.

The progression of T2DM is accompanied by pathological alterations in the islets of Langerhans, which are the consequences to the altered insulin signaling and β-cell failure (Dooley et al., 2016; Folli et al., 2018). In the present manuscript we describe that, despite the loss of β-cells occurring in T2DM patients, a significant regenerative process takes place, leading to the observation of larger islets and an increased islet mass, together with increased expression of the proliferation marker PCNA within the islet cells. In parallel, islet cells showed higher expression of apoptosis and cellular senescence markers. These observations indicate that islet damage during T2DM is accompanied by an activation of regenerative processes associated with proliferative senescence and apoptosis, limiting an appropriate and long-lasting renewal of β-cell pool.

The regenerative properties of endocrine pancreatic cells and the possible source of newly-formed pancreatic islets are the subject of investigations and lively discussions in the scientific community (Domínguez-Bendala et al., 2019). Lineage tracing studies produced contradictory results on the topic, both excluding and individuating a possible role for progenitor cells in endocrine pancreas renewal (Dor et al., 2004; Xiao et al., 2013; Song et al., 2015; Yuchi et al., 2015). Despite the possibility of mature endocrine cell replication (Meier et al., 2008; van der Meulen et al., 2017), several studies have identified cell populations with progenitor features in both the insulae and in the ductal compartment (Martin-Pagola et al., 2008; Huch et al., 2013; El-Gohary et al., 2016; Qadir et al., 2018; Wang et al., 2020). The results obtained in the present manuscript support that multiple regenerative pathways are occurring in T2DM pancreata: 1) the enlargement of islets and increased proliferation of islets cells support the concept of mature endocrine cell replication; 2) the individuation of an increased proportion of pancreatic islets in proximity with intra- and inter-lobular pancreatic duct branches suggests a role of pancreatic duct plasticity in islet generation; finally, 3) the appearance of signs of endocrine islet regeneration in PDGs, associated with larger pancreatic ducts, further delineates the involvement of this peculiar cell compartment.

It has been shown that remnants of the common hepato-bilio-pancreatic precursors are harbored within the biliary tree and pancreatic duct system postnatally (Carpino et al., 2012; Carpino et al., 2014; Carpino et al., 2016a). These cells display stem/

progenitor cell features and, particularly, potency towards mature endocrine pancreatic fate *in vitro* and/or in specific conditions *in vivo*. Cells isolated from the biliary tree and PDGs have shown the capability to differentiate into functional pancreatic islet-like structures without cell reprogramming when cultured in a hormonally-defined medium (Cardinale et al., 2015); the functional capabilities of these cells have also been demonstrated by transplanting the differentiated neo-islets in a murine model of diabetes, which led to an improvement in glycemic profile of mice (Wang et al., 2013). Moreover, modifications in the PBG compartment within the biliary tree have been observed both in human and murine diabetes. In these settings, PBGs showed cells with extensive signs of proliferation, and were characterized by the upregulation of pancreatic fate-related markers (e.g. MafA) (Carpino et al., 2016b). Similar evidence is now emerging for the role of the PDG cell compartment as a niche of committed precursors destined for pancreatic fates. These cells can be identified by the co-expression of endoderm stem/progenitor markers (i.e. Sox9) and pancreatic stem/progenitor markers (i.e. Pdx1 or Ngn3) (Yamaguchi et al., 2015; Carpino et al., 2016a; Qadir et al., 2020). In the present manuscript, we described the presence of islet-like structures within the PDG compartment in pancreatic ducts of T2DM patients; these structures contained insulin- and glucagon-positive cells, and showed a well-arranged microvascular network, suggesting functional properties. Therefore, these data further support the role of PDGs as a possible regenerative compartment in the pancreas. However, no specific marker/promoter for PDGs has been still individuated to distinguish PDG cells from the surface epithelium of the pancreatic duct; therefore, it is impossible to judge the actual cell of origin of PDG-associated islets.

Interestingly, ducts characterized by the appearance of neoislets also presented with dysplastic lesions of the epithelium and PDGs. T2DM has been linked with the development of pancreatic duct adenocarcinoma (PDAC) (Qadir et al., 2020) through several possible mechanisms including both systemic risk factors and local processes (Duvillié et al., 2020). Regarding the latter, it has been hypothesized that intrapancreatic hyperinsulinemia could trigger a response in ductal cells via insulin receptors and, particularly on transformed cells, by the IGF-1 signaling pathway. This could lead to proliferation within the exocrine compartment as well, and predispose to PDAC development (Andersen et al., 2017). Moreover, injured islet cells can acquire a senescence-associated secretory phenotype which can further support cancer development (Cantor and David, 2014; Thompson et al., 2019). Interestingly, previous observations have shown a relationship between the activation of the PDG compartment after injury and the development of PDAC (Strobel et al., 2010; Yamaguchi et al., 2015; Yamaguchi et al., 2016). Our results are in accordance with this evidence, suggesting how PDG activation in T2DM patients could be related to the emergence of dysplastic lesions of the pancreatic ducts, possibly predisposing to cancer development.

Finally, we investigated the possibility to induce pancreatic β-cell regeneration in a mouse model of diabetes (i.e. the STZ mouse) by administration of PDX1. In our model, we observed an increase in the portion of central islets and islet proximity to pancreatic duct compared to controls in all STZ mice and, especially, in PDX1-treated ones, which also showed a recovery in islet mass compared to STZ mice. However, PDX1 treatment was not effective in restoring a functional β-cell population and in rescuing diabetes in mice, which could be due to several aspects. Reprogramming strategies have been proved effective in converting cells in functional insulin-secreting cells *in vivo*, by inducing key pancreatic genes *NGN3, PDX1,* and *MAFA* (Zhou et al., 2008; Banga et al., 2012). Our approach was based on the intraperitoneal administration of a single factor and did not require genetic manipulation. With further improvements of conditions and administration methods, this could represent a feasible approach to be translated in the clinical setting in order to achieve positive results on insulin production and diabetes reversal. Furthermore, the extensive damage deriving from STZ administration and the continued injury during STZ washout could hamper the effective regeneration of functional β-cells in this model. Interestingly, the increase in alpha-cells in STZ-treated mice could represent a temporary compensatory mechanism in stressed beta-cells where they are reverting to a de-differentiated state. In this light, the time course of the experimental setting could represent a limitation of the study; a longer time course could allow to monitor the recovery of beta-cells mass. Nevertheless, our approach has been successful in supporting evidence of regenerative processes especially within the central pancreatic islets, representing a proof of concept for a possible role of PDX1 in supporting ductal-derived pancreatic islet regeneration.

In conclusion, we provide additional evidence that pancreatic islet regeneration occurs in T2DM patients, and that regenerating islets can be associated with the pancreatic duct system and PDG cell niche. Moreover, the proliferation induced in the ductal system in T2DM patients could have a role in PDAC development. Finally, we provide a report on the efficacy of PDX1 administration to support increased endocrine pancreatic regeneration in STZ mouse model of diabetes. Future studies are needed in order to develop effective and feasible strategies to use the same approach to revert the diabetic state and restore β-cell population within the islets.

DATA AVAILABILITY STATEMENT

The raw data supporting the conclusion of this article will be made available by the authors, without undue reservation.

ETHICS STATEMENT

The studies involving human participants were reviewed and approved by the Institutional Review Board of Policlinico Umberto I and Sapienza University of Rome. The patients/participants provided their written informed consent to

participate in this study. All animal experiments were approved by the institutional animal care and use committee of Sapienza University of Rome and by the Italian Ministry of Health (auth #172/2018-PR).

AUTHOR CONTRIBUTIONS

GC and DO were responsible for the study concept and design, acquisition of data, analysis and interpretation of data, drafting of the manuscript, and critical revisions of the manuscript for important intellectual content, statistical analysis, and study supervision. VC, MMo, LN, EDS, GF, LF, DS, MMa, and LR were responsible for the acquisition of data, analysis and interpretation of data, drafting of the manuscript, critical revision of the manuscript for important intellectual content, and technical or material support. AF, PO, LR, DA, and EG were responsible for the study concept and design, interpretation of data, drafting of the manuscript, critical revision of the manuscript for important intellectual content, obtainment of funding, and study supervision.

FUNDING

The study was supported by research project grants from Sapienza University of Rome (EG, PO, AF) and by Italian Federation of Juvenile Diabetes (FDG).

ACKNOWLEDGMENTS

The authors kindly thank the Italian Federation of Juvenile Diabetes, and its board composed of Prof. Giorgio Federici, Prof. Domenico Casa and Dr. Antonio Cabras, for the continuous support.

SUPPLEMENTARY MATERIAL

The Supplementary Material for this article can be found online at: https://www.frontiersin.org/articles/10.3389/fcell.2022.814165/full#supplementary-material

REFERENCES

Andersen, D. K., Korc, M., Petersen, G. M., Eibl, G., Li, D., Rickels, M. R., et al. (2017). Diabetes, Pancreatogenic Diabetes, and Pancreatic Cancer. *Diabetes* 66, 1103–1110. doi:10.2337/db16-1477

Banga, A., Akinci, E., Greder, L. V., Dutton, J. R., and Slack, J. M. W. (2012). *In Vivo* reprogramming of Sox9+ Cells in the Liver to Insulin-Secreting Ducts. *Proc. Natl. Acad. Sci. USA* 109, 15336–15341. doi:10.1073/pnas.1201701109

Cantor, D. J., and David, G. (2014). SIN3B, the SASP, and Pancreatic Cancer. *Mol. Cell Oncol.* 1, e969167. doi:10.4161/23723548.2014.969167

Cardinale, V., Puca, R., Carpino, G., Scafetta, G., Renzi, A., De Canio, M., et al. (2015). Adult Human Biliary Tree Stem Cells Differentiate to β-Pancreatic Islet Cells by Treatment with a Recombinant Human Pdx1 Peptide. *PloS one* 10, e0134677. doi:10.1371/journal.pone.0134677

Cardinale, V., Wang, Y., Carpino, G., Mendel, G., Alpini, G., Gaudio, E., et al. (2012). The Biliary Tree-A Reservoir of Multipotent Stem Cells. *Nat. Rev. Gastroenterol. Hepatol.* 9, 231–240. doi:10.1038/nrgastro.2012.23

Carpino, G., Cardinale, V., Gentile, R., Onori, P., Semeraro, R., Franchitto, A., et al. (2014). Evidence for Multipotent Endodermal Stem/progenitor Cell Populations in Human Gallbladder. *J. Hepatol.* 60, 1194–1202. doi:10.1016/j.jhep.2014.01.026

Carpino, G., Cardinale, V., Onori, P., Franchitto, A., Berloco, P. B., Rossi, M., et al. (2012). Biliary Tree Stem/progenitor Cells in Glands of Extrahepatic and Intraheptic Bile Ducts: an Anatomical *In Situ* Study Yielding Evidence of Maturational Lineages. *J. Anat.* 220, 186–199. doi:10.1111/j.1469-7580.2011.01462.x

Carpino, G., Puca, R., Cardinale, V., Renzi, A., Scafetta, G., Nevi, L., et al. (2016a). Peribiliary Glands as a Niche of Extrapancreatic Precursors Yielding Insulin-Producing Cells in Experimental and Human Diabetes. *Stem cells* 34, 1332–1342. doi:10.1002/stem.2311

Carpino, G., Renzi, A., Cardinale, V., Franchitto, A., Onori, P., Overi, D., et al. (2016b). Progenitor Cell Niches in the Human Pancreatic Duct System and Associated Pancreatic Duct Glands: an Anatomical and Immunophenotyping Study. *J. Anat.* 228, 474–486. doi:10.1111/joa.12418

Chomczynski, P., and Sacchi, N. (2006). The Single-step Method of RNA Isolation by Acid Guanidinium Thiocyanate-Phenol-Chloroform Extraction: Twenty-Something Years on. *Nat. Protoc.* 1, 581–585. doi:10.1038/nprot.2006.83

Domínguez-Bendala, J., Qadir, M. M. F., and Pastori, R. L. (2019). Pancreatic Progenitors: There and Back Again. *Trends Endocrinol. Metab.* 30, 4–11. doi:10.1016/j.tem.2018.10.002

Dooley, J., Tian, L., Schonefeldt, S., Delghingaro-Augusto, V., Garcia-Perez, J. E., Pasciuto, E., et al. (2016). Genetic Predisposition for Beta Cell Fragility Underlies Type 1 and Type 2 Diabetes. *Nat. Genet.* 48, 519–527. doi:10.1038/ng.3531

Dor, Y., Brown, J., Martinez, O. I., and Melton, D. A. (2004). Adult Pancreatic β-cells Are Formed by Self-Duplication rather Than Stem-Cell Differentiation. *Nature* 429, 41–46. doi:10.1038/nature02520

Duvillié, B., Kourdoughli, R., Druillennec, S., Eychène, A., and Pouponnot, C. (2020). Interplay between Diabetes and Pancreatic Ductal Adenocarcinoma and Insulinoma: The Role of Aging, Genetic Factors, and Obesity. *Front. Endocrinol.* 11, 563267. doi:10.3389/fendo.2020.563267

El-Gohary, Y., Wiersch, J., Tulachan, S., Xiao, X., Guo, P., Rymer, C., et al. (2016). Intraislet Pancreatic Ducts Can Give Rise to Insulin-Positive Cells. *Endocrinology* 157, 166–175. doi:10.1210/en.2015-1175

Folli, F., La Rosa, S., Finzi, G., Davalli, A. M., Galli, A., Dick, E. J., Jr., et al. (2018). Pancreatic Islet of Langerhans' Cytoarchitecture and Ultrastructure in normal Glucose Tolerance and in Type 2 Diabetes Mellitus. *Diabetes Obes. Metab.* 20 (Suppl. 2), 137–144. doi:10.1111/dom.13380

Huch, M., Bonfanti, P., Boj, S. F., Sato, T., Loomans, C. J. M., van de Wetering, M., et al. (2013). Unlimited *In Vitro* Expansion of Adult Bi-potent Pancreas Progenitors through the Lgr5/R-Spondin axis. *EMBO J.* 32, 2708–2721. doi:10.1038/emboj.2013.204

Lanzoni, G., Cardinale, V., and Carpino, G. (2016). The Hepatic, Biliary, and Pancreatic Network of Stem/progenitor Cell Niches in Humans: A New Reference Frame for Disease and Regeneration. *Hepatology* 64, 277–286. doi:10.1002/hep.28326

Leiter, E. H., and Schile, A. (2013). Genetic and Pharmacologic Models for Type 1 Diabetes. *Curr. Protoc. mouse Biol.* 3, 9–19. doi:10.1002/9780470942390.mo120154

Martin-Pagola, A., Sisino, G., Allende, G., Dominguez-Bendala, J., Gianani, R., Reijonen, H., et al. (2008). Insulin Protein and Proliferation in Ductal Cells in the Transplanted Pancreas of Patients with Type 1 Diabetes and Recurrence of Autoimmunity. *Diabetologia* 51, 1803–1813. doi:10.1007/s00125-008-1105-x

Mathieu, C., Martens, P.-J., and Vangoitsenhoven, R. (2021). One Hundred Years of Insulin Therapy. *Nat. Rev. Endocrinol.* 17, 715–725. doi:10.1038/s41574-021-00542-w

Meier, J. J., Butler, A. E., Saisho, Y., Monchamp, T., Galasso, R., Bhushan, A., et al. (2008). β-Cell Replication Is the Primary Mechanism Subserving the Postnatal Expansion of β-Cell Mass in Humans. *Diabetes* 57, 1584–1594. doi:10.2337/db07-1369

Merkwitz, C., Blaschuk, O. W., Schulz, A., Lochhead, P., Meister, J., Ehrlich, A., et al. (2013). The Ductal Origin of Structural and Functional Heterogeneity

between Pancreatic Islets. *Prog. Histochem. Cytochem.* 48, 103–140. doi:10.1016/j.proghi.2013.09.001

Qadir, M. M. F., Álvarez-Cubela, S., Klein, D., Lanzoni, G., García-Santana, C., Montalvo, A., et al. (2018). P2RY1/ALK3-Expressing Cells within the Adult Human Exocrine Pancreas Are BMP-7 Expandable and Exhibit Progenitor-like Characteristics. *Cel Rep.* 22, 2408–2420. doi:10.1016/j.celrep.2018.02.006

Qadir, M. M. F., Álvarez-Cubela, S., Klein, D., van Dijk, J., Muñiz-Anquela, R., Moreno-Hernández, Y. B., et al. (2020). Single-cell Resolution Analysis of the Human Pancreatic Ductal Progenitor Cell Niche. *Proc. Natl. Acad. Sci. USA* 117, 10876–10887. doi:10.1073/pnas.1918314117

Song, I., Patel, O., Himpe, E., Muller, C. J. F., and Bouwens, L. (2015). Beta Cell Mass Restoration in Alloxan-Diabetic Mice Treated with EGF and Gastrin. *PloS one* 10, e0140148. doi:10.1371/journal.pone.0140148

Strobel, O., Rosow, D. E., Rakhlin, E. Y., Lauwers, G. Y., Trainor, A. G., Alsina, J., et al. (2010). Pancreatic Duct Glands Are Distinct Ductal Compartments that React to Chronic Injury and Mediate Shh-Induced Metaplasia. *Gastroenterology* 138, 1166–1177. doi:10.1053/j.gastro.2009.12.005

Thompson, P. J., Shah, A., Ntranos, V., Van Gool, F., Atkinson, M., and Bhushan, A. (2019). Targeted Elimination of Senescent Beta Cells Prevents Type 1 Diabetes. *Cel Metab.* 29, 1045–1060. doi:10.1016/j.cmet.2019.01.021

van der Meulen, T., Mawla, A. M., DiGruccio, M. R., Adams, M. W., Nies, V., Dólleman, S., et al. (2017). Virgin Beta Cells Persist throughout Life at a Neogenic Niche within Pancreatic Islets. *Cel Metab.* 25, 911–926. doi:10.1016/j.cmet.2017.03.017

Wang, D., Wang, J., Bai, L., Pan, H., Feng, H., Clevers, H., et al. (2020). Long-Term Expansion of Pancreatic Islet Organoids from Resident Procr+ Progenitors. *Cell* 180, 1198–1211. doi:10.1016/j.cell.2020.02.048

Wang, Y., Lanzoni, G., Carpino, G., Cui, C. B., Dominguez-Bendala, J., Wauthier, E., et al. (2013). Biliary Tree Stem Cells, Precursors to Pancreatic Committed Progenitors: Evidence for Possible Life-long Pancreatic Organogenesis. *Stem cells* 31, 1966–1979. doi:10.1002/stem.1460

Xiao, X., Chen, Z., Shiota, C., Prasadan, K., Guo, P., El-Gohary, Y., et al. (2013). No Evidence for β Cell Neogenesis in Murine Adult Pancreas. *J. Clin. Invest.* 123, 2207–2217. doi:10.1172/jci66323

Yamaguchi, J., Liss, A. S., Sontheimer, A., Mino-Kenudson, M., Castillo, C. F.-d., Warshaw, A. L., et al. (2015). Pancreatic Duct Glands (PDGs) Are a Progenitor Compartment Responsible for Pancreatic Ductal Epithelial Repair. *Stem Cel. Res.* 15, 190–202. doi:10.1016/j.scr.2015.05.006

Yamaguchi, J., Mino-Kenudson, M., Liss, A. S., Chowdhury, S., Wang, T. C., Fernández-del Castillo, C., et al. (2016). Loss of Trefoil Factor 2 from Pancreatic Duct Glands Promotes Formation of Intraductal Papillary Mucinous Neoplasms in Mice. *Gastroenterology* 151, 1232–1244. doi:10.1053/j.gastro.2016.07.045

Yoneda, S., Uno, S., Iwahashi, H., Fujita, Y., Yoshikawa, A., Kozawa, J., et al. (2013). Predominance of β-Cell Neogenesis rather Than Replication in Humans with an Impaired Glucose Tolerance and Newly Diagnosed Diabetes. *J. Clin. Endocrinol. Metab.* 98, 2053–2061. doi:10.1210/jc.2012-3832

Yuchi, Y., Cai, Y., Legein, B., De Groef, S., Leuckx, G., Coppens, V., et al. (2015). Estrogen Receptor α Regulates β-Cell Formation during Pancreas Development and Following Injury. *Diabetes* 64, 3218–3228. doi:10.2337/db14-1798

Zhou, Q., Brown, J., Kanarek, A., Rajagopal, J., and Melton, D. A. (2008). *In Vivo* reprogramming of Adult Pancreatic Exocrine Cells to β-cells. *Nature* 455, 627–632. doi:10.1038/nature07314

Conflict of Interest: The Italian Federation of Juvenile Diabetes (FDG) holds a patent related to the recombinant Pdx1 utilized in this study.

The authors declare that the research was conducted in the absence of any commercial or financial relationships that could be construed as a potential conflict of interest.

Publisher's Note: All claims expressed in this article are solely those of the authors and do not necessarily represent those of their affiliated organizations, or those of the publisher, the editors and the reviewers. Any product that may be evaluated in this article, or claim that may be made by its manufacturer, is not guaranteed or endorsed by the publisher.

Advantages of publishing in Frontiers

OPEN ACCESS
Articles are free to read for greatest visibility and readership

FAST PUBLICATION
Around 90 days from submission to decision

HIGH QUALITY PEER-REVIEW
Rigorous, collaborative, and constructive peer-review

TRANSPARENT PEER-REVIEW
Editors and reviewers acknowledged by name on published articles

Frontiers
Avenue du Tribunal-Fédéral 34
1005 Lausanne | Switzerland

Visit us: www.frontiersin.org
Contact us: frontiersin.org/about/contact

REPRODUCIBILITY OF RESEARCH
Support open data and methods to enhance research reproducibility

DIGITAL PUBLISHING
Articles designed for optimal readership across devices

FOLLOW US
@frontiersin

IMPACT METRICS
Advanced article metrics track visibility across digital media

EXTENSIVE PROMOTION
Marketing and promotion of impactful research

LOOP RESEARCH NETWORK
Our network increases your article's readership